C 55. 2: C61/2/979

PENNSYLVANIA STATE UNIVERSITY
JUN 02 1980
DOCUMENTS COLLECTION

# Proceedings of the Fourth Annual Climate Diagnostics Workshop

Institute for Environmental Studies
University of Wisconsin
Madison, Wisconsin

October 16-18, 1979

**U.S. DEPARTMENT OF COMMERCE**
**National Oceanic and Atmospheric Administration**

# Proceedings of the Fourth Annual Climate Diagnostics Workshop

Held at the
Institute for Environmental Studies
University of Wisconsin
Madison, Wisconsin
October 16-18, 1979

U.S. DEPARTMENT OF COMMERCE
**Philip M. Klutznick, Secretary**
National Oceanic and Atmospheric Administration
**Richard A. Frank, Administrator**

U. S. Depository Copy

# Preface

In 1979 the Climate Analysis Center (CAC) took over NOAA's role in organizing the Annual Climate Diagnostics Workshop. I wish to express CAC's and NOAA's thanks to Prof. Reid Bryson, Director of the Institute for Environmental Studies for hosting this Fourth Annual Workshop at the University of Wisconsin. The contributions that he and Profs. John Kutzbach and Stefan Hastenrath made in organizing the program and making the local arrangements for the Workshop are much appreciated. Thanks are also due Joanne Mais, Susan (Cayan) Wurtz, Patsy Behling, and Melanie Woodworth for the fine logistical support at Wisconsin; Dr. Hassan Virji for very efficient handling of the projection facilities; and Luke Mannello and Norma Jaxel for preparation of these Proceedings for publication. I am also indebted to Drs. Donald Gilman, Lyle Horn, John Kutzbach, Stefan Hastenrath, and William Sprigg for effective chairing of the Workshop sessions. Finally, I thank all of the participants for their contributions to a very full, but lively and fast moving, two and a half days of informative and interesting presentations and discussions.

As in the three preceding years, these Proceedings are designed to provide synopses of the presentations at the Workshop. For the most part, papers are arranged here in the order of original presentation. One paper not given at the Workshop has been included here — Coughlan, Skinner, and Wright's discussion of Southern Hemisphere circulations of 1978-79 (end of Session 1). David Wright was originally scheduled to present it, but was unable to attend the Workshop. This paper helps to make the rather thorough review of the year's climate fluctuations over the globe (Session 1) even more complete.

Beyond the review of the past year's climate fluctuations, the Workshop concentrated principally on reports of a variety of ongoing climate diagnostic studies of the observed atmosphere (Session 2 and the third paper of Session 3) and of model atmospheres (Session 4). Also emphasized in Session 3 were the program of the CAC and the selection of indices and analyzed fields for inclusion in a real-time diagnostics data base at CAC. Session 3 also treated some of the opportunities as well as the problems involved in using the NMC and NESS data bases for climate analysis. Prediction was treated in only two papers — Spar's in Session 4 and Navato's in Session 5 (in addition to a few references to actual forecasts for the past year in Namias' and Douglas' papers in Session 1). A special topic for this year, volcanic activity and climate, was mainly addressed in Goodman and Bryson's paper (Session 5) and to a lesser extent in Navato's presentation.

Jay S. Winston
March 1980

## List of Participants
## Climate Diagnostics Workshop
## October 16-18, 1979

| | |
|---|---|
| Thomas Achtor | University of Wisconsin |
| Jon Ahlquist | University of Wisconsin |
| M. Al-Tasan | University of Wisconsin |
| Pat Behling | University of Wisconsin |
| Arthur D. Belmont | Control Data Corporation |
| Eugene J. Benuzzi | USAF/ETAC |
| Kenneth H. Bergman | National Science Foundation |
| George J. Boer | AES/Canadian Climate Centre |
| Reid A. Bryson | University of Wisconsin |
| Daniel Cayan | Scripps/University of California |
| Dennis G. Dartt | Control Data Corporation |
| Roger Davies | University of Wisconsin |
| Henry F. Diaz | NOAA/EDIS/NCC |
| Robert R. Dickson | NOAA/NWS/CAC |
| Gerald J. Dittberner | USAF/ETAC |
| Arthur V. Douglas | University of Nebraska |
| Yves Durocher | AES/Canadian Climate Centre |
| Harold J. Edmon, Jr. | University of Washington |
| Carl O. Erickson | NOAA/NWS/CAC |
| Joseph O. Fletcher | NOAA/ERL |
| Robert Gallimore | University of Wisconsin |
| Monique Gamache | University of Wisconsin |
| Catherine Gautier | University of Wisconsin |
| Donald L. Gilman | NOAA/NWS/CAC |
| Brian Goodman | University of Wisconsin |
| Kent L. Groninger | NOAA/ERL |
| David S. Gutzler | University of Washington |
| Douglas Hahn | NOAA/ERL/GFDL |
| Kirby J. Hanson | NOAA/ERL/GMCC |
| Robert P. Harnack | Rutgers University |
| Stefan Hastenrath | University of Wisconsin |
| Christopher M. Hayden | NOAA/NESS/MSL |
| Leroy D. Herman | NOAA/NESS/MSL |
| Edward Hopkins | University of Wisconsin |
| Lyle Horn | University of Wisconsin |
| David D. Houghton | University of Wisconsin |
| Arthur Kraus | University of Wisconsin |
| Arthur F. Krueger | NOAA/NWS/CAC |
| George J. Kukla | Lamont-Doherty/Columbia University |
| John E. Kutzbach | University of Wisconsin |
| Peter J. Lamb | Illinois State Water Survey |
| Ngar-Cheung Lau | NOAA/ERL/GFDL |
| Heinz Lettau | University of Wisconsin |
| Anne LeBlanc | University of Wisconsin |
| G. Robert Lofgren | University of Arizona |
| David Martin | University of Wisconsin |
| Michael Matson | NOAA/NESS/ESG |
| James P. McGuirk | Texas A&M University |
| Douglas R. McLain | NOAA/NMFS/PEG |

| | |
|---|---|
| Alvin J. Miller | NOAA/NWS/CAC |
| Kyung D. Min | University of Wisconsin |
| Ørnulf Moen | University of Wisconsin |
| Takio Murakami | University of Hawaii |
| Alfredo R. Navato | Massachusetts Institute of Technology |
| Bhim Namdeo Nimgade | University of Wisconsin |
| Bette Otto-Bliesner | University of Wisconsin |
| Jacob Padro | AES/Canadian Climate Centre |
| William H. Quinn | Oregon State University |
| Roderick S. Quiroz | NOAA/NWS/CAC |
| P. Krishna Rao | NOAA/NESS/MSL |
| Eugene M. Rasmusson | NOAA/NWS/CAC |
| Richard D. Rosen | Environmental Research & Technology, Inc. |
| James C. Sadler | University of Hawaii |
| David A. Salstein | Environmental Research & Technology, Inc. |
| Michael E. Schlesinger | Oregon State University |
| Robert Schlesinger | University of Wisconsin |
| James G. Schofield | USAF/ETAC |
| David Secora | University of Wisconsin |
| Curtis Smalls | University of Wisconsin |
| Jerome Spar | City University of New York |
| William A. Sprigg | NOAA/NCPO |
| Albert Swain | University of Wisconsin |
| Kevin E. Trenberth | University of Illinois |
| Harry van Loon | National Center for Atmospheric Research |
| Hassan Virji | University of Wisconsin |
| A. James Wagner | NOAA/NWS/CAC |
| Wayne Wendland | Illinois State Water Survey |
| Jay S. Winston | NOAA/NWS/CAC |
| Stanley F. Woronko | AES/Canadian Climate Centre |
| John A. Young | University of Wisconsin |
| Jim Zandlo | University of Wisconsin |
| John Zapotocny | University of Wisconsin |
| Shi-Feng Zhang | University of Nanking |

# TABLE OF CONTENTS

| | | Page |
|---|---|---|
| Preface . . . . . . . . . . . . . . . . . . . . . . . . . . . . . | | i |
| List of Participants . . . . . . . . . . . . . . . . . . . . . . . | | ii |

## Contributed Papers:

### Session 1: Review of Climate Fluctuations of the Year, September 1978-August 1979.

| | | |
|---|---|---|
| A Review of the Circulation and Weather of Fall and Winter 1978-79, With a Comparison of the Past Three Cold Seasons | A. James Wagner | 1 |
| The Circulation and Weather of Spring and Summer 1979. | Robert R. Dickson | 9 |
| Canadian Climate Extremes and Impacts for the Period September 1978 to August 1979. | Yves Durocher | 19 |
| 378-Year Occurrence of the 1976-77 and 1978-79 Winter Sea Level Pressure Patterns Over the North Pacific and North America. | G. Robert Lofgren<br>Geoffrey A. Gordon | 27 |
| Long-Wave Contributions to Tropospheric and Stratospheric Temperature Anomalies in Winter. | Roderick S. Quiroz | 37 |
| Circulation and Weather Changes From the Summer 1978 Through the Subsequent Winter. | Jerome Namias | 41 |
| Snow and Sea Ice in 1978-1979. | George J. Kukla<br>J. Gavin | 60 |
| Recent Variations of SST Along the East and West Coasts of the U.S. | Douglas R. McLain | 72 |
| Further Analysis of Recent Fluctuations in Circulation and Cloudiness (Rainfall) Over the Tropics. | Arthur F. Krueger<br>Jay S. Winston | 84 |
| Possible Causes for the Wet Winter of 1978-79 in the Southwestern United States and Mexico. | Arthur V. Douglas | 94 |
| The Large Scale Upper-Tropospheric Circulation Associated with Unusually Heavy Rainfall over the Southern United States, Spring 1979. | Carl O. Erickson | 108 |

## Session 1: Review of Climate Fluctuations of the Year, September 1978-August 1979 (con.)

| | | Page |
|---|---|---|
| TIROS-N Radiation Budget Over MONEX During 1979. | P. Krishna Rao | 120 |
| A Satellite View of the 1979 Indian Monsoon Circulation. | John A. Young | 137 |
| The Southern Hemisphere Circulations - September 1978 to August 1979. | M. Coughlan<br>T. Skinner<br>D. Wright | 149 |

## Session 2: Diagnostic Studies

| | | |
|---|---|---|
| A Diagnostic Study of the 1976-7 and 1977-8 Winters Over the Northern Hemisphere. | Harold J. Edmon, Jr. | 156 |
| Precipitation Along the West Coast of North America. | James P. McGuirk | 173 |
| The Statistical Relationship Between Mean Summer Precipitation in the United States and the Concurrent Tropospheric Pressure Distribution. | Robert Harnack | 188 |
| Airstream Source Regions of the Northern Hemisphere. | Wayne M. Wendland<br>Reid A. Bryson | 203 |
| Variations of Atmospheric Water Vapor and the Water Vapor Transport Vector During a Fifteen-Year Period. | David A. Salstein<br>Richard O. Rosen | 207 |
| Climatic Variability in the Northern Hemisphere. | George J. Boer<br>Kaz Higuchi | 218 |
| Trends of 700 mb Temperature in Winter and Their Connection with Changes in Stationary-Eddy Heat Fluxes. | Harry van Loon | 220 |
| A Statistical Model of Planetary Scale Waves in the 500 mb Geopotential. | Jacob Padro<br>Stanley F. Woronko | 226 |
| On the Heat Budget of Hydrosphere and Atmosphere in the Indian Ocean. | Stefan Hastenrath | 228 |
| Empirical Orthogonal Function Analysis of Satellite-Observed Outgoing Longwave Radiation During Winter. Part II. Short-Period (4-6 day) Oscillations. | Takio Murakami | 229 |

Session 2: Diagnostic Studies (con.)

| | | Page |
|---|---|---|
| The False El Niño and Recent Related Climatic Changes in the Southeast Pacific. | William H. Quinn | 233 |
| Coherent Fluctuations of the Ocean/ Atmospheric System on the Time Scale of Decades and Centuries. | Joseph O. Fletcher | 245 |
| Some Examples of Atmospheric Dynamical Effects on Atmospheric Trace Constituents. | Kirby Hanson<br>James Peterson<br>Bernard Mendonca<br>Walter Komhyr | 246 |

Session 3: CAC Program, Climate Indices

| | | |
|---|---|---|
| Current and Planned Activities of NOAA's Climate Analysis Center. | Jay S. Winston | 266 |
| Survey of Climate Indices Useful to the Climate Analysis Center. | Eugene M. Rasmusson<br>Wen-Yuan Chen | 282 |
| Horizontal Teleconnections During the Northern Hemisphere Winter Season. | John M. Wallace<br>David S. Gutzler | 296 |
| Trade Wind Anomalies Using Satellite Cloud Motion Vectors. | James C. Sadler | 307 |
| The NMC Operational Energy Code: Its Use in Data Base Evaluation. | Alvin J. Miller<br>T. G. Rogers | 319 |
| A Comparison Between Circulation Statistics Computed From Conventional Data and NMC Hough Analyses. | Richard D. Rosen<br>David A. Salstein | 334 |
| New Data and New Products: the NOAA/ NESS Continental Snow Cover Data Base. | Michael Matson<br>Donald A. Wiesnet<br>Craig P. Berg<br>E. Paul McClain | 351 |
| The Northern Hemisphere Sea Level Pressure Data Set: Trends, Errors and Discontinuities. | Kevin E. Trenberth<br>Daniel A. Paolino, Jr. | 365 |

Session 4. Modeling Results

| | | |
|---|---|---|
| Preliminary Analysis of the Seasonal and Interannual Variability Simulated by the OSU Two-level Atmospheric General Circulation Model. | Michael E. Schlesinger<br>W. L. Gates | 379 |

Session 4: Modeling Results (con.)

| | | Page |
|---|---|---|
| Simulation of Atmospheric Variability. | Douglas G. Hahn<br>Syukuro Manabe | 398 |
| The Three-Dimensional Structure of Monthly Anomalies Appearing in a 15-Year Simulation of a GFDL General Circulation Model. | Ngar-Cheung Lau | 403 |
| Prediction Experiments With a Coarse-Mesh Global Model. | Jerome Spar | 413 |

Session 5: Volcanic Activity and Climate

| | | |
|---|---|---|
| Observed Interannual Aerosol Optical Depth Variations for the Northern Hemisphere. | Brian Goodman<br>Reid A. Bryson | 424 |
| Influence of Volcanic Aerosols and Oceanic Surface Temperatures on Tropospheric Temperatures. | Alfredo R. Navato | 428 |

# A REVIEW OF THE CIRCULATION AND WEATHER OF FALL AND WINTER 1978-79, WITH A COMPARISON OF THE PAST THREE COLD SEASONS

by

A. James Wagner
Climate Analysis Center
NOAA/National Weather Service
Washington, D. C. 20233

## 1. FALL 1978

An unusually intense mean low centered between the North Pole and Spitzbergen contributed to a vigorous circulation at high latitudes during Fall 1978. The westerlies were remarkably strong across the Atlantic and European sectors, where seasonal 700 mb mean anomaly centers of -65m over Baffin Island and -86m over the Ural Mountains flanked an unusually strong ridge with a +89 anomaly center just west of the English Channel (Fig. 1A). These centers were all close to three standard deviations from the 1948-1970 mean.

A deeper than normal trough also extended south from Kamchatka over the western Pacific, while above normal 700 mb heights prevailed over much of Asia, the eastern Pacific and the United States east of the Rockies. A slightly stronger than normal trough was located over the southwestern United States.

The stronger than normal ridges over the eastern United States and western Europe were associated with pleasant mild and dry fall weather in those areas. Temperatures averaged 2°F to 4°F above normal over much of the southeastern United States, while extensive areas of the northwestern quarter of the country averaged more than 2°F below normal under the influence of enhanced northerly flow from Canada (Fig. 1B). New York and New England were also cooler than normal under the influence of Canadian air much of the time.

Precipitation was heaviest relative to normal over the Southwest, which was affected by moisture from Tropical Storm Norman dissipating just off the southern California coast in early September (Fig. 1C). Other than limited areas of the northern Great Plains and the upper Midwest, most of the remainder of the Nation had near normal or less precipitation. Drought conditions prevailed in sections of the Southeast.

September and November had circulation patterns similar to the fall pattern in the vicinity of the United States, and thus determined the prevailing seasonal mean. The pattern during October was the reverse, with a mild West and cool East. Several cities in Arizona and California reported one of their warmest Octobers. Stronger than normal northwesterly flow during this month also resulted in sparse precipitation over extensive areas. A number of cities from the West Coast to the Southeast reported one of the driest Octobers on record. A resurgence of the ridge over the Southeast the following month led to one of the mildest Novembers on record in that area, however.

## 2. WINTER 1978-79

Very long wavelengths characterized the 700 mb circulation during winter 1978-79. At middle latitudes principal troughs were located over the western Pacific, the western Atlantic and eastern Europe (Fig.2A). Above normal heights dominated the Pacific sector, while a band of below normal 700 mb heights extended from California eastward across the United States and southern Canada over the Atlantic to Europe. A deep low near the Tamyr Penisula (anomaly - 112m, approximately two standard deviations from the mean) along with above normal heights over central Asia provided a generally high index circulation over the eastern half of the Northern Hemisphere, while blocking extending from Alaska to Scandinavia, along with the previously noted band of below normal heights from North America to eastern Europe, gave a low index circulation over the western half of the Northern Hemisphere.

Winter temperatures averaged below normal over almost the entire mainland United States, and no stations were in the "above normal" category (Fig. 2B). A winter pattern with substantially below normal temperatures from coast to coast is quite rare, having occurred only twice before in the period of reliable records (1898-99 and 1909-10). Precipitation was heavier than normal over extensive areas of the country: The Southwest, much of the Rocky Mountain region and northern Great Plains, portions of the upper Mississippi Valley and almost the entire East and South (Fig. 2C). The active storm systems entering California and rejuvenating near the Gulf Coast, together with the cold air prevalent over the United States most of the time, produced heavier than normal snowfall over most of the country from the Rocky Mountains eastward.

During the course of the winter, progression of a deep trough over North America expanded the influence of cold air gradually eastward. In December, the dividing line between below and above normal temperatures lay close to the Mississippi River, with the coldest conditions over the northern Rockies. Record and near-record December cold was observed over the Northwest, the Rockies and the western Great Plains. An active storm track near the boundary between the cold west and mild east produced a record wet December at some places in and near the Ohio Valley. By January, below normal temperatures had extended to the Atlantic coast except for New England, while moderation began over California. A large area from the northern intermountain region through the Great Plains and Mississippi Valley eastward to the lower Ohio Valley had a record or near-record cold January. Record heavy snows fell in the Midwest, and many localities in the middle and north Atlantic States had their wettest January. In February, the main trough moved off the Atlantic coast and temperatures averaged well below normal over the entire country east of the Rocky Mountains. Several localities from the Mississippi Valley eastward had one of the coldest Februaries on record, and in the middle Atlantic States it was one of the snowiest as well.

## 3. COMPARISON OF THE LAST THREE COLD SEASONS

The occurrence of three consecutive unusually severe winters covering a large portion of the United States is a rare event. Although the area affected by the severest cold has been somewhat farther west each year, the Midwest has born the brunt of the cold. Fig. 3A shows this tendency for westward displacement and enlargement of the -8°F winter mean anomaly isoline, and discloses an area in Illinois where each of the past three winters has averaged more than 8°F below normal.

A more representative indication of how extreme or unusual a season has been is the probability of exceeding a given departure from normal. This method has been used to show how the last three cold seasons (taken from July 1 through June 30) rank as to total heating degree days (Figs. 3B, C, D). The principal pattern is determined by the three winter months, with somewhat smaller contributions from the fall and spring.

It can be seen that the cold season of 1976-77 was actually most extreme in the Midwest and South, where fewer than one in 50 seasons would be expected to be colder. During 1977-78, the most extreme cold relative to normal was centered over the central and southern Mississippi Valley, and in the most recent season it was over the northern and central Great Plains. The area enclosed by the one in 50 line was actually less extensive in 1978-79 than in the previous two years, even though the area within the -8°F isoline was larger. This is due to the fact that the north-central states and Great Plains have the highest temperature variability for any part of the country, while the South and Gulf Coast have considerably less.

## FIGURES

Fig. 1 (A) Mean 700 mb contours (solid) in dekameters and departures from normal (dashed) in meters, (B) departure from normal of average surface temperature (°F), and (C) percentage of normal precipitation for fall (September, October and November 1978).

Fig. 2 As in Fig. 1, except for winter (December 1978 and January and February 1979).

Fig. 3 Comparison of last three winters and cold seasons. (A) Areas where the past three winters averaged 8°F or more below normal, (B), (C), and (D) areas where the heating degree day totals for 1976-77, 1977-78 and 1978-79, respectively, were among the greatest 2%, 10% and 20% based on analysis of data from 1931-32 through 1977-78.

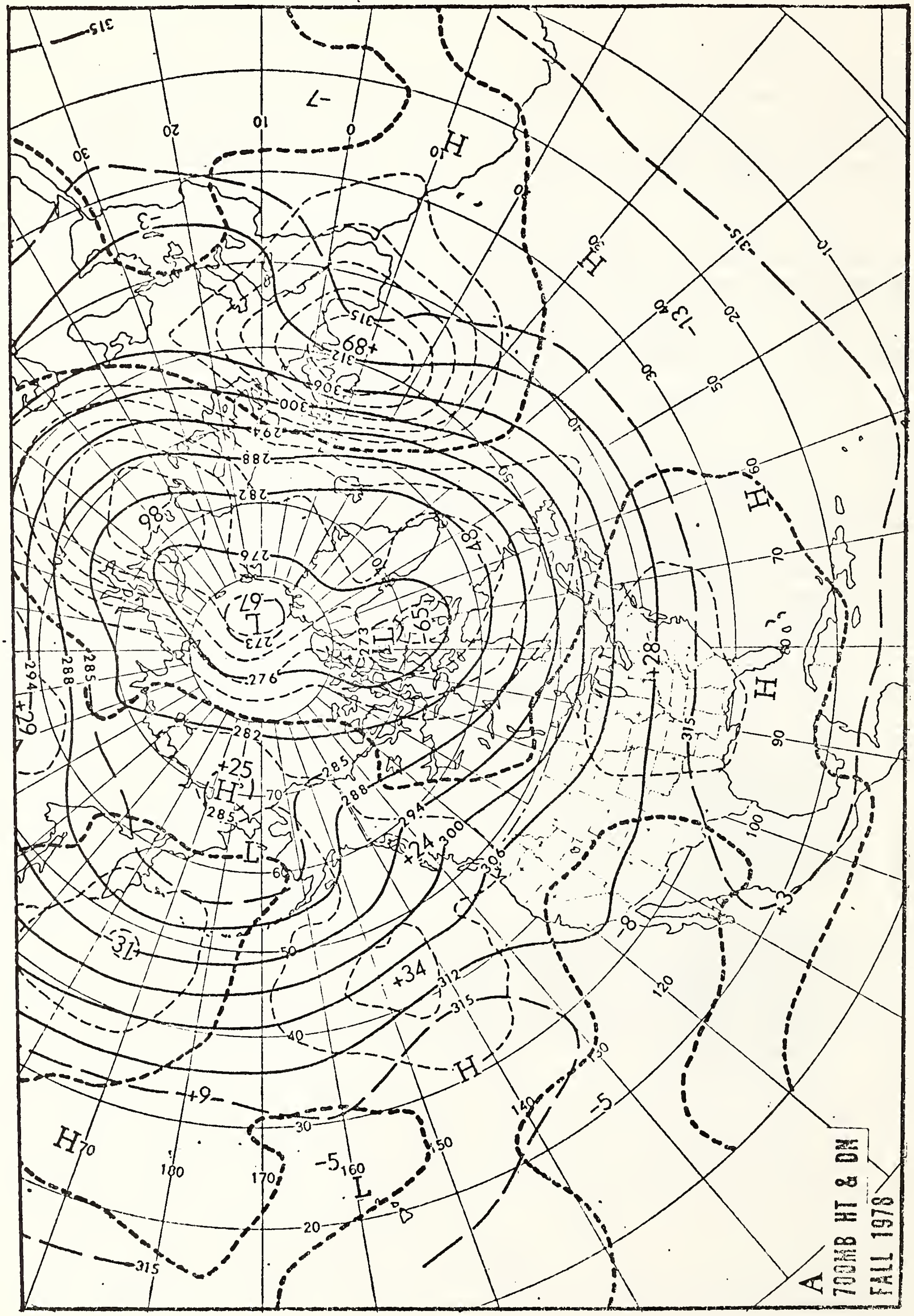

A
700MB HT & DN
FALL 1978

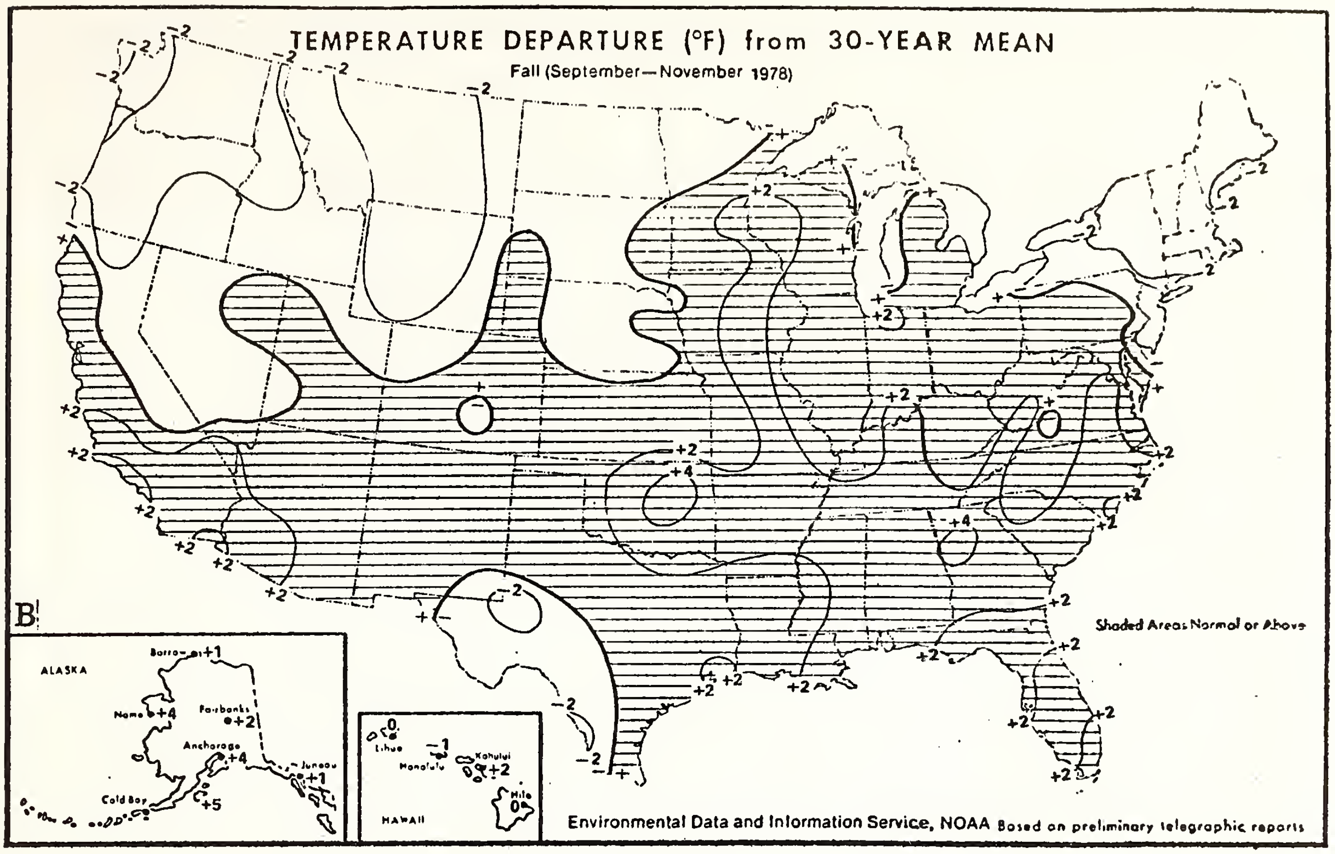

TEMPERATURE DEPARTURE (°F) from 30-YEAR MEAN

Fall (September—November 1978)

Environmental Data and Information Service, NOAA Based on preliminary telegraphic reports

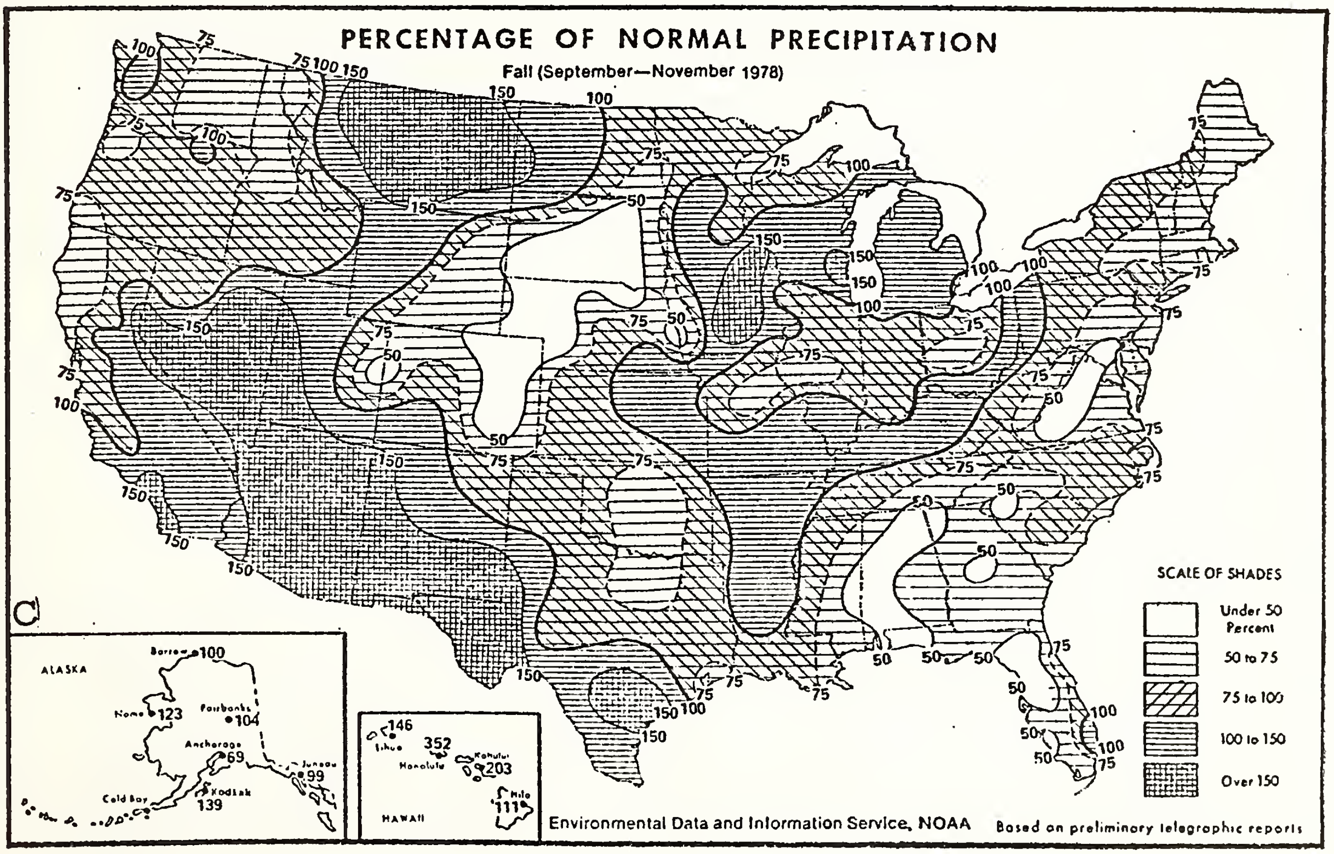

PERCENTAGE OF NORMAL PRECIPITATION

Fall (September—November 1978)

Environmental Data and Information Service, NOAA Based on preliminary telegraphic reports

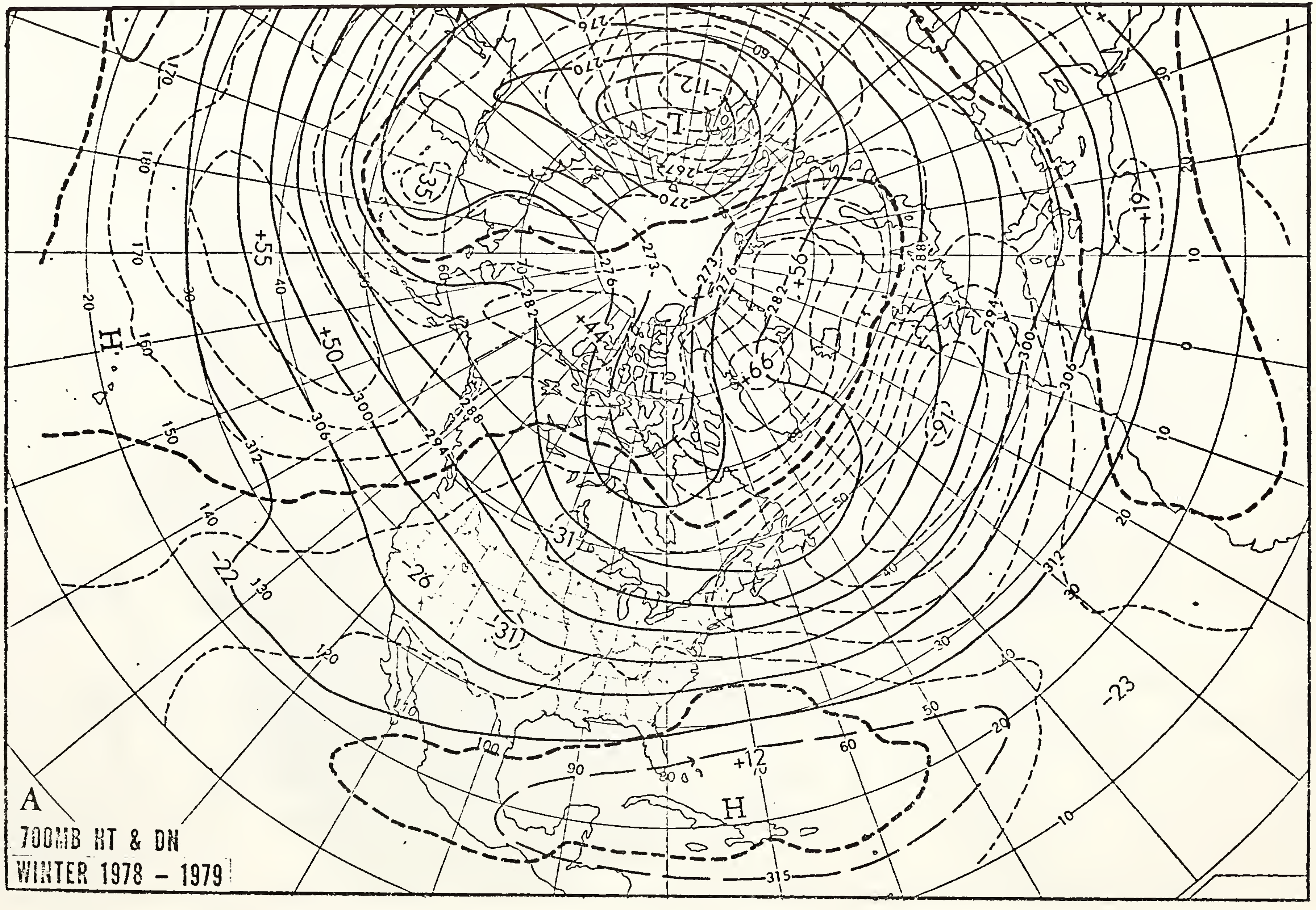

A

700MB HT & DN
WINTER 1978 - 1979

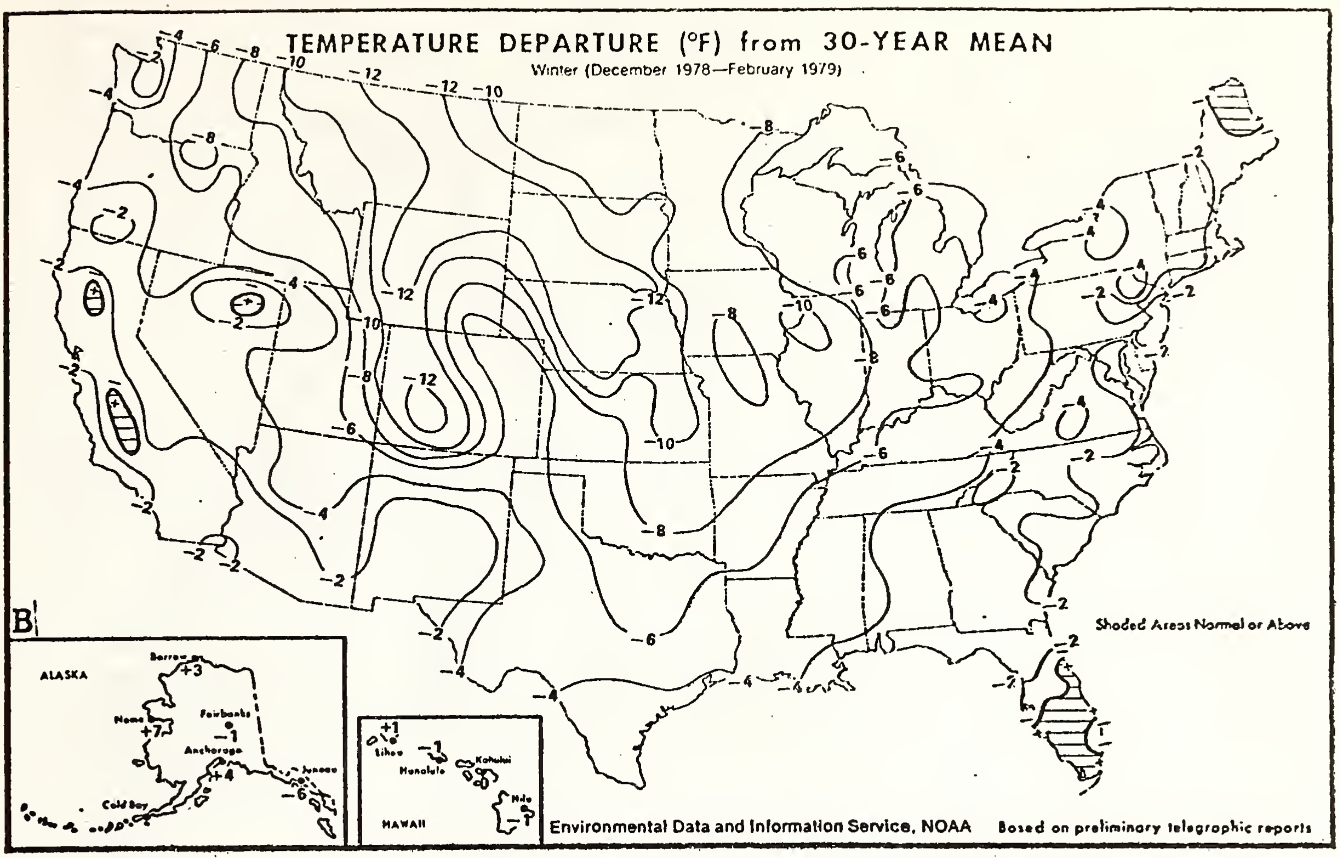
TEMPERATURE DEPARTURE (°F) from 30-YEAR MEAN
Winter (December 1978—February 1979)
B
ALASKA
Barrow +3
Nome +7
Fairbanks −1
Anchorage +4
Juneau −6
Cold Bay
HAWAII
Lihue +1
Honolulu −1
Kahului
Hilo −1
Shaded Areas Normal or Above
Environmental Data and Information Service, NOAA
Based on preliminary telegraphic reports

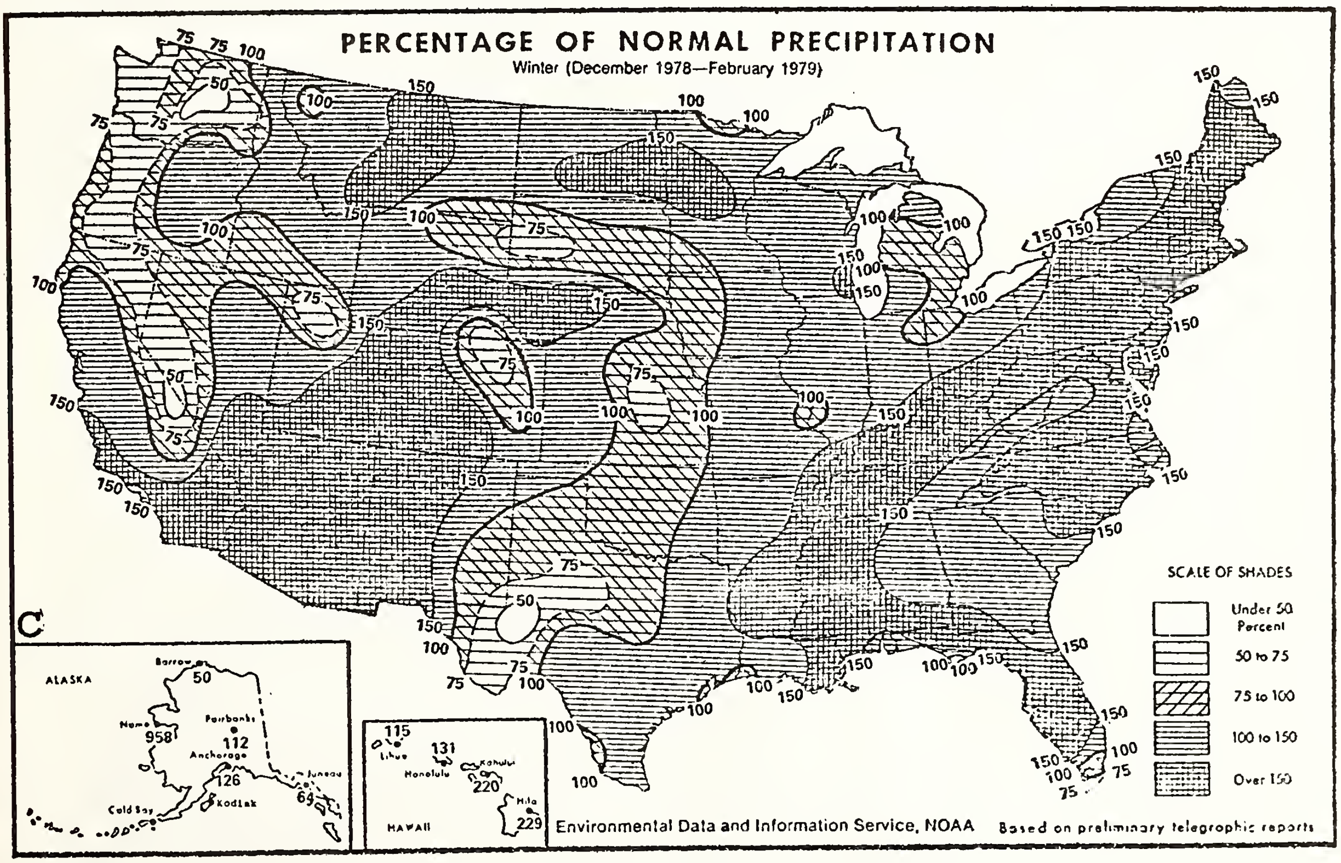
PERCENTAGE OF NORMAL PRECIPITATION
Winter (December 1978—February 1979)
C
ALASKA
Barrow 50
Nome 958
Fairbanks 112
Anchorage
Kodiak 126
Juneau 64
Cold Bay
HAWAII
Lihue 115
Honolulu 131
Kahului 220
Hilo 229
SCALE OF SHADES
Under 50 Percent
50 to 75
75 to 100
100 to 150
Over 150
Environmental Data and Information Service, NOAA
Based on preliminary telegraphic reports

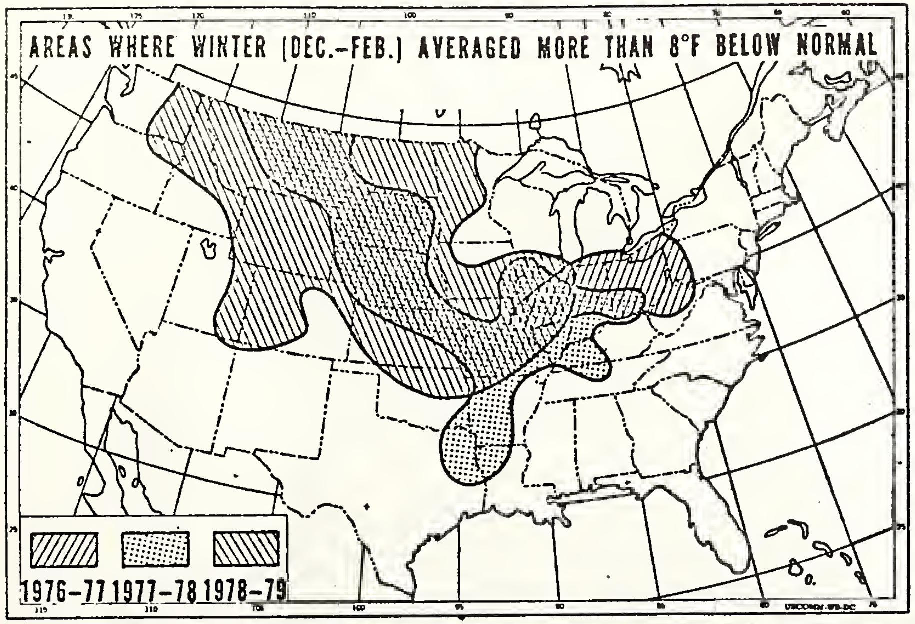
AREAS WHERE WINTER (DEC.-FEB.) AVERAGED MORE THAN 8°F BELOW NORMAL

| ▨ | ▒ | ▧ |
|---|---|---|
| 1976-77 | 1977-78 | 1978-79 |

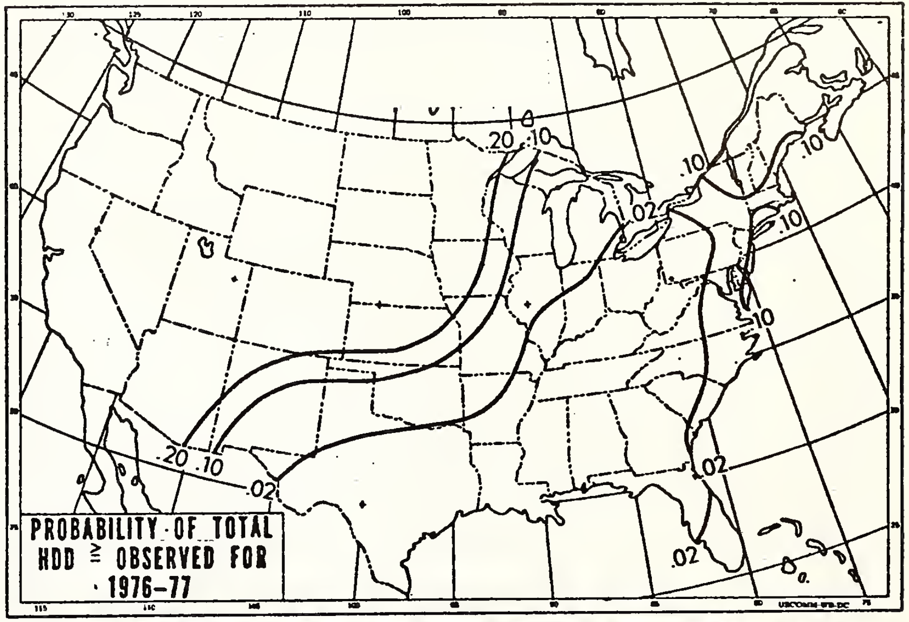
PROBABILITY OF TOTAL HDD ≧ OBSERVED FOR 1976-77

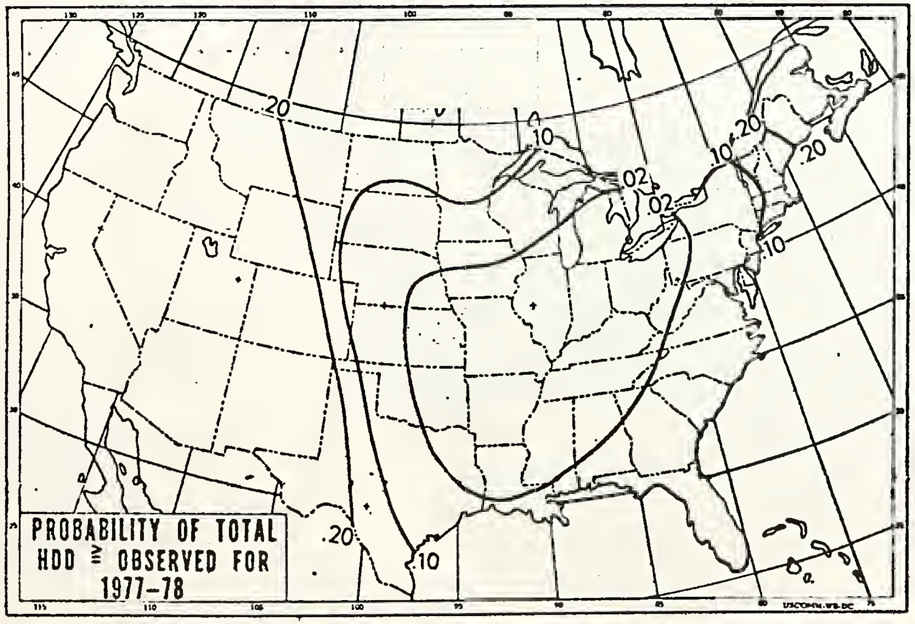
PROBABILITY OF TOTAL HDD ≧ OBSERVED FOR 1977-78

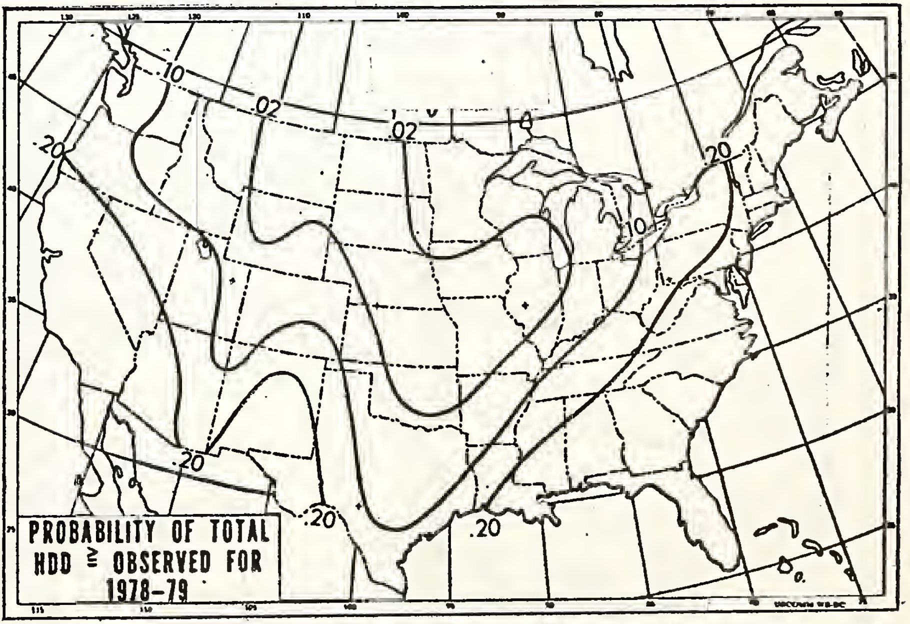
PROBABILITY OF TOTAL HDD ≧ OBSERVED FOR 1978-79

# The Circulation and Weather of Spring and Summer 1979

by

Robert R. Dickson
Climate Analysis Center
National Weather Service, NOAA

Spring 1979. The seasonal mean 700 mb circulation this spring had four well defined waves north of 50°N instead of the normal three (Fig. 1a); the deep trough over England was the principal anomaly. The strong high north of northeastern Siberia represents the retrogression of a winter mean anomaly. A westward displacement of the Canadian ridge coupled with a strong subtropical jet stream emanating from the southeast Pacific to bring deepening systems to mid-nation while the east coast trough was weaker than normal. Vorticity maxima and storm systems crossing the United States with the subtropical jet stream spread bountiful precipitation over most of the southern half of the country (Fig. 1b). Record or near record monthly precipitation was observed in parts of the central and southern Great Plains and the central Intermountain Region in March, in the South in April and in parts of the Southwest in May. This brought severe flooding to northeastern Mississippi, Texas and Louisiana in April. Melting of the anomalous winter snow cover, together with substantial rains gave flooding in the northern Mississippi Valley in March and in the Red River Valley in North Dakota in April. Temperatures this spring averaged above normal near the coastal ridges with cooler weather in the interior (Fig. 1c).

Summer 1979. The wave pattern north of 60°N was highly amplified this summer while the subtropical highs over both Atlantic and Pacific expanded in all directions, but most strongly northward (Fig. 2a). Retrogression associated with the seasonally declining westerlies brought a fairly deep mean trough to the east Pacific. This, together with the persistently strong subtropical jet stream emanating from the east Pacific again drove vorticity maxima deeply into the western United States. This produced greater than normal precipitation in much of the Intermountain Region (Fig. 2a) and contributed to the augmented flow of moisture into the United States across the south-central border. Most of the country from the Rocky Mountains to the Appalachians received greater than normal rainfall from a variety of causes -- migratory troughs, southward penetrating cold fronts and tropical storms. Hurricane Bob and Tropical Storm Claudette, both July storms, moved from the central Gulf Coast to the Ohio Valley. Rainfall amounts from the two storms exceeded 16 inches along the central Gulf Coast to 12 inches in Indiana and contributed to record or near record July rainfall and flooding in both areas. It was the wettest August of record in the upper Midwest and near record in parts of the Northwest (which helped control forest fires). Although June was also a wet month for much of the country, it was one of the driest Junes of record in parts of the northern Great Plains and New England. Summer mean temperatures exceeded normal in advance of the western trough but were subnormal over most of the rest of the country--

a result of advection and the insolation shielding effect of the frequent and extensive cloud cover (Fig. 2c). The mean summer temperature pattern over the United States closely matched the preferred pattern for the last 10 years (Fig 3), after the occurrence of dissimilar summers in 1977 and 1978.

This summer, tropical storms (including hurricanes ) were more frequent than normal in the Atlantic in contrast to both east and west Pacific; each region observed 6 tropical storms (including hurricanes). There were, however, about the usual quota of storms reaching hurricane strength in all three regions. The northward expansion of the Atlantic subtropical ridge, as observed this summer (Fig 2a), has been shown by Ballenziveig to accompany active Atlantic tropical storm seasons. Further, sea surface temperatures over the eastern part of the tropical Atlantic were generally above normal (Fig. 4). Tropical Storm Ana was the first tropical storm or hurricane to develop over the Atlantic or adjacent waters in June since 1975. The two flood producing July storms were followed after a month of quiet by Hurricane David which ravaged the Leeward Islands and the Island of Hispaniola at the end of August, prior to its September track over the East Coast States. Tropical Storms Elena and Frederic formed on the last day of August; Frederic became a very damaging Gulf storm in September.

Figure 5 was intended to contrast the energetics behavior of the atmosphere in the Northern Hemisphere during the year ending this August with the energetics of the last 4 or 5 years since such computations have been available at NMC. Unfortunately, the main thing that is apparently shown is the effect of a change in analysis methods at NMC. Both eddy available potential energy (AE) and eddy kinetic energy (KE) exceeded the multiyear mean by 5-30% in each month since September 1978. Significantly, in mid September 1978 spectral objective analysis based on Hough functions was replaced by a statistical procedure, optimum interpolation.

## Legend to Figures

Fig. 1a Mean 700 mb height contours (dam) and departures from normal (m) for spring 1979.

Fig. 1b Percentage of normal precipitation for spring 1979 from Weekly Weather and Crop Bulletin.

Fig. 1c Departure from normal of average surface air temperature (°F) for spring 1979 (from Weekly Weather and Crop Bulletin).

Fig. 2a Mean 700 mb height contours (dam) and departures from normal (m) for summer 1979.

Fig. 2b Percentage of normal precipitation for summer 1979 (from Weekly Weather and Crop Bulletin).

Fig. 2c Departure from normal of average surface air temperatures (°F) for summer 1979 from Weekly Weather and Crop Bulletin.

Fig. 3 Frequency of below, near and above normal temperature classes (left to right), summer 1969-1978.

Fig. 4 Departure from normal of mean sea surface temperature (°C), August 1-23, 1979.

Fig. 5 Time variation of monthly mean values of energetics parameters for the Northern Hemisphere, 1000 to 100 mb, September 1978 to August 1979. Solid line is 4 or 5 year average as indicated.

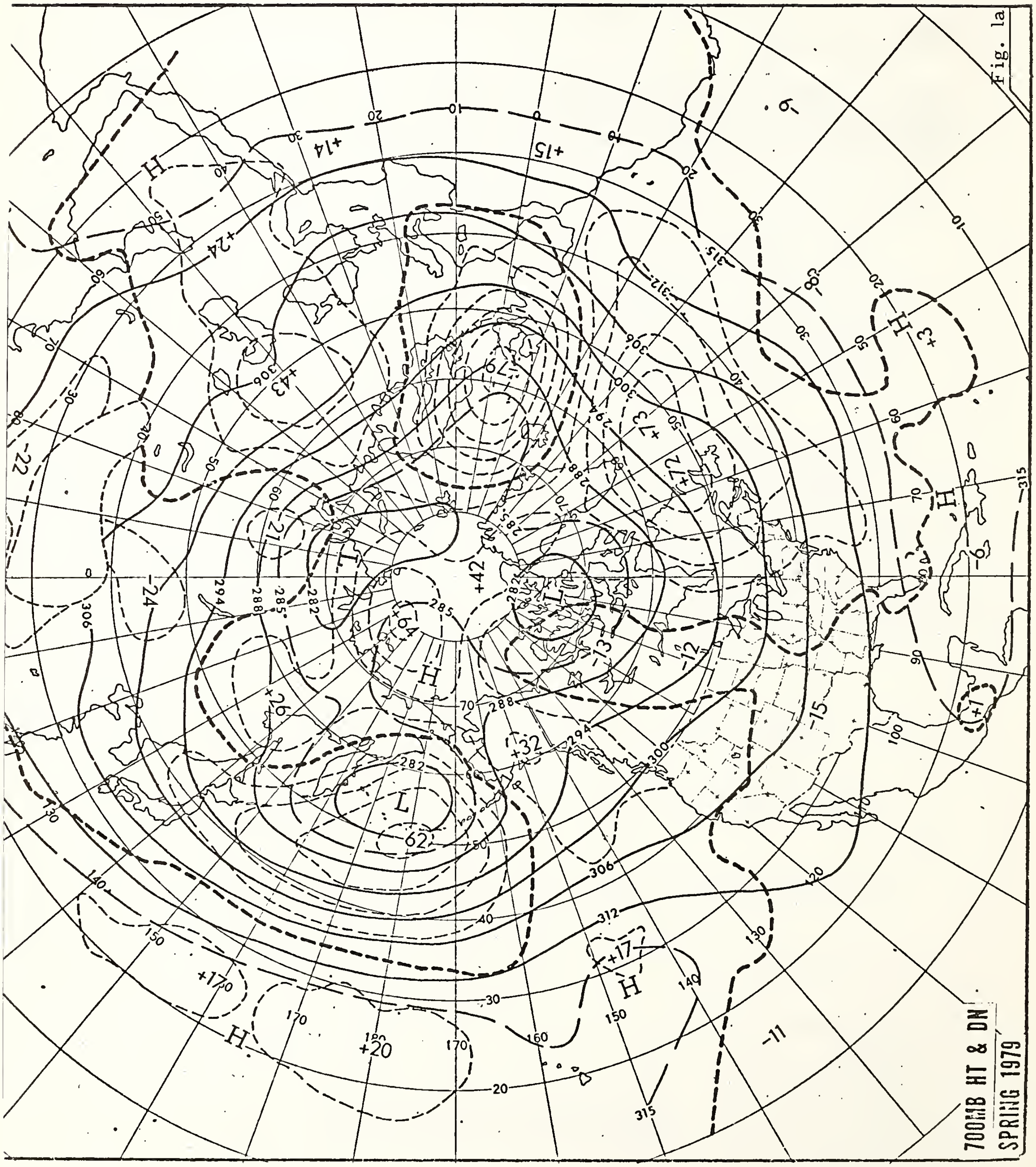

Fig. 1a

700MB HT & DN SPRING 1979

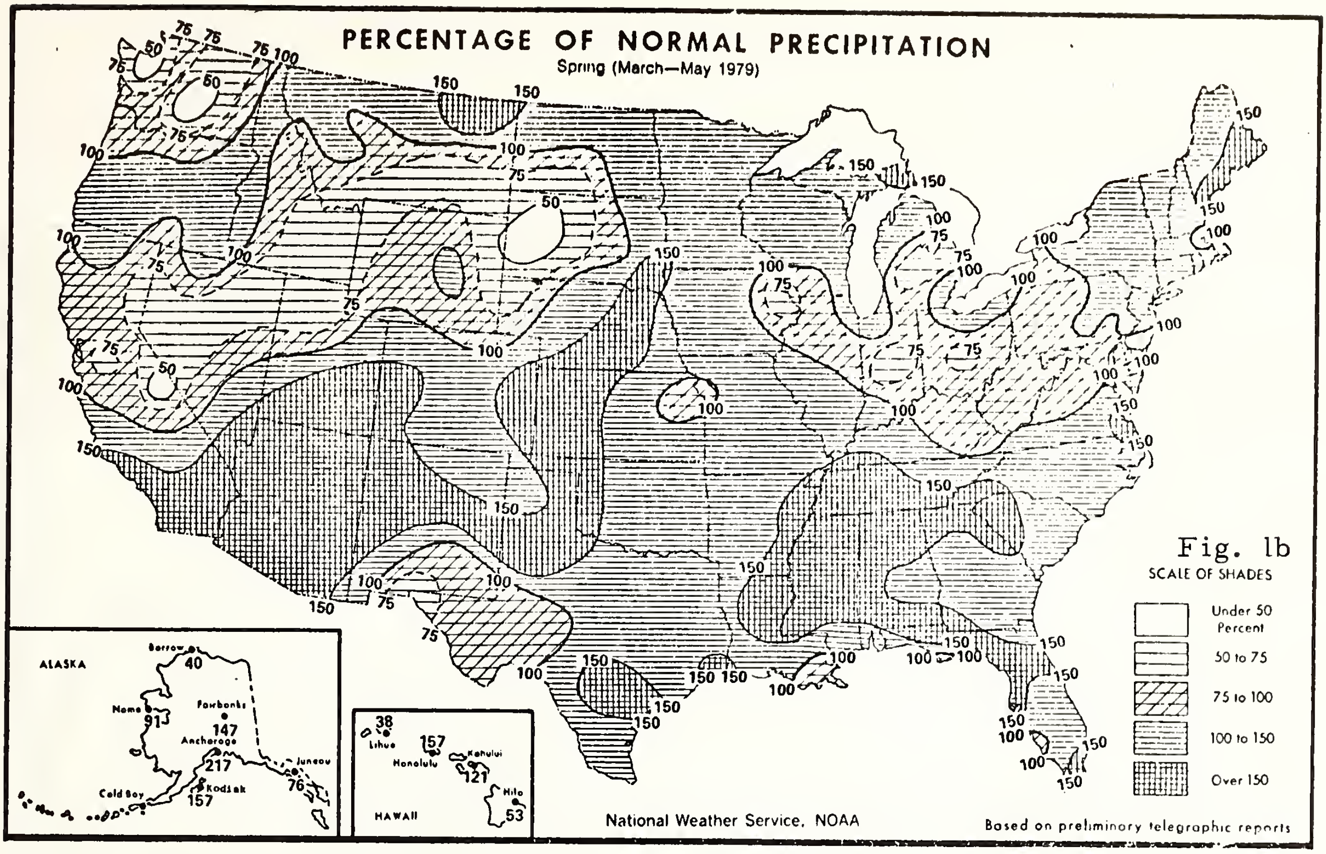

PERCENTAGE OF NORMAL PRECIPITATION

Spring (March—May 1979)

Fig. 1b

National Weather Service, NOAA

Based on preliminary telegraphic reports

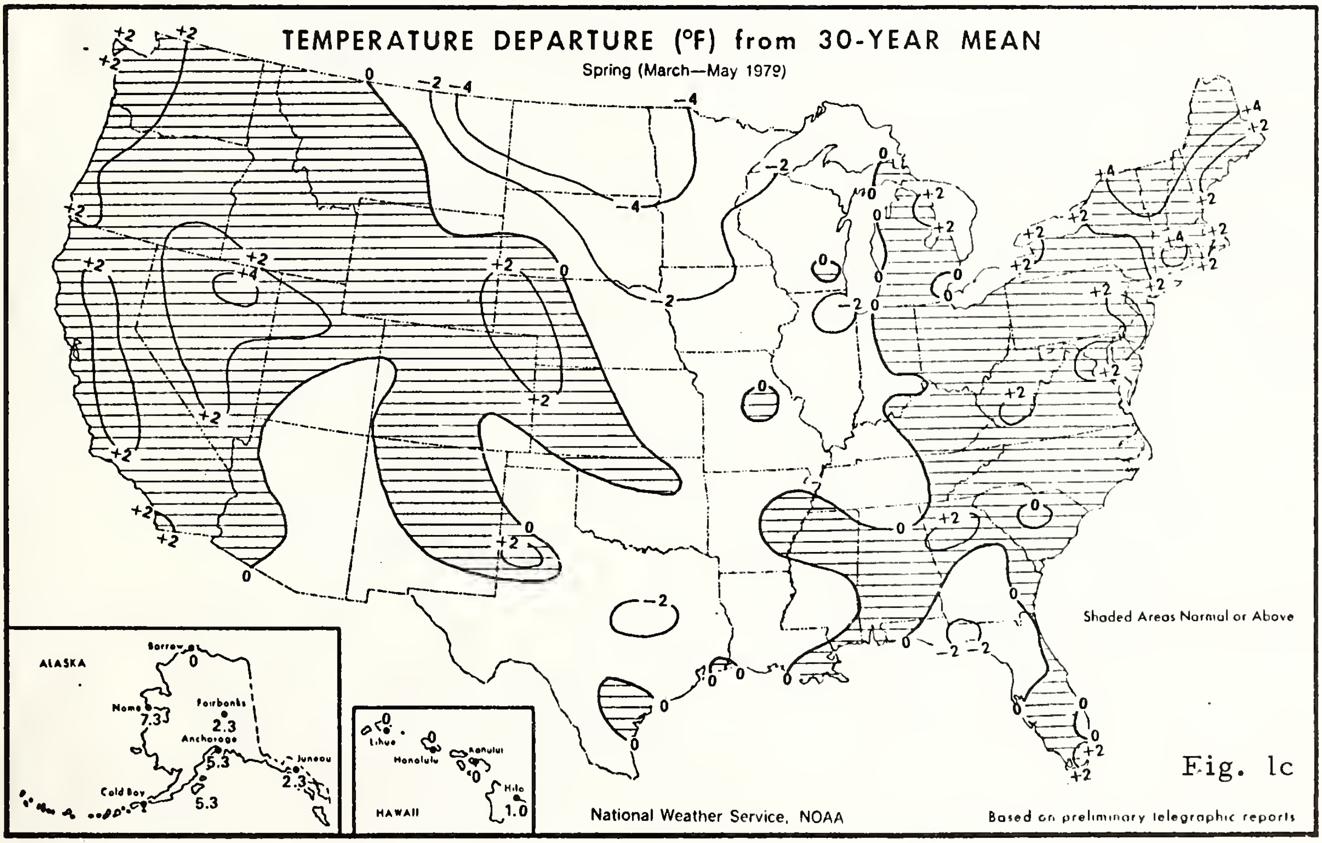

TEMPERATURE DEPARTURE (°F) from 30-YEAR MEAN

Spring (March—May 1979)

Fig. 1c

National Weather Service, NOAA

Based on preliminary telegraphic reports

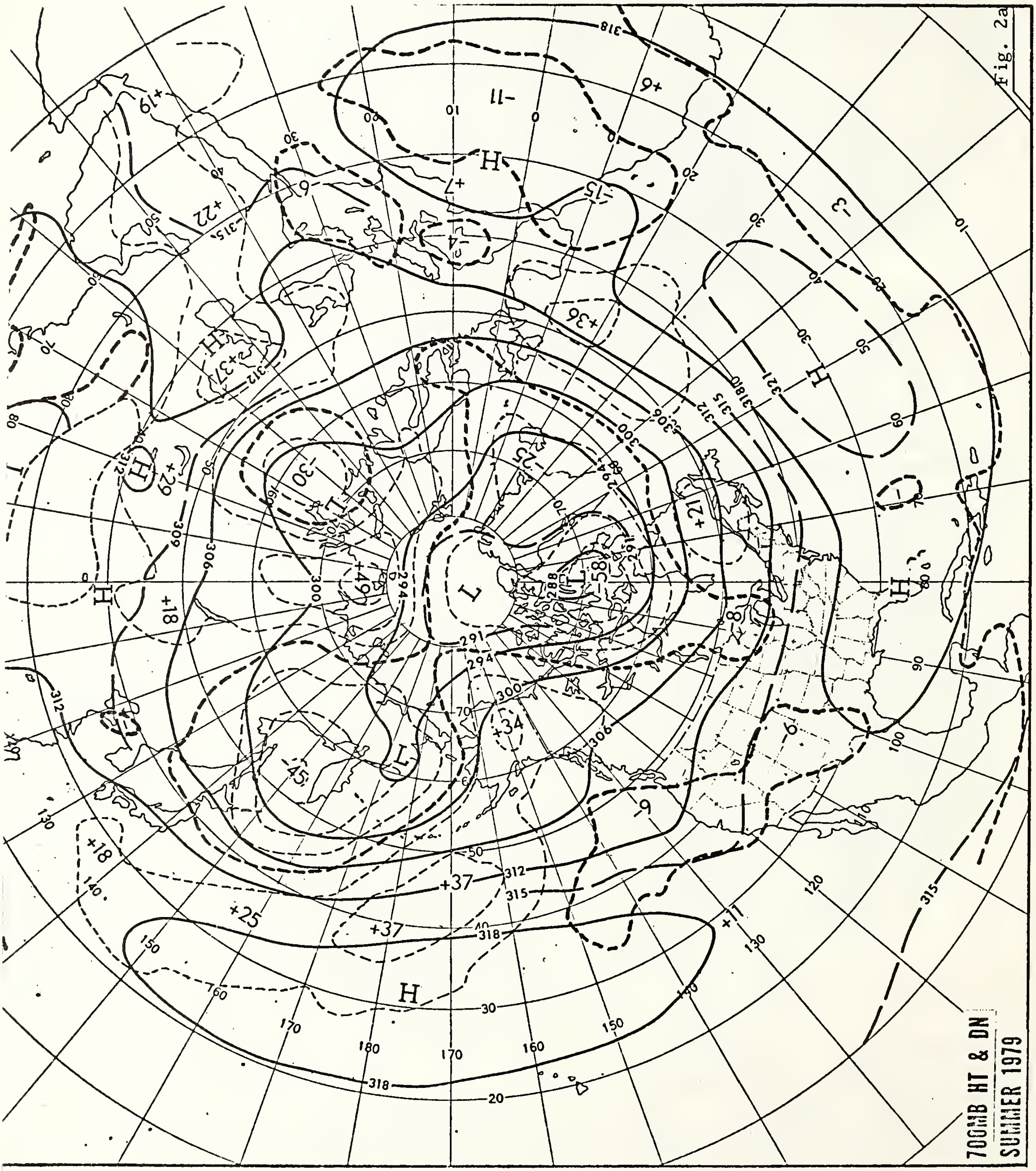

Fig. 2a

700MB HT & DN
SUMMER 1979

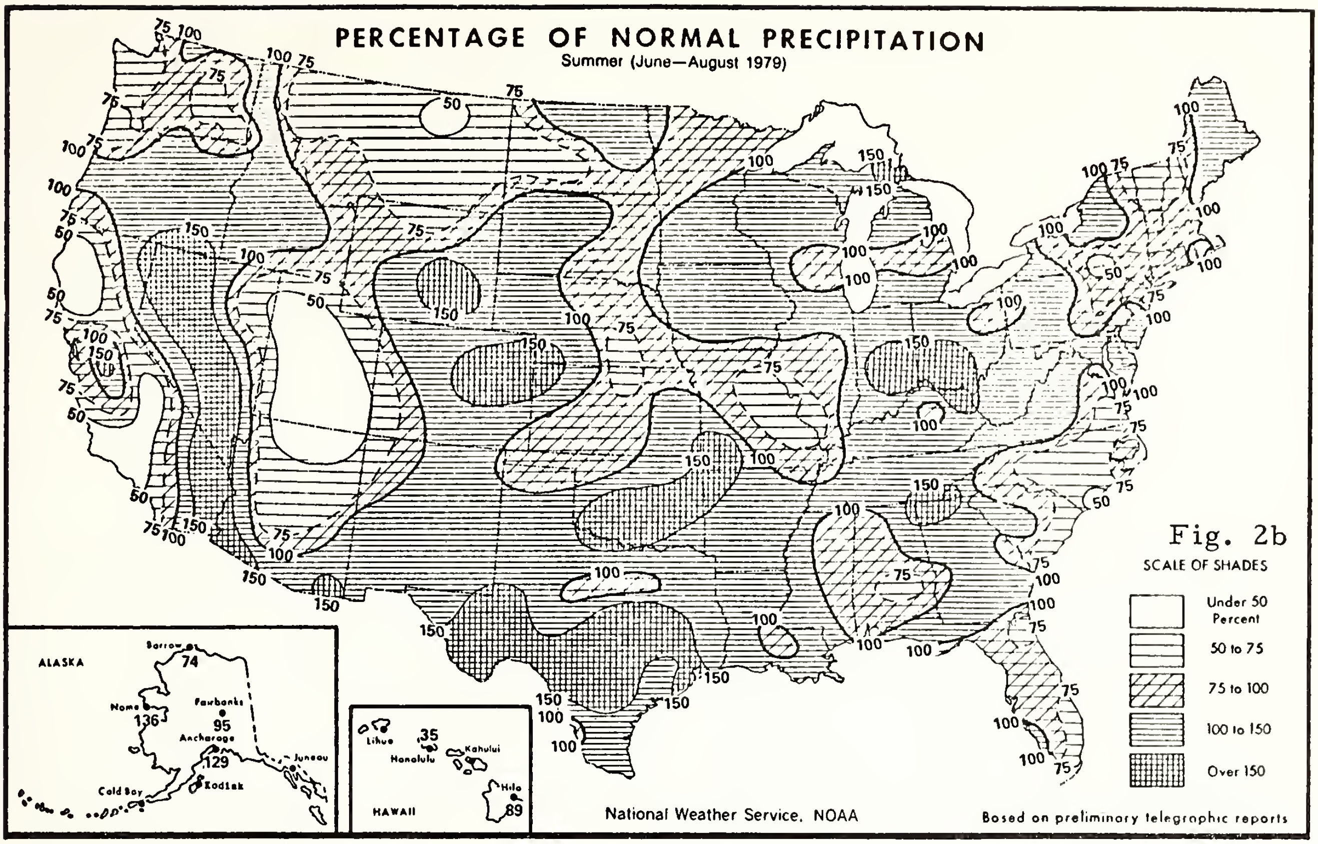

PERCENTAGE OF NORMAL PRECIPITATION

Summer (June—August 1979)

Fig. 2b

SCALE OF SHADES

National Weather Service, NOAA

Based on preliminary telegraphic reports

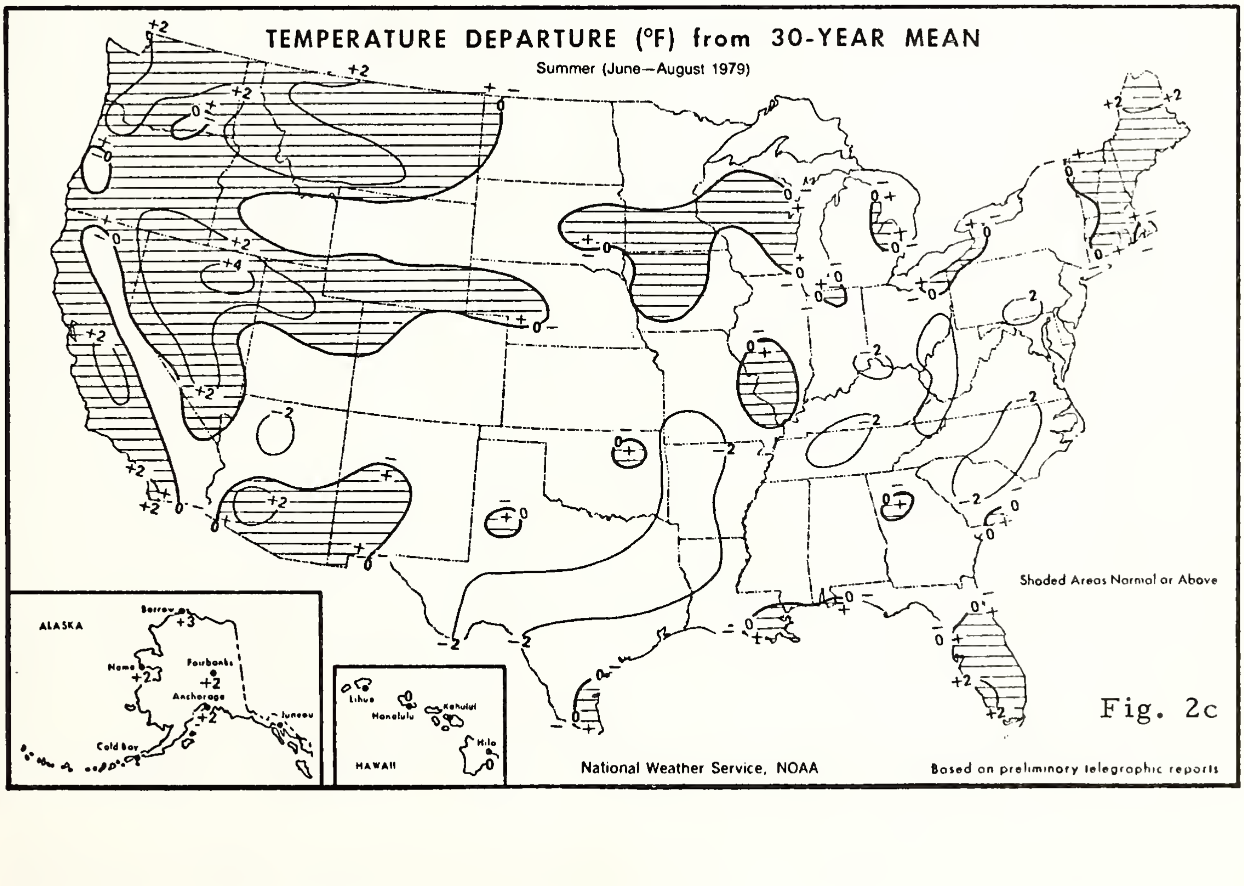

TEMPERATURE DEPARTURE (°F) from 30-YEAR MEAN

Summer (June—August 1979)

Fig. 2c

Shaded Areas Normal or Above

National Weather Service, NOAA

Based on preliminary telegraphic reports

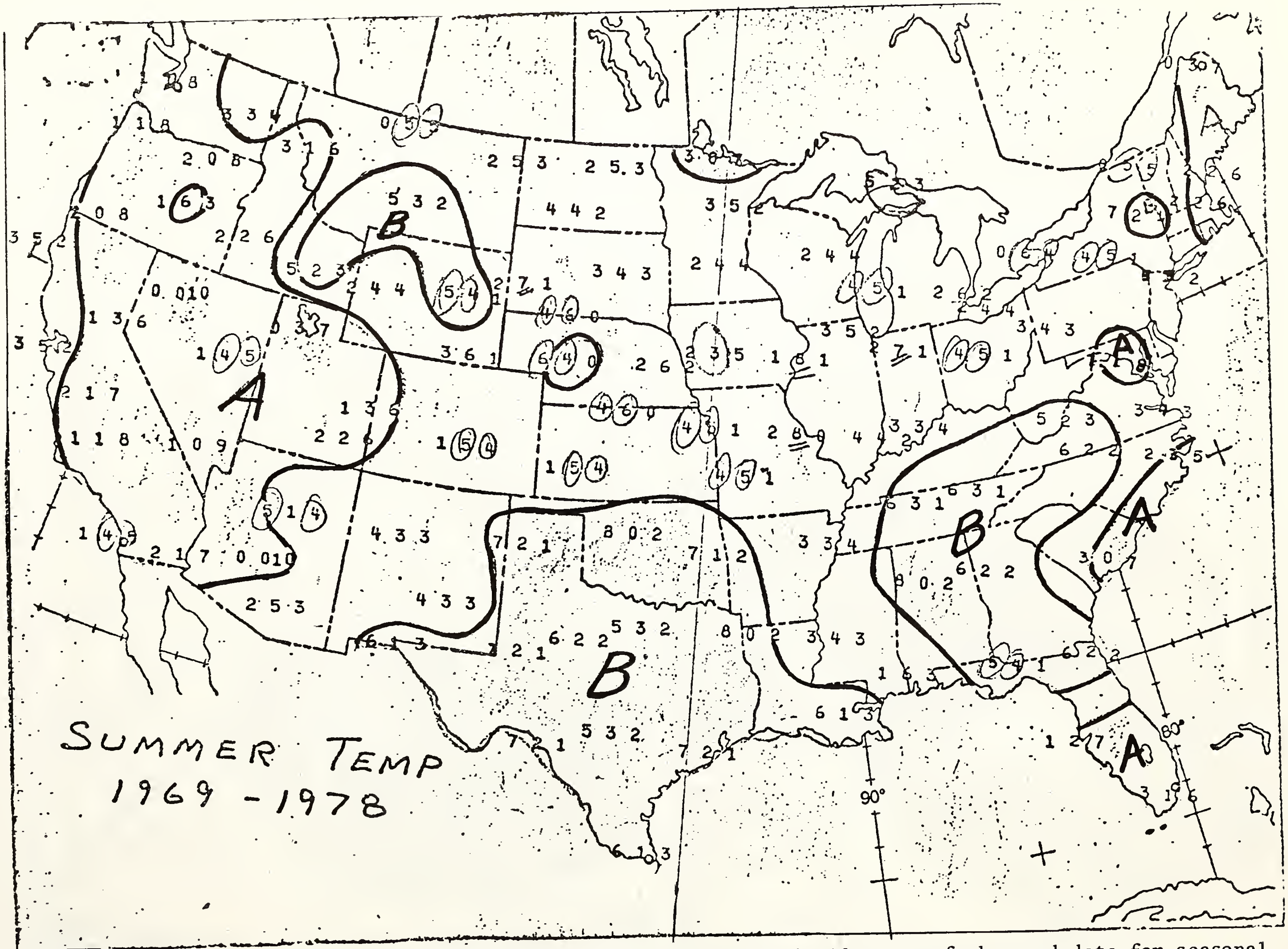

Figure 3.--Number of below, near, and above temperature classes in 10 cases of observed data for seasonal period beginning June 1, 1969 through seasonal period beginning June 1, 1978.

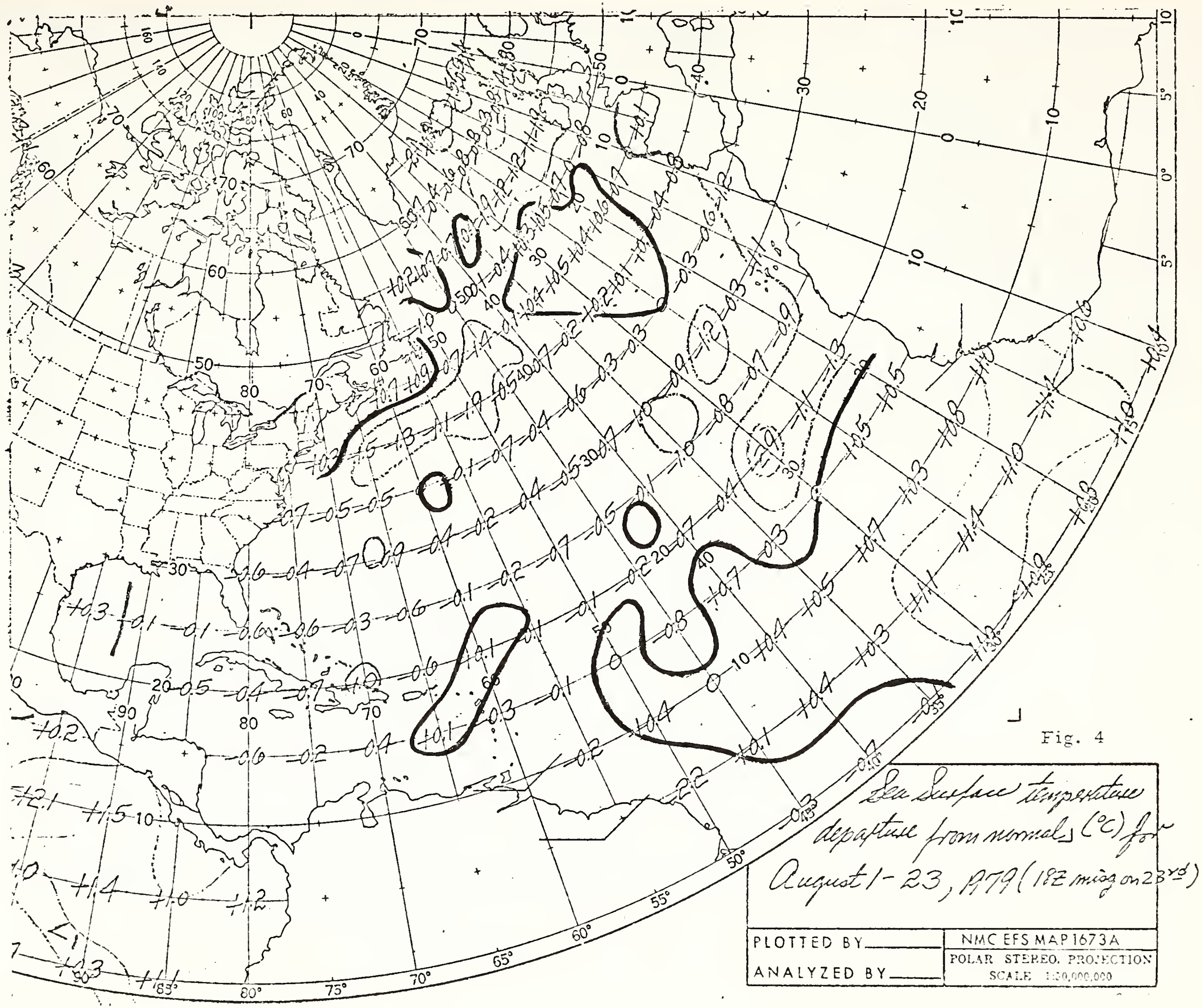

Fig. 4

Sea Surface temperature departure from normal (°C) for August 1-23, 1979 (12Z missing on 23rd)

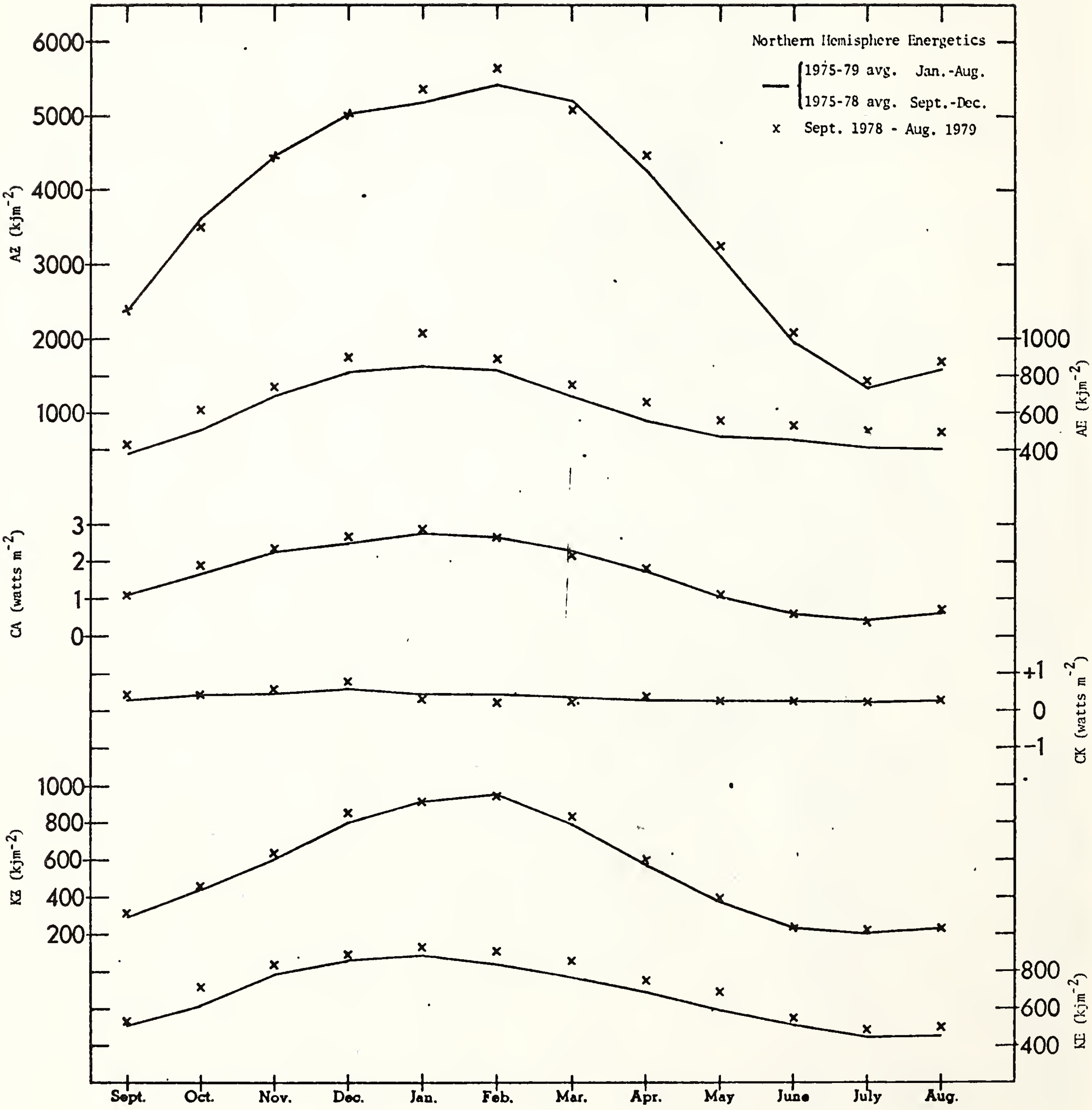
Northern Hemisphere Energetics
1975-79 avg. Jan.-Aug.
1975-78 avg. Sept.-Dec.
x Sept. 1978 - Aug. 1979
AZ (kjm$^{-2}$)
6000
5000
4000
3000
2000
1000
AE (kjm$^{-2}$)
1000
800
600
400
CA (watts m$^{-2}$)
3
2
1
0
CK (watts m$^{-2}$)
+1
0
-1
KZ (kjm$^{-2}$)
1000
800
600
400
200
KE (kjm$^{-2}$)
800
600
400
Sept.
Oct.
Nov.
Dec.
Jan.
Feb.
Mar.
Apr.
May
June
July
Aug.

Fig. 5

# Canadian Climate Extremes and Impacts for the Period September 1978 to August 1979

Yves Durocher
Atmospheric Environment Service

## Overview of September 1978 to August 1979 period

The twelve month period from September, 1978 to August, 1979 turned out to be colder than normal, except over eastern Quebec, the Maritimes as well as in the Mackenzie Delta region of the western Canadian Arctic. This colder climate resulted in increased multi-year ice in the central Arctic, disrupted Arctic navigation and considerably increased Canadian heating fuel consumption. Precipitation during this period was above normal over most of eastern Canada and parts of the Canadian Prairie Provinces. On the east coast in New Brunswick, Nova Scotia and Prince Edward Island, most of this precipitation occurred in the spring and summer, resulting in extremely poor agricultural conditions both at planting and at harvesting time. Over the Prairies most of the precipitation fell during the fall, fortunately before freeze-up, and therefore resulted in extremely good water reserves which saved crops that would otherwise have been victims of the very dry growing season over portions of the Prairies. Extremely dry conditions in northern Saskatchewan and the western District of Mackenzie, N.W.T., resulted in a very costly and devastating forest fire season in those areas; northwestern Ontario was also affected.

## Fall 1978 (September - November)

The weather during the fall was controlled by a mean 50 kPa trough over eastern Canada, which maintained the Prairie provinces, Ontario and Quebec under a northwesterly flow. As a result, seasonal and particularly November mean temperatures plunged below normal over the entire country, the Yukon, northern British Columbia and northern Alberta excepted. Over the eastern District of Keewatin, N.W.T., mean temperature anomalies reached -5°C. October - November mean temperatures were more than 7°C below normal in the eastern Arctic. In November Frobisher Bay was 9°C below normal; in fact, the entire country was below normal. This cold weather outbreak, following a colder than normal summer over the central Arctic, resulted in poor ice break-up and very early and rapid freeze-up in this area. This cold snap also forced the early end of the drilling season in the Beaufort Sea where oil drilling ships had to be brought into harbour as early as the beginning of October.

Abundant precipitation before freeze-up in the Prairies replenished soil water reserves to full capacity. This turned out to be the salvation of the 1979 crop which would otherwise have suffered considerably more from the summer drought.

## Winter 1979 (December 1978 - February 1979)

The winter of 1978-79 produced abnormal cold and snow in many parts of North America which was under the influence of a very broad trough. A northwesterly flow of cold Arctic air prevailed for most of the winter over all of Canada where, except for eastern and northern Quebec, winter mean temperatures were below normal. December to February temperature anomalies reached -6°C over the Prairies. The anomalies were highly influenced by an exceptionally cold February during which numerous cold records were set throughout the country. February, 1979 was the coldest on record at at least 9 long-term southern stations and 50 kPa height anomalies reached -17 dam over the District of Mackenzie. Mean monthly temperatures fell to more than 17°C below normal over the Yukon. The February mean temperature anomalies were greater than 3 standard deviations in Alberta and the Yukon and greater than 4 and 5 standard deviations respectively at Alert and Eureka in the high Arctic. The mean February temperature at Eureka fell to -47.9°C, the coldest ever recorded in North America. The temperature refused to rise above -48°C for 17 consecutive days.

Except for a small area over the Gulf of St. Lawrence, the November 1978 to March 1979 mean temperature was below normal for all of Canada. The monthly temperatures at Winnipeg, Man., remained below normal for 8 consecutive months and temperatures remained below freezing for 112 out of 113 days from November 1st, 1978 to February 28th, 1979. Similarly, the temperature at Brandon, Man., remained below zero for 126 consecutive days. This very cold temperature regime prevented any snow thaw; as a consequence, despite lower than average snowfall, the snow remained for the spring thaw resulting in devastating spring floods in southern Manitoba and Saskatchewan. Also, the cold weather combined with an unusually thin snow cover resulted in winter wheat killed by frost in some parts of the Prairies. Between 50% and 70% of the winter wheat suffered from killing frost and up to 95% in the Drumheller area of Alberta. It was also a very dry winter over the Northwest Territories, Yukon, Alberta and southern British Columbia. Those are the areas where forest fires were most severe the following summer.

## Spring 1979 (March - May)

The cold weather continued over most of the Prairies during the spring. Thawing was sudden and resulted in record flood levels over southern Saskatchewan and Manitoba. More than 200,000 hectares of agricultural land were flooded resulting in nearly $1,000,000 of grain lost in the Souris River area. More than 1500 sq km of land was flooded in the Red River area where water levels reached record heights. The $63,000,000 floodway finished in 1960 around Winnipeg certainly proved its worth by protecting the city from flood waters.

Precipitation was above normal in all agricultural regions but Alberta. In the Prairies and the Maritimes, because of the excess waters, it was very late before field work could begin and many farmers had to plant shorter maturing crops. Seed rotted in the ground and germination was poor. In Alberta, late emergence of crops because of cold weather coincided with insect infestations.

## Summer 1979 (June - August)

The summer was characterized by an east-west polarization of precipitation. From British Columbia to northwestern Ontario, many of the agricultural and forestry regions suffered from drought while eastern Canada received above normal precipitation.

The western drought resulted in a reduction in grain production; however, crop losses were reduced by the plentiful reserve of soil moisture resulting from copious precipitation during the previous fall. Forest fires raged in northern Alberta and Saskatchewan, in the Northwest Territories and British Columbia and northwestern Ontario. The province of Alberta had to boost its present fire fighting budget by $2,000,000 because of some 220 fires that burned more than 160,000 hectares. In the Maritimes, excessive precipitation combined with warm summer weather was very profitable to agriculture but harvesting was very difficult and late because of wet fields.

In the Arctic, summer 1979 was as much as 2°C below normal; ice break-up was slow and reduced. As a result, multi-year ice was abundant in the central Arctic.

## Summary

Overall, it was a cold 12-month period in Canada, in fact eastern Canada experienced its third consecutive cold winter. In the agricultural zones of the Canadian Prairies drought and early frost reduced cereal grain production by 19% when compared to 1978 production, as indicated by Statistics Canada's September forecast.

Mean Temperature – Departure from Normal (September 78 – August 79)

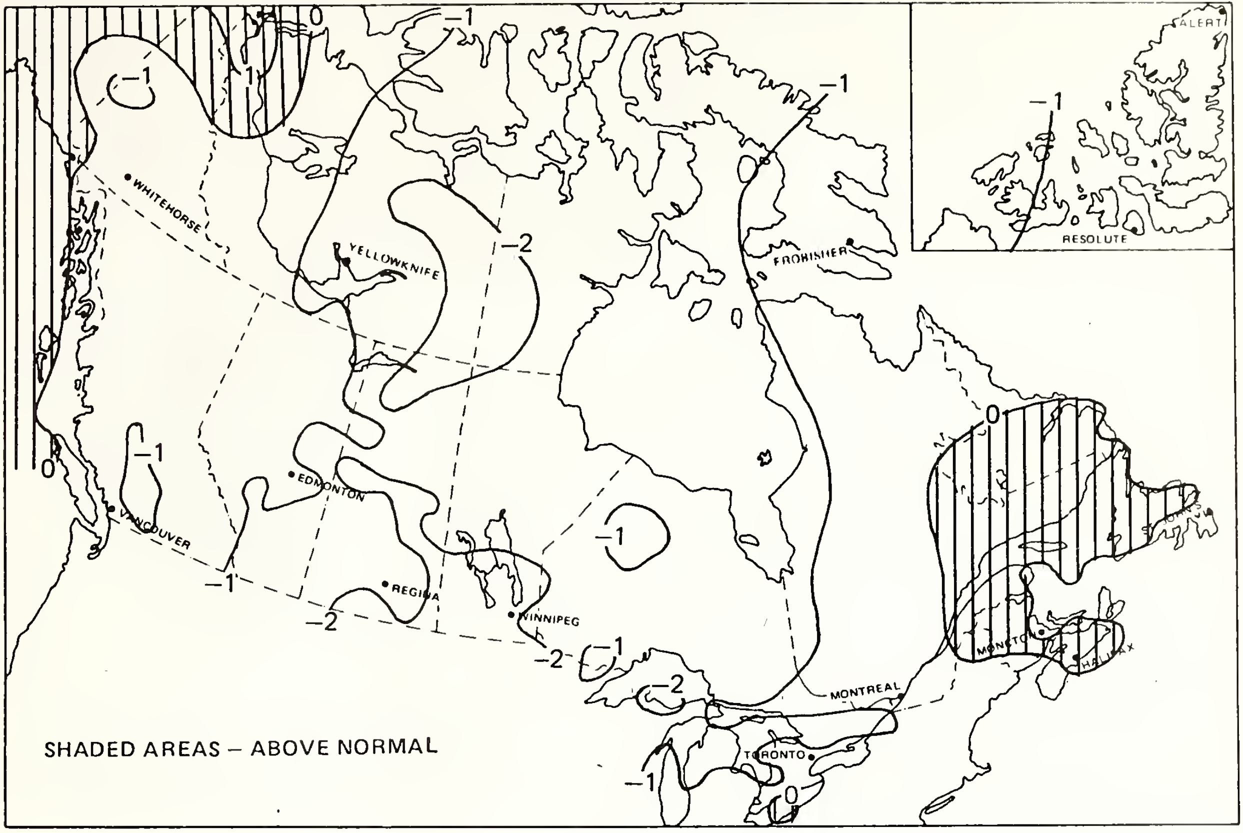

Total Precipitation – Percent of 1941-70 Normal (September 78 – August 79)

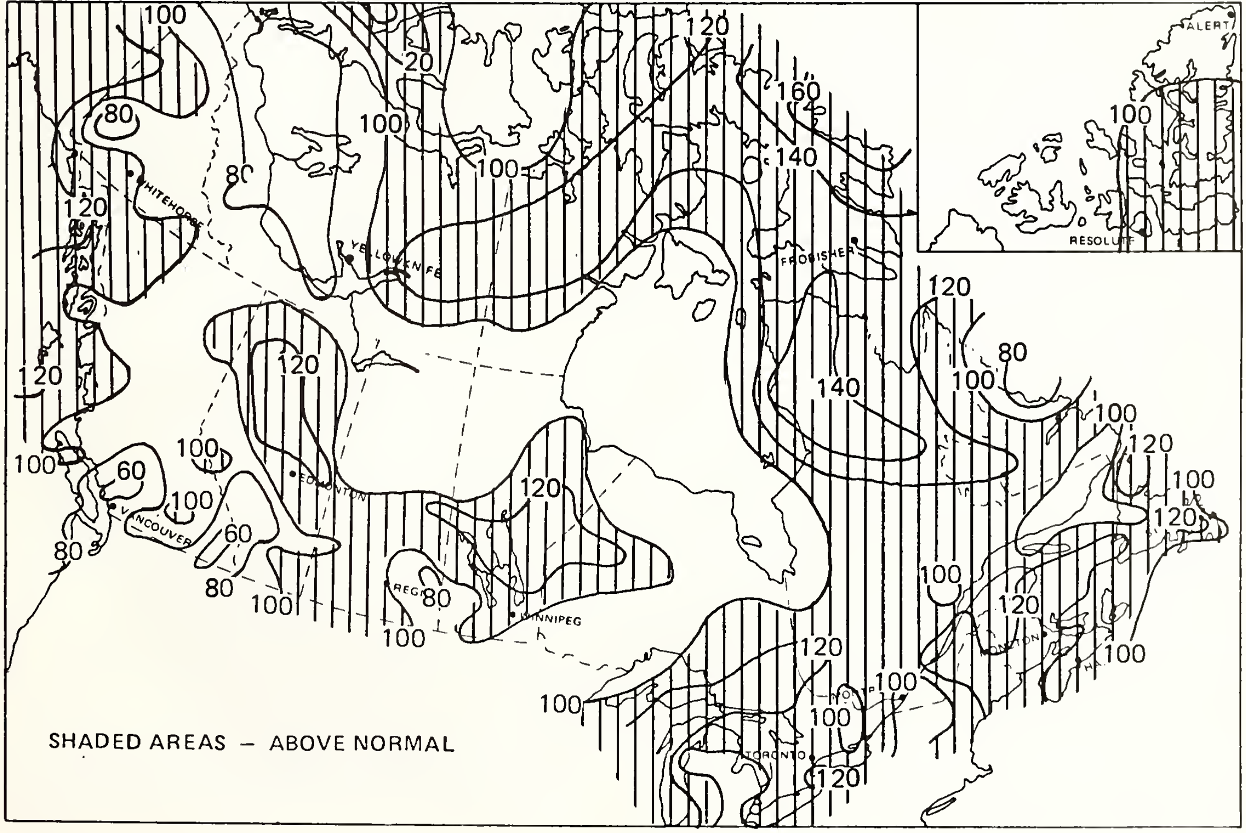

Mean Temperature – Departure from Normal (December 78 – February 79)

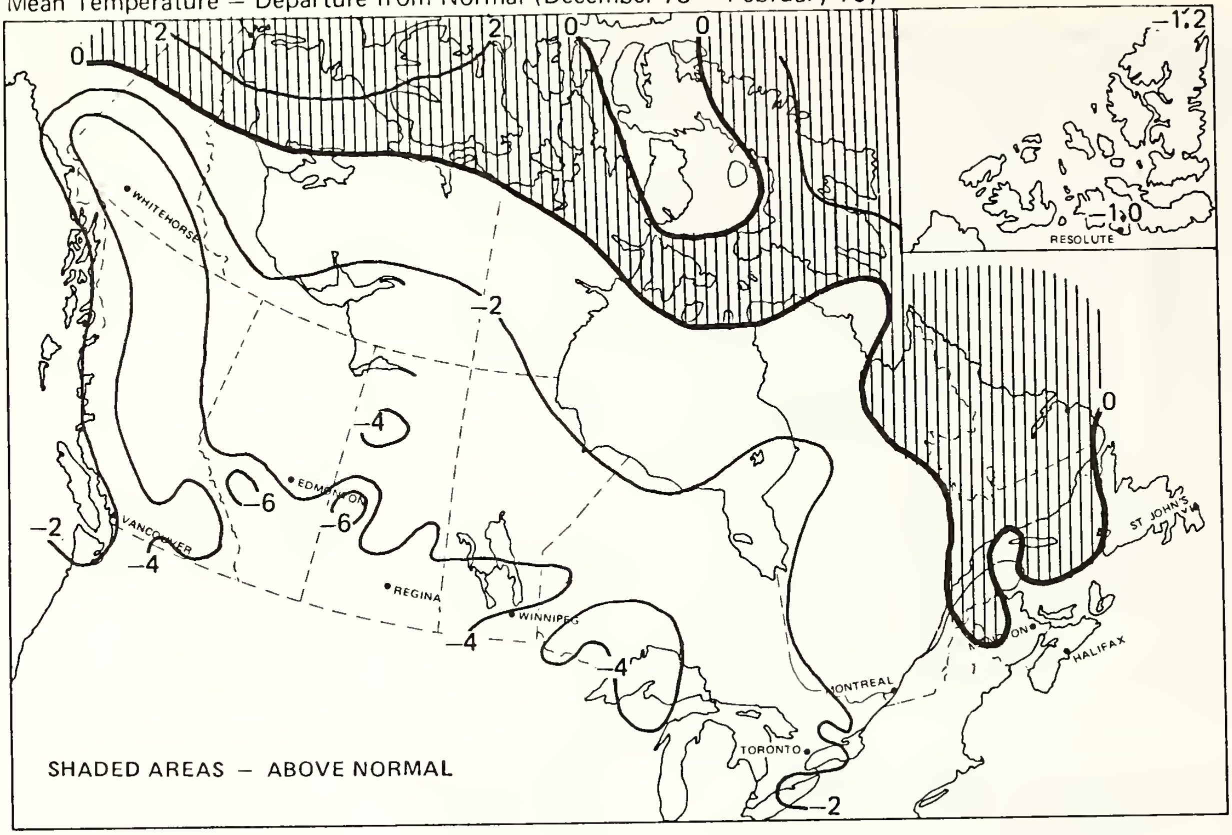

Total Precipitation – Percent of 1941-70 Normal (December 78 – February 79)

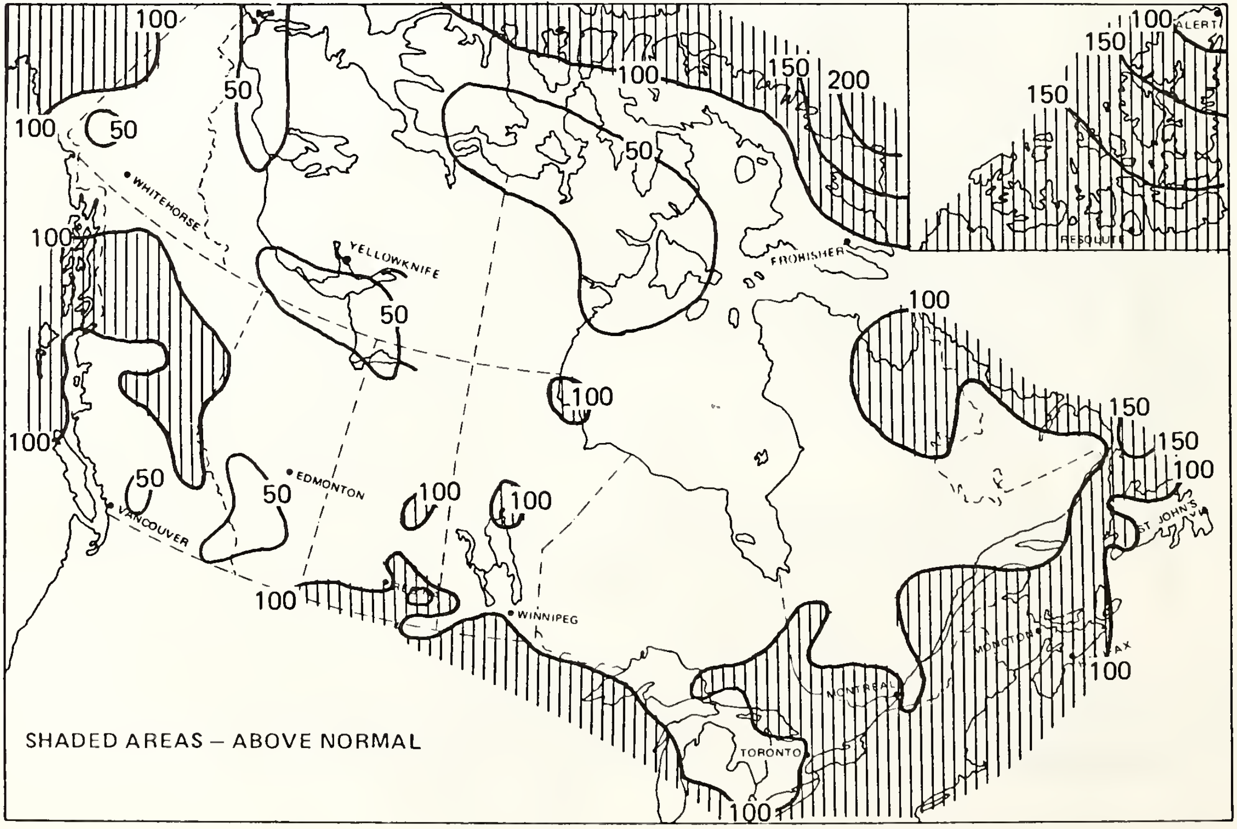

Mean Temperature – Departure from Normal (March 79 – May 79)

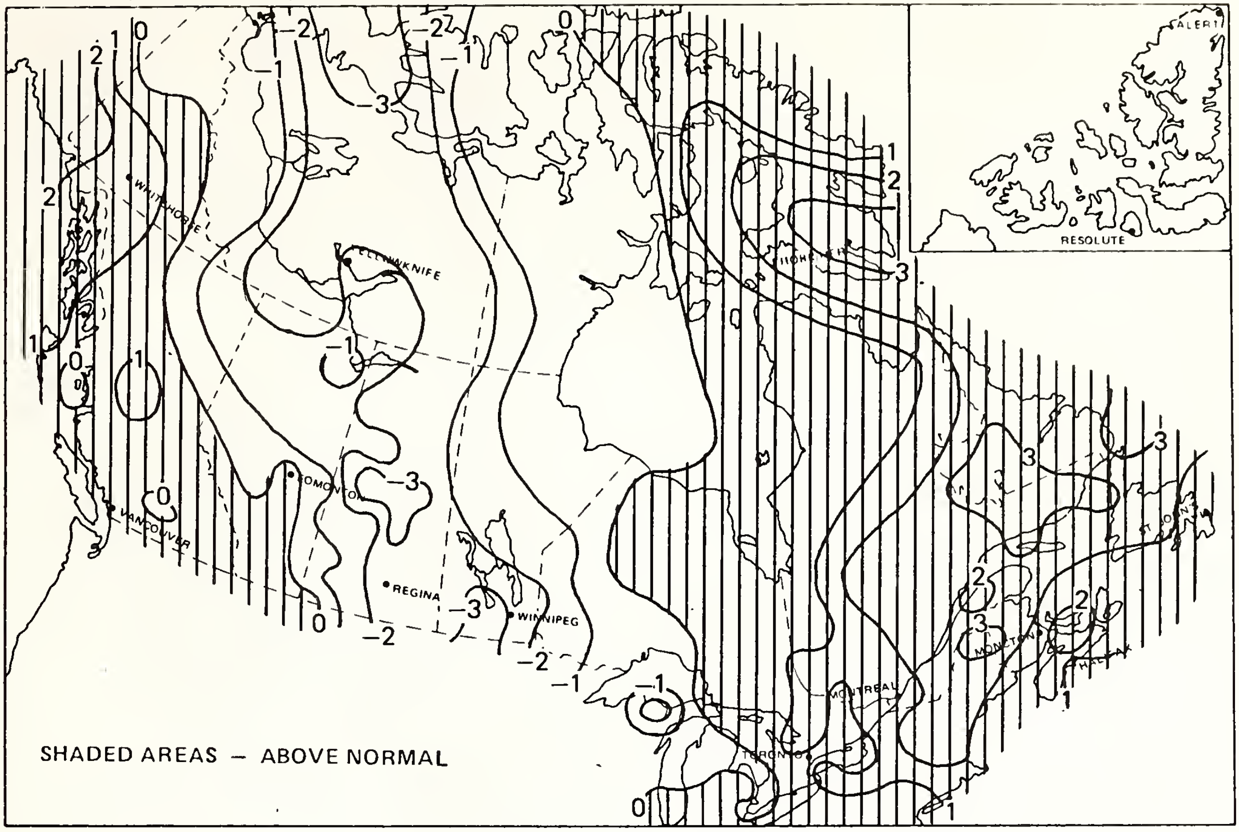

Total Precipitation – Percent of 1941-70 Normal (March 79 – May 79)

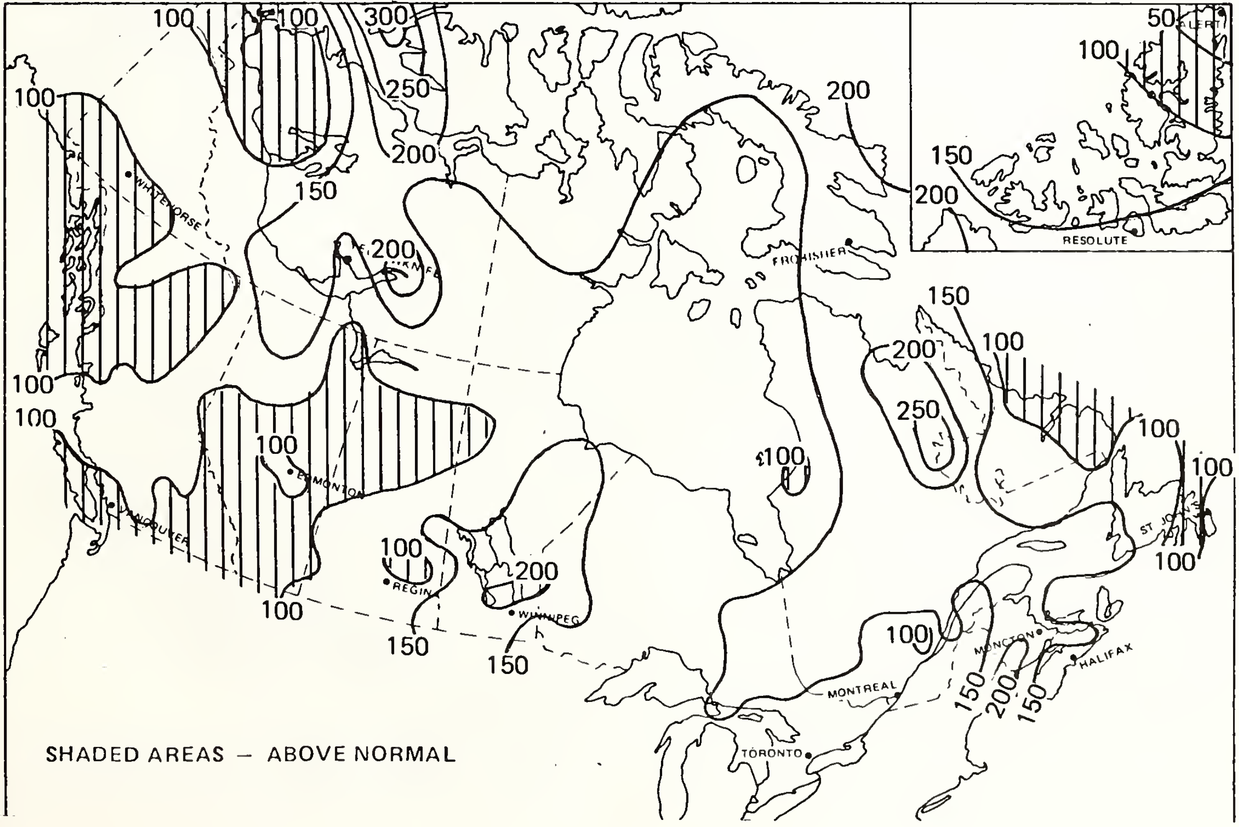

Mean Temperature – Departure from Normal (June 79 – August 79)

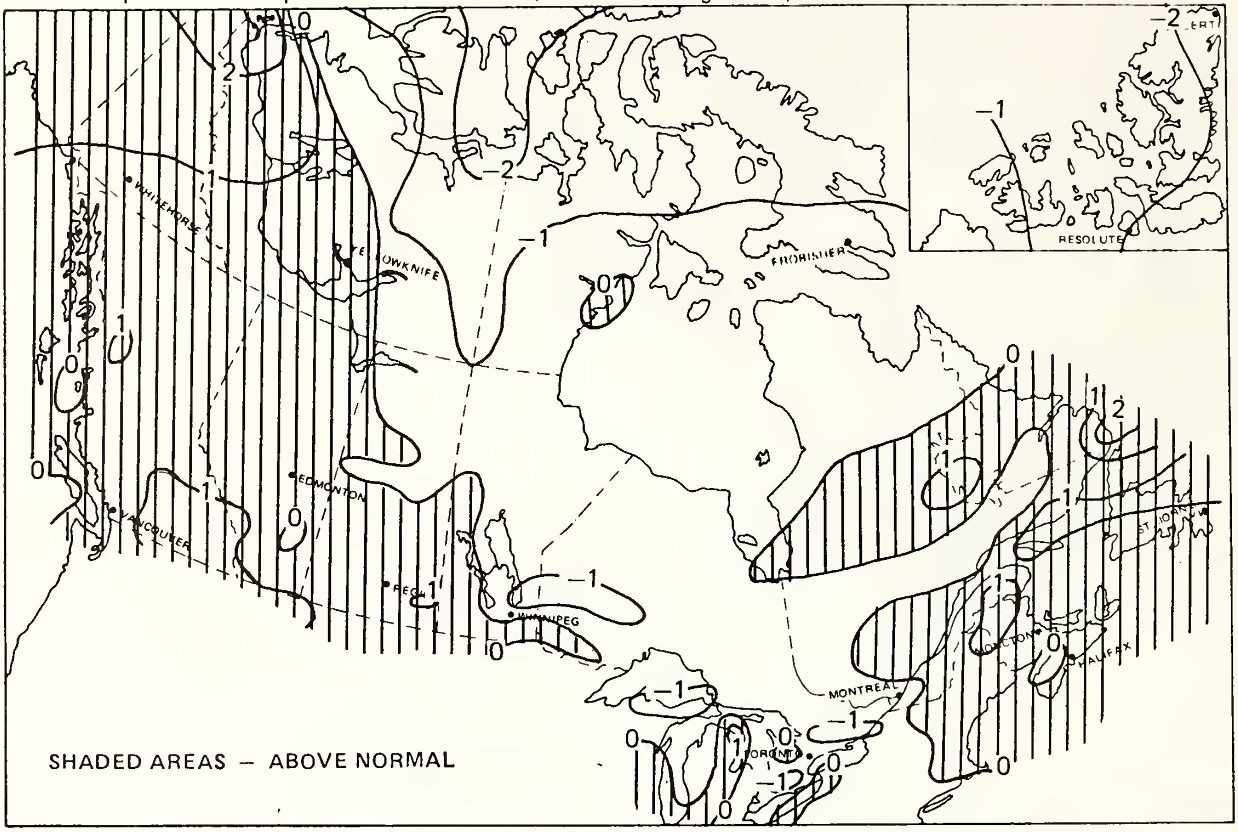

Total Precipitation – Percent of 1941-70 Normal (June 79 – August 79)

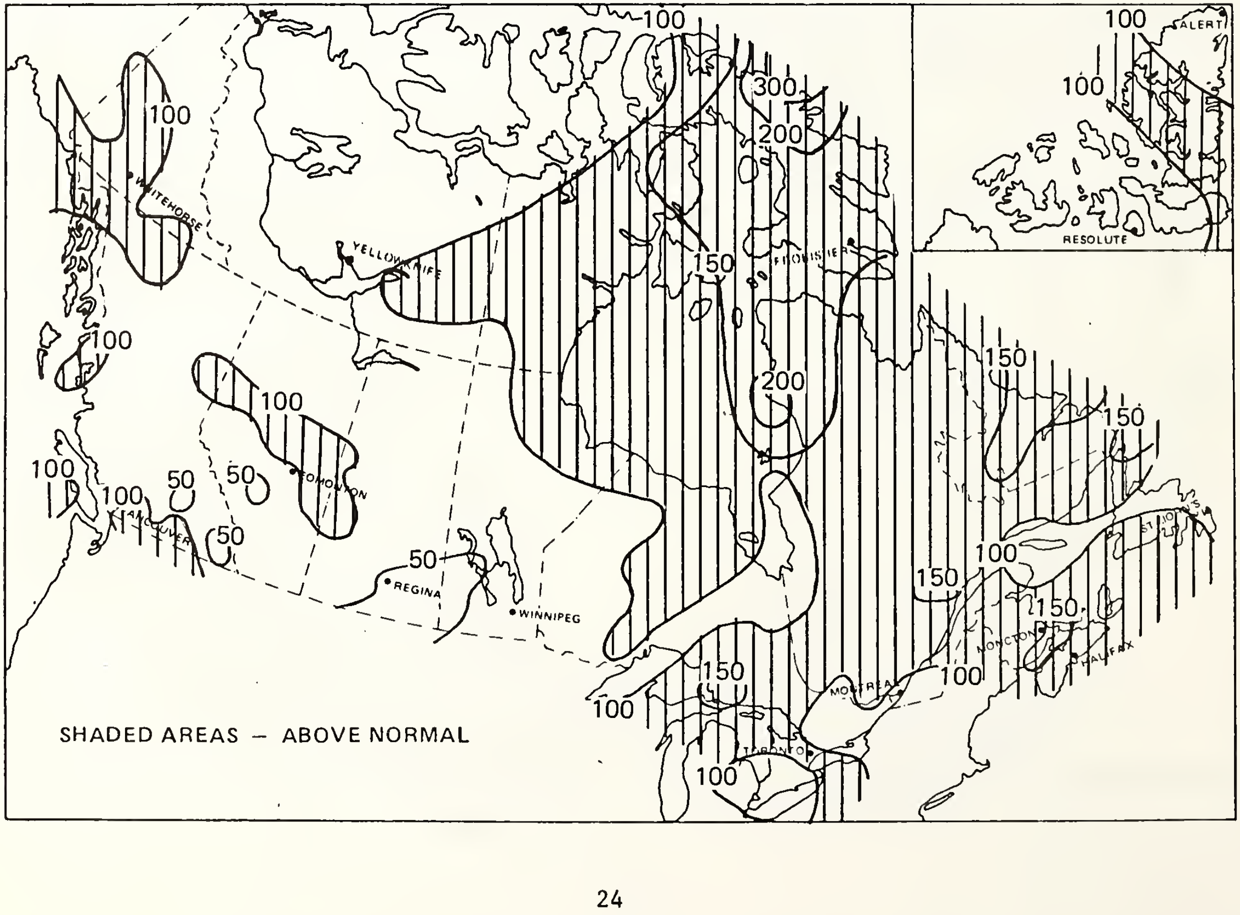

Total Precipitation – Percent of 1941-70 Normal (November 78 – March 79)

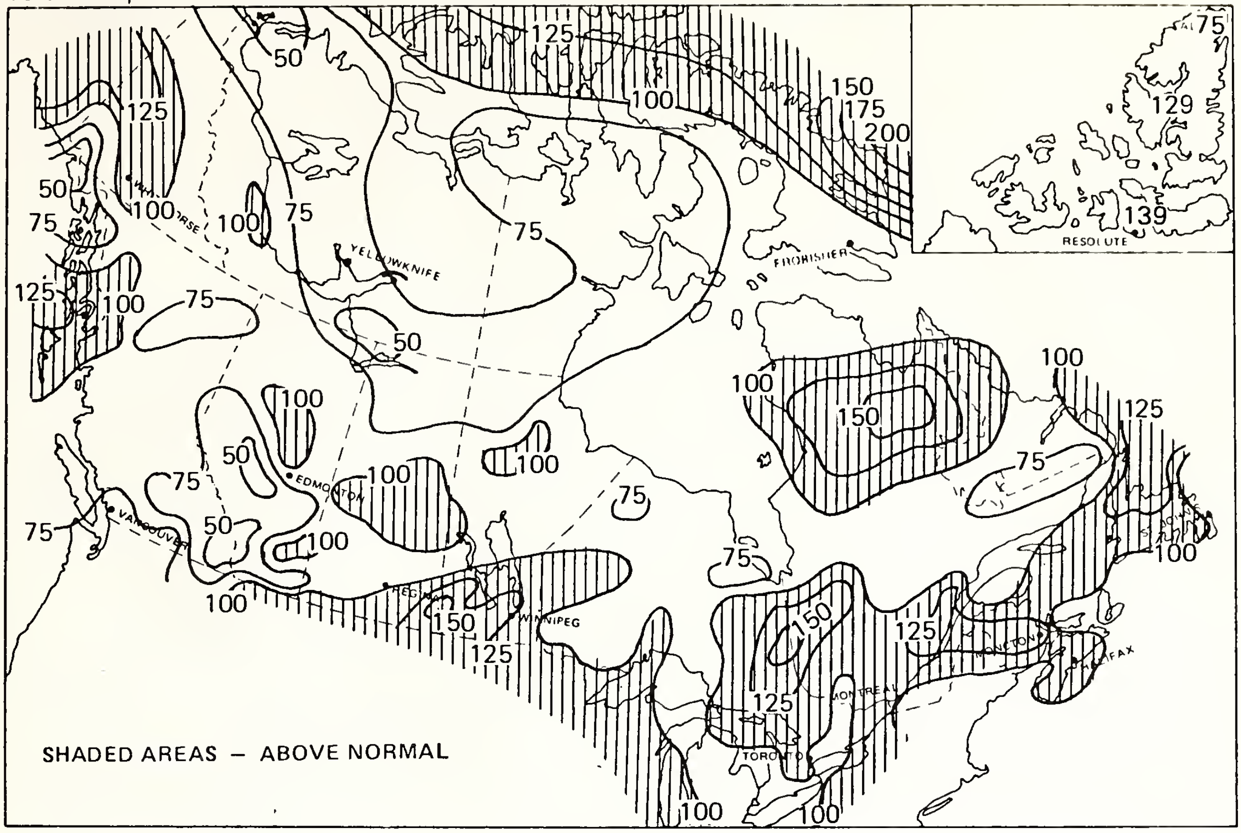

Mean Temperature – Departure from Normal (November 78 – March 79)

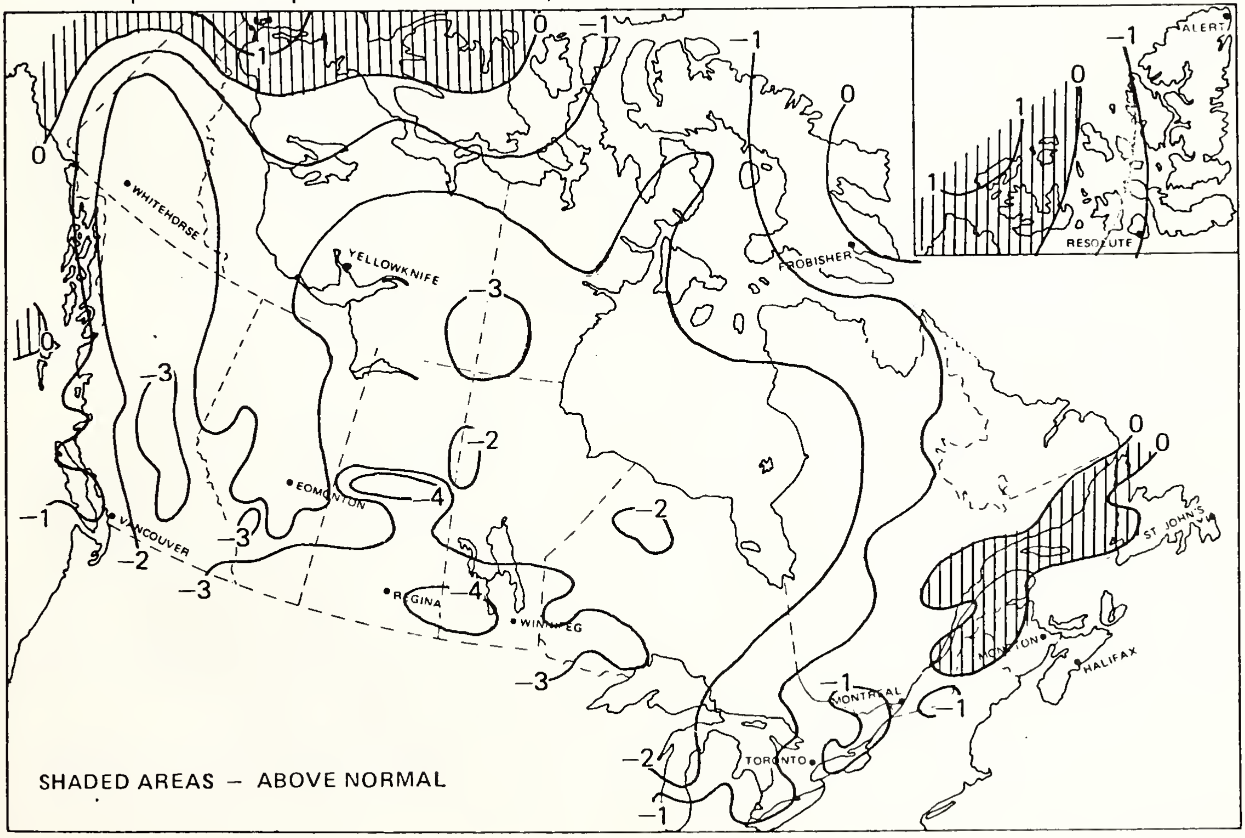

Mean Temperature – Departure from Normal (October 78 – November 78)

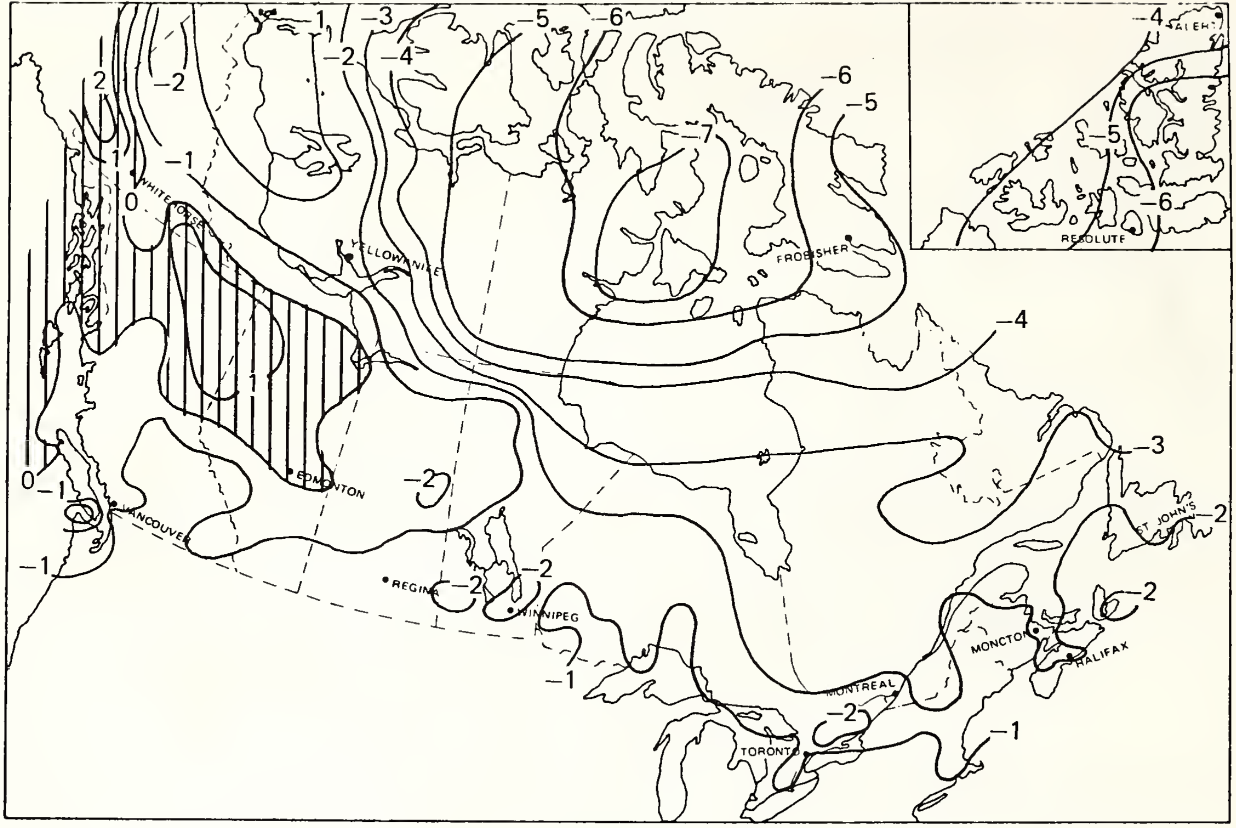

Mean Temperature – Departure from Normal (February 79)

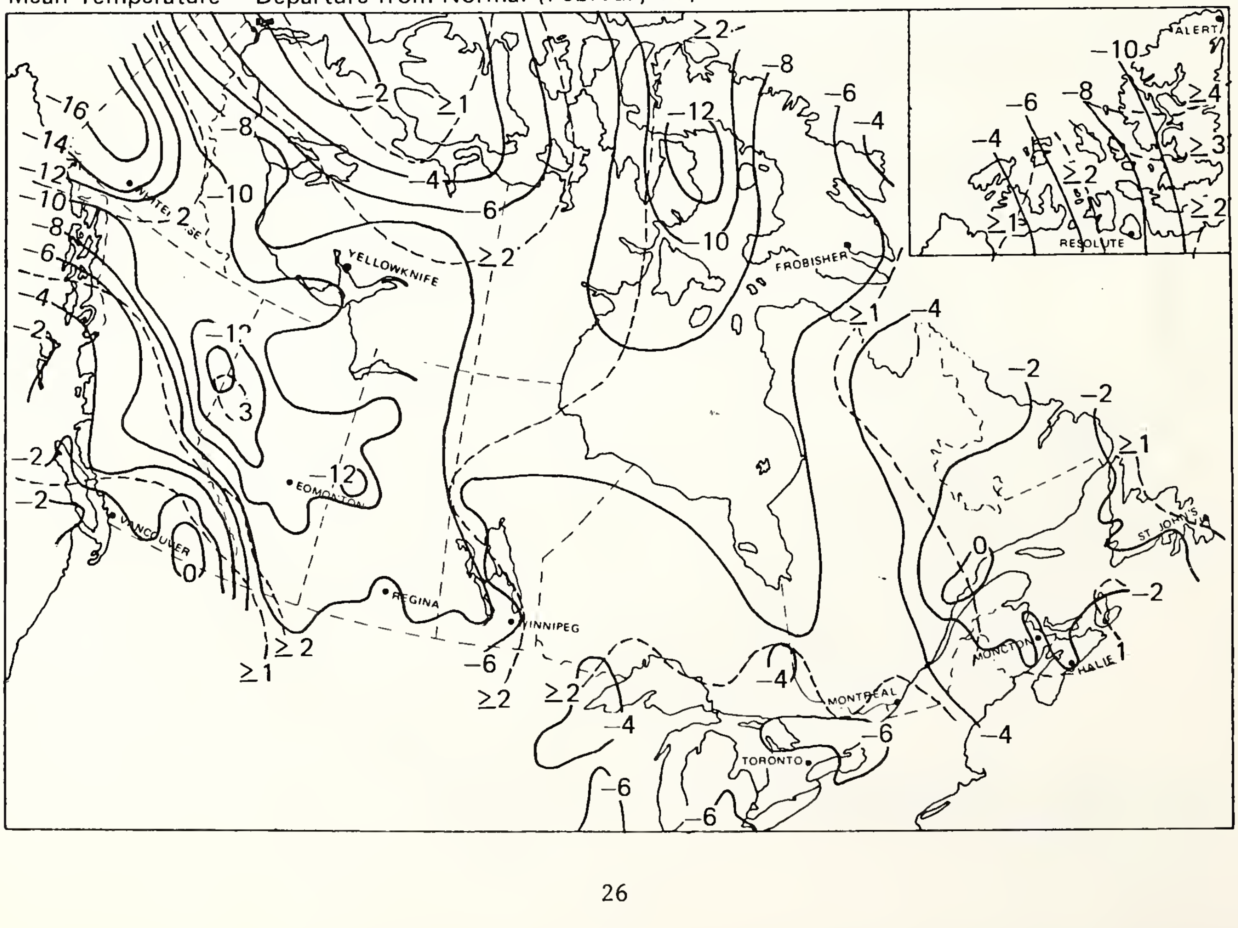

# 378-Year Occurrence of the 1976-1977 and 1978-1979 Winter Sea Level Pressure Patterns Over the North Pacific and North America

G. Robert Lofgren and Geoffrey A. Gordon
Laboratory of Tree-Ring Research
University of Arizona
Tucson, Arizona 85721

We have chosen to determine winters similar to those of the last three winters by examining sea level pressure data for persistent synoptic anomalies. Mean monthly sea level pressures over North America and the North Pacific (Fig. 1) averaged for the three months of December, January, and February give the persistent synoptic features that occurred for that particular winter. When the anomaly pattern is formed from the long-term mean, the synoptic variability has been filtered out and only the net effect during that particular winter season is shown. Then when anomaly maps are compared, maps with similar anomalous features can be grouped.

The period 1899 to 1970 has been chosen as the base period from which to compute the long-term seasonal mean maps. Winter anomaly maps have been computed for each year from 1899 to the present. Each pattern is compared to the patterns of the last three winters by a map-pattern correlation analysis. The correlation coefficient between two anomaly maps is used as the measure of their similarity. Experience has shown that when the correlation coefficient between maps exceeds 0.5, similar anomalous synoptic features usually occur. The associated temperature anomaly patterns will generally resemble each other. Dissimilarities are most likely to show up on the precipitation anomaly fields.

Climatic anomalies associated with the last three winters are shown in Figures 1, 2, and 3. The map-pattern correlation between the earlier two winters was 0.35. Thus, the winters of 1976-1977 and 1977-1978 are not classified as being similar. The winter of 1978-1979 displayed pressure features different from those of the previous two winters.

We want to determine the occurrence of winters similar to the two most dissimilar winters of 1976-1977 and 1978-1979. Table I shows those winters during the twentieth century for which the sea level pressure anomaly patterns were similar.

To show that there is a relationship between the sea level pressure field and point measurements of temperature and precipitation from the western United States, we have used these latter two variables as predictors of pressure. Data from 46 temperature and from 52 precipitation stations from the western United States have been used. Using a multivariate linear analysis which combines canonical correlation with canonical regression, 5 eigenvector amplitudes of temperature and 12 eigenvector amplitudes of precipitation have been calibrated against 11 eigenvector amplitudes of winter sea level pressure. Twentieth century data from 1901 to 1970 have been used to obtain the regression coefficients. Forty-nine percent of the original pressure variance was explained by this model. Figure 4 shows the spatial distribution of the variance explained.

Reconstructions have been made from 65 tree-ring chronologies over the western United States. Sixty-four years of data from the twentieth century have been used to calibrate 15 eigenvector amplitudes of tree growth for year t with 15 amplitudes for year t-1 against 15 eigenvector amplitudes of winter sea level pressure for year t. Yearly winter pressure anomaly patterns have been reconstructed beginning in 1602.

Each one of these patterns has been compared to the patterns just shown and the map correlation coefficient determined. Figure 5 is the plot of the correlations of each reconstructed pattern with the two recent winters. The smoothed overlaid curve is the 15-year average of the correlation coefficients. The distribution of these winter types over time is not uniform. Negative pressure anomalies over the North Pacific, similar to those occurring in 1976-1977, were especially common between about 1615 and 1670. Positive pressure anomalies over the North Pacific and North America occurred frequently during the middle and end of the nineteenth century.

Table II shows the percent of reconstructed occurrence by century of winters similar to these recent winters. Gathering statistics for the entire 378-year period from the combined reconstructed and actual occurrence, winters of the type similar to 1976-1977 occurred 17% of the time while those similar to 1978-1979 occurred 11% of the time. These 378-year figures are only slightly different from the twentieth century's percentages of 14 and 11, respectively.

Figure 6 shows the past occurrence of winters similar to 1976-1977 and 1978-1979 relative to their occurrence during the twentieth century. Winters characterized by below-normal pressures over the North Pacific and a blocking high situation over the Pacific Northwest occurred on an average of one out of every four years between 1602 and 1699. During the nineteenth century, winters similar to 1978-1979 occurred more than twice as often. It is not that these types of winters had increased occurrence in the past, but rather that the distribution in the past has not been consistent with the distribution during the present century.

## Figure Legends

Figure 1. Winter 1976-1977 (December, January, February) mean climatic anomalies. Monthly sea level pressure and temperature means are averaged and differenced from the 1898-1899 to 1969-1970 mean for pressure and from the 1900-1901 to 1969-1970 mean for temperature. Total winter precipitation is compared to the mean from 1900-1901 to 1969-1970.

Figure 2. Same as Figure 1 except for winter 1977-1978.

Figure 3. Same as Figure 1 except for winter 1978-1979.

Figure 4. Distribution of explained pressure variance from the calibration of 11 pressure eigenvectors with 5 temperature eigenvectors and 12 precipitation eigenvectors. The first eigenvectors of pressure, temperature, and precipitation account for 34%, 53%, and 22%, respectively, of the variance of the climatic variable.

Figure 5. Plot of the map-pattern correlations between winter sea level pressure anomaly patterns reconstructed from tree-growth anomalies and the patterns for winters 1976-1977 and 1978-1979. The smoothed overlaid curve is the 15-year running average of the correlation coefficients to emphasize the non-uniform distribution.

Figure 6. The 3-century distribution of occurrence of winters similar to the winters of 1976-1977 and 1978-1979 relative to their occurrence during the twentieth century.

## TABLE I

## 20th CENTURY WINTERS SIMILAR TO RECENT WINTERS

| 1976-1977 | 1978-1979 |
|---|---|
| 1899-1900 | 1909-1910 |
| 1901-1902 | 1914-1915 |
| 1928-1929 | 1921-1922 |
| 1930-1931 | 1936-1937 |
| 1935-1936 | 1948-1949 |
| 1939-1940 | 1951-1952 |
| 1944-1945 | 1965-1966 |
| 1952-1953 | |
| 1960-1961 | |
| 1969-1970 | |

## TABLE II

## PERCENT OCCURRENCE OF RECONSTRUCTED SEA LEVEL PRESSURE ANOMALY PATTERNS SIMILAR TO THOSE OF RECENT WINTERS

| | 1976-1977 | 1978-1979 |
|---|---|---|
| 1602-1699 | 25% | 5% |
| 1700-1799 | 16% | 5% |
| 1800-1899 | 14% | 23% |
| 1900-1979 | 14% | 11% |
| 1602-1979 | 17% | 11% |

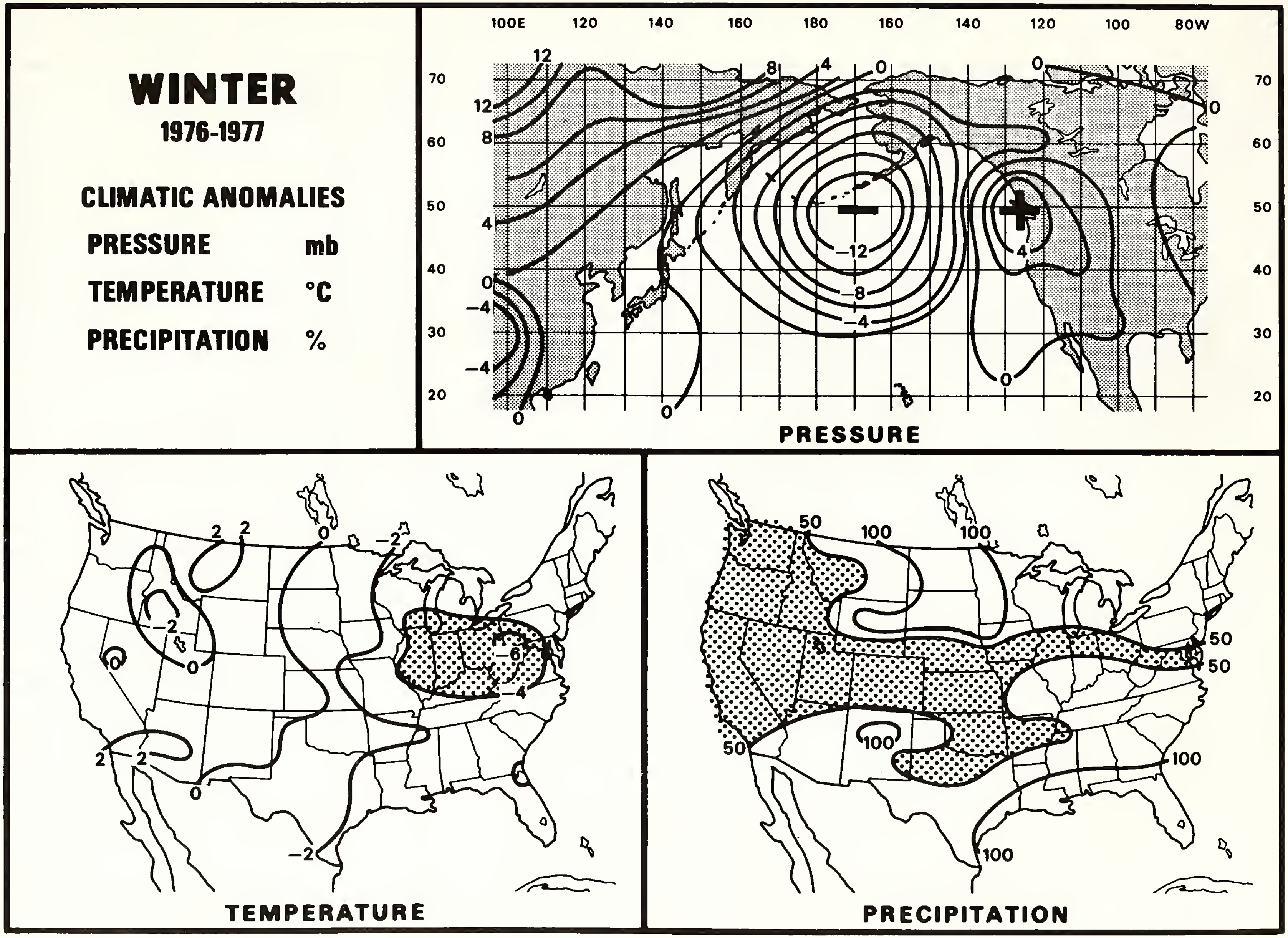
WINTER
1976-1977
CLIMATIC ANOMALIES
PRESSURE mb
TEMPERATURE °C
PRECIPITATION %
100E
120
140
160
180
160
140
120
100
80W
70
60
50
40
30
20
12
8
4
0
−4
−12
−8
PRESSURE
2
−2
−6
−4
TEMPERATURE
50
100
PRECIPITATION

FIGURE 1

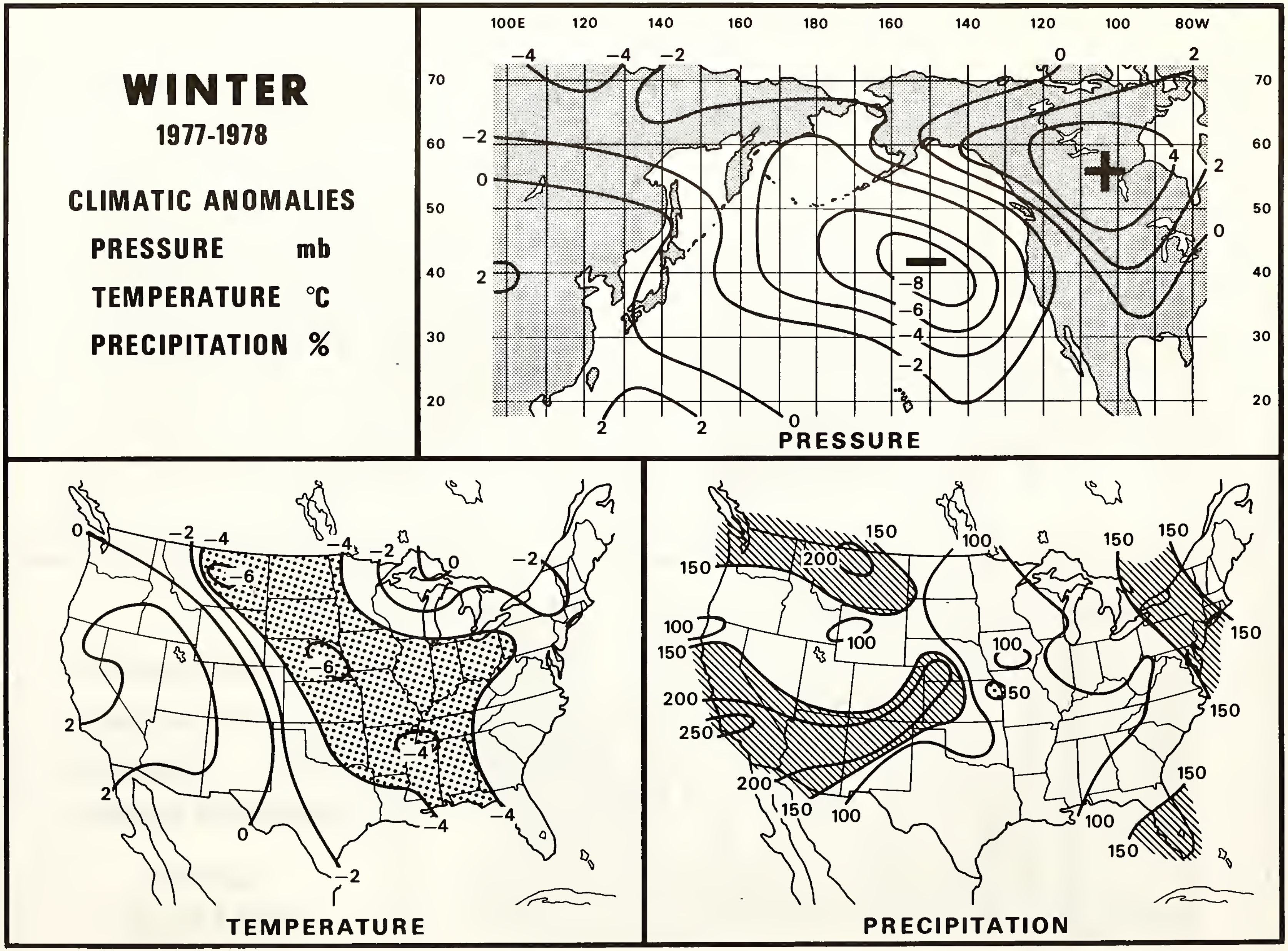

**WINTER**

**1977-1978**

**CLIMATIC ANOMALIES**

**PRESSURE mb**

**TEMPERATURE °C**

**PRECIPITATION %**

FIGURE 2

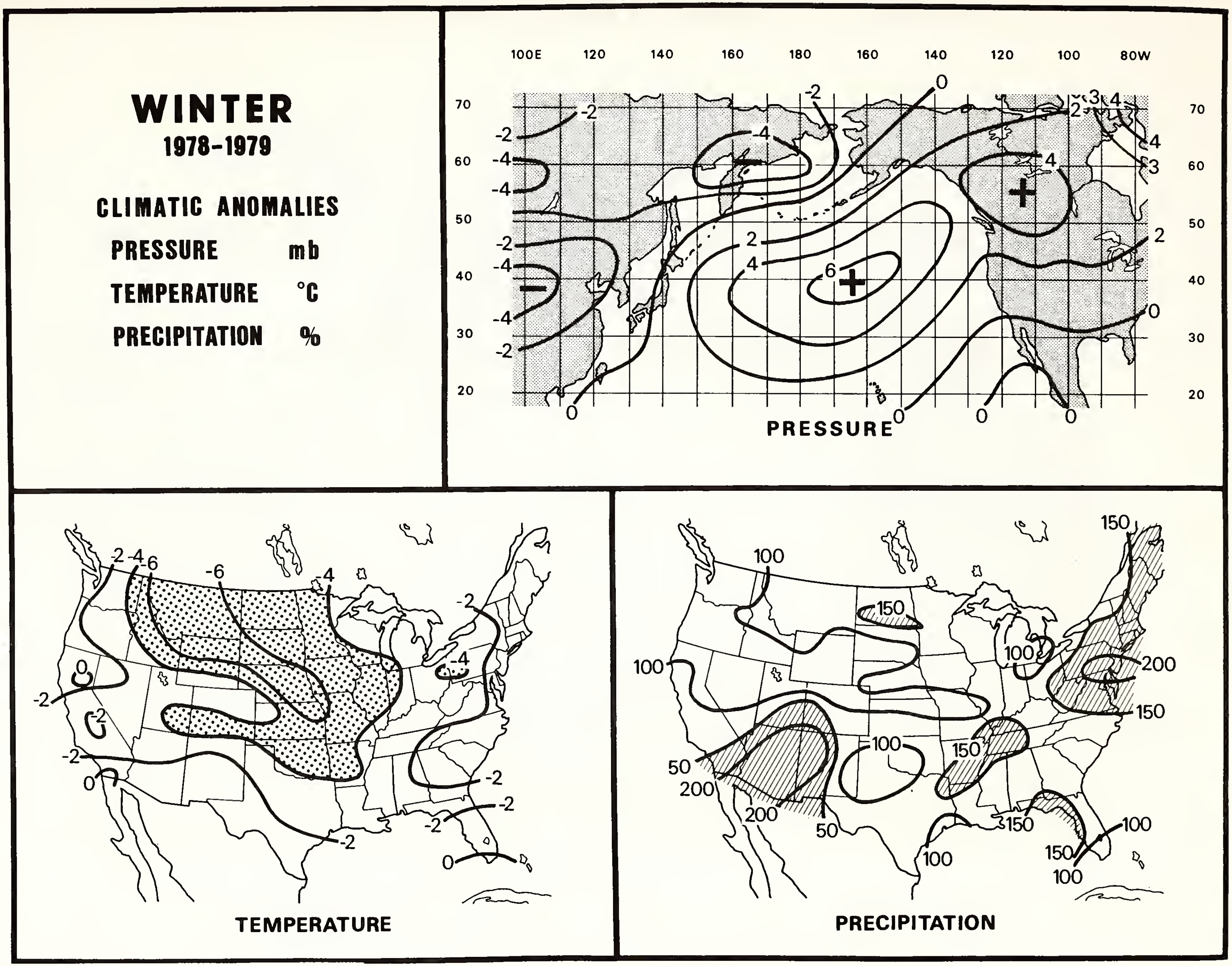

**WINTER**

**1978-1979**

**CLIMATIC ANOMALIES**

**PRESSURE** mb

**TEMPERATURE** °C

**PRECIPITATION** %

PRESSURE

TEMPERATURE

PRECIPITATION

FIGURE 3

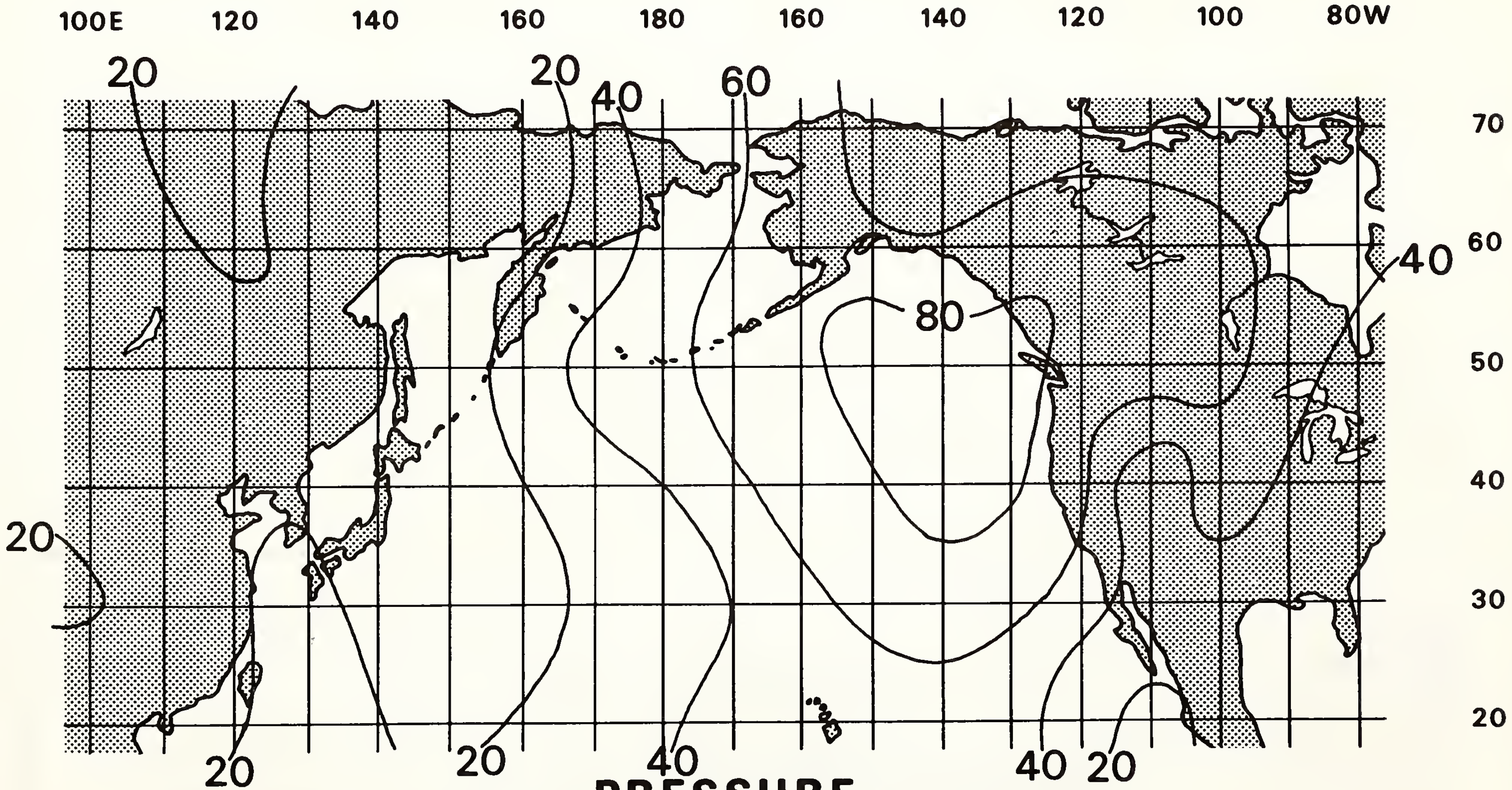

PRESSURE

CALIBRATED VARIANCE FOR MODEL 11P5T12R

FIGURE 4

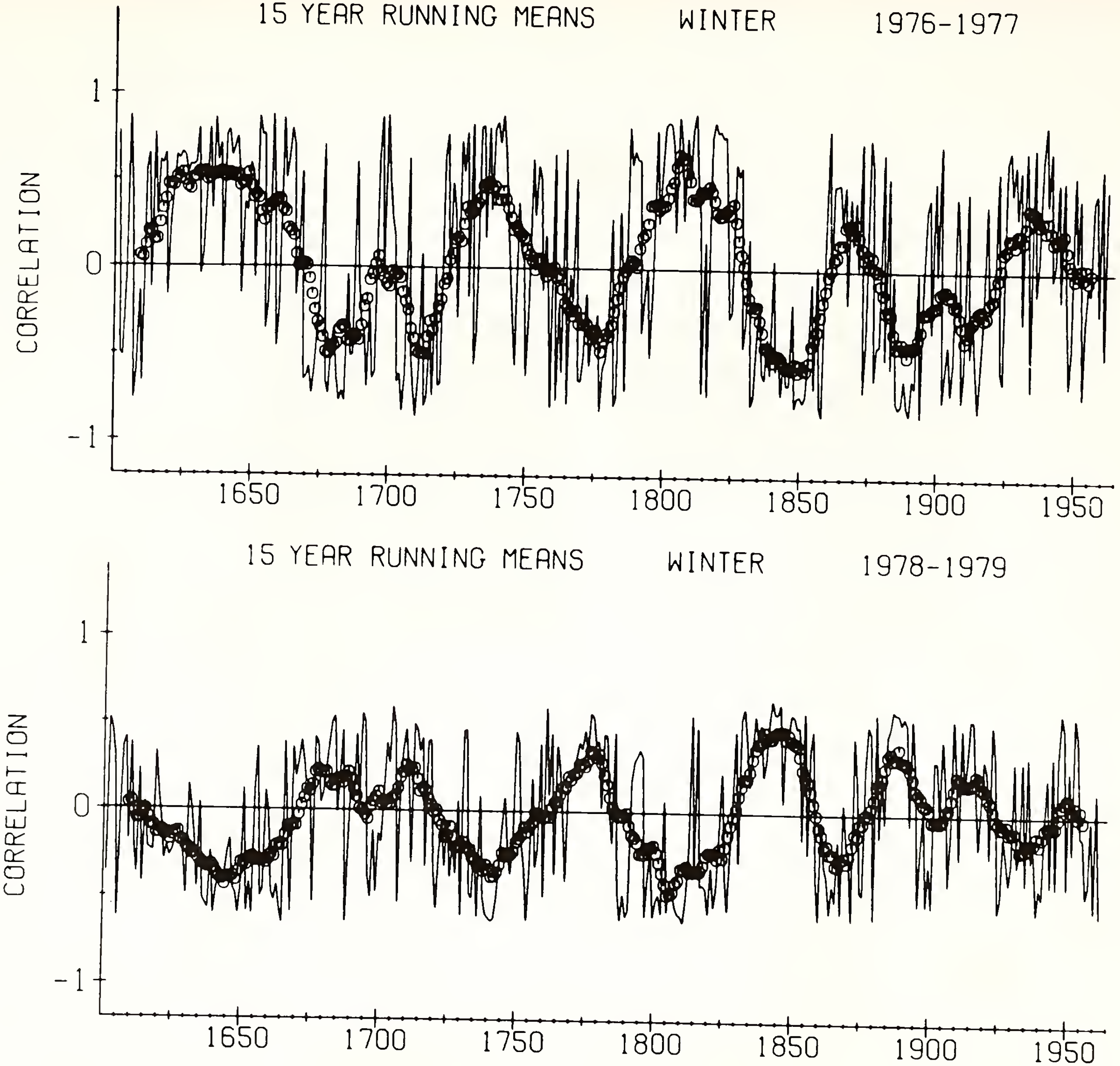
15 YEAR RUNNING MEANS WINTER 1976-1977
CORRELATION
1
0
-1
1650
1700
1750
1800
1850
1900
1950
15 YEAR RUNNING MEANS WINTER 1978-1979
CORRELATION
1
0
-1
1650
1700
1750
1800
1850
1900
1950

FIGURE 5

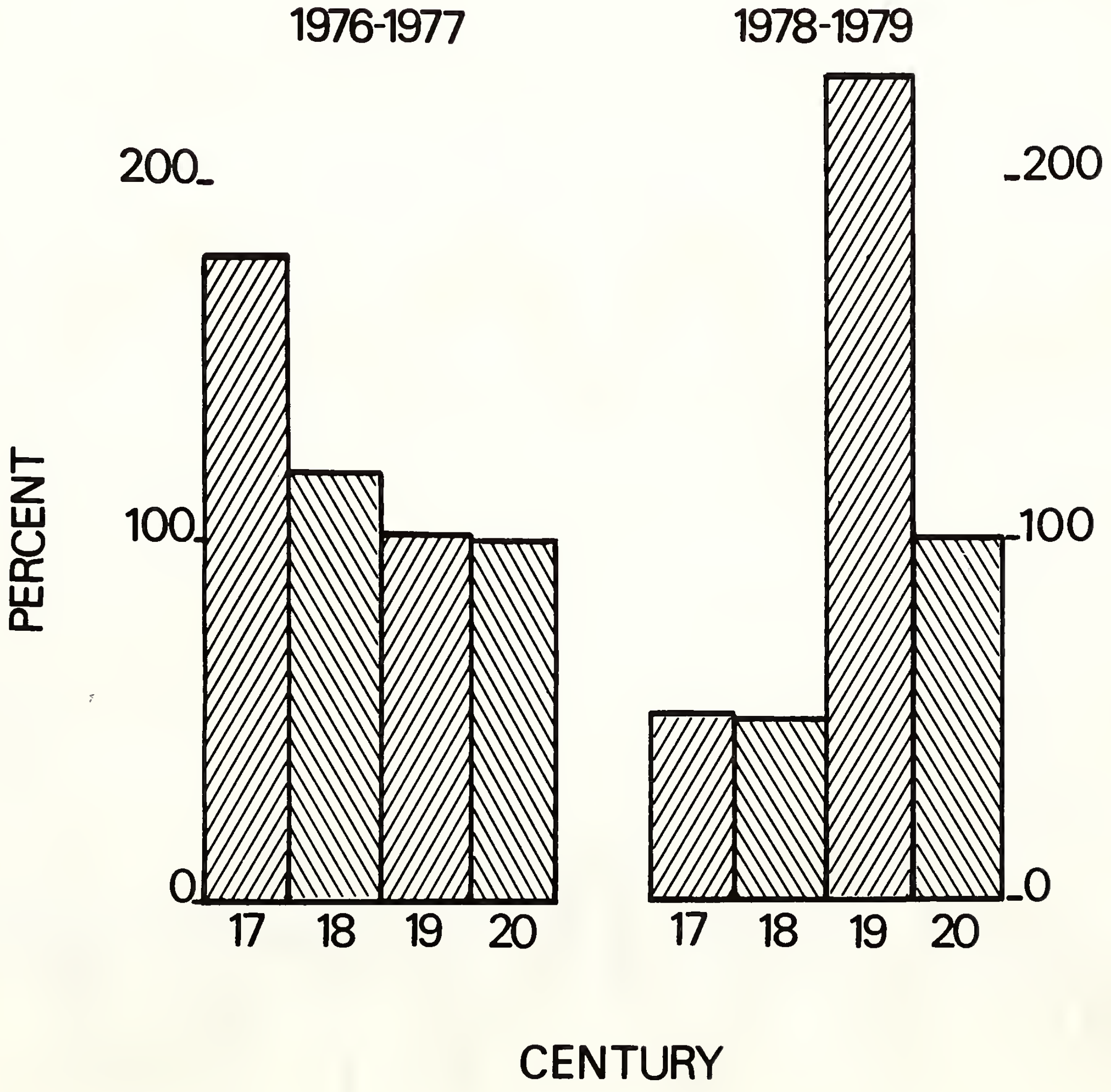
1976-1977
1978-1979
PERCENT
200
100
0
200
100
0
17
18
19
20
17
18
19
20
CENTURY

FIGURE 6

# Long-Wave Contributions to Tropospheric and Stratospheric Temperature Anomalies in Winter

by

R. S. Quiroz
Climate Analysis Center
NMC, NOAA
Washington, D. C. 20233

Planetary zonal waves 1 and 2 are of overriding importance for explaining anomalies in stratospheric zonal mean temperature. For the troposphere, it is shown that wave 2 is of crucial importance.

The morphology of daily planetary wave structure is illustrated by time-latitude sections of amplitude of waves 1-3 at 500 mb during the 1978-79 winter (figure not included here). Fig. 1 shows wave 1 and 2 amplitude at 65°N, from data for 700-10 mb, for January-February 1979 (from Geophys. Res. Letters, Aug. 1979). The major wave developments depicted, most notably the stratospheric wave 1 amplification in late January and the major tropospheric-stratospheric wave 2 amplification after February 10, had a profound influence on the temperature and wind fields of both the troposphere and stratosphere. Fig. 2, giving daily mean zonal wind in the vicinity of the tropospheric (200 mb, 30°N) and stratospheric jet stream cores (50 mb, 65°N) indicates a strong coupling of the two circulations. Note the enhanced (diminished) tropospheric (stratospheric) flow in late January and late February. Climatological aspects of this coupling in the circulation have been examined recently by the author (J. Pure and Appl. Geophys., January 1980).

Planetary waves 1-3 tend to extract heat from mid-latitudes, through horizontal heat transport (as has been shown by van Loon, MWR,1979), and tend to deposit heat in high latitudes. In February 1979, wave 2 amplified greatly in moderately high latitudes (Fig. 3), accounting for maximum cooling (as defined by zonal mean temperature at 850-500 mb) at latitudes 60-80°N (Fig. 3, bottom right). This was in contrast to maximum cooling in mid-latitudes in the 1976-77 winter which was associated with sustained high amplitude of wave 2 (500 mb) near 50°N. The "standing" component of wave 2 (defined by Fourier analysis of monthly mean charts) evidently largely accounts for the major temperature trends.

Fig. 3 shows the amplitude of 500 mb height wave 2 (standing) and the monthly temperature anomaly, as a function of latitude and month, during the last 4 winters (October-March). Note certain similarities of pattern, particularly in 1976-77 and 1978-79. In the temperature data, note the changeover from warm to cold temperature in mid-latitudes from 1975-76 to 1976-77; the meridional diffusion of cold anomaly in 1977-78; and the poleward displacement of cold anomaly in 1978-79. Anomaly, here, is defined as the departure, in deg C, of zonal mean temperature from the 4-year mean for each month.

Fig. 4 quantifies the relationship between horizontal eddy heat flux and zonal mean temperature, at left. Data consist of the correlation between one property at a specified latitude and the other property at all latitudes. At right are correlations between the amplitude of height wave 2 (standing) and zonal mean temperature. The sample consisted of 12 monthly values (Dec., Jan., Feb.; 4 winters) of each property, for each pair of latitudes. The results at the left agree qualitatively with the eddy heat flux comparison made previously by van Loon (1979) on the basis of 20 winters (seasonal values). The results on the right further show that the amplitude of standing wave 2 (without specification if innate properties such as vertical tilt and actual heat fluxes) is highly correlated with mean zonal temperature, negatively in mid-latitudes and positively for mid-latitude waves and high latitude temperature.

These results emphasize the importance of quasi-stationary wave 2 for explaining hemispheric temperature anomalies. Further work is needed, particularly on the questions of (1) relating regional anomalies to hemispheric anomalies, and (2) seeking to determine the physical origin of large wave 2 amplifications.

## Figure Legends

Fig. 1 Amplitude of wave 1 (above) and wave 2 (below) in height of pressure surfaces 700-10 mb, at 65°N, respectively.

Fig. 2 Tropospheric and stratosphere jet flows during early 1979, as represented by the mean zonal wind at 200 mb, 30°N, and 50 mb, 65°N, respectively.

Fig. 3 Monthly amplitude, October-March, 1975-76 to 1978-79, of 500 mb height wave 2 (standing) (above); and monthly departure of zonal mean temperature at 500 mb from 4-yr. mean (below).

Fig. 4 Correlation for each pair of latitudes, between monthly average of daily eddy heat flux and monthly zonal mean temperature (at left); and between monthly amplitude of height wave 2 (standing) and zonal mean temperatures at 500 mb.

FIG. 1.

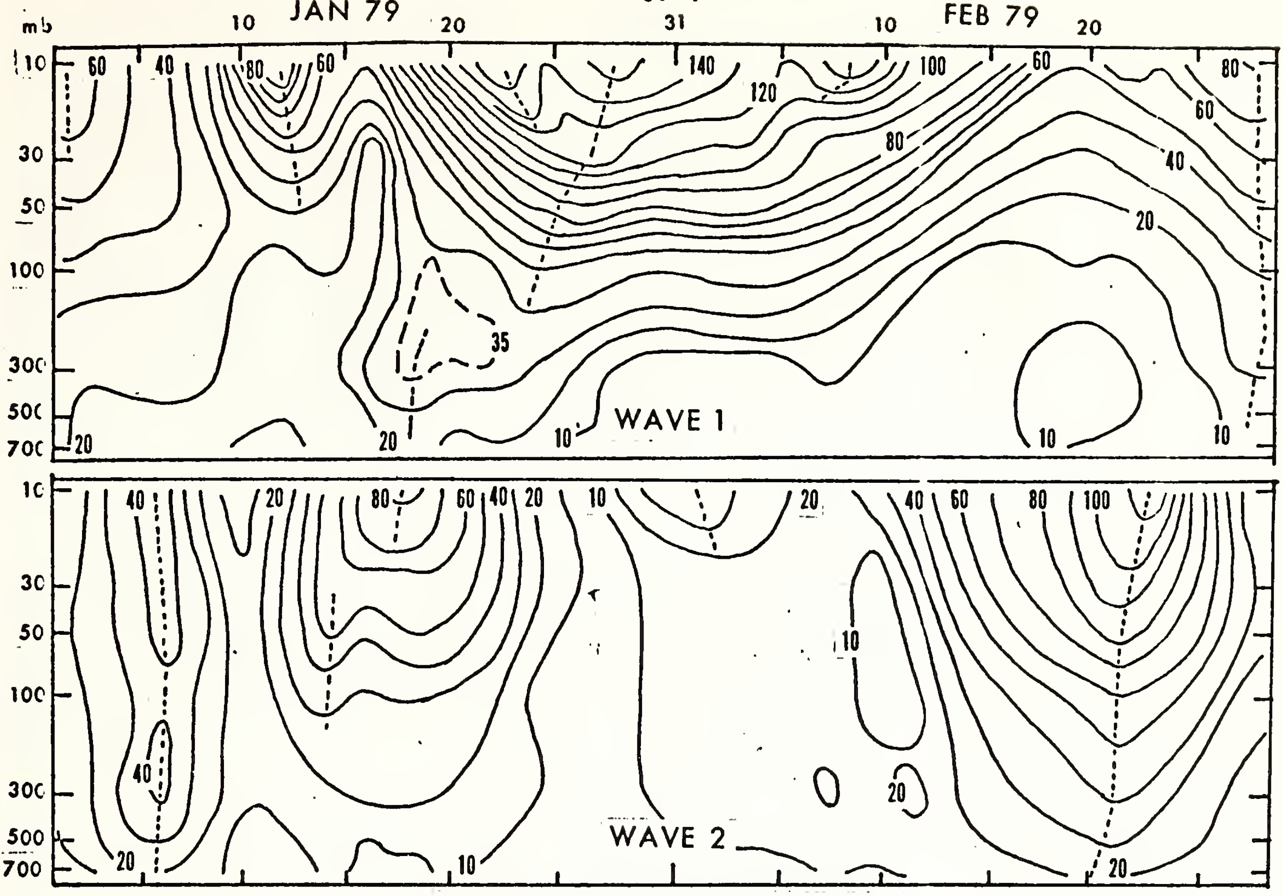

AMPLITUDE (HEIGHT), DECAMETERS

FIG. 2

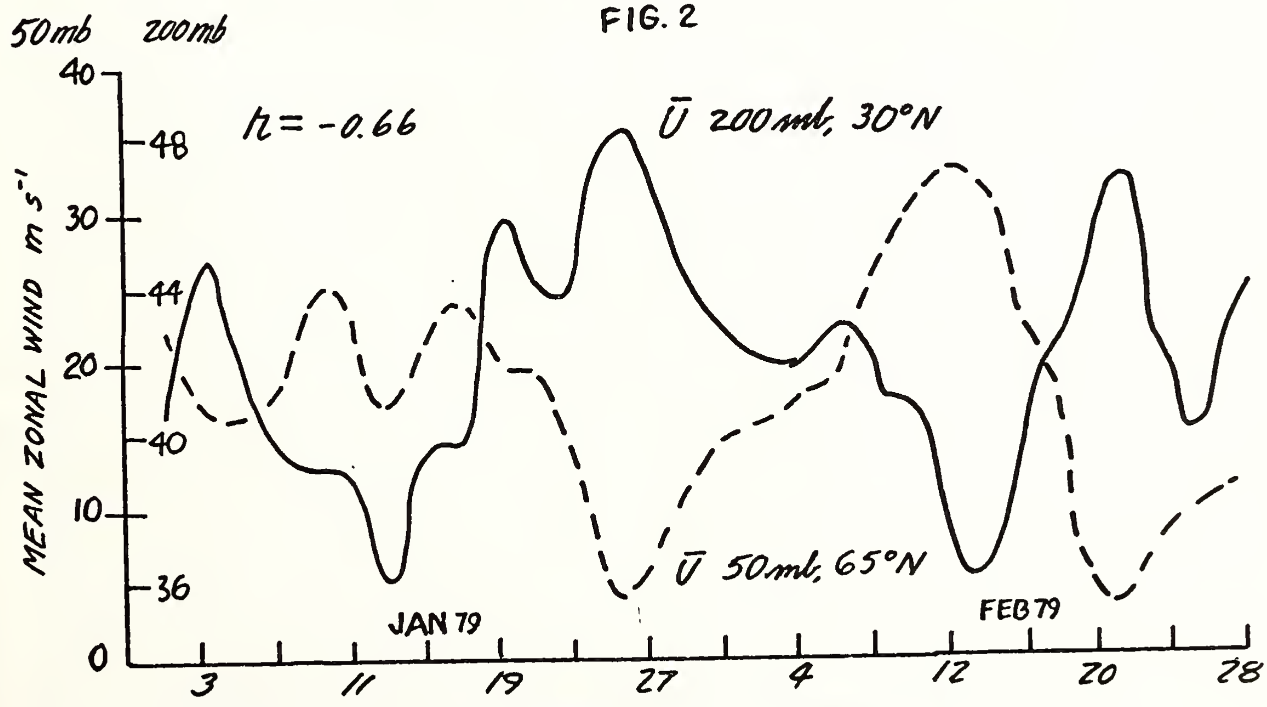

COMPARISON OF STRATOSPHERIC AND TROPOSPHERIC ZONAL WIND

FIG. 3

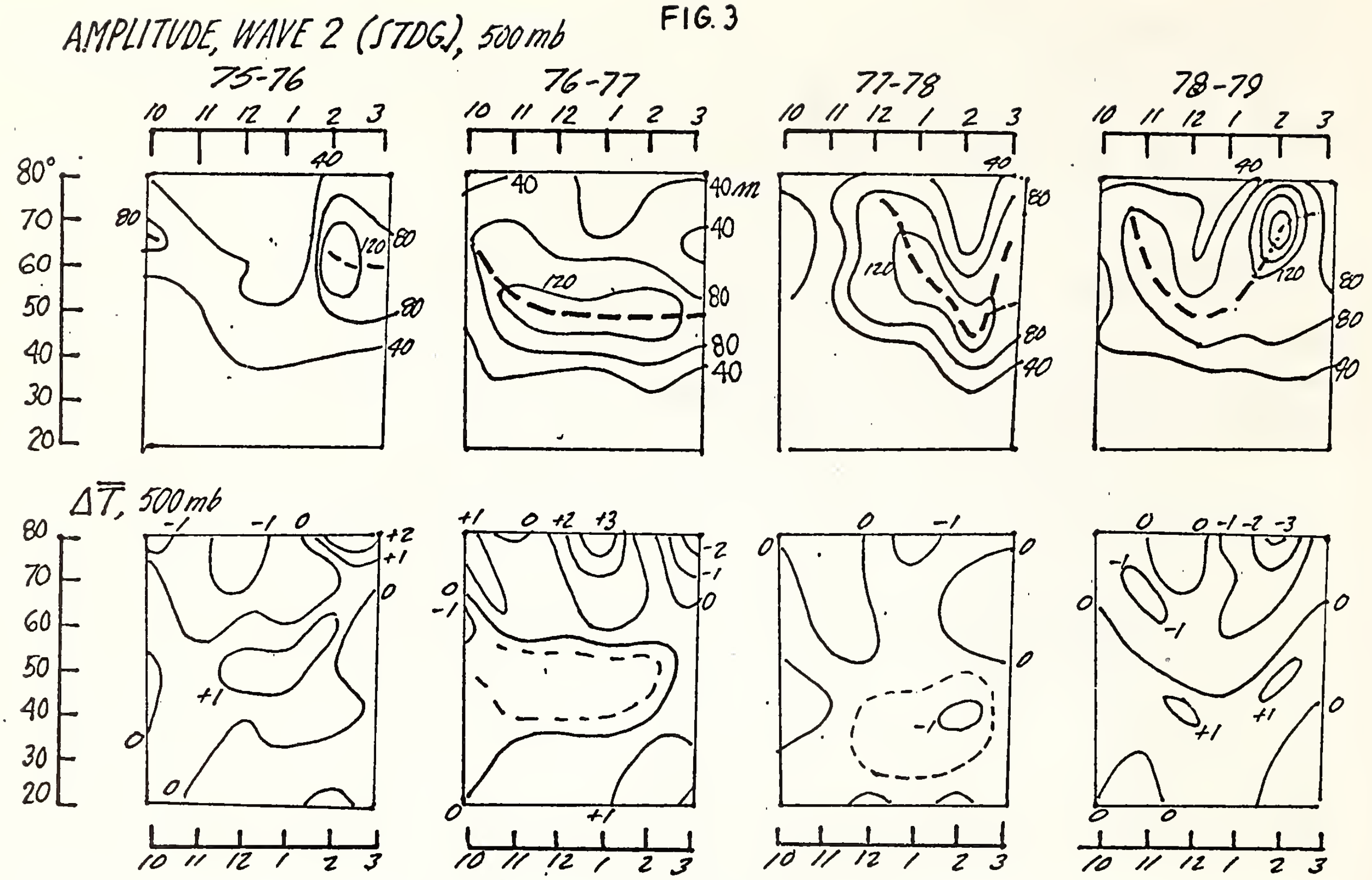

FIG 4. CORRELATION BETWEEN MEAN (TOTAL) EDDY HEAT FLUX AND MEAN ZONAL TEMPERATURE (LEFT) AND BETWEEN AMPLITUDE OF WAVE 2 HT (STDG.) AND MEAN ZONAL TEMPERATURE (RIGHT), BASED ON DEC, JAN, FEB 1975-76 TO 1978-79 (N=12)

500 MB

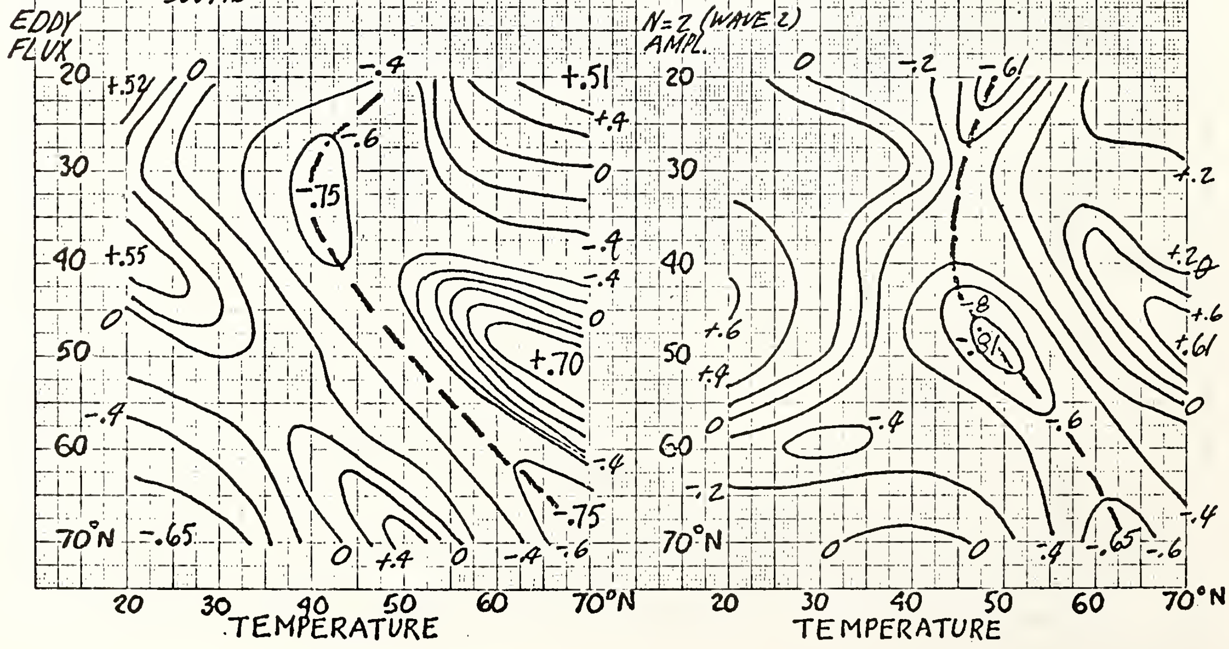

# ABSTRACT

## "Circulation and Weather Changes from the Summer 1978 through the Subsequent Winter"

Jerome Namias†
Scripps Institution of Oceanography
La Jolla, California

The winter of 1978-79 had some intense and extensive anomalies in various wind, weather and sea elements. Ranking high among these was exceptional cold over practically the entire United States and frequent storminess associated with recurrent snows. In fact, taking the winter as a whole (Dec., Jan. and Feb.) and considering terciles of temperature, there were no areas of above normal in the continental United States and only a few very small areas of near normal—all the rest of the nation averaged below normal. Such extensive cold patterns over the United States occur rarely, perhaps less than once in twenty winters, and such a pattern has not been observed during the winters of the past two decades. However, it will be remembered that the two preceding winters, 1976-77, 1977-78, were both extremely cold over the Central and Eastern portions but not over the West.

Obviously, the general circulation of the atmosphere influencing this large area must have been highly abnormal. Because of this peculiar condition, not foreseen by the author nor by any of his colleagues in the U.S., a case study has been made of conditions preceding and during the winter. This study necessarily includes the atmosphere circulation and its evolution as well as oceanic thermal conditions over the adjacent oceans and conditions in the Arctic.

---

†Paper delivered by Mr. Daniel Cayan of Scripps Institution of Oceanography to whom I am indebted.

It turns out that a strong ridge developed in the Eastern Pacific late in the fall of 1978, and this was associated with a coherent warm pool of surface water. The change in SST's was such that cold water off the coast also developed so that a strong west-east SST gradient was established late in the fall and remained through the winter. This SST gradient fed into the overlying atmosphere so as to reinforce north to south thermal winds (and total winds) to the east of the ridge as a persistent winter feature. Downstream redistribution of vorticity led to deployment of cold air in the Far West. However, while the East usually responds by developing a ridge and strong Bermuda High, this did not take place during the 1978-79 winter because of the establishment of a strong quasi-stationary high latitude block extending from Scandinavia to Alaska. The block suppressed storm tracks and was completely at variance with statistically derived teleconnections from the North Pacific ridge. While no good explanation of the blocking is at hand, the North Pacific situation seems to have responded in a manner earlier described by the author, wherein cold water in the Eastern Pacific in summer and early fall causes a ridge to develop in fall, (negative feedback). This mean pattern remained stable during the entire winter because of air-sea coupling.

Premonitory signs of the North Pacific activity were indicated by kinematic (advective) prognoses of SST patterns made as early as November, and also by specification patterns of SST from atmospheric 700 mb pattern generated in November. The latter indicated the possible amplification of the warm water pool.

# LEGENDS TO FIGURES

Fig. 1 Thickness departures from normal in tens of feet (anomalies) for seasons of Summer and Fall, 1978 and Winter, 1978-79. Isopleths are for every 30 feet with centers labelled in tens of feet. Hatched areas are below normal; stippled, above normal.

Fig. 2 700 mb contours (solid lines, labelled in tens of feet), and sea surface temperature (SST) anomalies (°F) for the seasons indicated. Hatched areas show below normal SST and stippled, above normal SST. Centers labelled in tens of feet.

Fig. 3 (Upper) 700 mb height anomalies (tens of feet), and (Lower) SST anomalies (°F) for Fall, 1978.

Fig. 4 As in Fig. 3, except for Winter, 1978-79.

Fig. 5 Predicted and observed anomaly patterns of temperature (above) and precipitation (below) for Winter, 1979. Terciles are employed—(B) below normal, (N) normal, (A) above normal for temperature. H, M, and L stand for light, moderate and heavy precipitation respectively. Although poor in the East, the nationwide forecast exhibited positive skill because of correct prognosis of western half.

Fig. 6 700 mb contours (solid, labelled in tens of feet) and anomalies of SST (°F) for months shown.

Fig. 7 As in Fig. 6.

Fig. 8 Advective forecasts of SST anomalies made from initial state (November, 1978) up to February, 1979. Advection assumes conservation of anomalies as they are carried

by normal surface currents. Hatched areas are more negative than -.85°F; shaded areas above +.85°F.

Fig. 9 Specification of SST anomalies for November 1978, based on contemporaneous 700 mb anomaly pattern. Contour interval 1°F.

Fig. 10 (Top and middle) SST monthly anomaly (solid) at 40°N 150°W and 40°N 125°W and also 700 mb anomalies (dashed) at these points. (Lowest graph) Difference, or west to east gradients of the above.

Fig. 11 Daily surface and 500 mb charts for December 6, 1978 (from NWS, NOAA).

Fig. 12 Mean 700 mb contours (solid, labelled in tens of feet) and isopleths of anomaly (broken) for December, 1978.

Fig. 13 700 mb height anomalies for winter, 1978-79.

Fig. 14 Point correlations between SST anomalies in summer vs. 700 mb anomalies in the subsequent fall.

Fig. 15 Cross-correlations between 700 mb height at 40°N 140°W and heights elsewhere. Stippled areas are positive, hatched negative. Isopleths are drawn for each .10.

1000-700mb THICKNESS$_{DM}$ (TENS OF FEET)

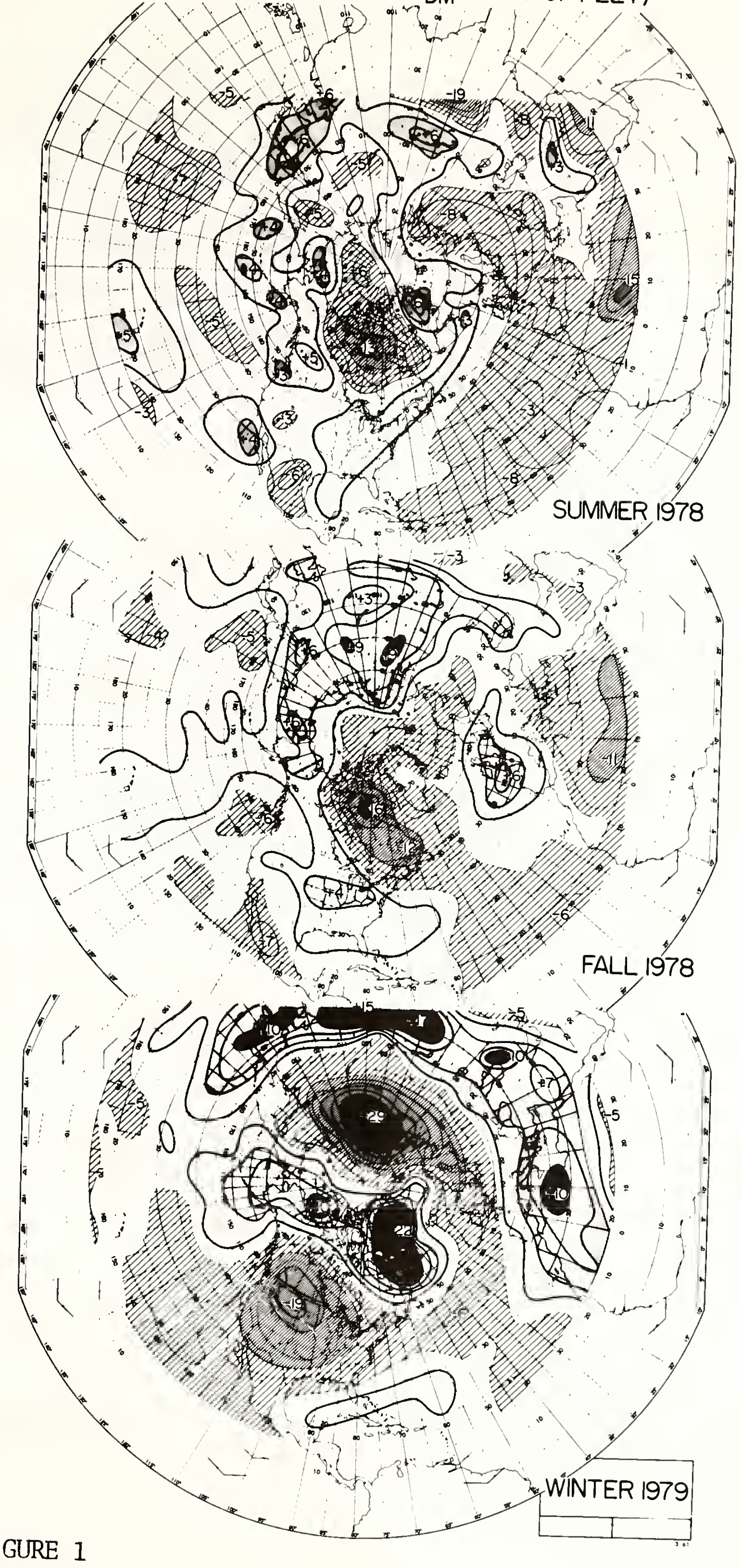

FIGURE 1

700 mb HT (ft. x 10) & $SST_{DM}$

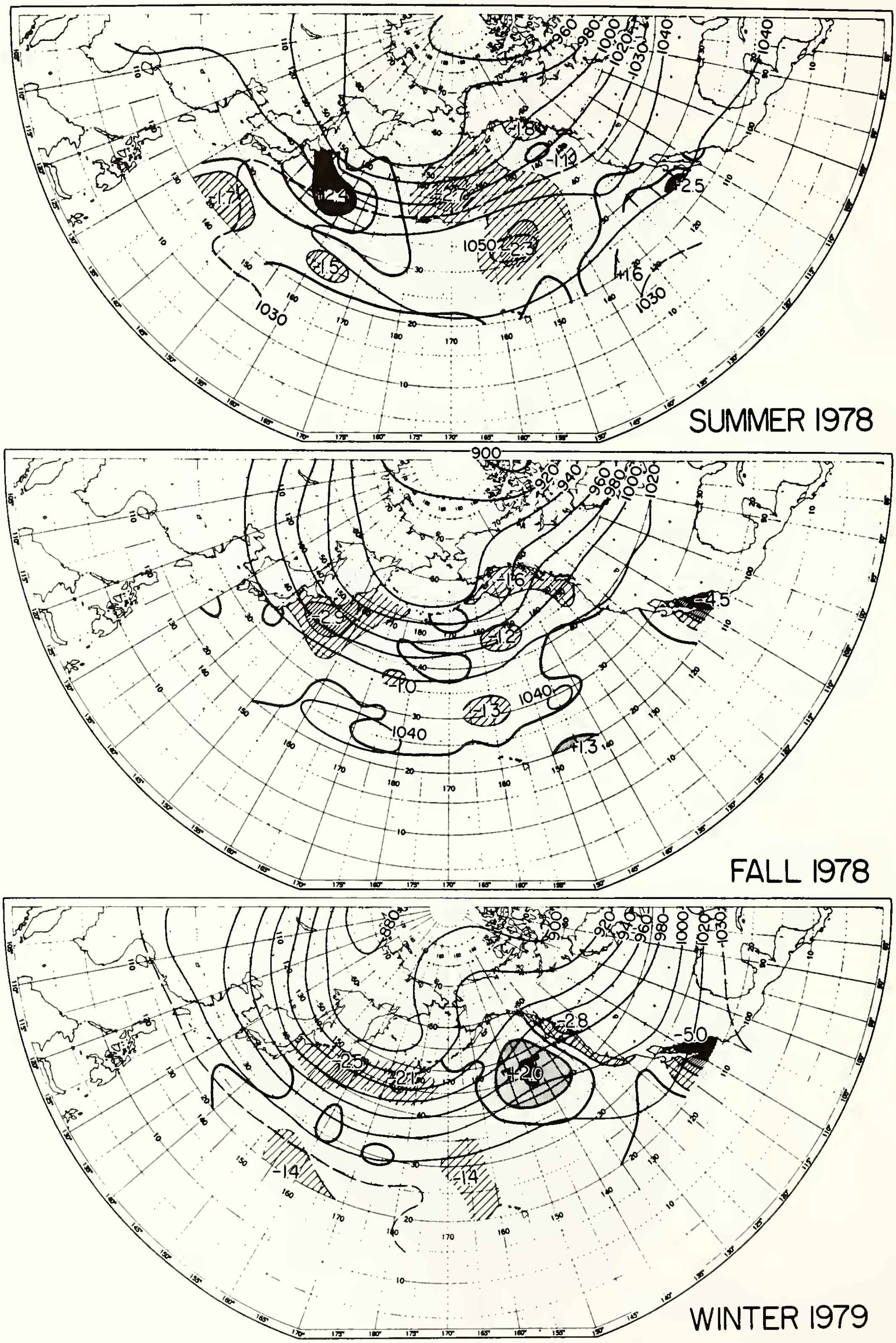

FIGURE 2

FALL 1978

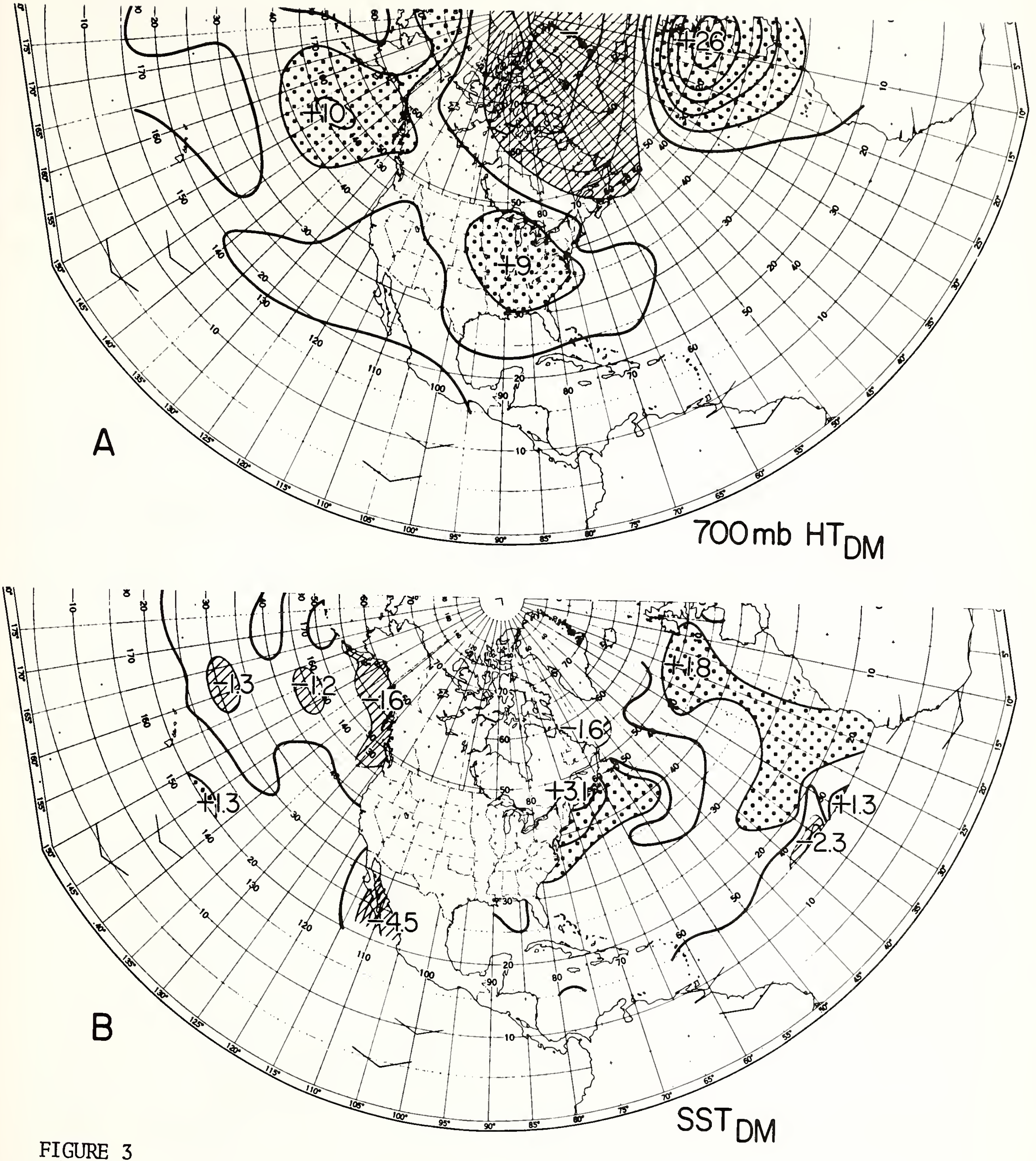

FIGURE 3

WINTER 1979

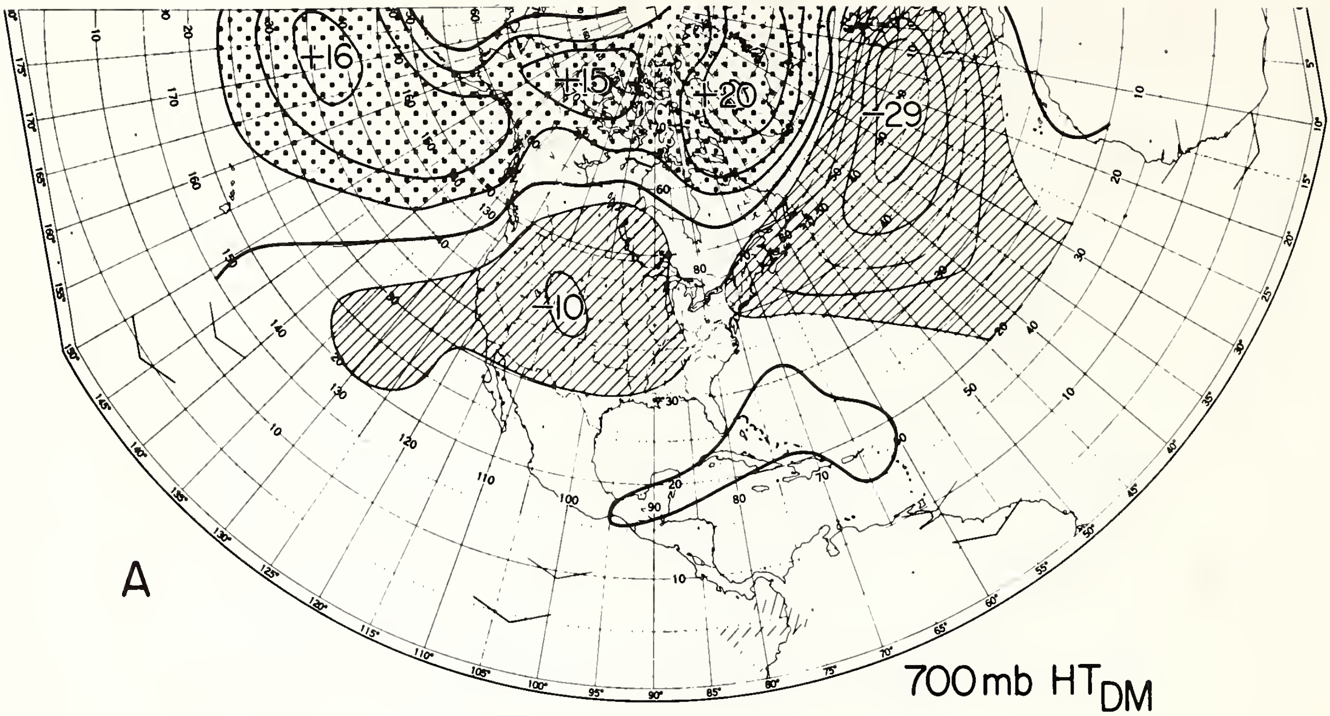

A

700 mb $HT_{DM}$

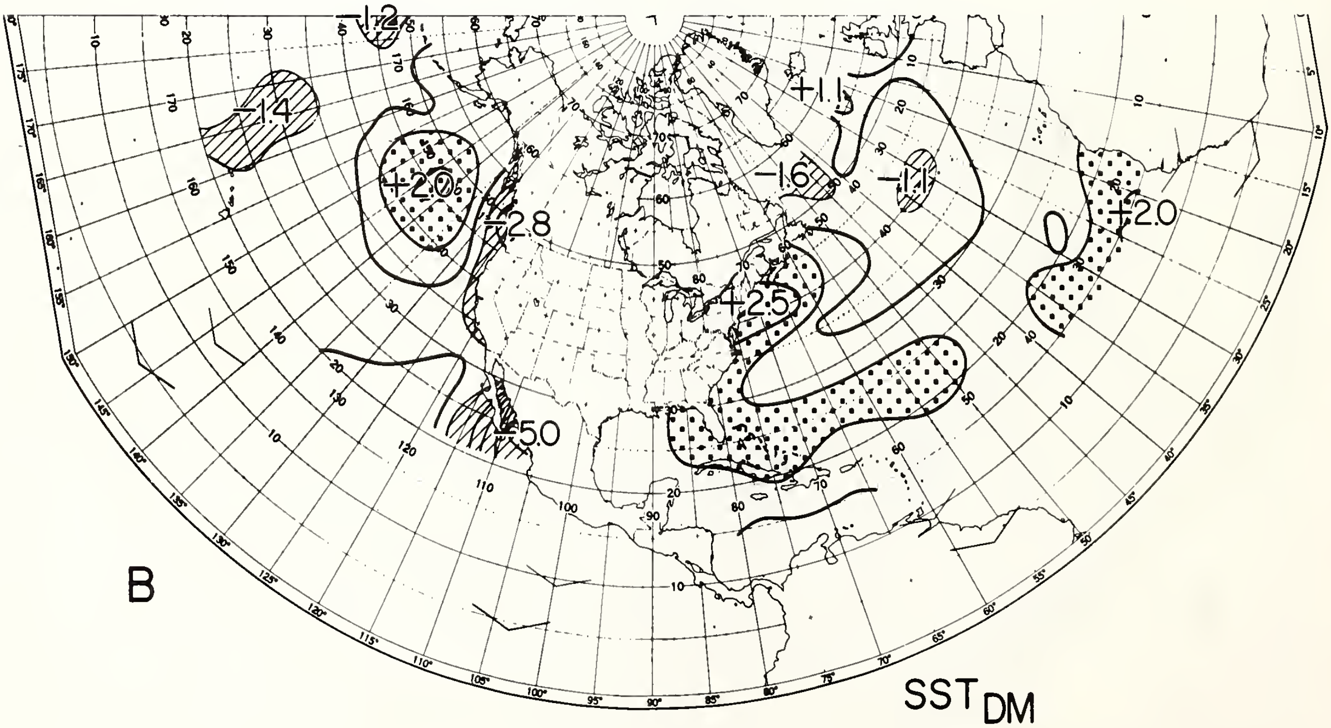

B

$SST_{DM}$

FIGURE 4

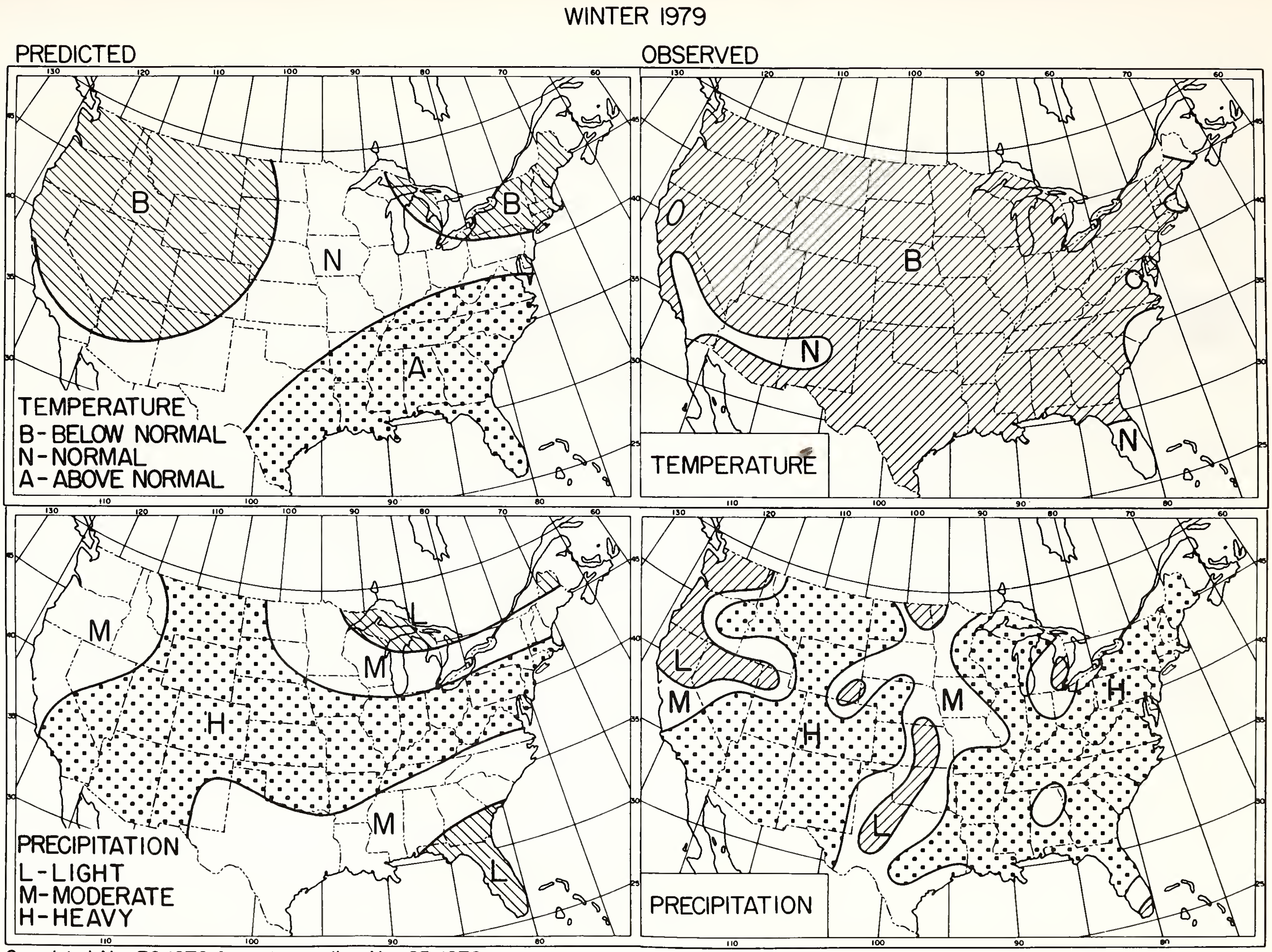

Completed Nov. 30, 1978, from data ending Nov. 25, 1978

FIGURE 5

## $SST_{DM}$ & 700mb Ht.

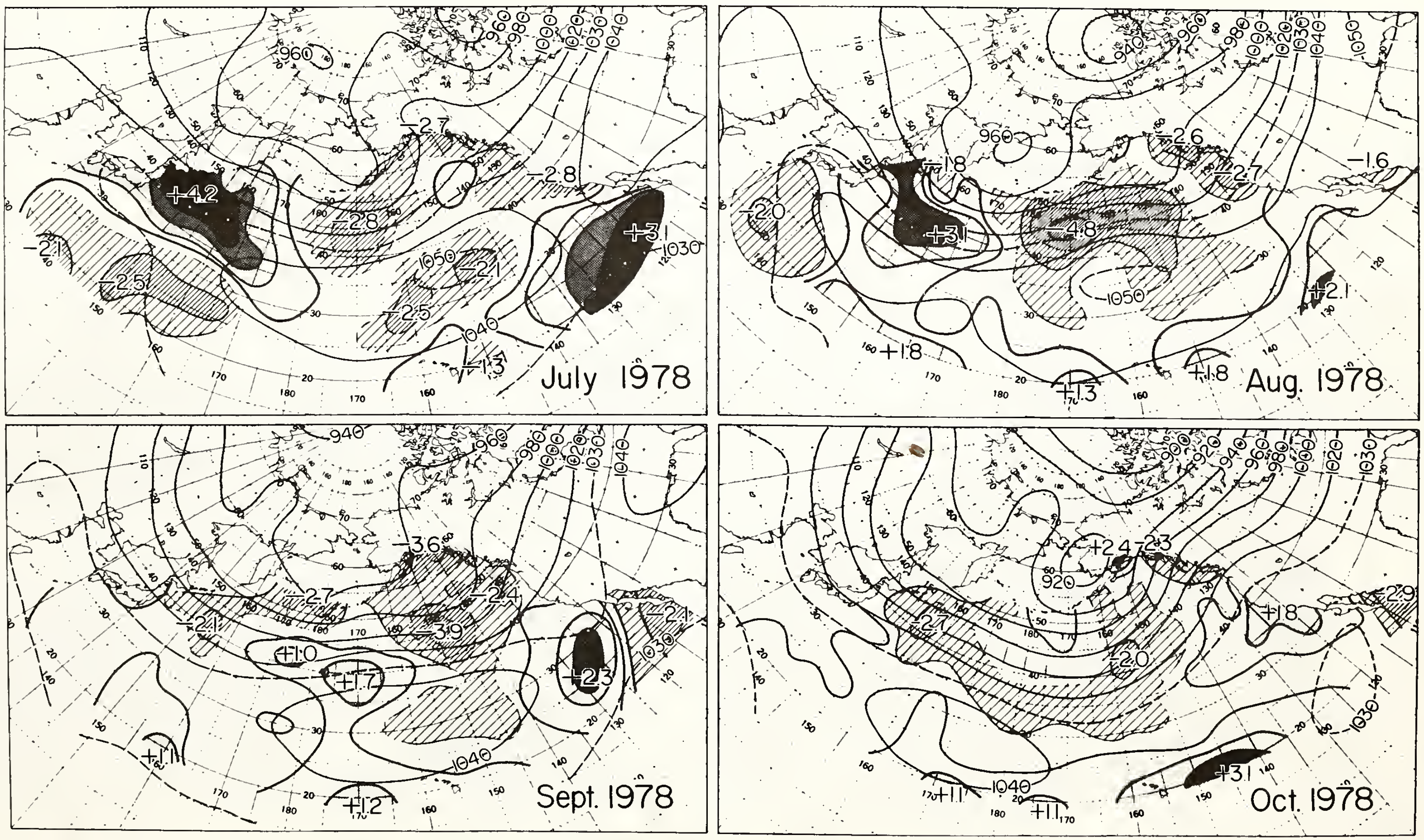

FIGURE 6

$SST_{DM}$ & 700mb Ht.

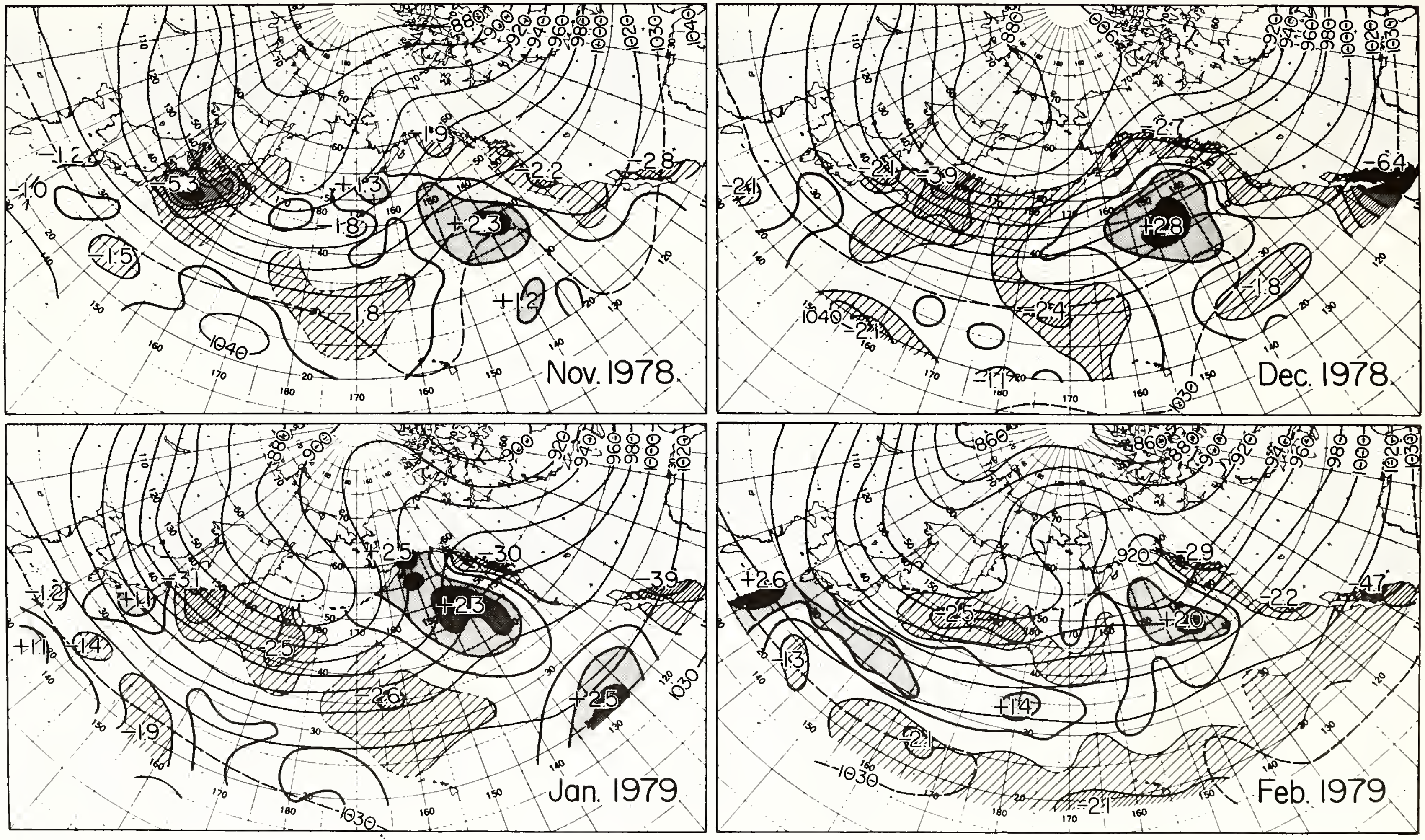

FIGURE 7

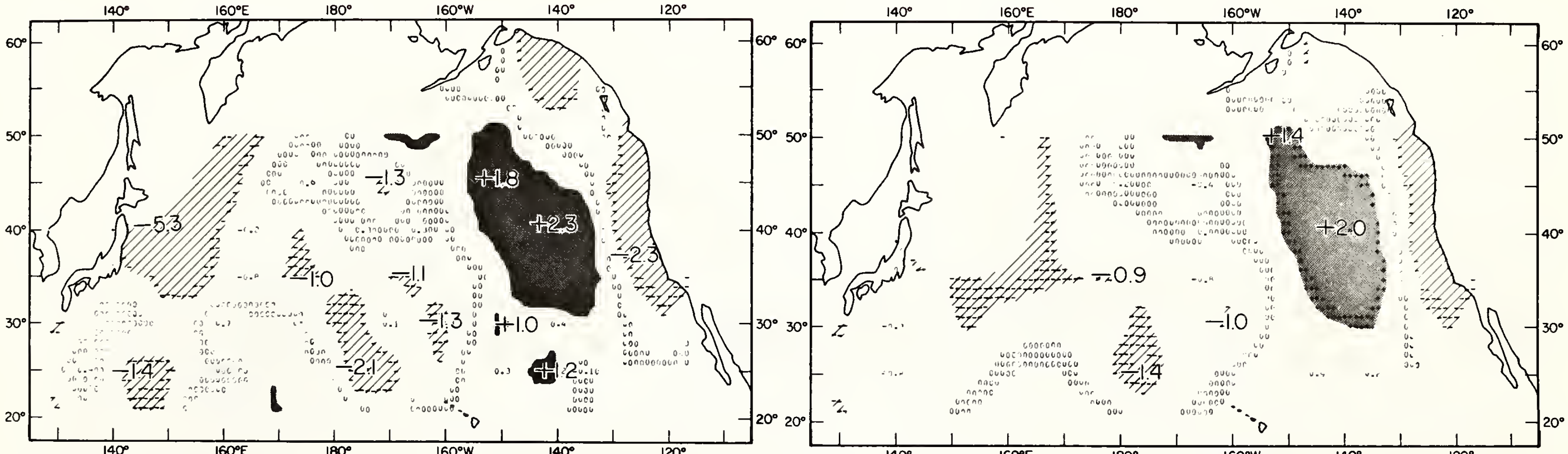

SST$_{DM}$ Nov. '78

Fcst. for Dec. '78

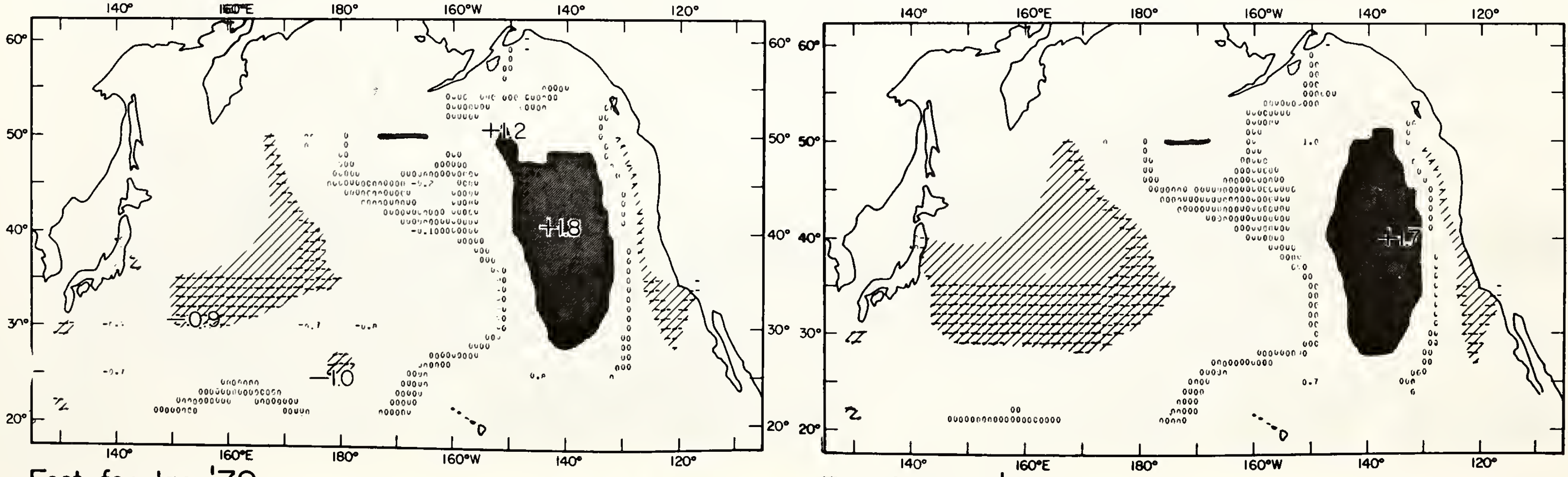

Fcst. for Jan. '79

Fcst. for Feb. '79

FIGURE 8

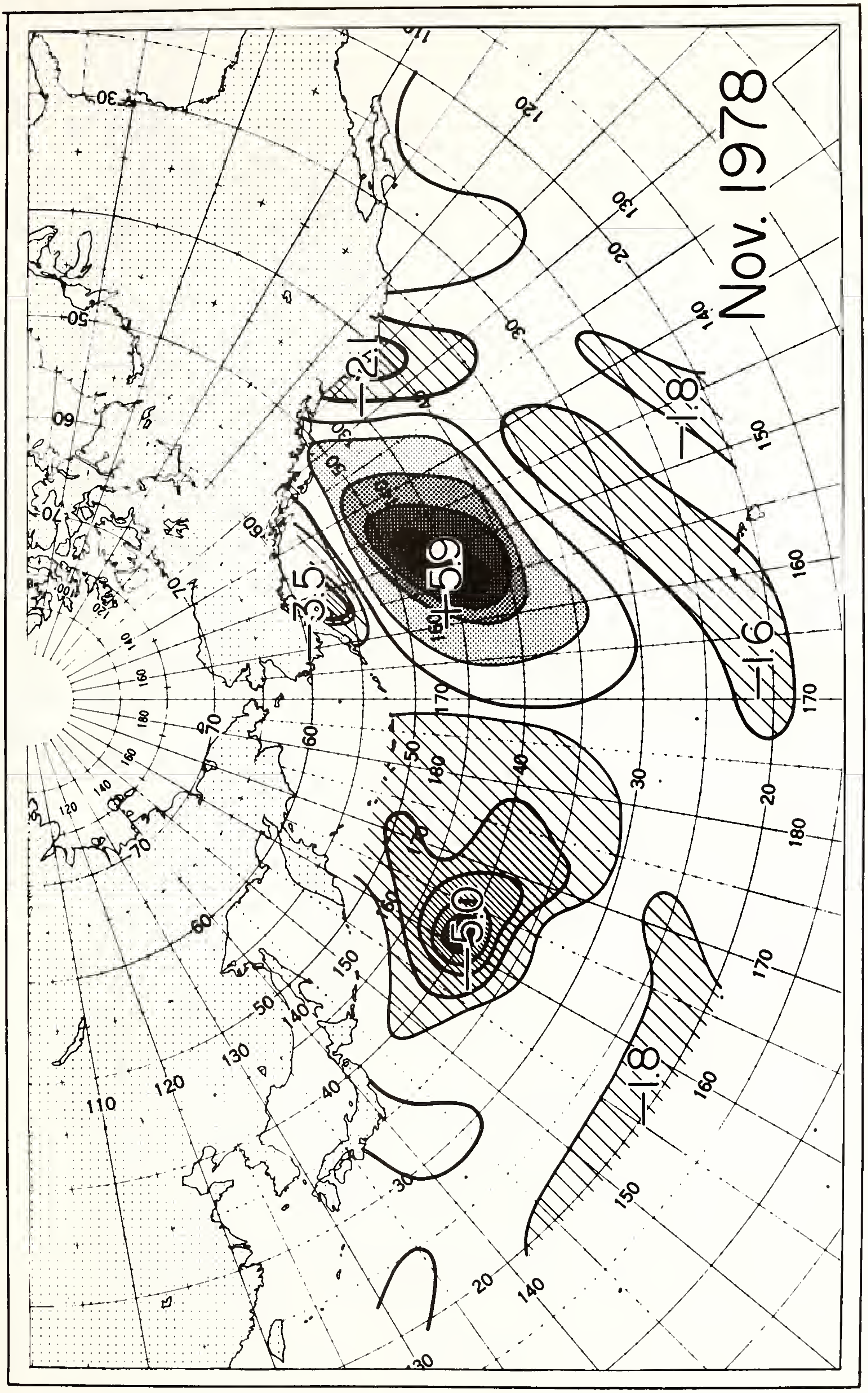

$SST_{DM}$ Specified from $700mb_{DM}$

FIGURE 9

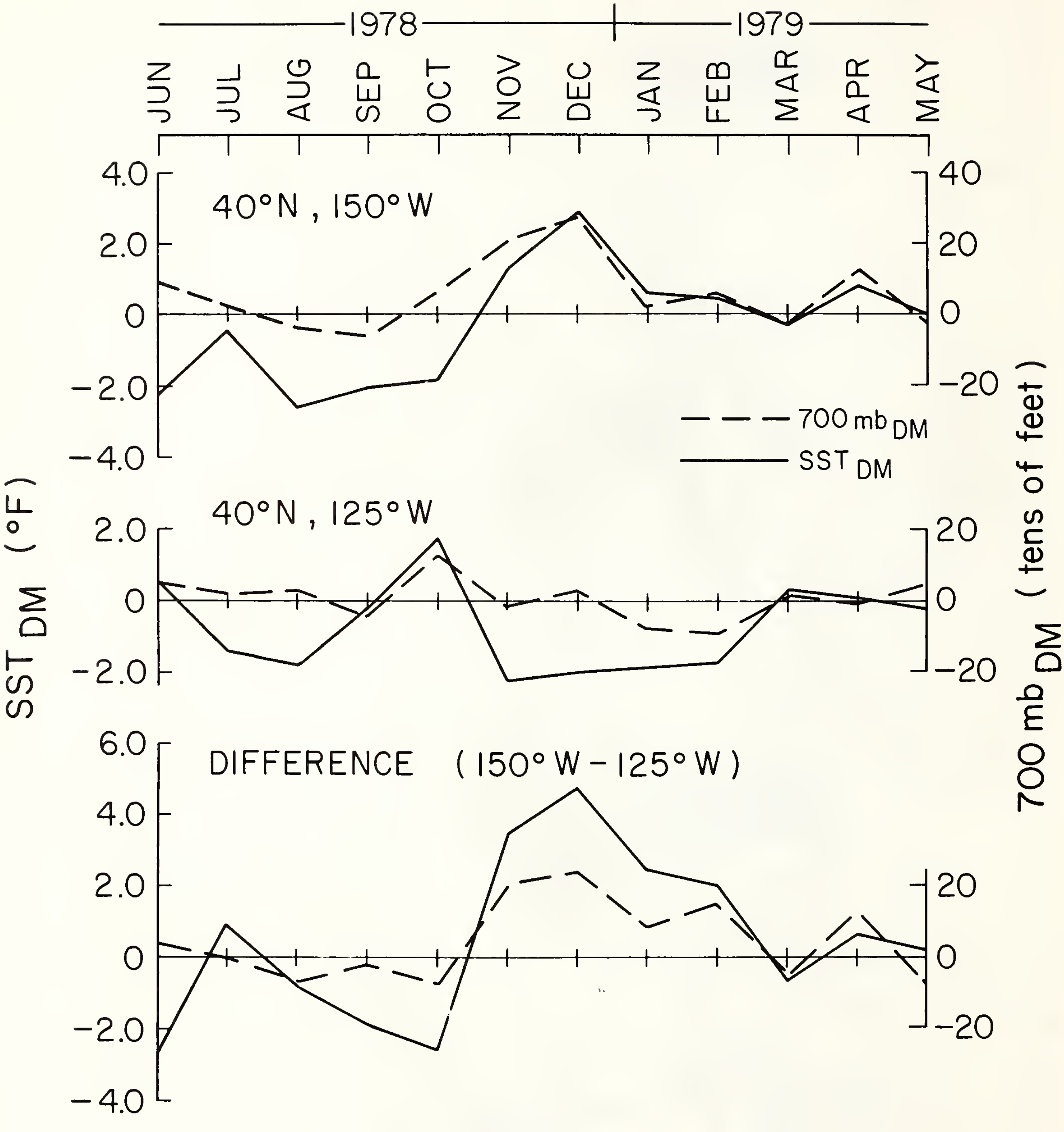
1978
1979
JUN
JUL
AUG
SEP
OCT
NOV
DEC
JAN
FEB
MAR
APR
MAY
40°N, 150°W
4.0
2.0
0
−2.0
−4.0
40
20
0
−20
700 mb$_{DM}$
SST$_{DM}$
40°N, 125°W
2.0
0
−2.0
20
0
−20
DIFFERENCE (150°W − 125°W)
6.0
4.0
2.0
0
−2.0
−4.0
20
0
−20
SST$_{DM}$ (°F)
700 mb$_{DM}$ (tens of feet)

FIGURE 10

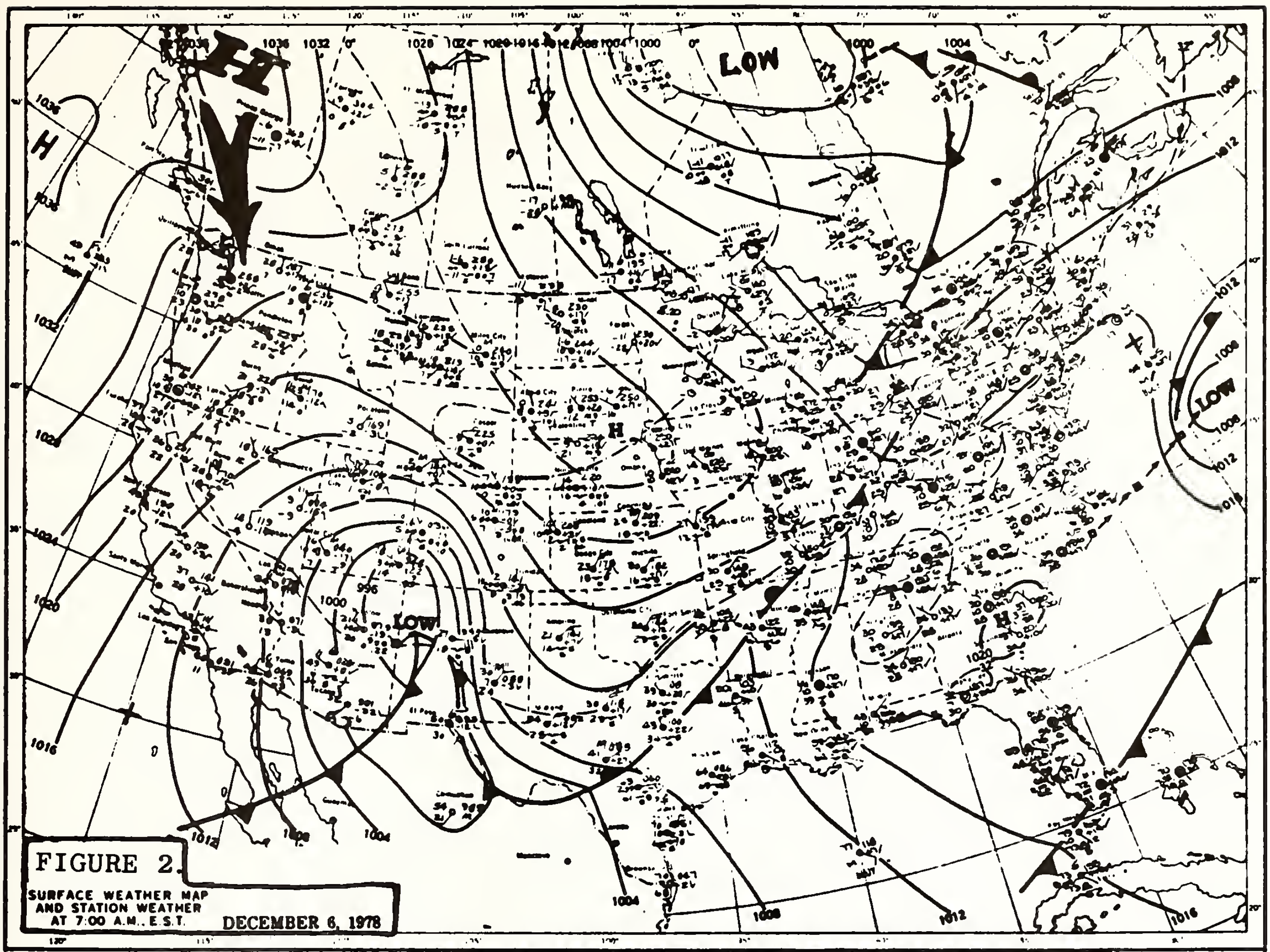

FIGURE 2.

SURFACE WEATHER MAP AND STATION WEATHER AT 7:00 A.M., E.S.T. DECEMBER 6, 1978

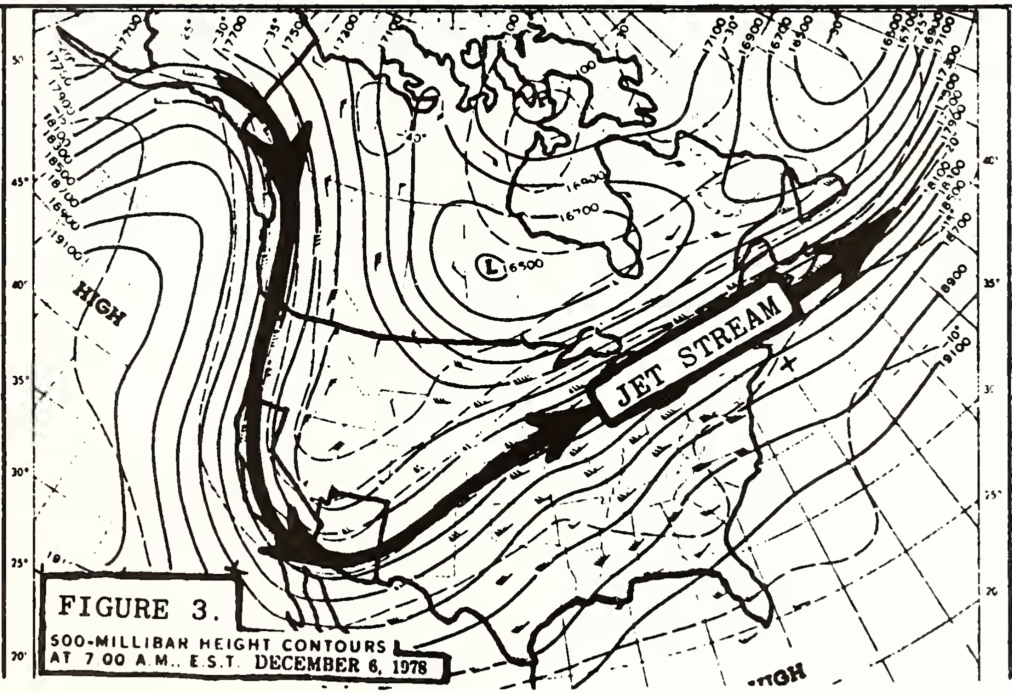

FIGURE 3.

500-MILLIBAR HEIGHT CONTOURS AT 7:00 A.M., E.S.T. DECEMBER 6, 1978

FIGURE 11

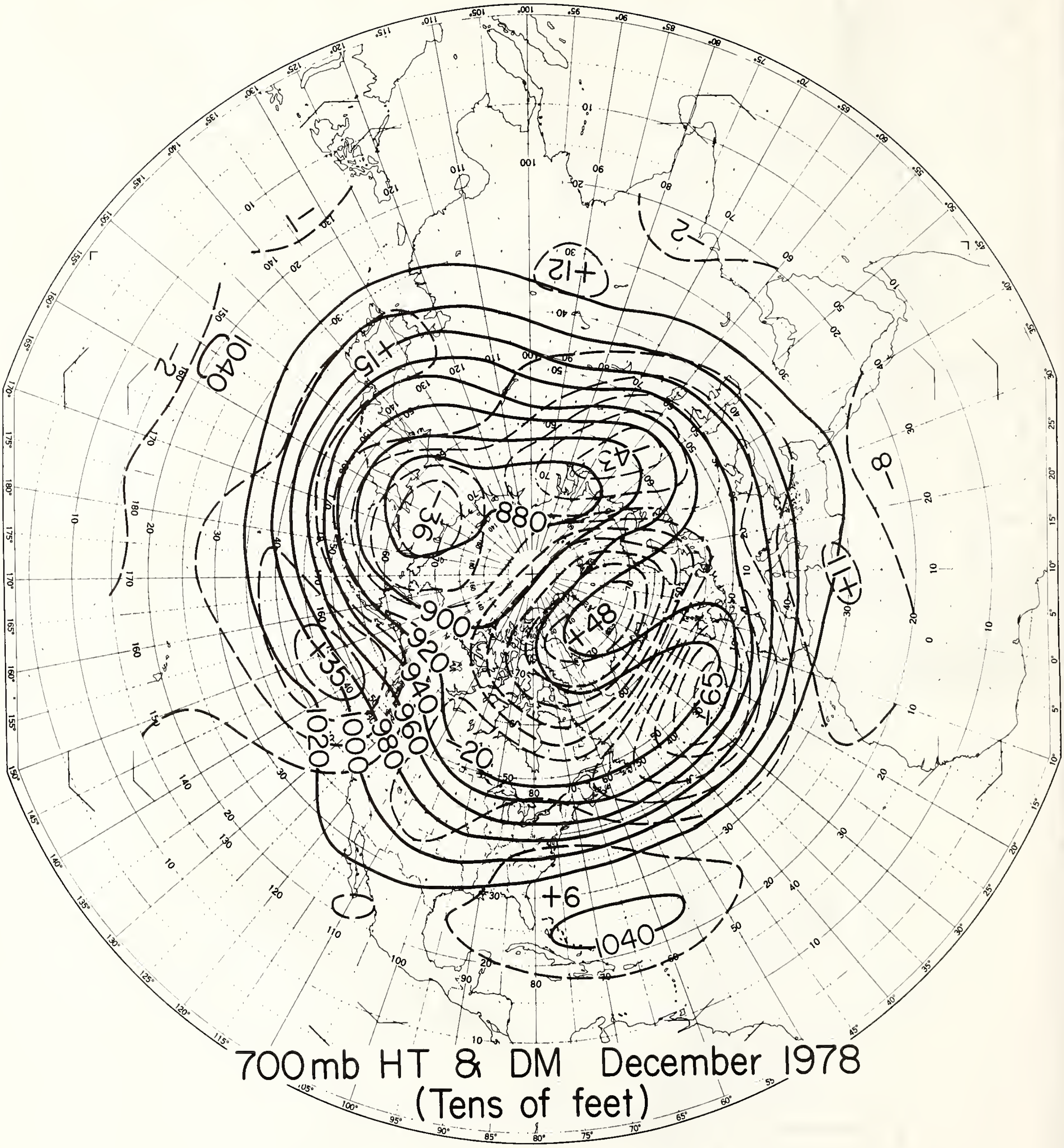

700 mb HT & DM December 1978
(Tens of feet)

FIGURE 12

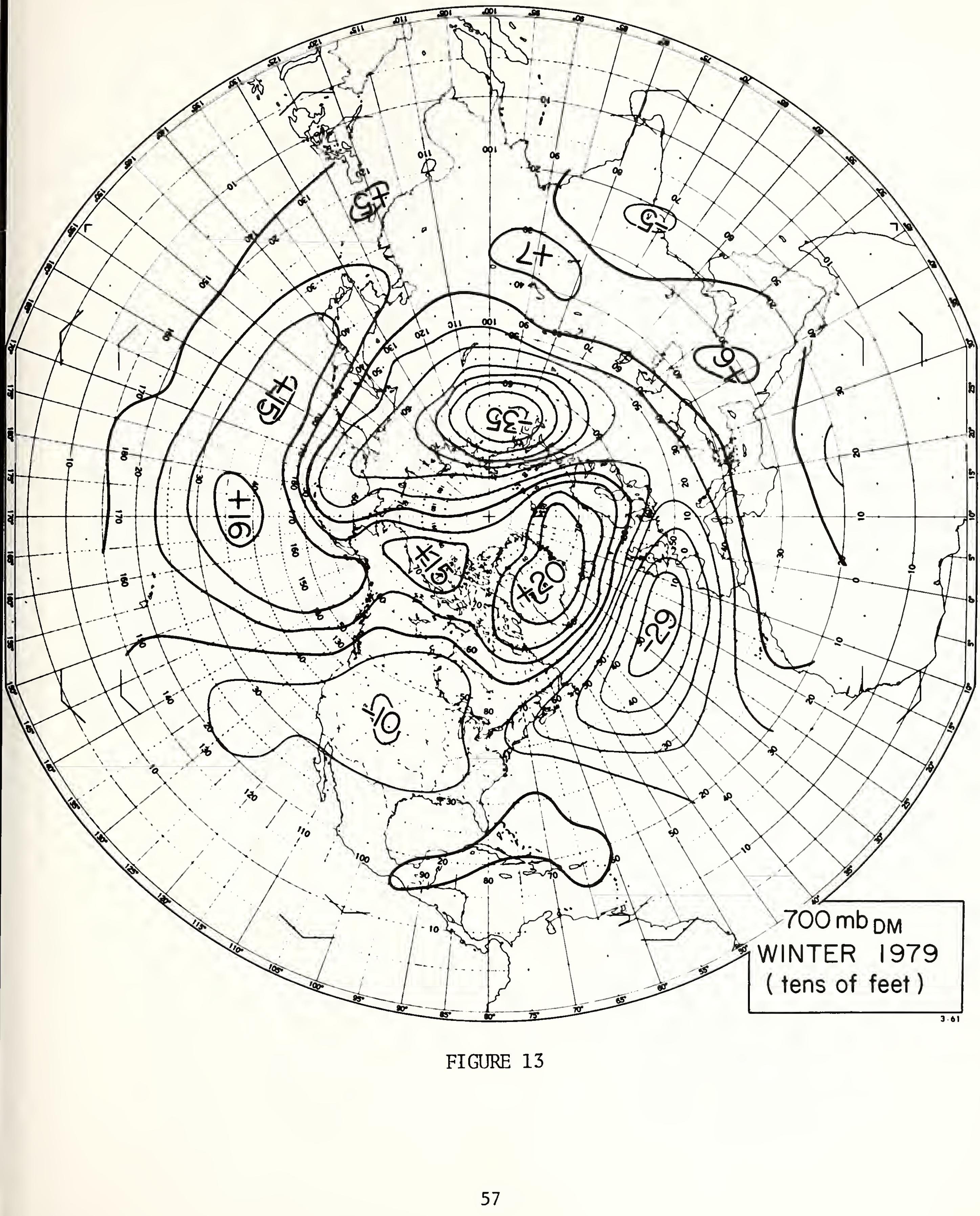

FIGURE 13

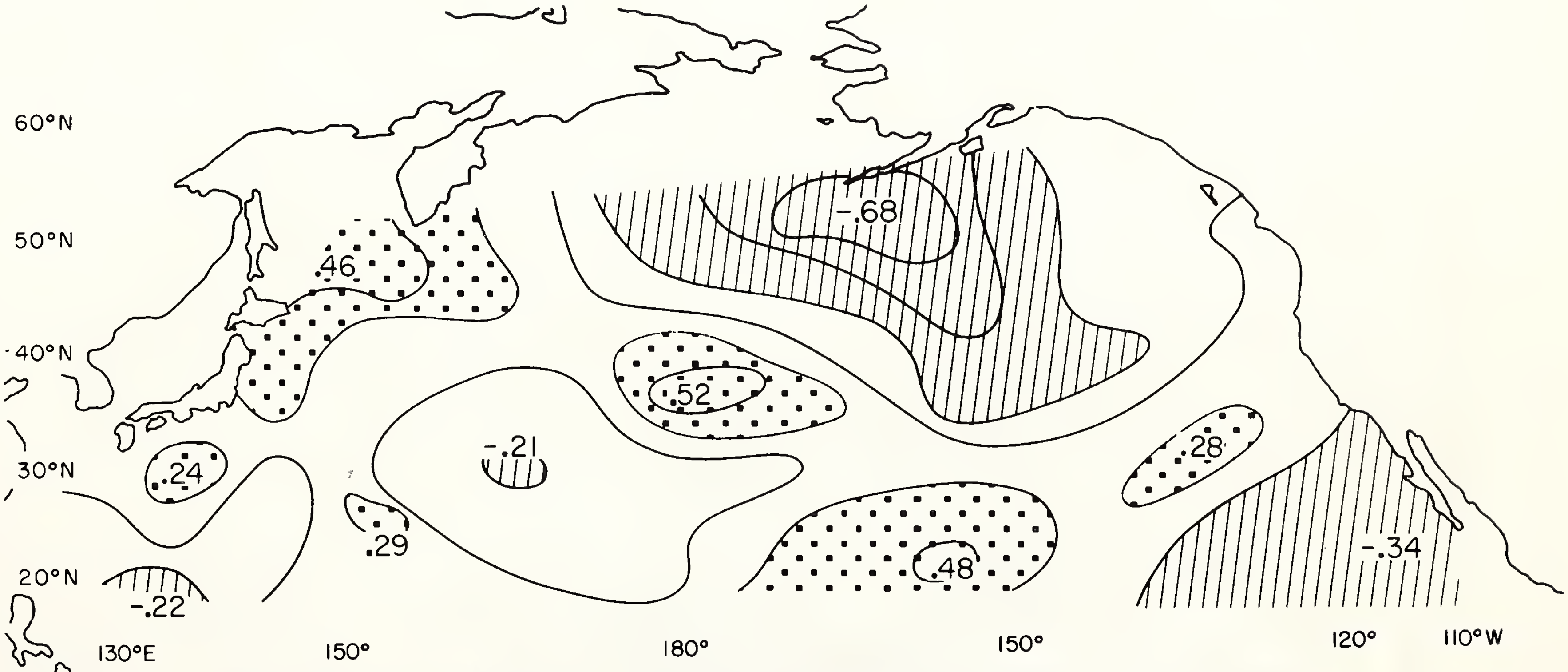

$SST_{DM}$ SUMMER VS $700_{DM}$ AUTUMN 1948-1974

FIGURE 14

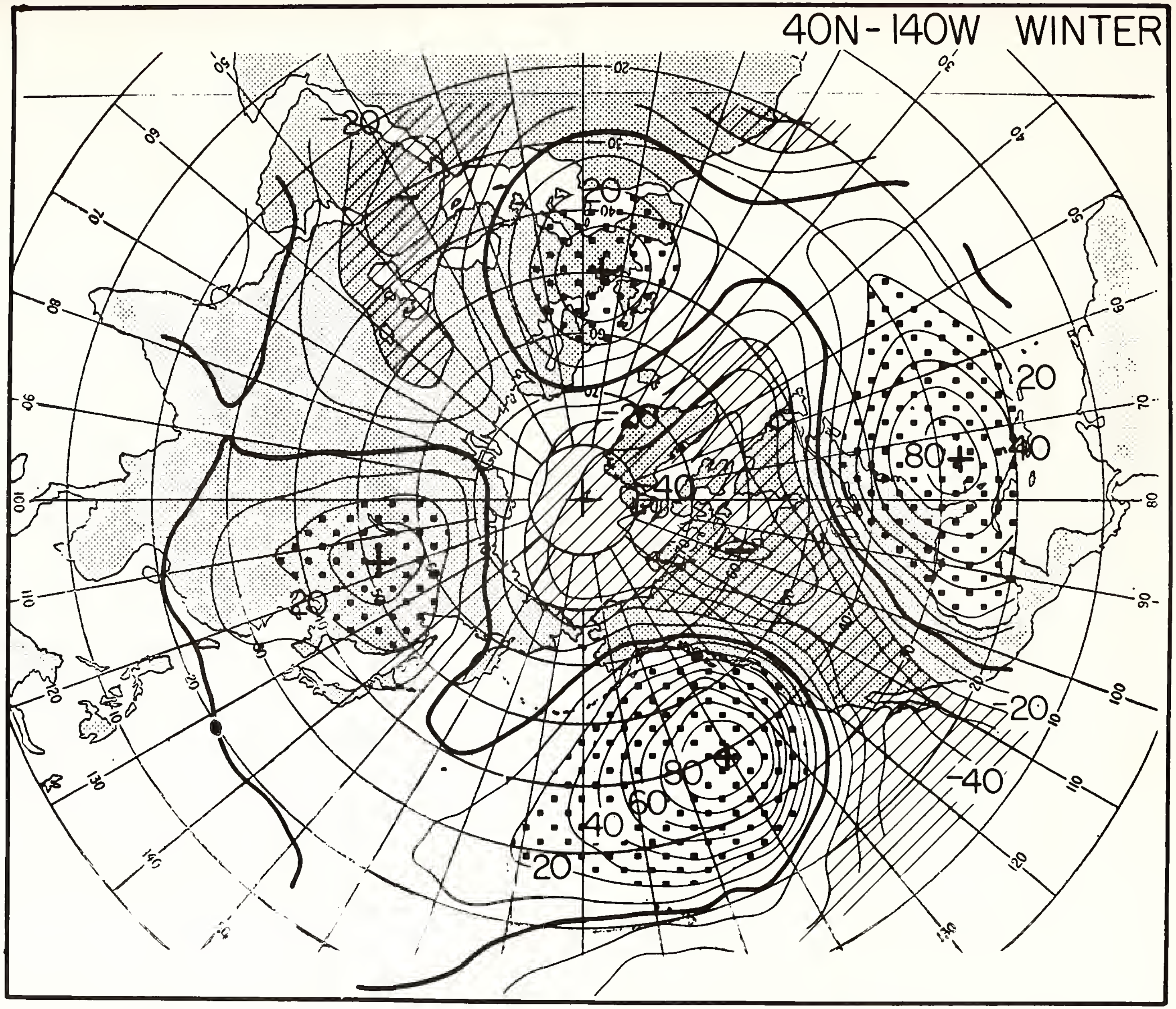

TELECONNECTIONS OF 700 DM

FIGURE 15

# SNOW AND SEA ICE IN 1978-1979

G.J. Kukla and J. Gavin

Lamont-Doherty Geological Observatory
of Columbia University
Palisades, New York 10964

Snow and sea ice indices were updated from information contained in NOAA and Navy charts. The surface albedo index was obtained using fixed parametrized values for snow in each reflectivity class and for sea ice in five separate concentration classes. Details in Kukla and Robinson (in press). The albedo of water was taken as 10% and snow-free land as 17%.

The following general observations pertain to the season beginning September 1978 and ending August 1979.

1) Snow in the Northern Hemisphere continued to be extensive, although less so than the previous year (cf. Fig. 4).
2) Sea-ice cover in the Southern Hemisphere continued to be light, although less so than the previous two years.
3) The year-to-year departures in land surface albedo north of 30°N and south of 50°S were partly out of phase in the two hemispheres (cf. Fig. 5).
4) The 1978/1979 season was marked by record-breaking positive and negative snow and ice anomalies associated with pronounced meridional flow. For the first time in living memory snow covered the ground

in Ghardaia and in several other localities in the Sahara (February 19, 1979). Also, for the first time since available satellite observations began, large polynyas with broken ice occurred in the close vicinity of the North Pole, permitting a record northward penetration of a Coast Guard cutter in the area (cf. Fig. 2).

5) In April 1979 in eastern Europe (ERE) the highest extent of snow during the 1974-1979 interval was observed (Fig. 6). Possible links of this anomaly with the preceding positive snow anomaly in western Europe (EUR), and with the failure of the 1979 monsoon is being investigated.

6) Anomalous sea ice distribution in the North Atlantic during March and April 1979 (cf. Fig. 2) resembled that of 1969. On both occasions a positive snow anomaly and cold spring occurred in Europe (Haupt and Kant, 1976)

Additional observations are documented in Figures 1-10. Method by which the indices were obtained is described in Kukla and Gavin (1979).

References

Kukla, G. and Gavin, J. (1979) Snow and Pack Ice Indices. Glaciological Data, Report GD-6, 9-14.

Kukla, G. and Robinson, D. (in press) Annual Cycle of Surface Albedo. Monthly Weather Review.

Haupt, I. and V. Kant (1976) Satellite ice surveillance studies in the Arctic in relationship to the general circulation. In: Proc. on Met. Obs. from Space: their Contribution to the First GARP Global Experiment. NCAR, Boulder, Colo. 110-113.

# SNOW AND SEA ICE IN 1978-1979

G.J. Kukla and J. Gavin

Lamont-Doherty Geological Observatory
of Columbia University
Palisades, New York 10964

Snow and sea ice indices were updated from information contained in NOAA and Navy charts. The surface albedo index was obtained using fixed parametrized values for snow in each reflectivity class and for sea ice in five separate concentration classes. Details in Kukla and Robinson (in press). The albedo of water was taken as 10% and snow-free land as 17%.

The following general observations pertain to the season beginning September 1978 and ending August 1979.

1) Snow in the Northern Hemisphere continued to be extensive, although less so than the previous year (cf. Fig. 4).
2) Sea-ice cover in the Southern Hemisphere continued to be light, although less so than the previous two years.
3) The year-to-year departures in land surface albedo north of 30°N and south of 50°S were partly out of phase in the two hemispheres (cf. Fig. 5).
4) The 1978/1979 season was marked by record-breaking positive and negative snow and ice anomalies associated with pronounced meridional flow. For the first time in living memory snow covered the ground

in Ghardaia and in several other localities in the Sahara (February 19, 1979). Also, for the first time since available satellite observations began, large polynyas with broken ice occurred in the close vicinity of the North Pole, permitting a record northward penetration of a Coast Guard cutter in the area (cf. Fig. 2).

5) In April 1979 in eastern Europe (ERE) the highest extent of snow during the 1974-1979 interval was observed (Fig. 6). Possible links of this anomaly with the preceding positive snow anomaly in western Europe (EUR), and with the failure of the 1979 monsoon is being investigated.
6) Anomalous sea ice distribution in the North Atlantic during March and April 1979 (cf. Fig. 2) resembled that of 1969. On both occasions a positive snow anomaly and cold spring occurred in Europe (Haupt and Kant, 1976)

Additional observations are documented in Figures 1-10. Method by which the indices were obtained is described in Kukla and Gavin (1979).

## References

Kukla, G. and Gavin, J. (1979) Snow and Pack Ice Indices. Glaciological Data, Report GD-6, 9-14.

Kukla, G. and Robinson, D. (in press) Annual Cycle of Surface Albedo. Monthly Weather Review.

Haupt, I. and V. Kant (1976) Satellite ice surveillance studies in the Arctic in relationship to the general circulation. In: Proc. on Met. Obs. from Space: their Contribution to the First GARP Global Experiment. NCAR, Boulder, Colo. 110-113.

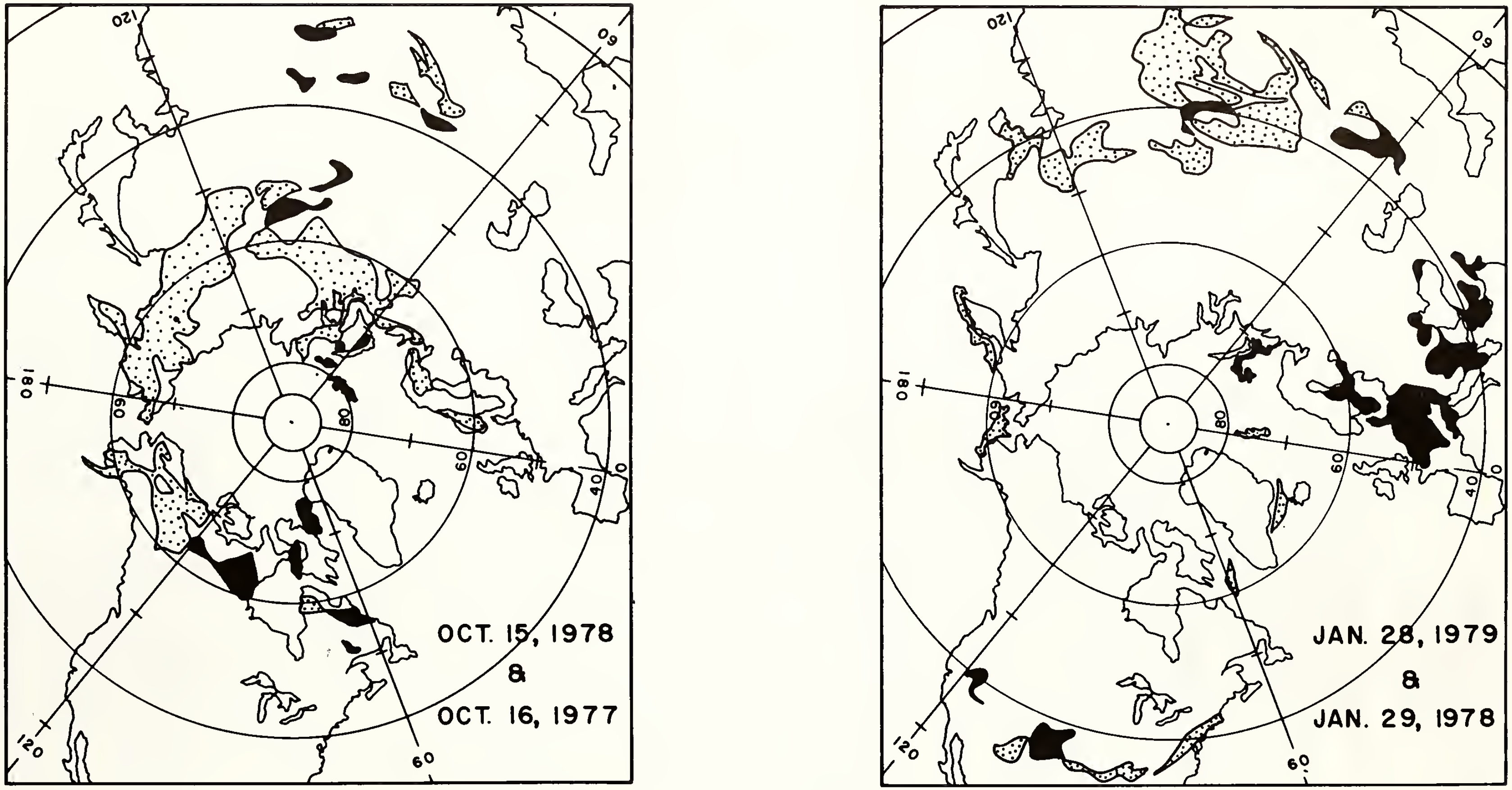

Fig. 1. Extent of snow (reflectivity classes 1-3) and sea-ice (concentration>1 octa) on October 15, 1978 and January 28, 1979 compared to previous year. Excess cover in black, missing cover dotted. Note less snow in fall of 1978 over much of the hemisphere, except Canada, but a negligible difference in sea ice extent. In the winter of 1979 snow was extensive in Europe and Asia Minor but reduced in central and eastern Asia. Ice cover was greater in the Barents Sea and less around Kamchatka and in the Bering Sea. Compensating positive and negative anomalies are shown in North America. Dates refer to the end of the charted week.

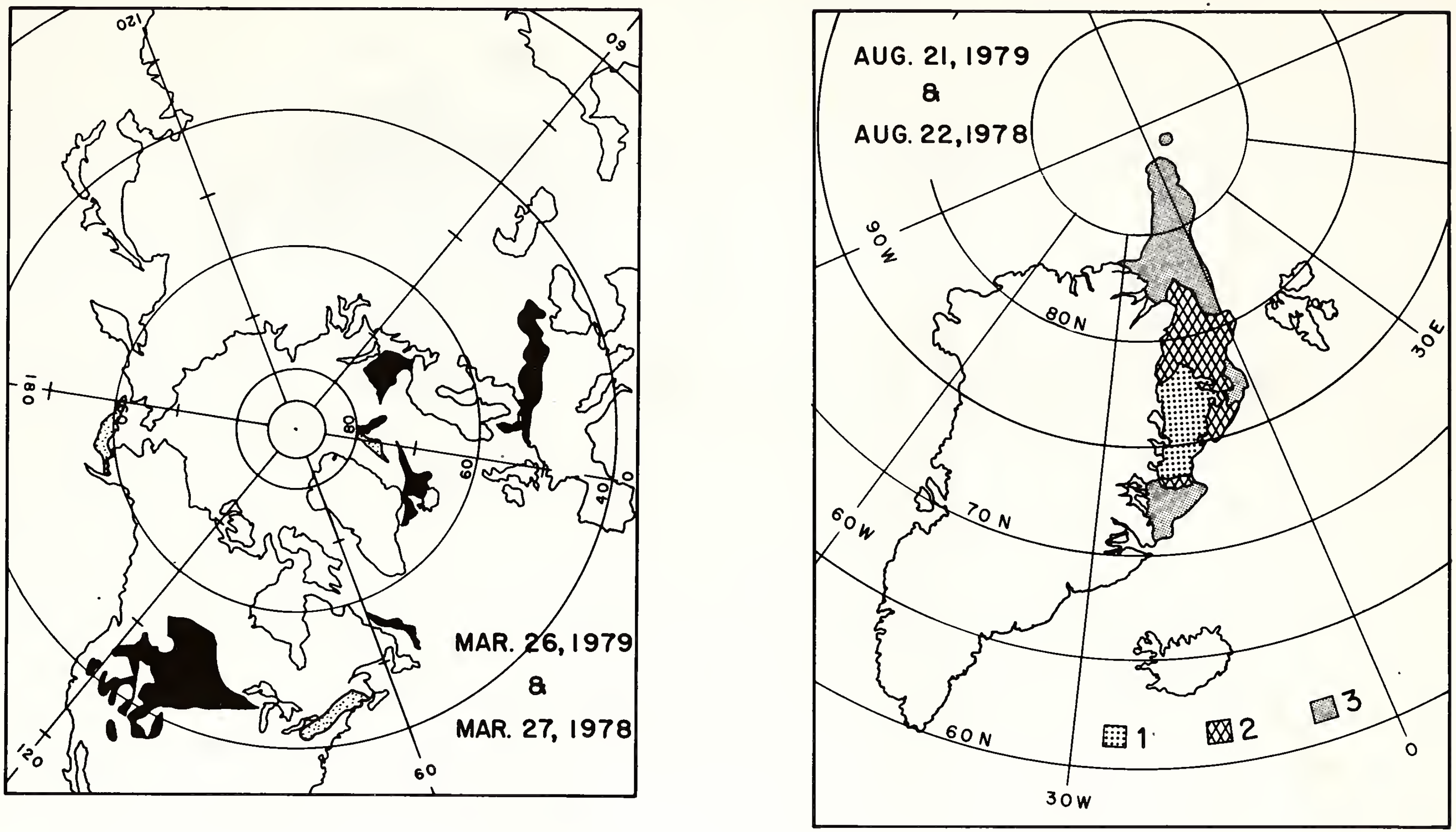

Fig. 2. The extent of snow and sea ice on March 26, 1979 compared with the previous year. Note excess snow in Europe and western North America, and the near record sea ice expansion in the Barents Sea and off Iceland. Similar conditions occurred in 1969. Ice in the Bering Sea continued to be less. Comparison of sea ice concentration in East Greenland Sea on August 21, 1979 with the previous year is also shown. (1) Concentration heavier by at least two octas; (2) approximately same; (3) lighter by at least two octas. Note exceptionally light concentration reaching approximately 100 km of the North Pole.

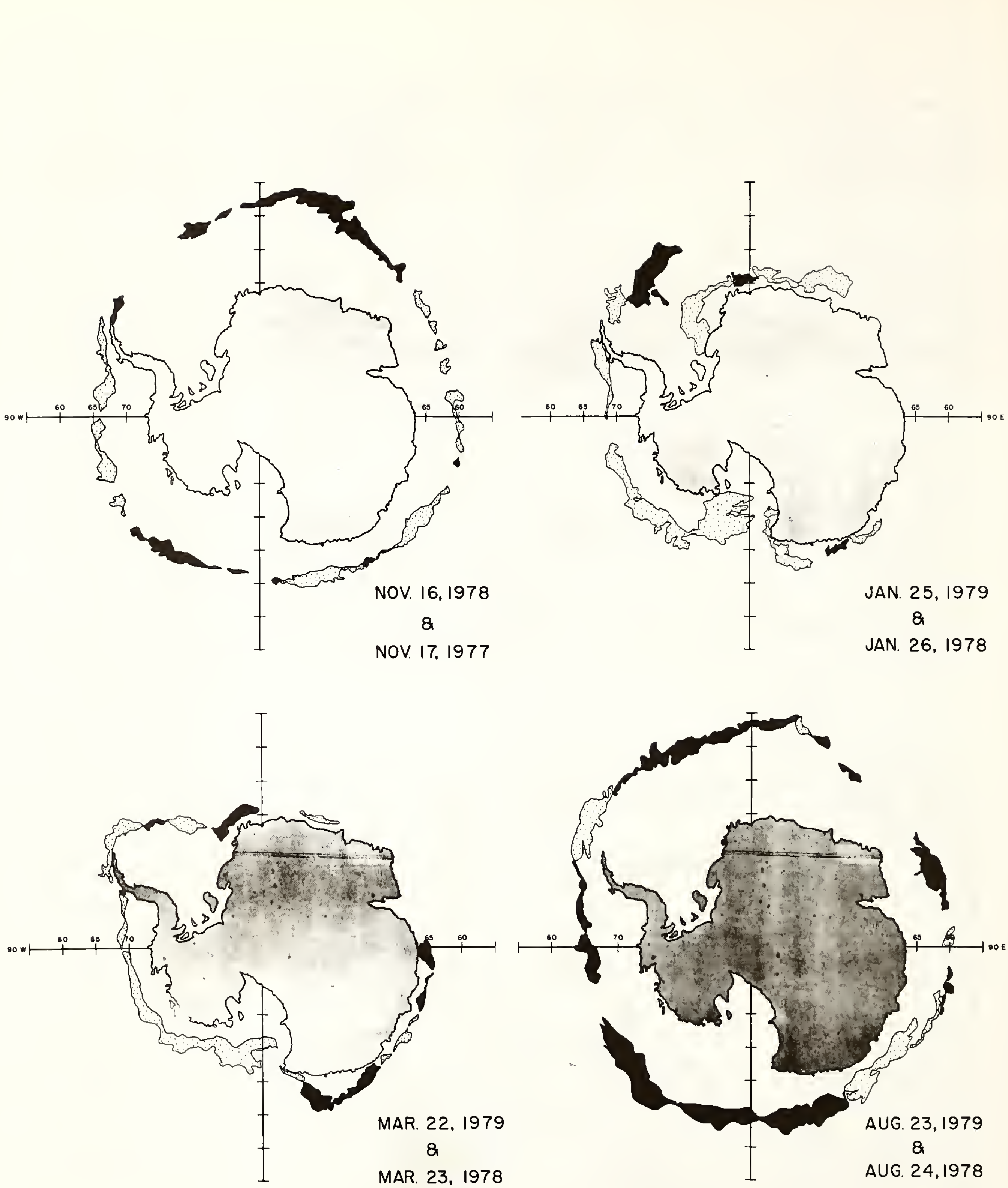

NOV. 16, 1978
&
NOV. 17, 1977

JAN. 25, 1979
&
JAN. 26, 1978

MAR. 22, 1979
&
MAR. 23, 1978

AUG. 23, 1979
&
AUG. 24, 1978

Fig. 3. Sea ice around Antarctica at four characteristic intervals of the 1978/79 season compared with the previous year. Excess ice shown in black, missing cover dotted. Spring (November) was characterized by compensating positive and negative anomalies along the N-S and E-W axis. Exceptionally less ice was present during the summer of 1979. Autumn (March) conditions show less ice in the area of the Ross Sea and around the peninsula with slightly greater amounts present around the eastern sector. Considerably more ice during the winter of 1979 is noted.

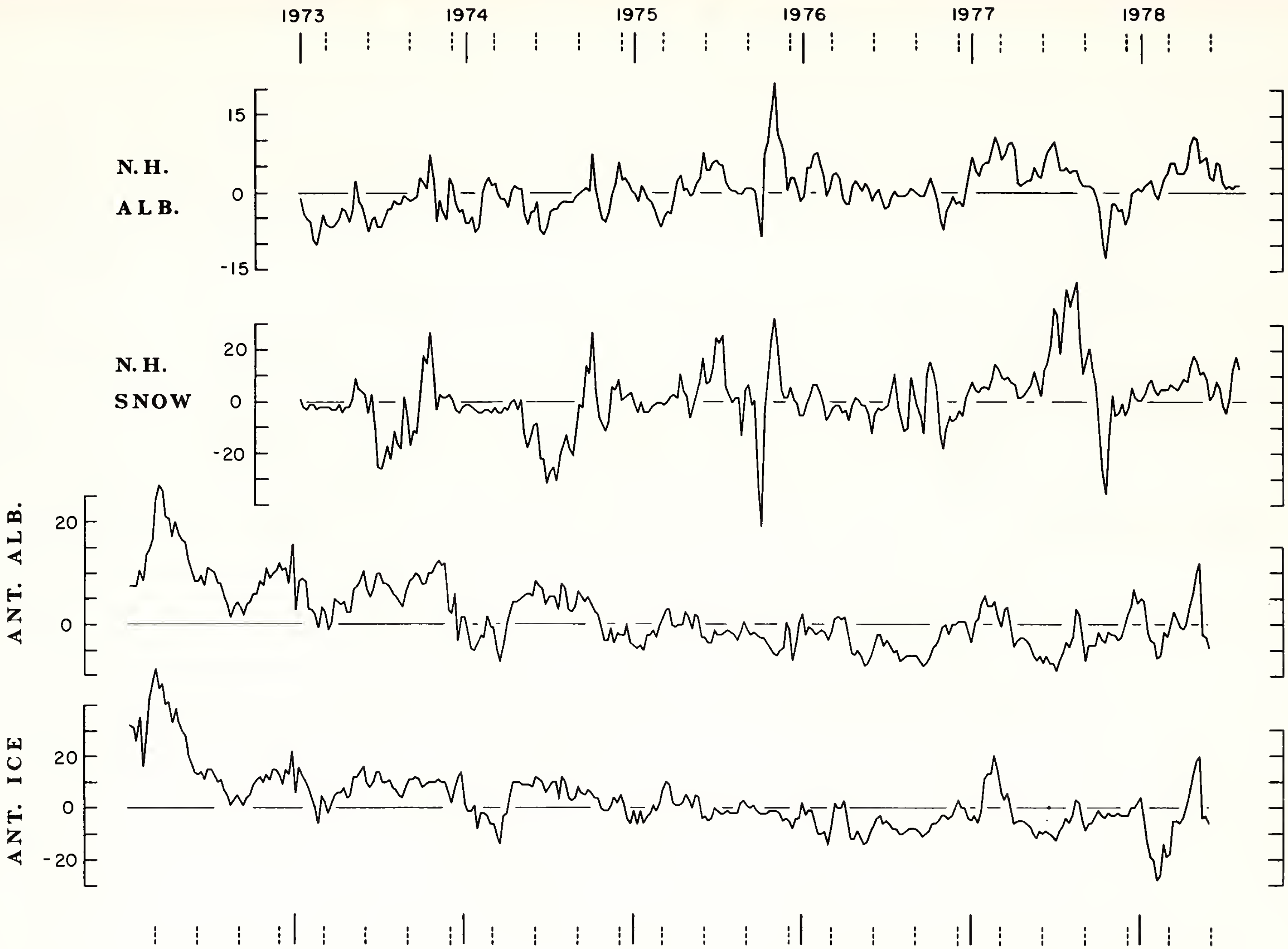

Fig. 4. Weekly departures as percent difference from the 1974-1978 weekly means for Northern Hemisphere snow extent and land surface albedo (N.H. ALB) poleward of 30°N (Arctic ice not included). Similar departures shown for Antarctic pack-ice extent and ocean surface albedo poleward of 50°S (continent not included). End of each year is marked. Note gradual increase of snow covers and albedo in the Northern Hemisphere and decrease in the Southern Hemisphere.

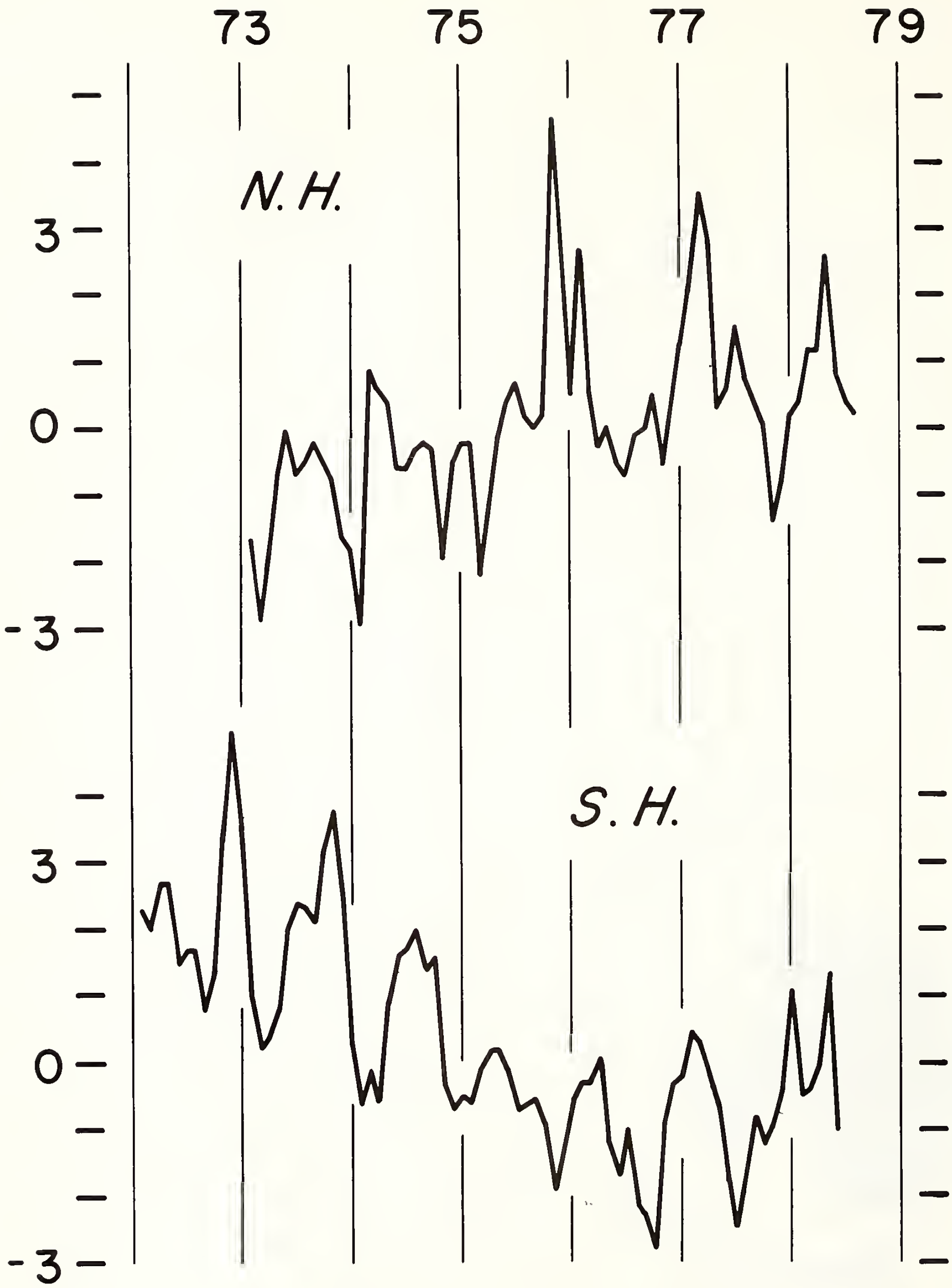

Fig. 5. Area weighted monthly mean surface albedo of Northern Hemisphere (NH) land (north of 30°N) and Southern Hemisphere (SH) ocean (south of 50°S) expressed as departures from the 1974-1978 monthly means. Units in percent albedo. Year ending in December is marked. Note opposite trends in the two hemispheres. NH record ends in July, SH in May.

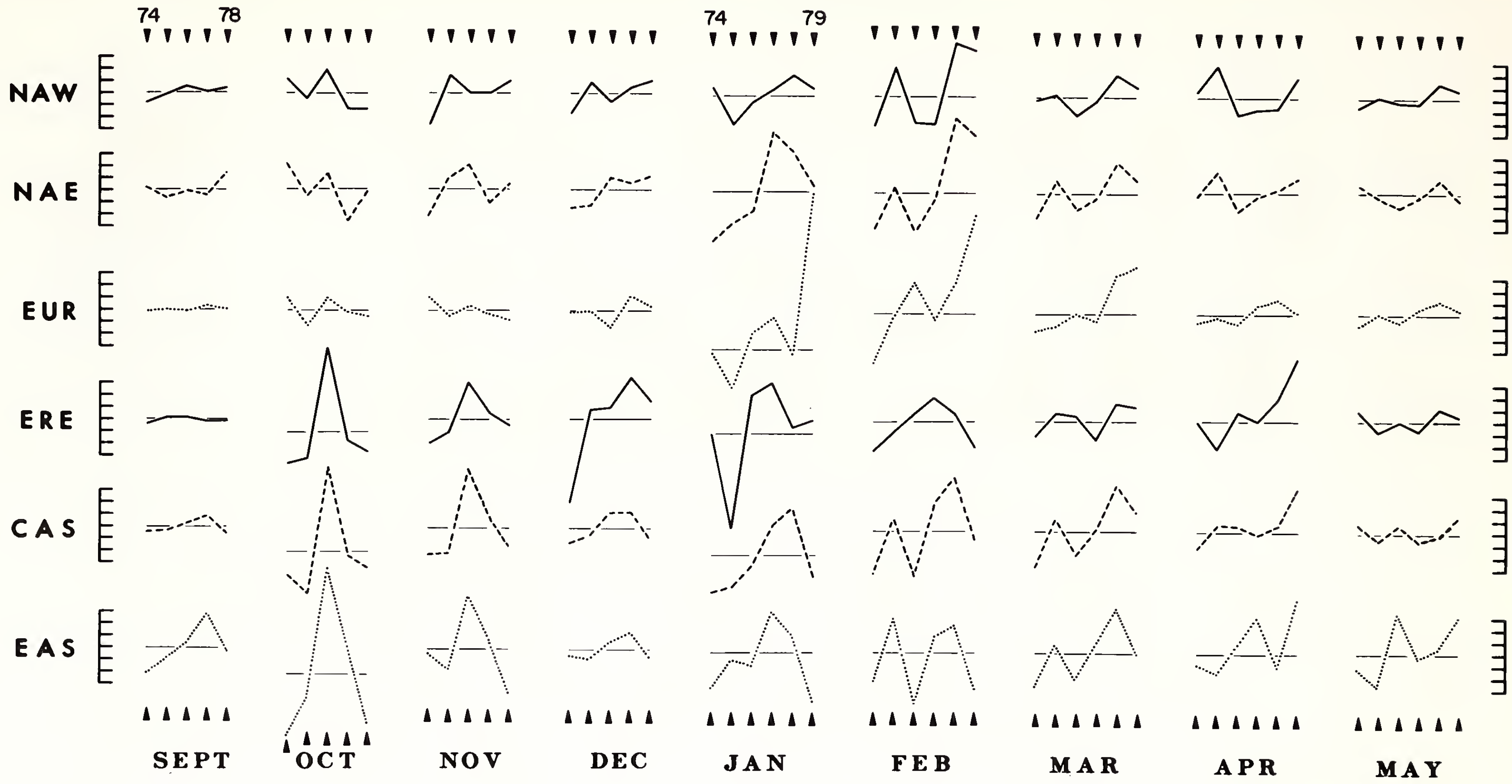

Fig. 6. Average monthly surface albedo of land segments north of 30°N expressed as departure from the 1974-1978 monthly means. Units in increments of 1% albedo. NAW: North America 170-100W; NAE: North America and Greenland east of 100W; EUR: Europe to 30E; ERE: 30-60E; CAS: 60-120E; EAS: 120-170W. Note 1979 record highs in Europe from January through March; in ERE, CAS and EAS in April; near record high in NAW and NAE in February and the record and near record low in EAS in October, November, January and February.

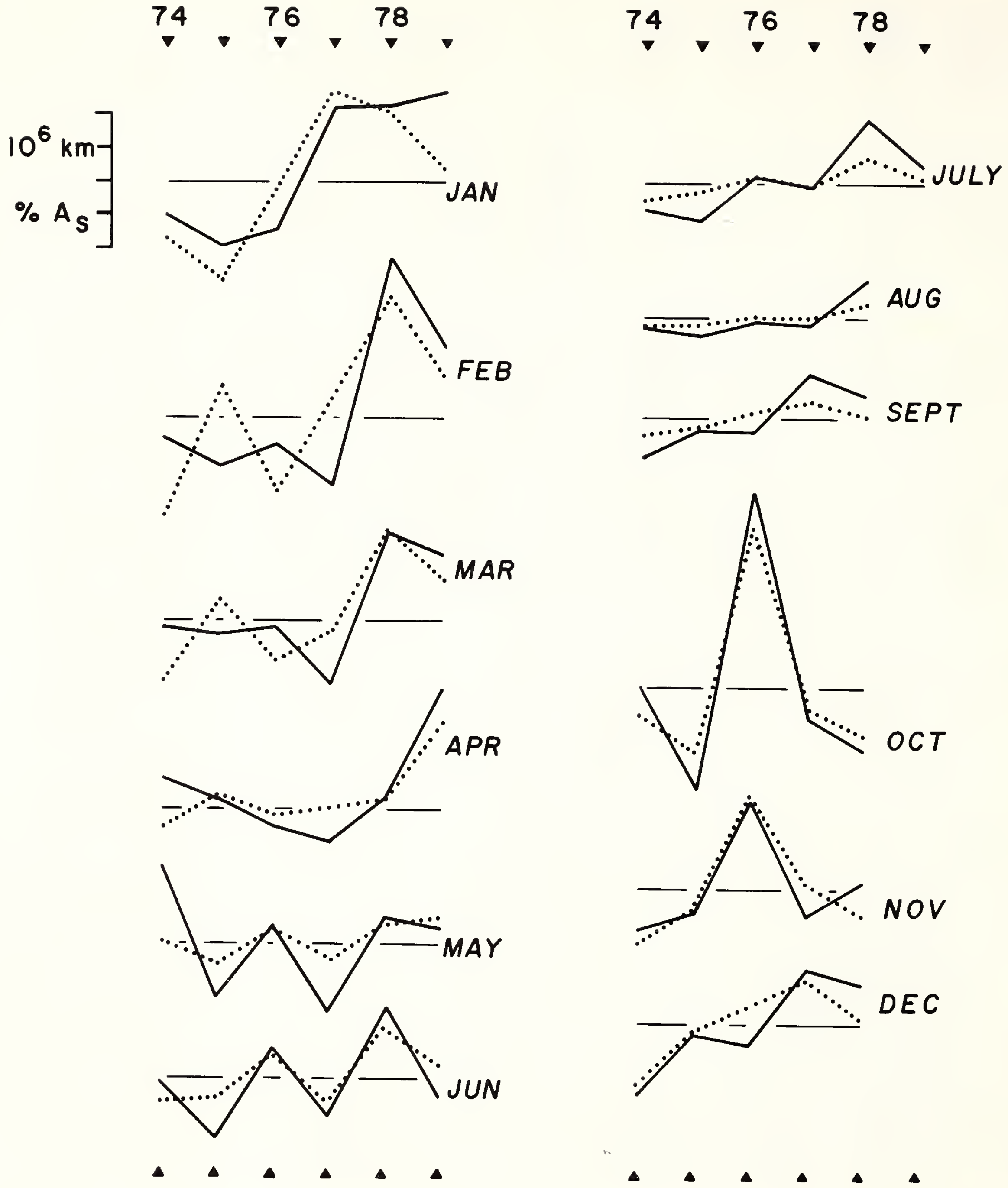

Fig. 7. Average monthly total snow extent (full line) and surface albedo of land (dotted line) poleward of 30°N from 1974 through 1979. Plotted as a departure from 1974-1978 monthly means. Units in increments of 1% albedo and 1 million square kilometers of snow. Note record 1979 albedo in January and April.

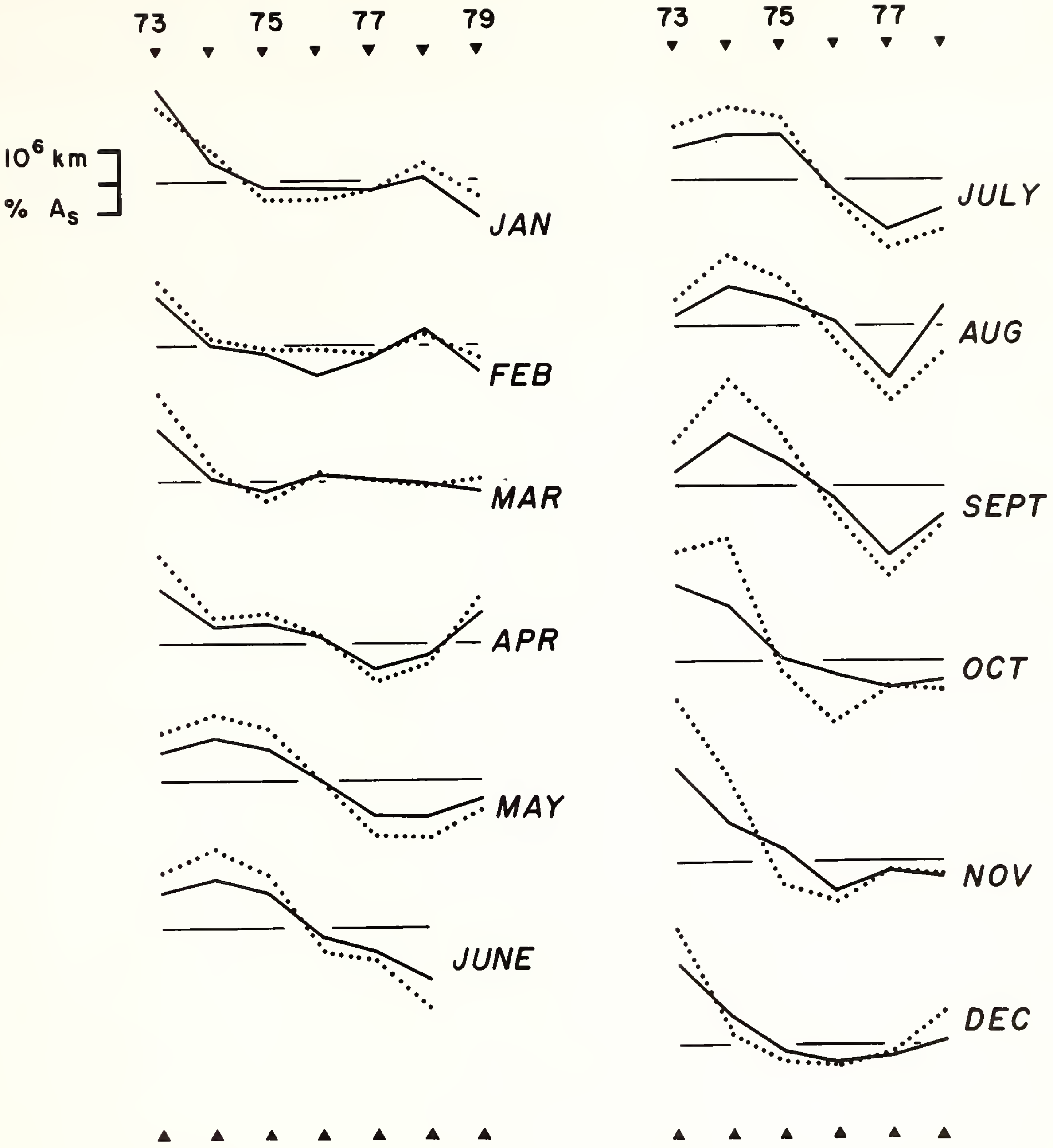

Fig. 8. Average monthly sea ice extent (full line) and ocean surface albedo (dotted line) poleward of 50°S from 1973 through 1979. Plotted as a departure from 1974-1978 monthly mean. Units same as in Fig. 7. Note record or near record lows in January and February 1979.

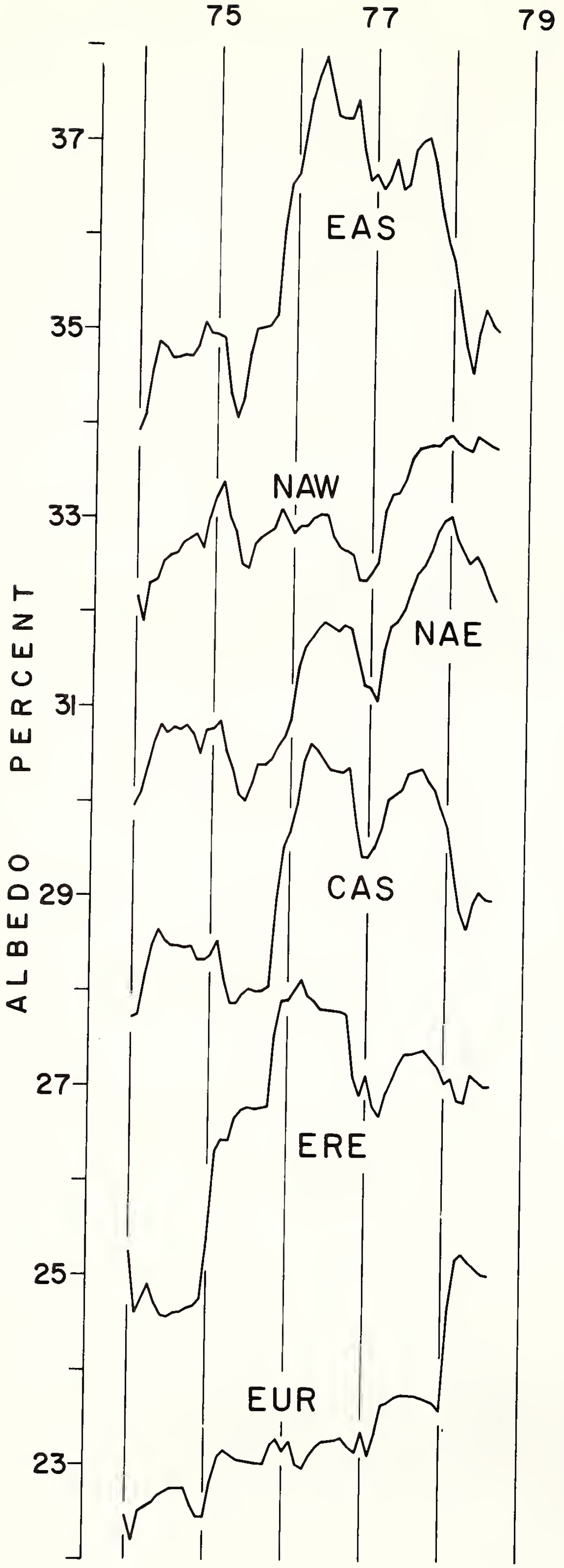

Fig. 9. Twelve month running means of land surface albedo north of 30°N. Meridional segments same as in Fig. 6. Indicated years represent period ending in December. Note record and near record 1979 high in Europe and western North America and the general increase over 1974 levels in all segments. Plotted at the ending date.

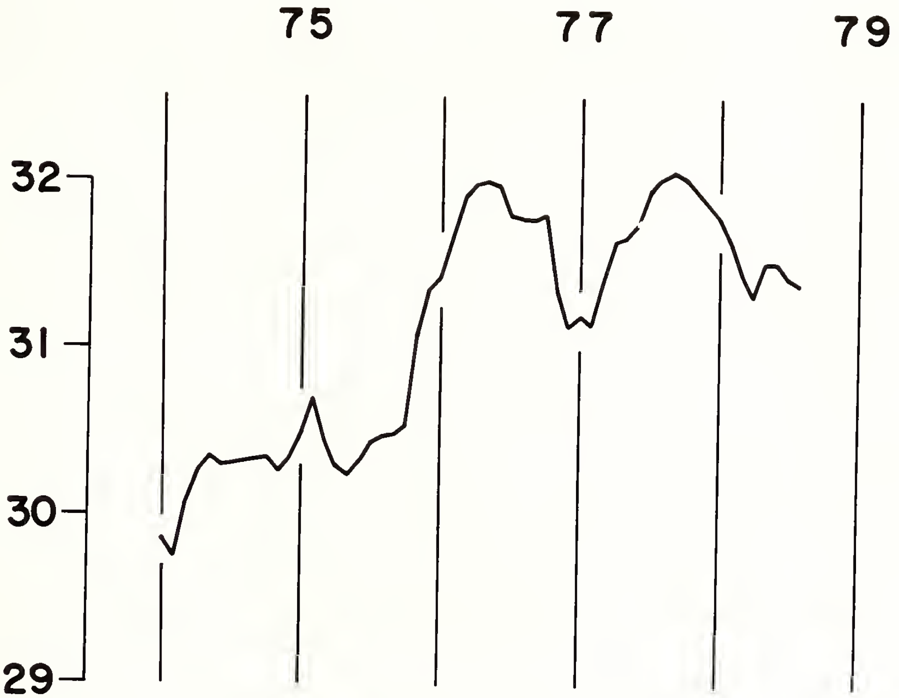

Fig. 10. Twelve month running means of land albedo for the Northern Hemisphere north of 30°N. Units in percent albedo, end of the year marked. Plotted on the ending date.

# Recent Variations of SST Along the East and West Coasts of the U.S.

Douglas R. McLain

NOAA, NMFS - PEG, Monterey, CA

Fluctuations of sea surface temperature (SST) in coastal areas are of importance for monitoring the environment of coastal fish populations. A major factor causing fluctuations of SST is the wind and its variations in time and space. If winds are from the north in the northern hemisphere, SST's are often below normal and if winds are southerly, SST's often are above normal. Thus if a ridge of upper air circulation forms, southerly winds under its western limb will cause positive SST anomalies and northerly winds under its eastern limb will cause negative SST anomalies. This has happened over North America in recent winters. In the winter of 1976-77 a strong ridge of upper air circulation formed over the west coast with a trough over the eastern U.S. (Fig 1). I use the single month, February, to represent the average winter circulation because the pattern was relatively persistent all winter. Also February is often the month of maximum SST anomalies. The ridge brought warm, maritime air towards the coast of Alaska and the Pacific Northwest causing mild air temperatures and abundant precipitation. The storms were diverted north of California and drought resulted there. Strong winds occurred over the central North Pacific.

The west coast ridge was associated with a large region of negative SST anomaly (Fig 2)in the central North Pacific and positive anomalies along the west coast. Downstream along the eastern seaboard, cold outbreaks of arctic air lowered SST's to below normal values over the coastal region from the western Gulf of Mexico to the central North Atlantic. SST's were as much as 3.4° C below normal in the Gulf of Mexico and near Cape Hatteras.

The west coast ridge occurred again in the winter of 1977-78 (Fig 3) as it had the previous winter. This winter, however, the ridge allowed storms to come in over California, bringing abundant precipitation, and breaking the California drought. Note again the strong winds over the central North Pacific.

The distribution of SST in February 1978 (Fig 4) was similar to that of the previous winter with the large pool of below normal SST water in mid Pacific, positive anomalies along the west coast, and negative anomalies along the east coast from the Gulf of Mexico to the central North Atlantic. Largest anomalies were up to -4.7° C, again centered in the northern Gulf of Mexico and off Cape Hatteras.

During the winter of 1978-79 the ridge occurred again but was shifted several thousand miles off the west coast. By February 1979 (Fig 6) it had formed into an "omega" type blocking ridge over the Bering Sea but still strong winds persisted over the eastern United States.

This pattern created a different pattern of anomaly of SST's — negative anomalies occurred along the both east and west coasts (Fig 6). Large negative anomalies again occurred in the northern Gulf of Mexico and off Cape Hatteras and also off Nova Scotia where SST's were up to 4.5° C below normal.

To look at these fluctuations in a time series sense, I have plotted time series of anomaly of SST from the long term mean for a series of 5 degree squares along the coast lines of North America (Fig 7). Along the Aleutian Chain (Marsden 5 degree squares 198-1 and 197-1, Fig 8) SST's in the late 1960's were near or above normal, much below normal in the early 1970's, above normal in 1977, and more nearly normal since then. The cold conditions in the early 1970's had been associated with northerly winds on the eastern limb of a large ridge then centered over the Central North Pacific. The recent warm conditions were associated with southerly winds on the western limb of a ridge centered to the east, over the west coast. As a result of the cold weather in the early 1970's, stocks of salmon in Alaska were severly depressed but with the recent mild conditions, catches have recovered remarkably.

Conditions in the Gulf of Alaska and off the Pacific Northwest have followed somewhat similar trends. Off California (Squares 121-3 and 120-2) similar anomalies of SST occurred with above normal temperatures in the late 1960's, below normal SST's in the early 1970's, and more normal temperatures in recent years. Recent mild conditions off California have been associated with catches of tropical species along the coast.

From California and south to Peru, (Fig 9) periods of above normal SST's are associated with the El Nino disturbances. Note the above normal SST's in 1957-9, 65, 69, 72, and 76. These periods were associated with similar periods of high sea levels and reduced upwelling of cold, nutrient rich water.

Time series of anomalies of SST from Nova Scotia to the Gulf of Mexico (Fig 10) follow quite different trends. Off New England (Square 151-1), SST's were below normal in the early 1940's, reached a peak in the early 1950's, and cooled to a second minimum in 1965-66. I don't have data for 1968-70 processed yet, but since 1970 SST'S have been generally below normal particularly in the inshore waters in the northern Gulf of Mexico and off the southeastern states (Squares 81-4 and 116-2). There have been numerous effects of the recent cold winters on marine populations in the area, including a disastrous decline of white shrimp stocks.

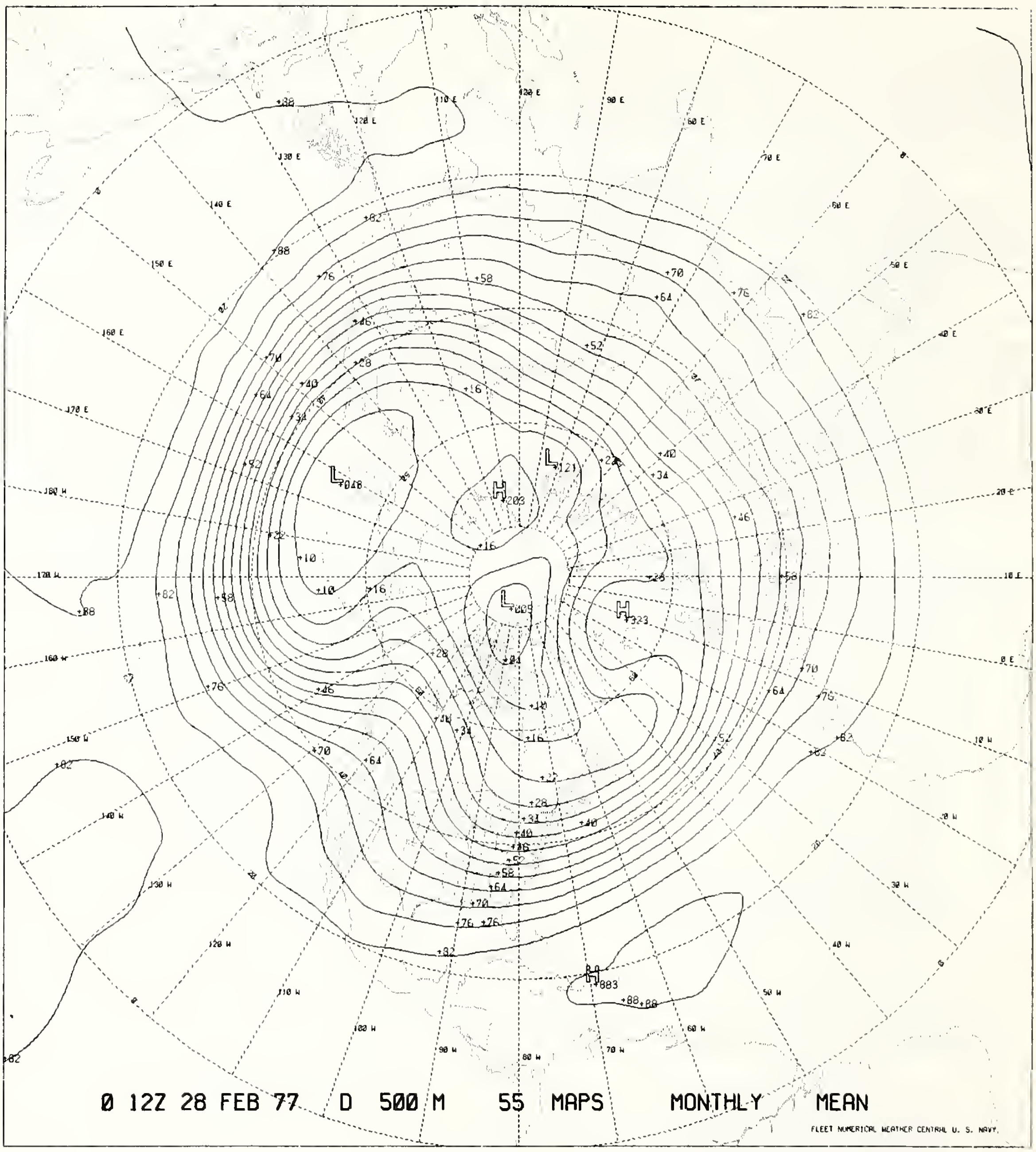

Figure 1. Monthly mean height of 500 mb surface in meters for February 1977. Data from Fleet Numerical Weather Central.

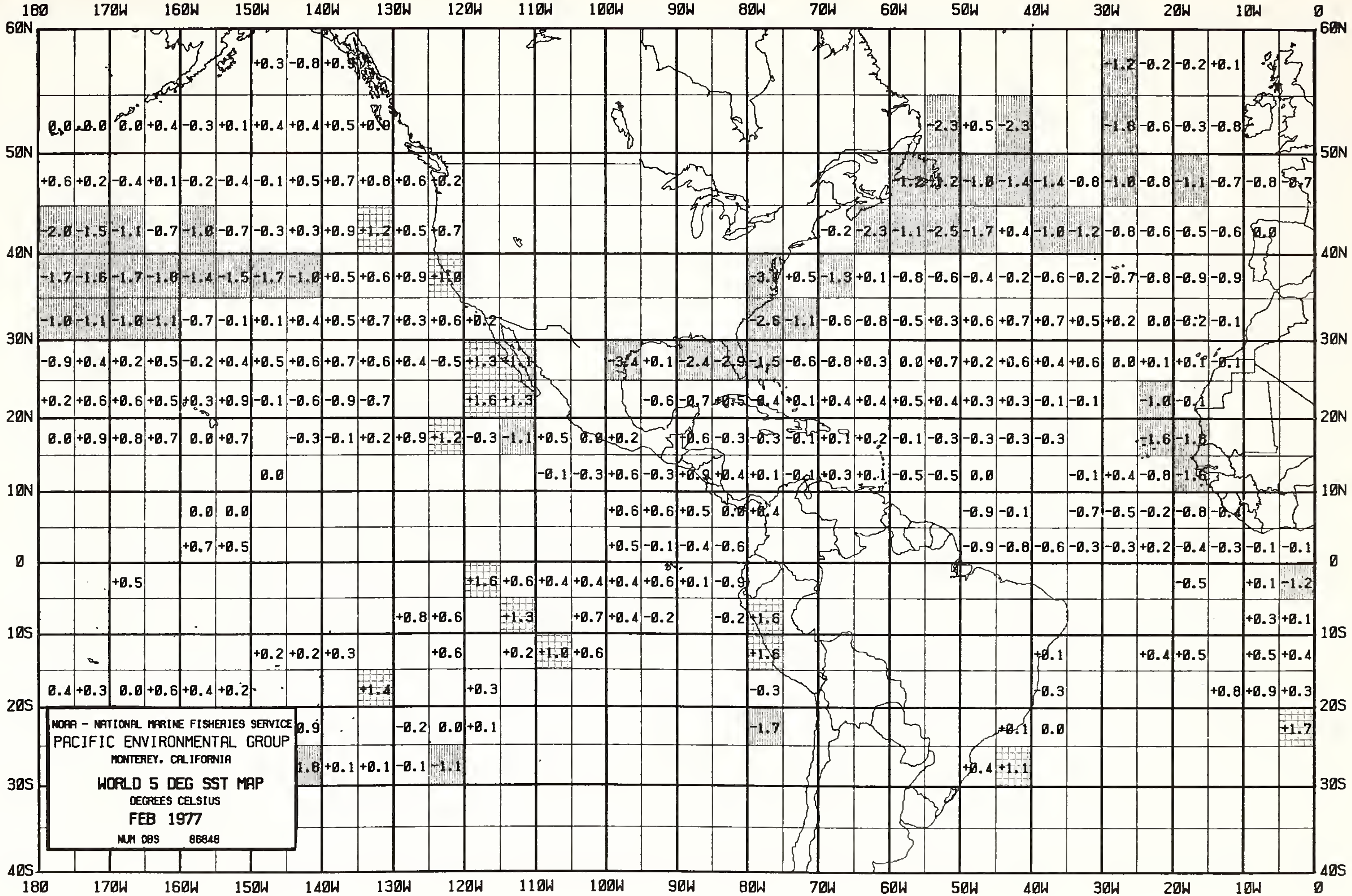

Figure 2. Monthly mean anomaly of sea surface temperature in °C by 5 degree squares for February 1977 relative to long term mean for reference period 1948-67.

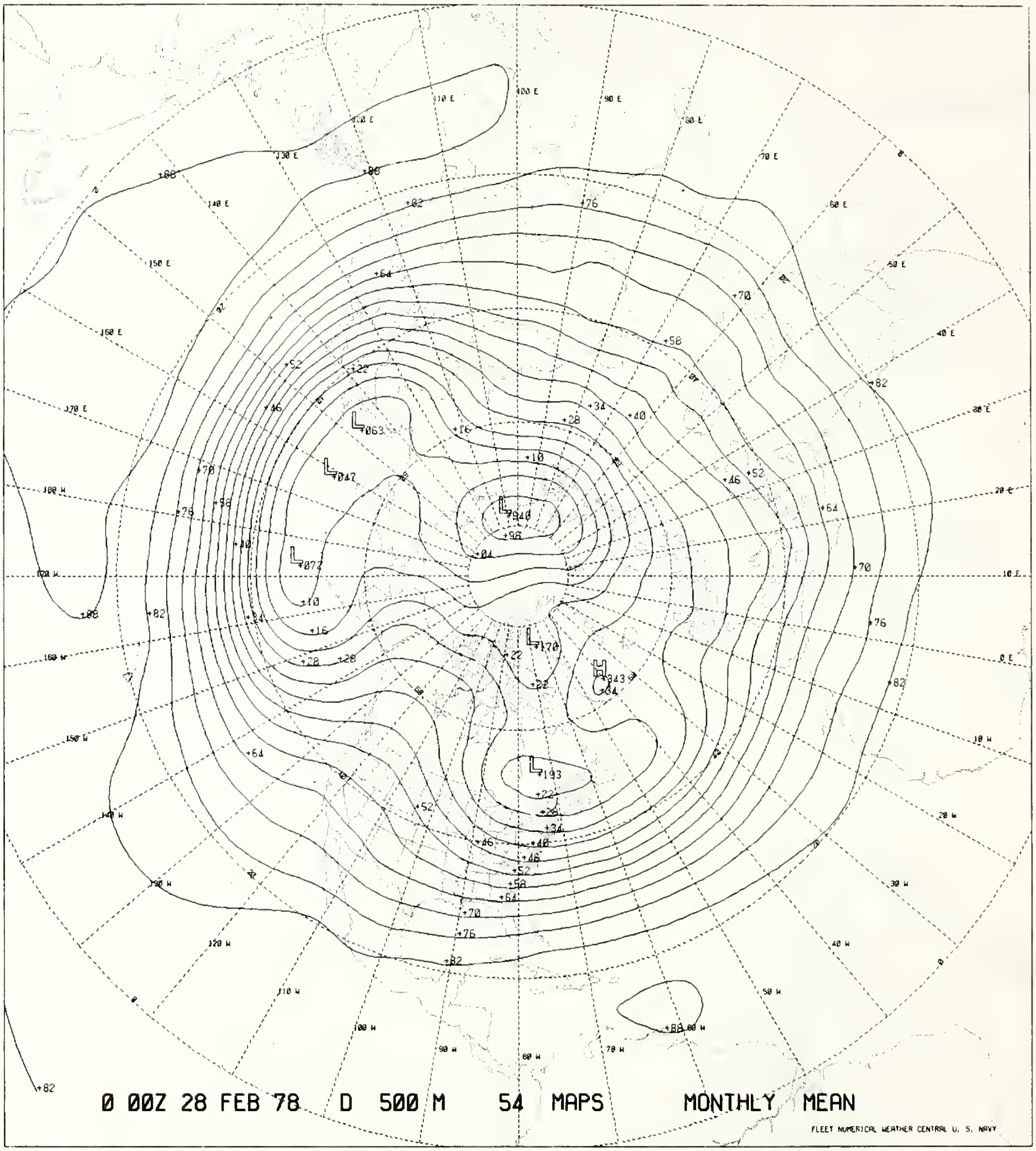

Figure 3. Monthly mean height of 500 mb surface in meters for February 1978. Data from Fleet Numerical Weather Central.

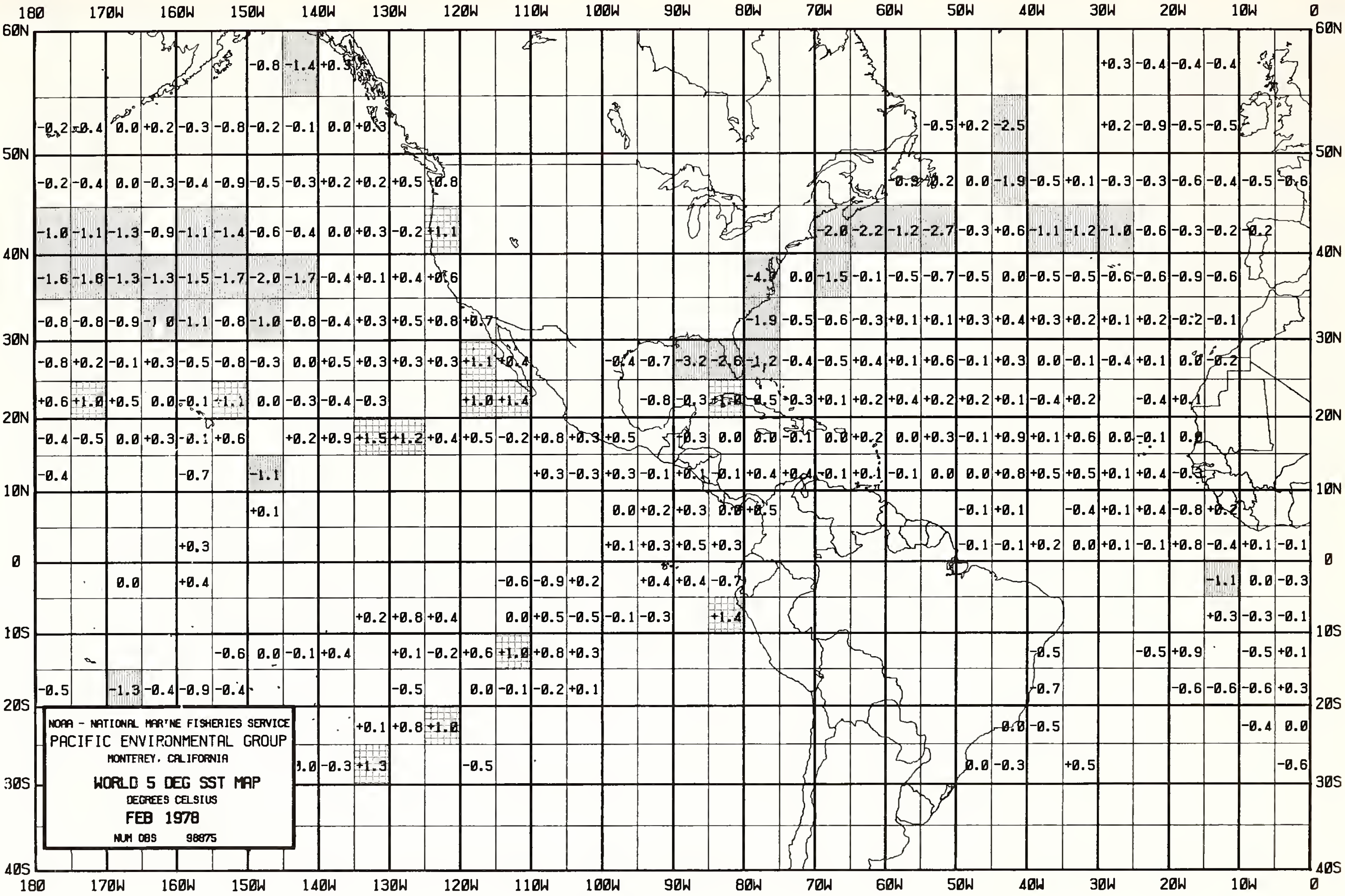

Figure 4. Monthly mean anomaly of sea surface temperature in °C by 5 degree squares for February 1978 relative to long term mean for reference period 1948-67.

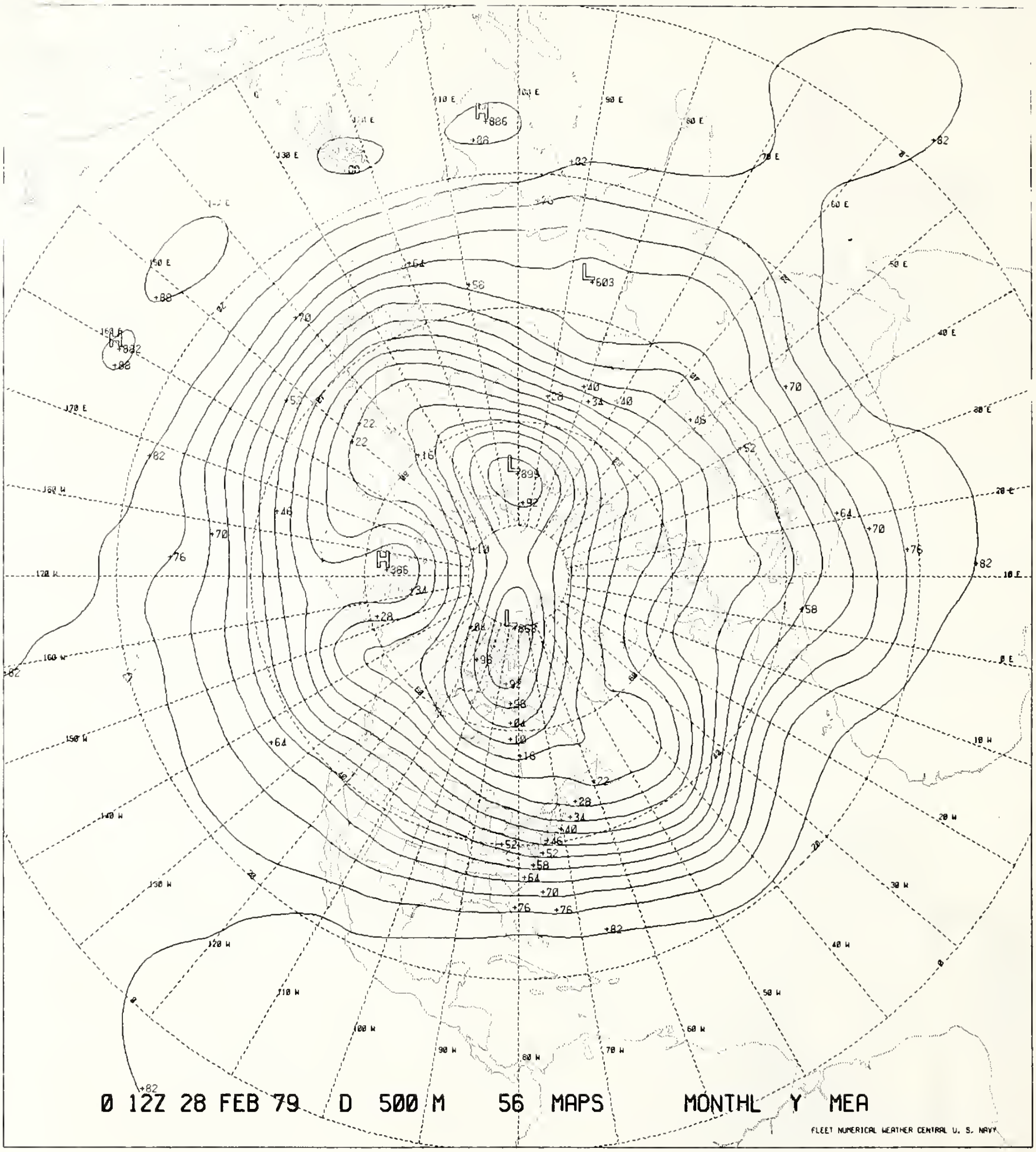
0 12Z 28 FEB 79 D 500 M 56 MAPS MONTHL Y MEA
FLEET NUMERICAL WEATHER CENTRAL U. S. NAVY
H
L
L
H
L
H

Figure 5. Monthly mean height of 500 mb surface in meters for February 1979. Data from Fleet Numerical Weather Central.

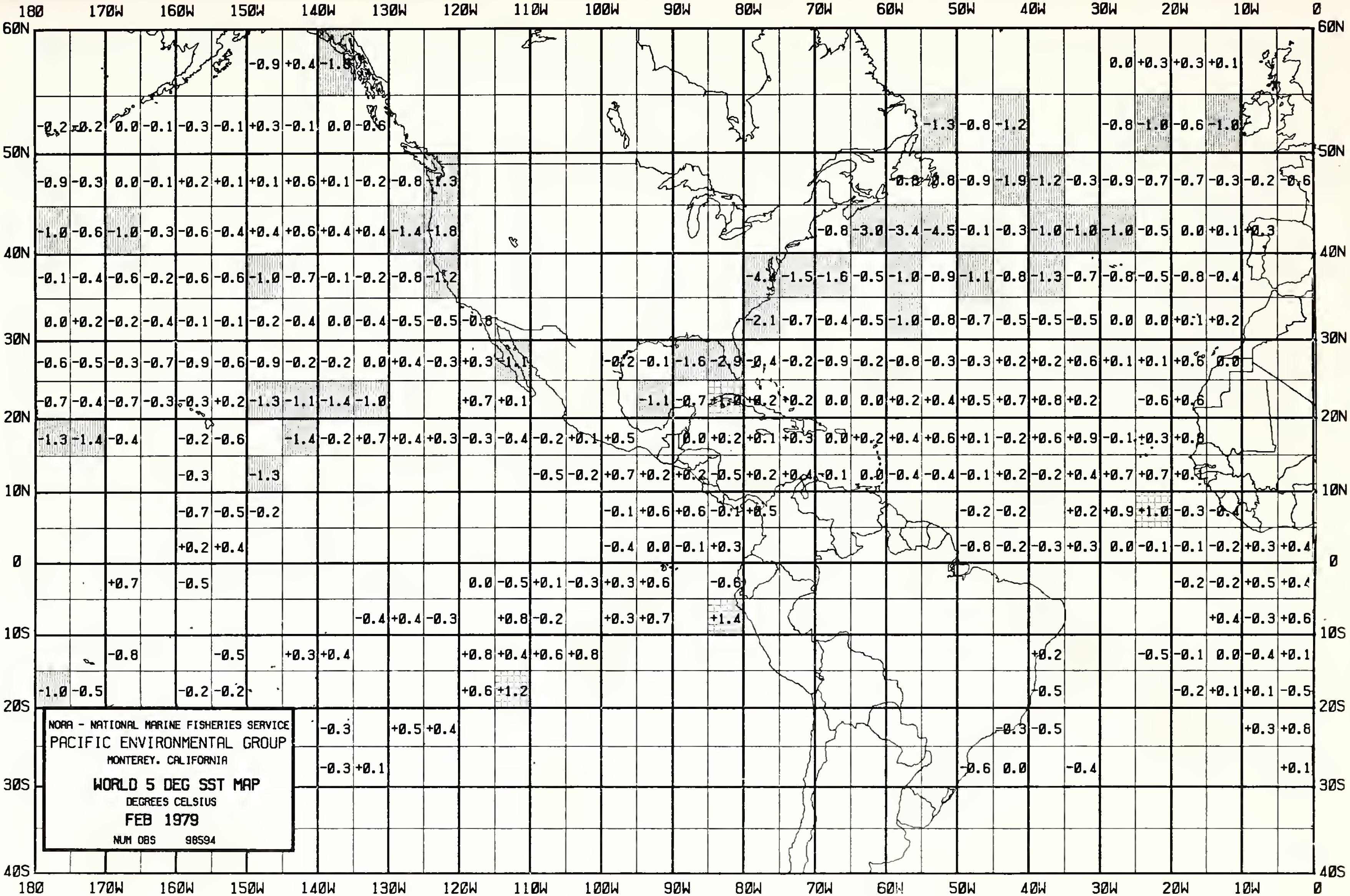

Figure 6. Monthly mean anomaly of sea surface temperature in °C by 5 degree squares for February 1979 relative to long term mean for reference period 1948-67.

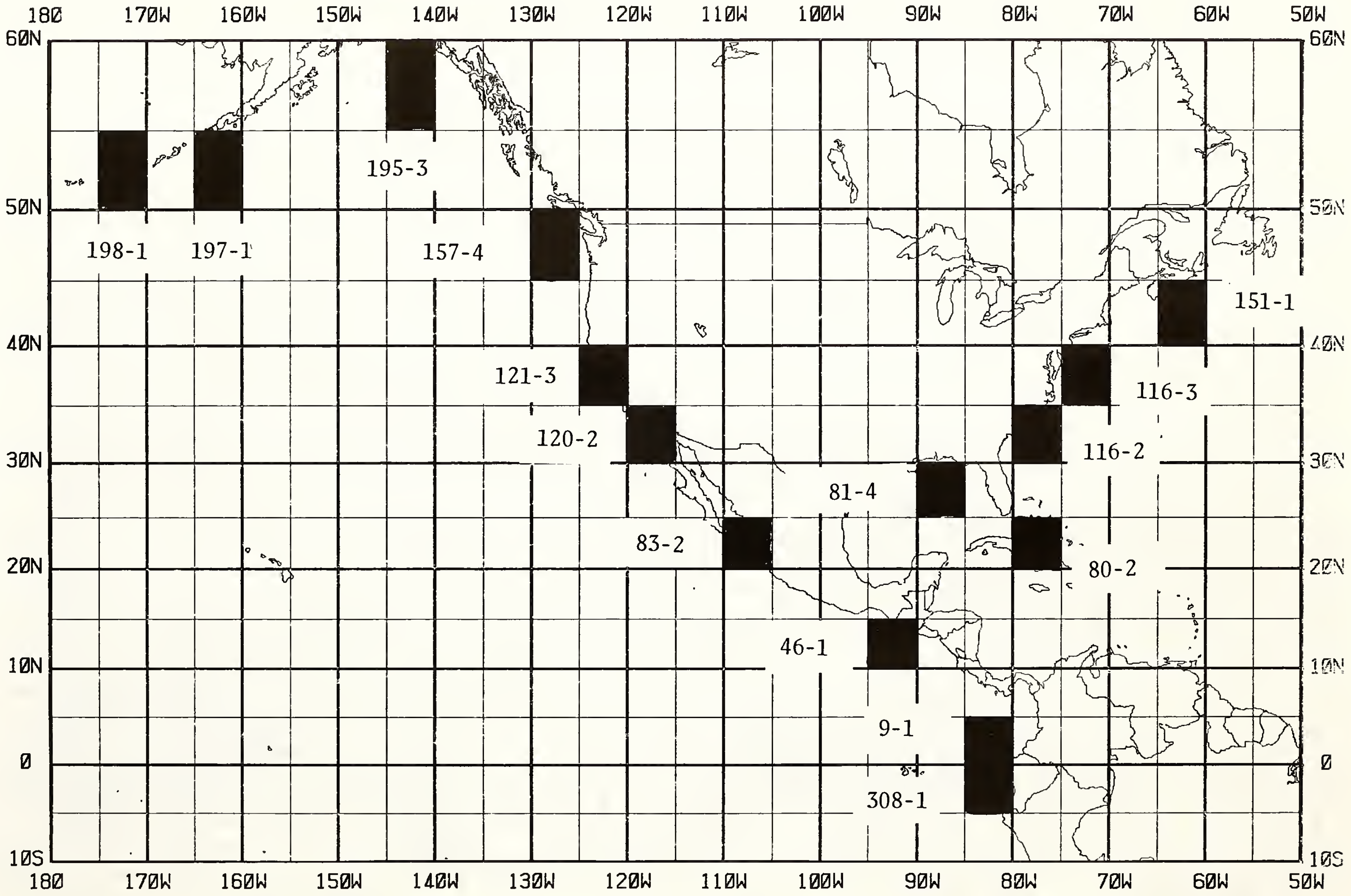

Figure 7. Location of selected 5 degree squares along U.S. coasts where time series plots of sea surface temperature were made.

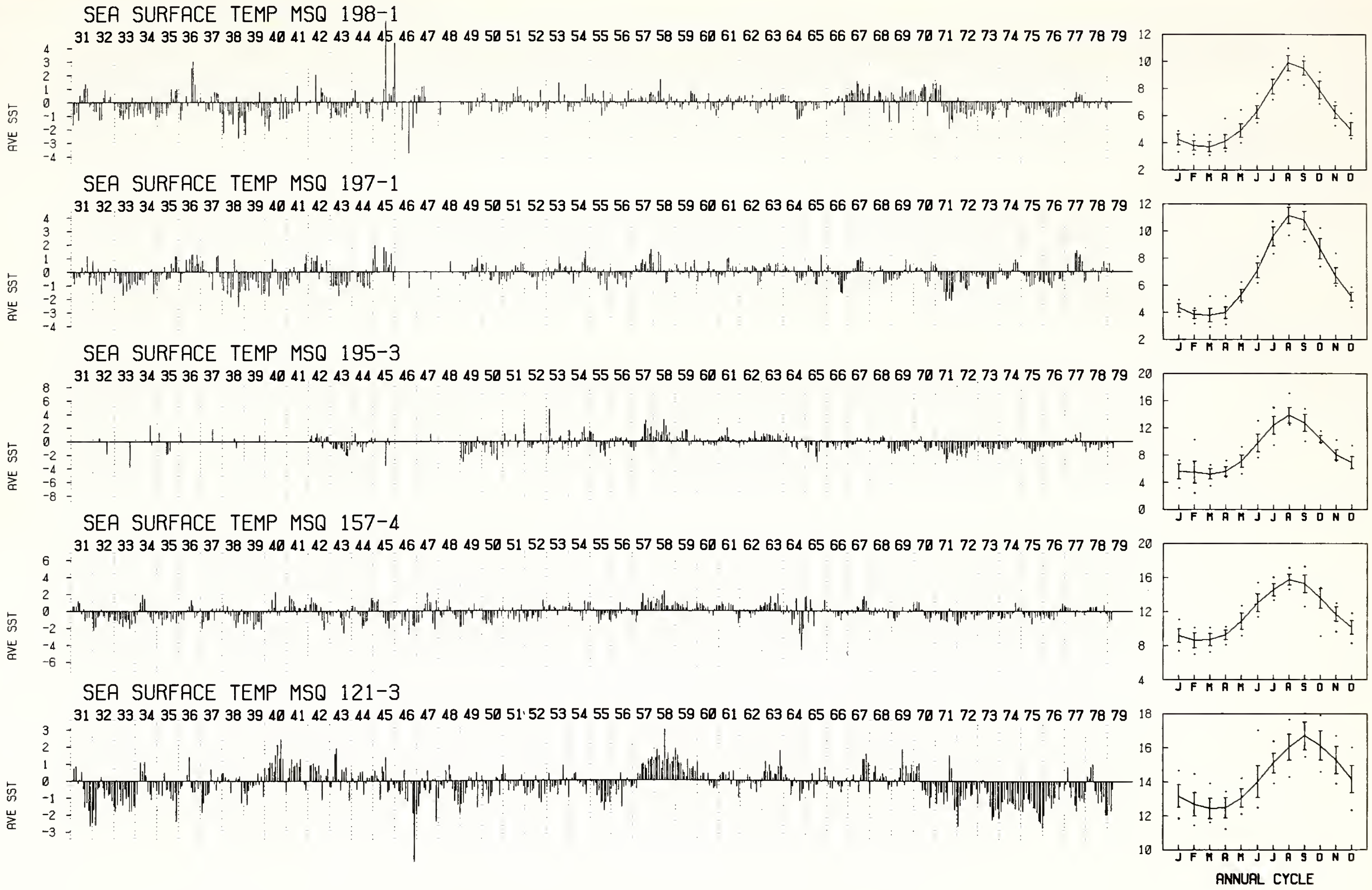

Figure 8. Time series of monthly mean anomaly of sea surface temperature in °C for 1931-79 relative to long term means for 5 degree squares along the West Coast from the Central Aleutian Islands to Central California.

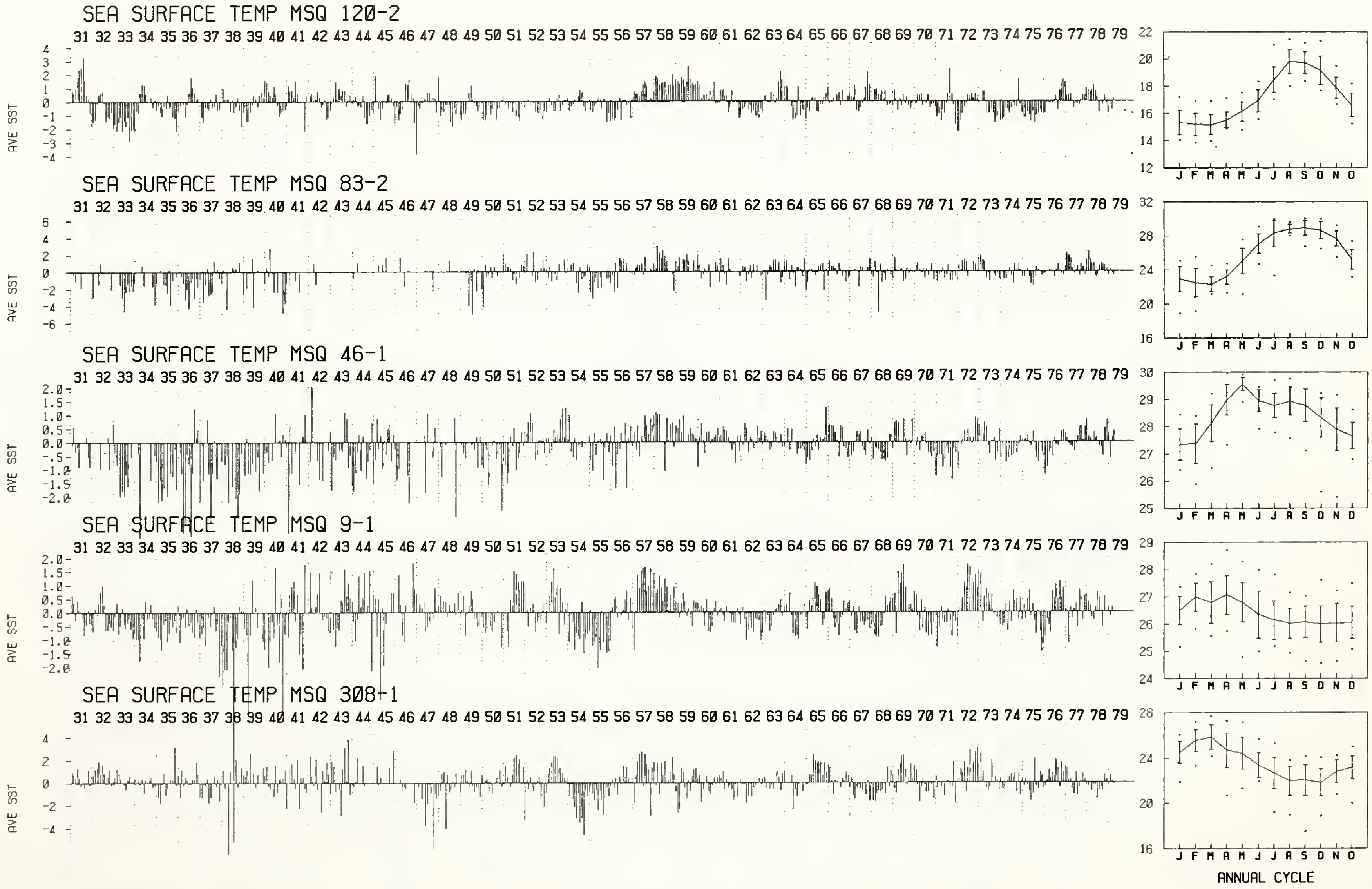

Figure 9. Time series of monthly mean anomaly of sea surface tempeature in °C for 1931-79 relative to long term means for 5 degree squares along the West Coast from Southern California to Equador.

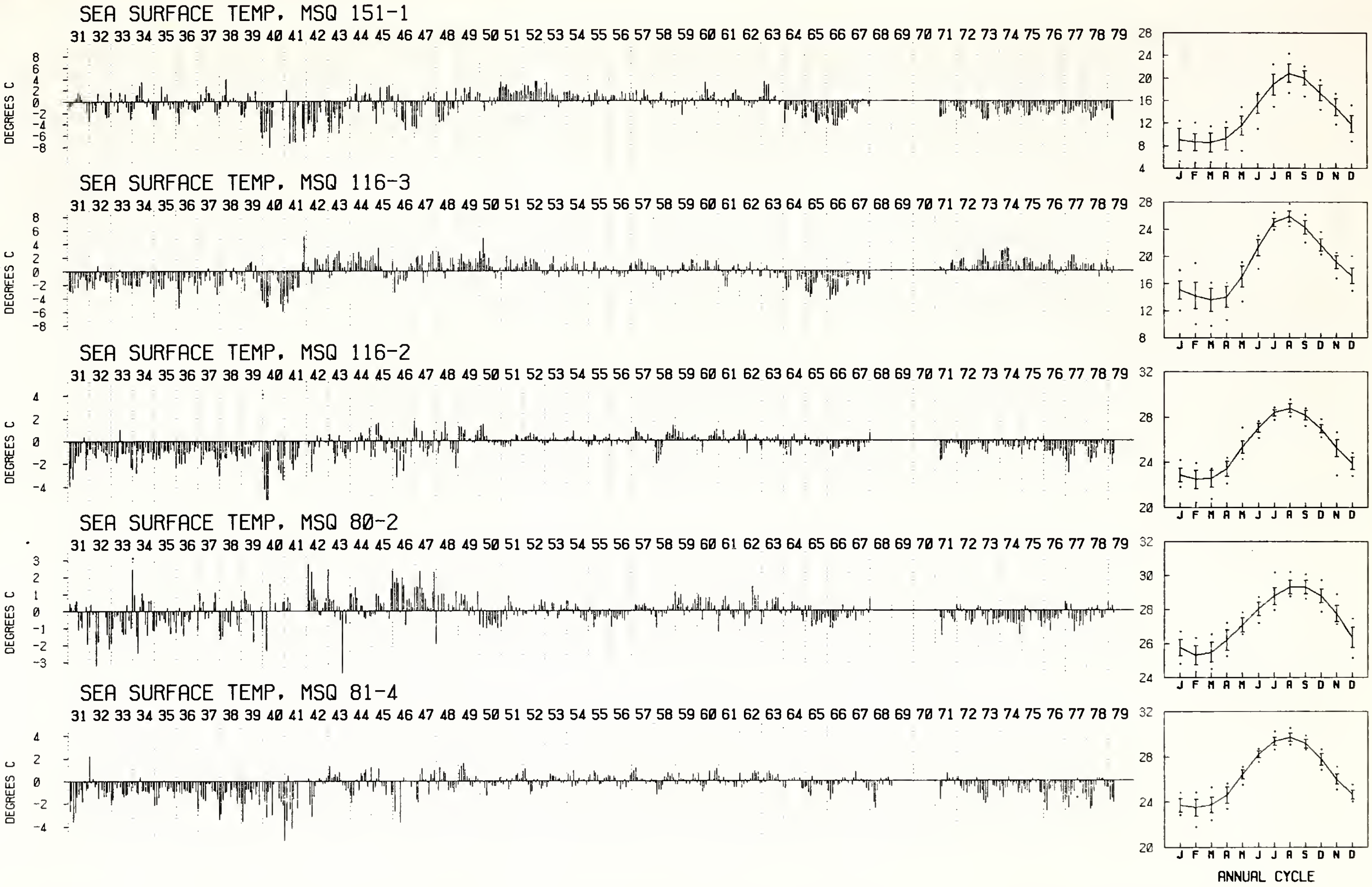

Figure 10. Time series of monthly mean anomaly of sea surface temperature in°C for 1931-79 relative to long term means for 5 degree squares along the West Coast from Nova Scotia to northern Gulf of Mexico.

# Further Analysis of Recent Fluctuations in Circulation and Cloudiness (Rainfall) over the Tropics

Arthur F. Krueger and Jay S. Winston
NOAA, NWS, CAC, Washington, D. C.

In many respects the circulation over the tropical Pacific in the winter of 1978-79 resembled that of the previous two winters. This is rather interesting in light of the similar persistence of the North American wintertime circulation. It has already been noted that the North American subtropical jetstream on the average has been abnormally strong and south of normal during the past three winters. Figure 1 which shows 200 mb zonal wind components for the past four winters, illustrates the greater strength and extent of the westerlies over eastern North America during the last three winters as compared with the winter of 1975-76 (top). In contrast, the high level zonal flow over the eastern equatorial Pacific has been averaging below normal these past three winters, and this too represents a decided change from the 1975-76 winter circulation. This is shown in figures 2 and 3.

In figure 2 three time series for the 200 mb zonal wind speed over the eastern tropical Pacific (165 W-110 W) are shown. These are anomalies about a ten-year mean with a 1-2-1 smoother applied. The upper and lower time series are for 24° N and 24° S latitude respectively, while the middle series is for the equator and can be considered as a measure of the "Walker circulation". Note the continued weakness of the equatorial westerly flow ever since the 1975-76 winter when it averaged unusually strong. Also note that the equatorial flow generally varies inversely with the subtropical westerlies both north and south of the equator. Thus the subtropical westerlies over the eastern Pacific both north and south of the equator have been averaging "above normal" for the past three years.

These recent 200 mb zonal wind anomalies are a manifestation of large scale circulation changes that have occurred over the tropics. The nature of these changes can be seen in figure 3 where the 200 mb streamfunction anomalies for the past four winters are shown. Over the eastern Pacific these zonal wind anomalies appear symmetric about the equator with a meridional wavelength varying from about 40 to 60° of latitude. These past three winters have essentially been characterized by more anticyclonic anomalous flow both north and south of the equator than the 1975-76 winter, which in contrast consisted of cyclonic anomalous flow north and south of the equator. It should be noted however, that these anticyclonic anomalies and the relative easterly flow at the equator were considerably reduced during this past winter. Yet the subtropical westerlies north and south of the equator remained strong, but were more confined to latitudes nearer 20° N and 20° S (i.e., the meridional wavelength was smallest in this past winter).

The recent changes over the tropical Atlantic are also interesting and are in marked contrast to those over the Pacific. Particular striking is the stronger relative westerly flow along the equator (stronger Atlantic Walker circulation) during the past three winters in contrast to that of 1975-76.

As would be expected these changes in the large scale circulation were accompanied by major changes in cloudiness and rainfall over the tropics. These can be monitored by using satellite outgoing longwave radiation measurements as shown in figures 4 and 5. The most striking feature of the past three winters is the abnormal eastward displacement of the South Pacific's tropical convergence zone. Normally it extends southeastward from the maritime continent of Indonesia-New Guinea as occurred during the 1975-76 winter (fig. 5, top). Since 1977 however, the cloudiness and precipitation associated with this convergence has extended eastward into the equatorial dry zone. Note, for example, the eastward trend in the shaded area which represents radiation less than 250 $Wm^{-2}$ and hence the most cloudy areas. Cloudiness over the northeastern tropical Pacific, particularly during this past winter, has also increased (fig. 4).

Bjerknes has suggested that these events are "regulated" or at least accompanied by a warming of the South Equatorial current which arises in response to a weakening of the Southern Hemisphere's tradewinds. This seems to be the case initially. Note for example, the warming at 5° S, 85° W, and also 0°, 110° W that occurred during 1976 with above normal temperatures continuing through the 1976-77 winter (fig. 6, middle two time series). During 1977 however, both of these time series showed rapid cooling to below normal temperatures which then persisted for nearly two years. Thus the anomalous tropical circulation over the Pacific these past two winters was accompanied by below normal temperatures in the eastern equatorial Pacific in contrast to the 1976-77 winter. It is interesting that the sea surface temperatures 10° north and south of the equator also went above normal during 1976 (fig. 6 top and bottom time series). They, however, remained above normal for the past two winters. Considering that these anomalies represent temperatures of 27° C or more, this may be a significant factor in accounting for the anomalous eastward displacement of the tropical convection during these past three winters. Such temperatures appear to be a necessary, although not a sufficient condition, for initiating and sustaining convection over the tropics.

During spring 1979 above normal cloudiness continued over the South Pacific near French Polynesia (fig. 7 and 8, upper). North of the equator it was also above normal over much of the western and eastern Pacific as well as the Caribbean and Atlantic.

The major abnormality of the summer circulation was the weakness of the Indian monsoon. Decreased cloudiness and rainfall associated with this is indicated by the + 15 $Wm^{-2}$ contour over India (fig. 7, lower). It is interesting that increased cloudiness (rainfall) occurred over the western tropical Pacific and Indian Ocean as well as Central America and the Caribbean. Again, as for 1972, a possible relation between summertime convection over the western Pacific and the intensity of the Indian monsoon appears to be worth considering.

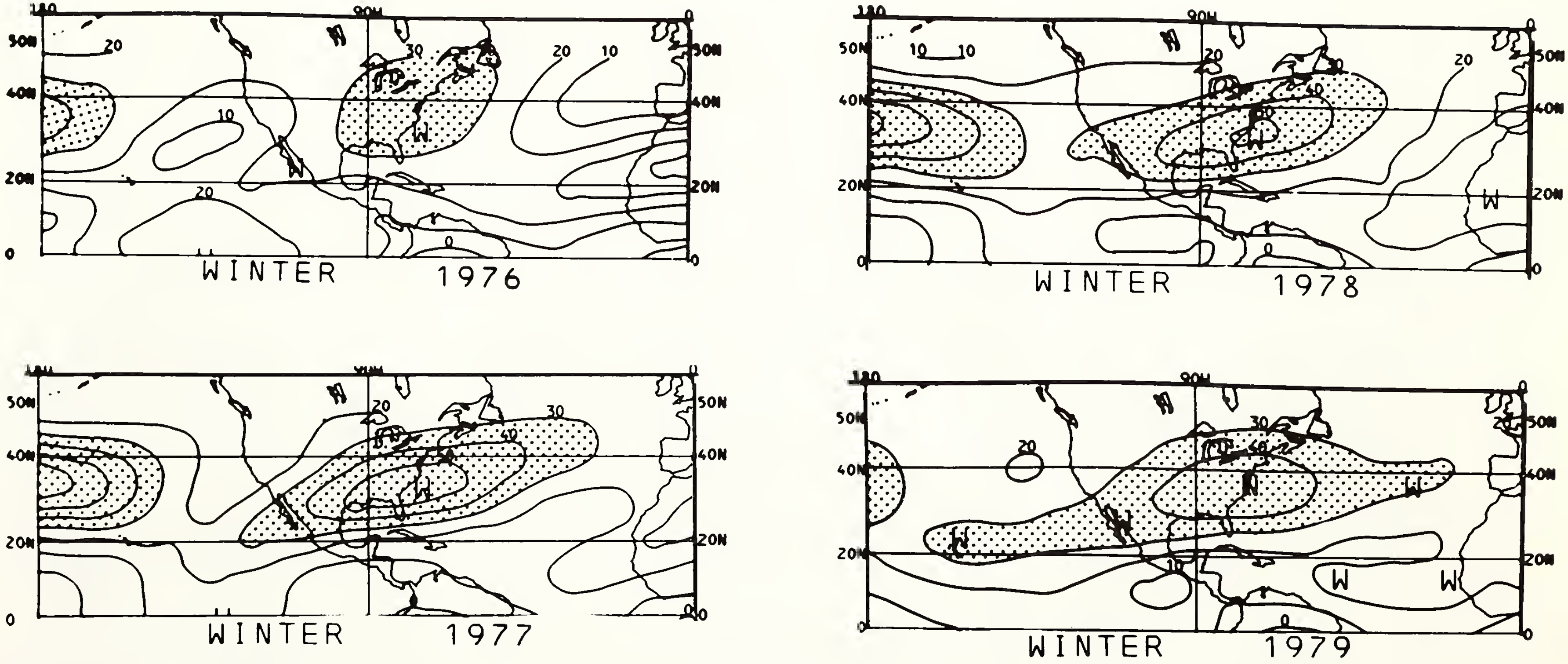

200MB ZONAL WIND ($MS^{-1}$)

Figure 1

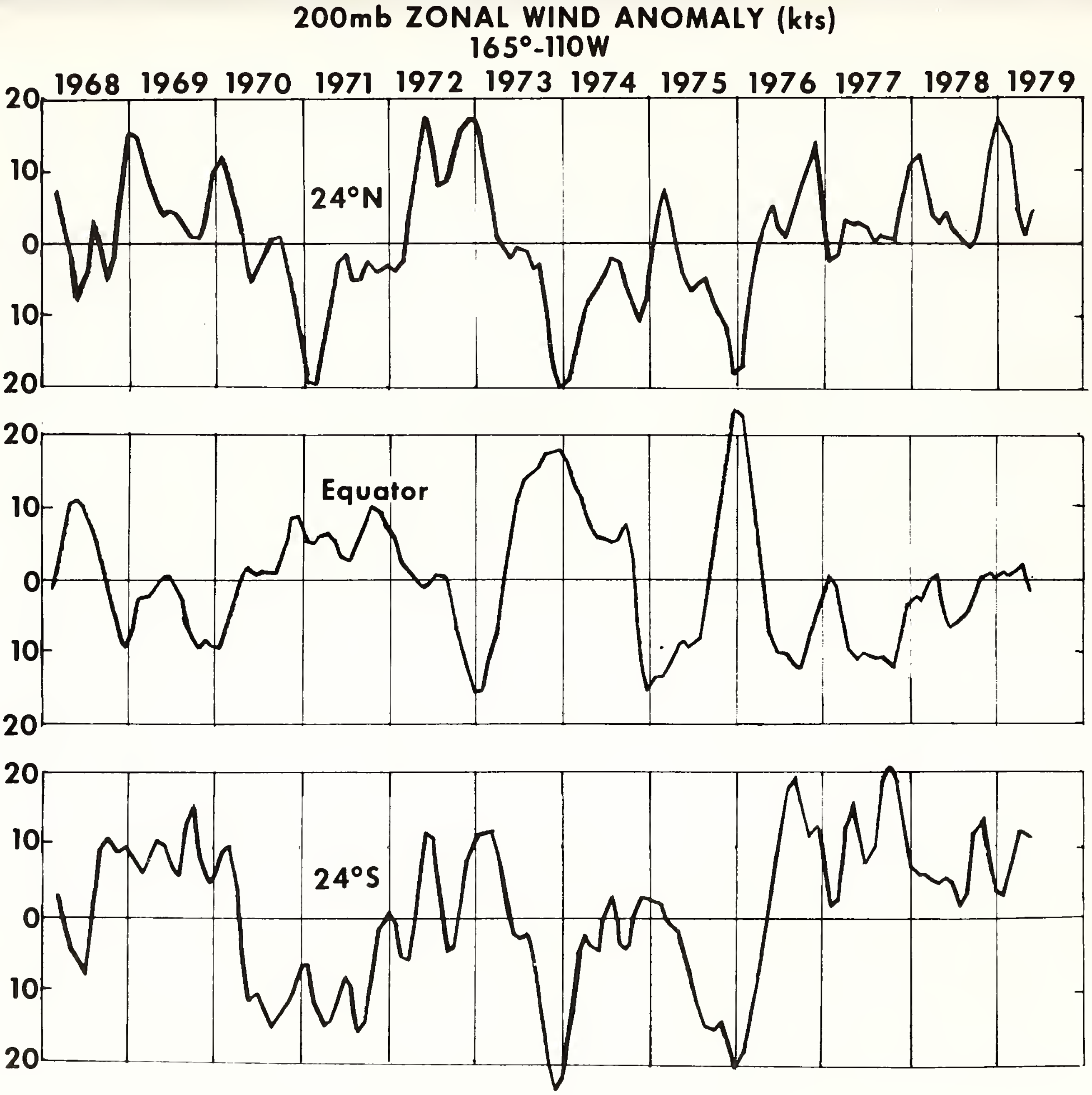
200mb ZONAL WIND ANOMALY (kts)
165°-110W
1968
1969
1970
1971
1972
1973
1974
1975
1976
1977
1978
1979
20
10
0
10
20
24°N
Equator
24°S

Figure 2

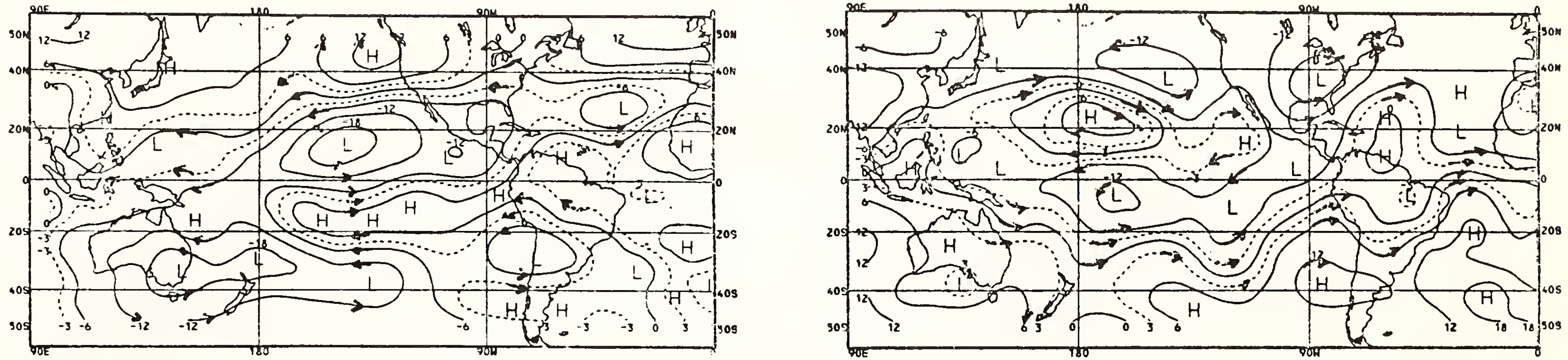

WINTER 1976

WINTER 1978

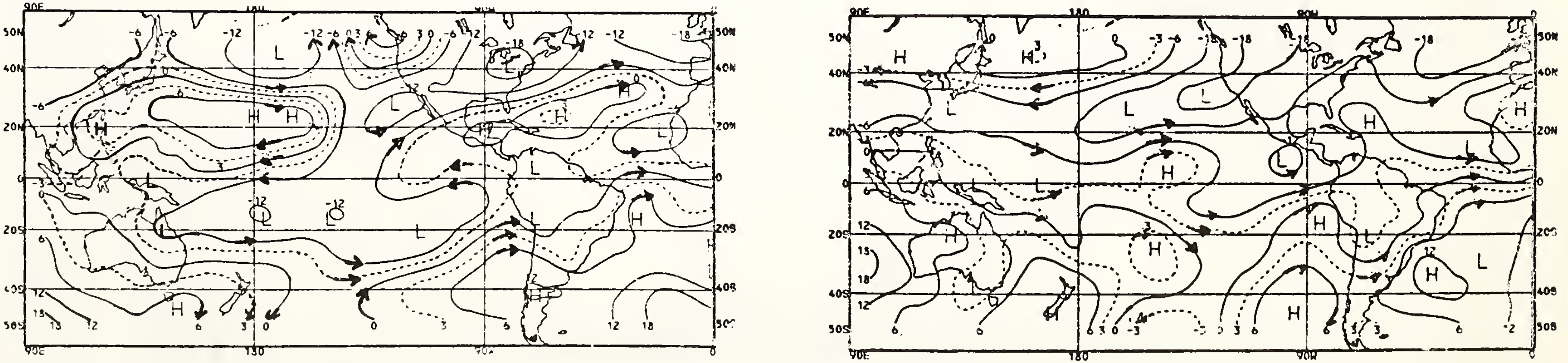

WINTER 1977

WINTER 1979

200 MB STREAMFUNCTION ANOMALY

Figure 3

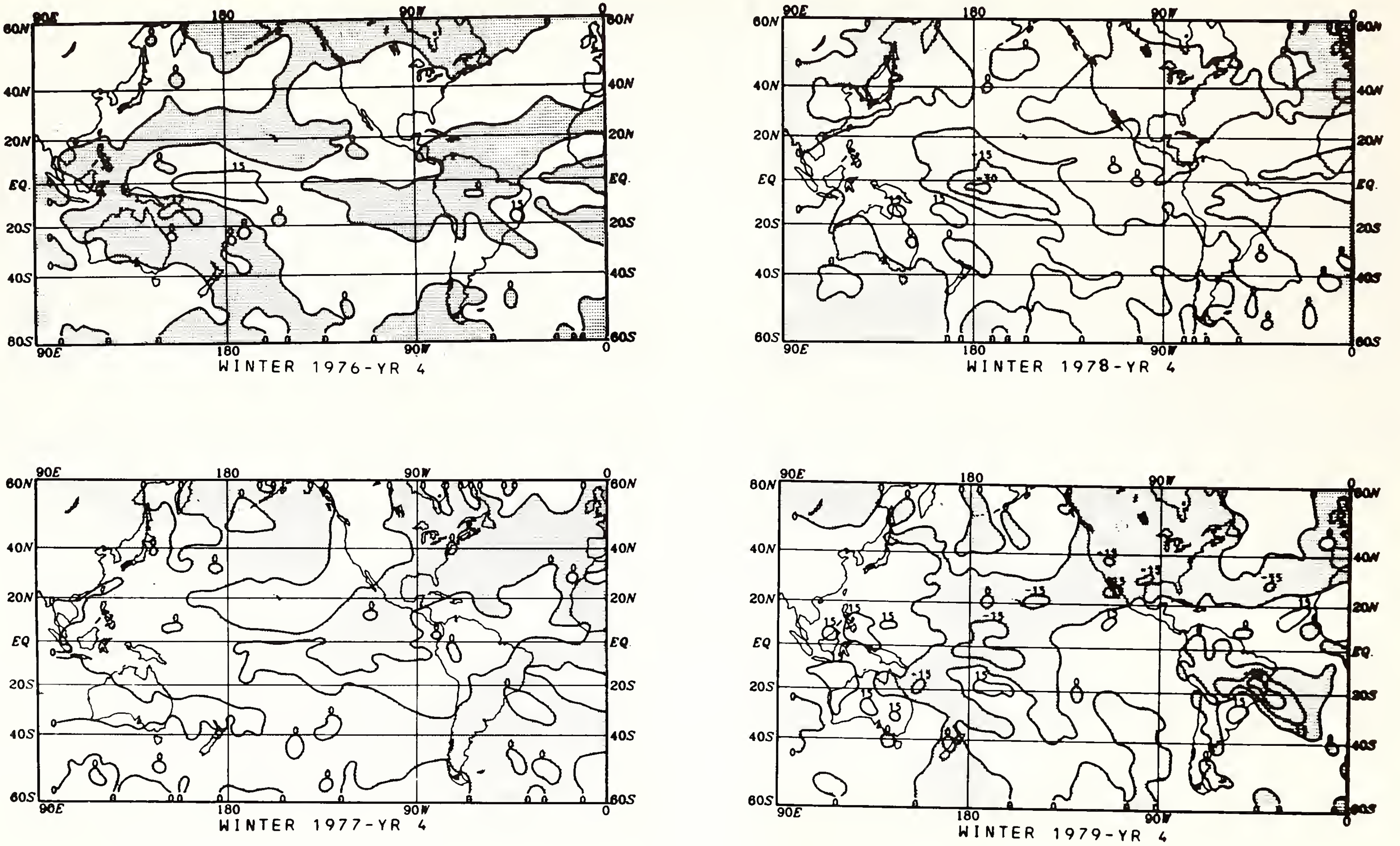

WINTER 1976-YR 4

WINTER 1978-YR 4

WINTER 1977-YR 4

WINTER 1979-YR 4

**OUTGOING LONGWAVE RADIATION ANOMALY ($WM^{-2}$)**

Figure 4

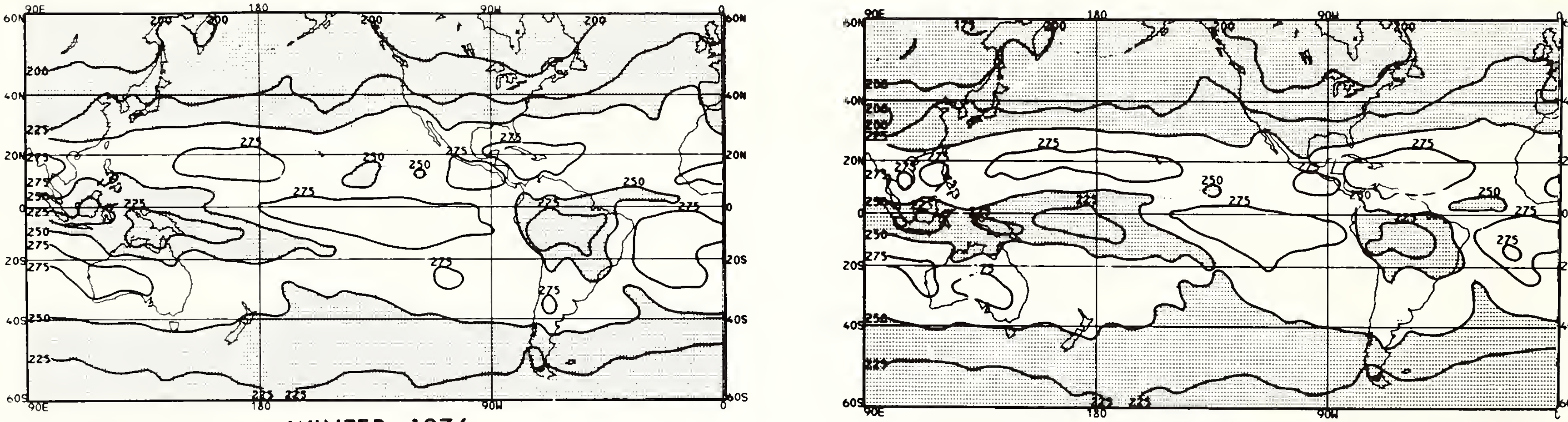

WINTER 1976

WINTER 1978

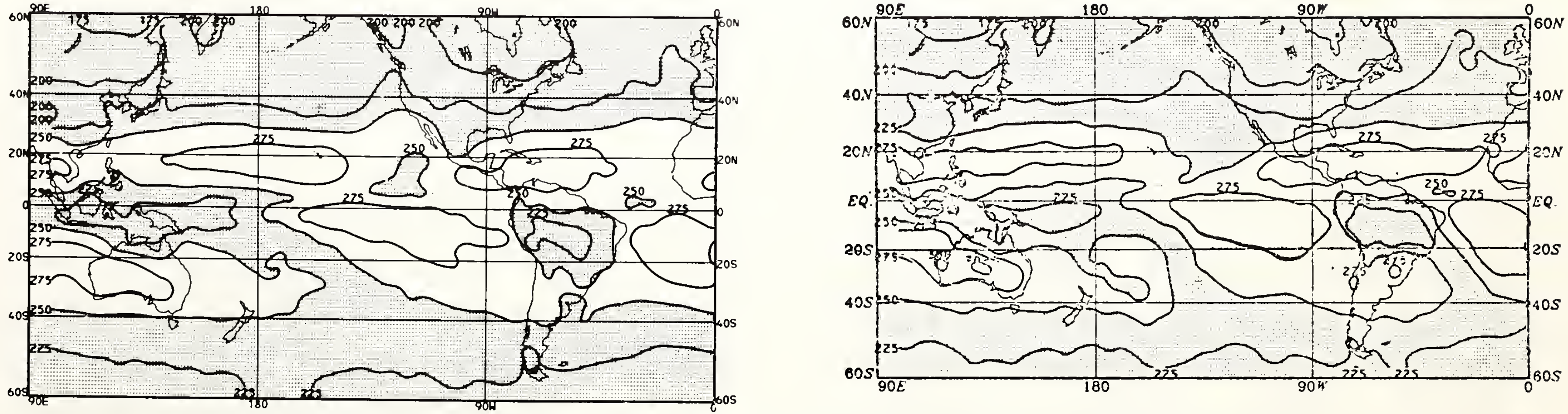

WINTER 1977

WINTER 1979

OUTGOING LONGWAVE RADIATION $(WM^{-2})$

Figure 5

Pacific Sea Surface Temperature Anomalies

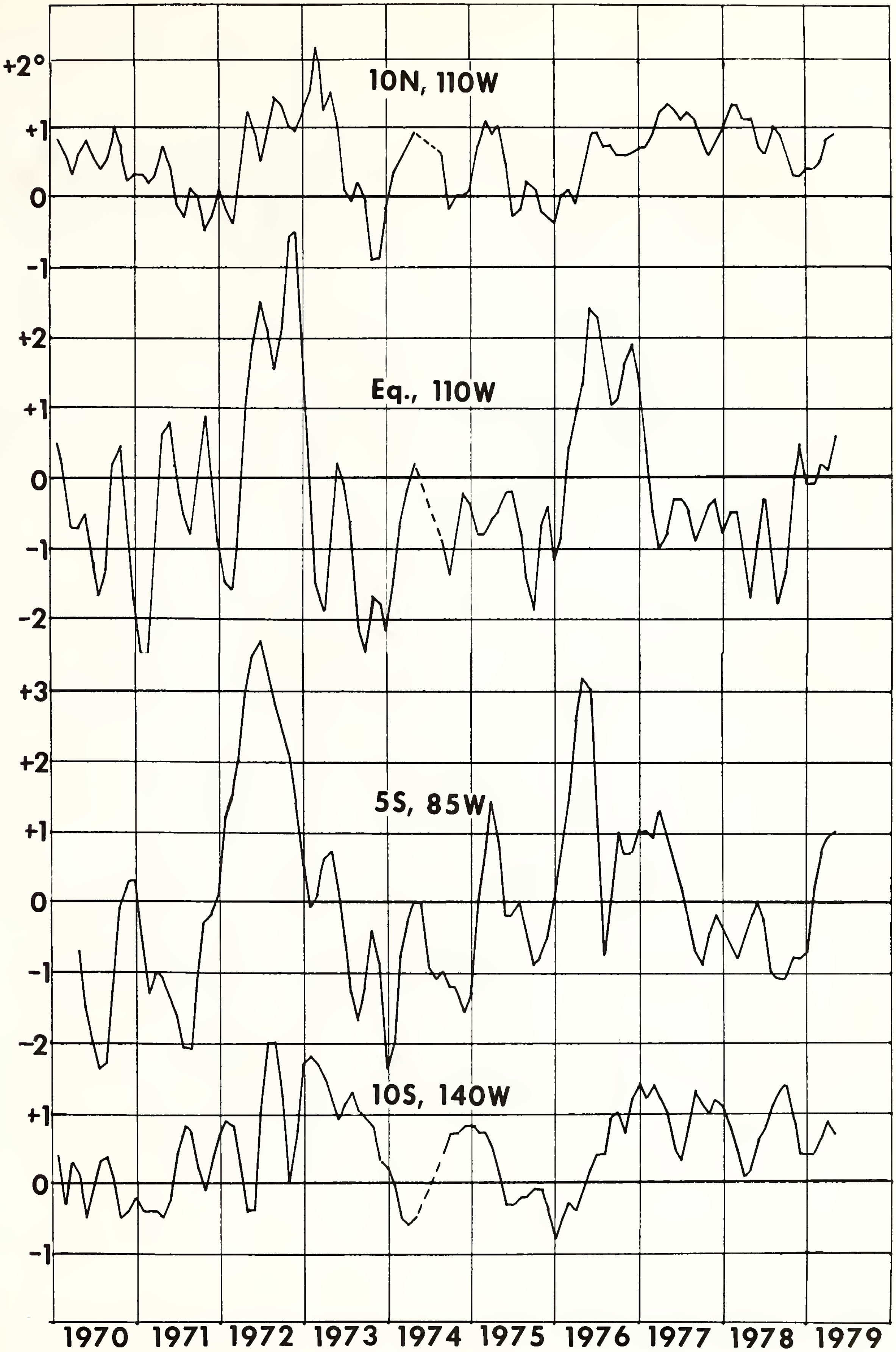

Figure 6

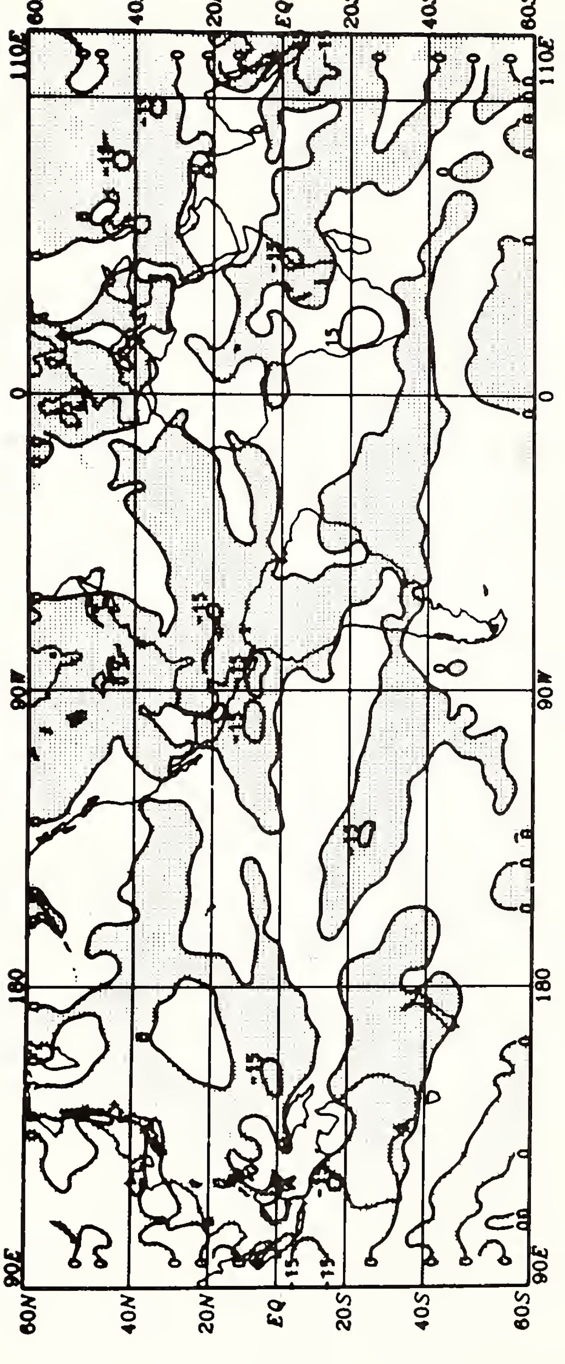

OUTGOING LONGWAVE RADIATION ($WM^{-2}$)

DIFFERENCE SPRING 1979-YR 4 PRE

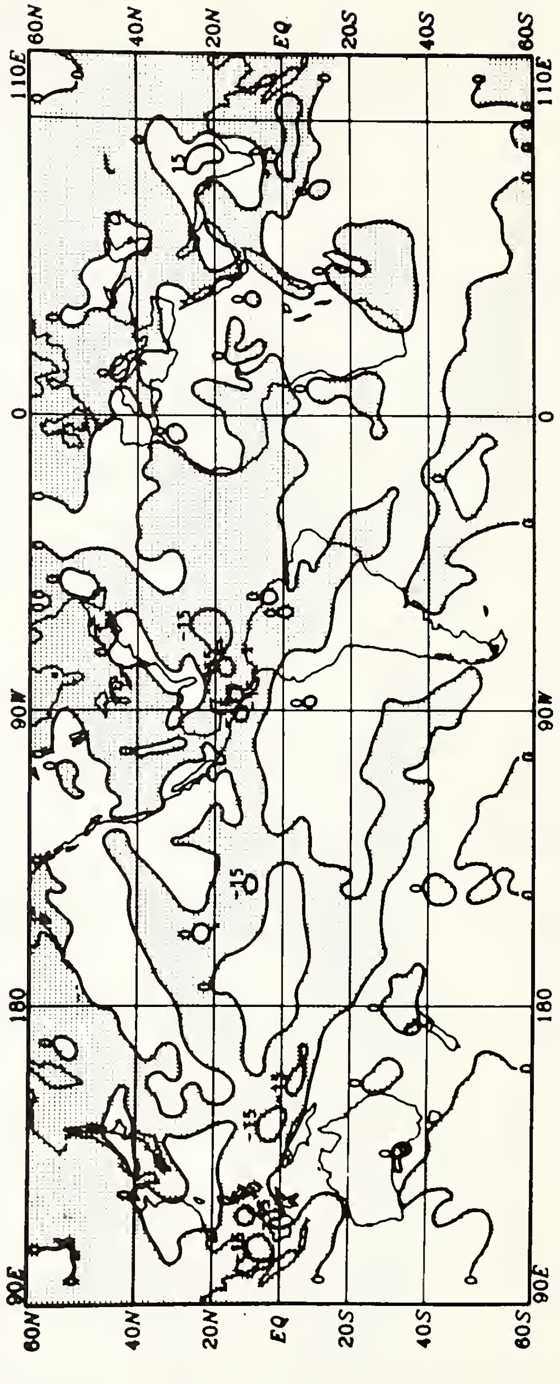

OUTGOING LONGWAVE RADIATION ($WM^{-2}$)

DIFFERENCE SUMMER 1979-YR 4 PRE

Figure 7

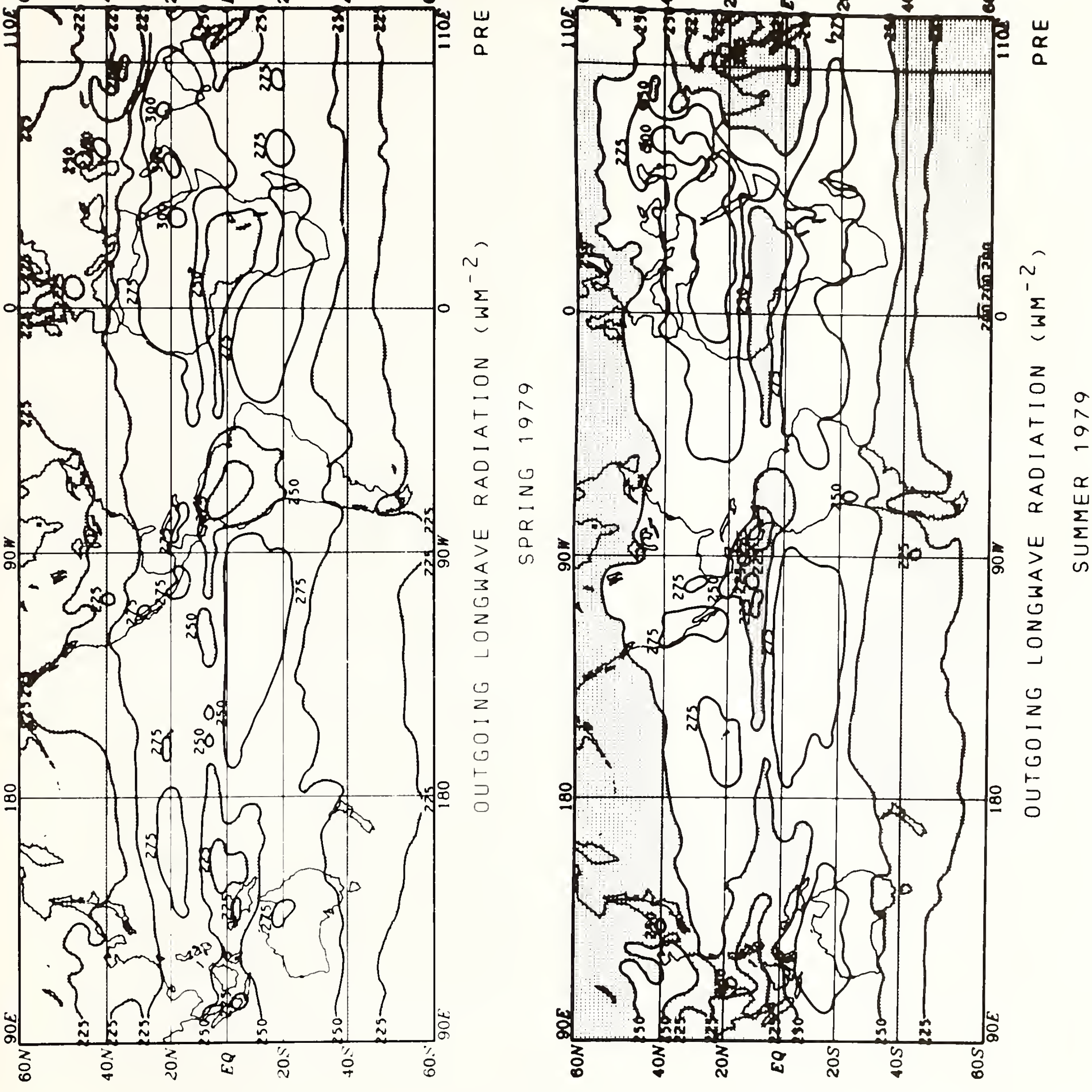
OUTGOING LONGWAVE RADIATION (WM$^{-2}$)

SPRING 1979

OUTGOING LONGWAVE RADIATION (WM$^{-2}$)

SUMMER 1979

Figure 8

# Possible Causes for the Wet Winter of 1978-79 in the Southwestern United States and Mexico

Arthur V. Douglas
Climatology Program
Department of Geography
University of Nebraska
Lincoln, Nebraska 68588

During the winter of 1978-79, unusually heavy precipitation developed in the southwestern United States and northwestern Mexico. While the heavy precipitation was primarily a result of strong upper-level troughing over the region, baroclinic enhancement of the trough may have occurred in response to anomalous air-sea interactions over the eastern North Pacific. For example, SST's were observed to be more than 1°C warmer than normal on the south side of the trough (Figure 1), following a prolonged period of weakened trades and increased solar radiation which began in June, 1978. Another pool of anomalously warm SST's developed far to the northwest of the trough in response to decreased fall storm activity and the offshore retrogression of the West Coast ridge (Figure 1).

Preliminary research aimed at predicting mid-winter precipitation in the southwestern United States indicates that late fall ridging in the east central North Pacific, when associated with warmer than normal SST's, often foreshadows heavy precipitation in the Southwest. With respect to the winter of 1978-79, it is believed that the upper-level ridge forced colder than normal air into the trough off Baja, California, while at the same time warm-moist air was advected into the south side of the trough from the anomalously warm eastern North Pacific.

An examination of past Novembers (1948-77) with warm SST's near 50°N/150°W, indicates that these years were followed by persistent ridging in the same area during December and January. The 700mb height anomalies in December and January of warm water falls are considerably different than those following cold water falls (Figure 2). Following a warm fall in the east central North Pacific (40°N to 50°N/150°W to 160°W), there is a strong tendency for early winter height anomalies (December and January) to be positive in the Gulf of Alaska and negative off Baja, California. Teleconnection charts from O'Connor indicate that positive height anomalies near 50°N/150°W are strongly associated with negative height anomalies near Baja, California - a teleconnection which was very active in the winter of 1978-79.

During early winter there is a marked difference in storm tracks following warm falls compared to cold falls (Figure 3). Following a warm fall, there is a paucity of storms off the Pacific Northwest and an increase in Colorado lows. The observed storm tracks for December and January, 1978-79, were similar to those of previous warm water years (Figure 4B). The dry conditions in the Pacific Northwest during this same winter can be linked to a decrease in local storm numbers and storms originating from the southwest (greater moisture potential).

In January, 1979, the West Coast trough was located just north of the warm water pool in the eastern tropical Pacific (Figure 5A). Due to this positioning, the warm water pool remained entact despite repeated storminess to the immediate north. Based on surface observations and satellite data, the heaviest precipitation for the month occurred during the period January 16-20, when the subtropical jetstream was actively transporting moisture towards Baja, California. The subtropical moisture was advected northeastward across the warm water pool and appears to have entered the circulation of a deep cut-off low centered west of northern Baja, California. The heavy precipitation associated with this surge of subtropical moisture was probably enhanced by the colder air aloft, as well as the forced ascent over the fairly rugged terrain. These synoptic events resulted in precipitation totals of one to three inches in southern Arizona, and by the end of the month precipitation exceeded 300% of normal in Arizona and northwest Mexico (Figure 6).

Central Mexico and Texas remained dry during January, 1979, and current research indicates that this region would probably have been wet had the 700mb trough been shifted southeastward into northeast Mexico (compare Figures 5, 7, and 8B). Overall, the precipitation pattern for January, 1979, appears to be a combination of both eigenvector 1 (positive sense) and eigenvector 2 (negative sense) (Figure 9). Eigenvector 2 of January precipitation is strongly associated with height anomalies in northern Mexico (Figure 8A), as is precipitation in central Mexico. An examination of Figures 7 and 8 indicates that similar 700mb height patterns are associated with precipitation not only in Texas and central Mexico, but also in the dry zone region of the central equatorial Pacific. This may suggest that the coupling of tropical and midlatitude circulations is an important factor which, at times, influences the precipitation regimes of the southern United States and Mexico.

In an attempt to better understand the relationship between southern United States precipitation and a number of the variables discussed above, regression equations were developed using divisional precipitation as the dependent variable, and previous monthly SST anomalies, 700mb anomalies, and equatorial rainfall anomalies as the independent variables (Figure 10). In a hindcast experiment it was found that January, 1979, showed relatively good predictability (Figure 11). Important predictors were the SST's from off Baja, California and 50°N/150°W, and the 700mb height anomalies near 25°N/125°W.

# FIGURE CAPTIONS

Figure 1. Sea surface temperature anomalies for January, 1979. Eastern North Pacific sea surface temperature anomalies for January, 1979, are given, as well as the mean location of the 700mb trough for November through December, 1978-79.

Figure 2. Difference in the observed 700mb height anomalies for early winters preceded by cold falls in the east central North Pacific versus early winters preceded by warm falls. Height anomalies (December and January) for the cold years (1950, '53, '63, and '69) were subtracted from the height anomalies for the warm years (1948, '61, '71, and '72). In years with warm November SST's near $50^{o}N/150^{o}W$, strong ridging usually occurs in the Gulf of Alaska during the following December and January (e.g. fall and winter, 1948-49).

Figure 3. December and January storm tracks for warm water years (top) and cold water years (bottom). Years selected were the four warmest and four coldest for November based on SST records 1948-1977.

Figure 4. Top map shows the correlation between SST's in a $10^{o}$ square of Pacific Northwest and divisional precipitation in the southwestern United States (period of analysis 1948-1977). Bottom map shows the observed storm track data for December and January, 1978-1979.

Figure 5. Top map shows the 700mb height anomalies for January, 1979, and the location of positive SST anomalies off Baja, California for the same month. Bottom map shows the mean 700mb height fields for January 16-20, 1979 and observed cloudiness (IR) for January 16, 1979.

Figure 6. Percentage of normal precipitation for January, 1979, in the southern United States and Mexico.

Figure 7. Correlation between January precipitation at Leon, Mexico, (Located near the -0.58 value) and concurrent 700mb height anomalies. Period of analysis 1948-76.

Figure 8. Top map shows the correlation between the time coefficients for eigenvector 2 (1948-1976) and concurrent 700mb heigh anomalies. Bottom map shows a similar correlation but between equatorial rainfall and 700mb height anomalies. The spatial pattern of eigenvector 2 is shown in Figure 9, and the locations of equatorial rainfall stations are shown in Figure 10.

Figure 9. The first and second eigenvectors of January precipitation for the southern United States. Analysis was performed on divisional precipitation data (1948-76).

Figure 10. Location map for variables used in regression analysis with southern United States precipitation. The rainfall for the equatorial dry zone has been analyzed into an index by Wright (Univ. of Hawaii).

Figure 11. Top map shows predicted precipitation for January, 1979, bottom map shows observed precipitation for January, 1979. All divisional precipitation equations significant at the 95% level.

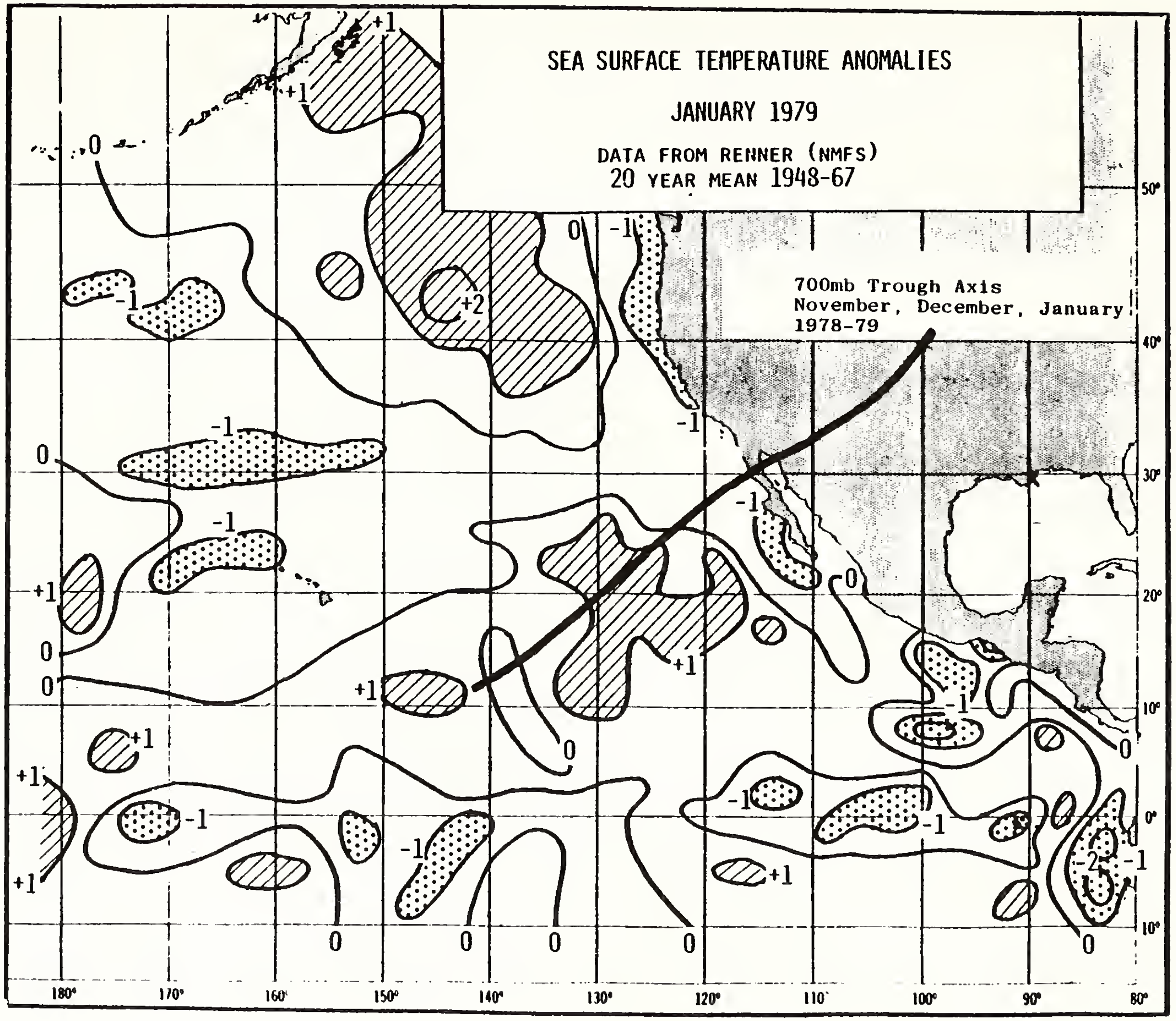

SEA SURFACE TEMPERATURE ANOMALIES

JANUARY 1979

DATA FROM RENNER (NMFS)
20 YEAR MEAN 1948-67

700mb Trough Axis
November, December, January
1978-79

FIGURE 1

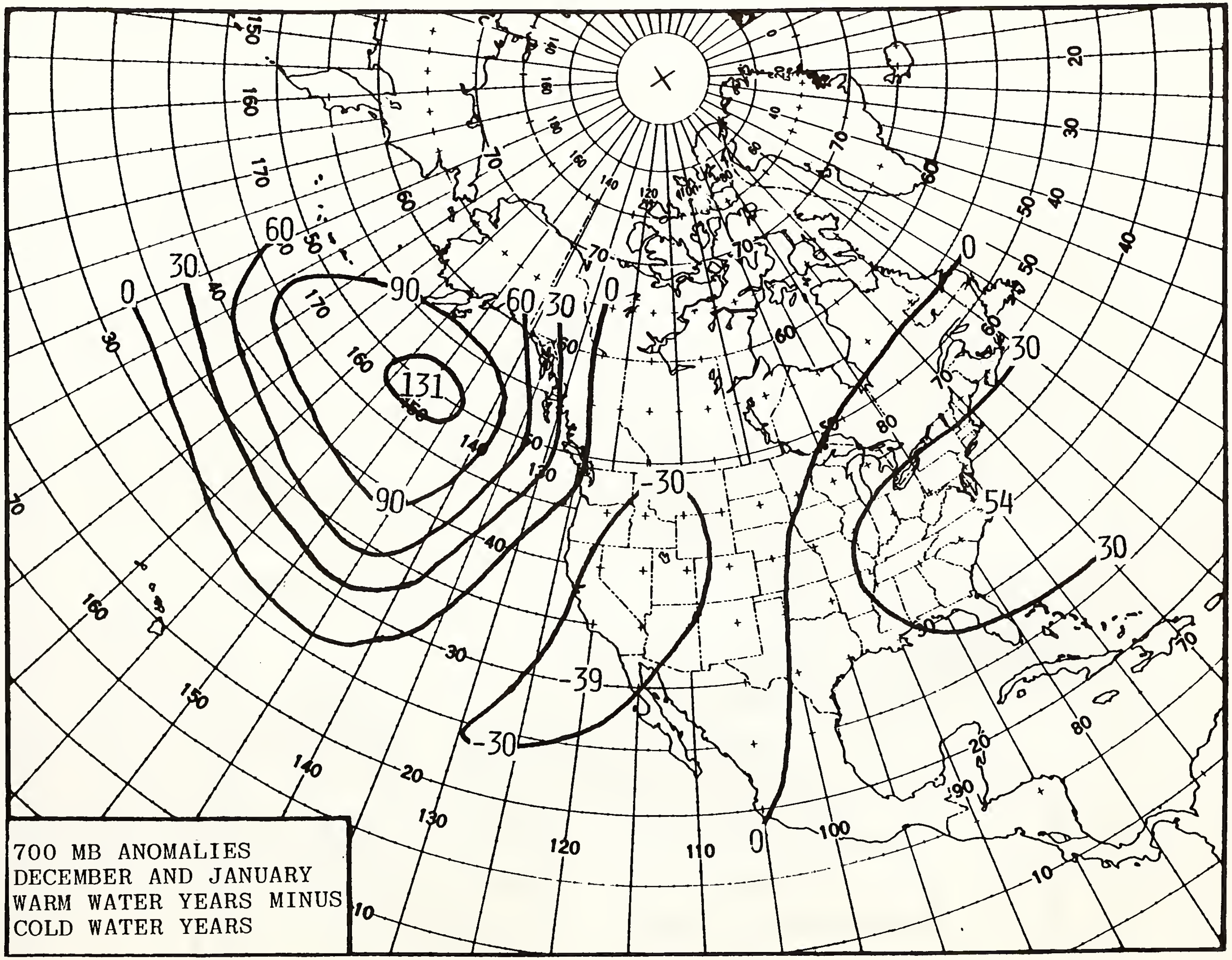
700 MB ANOMALIES
DECEMBER AND JANUARY
WARM WATER YEARS MINUS
COLD WATER YEARS
131
90
90
60
30
0
-30
-39
-30
0
0
30
54
30
60
30
0

FIGURE 2

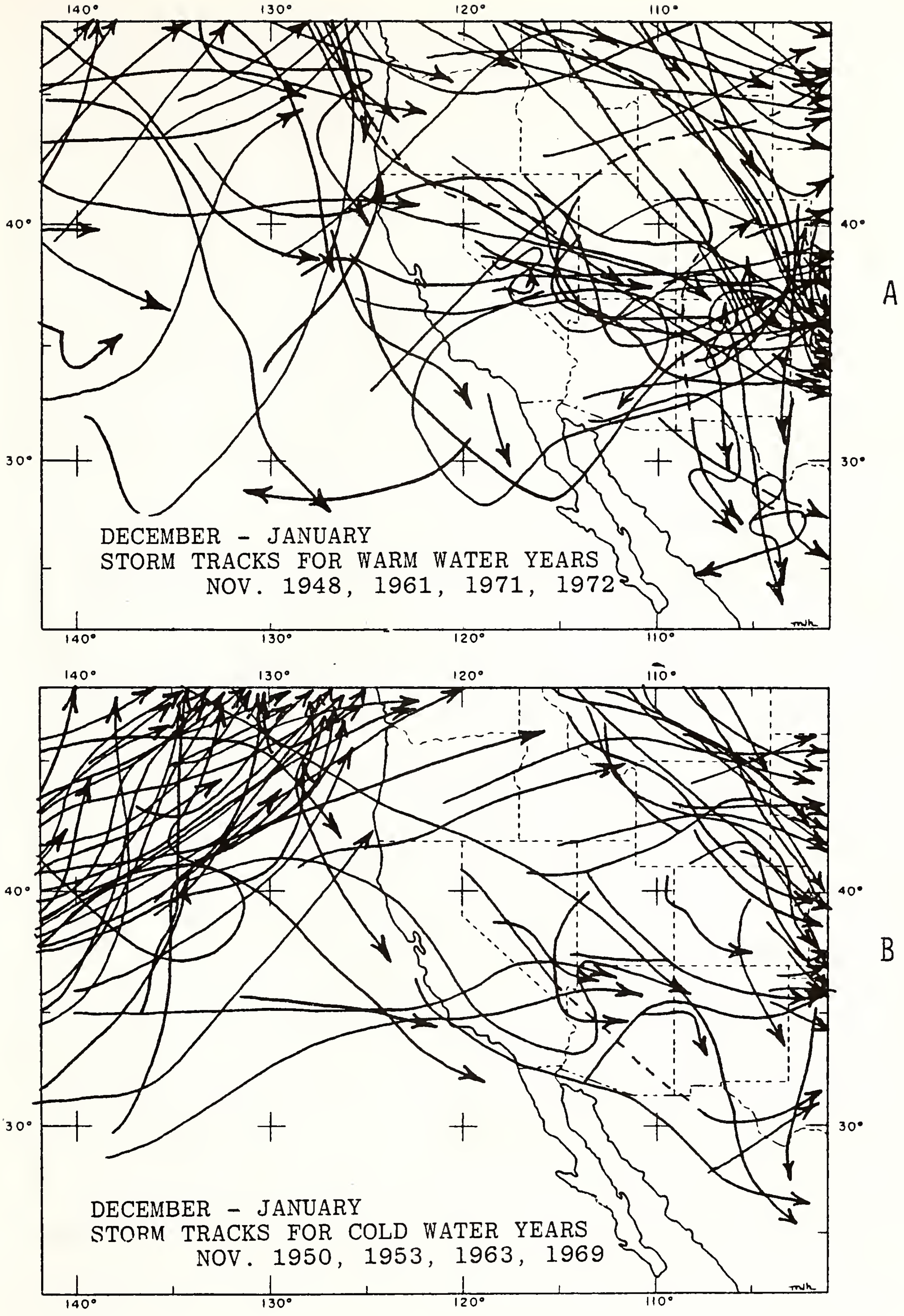
140°
130°
120°
110°
40°
30°
DECEMBER - JANUARY
STORM TRACKS FOR WARM WATER YEARS
NOV. 1948, 1961, 1971, 1972
A
DECEMBER - JANUARY
STORM TRACKS FOR COLD WATER YEARS
NOV. 1950, 1953, 1963, 1969
B

FIGURE 3

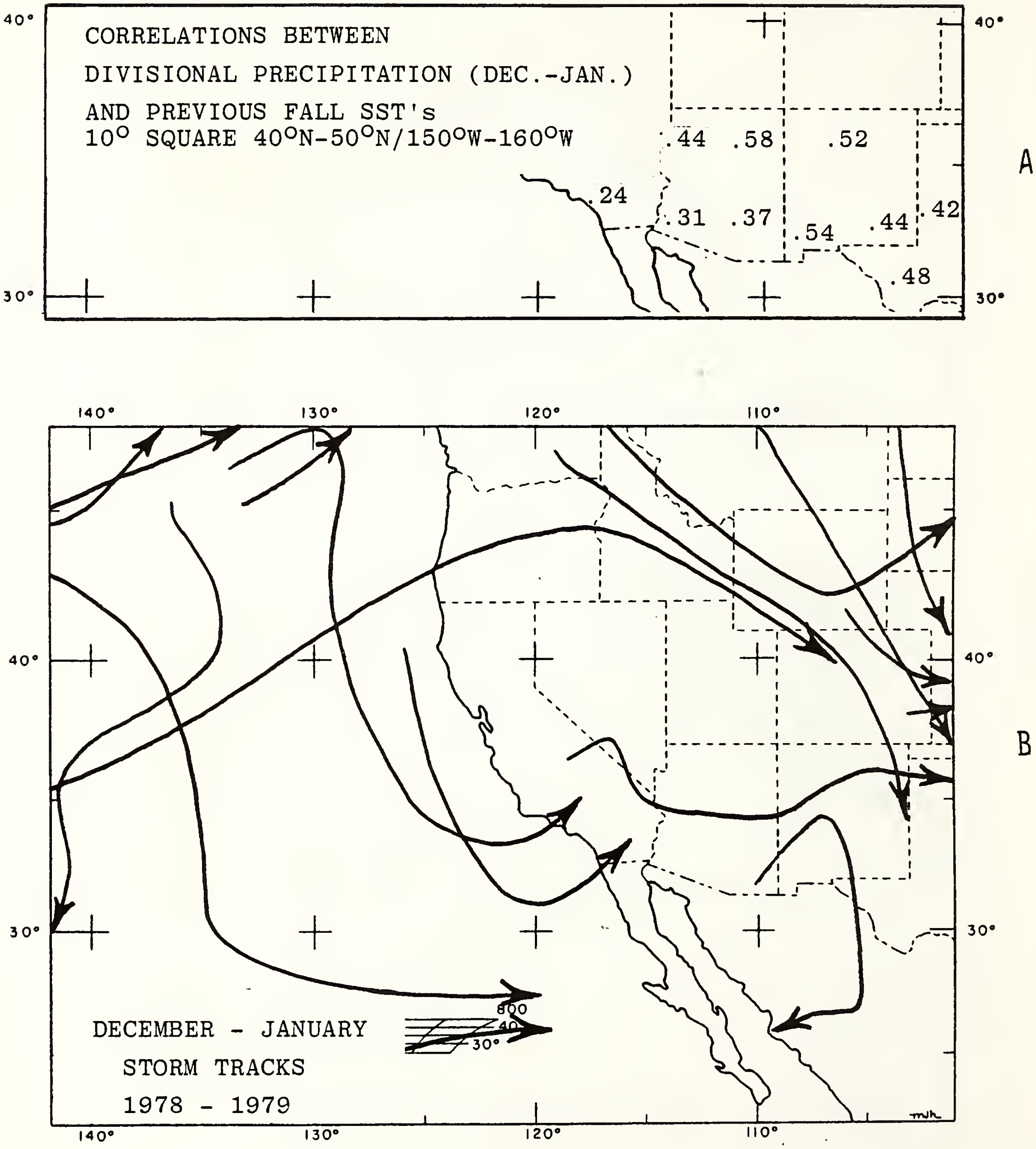
40°
40°
CORRELATIONS BETWEEN
DIVISIONAL PRECIPITATION (DEC.-JAN.)
AND PREVIOUS FALL SST's
10° SQUARE 40°N-50°N/150°W-160°W
.44
.58
.52
.24
.31
.37
.54
.44
.42
.48
30°
30°
A
140°
130°
120°
110°
40°
40°
B
30°
30°
800
40
30°
DECEMBER - JANUARY
STORM TRACKS
1978 - 1979
140°
130°
120°
110°
mh

FIGURE 4

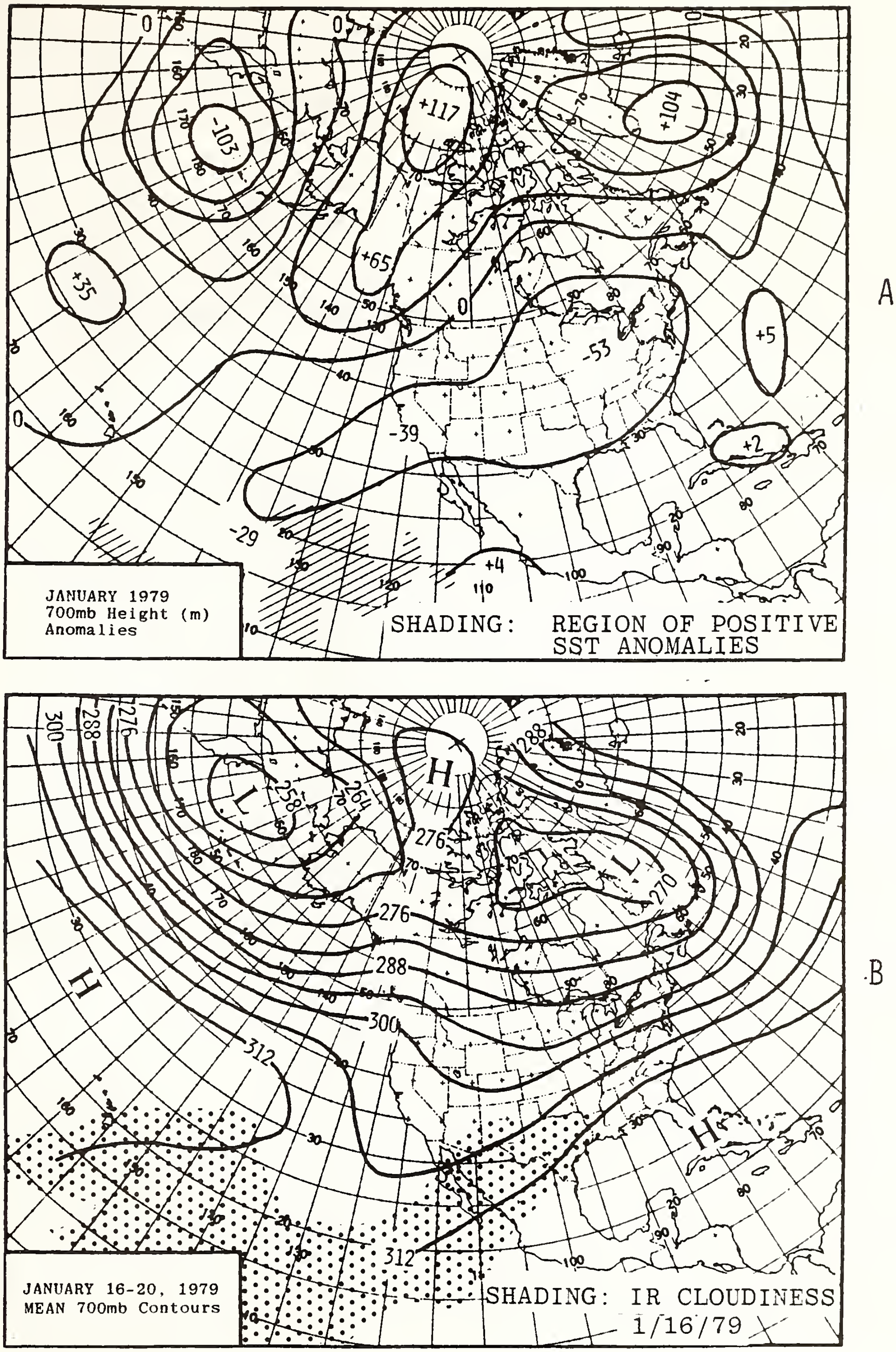 A
JANUARY 1979
700mb Height (m)
Anomalies
SHADING: REGION OF POSITIVE SST ANOMALIES
-103
+117
+104
+65
+35
0
-53
+5
-39
+2
-29
+4
B
JANUARY 16-20, 1979
MEAN 700mb Contours
SHADING: IR CLOUDINESS 1/16/79
H
L
258
264
276
288
300
312
270

FIGURE 5

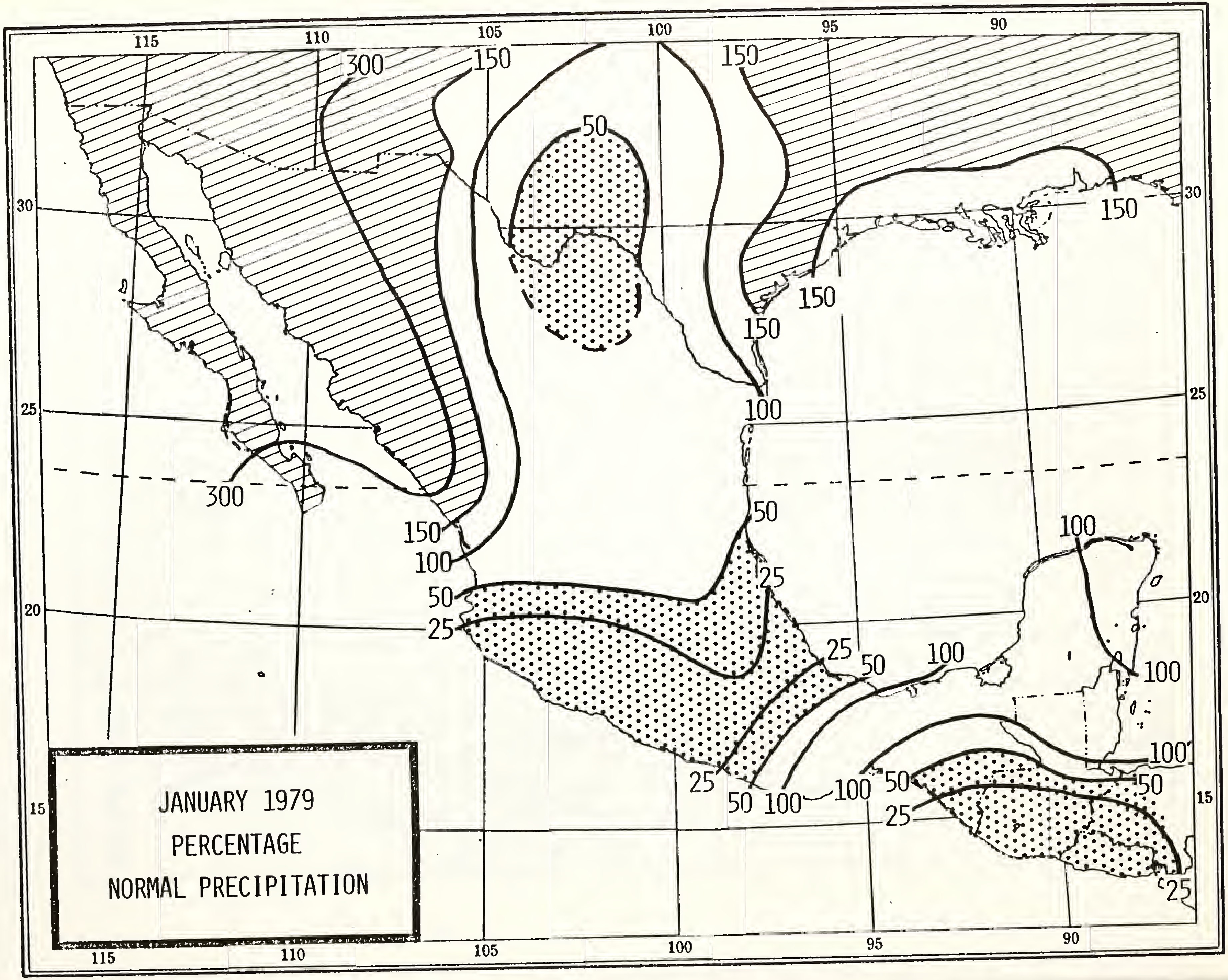
JANUARY 1979
PERCENTAGE
NORMAL PRECIPITATION
115
110
105
100
95
90
30
25
20
15
300
150
50
150
150
150
150
100
300
150
100
50
25
50
25
25
50
100
100
100
100
100
50
25
50
100
100
50
25
25

FIGURE 6

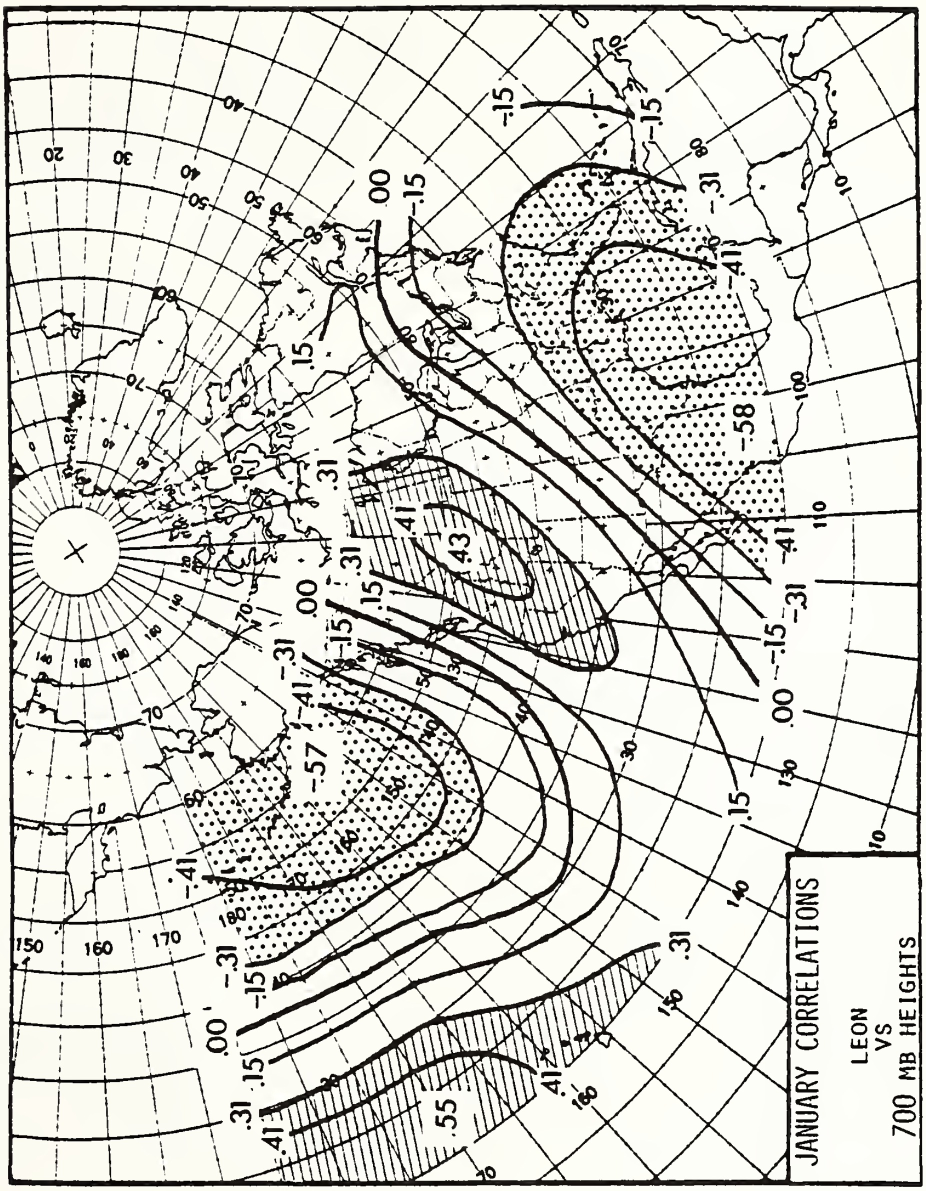
JANUARY CORRELATIONS
LEON
VS
700 MB HEIGHTS
.55
.41
.31
.15
.00
-.15
-.31
-.41
-.57
-.58
.43
150
160
170
10
110
130
140

FIGURE 7

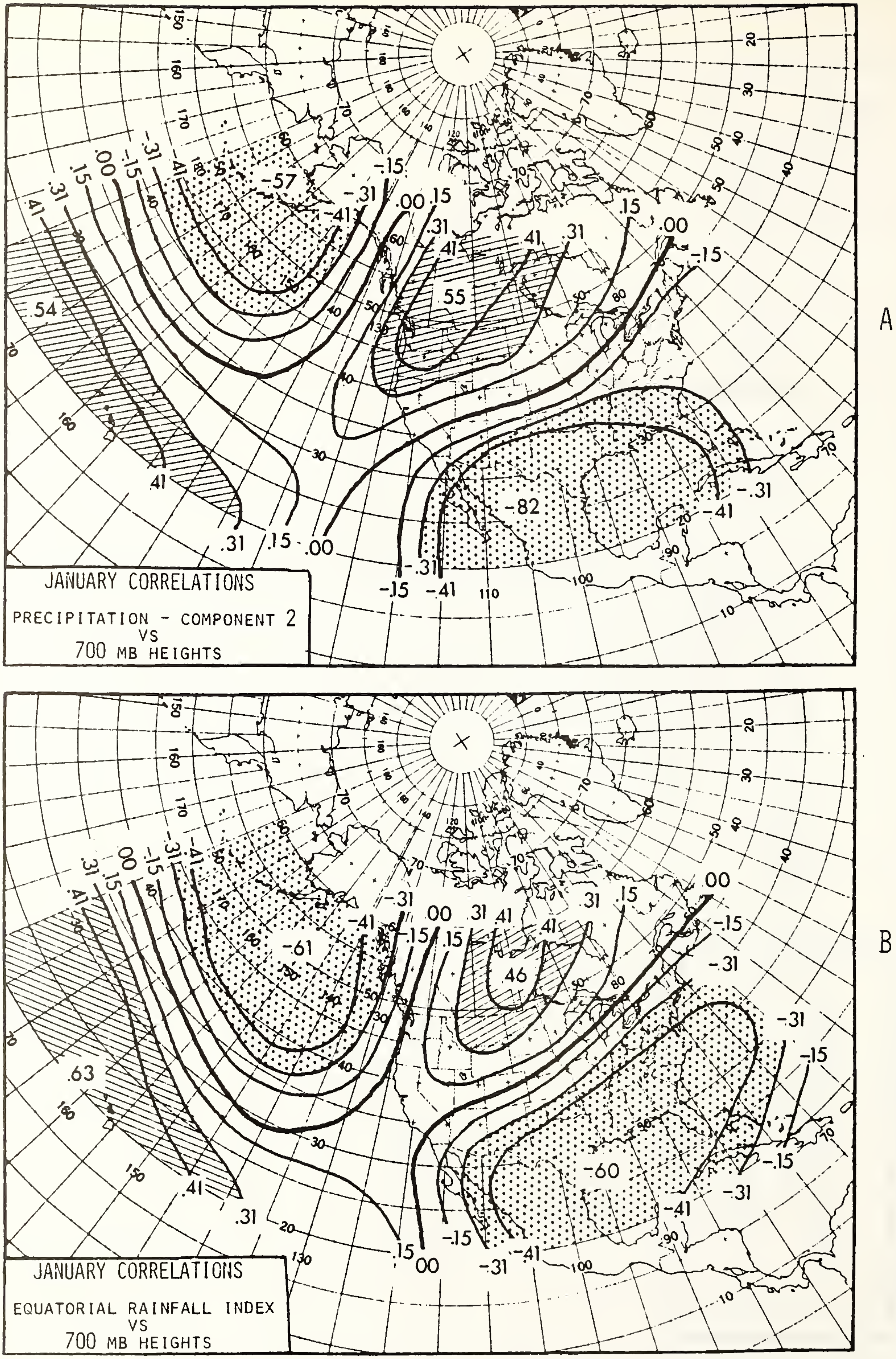

JANUARY CORRELATIONS

PRECIPITATION - COMPONENT 2
VS
700 MB HEIGHTS

JANUARY CORRELATIONS

EQUATORIAL RAINFALL INDEX
VS
700 MB HEIGHTS

FIGURE 8

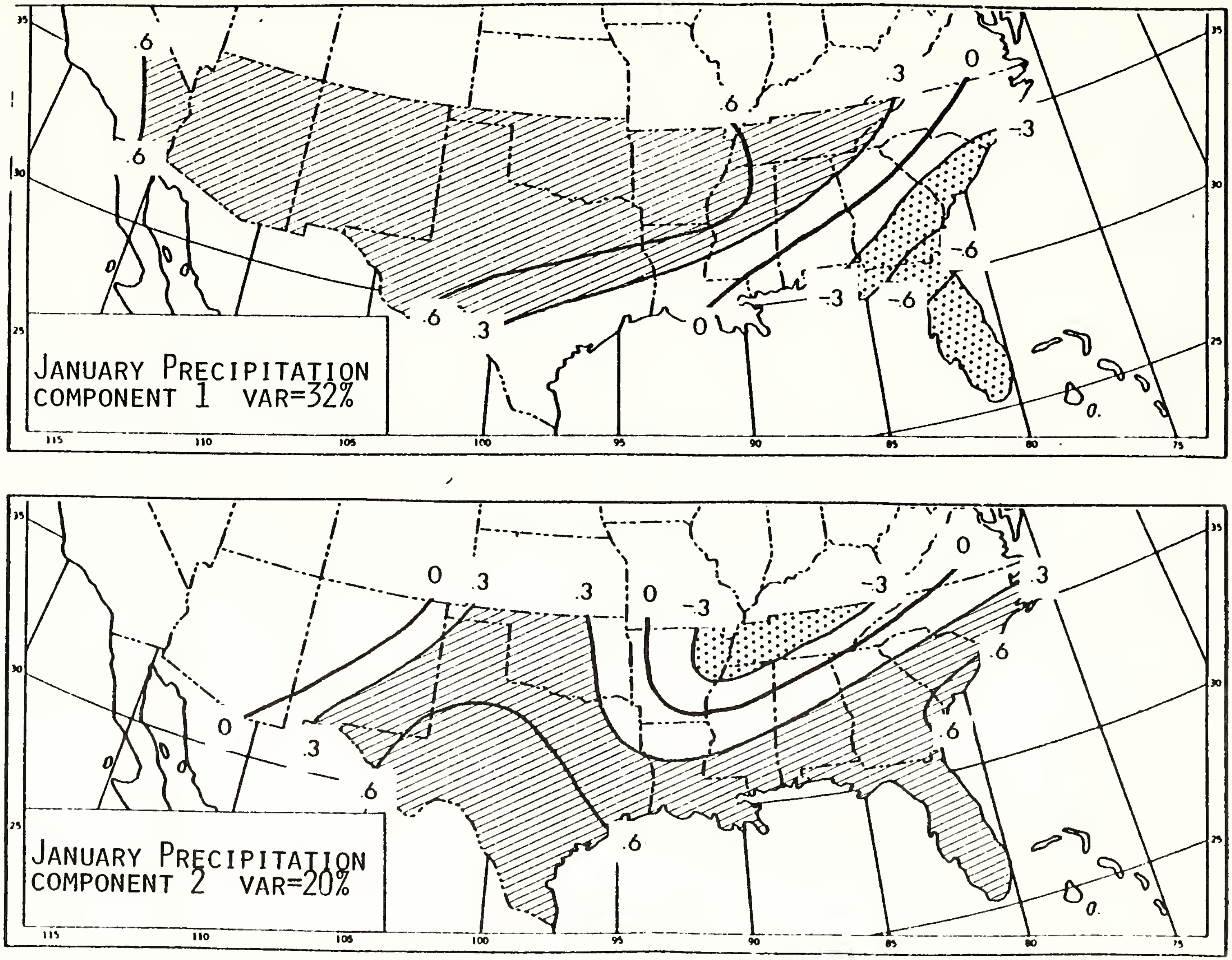
JANUARY PRECIPITATION COMPONENT 1 VAR=32%

JANUARY PRECIPITATION COMPONENT 2 VAR=20%

FIGURE 9

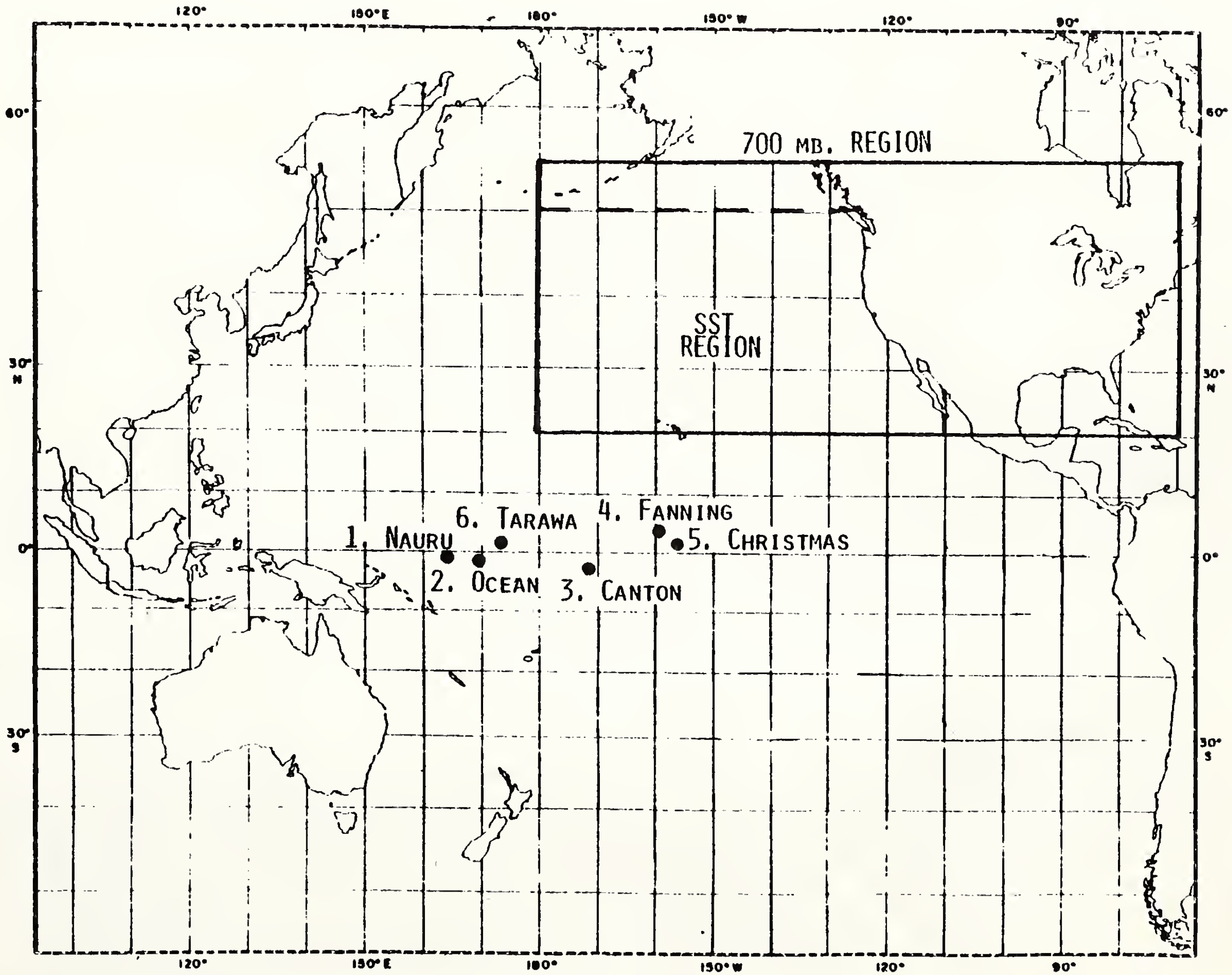
120°
150°E
180°
150° W
120°
90°
60°
30° N
0°
30° S
700 MB. REGION
SST REGION
1. NAURU
2. OCEAN
3. CANTON
4. FANNING
5. CHRISTMAS
6. TARAWA

FIGURE 10

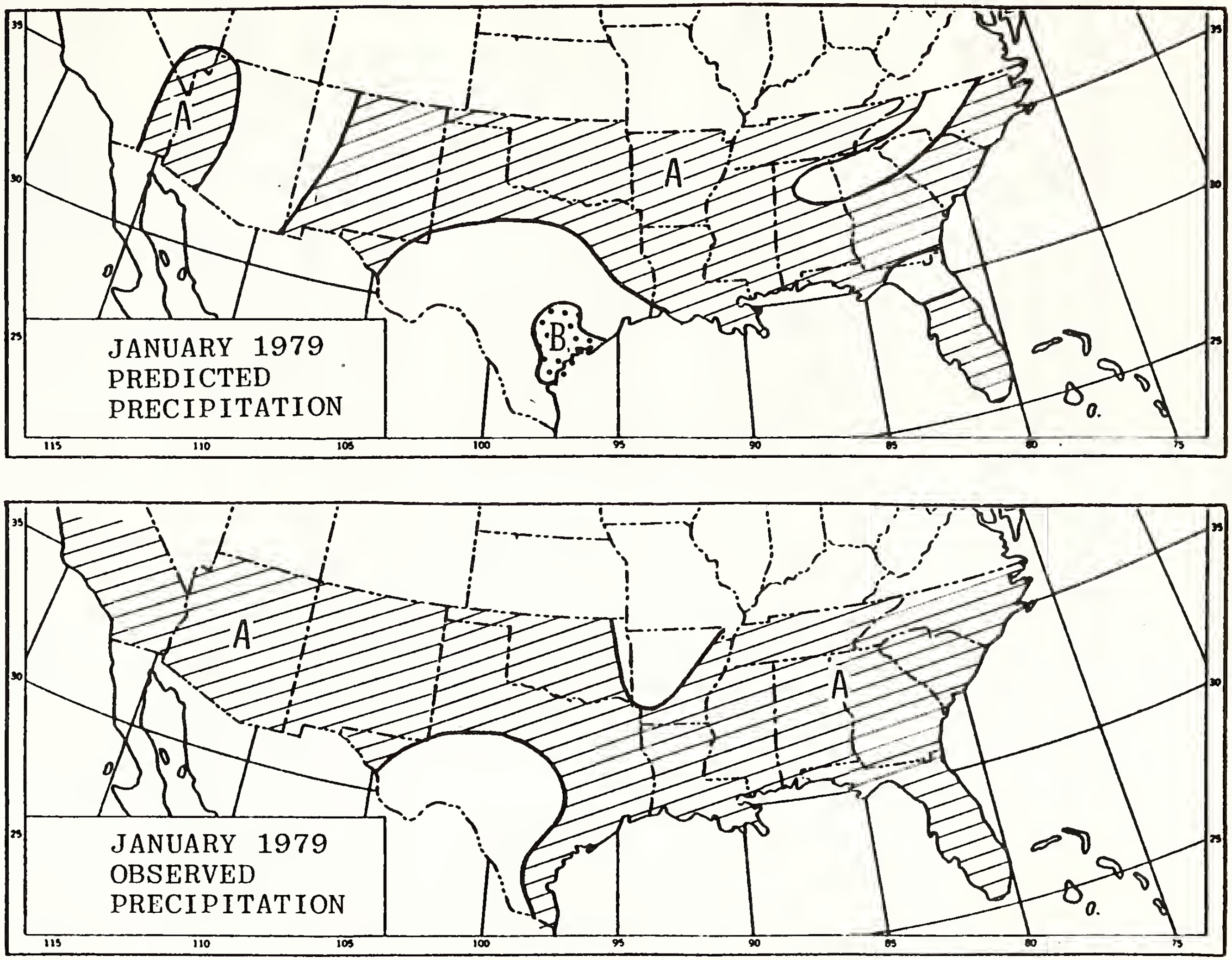
JANUARY 1979
PREDICTED
PRECIPITATION
A
A
B
JANUARY 1979
OBSERVED
PRECIPITATION
A
A
35
30
25
115
110
105
100
95
90
85
80
75

FIGURE 11

# The Large Scale Upper-Tropospheric Circulation Associated with Unusually Heavy Rainfall over the Southern United States, Spring 1979

Carl O. Erickson
NOAA/NMC/CAC
Washington, D. C.

During both winter and spring 1979, large areas of the southern United States received more than 150% of normal precipitation (see papers by Wagner and Dickson). Within this generally widespread wet period were some extremely heavy rainfalls over local or statewide areas (Table 1). New records for monthly or 24h totals were set at several stations. Floods occurred.

The purpose of this report is to show that the widespread excessive precipitation was closely associated with a persistent large-scale southward displacement of the upper-tropospheric westerly flow and mean subtropical jet stream position, leading to increased cyclonic activity over the lower latitudes of the southern United States. Additionally, the upper level westerly flow was generally stronger than normal, thus providing increased kinetic energy for cyclone development.

Although other factors, such as abundant moisture and slowly moving weather systems, obviously contributed to the heavy rainfalls, the large-scale southward displacement and stronger than normal upper-tropospheric flow was a continuing and seemingly vital feature. This anomaly existed not only over the U. S. but over much of the Northern Hemisphere as well, and it persisted for many months. Because of its persistence and near-hemispheric character, it is the feature emphasized in this report.

Figure 1 shows the numerical operational 200-mb synoptic data and analysis over the eastern U. S. for 0000 GMT, 4 March 1979 -- a time of extremely heavy rainfall over Alabama and the western Florida Panhandle. The pattern is typical of many individual heavy rain situations. A deep trough is approaching from the west. The subtropical jet is displaced southward over the Gulf of Mexico. Similarly, the polar jet is displaced far southward over Texas, almost merging with the subtropical jet. Strongly difluent flow exists over the heavy rain areas of Alabama and western Florida, between the two jet streams.

Mean 200-mb isotachs for each of the three spring months, March, April, and May 1979, are presented in Figure 2. Also shown are the axes of mean wind maxima (heavy dashed lines). The analyses cover the somewhat larger area of 0-48N, 75-150W -- essentially, most of North America and the eastern North Pacific. In each of the three months, it is seen that the mean wind maxima are located south of their ten-year (1968-78) monthly average positions and have above-average core speeds. The mean isotach patterns in Figure 2 are derived from once-a-day grid point values from the global (48N to 48S) wind analyses prepared by the NMC.

Table 1. --Eight episodes of extremely heavy rainfall over the southern United States during winter - spring 1979.

| | | | |
|---|---|---|---|
| JAN 13-15 | Hilo, Hawaii | 13.49" | (3-day total) |
| | | | (January total 32.24") * |
| | Kukaiau, Hawaii | 12.98" | (Jan 15) |
| | | 32.04" | (3-day total) |
| | | | (January total 60.44") |
| FEB 19-20 | Hilo, Hawaii | 22.28" | (24h total) * |
| | | 28.37" | (2-day total) |
| | | | (February total 45.55") |
| MAR 3-4 | Pensacola, Fla | 11.10" | (Mar 3) * |
| | Hickory, Miss | 11.62" | (Mar 4) |
| | | 13.09" | (2-day total) |
| | SW Ala. (several stns) | (2-day totals of 6.00" to 10.00") | |
| | remainder of Alabama | (generally 3.00" to 8.00") | |
| | Lake Toxaway, N.C | (approximately 10.00" in 24h) | |
| | Jocassee, S.C | (approximately 9.00" in 24h) | |
| APR 12-13 | Louisville, Miss | 10.25" | (Apr 13) |
| | | 19.60" | (2-day total) |
| | Reform, Ala | 12.72" | (Apr 13) |
| | | 15.90" | (2-day total) |
| | several other stations in E. Miss. and W. Ala | (2-day totals of 10.00" to 15.00") ** | |
| APR 18-20 | Conroe, Tex | 11.61" | (Apr 19) |
| | | 15.61" | (2-day total) |
| | Mountain Home, Tex | 4.00" | in one hour (Apr 18) |
| | Beaumont, Tex | 8.83" | (Apr 20) |
| APR 21-22 | Jeanerette, La | 10.15" | (Apr 22) |
| | | 11.31" | (2-day total) |
| | Lafayette, La | 10.55" | (2-day total) |
| | Baton Rouge, La | 8.80" | (2-day total) |
| APR 25 | Hialeah, Fla | 16.39" | |
| | Ft. Lauderdale, Fla | 14.59" | |
| | Miami, Fla | (24h total of over 16.00" on April 24-25) * | |
| MAY 8 | Tampa, Fla | 11.45" | |
| | Tarpon Springs, Fla | 11.09" | |

* new records for individual stations.

** beginning of record floods in the Pearl River Valley of Mississippi. Widespread but less severe flooding elsewhere in the Deep South.

Table 2 shows that area-averaged 200-mb wind speeds and area-averaged kinetic energy for the entire analysis area of Figure 2 were also above their ten-year monthly averages. As with the southward displacement of the jet stream, this was true for each of the three months, March, April, and May 1979.

Table 2. --Percentage departures from 1968-78 base period for area-mean values of 200-mb zonal wind, total wind, and kinetic energy. Area is 75-150W, 0-48N.

| | Zonal Wind | Total Wind | K.E. |
|---|---|---|---|
| March 1979 | + 7.4 | + 7.8 | + 15.5 |
| April 1979 | + 8.9 | + 11.0 | + 20.3 |
| May 1979 | + 11.5 | + 12.9 | + 21.5 |

Figures 3, 4, and 5 together show large-scale analyses of the 200-mb streamfunction anomaly for each of nine months, beginning with October 1978 and continuing through June 1979. Each figure contains three months. The anomalies are calculated from NMC gridpoint u and v components and are with reference to monthly mean wind data for the 1968-78 base period. A 1-2-1 smoothing has been applied for better month-to-month continuity. Negative anomalies (in the Northern Hemisphere) correspond to a southward displacement of the westerly flow and generally above normal cyclonic activity. Thus, enhanced mean westerly flow exists equatorward of negative centers, and reduced mean westerly flow exists poleward of such centers. In Figures 3, 4, and 5, northern hemisphere anomalies $<-6$ are lightly shaded; anomalies $<-18$ are heavily shaded.

Overall, two features stand out:

(1) the large and increasingly negative anomaly over the western half of the Northern Hemisphere during late fall 1978 and winter 1979, and its persistence (with only moderate weakening) through June 1979;

(2) within the large negative area, the maintenance of individual low centers over periods of several consecutive months.

Over the Gulf of Mexico and southern United States it is obvious that during March and April 1979, (1) and (2) above would tend to result in increased cyclonic activity and increased rainfall. A similar argument applies to Hawaii during the earlier January-February period. The timing and locations of some of the extreme rainfalls in Table 1 are consistent with this idea.

The correlogram of Figure 6 gives evidence that mean monthly zonal wind components at 200 mb (at subtropical latitudes) tend to propagate from west to east. The data base is 11 years of monthly mean zonal wind components, March 1968 through February 1979 (annual cycle removed). For simultaneous data (zero lag), the correlation between the gridpoint data at 28.7N, 90W and the data at the same latitude at 140W is +.23. This is just at the 99% level of significance for 132 pairs. However, for lags of -1 to -2 months, the coefficients are larger, indicating the eastward-moving tendency.

The foregoing reinforces the visual impression one gets from the anomaly patterns of Figures 3, 4, and 5. In those figures there is the suggestion of a gross but ill-defined eastward propagation of the large area of negative anomaly during winter and spring 1979.

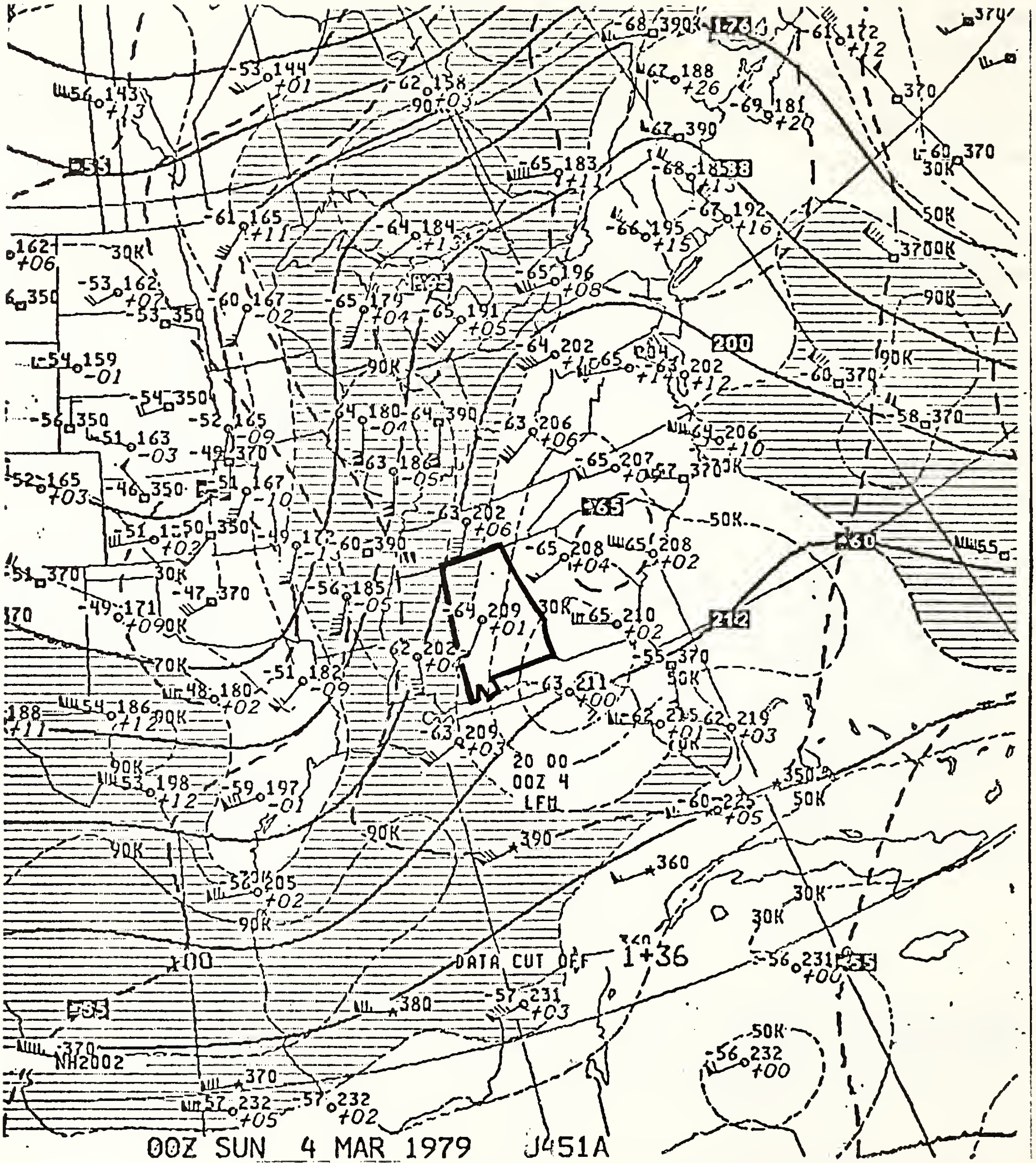

Figure 1. --Numerical operational 200-mb analysis for 0000 GMT, 4 March 1979.

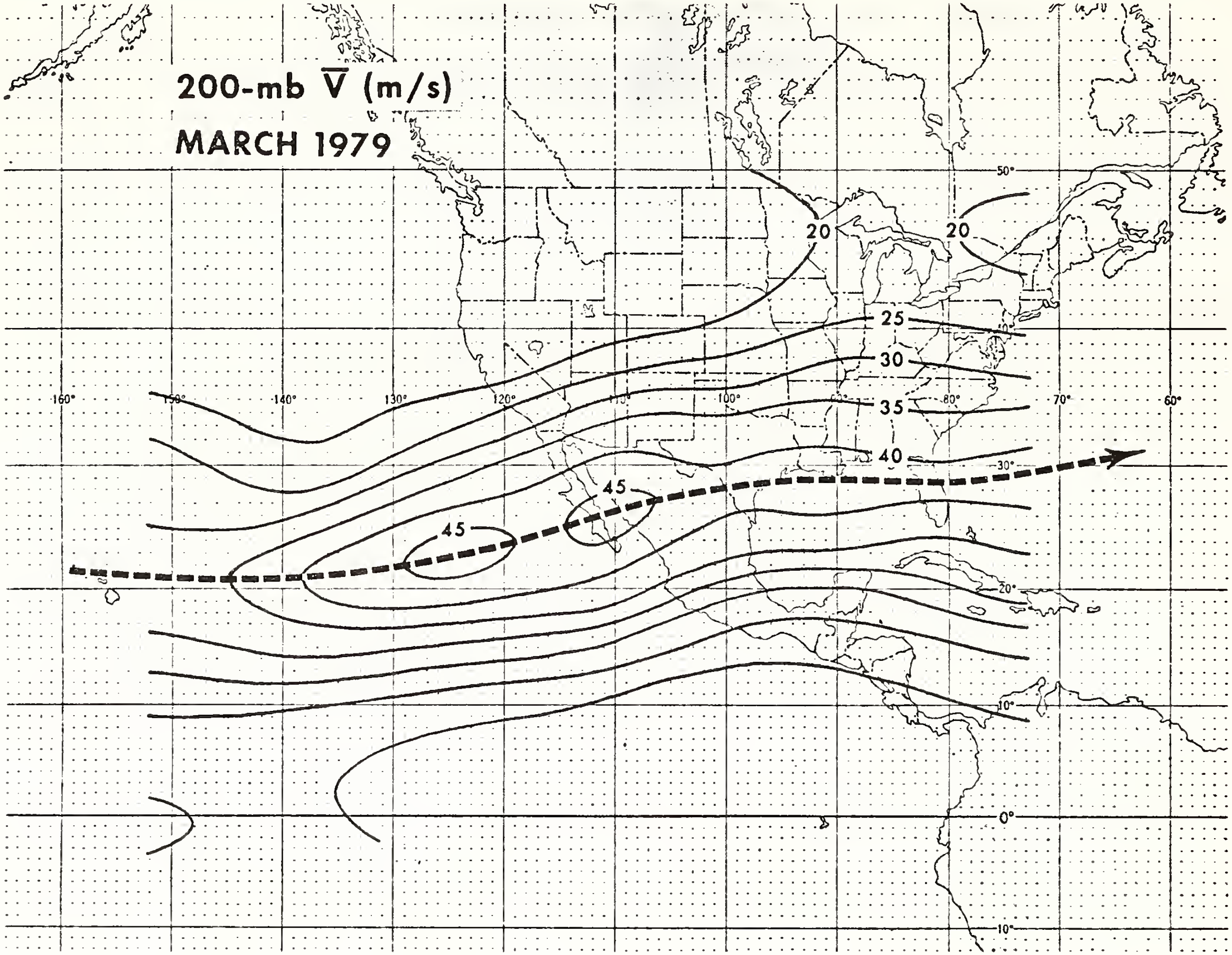

Figure 2a --Monthly mean 200-mb isotachs (m $s^{-1}$) for March 1979. Heavy dashed line marks mean windspeed maximum.

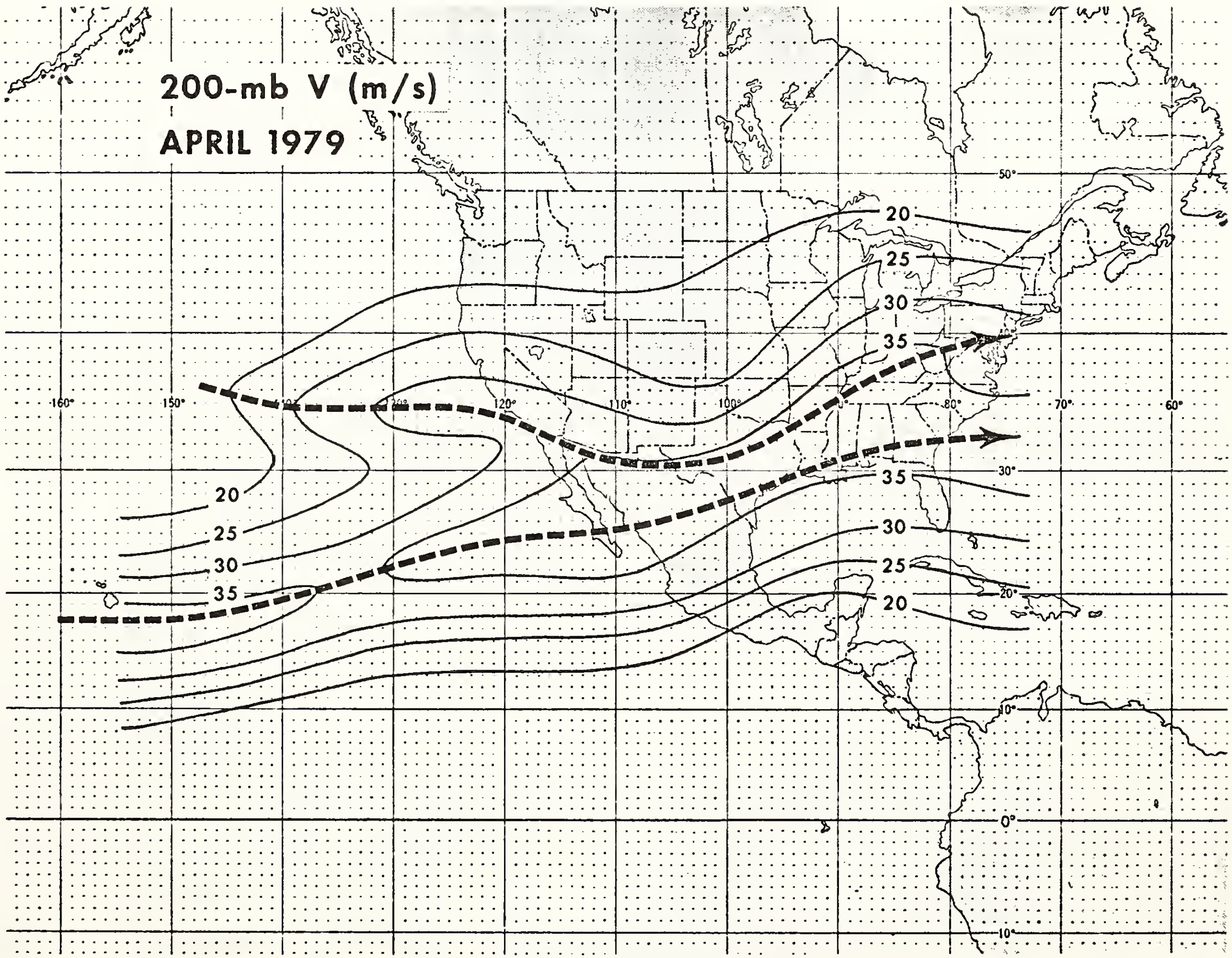

Figure 2b. --Same as Figure 2a, but for April 1979.

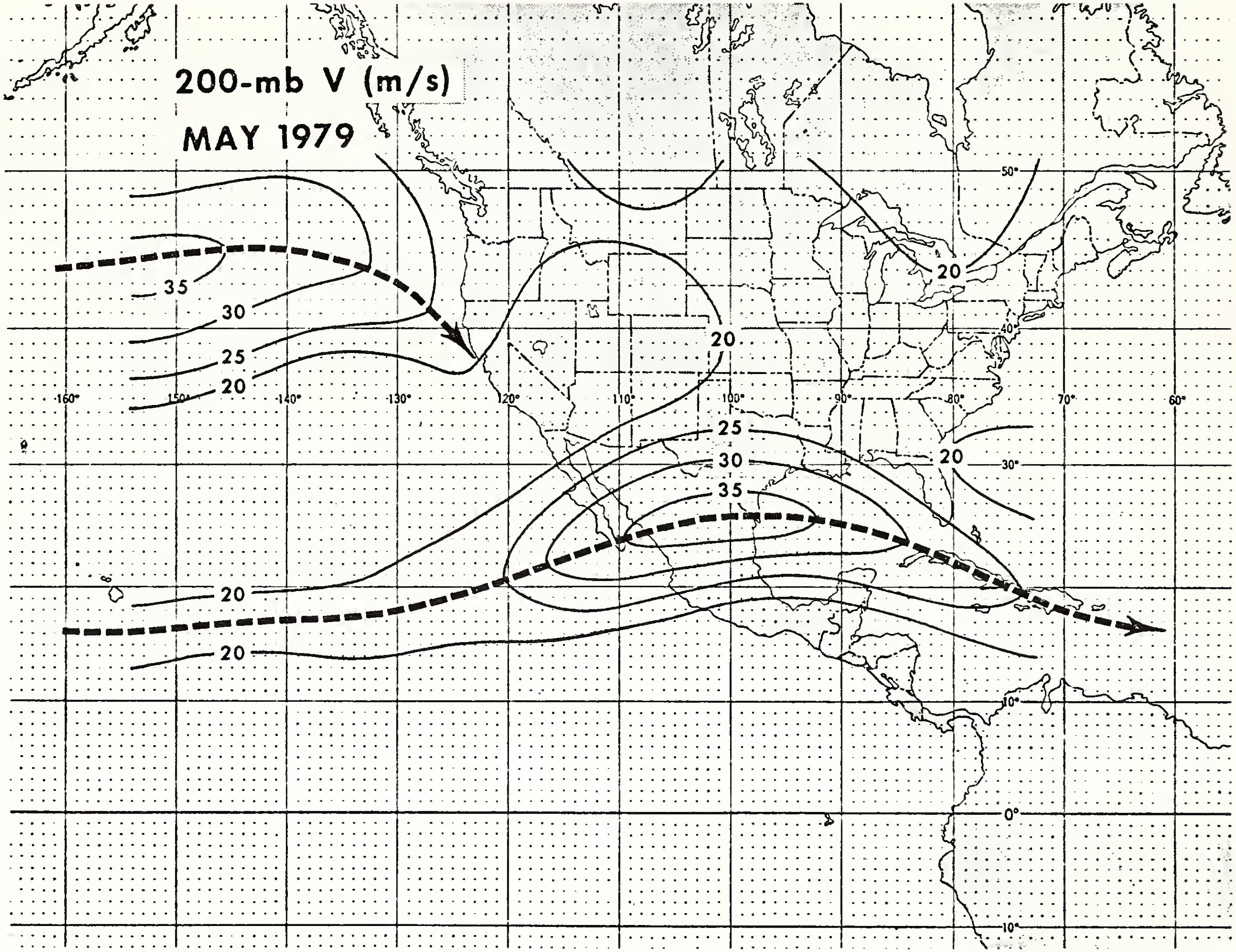

Figure 2c. --Same as Figure 2a, but for May 1979.

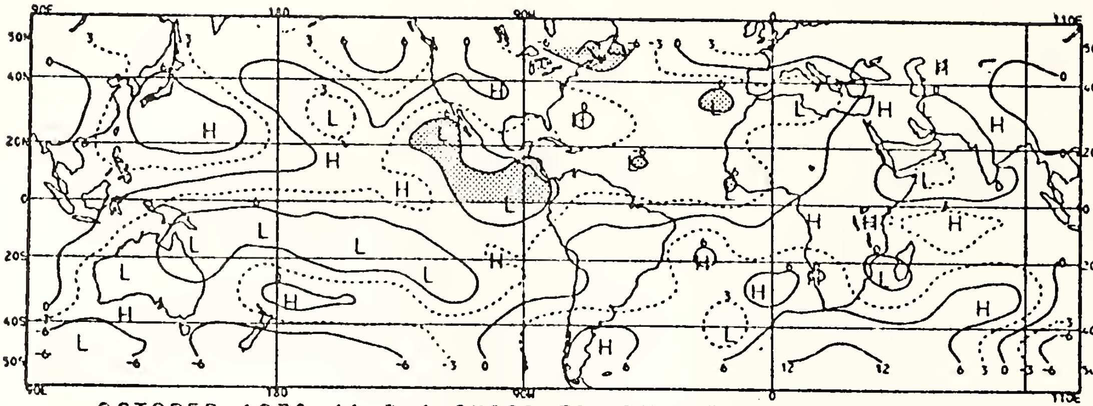

OCTOBER 1978 (1+2+1 SMOOTHED) STREAMFUNCTION ANOMALY(10)200MB

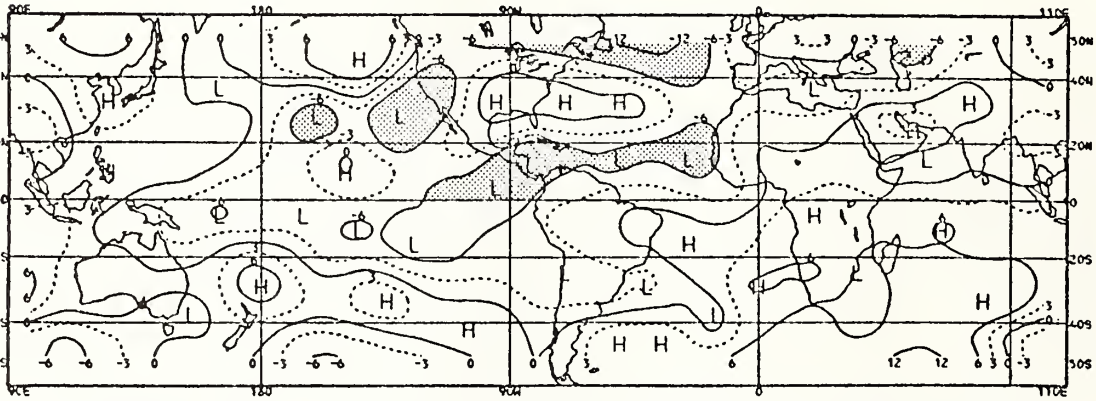

NOVEMBER 1978 (1+2+1 SMOOTHED) STREAMFUNCTION ANOMALY(10)200MB

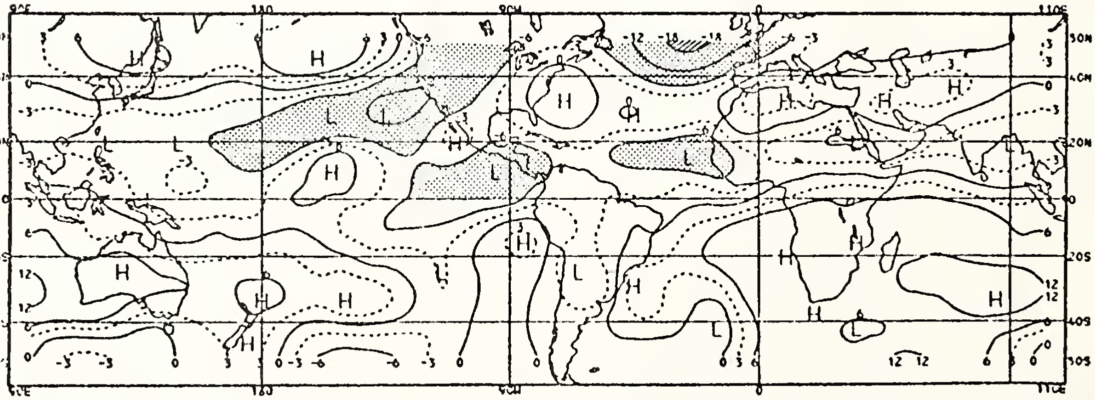

DECEMBER 1978 (1+2+1 SMOOTHED) STREAMFUNCTION ANOMALY(10)200MB

Figure 3. --Monthly mean anomalies of the 200-mb streamfunction for October 1978, November 1978, and December 1978. Anomalies are with respect to monthly means from the ten-year base period 1968-78. Northern hemisphere areas of negative anomaly < -6 are lightly shaded; areas < -18 are heavily shaded.

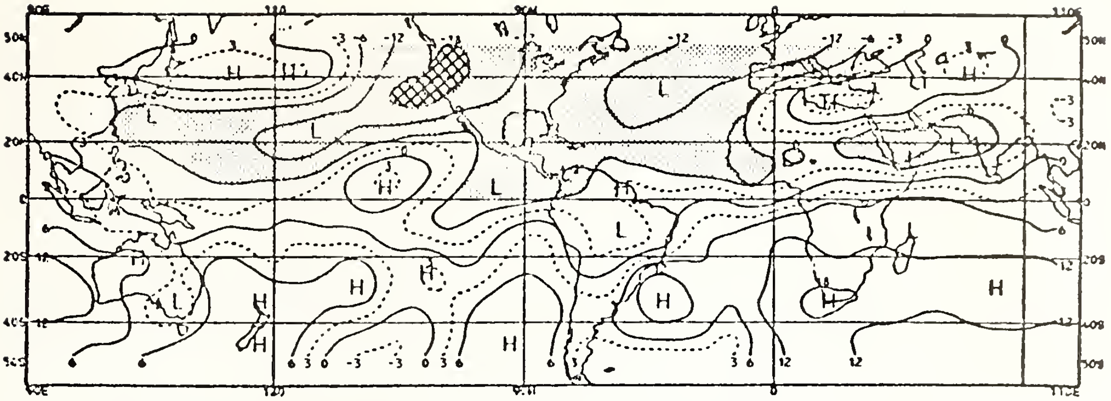

JANUARY 1979 (1+2+1 SMOOTHED) STREAMFUNCTION ANOMALY(10)200MB

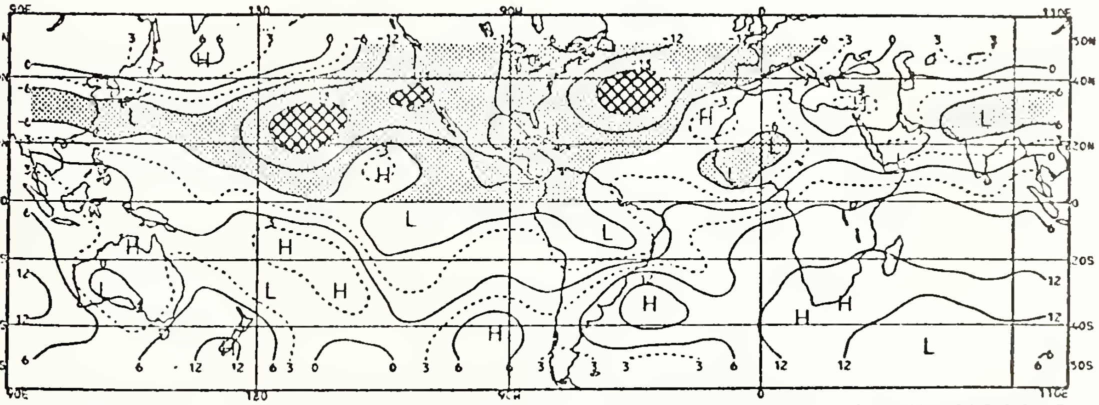

FEBRUARY 1979 (1+2+1 SMOOTHED) STREAMFUNCTION ANOMALY(10)200MB

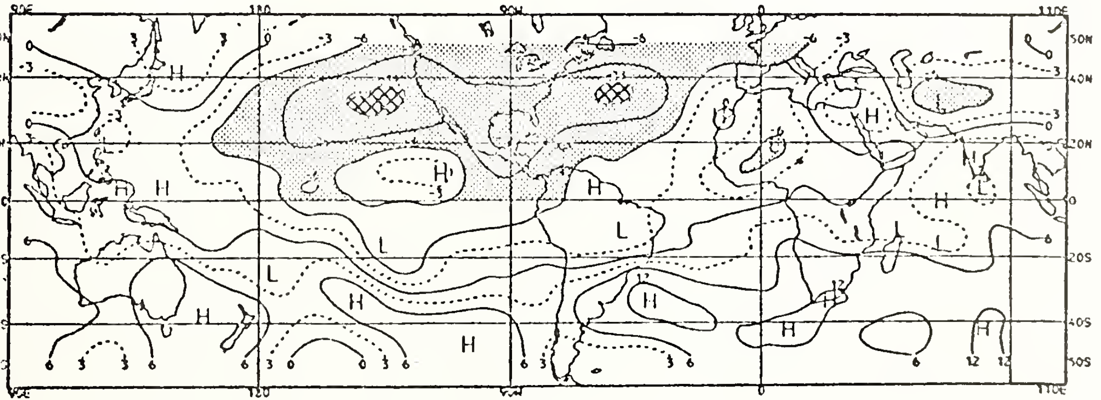

MARCH 1979 (1+2+1 SMOOTHED) STREAMFUNCTION ANOMALY(10)200MB

Figure 4. --Same as Figure 3, for January 1979, February 1979, and March 1979.

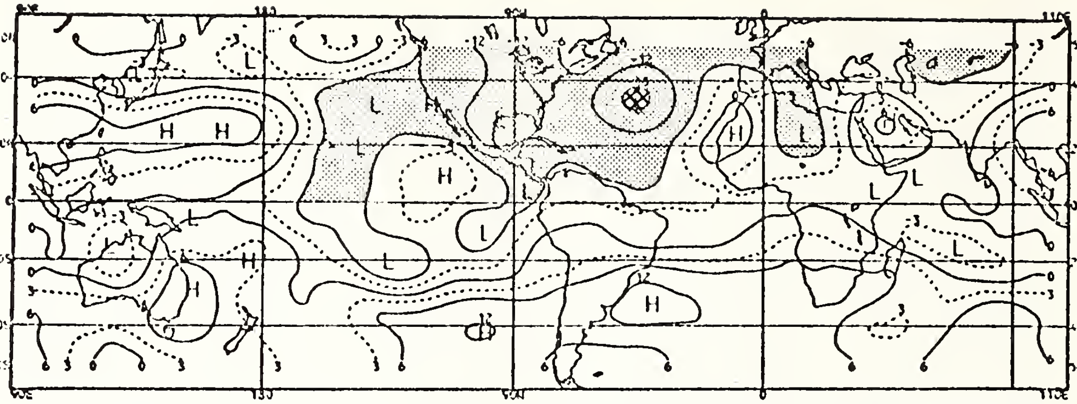

APRIL 1979 (1+2+1 SMOOTHED) STREAMFUNCTION ANOMALY(10)200MB

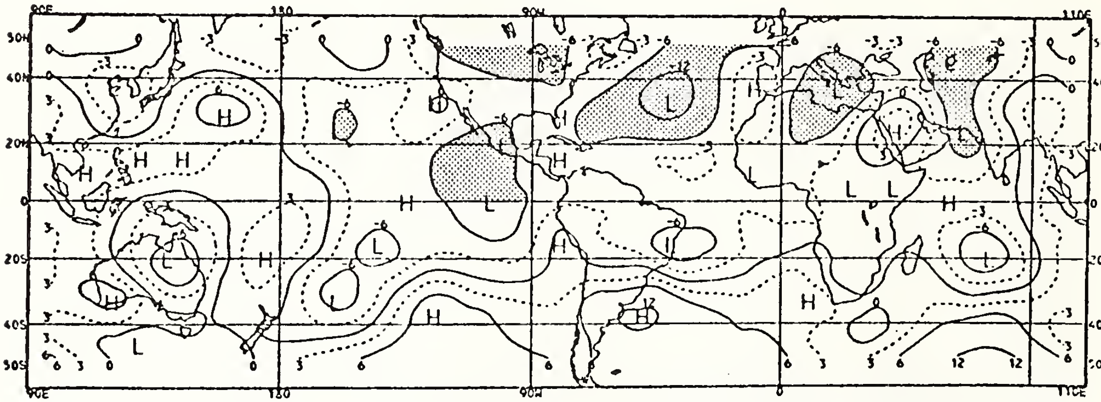

MAY 1979 (1+2+1 SMOOTHED) STREAMFUNCTION ANOMALY(10)200MB

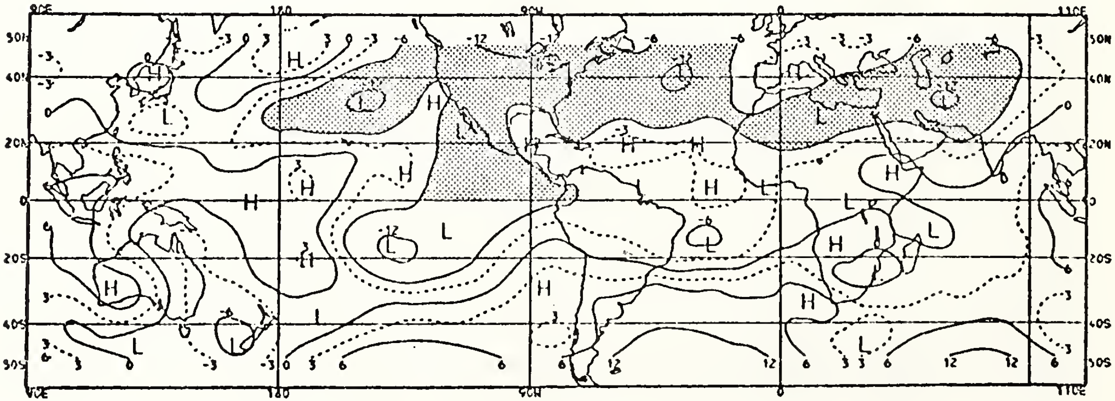

JUNE 1979 (1+2+1 SMOOTHED) STREAMFUNCTION ANOMALY(10)200MB

Figure 5. --Same as Figure 3, for April 1979, May 1979, and June 1979.

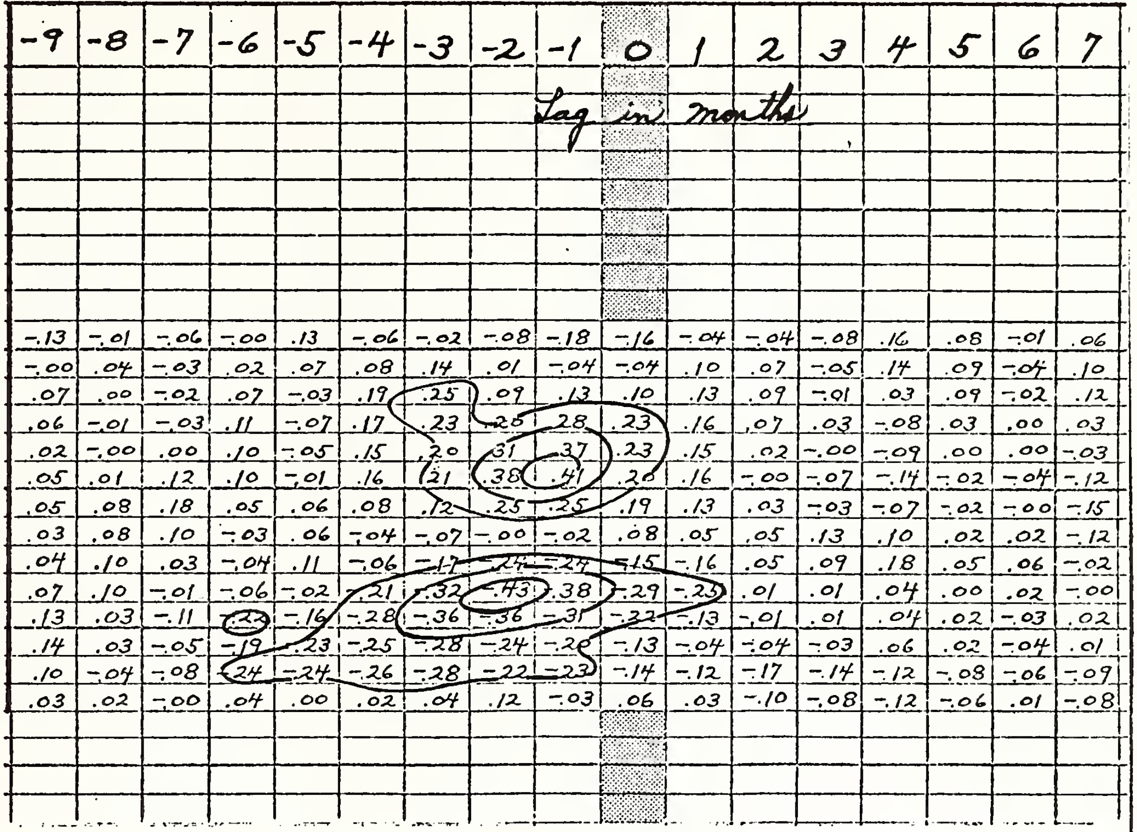

| Latitude | -9 | -8 | -7 | -6 | -5 | -4 | -3 | -2 | -1 | 0 | 1 | 2 | 3 | 4 | 5 | 6 | 7 |
|---|---|---|---|---|---|---|---|---|---|---|---|---|---|---|---|---|---|
| | | | | | | | | | Lag in months | | | | | | | | |
| 44.7 | -.13 | -.01 | -.06 | -.00 | .13 | -.06 | -.02 | -.08 | -.18 | -.16 | -.04 | -.04 | -.08 | .16 | .08 | -.01 | .06 |
| 41.0 | -.00 | .04 | -.03 | .02 | .07 | .08 | .14 | .01 | -.04 | -.04 | .10 | .07 | -.05 | .14 | .09 | -.04 | .10 |
| 37.2 | .07 | .00 | -.02 | .07 | -.03 | .19 | .25 | .09 | .13 | .10 | .13 | .09 | -.01 | .03 | .09 | -.02 | .12 |
| 33.1 | .06 | -.01 | -.03 | .11 | -.07 | .17 | .23 | .25 | .28 | .23 | .16 | .07 | .03 | -.08 | .03 | .00 | .03 |
| 28.7 | .02 | -.00 | .00 | .10 | -.05 | .15 | .20 | .31 | .37 | .23 | .15 | .02 | -.00 | -.09 | .00 | .00 | -.03 |
| 24.2 | .05 | .01 | .12 | .10 | -.01 | .16 | .21 | .38 | .41 | .20 | .16 | -.00 | -.07 | -.14 | -.02 | -.04 | -.12 |
| 19.6 | .05 | .08 | .18 | .05 | .06 | .08 | .12 | .25 | .25 | .19 | .13 | .03 | -.03 | -.07 | -.02 | -.00 | -.15 |
| 14.7 | .03 | .08 | .10 | -.03 | .06 | -.04 | -.07 | -.00 | -.02 | .08 | .05 | .05 | .13 | .10 | .02 | .02 | -.12 |
| 9.9 | .04 | .10 | .03 | -.04 | .11 | -.06 | -.17 | -.24 | -.24 | -.15 | -.16 | .05 | .09 | .18 | .05 | .06 | -.02 |
| 5.0 | .07 | .10 | -.01 | -.06 | -.02 | -.21 | -.32 | -.43 | -.38 | -.29 | -.23 | .01 | .01 | .04 | .00 | .02 | -.00 |
| EQUATOR | .13 | .03 | -.11 | -.22 | -.16 | -.28 | -.36 | -.36 | -.31 | -.22 | -.13 | -.01 | .01 | .04 | .02 | -.03 | .02 |
| - 5.0 | .14 | .03 | -.05 | -.19 | -.23 | -.25 | -.28 | -.24 | -.20 | -.13 | -.04 | -.04 | -.03 | .06 | .02 | -.04 | .01 |
| - 9.9 | .10 | -.04 | -.08 | -.24 | -.24 | -.26 | -.28 | -.22 | -.23 | -.14 | -.12 | -.17 | -.14 | -.12 | -.08 | -.06 | -.09 |
| -14.7 | .03 | .02 | -.00 | .04 | .00 | .02 | .04 | .12 | -.03 | .06 | .03 | -.10 | -.08 | -.12 | -.06 | .01 | -.08 |

Figure 6. --Cross correlations between 200-mb monthly mean zonal wind components at 28.7N, 90W, and various latitudes at 140W. Negative lag means that the data at 140W lead the data at 28.7N, 90W. Positive lag means the reverse.

# TIROS-N Radiation Budget Over MONEX
# During 1979

P. Krishna Rao
Meteorological Satellite Laboratory, NESS, NOAA
Camp Springs, MD. 20233

The summer MONEX, an international scientific experiment to study the monsoon over India and adjacent regions, was carried out between May 1 and August 31, 1979. The experiment was a part of the Global Weather Experiment and observations were collected from aircraft, ships, satellites and other platforms for future analyses and interpretation. The Southwest monsoon came late in 1979 and was erratic during July and August. Some features of the monsoon circulation as seen in the earth-atmosphere radiation budget data derived from the TIROS-N satellite are illustrated in this study.

The radiation budget values were derived from the Advanced Very High Resolution Radiometer (AVHRR) data on board the TIROS-N operational satellite. The outgoing longwave radiation values were derived from the infrared window measurements and is an average of both day and night observations; the albedo values were derived from the visible channel measurements and correspond to daytime values. Some assumptions have been made in deriving these radiation budget quantities and caution should be exercised in using these data as absolute values in quantitative studies to estimate net heating. For example, it was assumed that the reflected solar radiation is diffuse and no corrections due to angular variations were incorporated. Similarly, the total outgoing longwave fluxes were derived from narrow spectral window channel values based on a relationship developed from model atmospheres.

The 1979 parameters are compared with the 1975 parameters because in 1975 the monsoon was considered to be very good.

Figure Legends

1. Outgoing longwave radiation, May 1979.

   High values of outgoing longwave radiation are over the Indian sub-continent and Saudi Arabia (310 $Wm^{-2}$) indicating relatively cloud free conditions. Shaded areas represent values less than 250 $Wm^{-2}$ and are located near the equator. These low values generally represent cloudy regions.

2. Outgoing longwave radiation, June 1979.

   The high values over India shifted northwestward to Pakistan and the high values over Saudi Arabia remained the same (310 $Wm^{-2}$). Low values over South India are associated with the advancing monsoon cloudiness and note that there are low values near the equator indicating persistent clouds in that region. A comparison of June 1979 radiation data with June 1975 indicated that the values in 1979 over Southern India were higher than in 1975, and this can be translated in terms of a weak monsoon in June 1979 compared to 1975.

3. Outgoing longwave radiation, July 1979.

   The high values of outgoing longwave radiation over India shifted more northwestward. High values are still 310 $Wm^{-2}$ indicating relatively no change in cloud conditions over these areas. However, the low values shifted more northeastward indicating a well established monsoon over most of India. During this period monsoon was very active over Southwest India.

4. Outgoing longwave radiation, August 1979.

   Relatively no change is shown in the high values over Pakistan and Saudi Arabia. A remarkable change in the low values occurred during this month which indicated a split in the radiation field. One part of the low values are located over the northern part of Bay of Bengal and another part was located near the equator. The split in the radiation field indicates the break in the cloud field and during this month, the monsoon was erratic.

5. Outgoing longwave radiation, September 1979.

   The radiation field shows that the monsoon circulation is near normal. Low radiation values associated with monsoon cloudiness covered most of South and Northeast India. These values are comparable to September 1975 values during which period the monsoon was considered to be a normal one.

6. Outgoing longwave difference, May (1979 - 1975)

   In 1975, the monsoon was active and it was considered to be one of the best monsoons during the last decade. The 1979 data are compared with the 1975 data; the shaded areas show that the outgoing longwave radiation was lower in 1979 compared to 1975 and this represents more clouds in 1979 than in 1975. More cloudiness existed near the equator and over the extreme northern sections of India during 1979. The cloudiness near the equatorial zone could be associated with the ECZ.

7. Outgoing longwave difference, June (1979 - 1975)

   Cloud cover during 1979 was confined more towards Arabian Sea rather than the Indian Subcontinent. The monsoon seems to be weak in 1979 compared to 1975.

8. Outgoing longwave difference, July (1979-75).

   The major difference is over Bay of Bengal and in this region more cloudiness prevailed over Central and Southern parts of the Bay of Bengal and Central Indian Ocean in 1979 than in 1975. Monsoon activity was weak over most of Indian Subcontinent during this period.

9. Outgoing longwave difference, August (1979-75).

   One could notice the major difference in the radiation fields. In 1979 there were fewer clouds over the Indian subcontinent indicating a weak monsoon. The monsoon activity seems to have affected only the northeast part of India and Burma.

10. Outgoing longwave difference, September (1979-75)

    In 1979, the maximum cloudiness is confined to East coast of India; other regions seems to be less active compared to 1975. Equatorial Indian Ocean area also shows fewer clouds in 1979 compared to 1975.

11. Difference (1979-75) in latitudinal average (47.5E - 105E) Outgoing longwave radiation. The shaded areas indicate that the monsoon to be relatively **more active** in 1979 compared to 1975. The figure shows that in 1979 the monsoon was relatively more active in July and September than in 1975 at the lower latitudes (up to 15N) and erratic during July and August.

12. 200mb zonal wind.

    Weekly average values of 200mb zonal wind for the region were used. Only the zero contour (ridge line) is shown to show the separation between the westerlies and the easterlies. During the early part of June the westerlies extended up to 20N and started moving northward during the week of June 16. The onset of the monsoon (about June 15) which was delayed in

1979, was probably due to the southward extension of the zonal westerlies. As they shifted north, the monsoon advanced northward and eastward from the Indian Ocean.

An extensive study has to be performed relating the satellite data with other conventional data collected during MONEX to understand the 1979 situation.

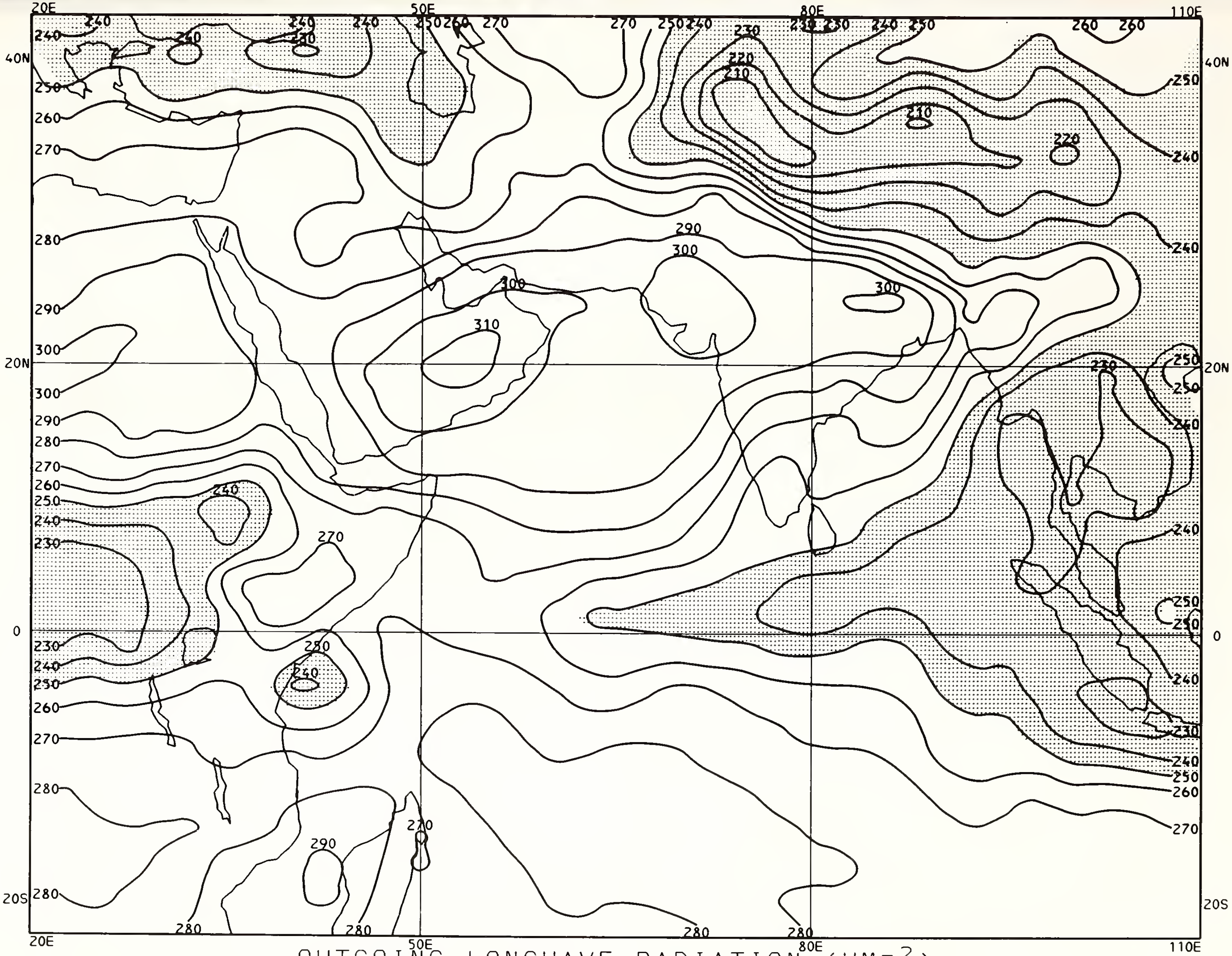

OUTGOING LONGWAVE RADIATION $(WM^{-2})$
31 DAYS ENDING MAY 31, 1979 TIROS-N

Figure 1

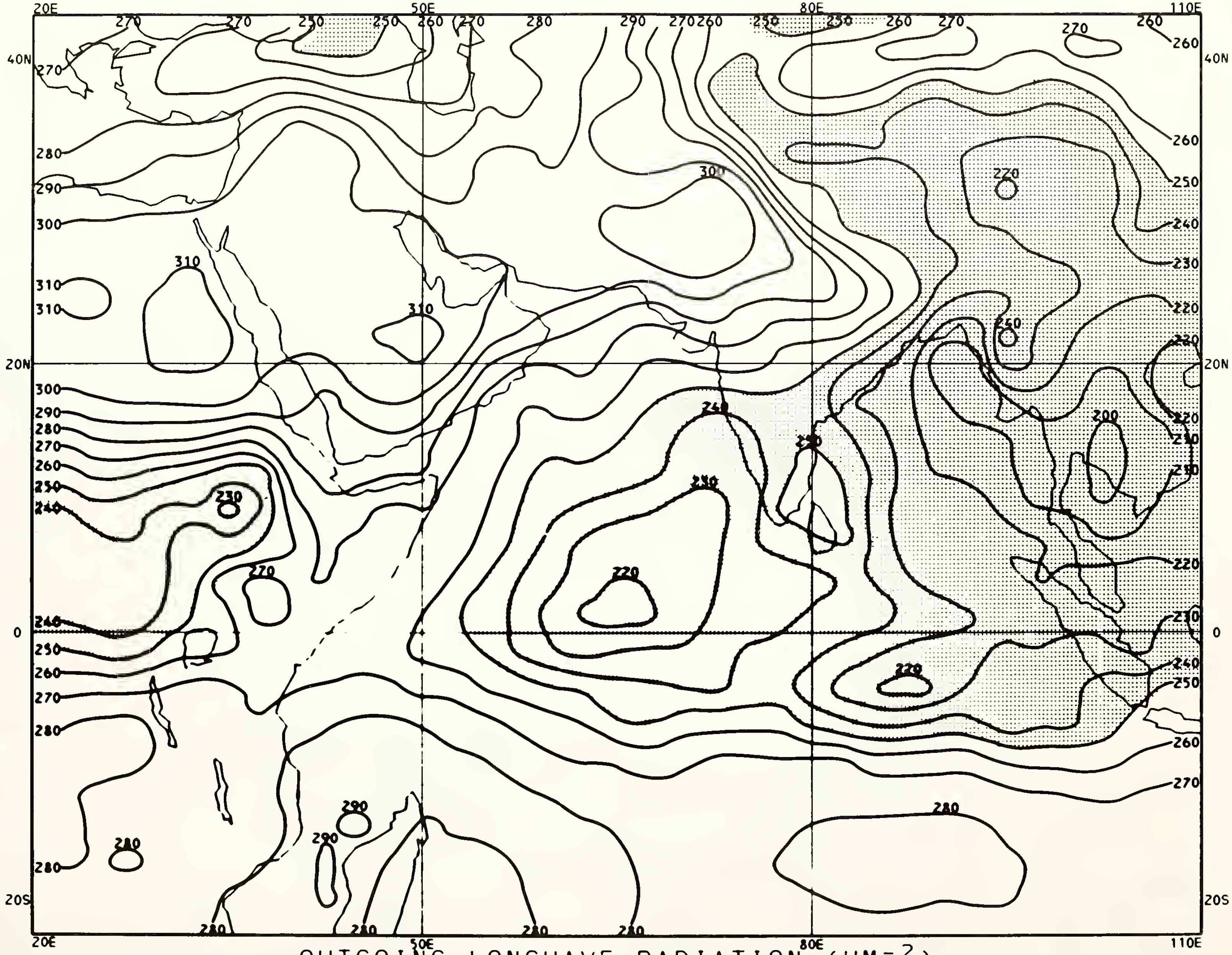

OUTGOING LONGWAVE RADIATION (WM$^{-2}$)
26 DAYS ENDING JUNE 30, 1979 TIROS-N

Figure 2

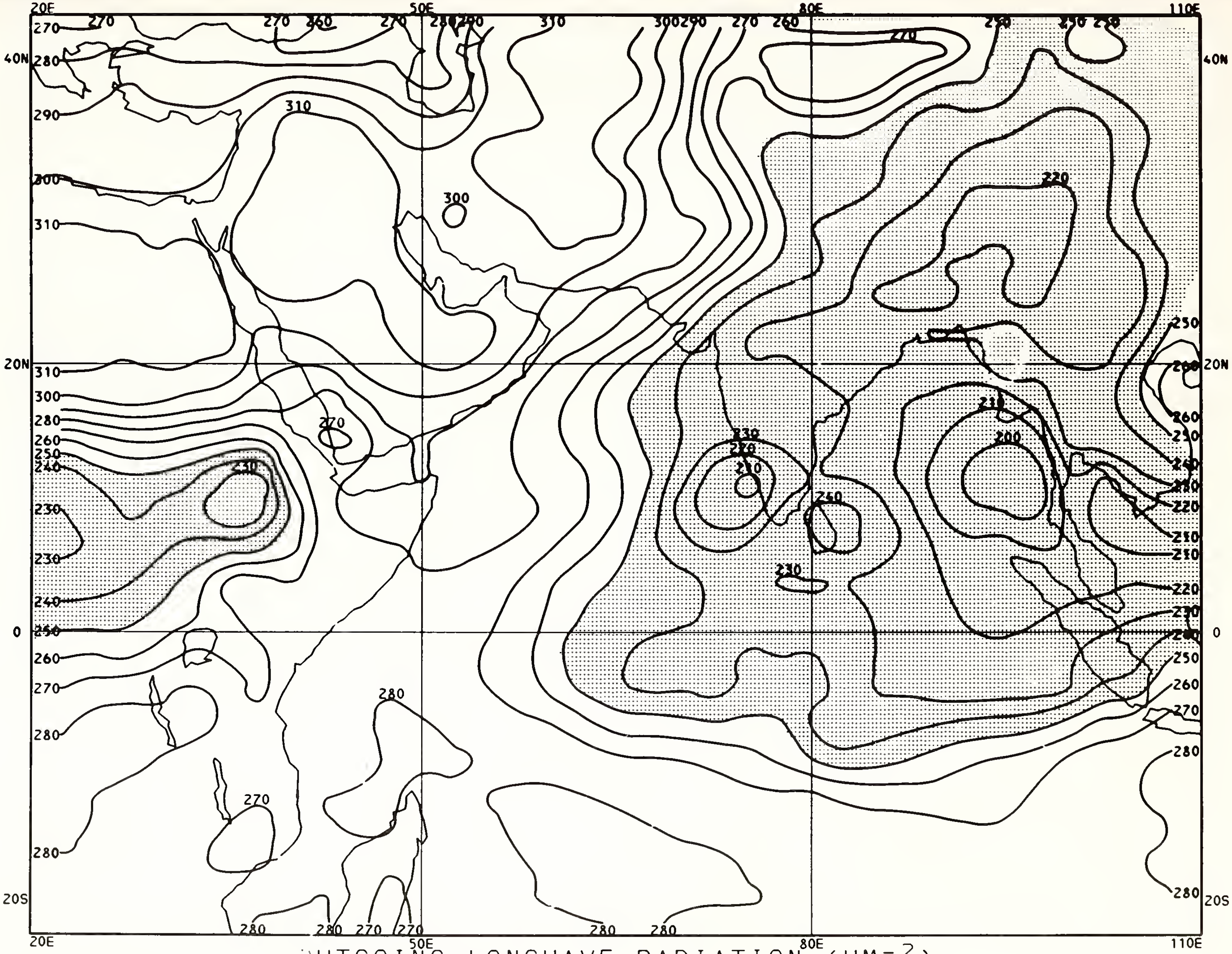

OUTGOING LONGWAVE RADIATION (WM$^{-2}$)
29 DAYS ENDING JULY 31, 1979 TIROS-N

Figure 3

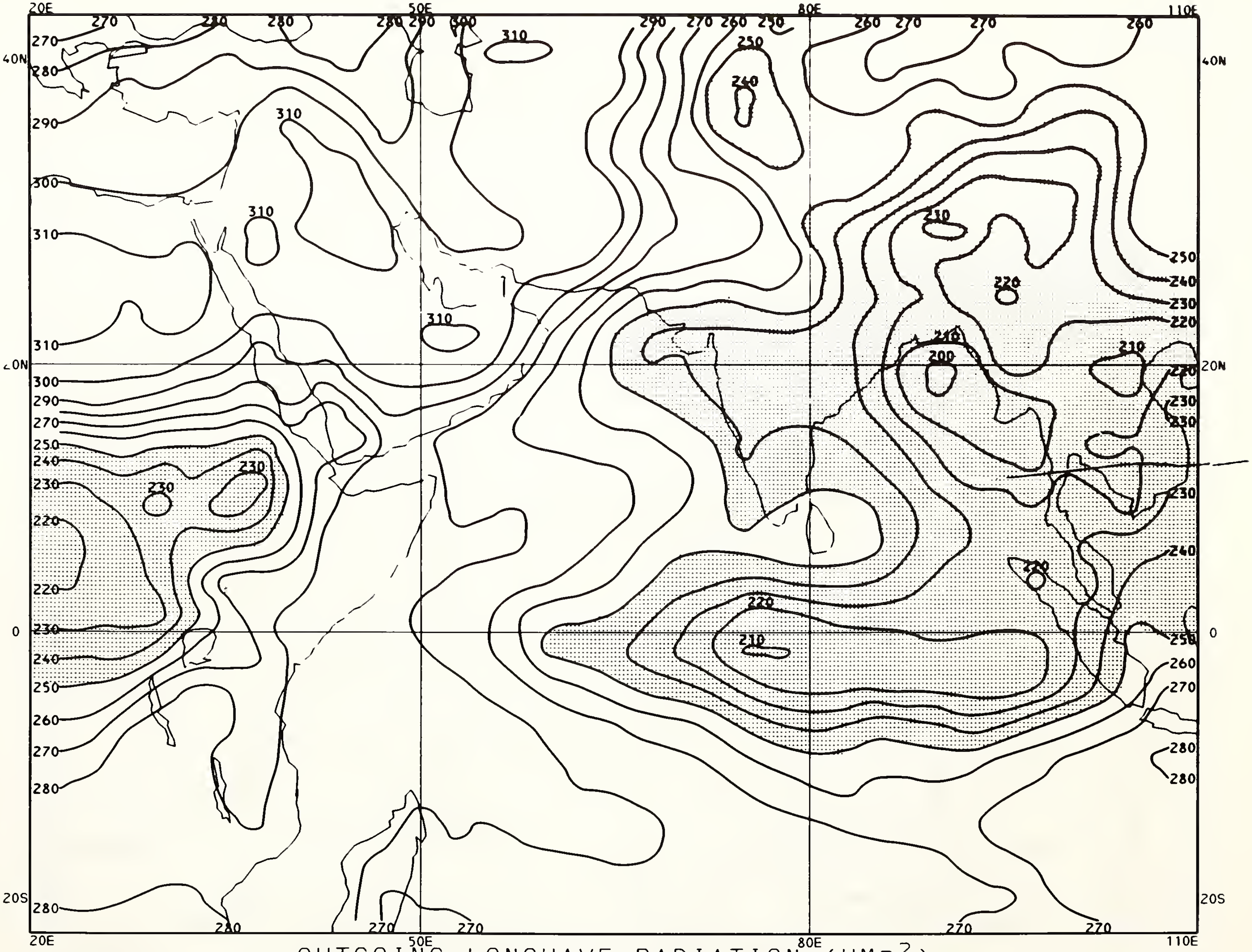

OUTGOING LONGWAVE RADIATION (WM-2)
31 DAYS ENDING AUGUST 31, 1979 TIROS-N

Figure 4

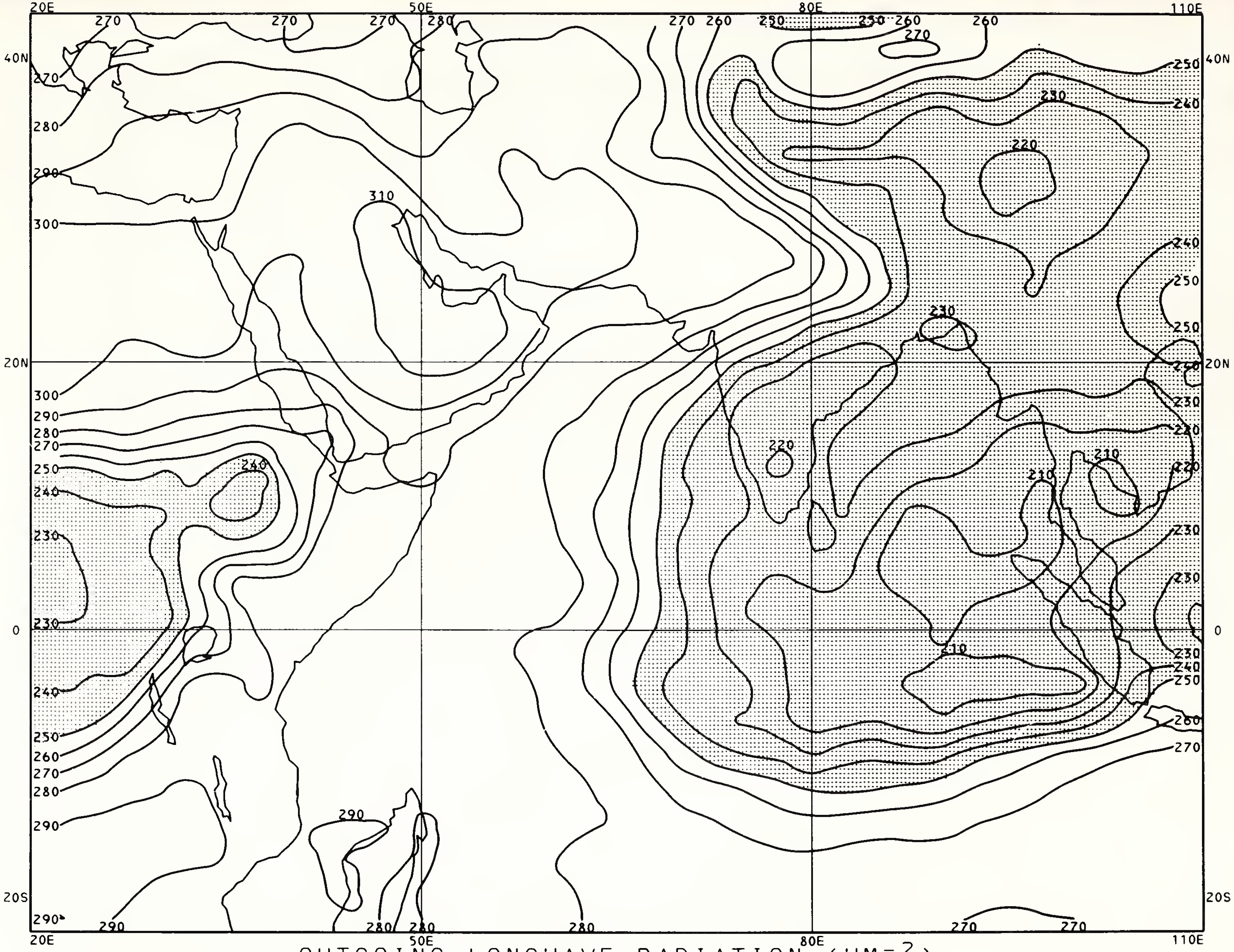

OUTGOING LONGWAVE RADIATION $(WM^{-2})$
30 DAYS ENDING SEPTEMBER 30, 1979 TIROS-N

Figure 5

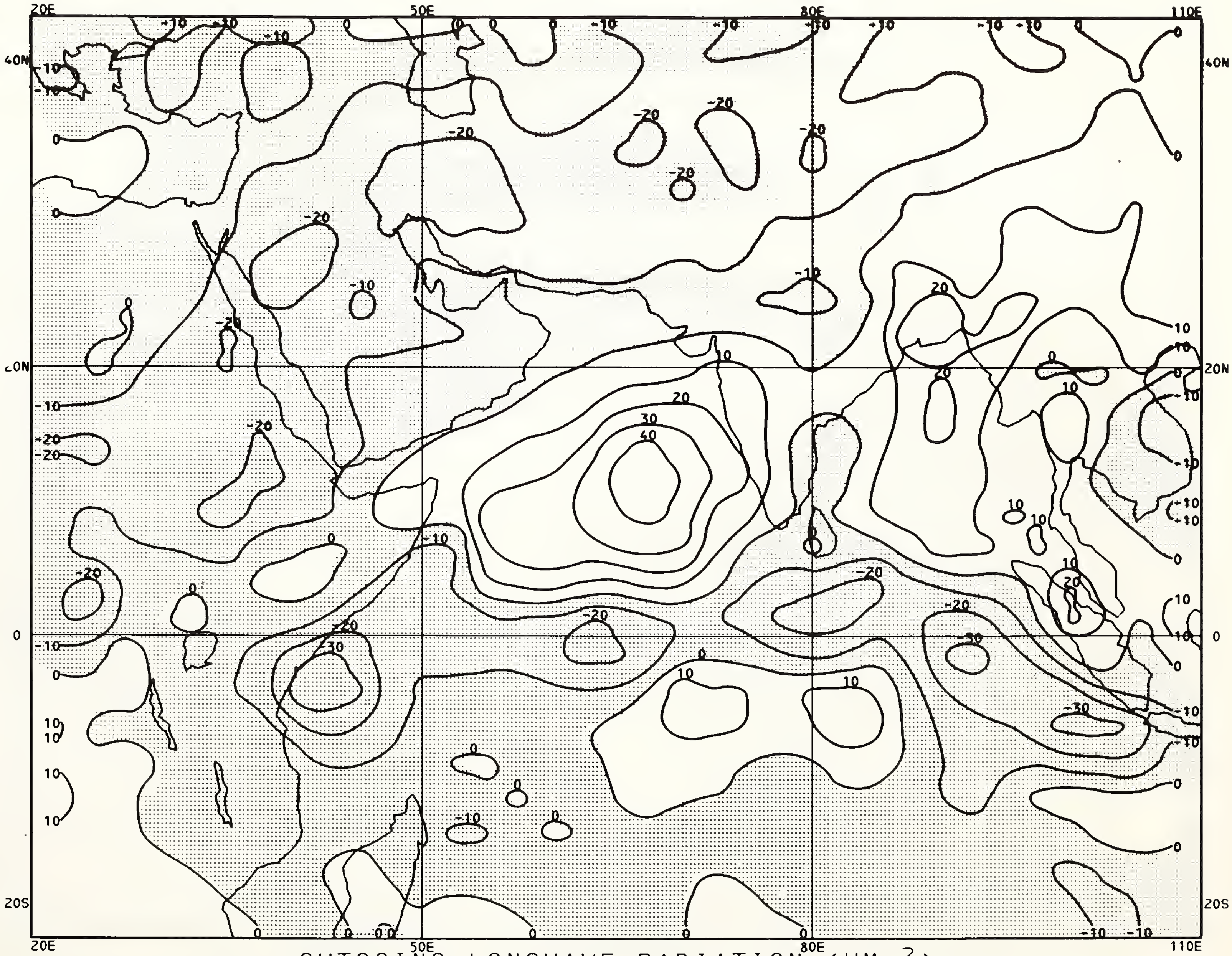

OUTGOING LONGWAVE RADIATION (WM$^{-2}$)
DIFFERENCE MAY 1979-1975 (TIROS-N - NOAA SR)

Figure 6

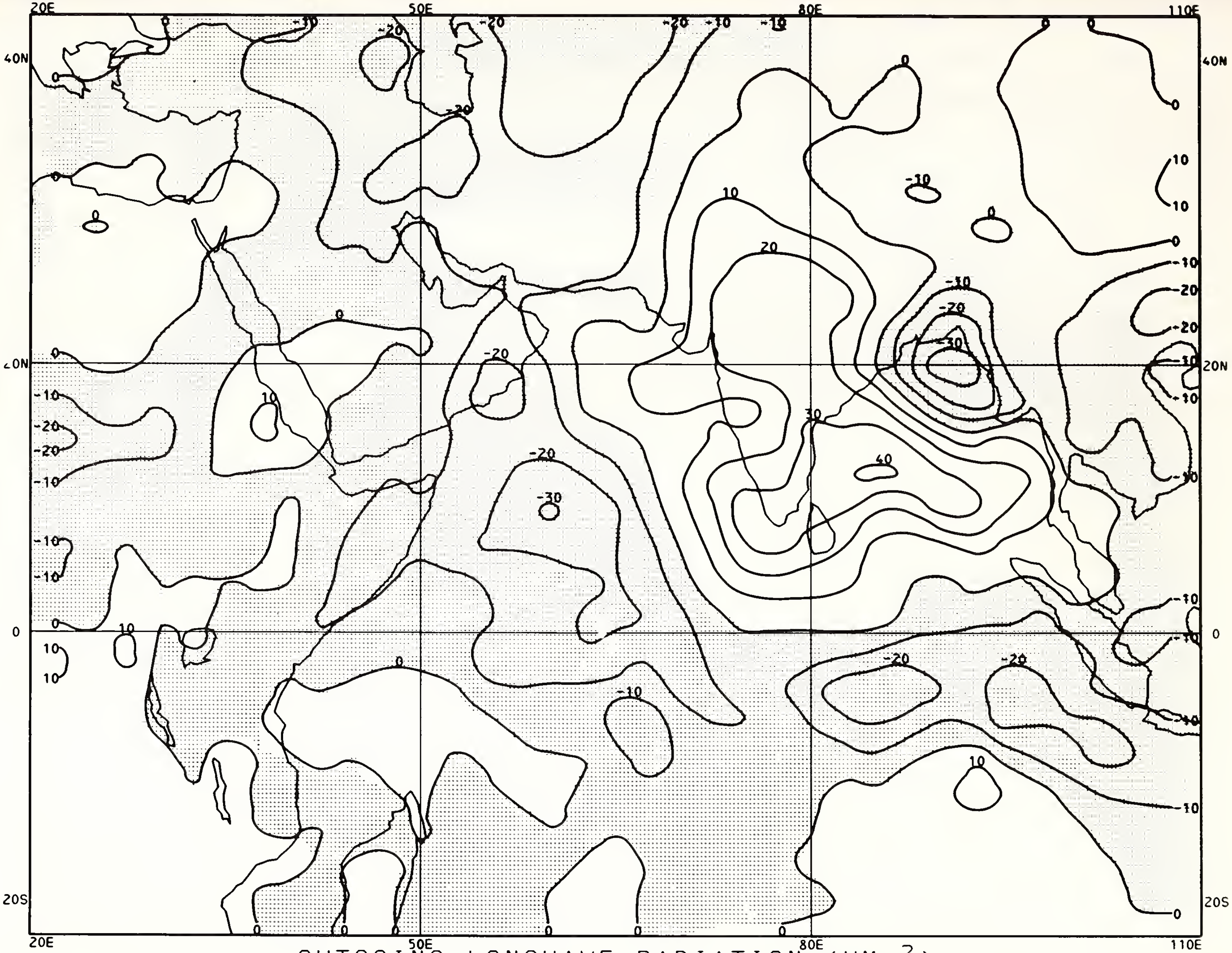

OUTGOING LONGWAVE RADIATION $(WM^{-2})$
DIFFERENCE JUNE 1979-1975 (TIROS-N - NOAA SR)

Figure 7

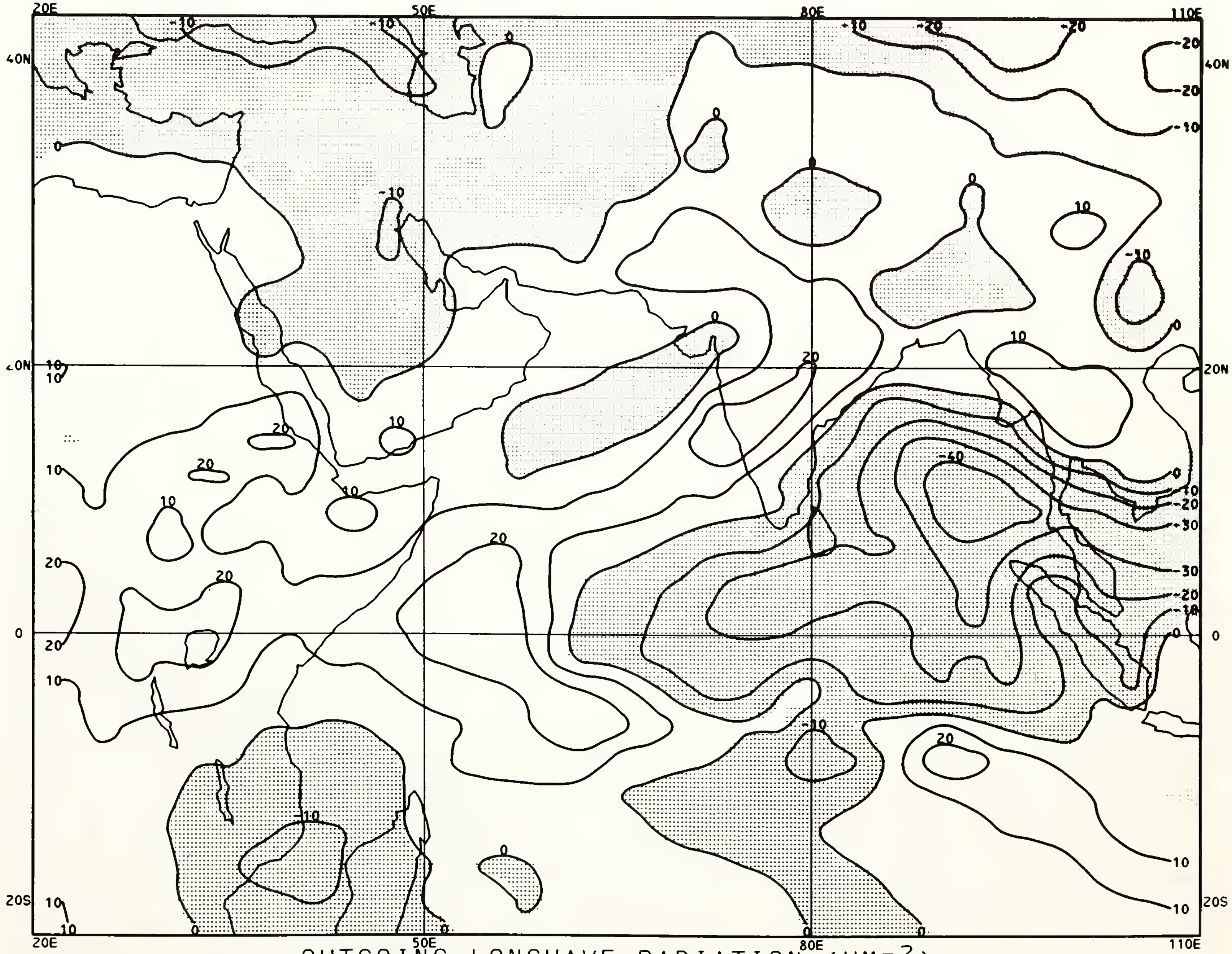

OUTGOING LONGWAVE RADIATION (WM$^{-2}$)
DIFFERENCE JULY 1979-1975 (TIROS-N - NOAA SR)

Figure 8

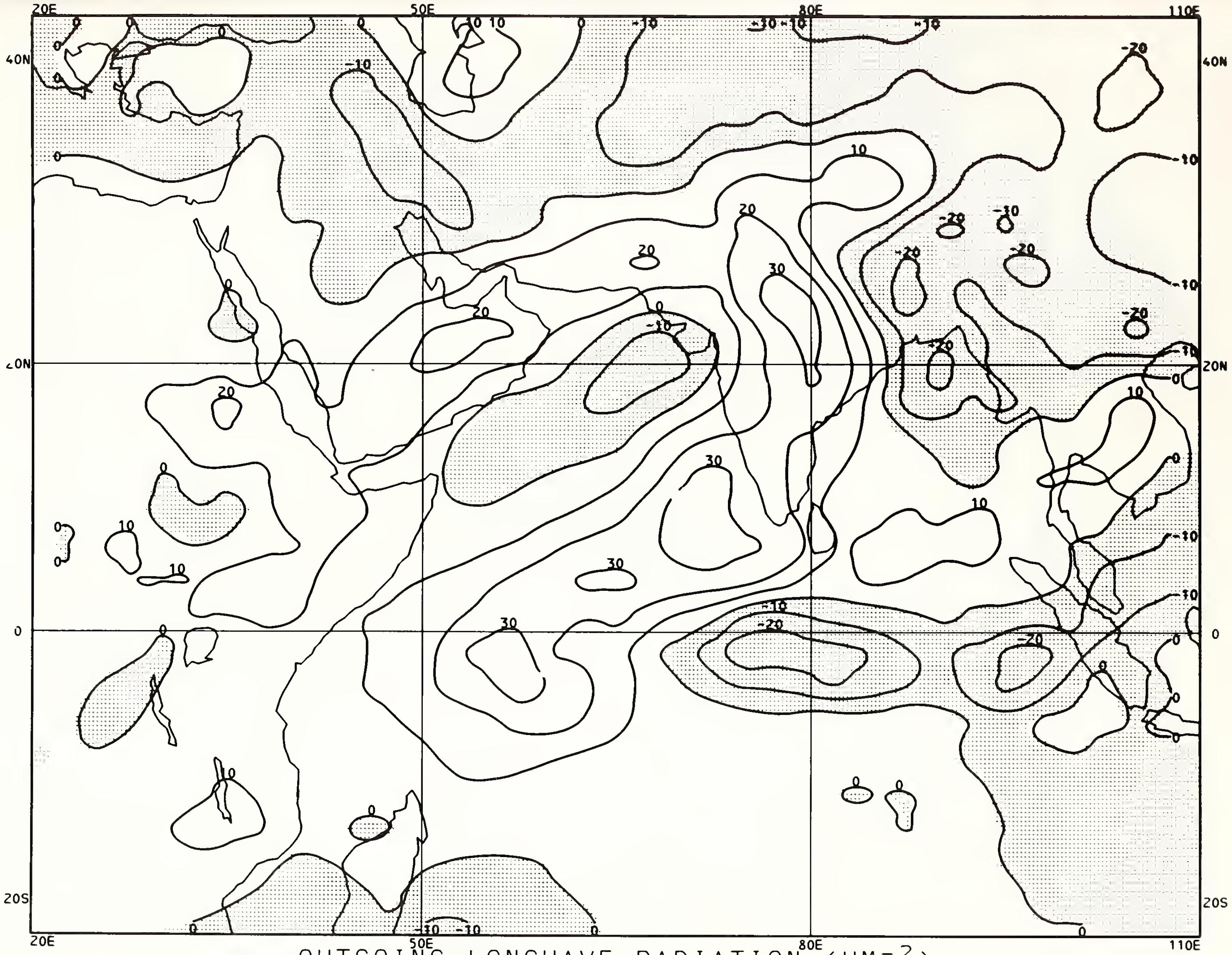

OUTGOING LONGWAVE RADIATION (WM$^{-2}$)
DIFFERENCE AUGUST 1979-1975 (TIROS-N - NOAA SR)

Figure 9

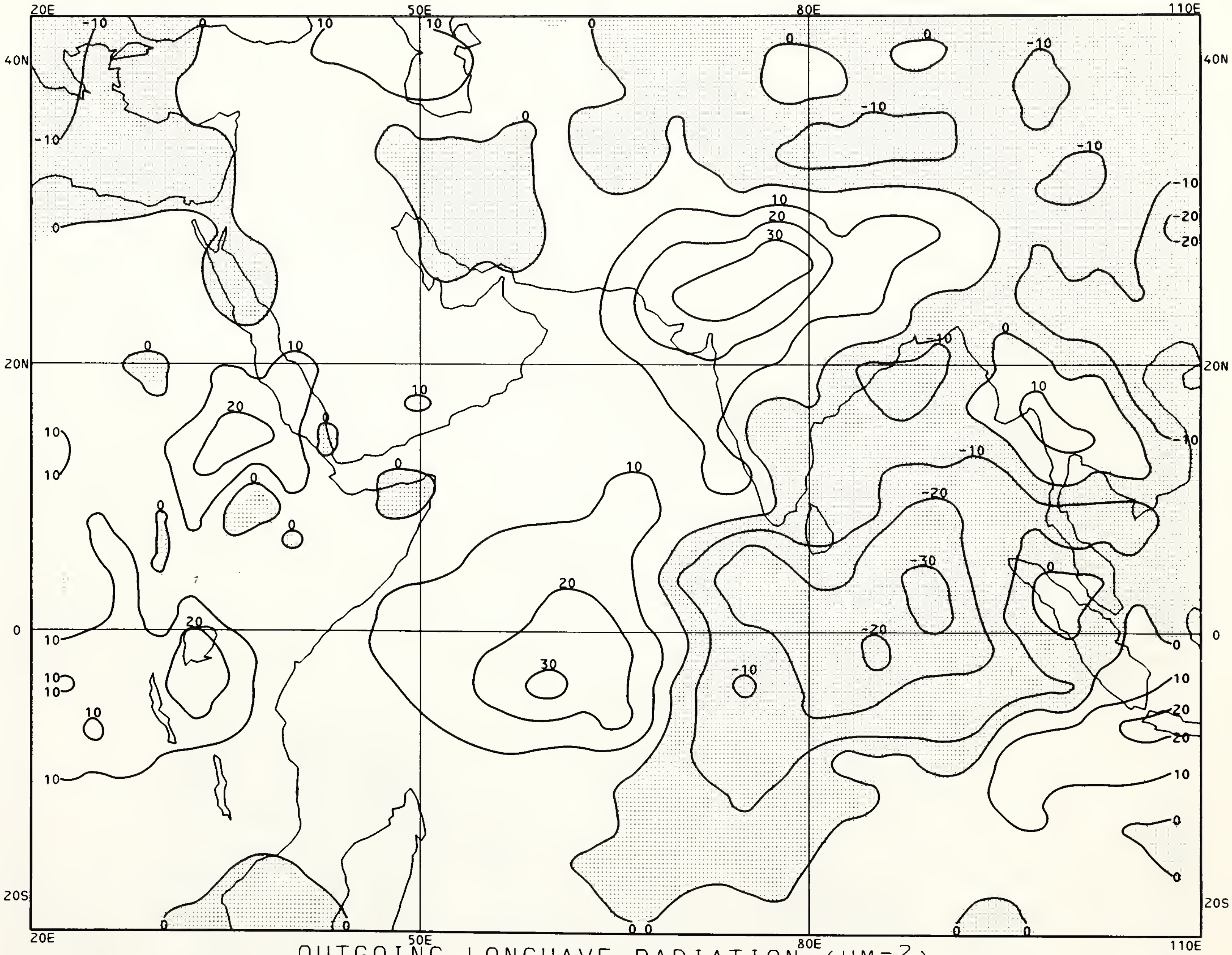

OUTGOING LONGWAVE RADIATION (WM-2)
DIFFERENCE SEPTEMBER 1979-1975.

Figure 10

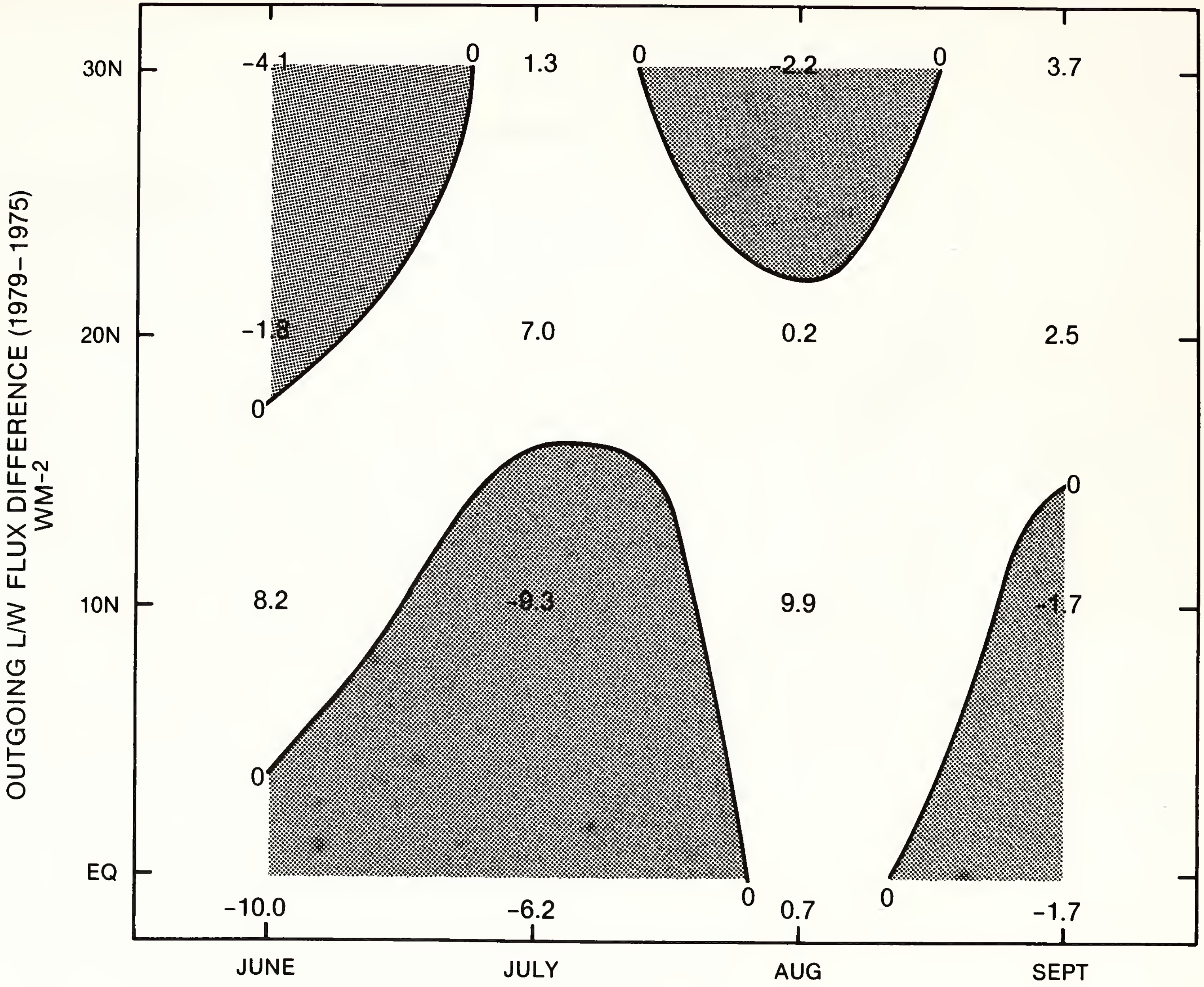
OUTGOING L/W FLUX DIFFERENCE (1979–1975)
WM-2
30N
20N
10N
EQ
JUNE
JULY
AUG
SEPT
-4.1
1.3
-2.2
3.7
-1.8
7.0
0.2
2.5
8.2
-9.3
9.9
-1.7
-10.0
-6.2
0.7
-1.7
0

Figure 11

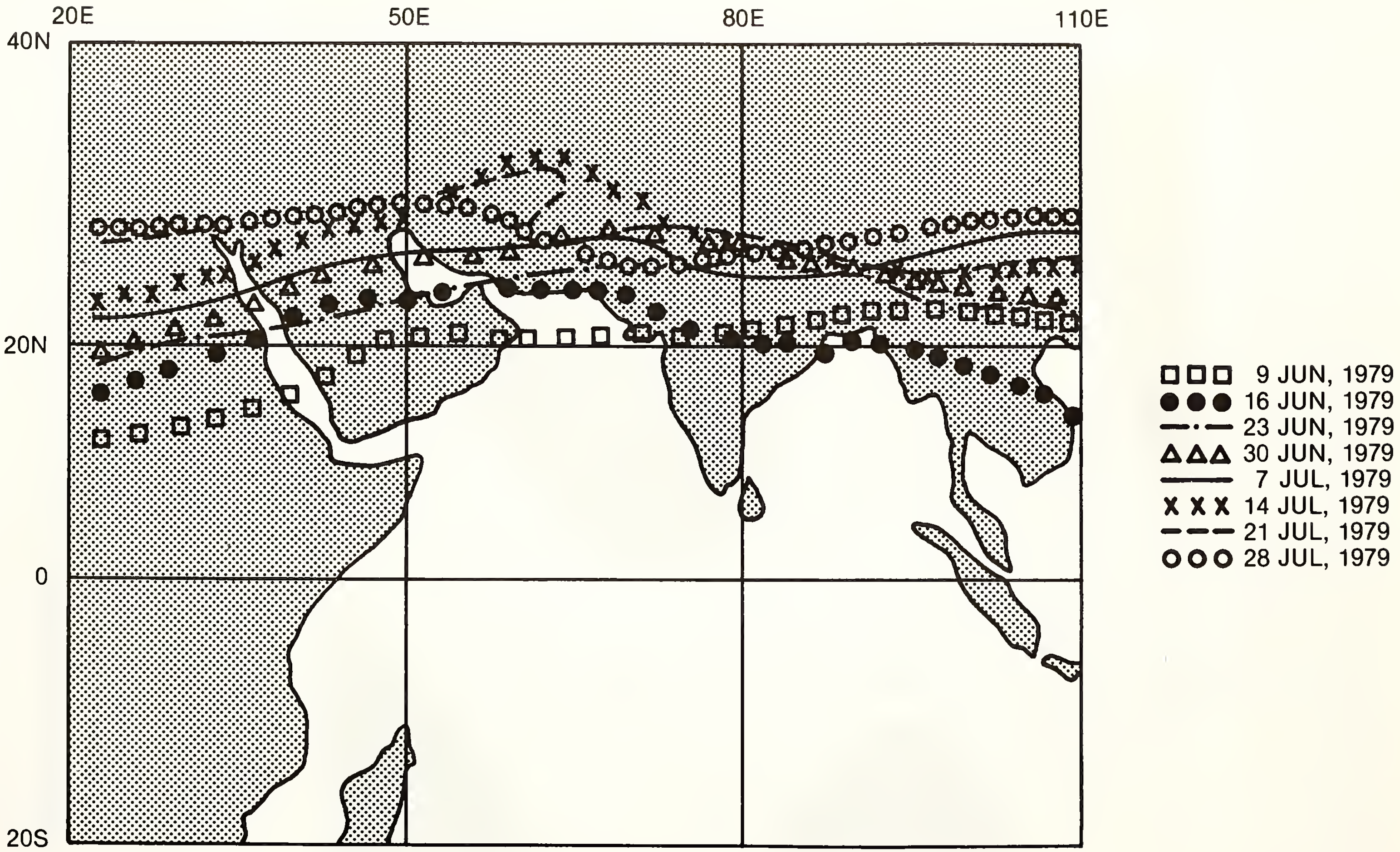

200 MB ZONAL WIND (ZERO LINE)

Figure 12

# A SATELLITE VIEW OF THE 1979 INDIAN MONSOON CIRCULATION

John A. Young
Space Science and Engineering Center and Department of Meteorology
The University of Wisconsin-Madison

## Abstract

During 1979 the GOES satellite over the Indian Ocean gave researchers the first opportunity to view the entire monsoon system during one complete annual cycle. Special efforts at the University of Wisconsin allowed relatively complete synoptic wind coverage for the summer monsoon at two levels to be obtained. This coverage included the two experimental areas of summer MONEX (Arabian Sea and Bay of Bengal) as well as the southern equatorial Indian Ocean during both the "onset" and "established" periods of evolution. Examples of lower and upper tropospheric wind fields for each phase of the monsoon's evolution are shown. These fields illustrate the applicability of the data for further diagnostic study of the development as well as intra-seasonal anomalies of the great monsoonal "climate machine".

## 1. Introduction

The monsoon winds - seasonally varying circulations associated with the annual cycle of heating and cooling - are among the most important yet least understood aspects of global flow. These winds induce evaporation into the atmosphere and transport water vapor to preferred regions where it is released as variably plentiful monsoon rainfall. The resulting latent heating of the atmosphere acts as an important focussed energy source for the winds supplying this "fuel". The Asian monsoon is indeed a great "climate machine" and understanding of its workings must be mastered before either of the twin goals of the Global Atmospheric Research Project (GARP) can be achieved: The large scale and interhemispheric coupling of the monsoon circulation make it of obvious importance to the forecasting of synoptic systems several days in advance, and the enhanced activity of small and large scale physical processes make it an attractive system to study in order to better understand the physical basis of climate.

In the past our knowledge of the wind fields over the Indian Ocean on individual days was sketchy. Upper air observations over the Arabian Sea and Bay of Bengal were essentially absent except for a few limited term observational programs (IIOE, 1963-64; ISMEX, 1973; Monsoon-77). No geosynchronous satellites operated over the summer monsoon area. With the advent of FGGE (First GARP Global Experiment) this situation changed dramatically: a GOES satellite operated during 1979 over the Arabian Sea at (0°N, 60°E). Thus, 1979 was the first opportunity to view the entire Indian monsoon system during one complete annual cycle.

The importance of the monsoon as a fundamental seasonal element was recognized by conducting the GARP sub-program known as MONEX (The Monsoon Experiment) simultaneously and in coordination with FGGE. The summer portion consisted of two phases, the Arabian Sea Experiment and the Bay of Bengal Experiment. Detailed descriptions of MONEX plans can be found in the international document "The Monsoon Experiment" (GARP Pub. Series No. 18, Oct. 1976) and the "Plan for U.S. Participation in MONEX" (Report of U.S. MONEX Panel to the U.S. GARP Committee, published by the National Academy of Sciences, 1977).

One of the year-long FGGE projects conducted at the University of Wisconsin's Space Science and Engineering center was the production of wind fields from infra-red and visible geostationary satellite images using the McIDAS (Man-Computer Interactive Data Access System). In order to obtain unique synoptic wind coverage, a special effort was employed to augment the

FGGE wind sets (produced at Madison) with additional sets in selected synoptic areas during the monsoon (at the Milwaukee terminal in Prof. D.N. Sikdar's group). Quality control of the MONEX augmentation was enhanced by supervisors Dr. D.P. Wylie (Milwaukee and Madison) and Dr. H. Virji (Madison).

The resulting combined Indian Ocean data consists of several hundred vectors at two or three altitudes, up to two times per day, for the period 1 May - 10 August 1979. The data has been included in the international FGGE IIb data set and can be used to study: (a) phases of the developing 1979 summer monsoon (pre-monsoon, onset, and established phases), (b) inter-weekly anomalies during the established phase, and (c) the character of day-to-day fluctuations which alter the circulation. In this paper we present a sampling of lower and upper tropospheric wind fields which illustrate (a) the three primary phases, and (b) the applicability of the data for future diagnostic studies of the great monsoonal "climate machine".

## 2. Five Phases of the Monsoon Circulation

This section shows five examples of upper (top diagram) and lower (bottom diagram) tropospheric wind fields for separate phases of the 1979 summer monsoon. Full barbs are 5 m $s^{-1}$, flags are 25 m $s^{-1}$. The data are "raw"; they have not been subjected to any space or time filtering. Data holes are mainly due to lack of cloud tracers at that level or obscuration of low clouds by higher clouds.

The figures are ordered chronologically during the evolution. It is easiest to begin by consulting representative examples of established monsoon flows shown in Fig. 5. At low levels, a giant S-shaped streamline pattern links major parts of the two hemispheres in this sector; this is similar to the surface climatological pattern. The Southeast Trades of the Southern Hemisphere approach and cross the equator on a long curved path. Near and downstream from the

Equator the flow often develops a well defined sub-synoptic structure of strong winds known as the East African or Somali Jet.

The southerly wind stress and its curl (negative along the Equator) provide fundamental driving for the three-dimensional summer circulations within the upper layers of the western Indian Ocean. In the jet exit region off Somalia, the left edge of the jet is cloud-free, confluent, and cyclonic; its location is an index of the northward penetration of the monsoon circulation from the Southern Hemisphere.

Further downstream the flow continues down the pressure gradient, but under increasing Coriolis influence, and forms the relatively broad and strong "Southwest Monsoon" over the Arabian Sea. This is a region of exceptionally strong air-sea interaction (exchange of latent heat, momentum, and sensible heat) that modifies the flow as it progresses toward India, the Bay of Bengal, and the regions of strongest monsoonal rainfall in the general area of the monsoon trough. This air-sea interaction also cools the upper layers of the ocean, and so the evaporation rates are modulated by the past history of the strong interaction. It is believed that the net water vapor transport toward India and the convective stability of the flow are influenced by these processes. Several investigators believe these properties may also be influenced by synoptic disturbances propagating along the flow from the Southern to Northern Hemispheres, so that a history of the flow at upstream locations is important. No previous data set has provided a complete view of these circulations or fully documented the variability in the climatological flow features.

The upper part of Fig. 5 shows that the high-level flow is similar to climatological expectations. It is more zonal than that at low levels, with the Tropical Easterly Jet found near and to the north of the Equator. Cross-equatorial motions are more pronounced on this and other individual maps (e.g. Figs. 3, 4) compared to climatology.

Considering both flow levels, a great thermally direct mass circulation in the Northern Hemisphere is described in a vertical plane oriented southwest to northeast along the low-level streamlines; the implied vertical connection is rising motion in monsoon rain regions. The displacement of this rising motion to a position well north of the Equator, and sinking implied to the south, characterizes this as a kind of reverse Hadley circulation.

The sequence of Figs. 1-5 illustrates the march of the monsoon circulation during summer 1979. The development of this flow was nearly two weeks later than normal; once it was established, the monsoon rains were relatively erratic.

### 6 May - Pre-Monsoon (Fig. 1)

Low level: weak cross-equatorial flow is seen, with strong westerlies to the south of India near the Equator. At 75°E, the confluence line separating air with recent histories in different hemispheres is slightly to the north of the Equator.

High level: the monsoonal easterly flow is undeveloped.

### 21 May - Pre-Monsoon (Fig. 2)

Low level: cross-equatorial flow is partly established, but the East African Jet is not present yet. The confluence line at 75°E has shifted northward to about 5°N.

High level: conditions are convectively inactive, so few cloud tracers are present and the flow is still relatively weak and disorganized.

### 14 June - Onset Imminent (Fig. 3)

Low level: cross-equatorial flow is now organized and the southwesterlies are becoming established in the western Arabian Sea. The confluence at 75°E has drifted further northward but is not clearly defined due to obscuration of low clouds by high cloud convective debris (e.g., 10°N, 75°E).

High level: many cloud tracers are present due to convection. Easterlies are present over the western Arabian Sea and Bay of Bengal. A major outburst of strong northeasterly flow extends from India southward across the Equator.

24 June - Newly Established (Fig. 4)

Low level: cross-equatorial flow, the East African Jet, and the southwesterlies are firmly established.

High level: the easterlies are present, but a significant southward component across the equator is found near 75°E.

14 July - Fully Established (Fig. 5)

The flows at both levels were discussed previously and resemble the normal climatological states.

### 3. Final Comments

The complete data set from which these samples have been selected will be interpolated onto a two degree grid and made available for climate diagnostic work. Current plans at Wisconsin call for decomposition of the fields into various time scales ranging from seasonal down to inter-diurnal synoptic variations. The low level fields will be used as a basis for estimating the time history of the wind stress on the Indian Ocean. The eventual optimum use of the data will result from integration with other satellite and special FGGE/MONEX data sets. It is hoped that a geostationary satellite will provide data over the Indian Ocean in future years in order to study interannual circulation variability in the region.

# Acknowledgments

In addition to the individuals named in the text, production of these wind fields was assisted by the diligent efforts of Dr. Fred Mosher, Carl Norton and numerous FGGE wind trackers at Madison, and wind trackers Robert Mack, Mark Wysocki, Richard Albrecht, and Margret Nowak at Milwaukee. The over-all encouragement given by the NOAA FGGE Project Office was most helpful; FGGE winds were produced under NOAA contract 7-35217. The MONEX winds were produced under NSF Grant ATM 78-21873 to the Space Science and Engineering Center; partial support (JAY) was provided by NSF Grant ATM 78-25503 to the Department of Meteorology.

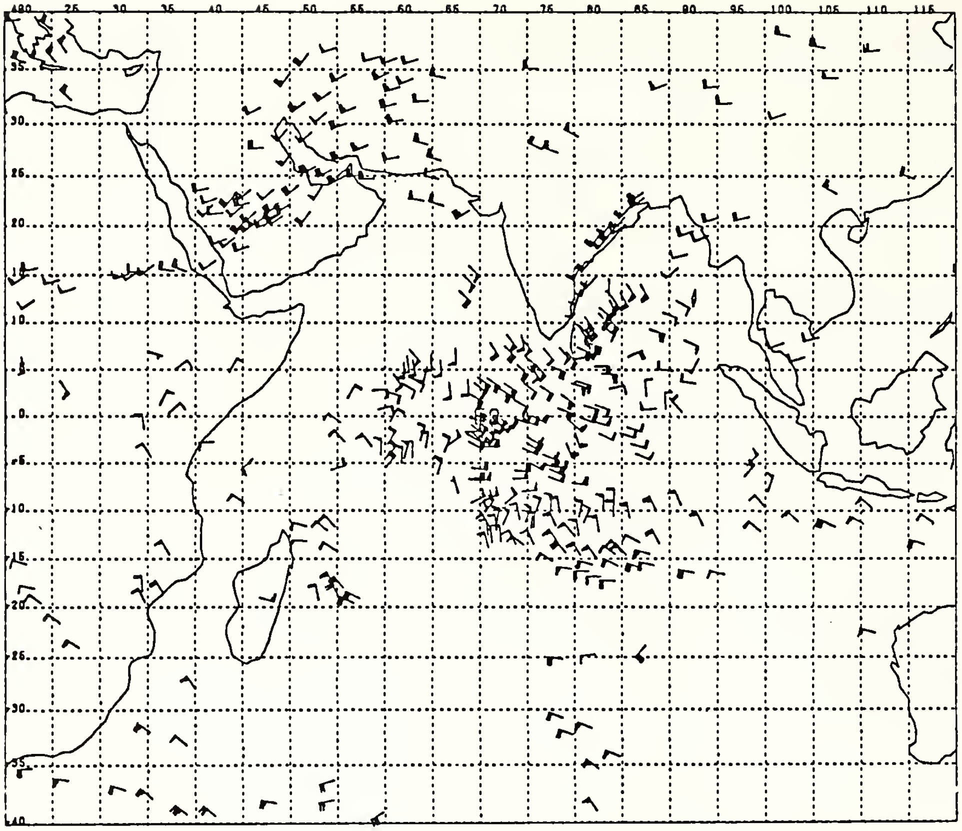

DAY 79126 TIME 83000 300- 100 MB WINDS

Upper Troposphere

**Figure 1**

6 May 1979
Pre-Monsoon

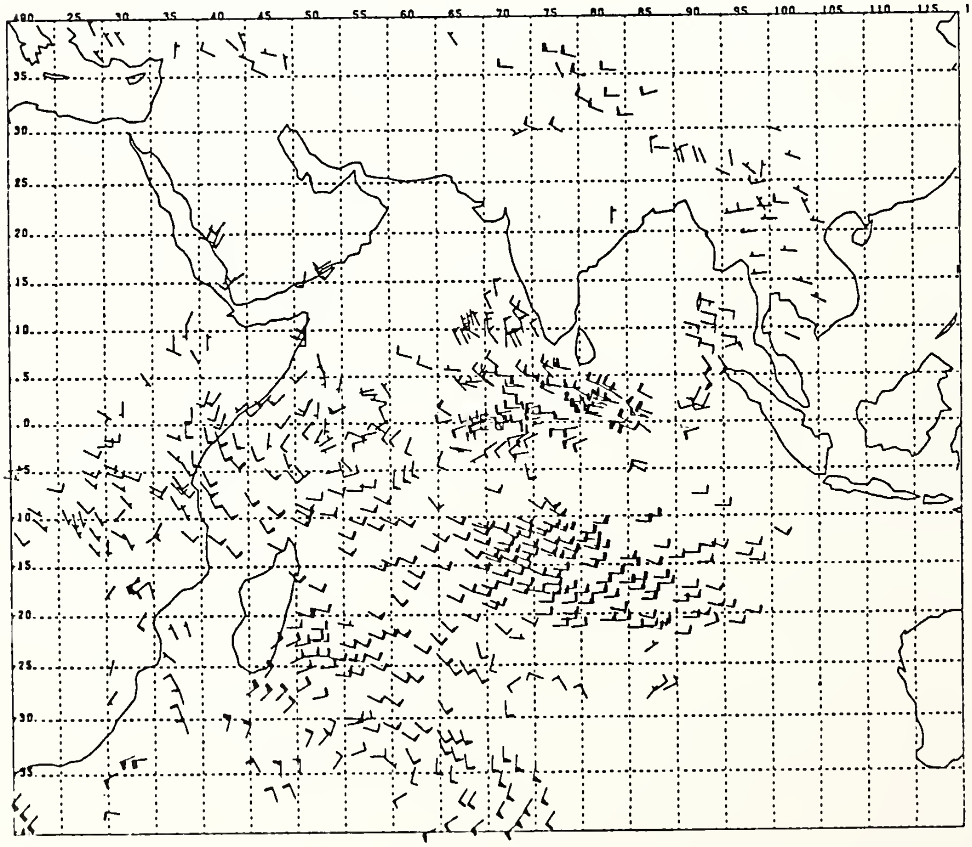

DAY 79126 TIME 83000 999- 850 MB WINDS

Lower Troposphere

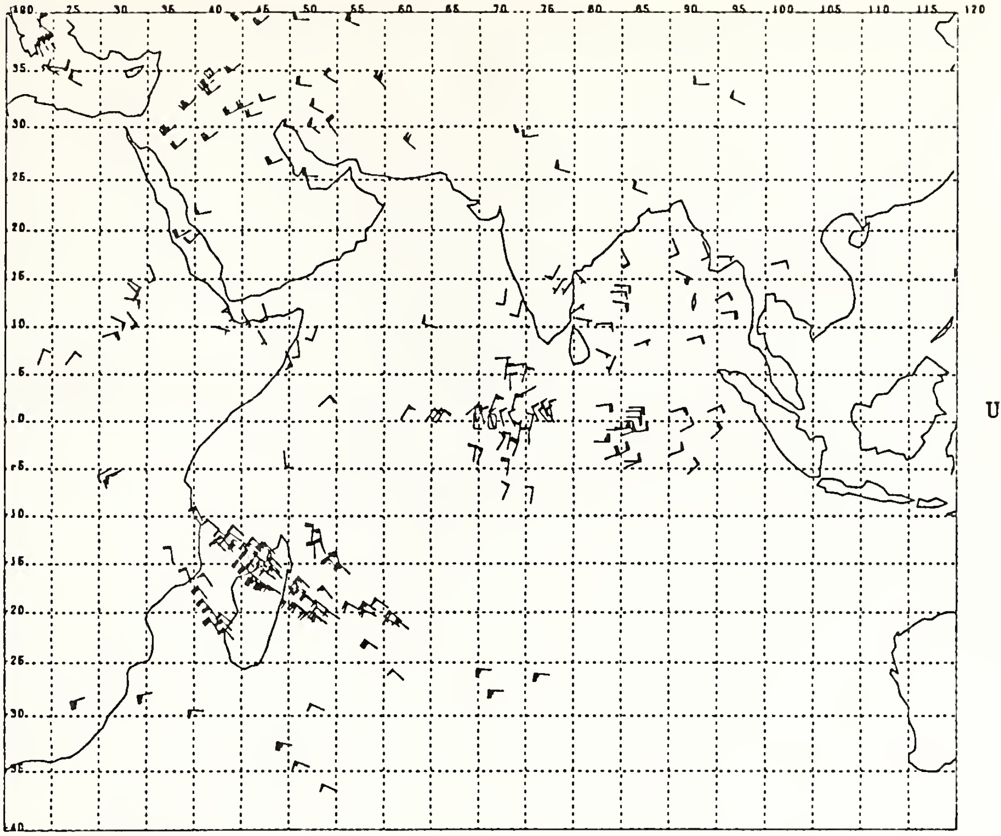

DAY 79141 TIME 83000 300- 100 MB WINDS

Upper Troposphere

Figure 2

21 May 1979
Pre-Monsoon

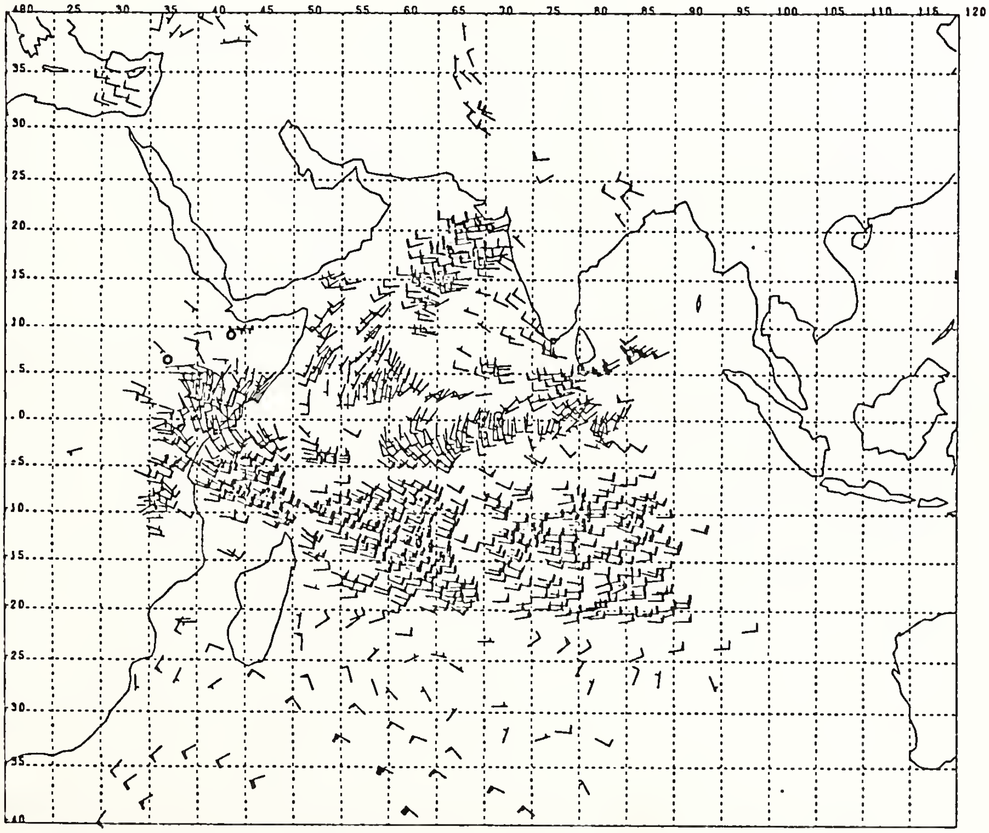

Lower Troposphere

DAY 79141 TIME 83000 999- 850 MB WINDS

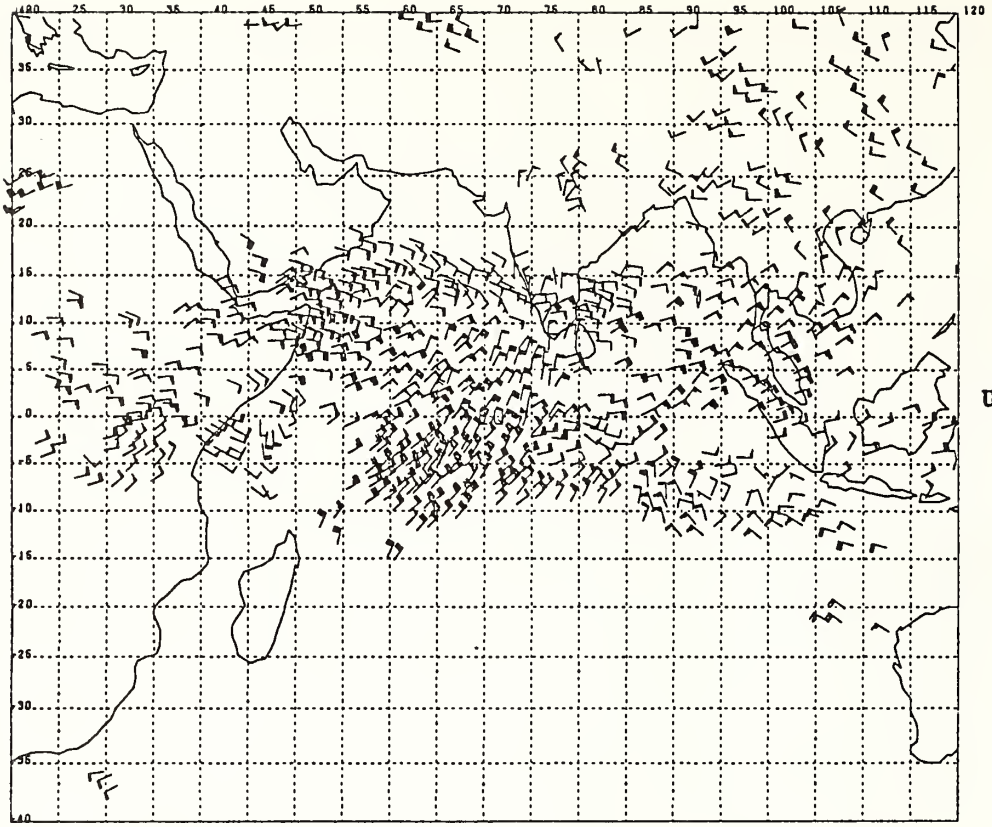

DAY 79165 TIME 83536 300- 100 MB WINDS

Upper Troposphere

**Figure 3**

**14 June 1979**
**Onset Imminent**

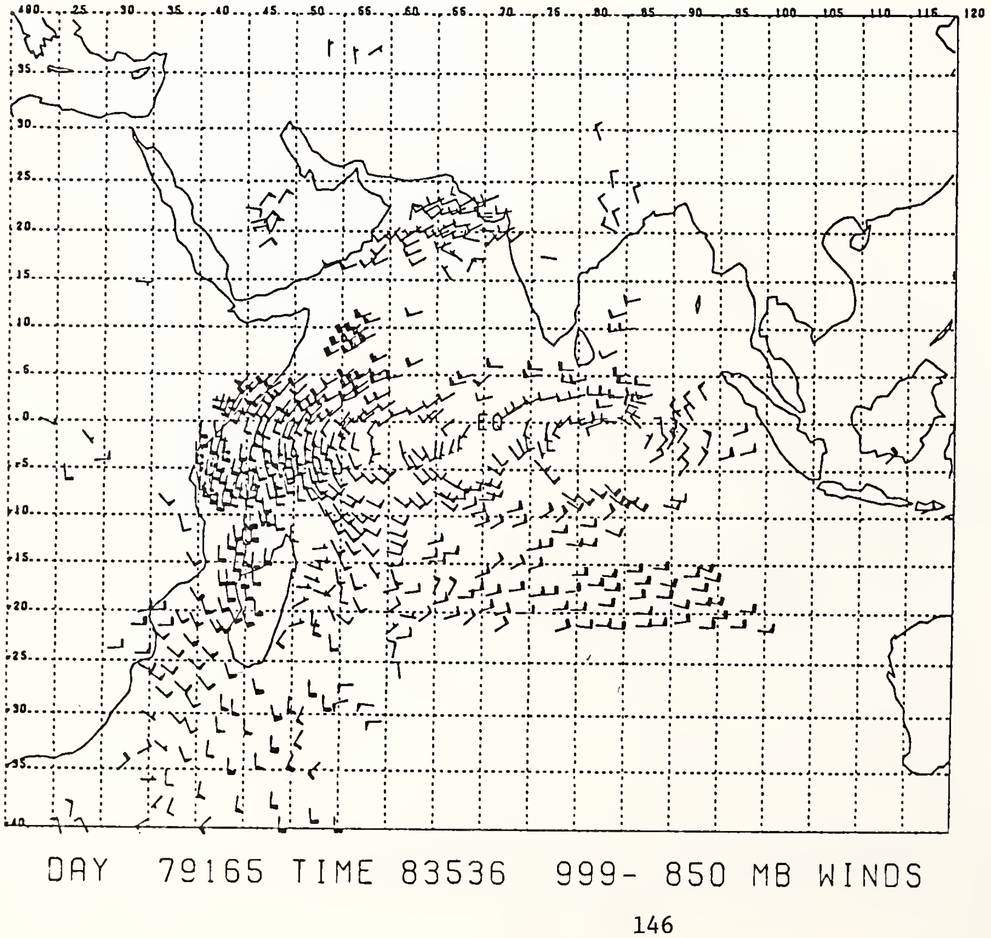

DAY 79165 TIME 83536 999- 850 MB WINDS

Lower Troposphere

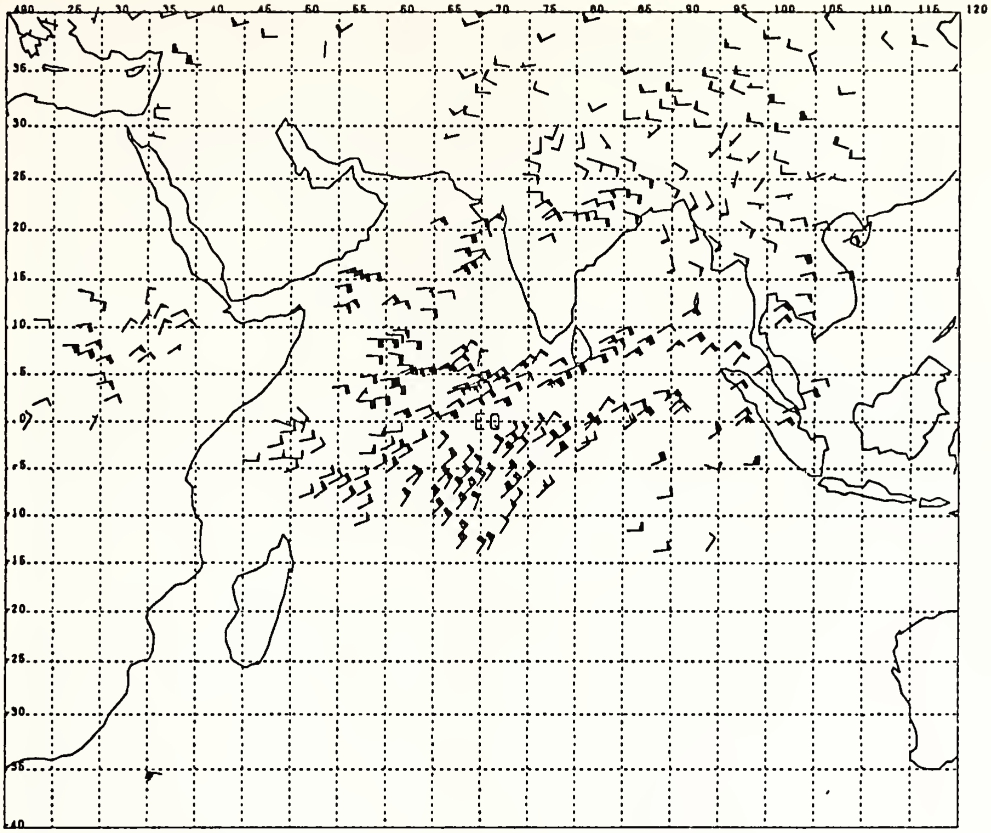

DAY 79175 TIME 93000 300- 100 MB WINDS

Upper Troposphere

**Figure 4**

24 June 1979
Newly Established
Monsoon Flow

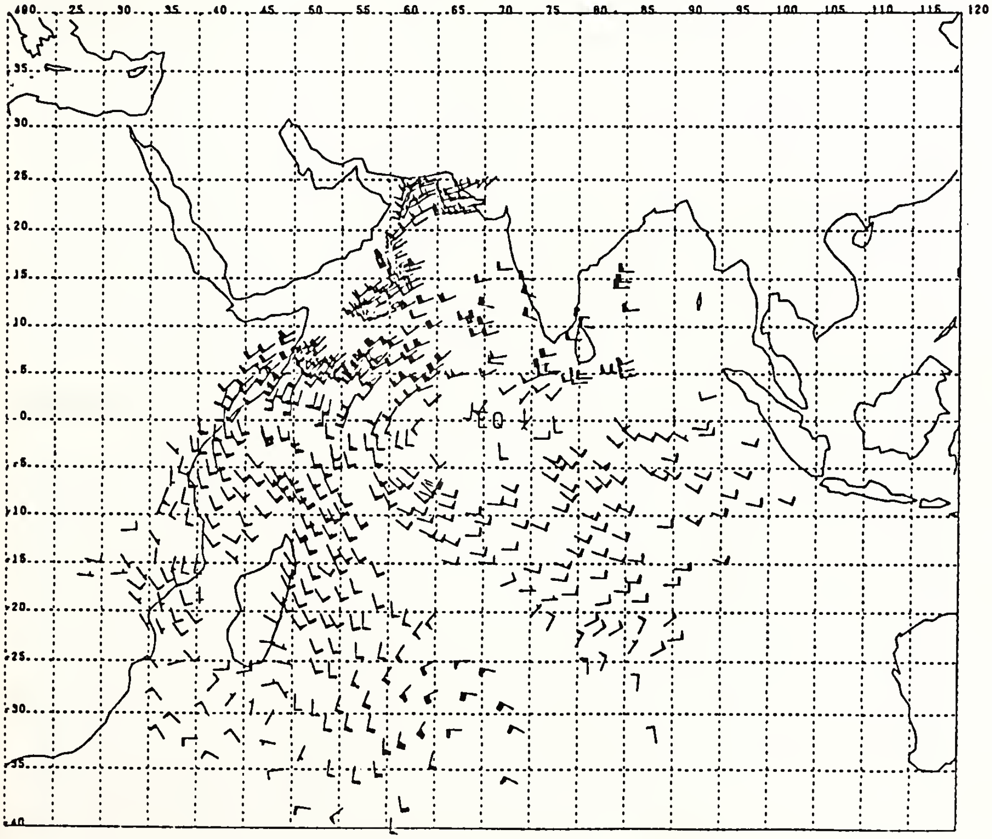

DAY 79175 TIME 93000 999- 850 MB WINDS

Lower Troposphere

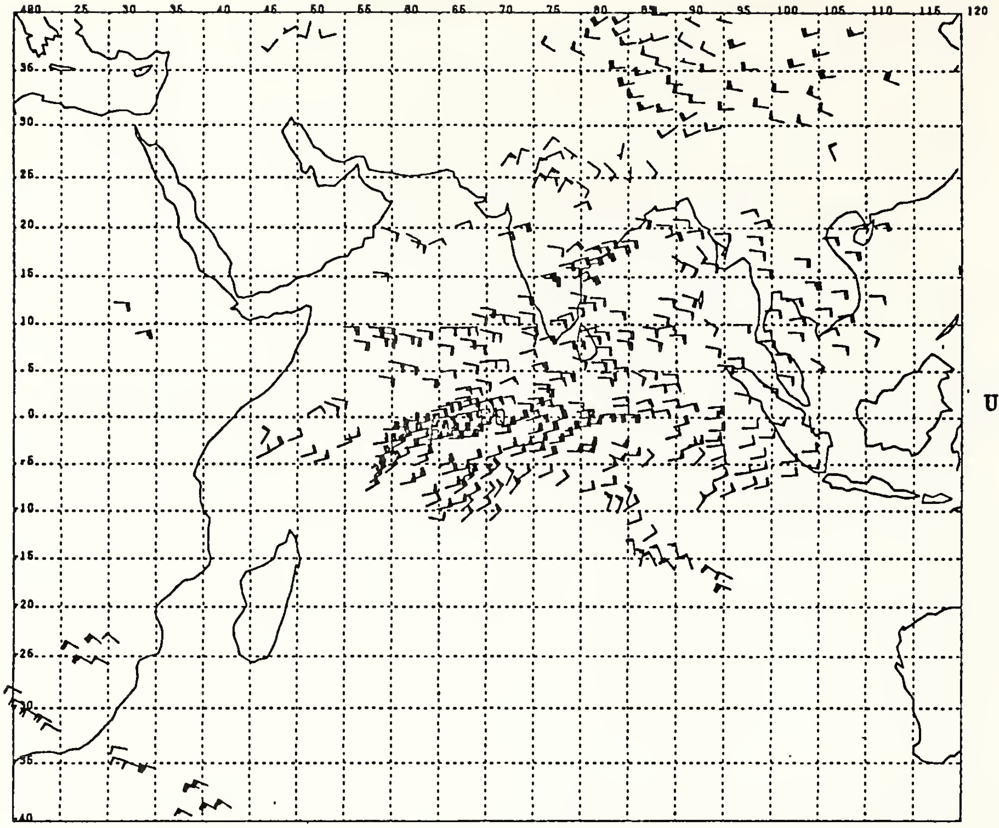

Upper Troposphere

DAY 79195 TIME 83533 300- 100 MB WINDS

**Figure 5**

**14 July 1979**
**Fully Established**
**Monsoon Flow**

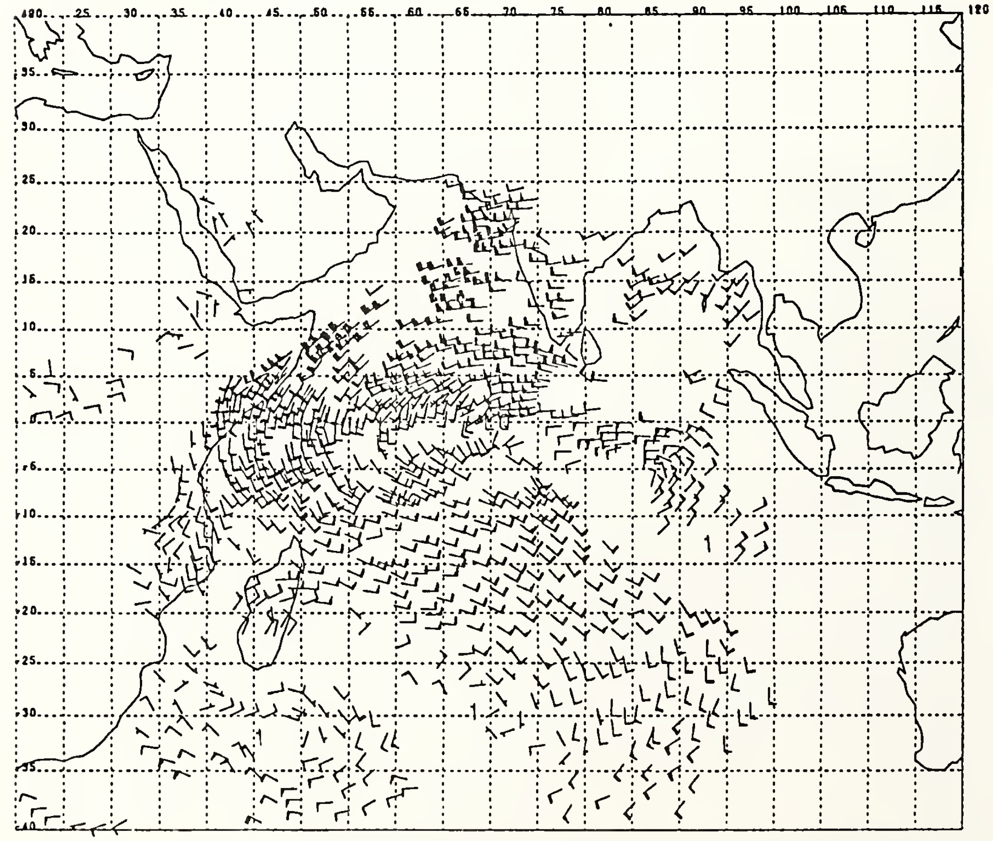

Lower Troposphere

DAY 79195 TIME 83533 999- 850 MB WINDS

# THE SOUTHERN HEMISPHERE CIRCULATIONS --- SEPTEMBER 1978 TO AUGUST 1979

M. Coughlan, T. Skinner and D. Wright

Australian Bureau of Meteorology, Melbourne

The atmospheric circulations of the Southern Hemisphere during the twelve months to August 1979 were characterised by unusual persistence of time averaged fields, particularly over the Pacific Ocean, Antarctica and the lower middle latitudes of the Indian Ocean. Monthly and seasonal mean fields in other regions displayed about normal variability.

The circulations over the South Pacific were characterised by well below average pressure and geopotential near 90°W during the spring and summer months (Figures 1 and 2) and at more western latitudes during the autumn and winter (Figures 3 and 4). The anomalies of about -100m and -120m during spring and summer, which respresented several times the standard deviation of seasonal means, resulted not from occasional very large departures but from persistent negative anomalies (See Figure 5). The accumulated seasonal anomalies for the autumn and winter also resulted from persistent negative departures, although, as evidenced in Figure 5, a marked change occurred in August as a belt of strong positive anomalies emerged at high latitudes of the south-western Pacific.

Unusual persistence was also a feature of the circulations over Antarctica, particularly in the nine months to May 1979. As is evident in Figures 1, 2 and 3, positive anomalies dominated over Antarctica through the spring, summer and autumn. The winter, however, saw a marked reversal, with intense and extensive negative anomalies emerging over the continent. The occurrence of the very intense centre of negative anomaly near the Eastern Antarctic coast together with the maintainance of a belt of positive anomalies across the lower mid latitudes of the Indian Ocean, resulted in very much stronger then normal westerly flow at high latitudes of almost all the eastern half of the hemisphere.

The occurrence of strong and persistent anomalies in the mean circulations, particularly over what was previously the data sparse South Pacific, prompted one to question whether these anomalies were genuine or whether the use of new data was providing new light on the real circulation patterns of this region. Zillman (1979) for instance pointed out that the use of drifting buoy data resulted in the analysis of more intense southern disturbances than had been analysed prior to the availability of these data. When one realises that the 'normals' used to calculate the anomalies are those published by Taljaard et al in 1969, and that the analyses from which data were extracted to produce the 'normals' were based on very sparse data coverage over large tracts of the southern oceans, one may conclude that the normals do not truly reflect the normal circulations of the Southern Hemisphere.

It may now be necessary to re-define the 'normal' circulations of the Southern Hemisphere using analyses only from the period in which improved data coverage was available.

REFERENCES

Taljaard, J. J., H. Van hoon, H. L. Crutcher and R. L. Jenne. Climate of the Upper Air, Part 1 - Southern Hemsiphere. Volume 1 - Temperatures, Dew Points, and Heights at Selected Pressure Levels. NAVAIR 50-1C-55 September 1969.

Zillman, J. W. Comments to WMO 8th Congress, Geneva, 1979.

FIGURE 1

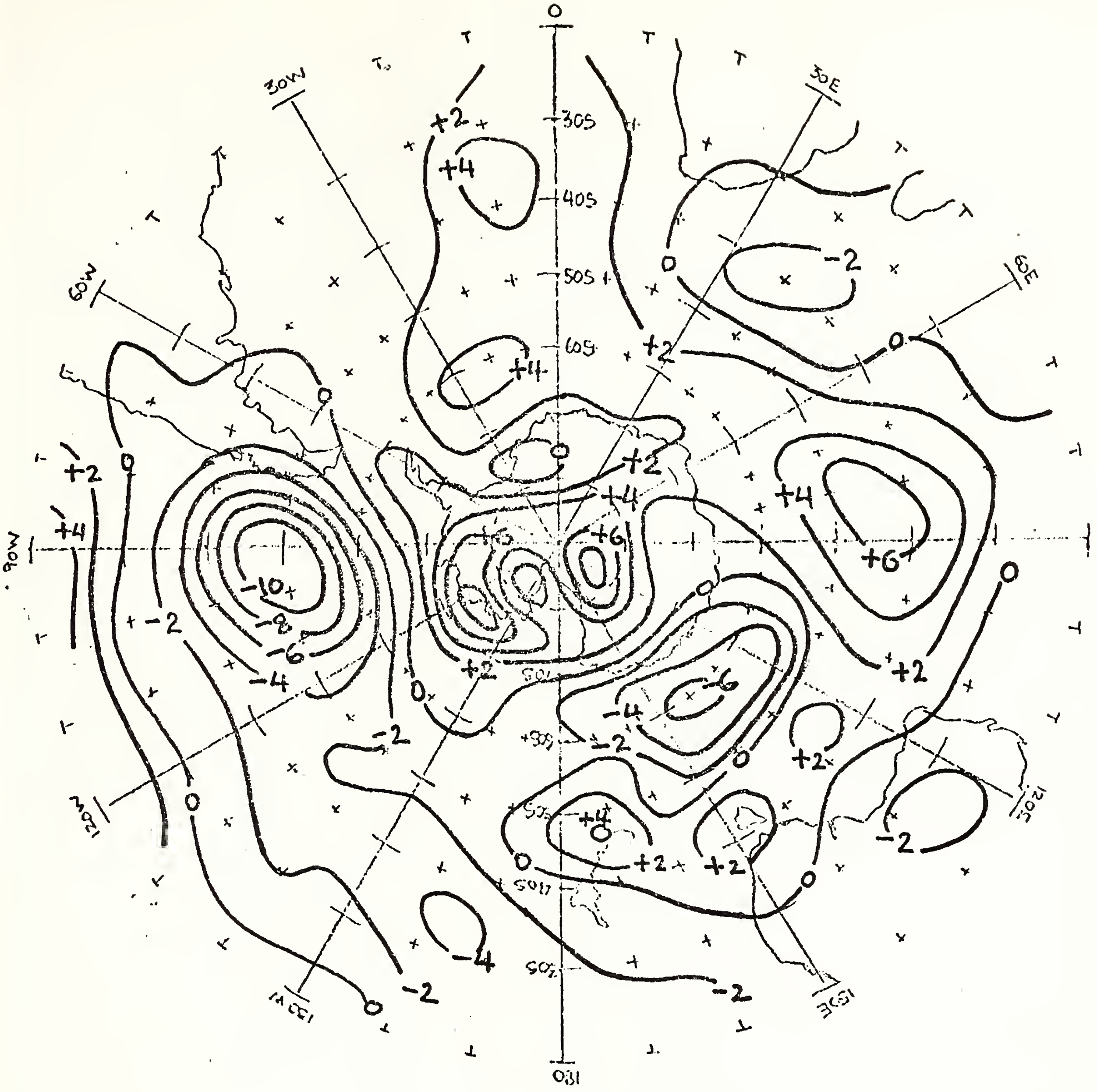

500 mb Geopotential Anomalies (gpdm) - Seasonal Means.

Data Extracted from Hemispheric Analyses Produced at the
National Meteorological Analysis Centre, Melbourne

September - November 1978 (Spring)

FIGURE 2

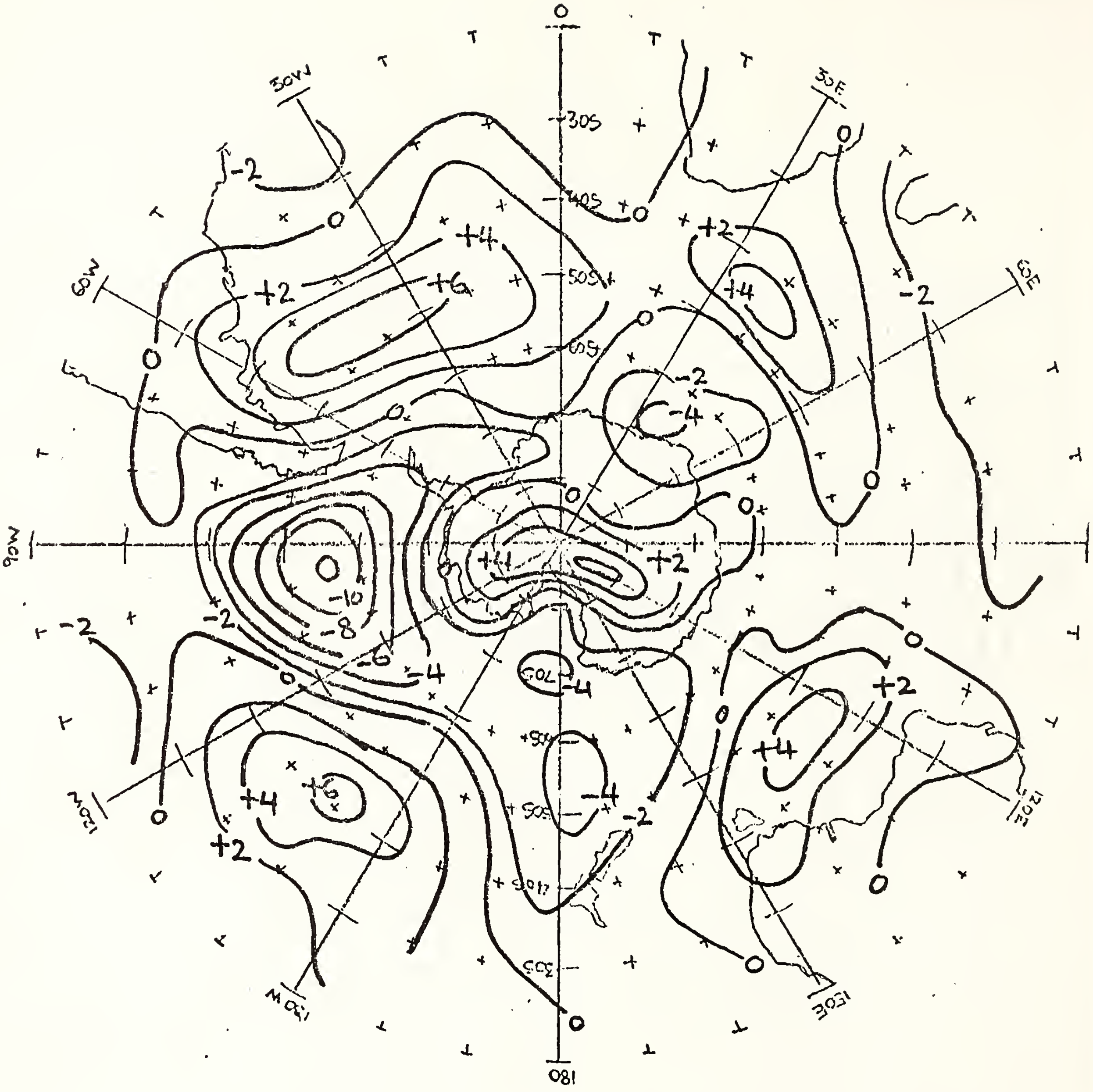

500 mb Geopotential Anomalies (gpdm) - Seasonal Means.

Data Extracted from Hemispheric Analyses Produced at the National Meteorological Analysis Centre, Melbourne

December 1978 - February 1979 (Summer)

FIGURE 3

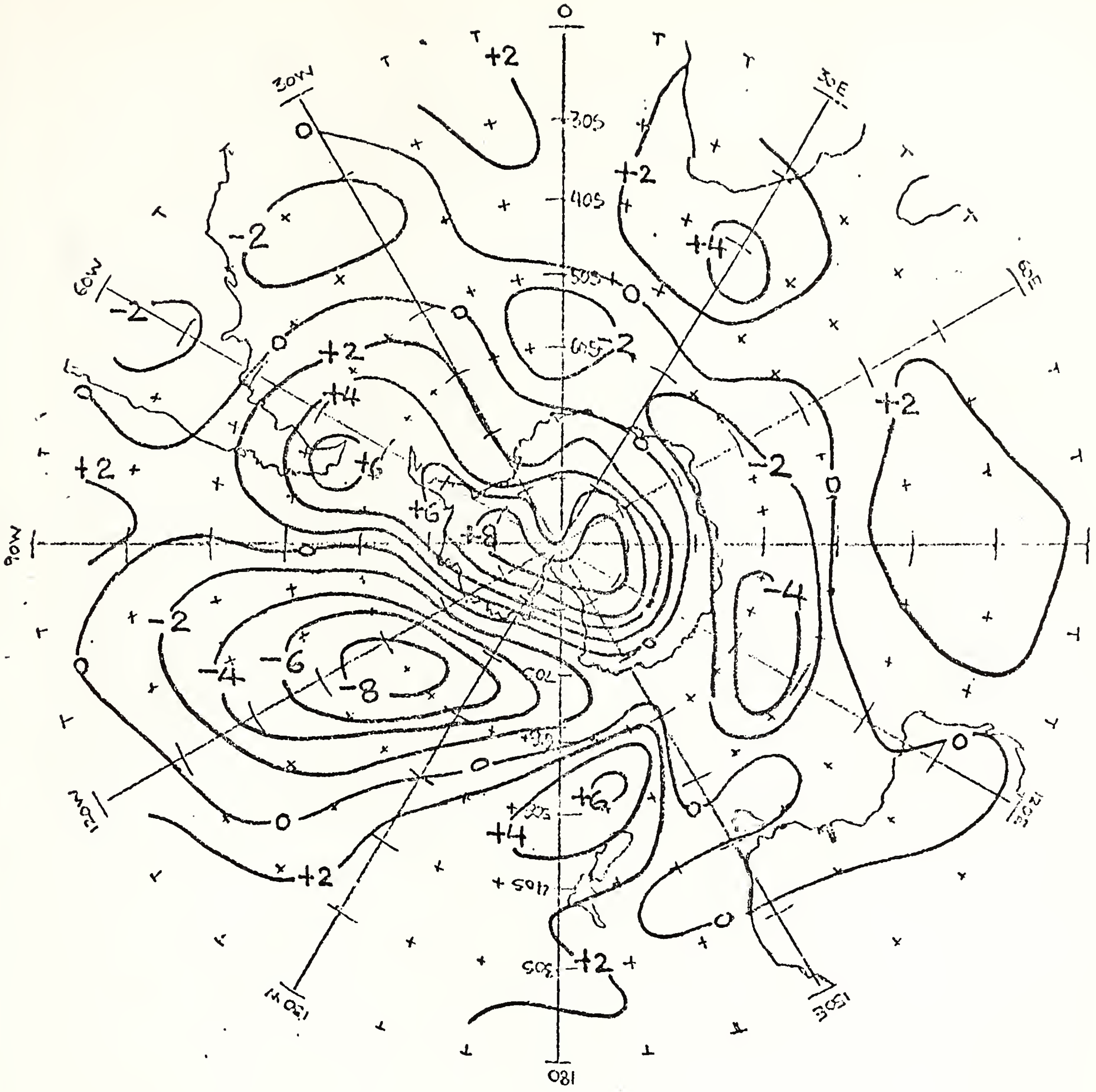

500 mb Geopotential Anomalies (gpdm) - Seasonal Means.

Data Extracted from Hemispheric Analyses Produced at the
National Meteorological Analysis Centre, Melbourne

March - May 1979 (Autumn)

FIGURE 4

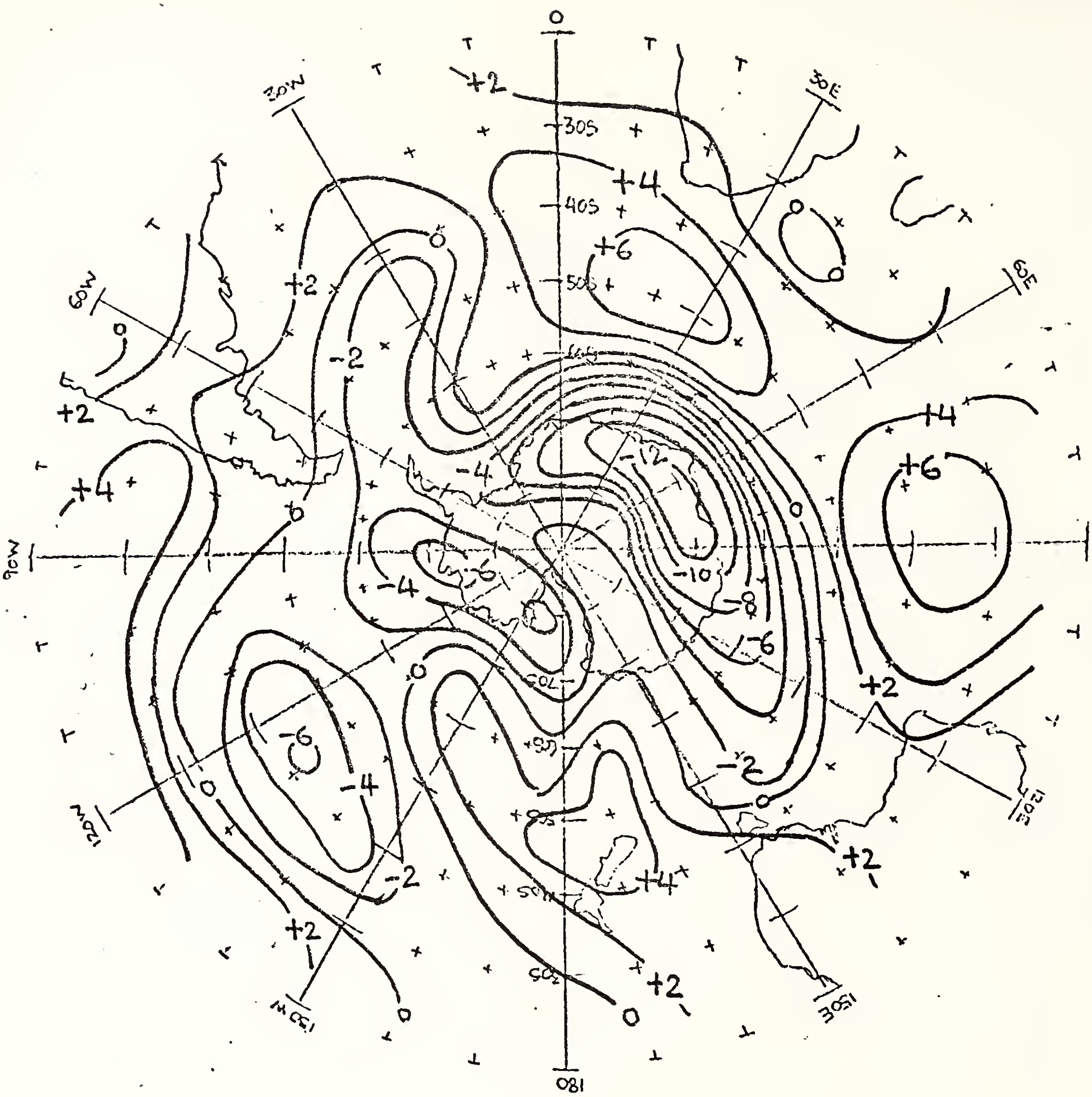

500 mb Geopotential Anomalies (gpdm) - Seasonal Means.

Data Extracted from Hemispheric Analyses Produced at the National Meteorological Analysis Centre, Melbourne

June - August 1979 (Winter)

FIGURE 5

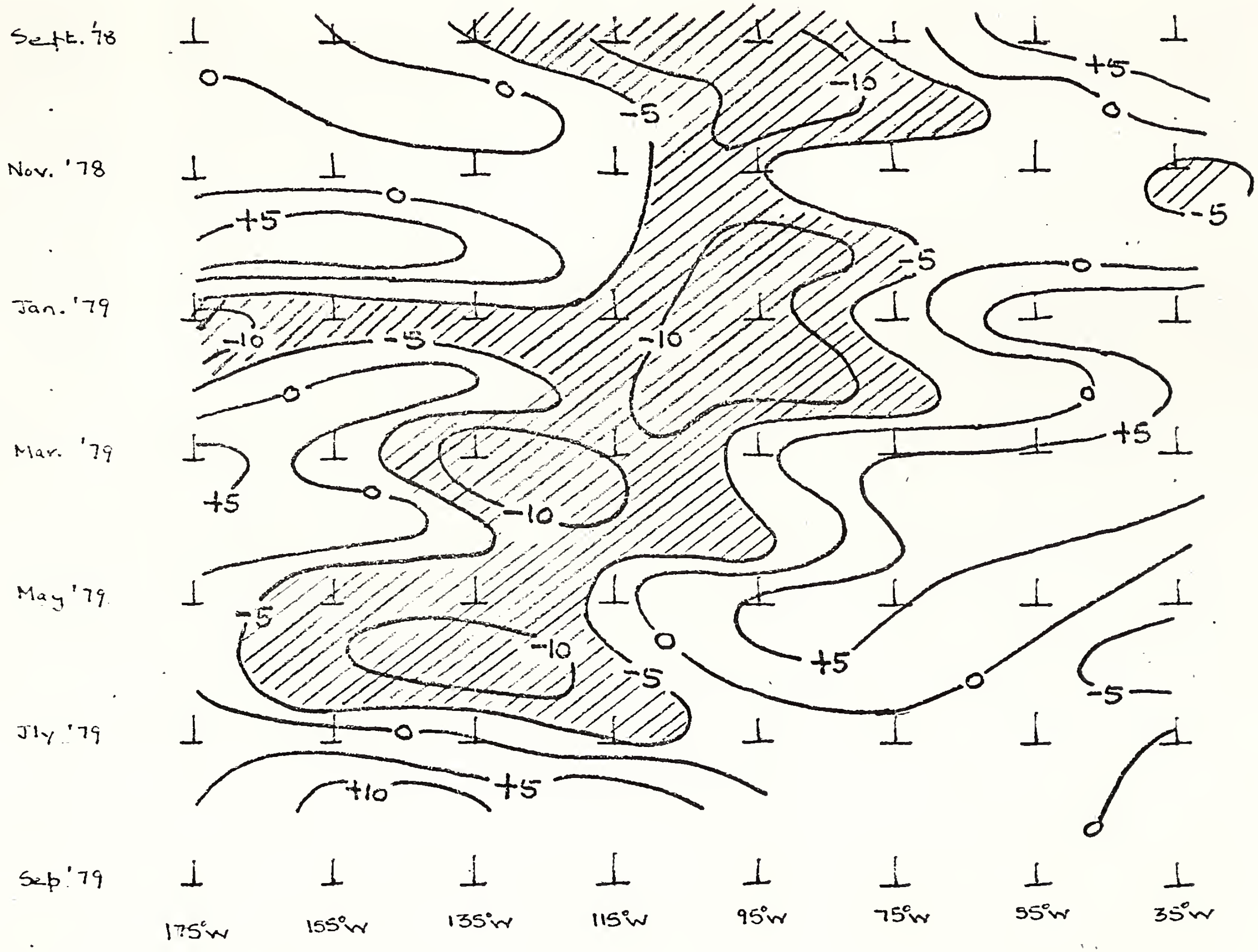

Longitude - Time Section
500 mb monthly mean anomalies (gpdm)
Latitude - 55 S.

# A diagnostic study of the 1976-7 and 1977-8 winters over the Northern Hemisphere

Harold J. Edmon, Jr.
The Joint Institute for the Study of the Atmosphere and Ocean
AK-40, University of Washington
Seattle, 98195

This paper will examine the horizontal and vertical structure of winters of 1976-7 and 1977-8 (W77 and W78, respectively) over the Northern Hemisphere. This study has two main objectives. One objective is to document the atmospheric conditions during two winters which had record cold temperatures in the eastern United States and yet had very different precipitation patterns, especially over the western United States. The second objective is to see if individual winters show the same relationships between mean and eddy fluxes and other circulation statistics as the eleven year mean winter reported on in a series of papers by Ngar-Cheung Lau. The data source for this study is the NMC octagonal grid analyses. The eleven year mean winter is an average of the winters of 1965-6 through 1975-6. The winter period is taken to be the 120 days starting 15 November except for W77 which is the 99 days starting 13 November.

The geopotential height anomalies (Figs. 1-4) are restricted mainly to the Western Hemisphere in both winters. Both have a stronger than normal Aleutian low which is south and west of its normal position. The high anomaly stretches the whole length of the west coast of the United States in W77, but is restricted to Canada in W78. The zonally-averaged anomalies increase with height in W77, but maximize at 300 mb in W78. The anomaly in the lower polar stratosphere is also very different in the two winters. The longitude-height cross-sections reveal the equivalent barotropic nature of the anomalies, with no tilt to the anomalies. The anomalies at 45°N maximize at the tropopause.

The temperature anomalies (Figs. 5-7) are nearly in phase with the height anomalies. They show warm anomalies over Alaska and Greenland and cold over the eastern United States. The temperature anomalies at 45°N maximize in the middle troposphere and reverse sign at the tropopause. Figs. 5 and 6 also show the transient eddy heat flux arrows. The fluxes show a tendency to be directed down the local temperature gradient in the zonal and meridional directions. This has also been noticed for the eleven year average winter. Anomalies of thermal advection by the time mean flow (Figs. 8 and 9) are almost in phase with the temperature anomalies. Thus the temperature anomalies are partially maintained by the time mean flow. There were no significant anomalies in the transient eddy heat flux convergence.

The zonal wind distribution (Figs. 10 and 11) shows stronger than normal jets displaced to the south of their normal positions. In W77 the exit region for the Pacific jet is displaced to the north of its normal position. Thus, the storm track was displaced into Alaska. In W78 the exit region was over California, resulting in a similar displacement of the storm track. Divergence anomalies, calculated by using the vorticity equation and assuming the time rate of change, twisting term and friction at 300 mb are zero, are shown in Figs. 12-14 with the corresponding precipitation anomalies. There is good correspondence between excess precipitation and excess divergence, which indicates excess upward motion. The converse of the previous statement is also true. Since the main features of the divergence pattern can be obtained from the time mean vorticity advection without the transient eddy convergence, these results indicate that precipitation anomalies can be inferred from knowledge of vorticity advection, which can be obtained from the height field.

Fig. 15 shows the 1000 mb heights and the irrotational component of the potential vorticity flux by the time mean flow at 200 mb for W77. The flux has a tendency to be directed out of surface highs, which are source regions of potential vorticity, into surface lows, which are sink regions. This tendency was observed for the eleven year mean, W77 and W78 for both the time mean flux and the transient eddy flux.

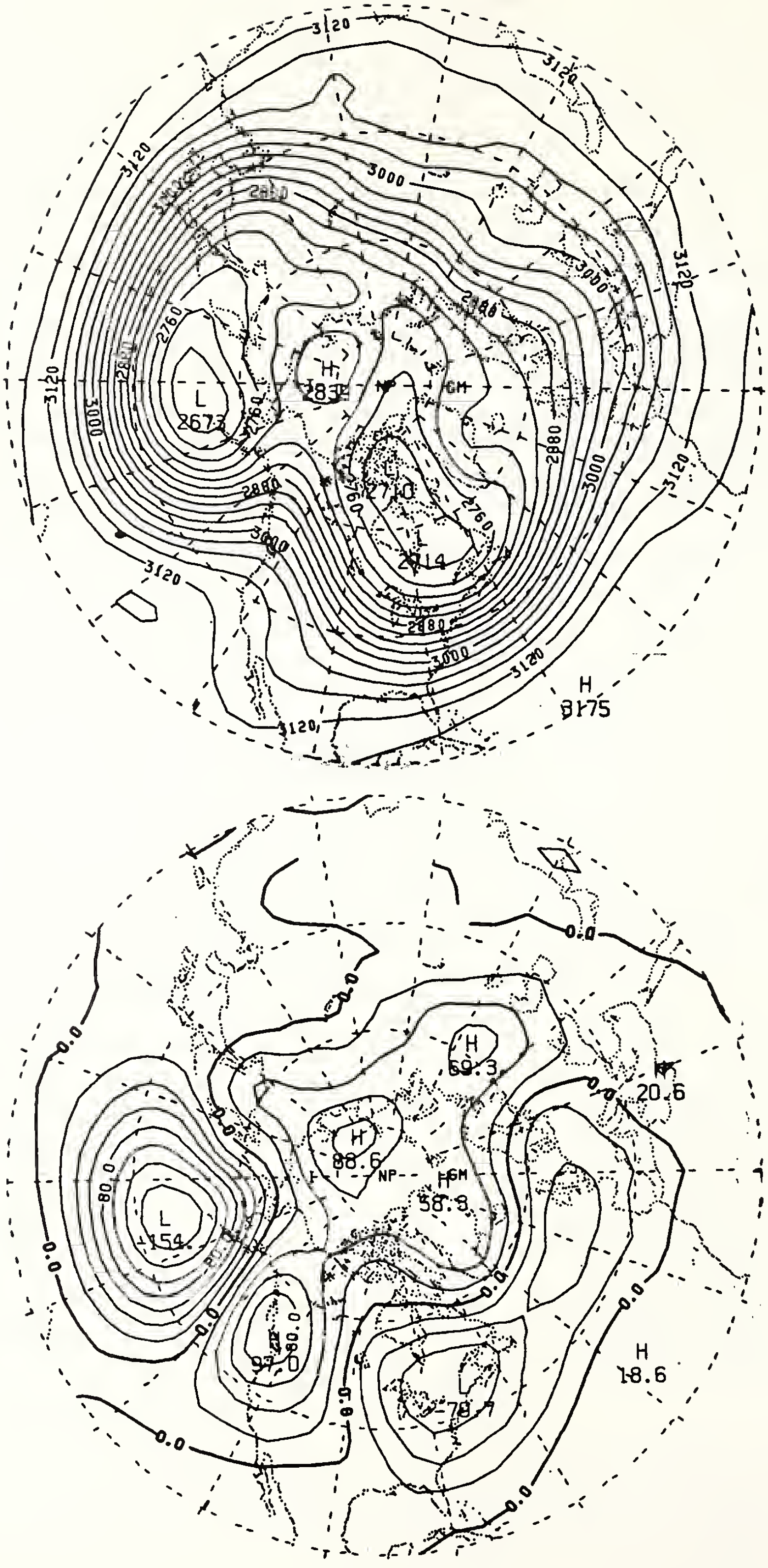

Fig. 1 700 mb height (upper) and anomaly from eleven year mean (lower) for W77. Contour interval is 30 m for height and 20 m for anomaly.

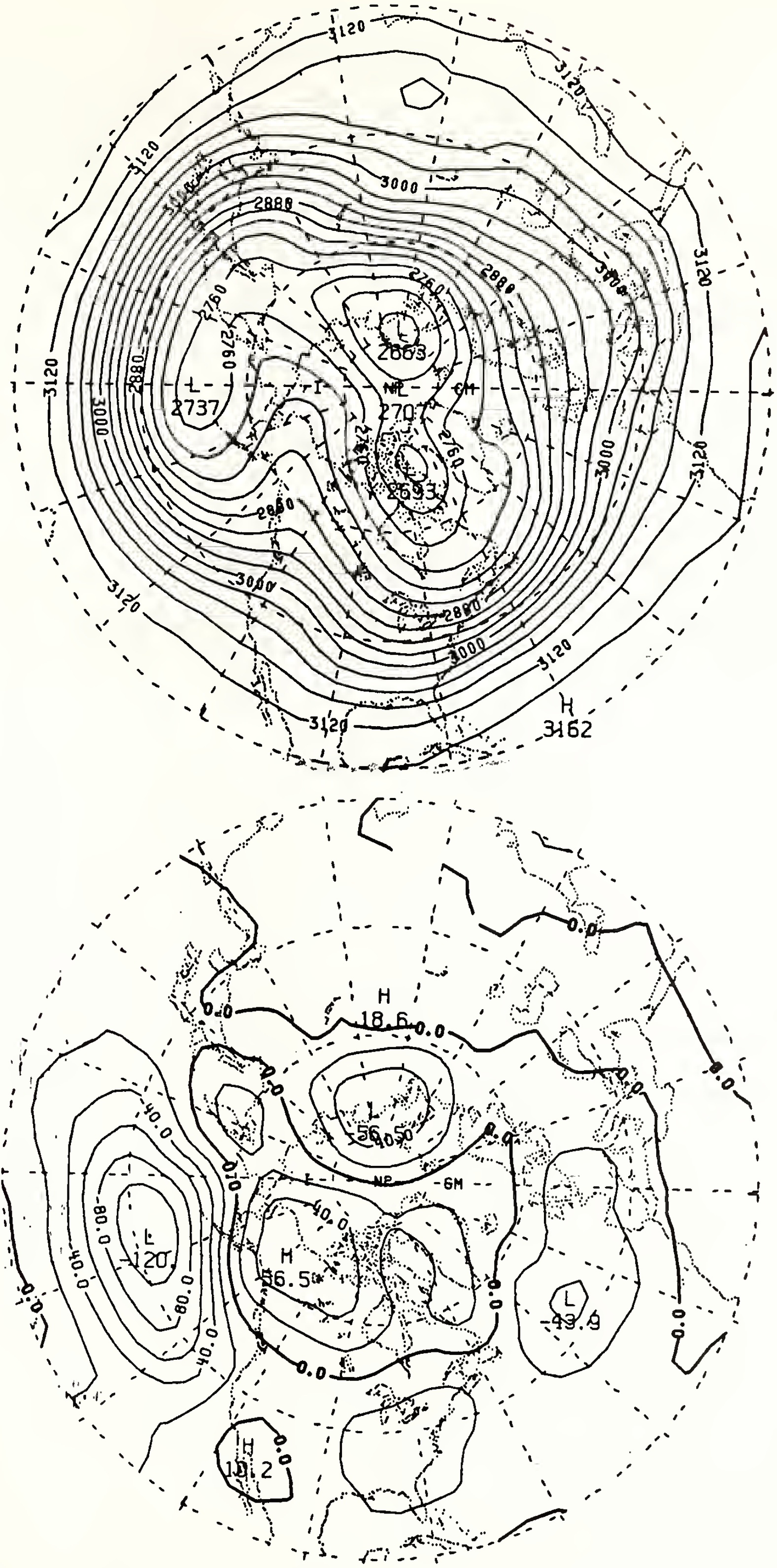

Fig. 2 Same as Fig. 1 for W78.

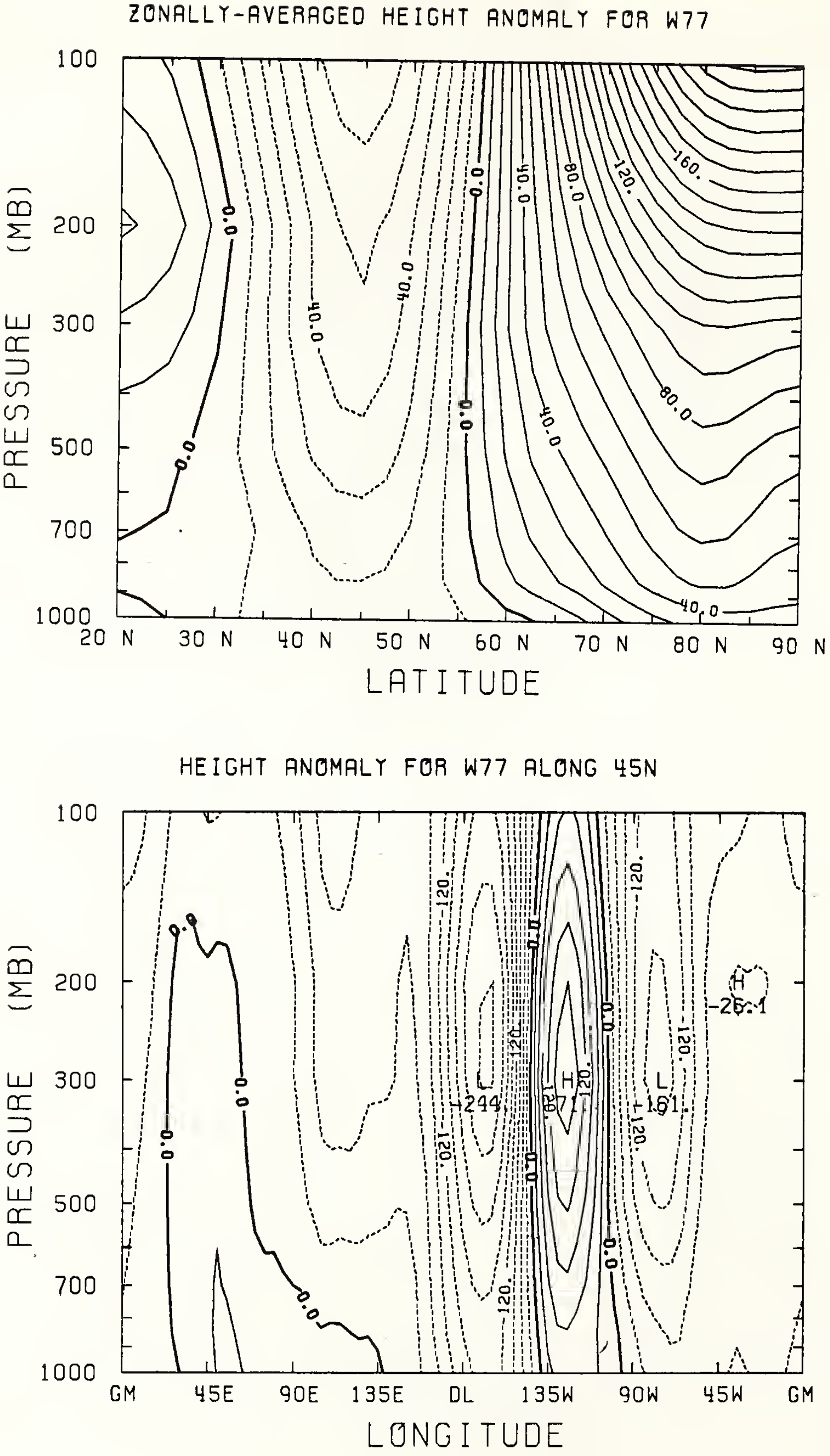

Fig. 3 Zonally-averaged height anomaly (upper) and height anomaly along 45°N for W77. Contour interval is 10 m for top figure and 30 m for lower figure.

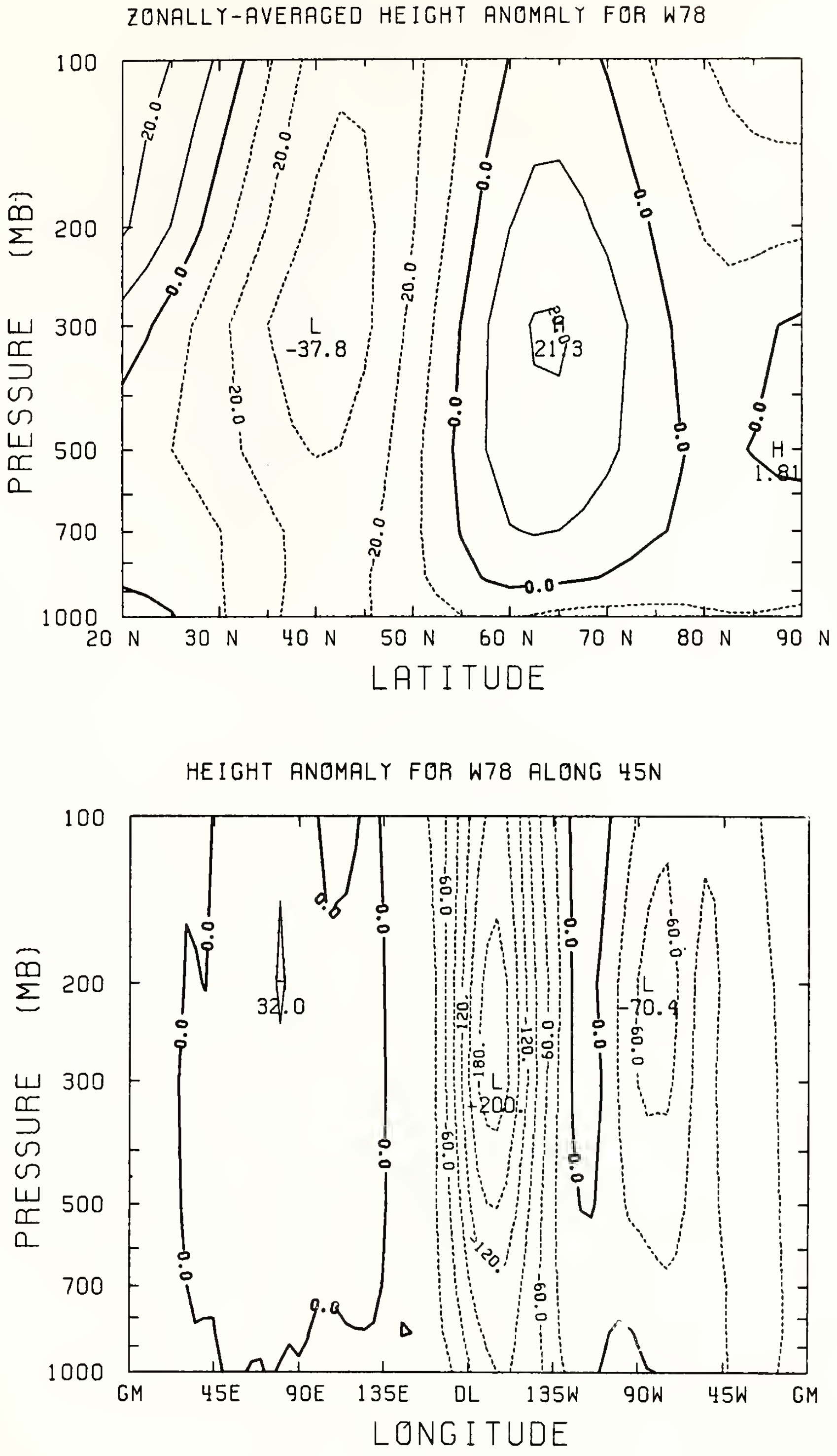

Fig. 4 Same as Fig. 3 for W78.

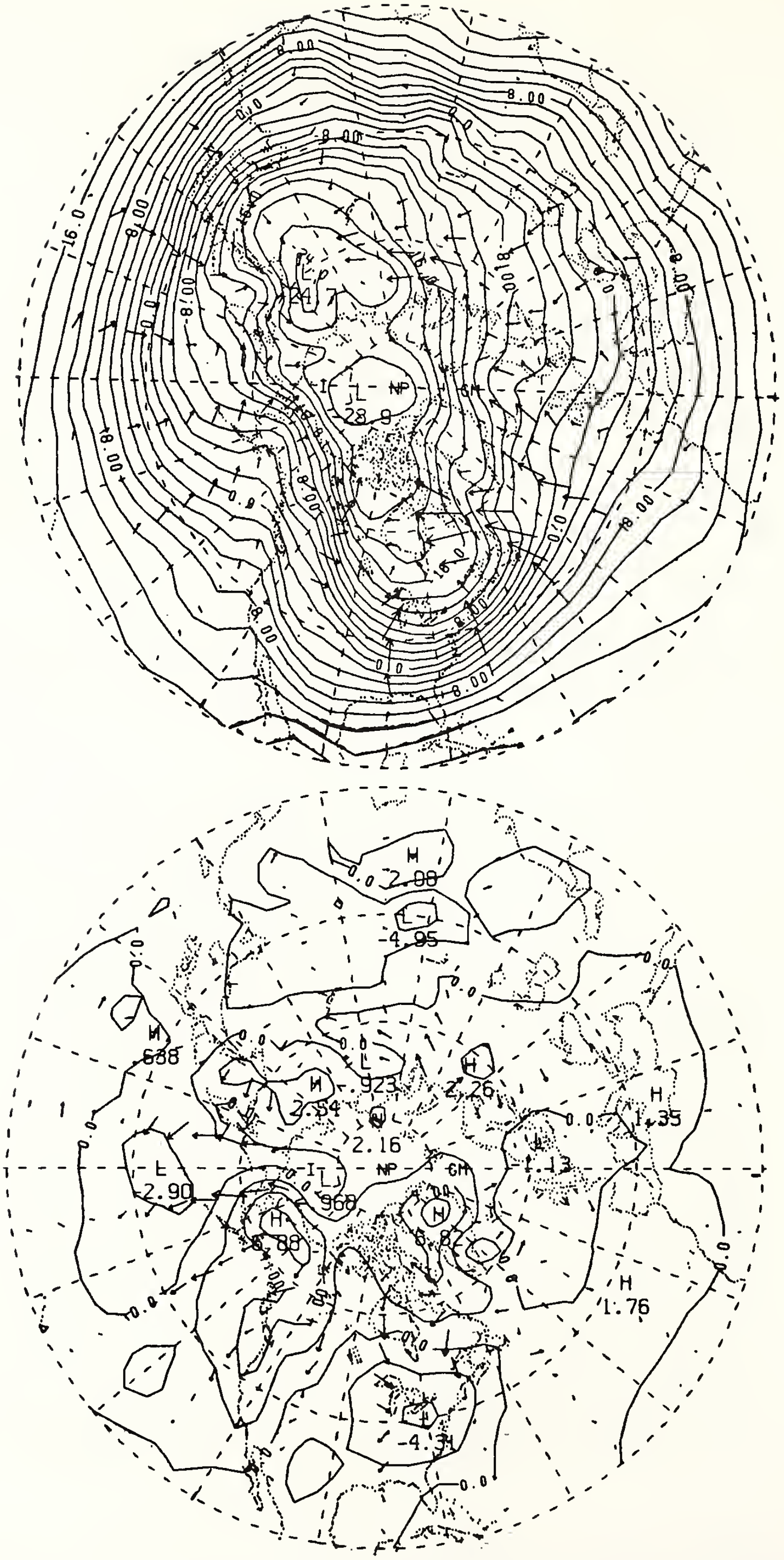

Fig. 5 850 mb temperature and transient eddy heat flux (upper) and anomalies from eleven year mean (lower) for W77. Contour interval is 2°C.

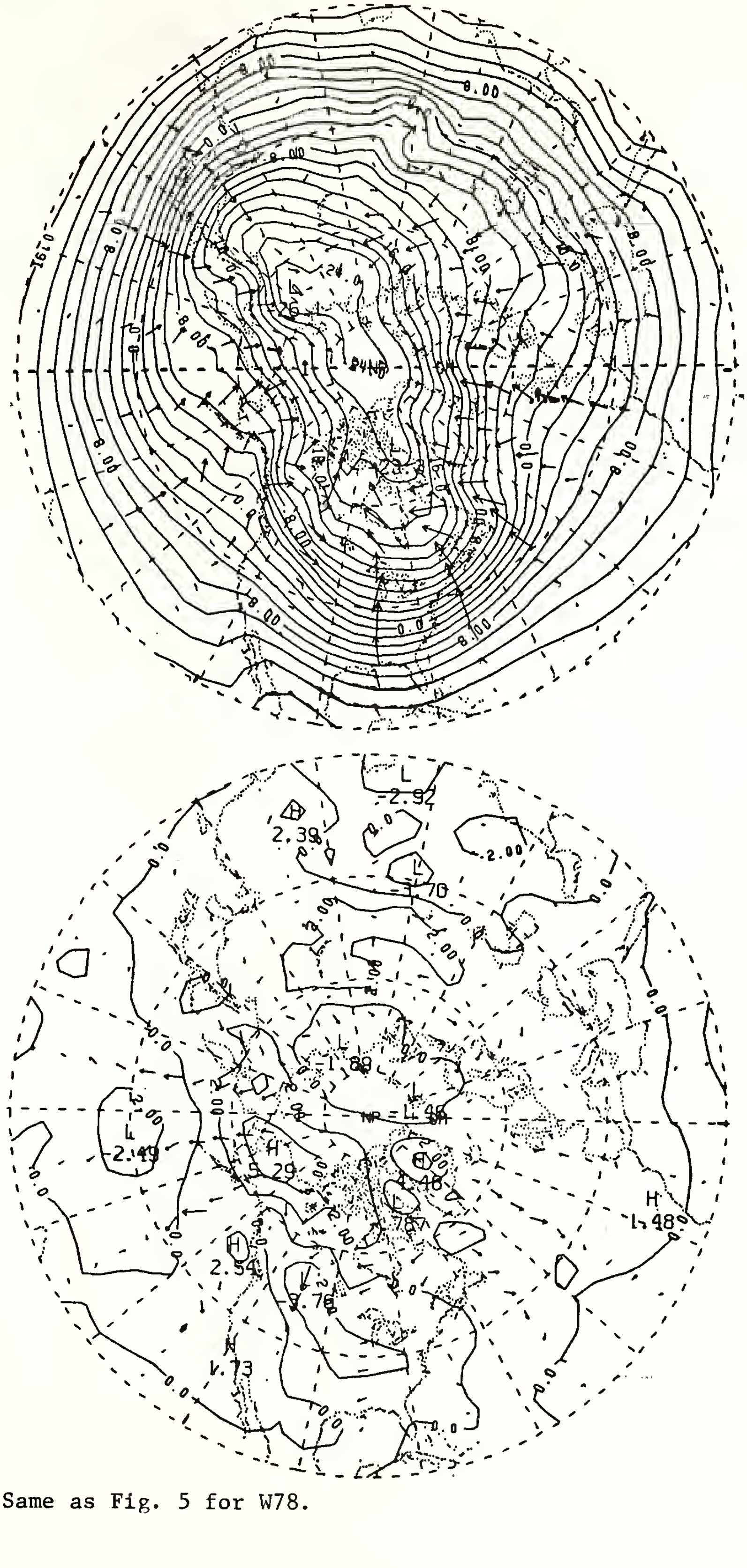

Fig. 6 Same as Fig. 5 for W78.

TEMPERATURE ANOMALY FOR W77 ALONG 45N

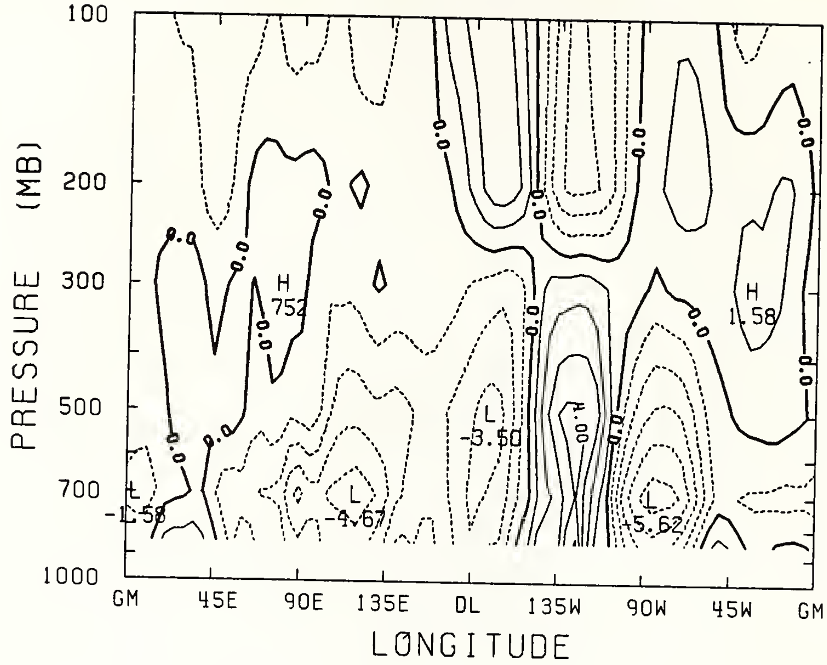

TEMPERATURE ANOMALY FOR W78 ALONG 45N

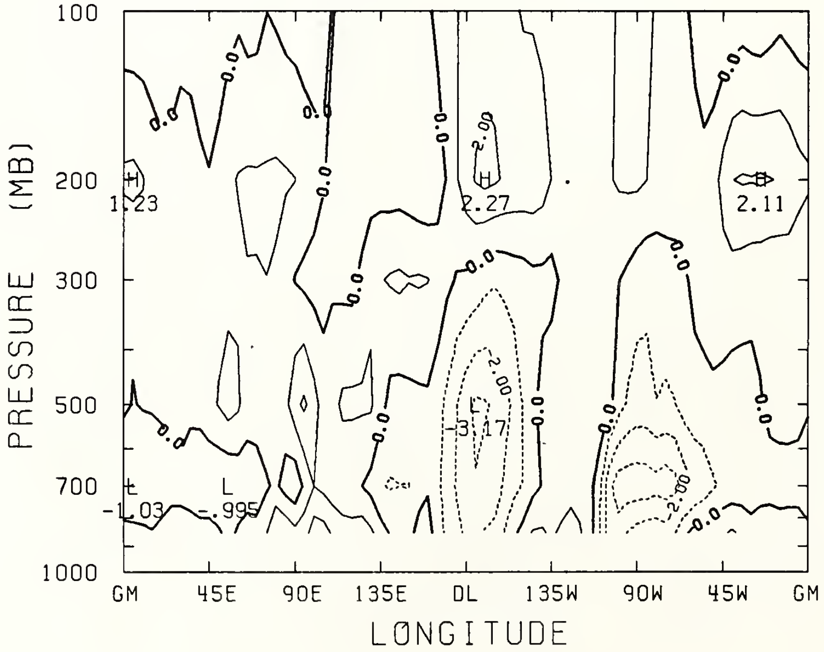

Fig. 7 Temperature anomaly along 45°N for W77 (upper) and W78 (lower). Contour interval is 1°C.

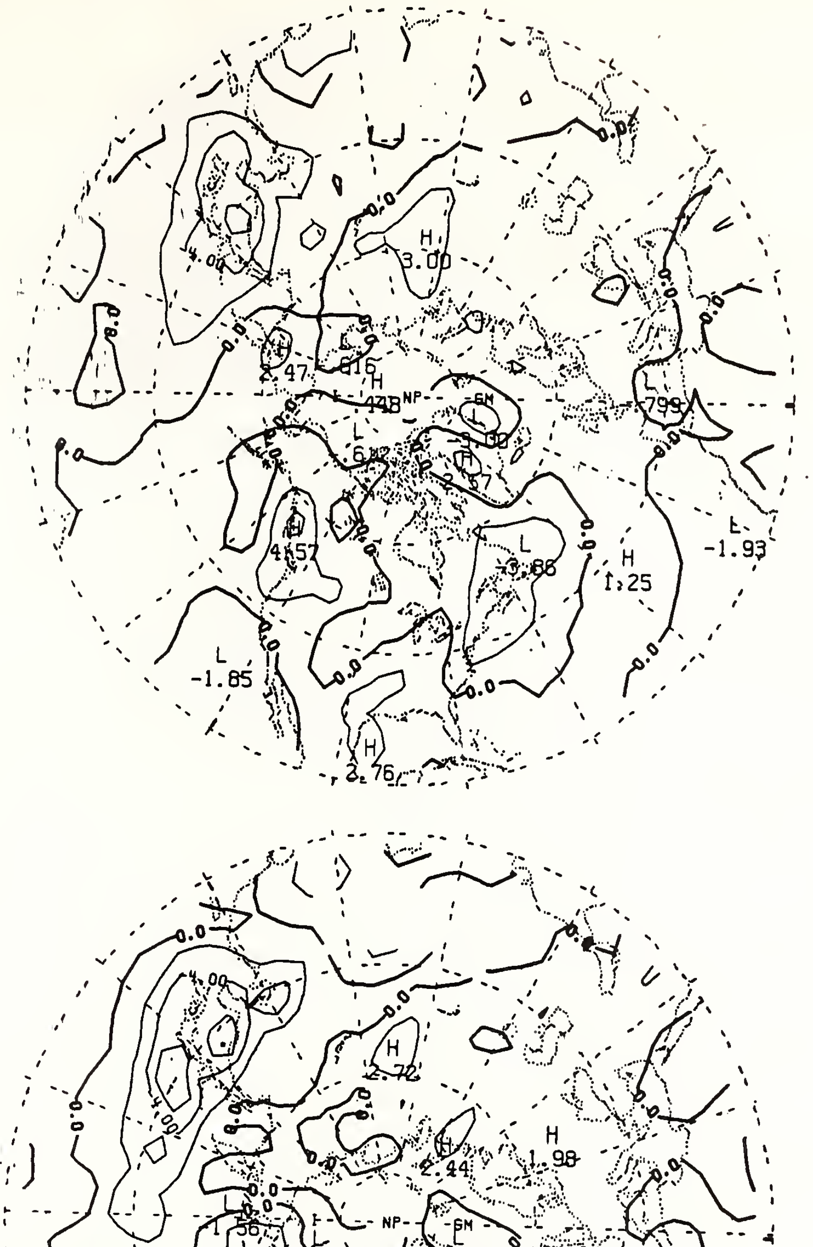

Fig. 8 850 mb temperature advection by time mean flow for eleven year winter (upper) and W77 (lower). Contour interval is 2°C $d^{-1}$.

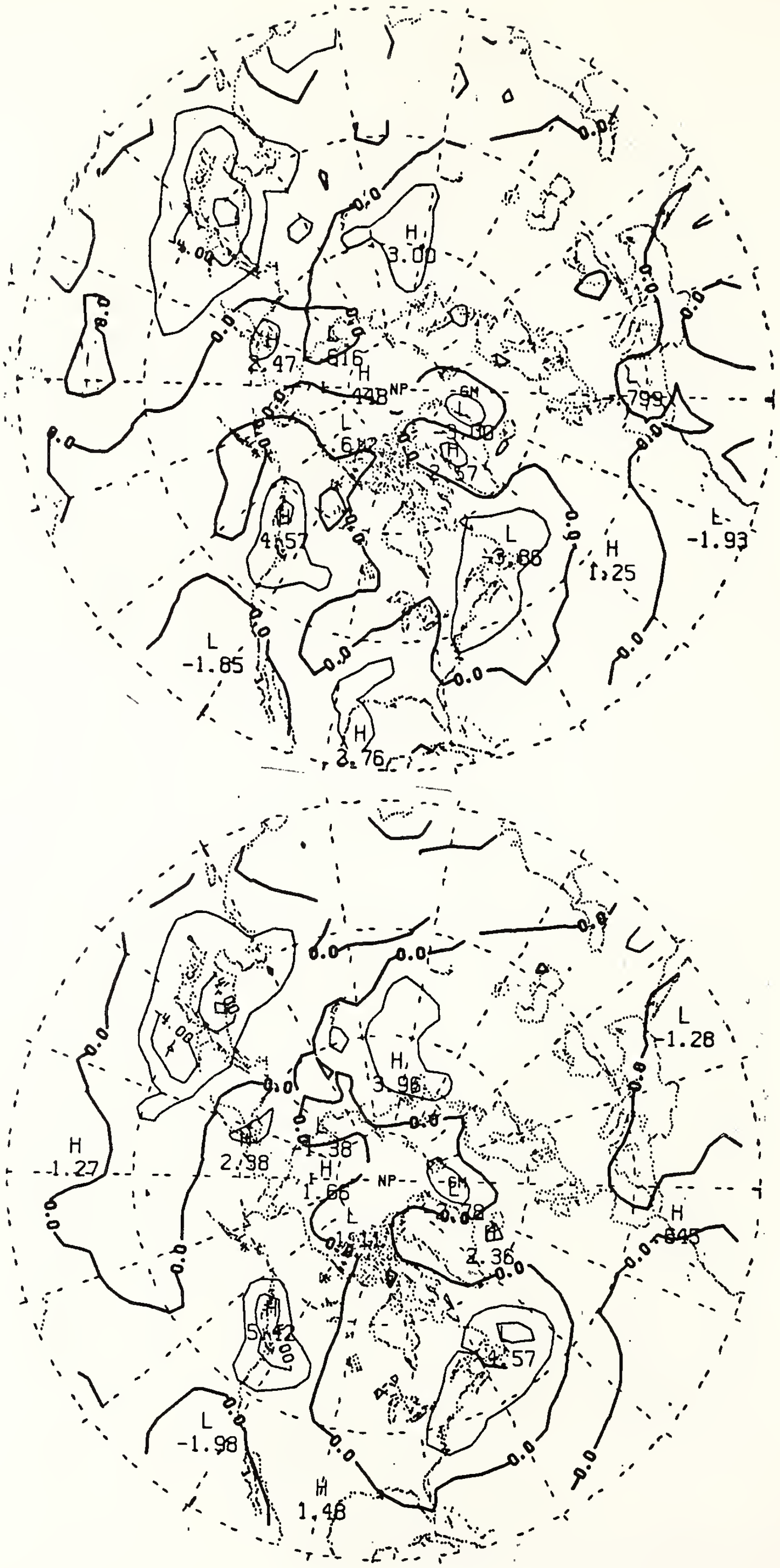

Fig. 9 Same as Fig. 8 except W78 (lower).

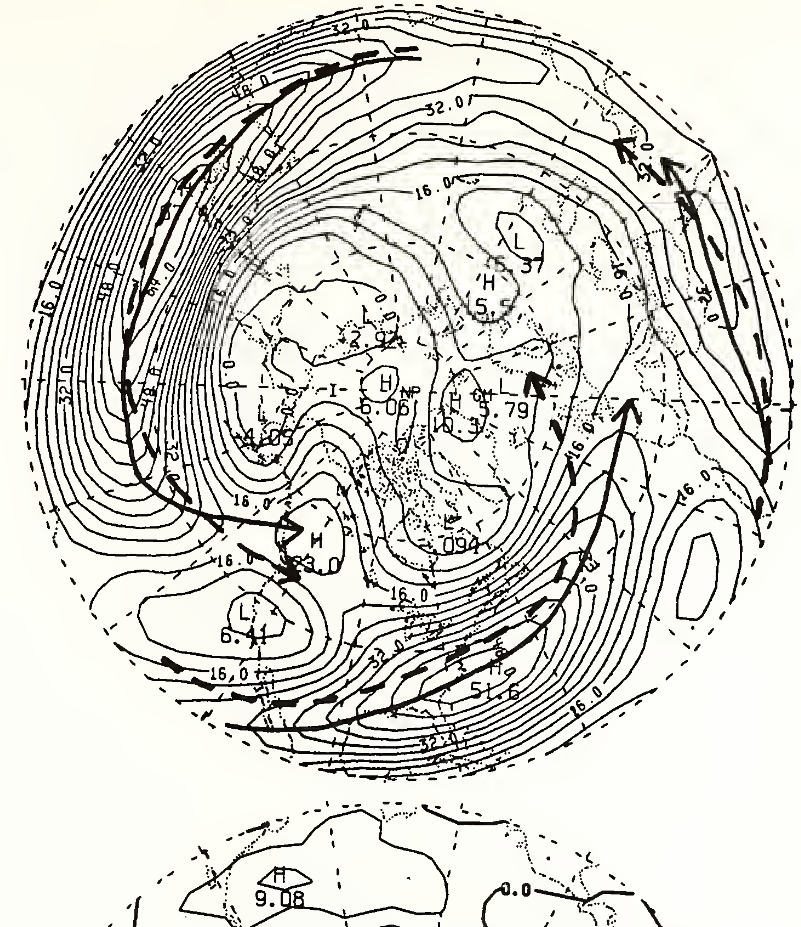

Fig. 10 Same as Fig. 1 except for 300 mb zonal wind for W77. Contour interval is 4 m $s^{-1}$. Jet core for eleven year mean given as dashed arrow, for W77 as solid arrow.

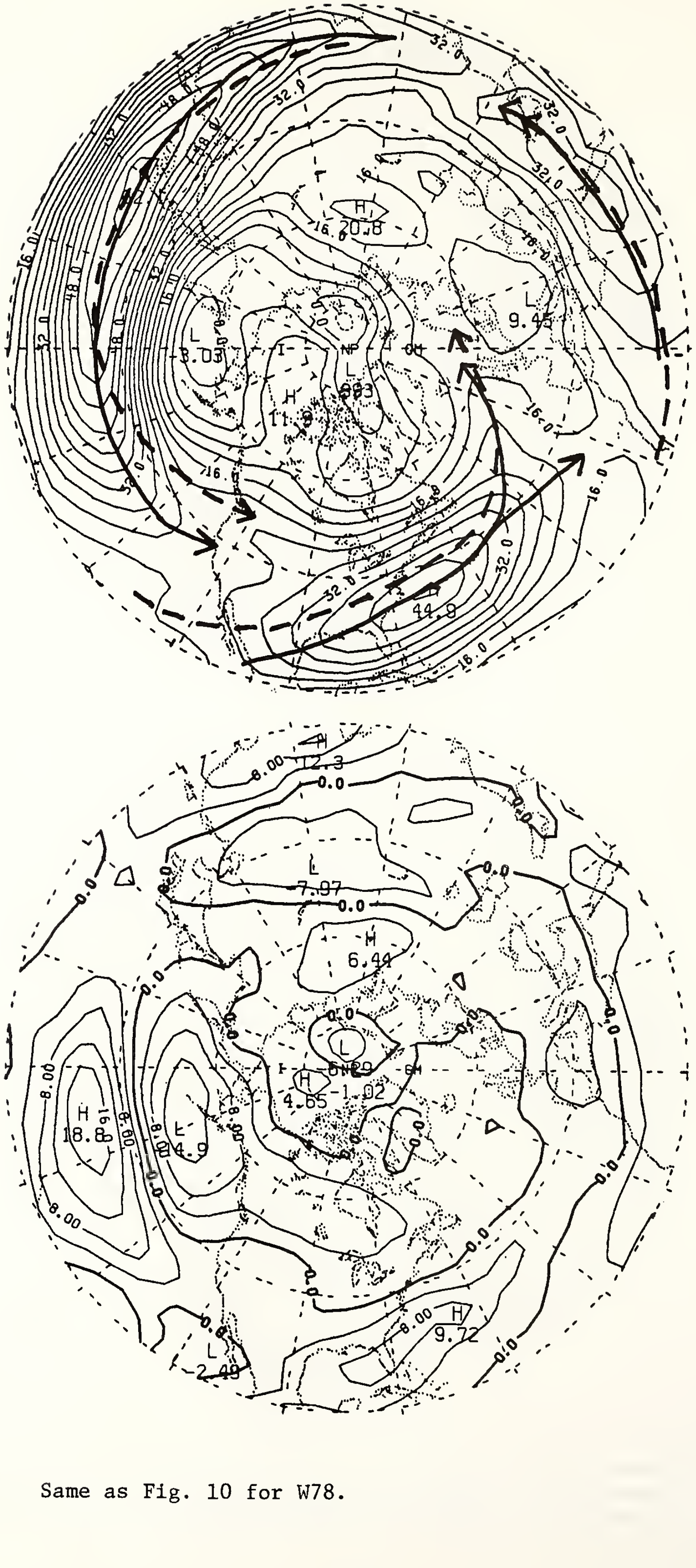

Fig. 11 Same as Fig. 10 for W78.

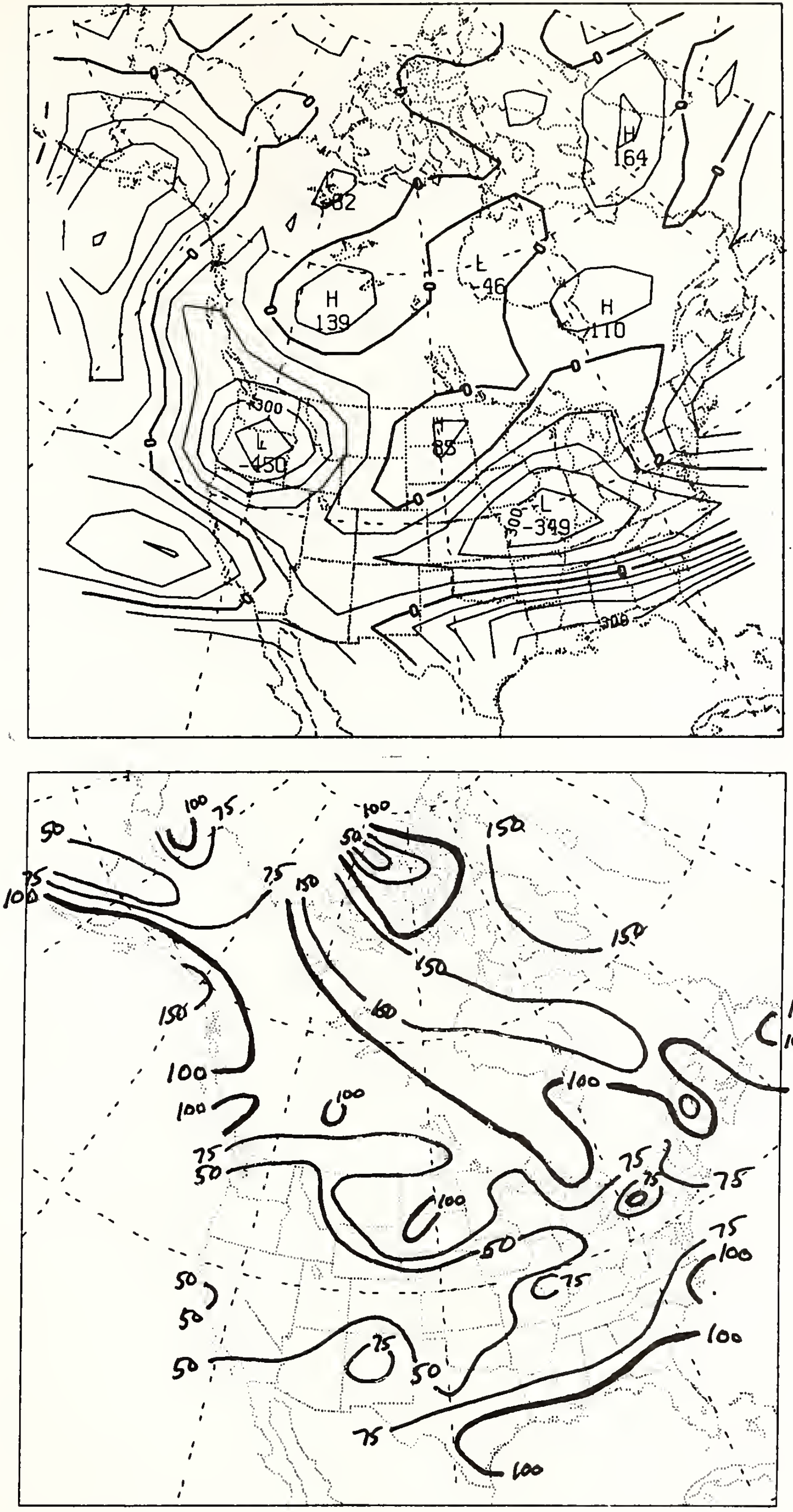

Fig. 12 Divergence anomaly at 300 mb from eleven year mean (upper) and percentage of normal precipitation (lower) for W77. Divergence contour interval is 7.5 x $10^{-7}$ $s^{-1}$.

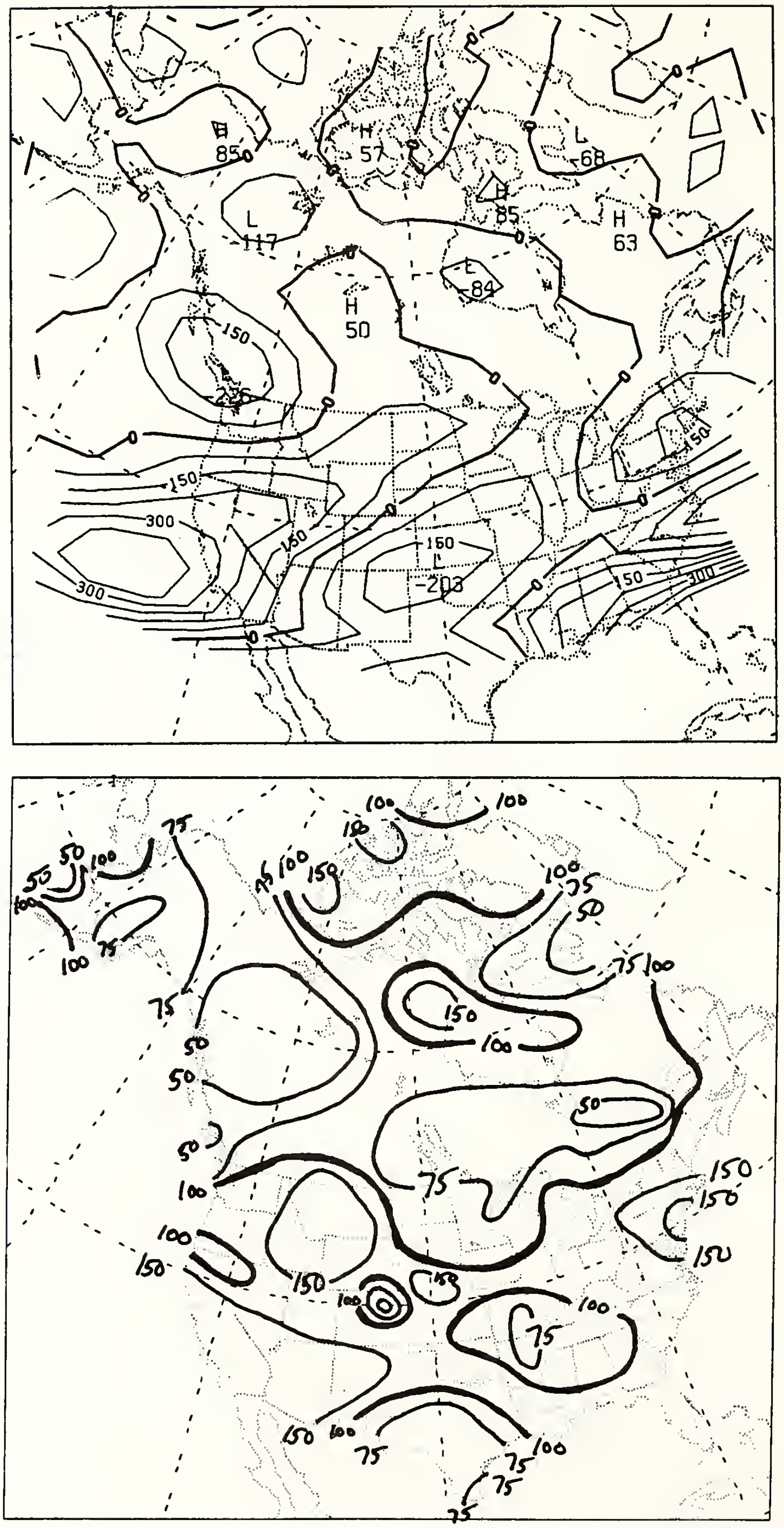

Fig. 13 Same as Fig. 12 for W78.

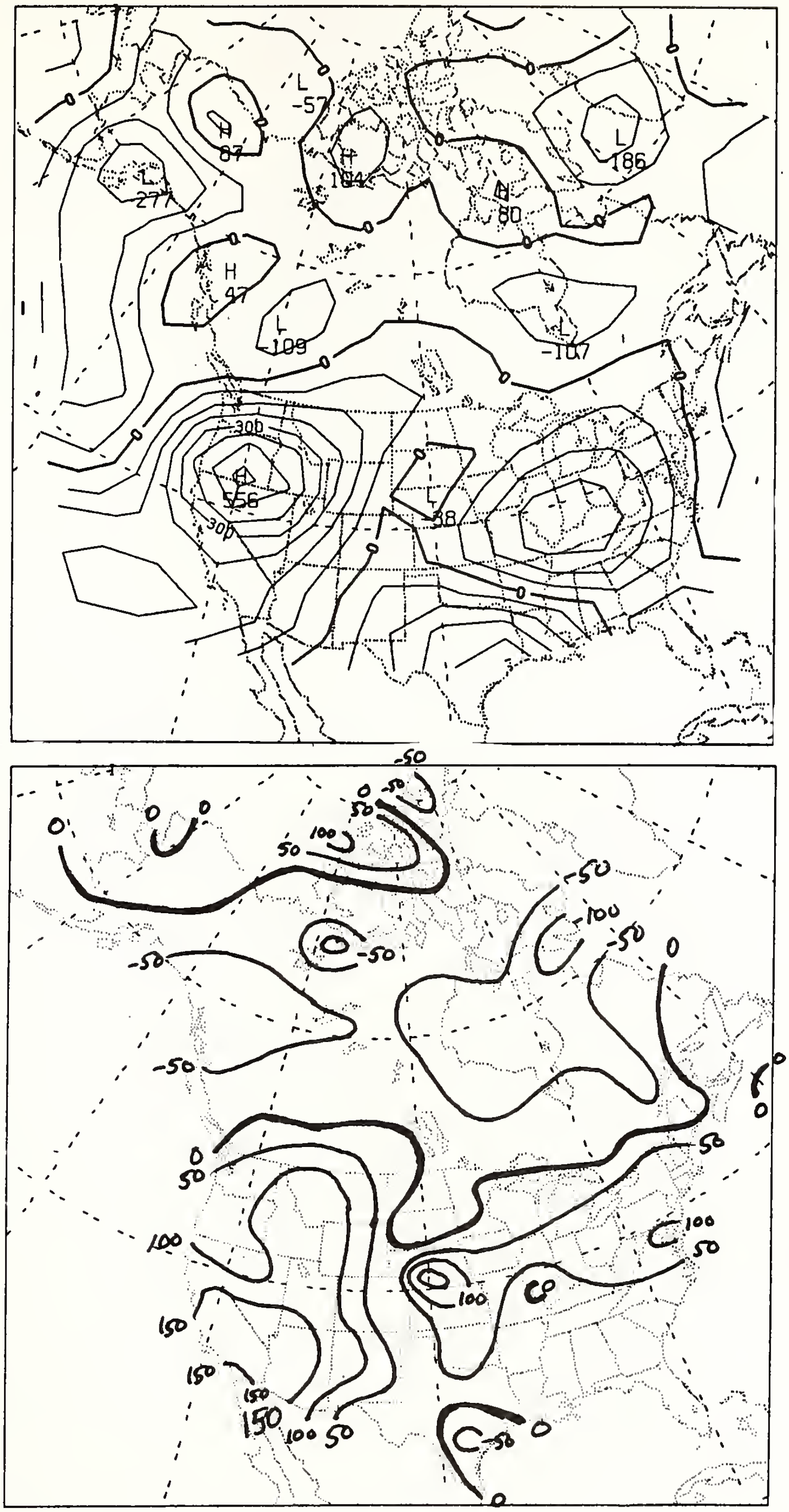

Fig. 14 Divergence change at 300 mb (upper) and change in percentage of normal precipitation (lower) from W77 to W78. Divergence contour interval is 7.5 x $10^{-7}s^{-1}$.

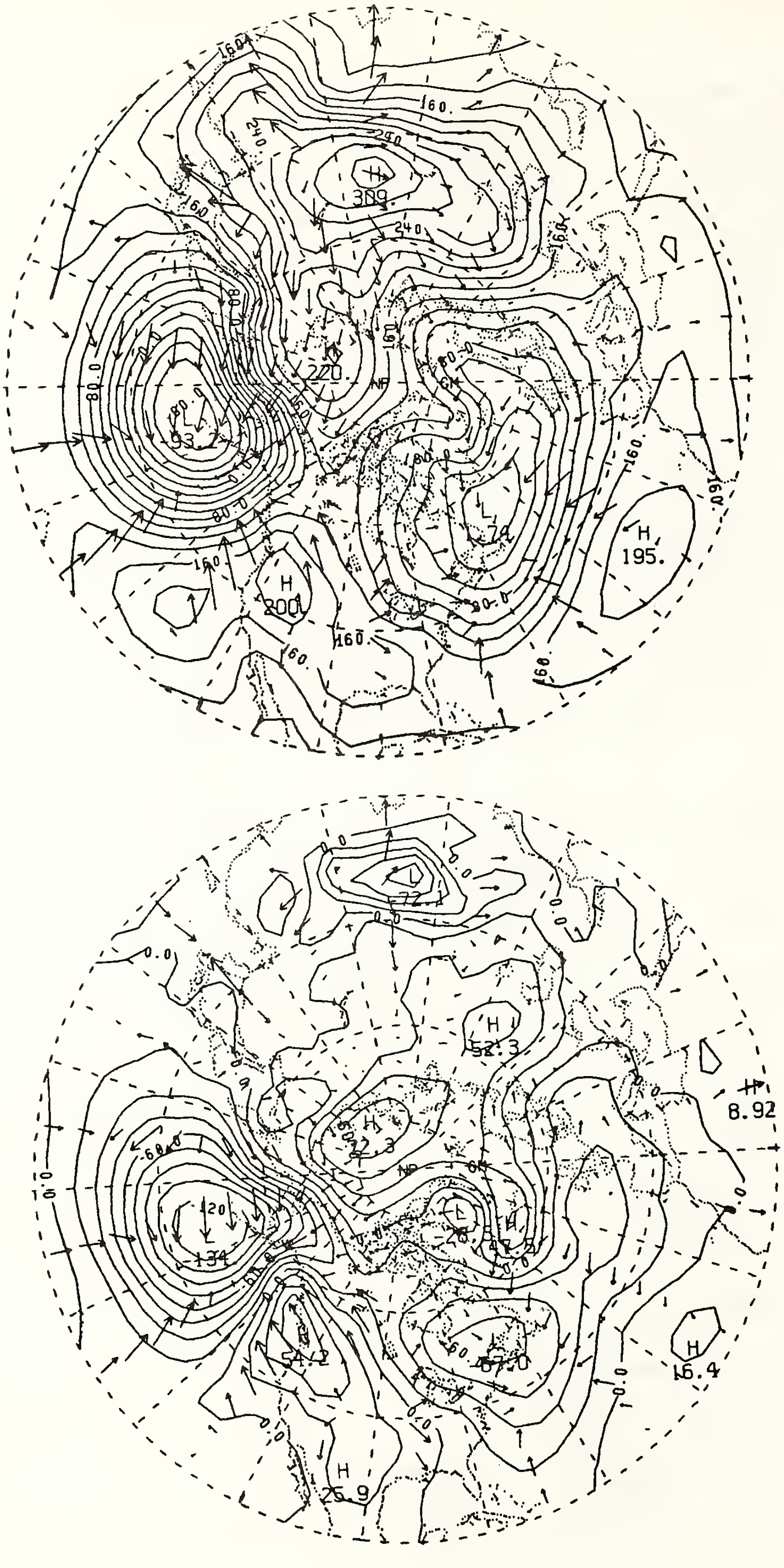

Fig. 15 1000 mb height and 200 mb irrotational component of time mean potential vorticity flux (upper) and anomalies from eleven year mean (lower) for W77. Contour interval is 20 m height and 15 m for anomaly.

# Precipitation Along the West Coast of North America

James P. McGuirk
Department of Meteorology
Texas A&M University
College Station, Texas

Monthly precipitation at seven stations along the West Coast of North America (fig.1) is analyzed. The record length at six of the stations exceeded 100 years (67 years at Prince Rupert). A variety of analysis procedures were employed to smooth the data or highlight certain features, the primary shortcoming of the data set being that it contains too much signal or too much noise to easily identify and interpret specific physical characteristics. The first objective of the analysis was to identify consistent long term patterns in the data relevant to large-scale atmospheric circulation. Important findings were:

(i) Although the data exhibited no uniform long-term trends, secular anomalies of periods up to 30 years duration were observed. The relative dryness at Eureka for about 1910 to 1940 is one example. (fig.4)

(ii) Fluctuations with a mean period of about 20 years were observed, although not strongly at all stations. The steadiest and most persistant signal is observed at Portland (fig. 3b.) The nature of the data and the length of the records preclude an assessment of statistical significance or physical meaning.

(iii) Perhaps even more interesting is the tendency for the extrema of the long-period fluctuations to migrate northwards with time. Fig.6 demonstrates this tendency. Additionally, time domain Fourier analysis of the precipitation at each station show relative spectral peaks in the 20-25 year periodicity range with a phase which progresses uniformly northward.

(iv) A high correlation (correlation coefficient of .64) exists between the variations in winter season precipitation and the variations in the strength of the 200 mb geostrophicly determined westerlies at about the same locations as the stations (fig. 5). Presumably, the correlation is a result of the synoptic origin of the precipitation and the correspondence between cyclones and jet streams. Thus trends in precipitation can be used to monitor trends in the westerlies (at least at longitudes near the Pacific Coast of North America.)

(v) Long-term persistence in the sign of the precipitation anomalies seems to correlate well with persistent sea surface temperature anomalies under the Pacific subtropical high, in general agreement with (fig. 7) Namias's observations.

A second analysis objective was to gain some perspective of the last several year's precipitation anomalies along the coast.

(vi) Compared to the records (which exceed 100 years in length) the only record setting observations occurred in the 1977 winter season along the northern coast. Several other large anomaly observations, both positive and negative, were recorded since 1976.

(vii) The drought conditions of the latter part of the 1970's were preceeded by large average positive anomalies for the preceeding ten years, compared to the long term mean. Thus, the dry conditions appeared to be more severe than if they had been preceeded by more normal amounts of precipitation.

(viii) In only five winter seasons of the record have precipitation deficiencies in excess of 30% of the mean been observed for at least four of the six in U.S. stations: 1977 and four years in the eleven year span between 1924 and 1934.

(ix) An empirical orthogonal function analysis demostrates that conditions of everywhere dry or everywhere wet along the U.S. Pacific coast explains 40% of West Coast precipitation variability (figs. 9 and 10).

(x) The second eigenfunction consisting of North and South coast anomalies of opposite signs, describes another 36% of the variance.

(xi) The third eigenfunction of the analysis including Prince Rupert indicates that that station varies nearly independently of all the U.S. stations (fig. 10.).

(xii) The time series of the amplitude of the first eigenfunction indicates the extent of the 1977 anomaly, as well as the generally dry years of the 1920's and 30's. Also indicated is the relatively increased occurrence of extremely wet years from the late 1930's through the 60's.

(xiii) The amplitudes of the second eigenfunction are strongly suggestive of a long-term trend in the distribution of precipitation along the west coast: highly variable, but generally wet northern regions through the first decade of the 1900's, an increase in variability and a return to northern wet conditions almost to the present, with a suggestion of a contemporary return to drier conditions. Anomalies of the opposite sign for the South coast follow from the shape of the eigenfunction. No cause for these fluctuations is suggested.

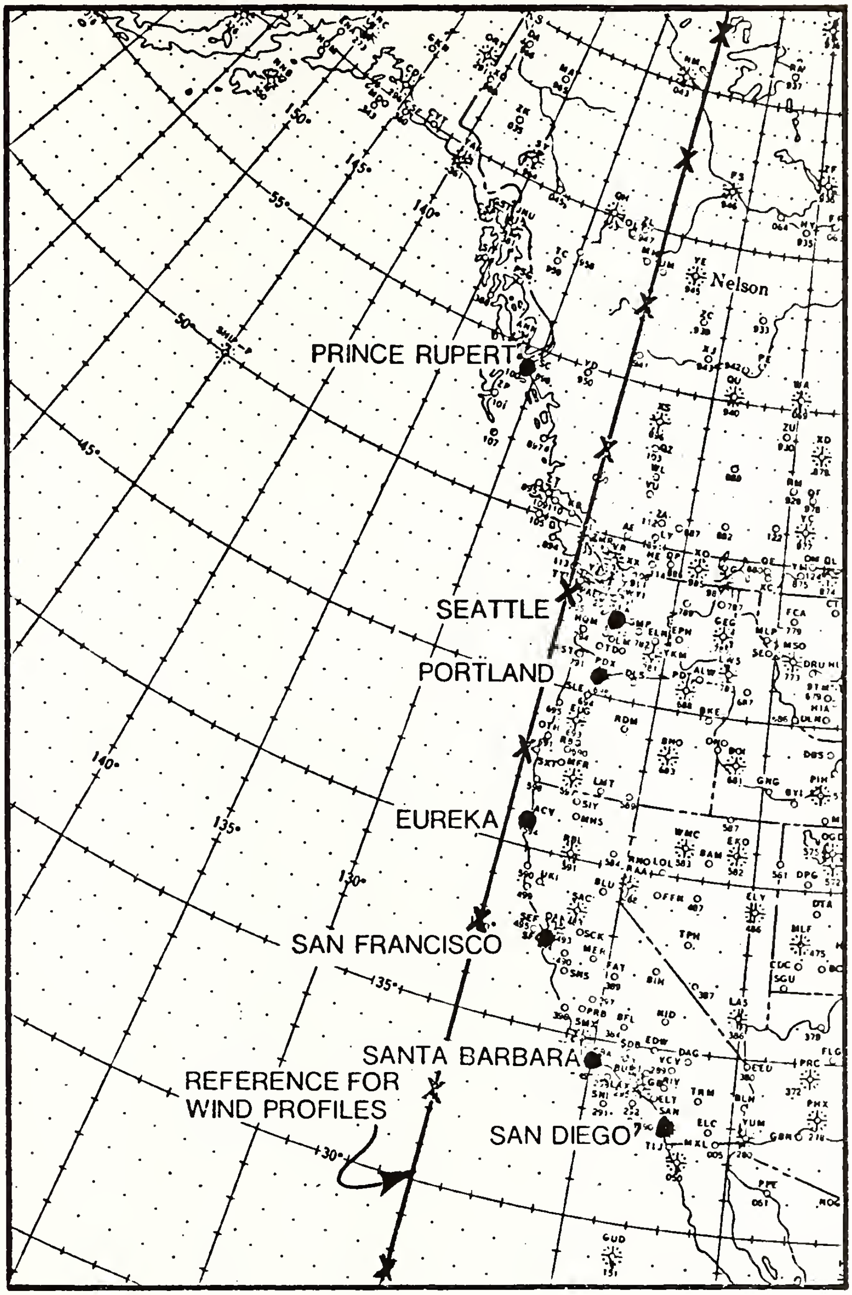

Fig. 1 DISTRIBUTION OF STATIONS FOR PRECIPATION DATA. LONGITUDINAL LINE INDICATES LOCATION OF WIND PROFILES.

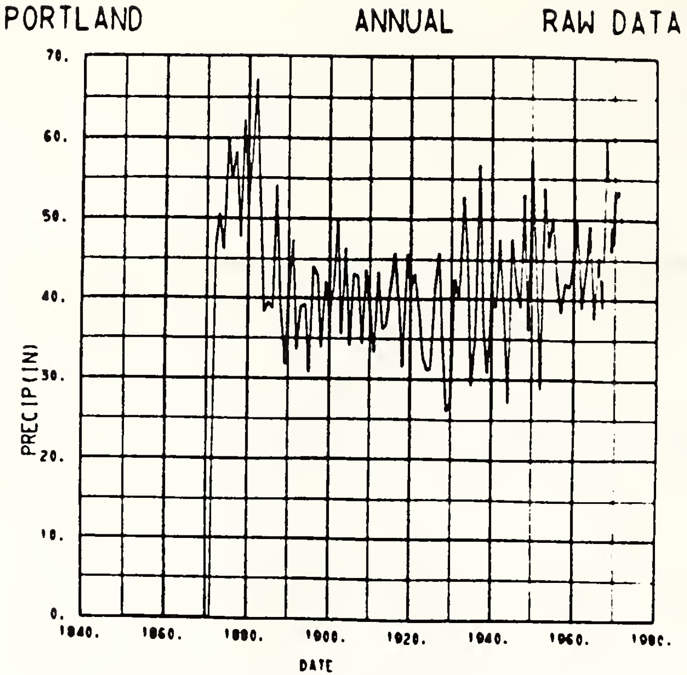

Fig. 2A Observed annual precipitation at Portland.

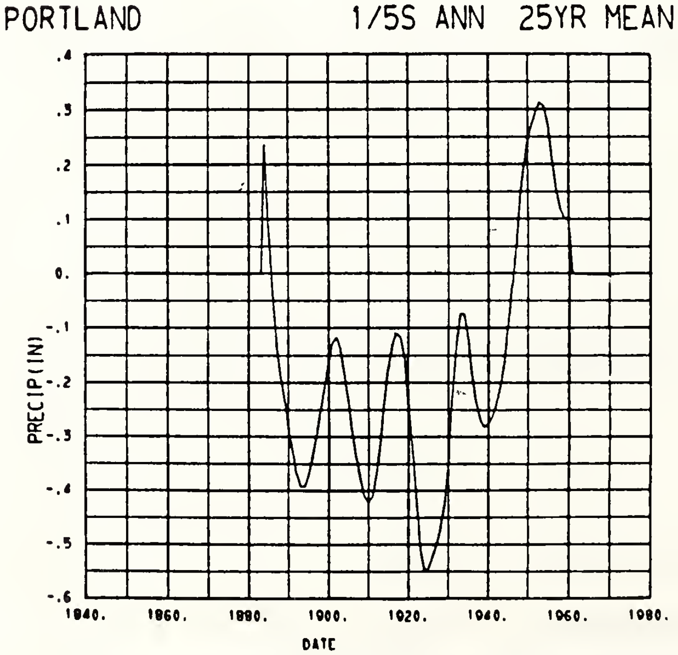

Fig. 2B Annual precipitation at Portland, divided into quintiles, weighted (+1, +.5, 0, -.5, and -1.0) according to intensity, and smoothed with a 25-year binomial filter.

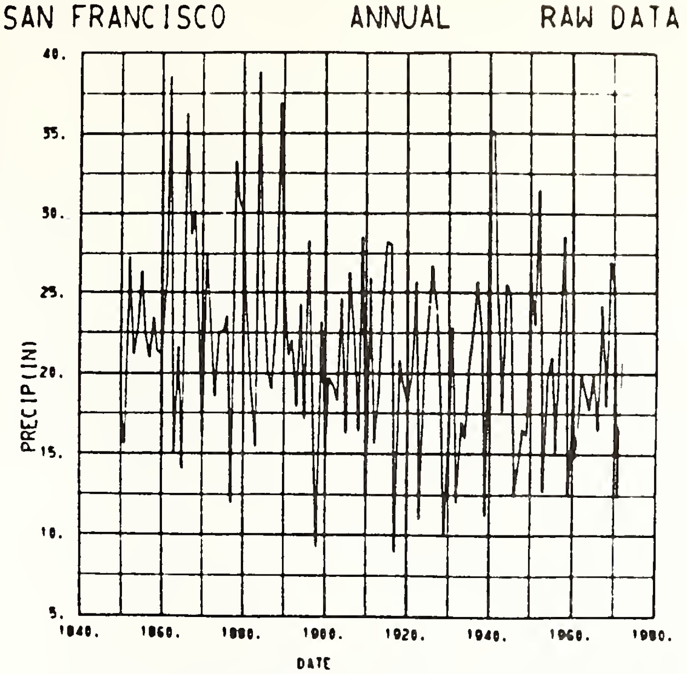

FIG. 3A OBSERVED ANNUAL PRECIPITATION AT SAN FRANCISCO

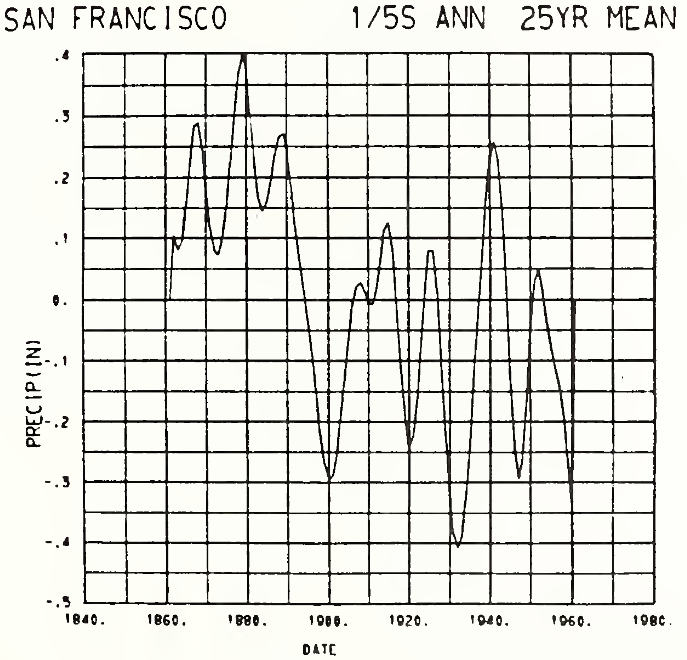

FIG. 3B ANNUAL PRECIPITATION AT SAN FRANCISCO, DIVIDED INTO QUINTILES, WEIGHTED (+1, +.5, 0, -.5, AND -1.0) ACCORDING TO INTENSITY, AND SMOOTHED WITH A 25-YEAR BINOMIAL FILTER.

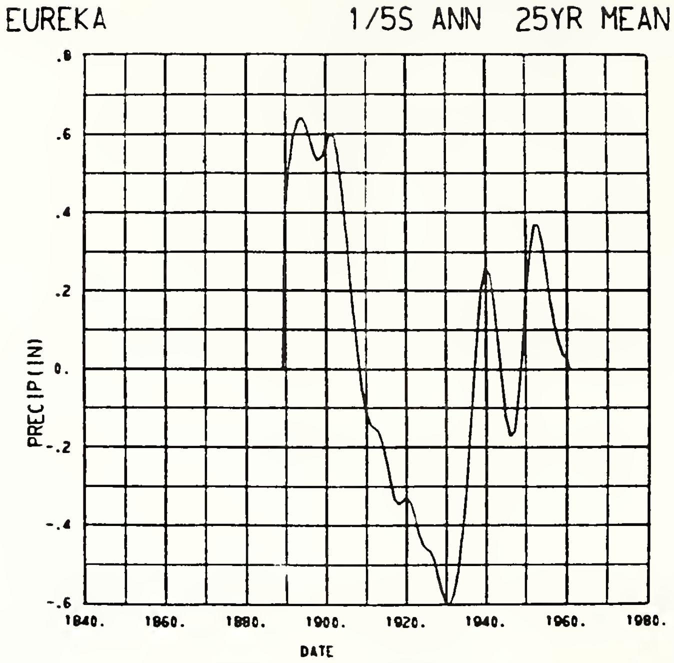

FIG. 4. ANNUAL PRECIPITATION AT EUREKA, DIVIDED INTO QUINTILES, WEIGHTED (+1, +.5, 0, -.5, AND -1.0) ACCORDING TO INTENSITY, AND SMOOTHED WITH A 25-YEAR BINOMIAL FILTER.

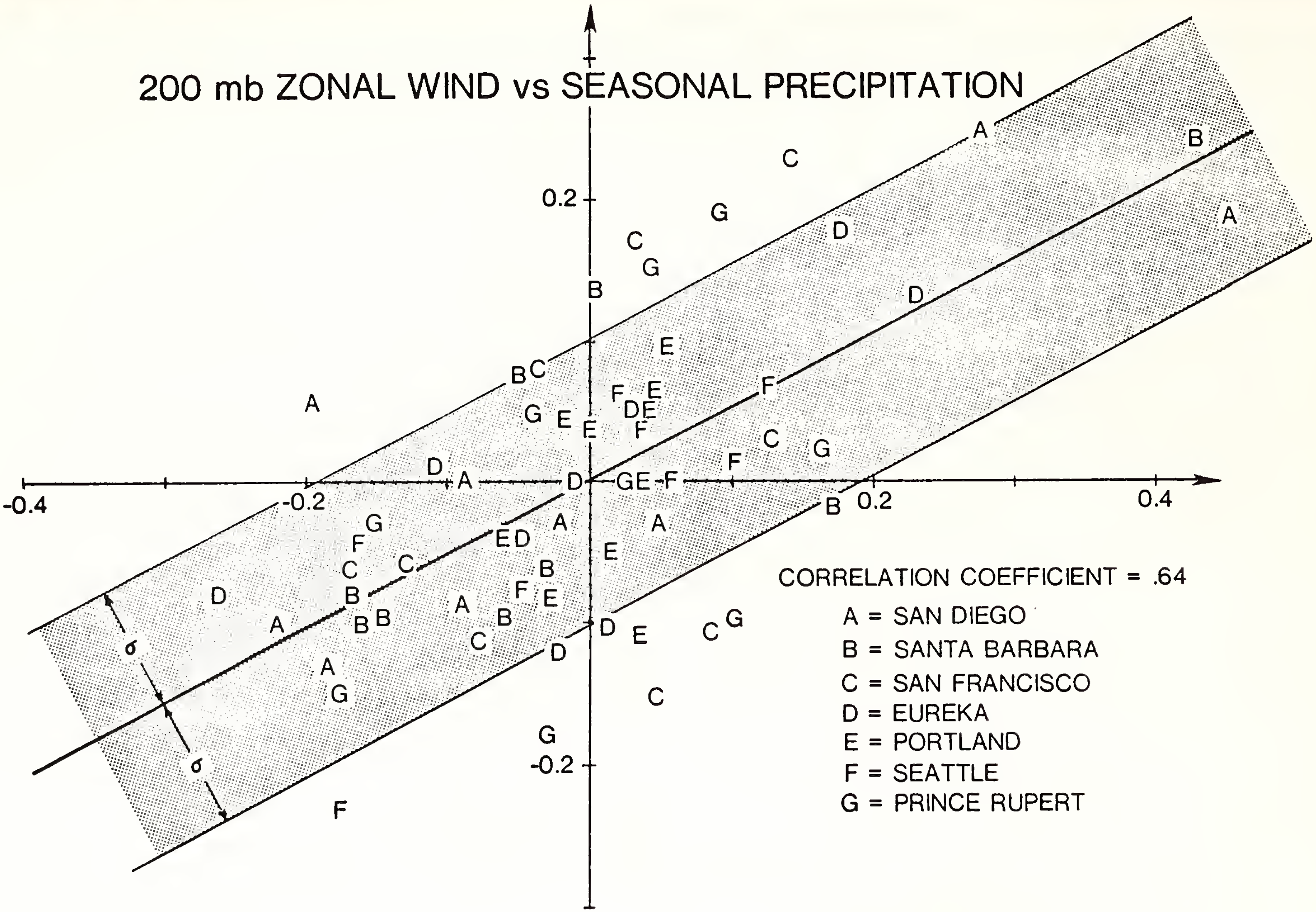

FIG. 5 LINEAR REGRESSION LINE OF MEAN ZONAL GEOSTROPHIC WIND AT 200 MB (VERTICAL AXIS) AND PRECIPITATION (HORIZONTAL AXIS) AT THE SAME LATITUDE FOR THE OCTOBER-MARCH SEASON FOR 1964-1972. DATA ARE PLOTTED IN TERMS OF NORMALIZED DEVIATIONS AND SCALED SO THAT THE DATA AT EACH STATION CONFORM TO A REGRESSION SLOPE OF 1/2. SHADED AREA SHOWS THE BOUNDS FOR PLUS AND MINUS ONE STANDARD DEVIATION.

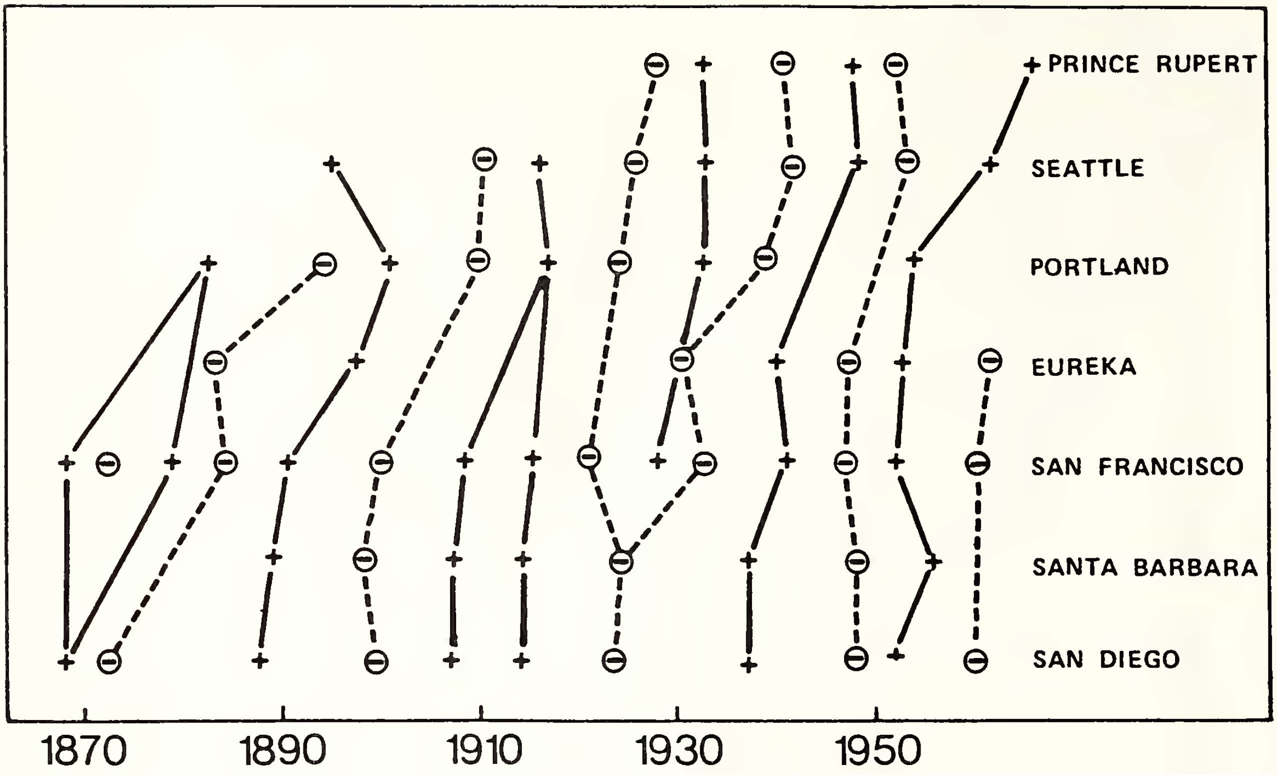

FIG. 6 TIME-LATITUDE CROSS SECTION OF EXTREME OF PRECIPITATION ANOMALIES DETERMINED FROM DATA CORRESPONDING, IN FORM, TO FIGS. 2B, 3B, AND 4B. DATA SHOWS BOTH ALTERNATING WET AND DRY PERIODS AND THE TENDENCY FOR A NORTHERLY MIGRATION OF EXTREMA WITH TIME.

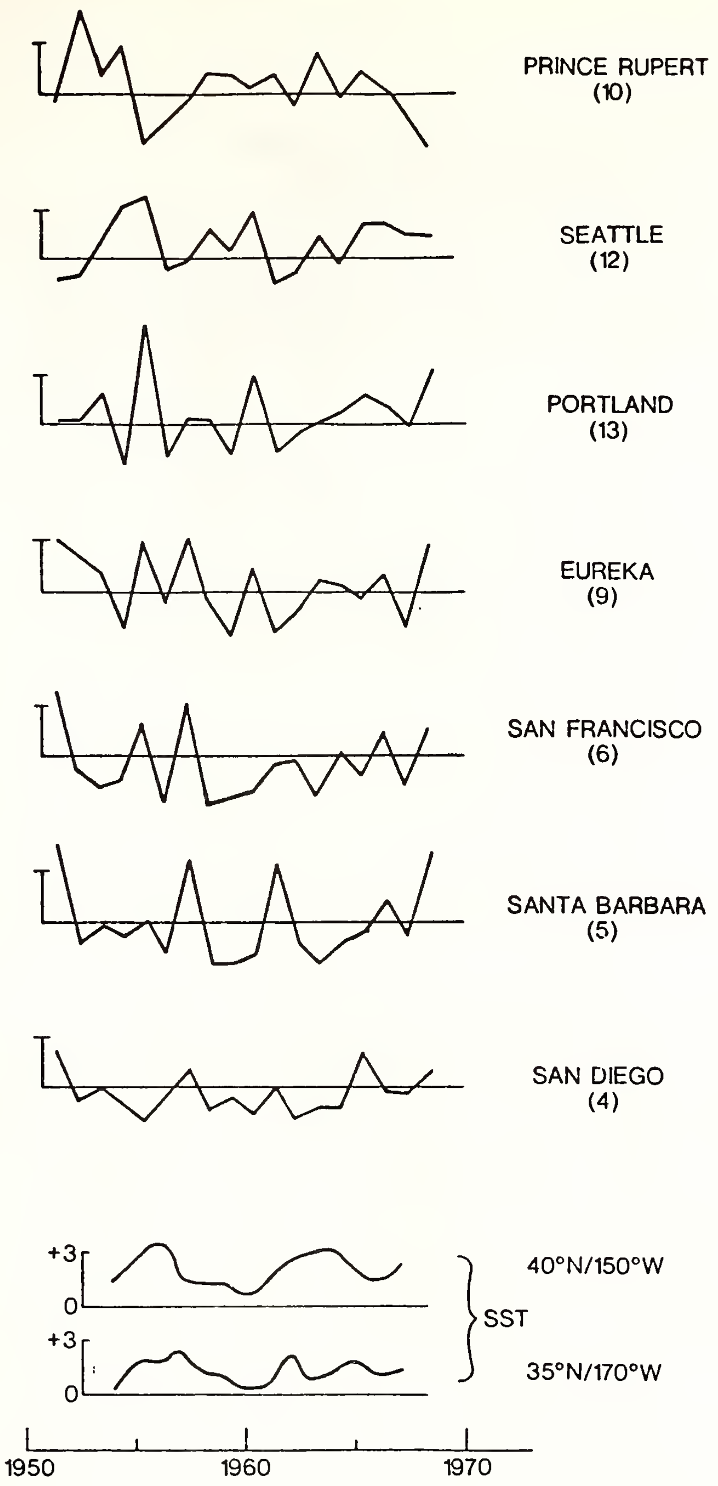

FIG. 7 COMPARISON OF ANOMALIES OF SEASONAL PRECIPITATION (HORIZONTAL AXIS CORRESPONDS TO LONG TERM MEAN) AND ANOMALIES OF SEA SURFACE TEMPERATURE AT TWO POINTS IN THE CENTRAL PACIFIC DURING A PERIOD OF ABNORMALLY WARM "CENTERS OF ACTION" (NAMIAS). NUMBERS IN PARENTHESES REFER TO THE NUMBER OF YEARS OF ABOVE NORMAL PRECIPITATION (OUT OF 17 POSSIBLE).

## YEARS OF GENERAL DROUGHT ALONG THE WEST COAST

(Negative Anomalies Exceeding 30% at 4 or more stations)

| | SD | SB | SF | EU | PD | SE | PR | = Σ |
|---|---|---|---|---|---|---|---|---|
| 1924 | X | X | X | X | X | X | +54% | 6 |
| 1926 | | X | | X | X | X | - 3% | 4 |
| 1931 | | X | X | X | X | | + 3% | 4 |
| 1934 | X | | X | X | | X | +30% | 4 |
| 1977 | | X | X | X | X | X | - 2% | 5 |
| Sample Size | 27 | 28 | 19 | 15 | 17 | 10 | 11* | |

*Anomalies Exceeding 20%

## 1960's and 1970's: WET FOLLOWED BY DRY

| Station | 10 Yr. Mean Preceeding Dry Period | Dry Period | Duration | Deficiency | |
|---|---|---|---|---|---|
| | | | | Total | Seasonal |
| Seattle | +4.6 in/yr | 1977-79 | 3 yr. | 18.59 in. | 6.2 in/yr |
| Portland | +6.1 in/yr | 1977-79 | 3 yr. | 26.87 in. | 9.0 in/yr |
| Eureka | +3.7 in/yr | 1976-79 | 4 yr. | 42.52 in. | 10.6 in/yr |
| San Francisco | +1.2 in/yr | 1975-77 | 3 yr. | 27.57 in. | 9.3 in/yr |
| Santa Barbara | +0.8 in/yr | 1976-77 | 2 yr. | 16.41 in. | 8.2 in/yr |

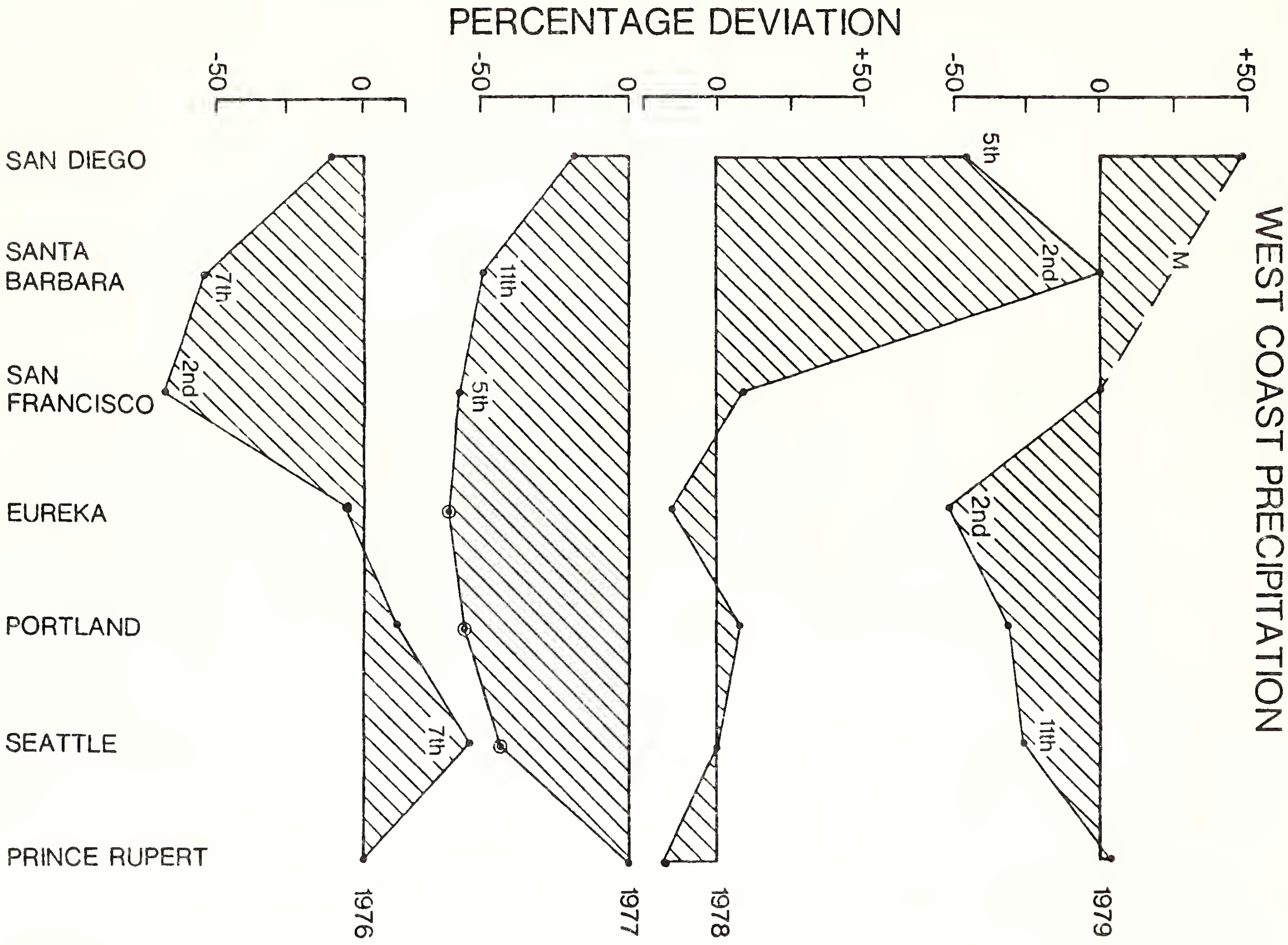

FIG. 8 DISTRIBUTION OF WINTER SEASON PRECIPITATION ALONG THE WEST COAST FOR THE FOUR MOST RECENT WINTERS IN UNITS OF PERCENT DEVIATION OF SEASONAL MEAN. CIRCLED VALUES (1977) INDICATE STATION RECORDS OF EXTREMA. NUMBERS GIVE RELATIVE RANKING OF EXTREMA FOR ABNORMALLY WET OR DRY YEARS.

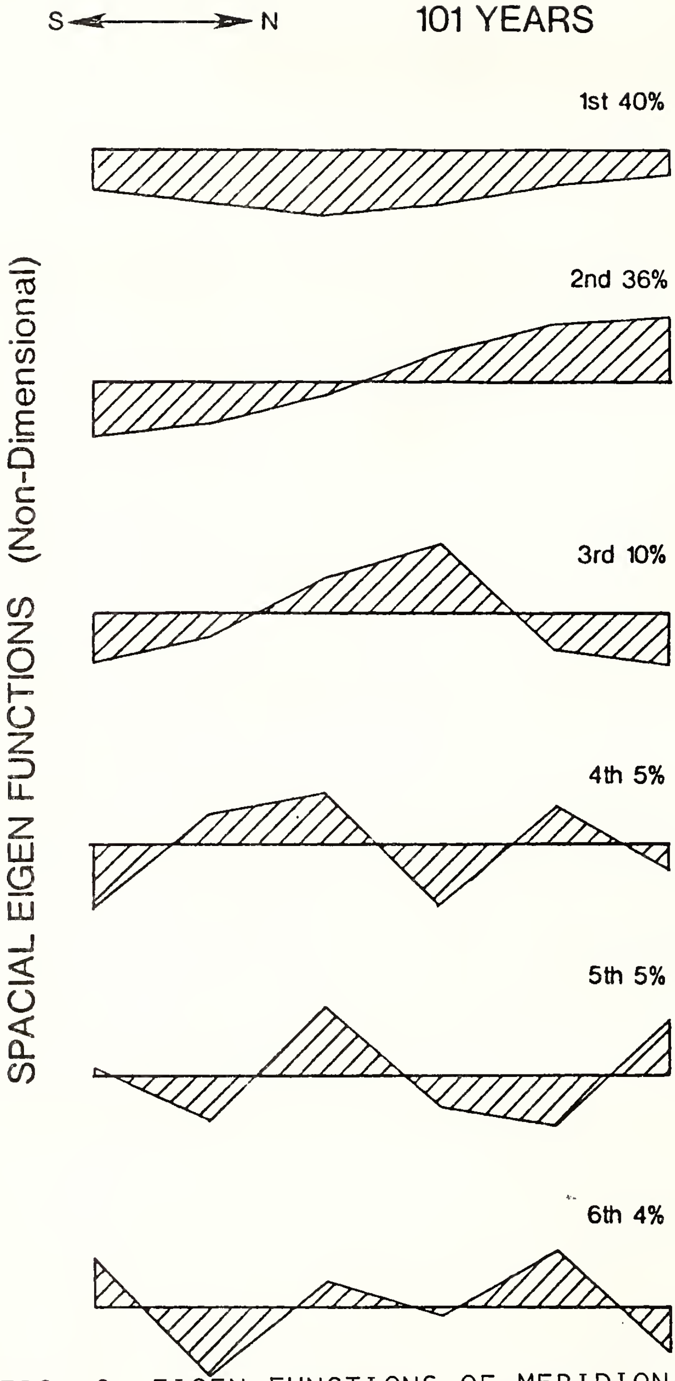

FIG. 9 EIGEN FUNCTIONS OF MERIDIONAL DISTRIBUTION OF SEASONAL PRECIPITATION RESULTING FROM AN EMPIRICAL ORTHOGONAL FUNCTION ANALYSIS OF 101 SEASONS OF PRECIPITATION AT 6 STATIONS. NUMBERS AT RIGHT CORRESPOND TO PER CENT OF EXPLAINED VARIANCE FOR EACH EIGENFUNCTION.

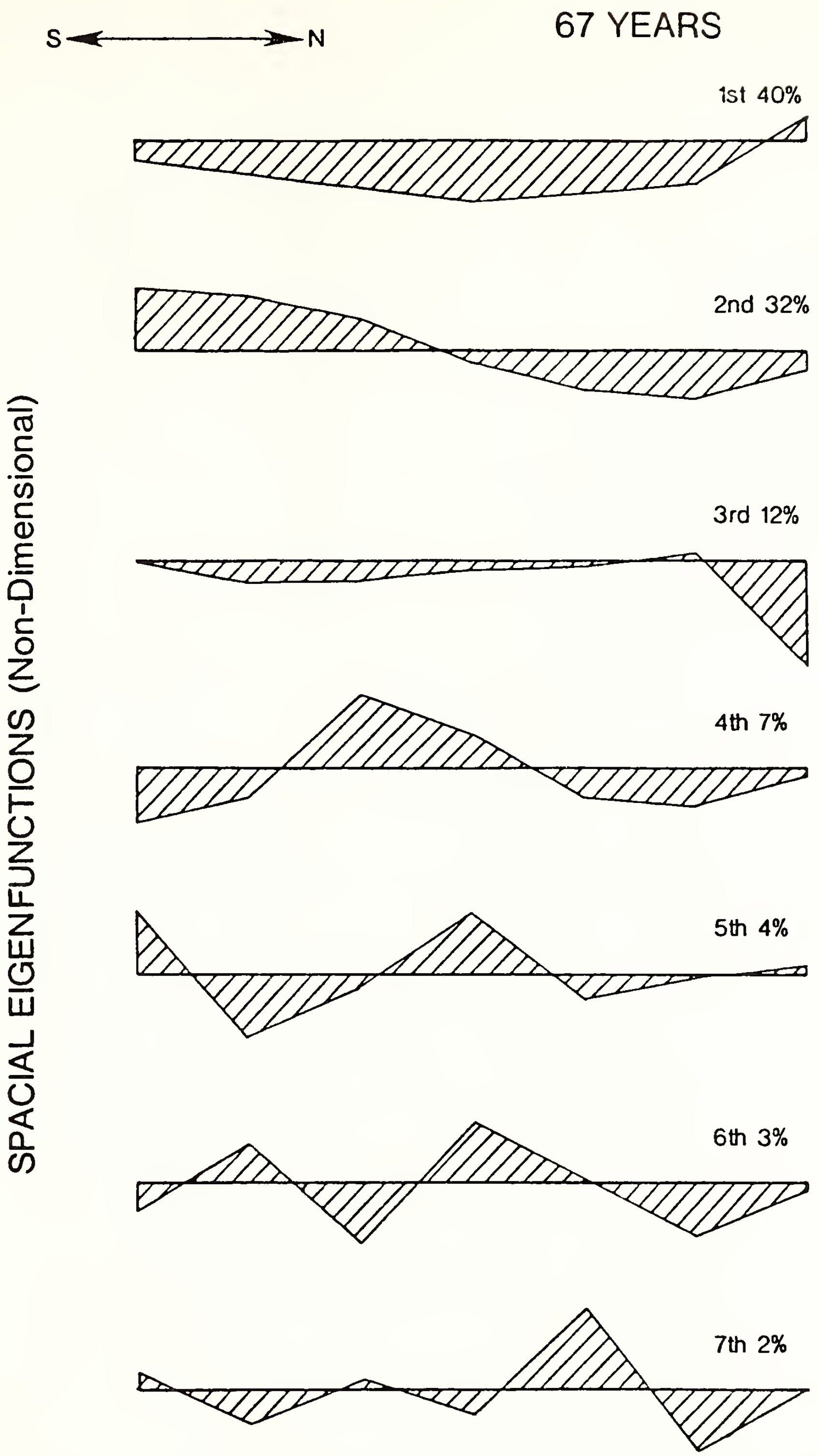

FIG. 10 EIGEN FUNCTIONS OF MERIDIONAL DISTRIBUTION OF SEASONAL PRECIPITATION RESULTING FROM AN EMPIRICAL ORTHOGONAL FUNCTION ANALYSIS OF 67 SEASONS OF PRECIPITATION AT 7 STATIONS (PRINCE RUPERT INCLUDED). NUMBERS AT RIGHT CORRESPOND TO PER CENT OF EXPLAINED VARIANCE FOR EACH EIGENFUNCTION.

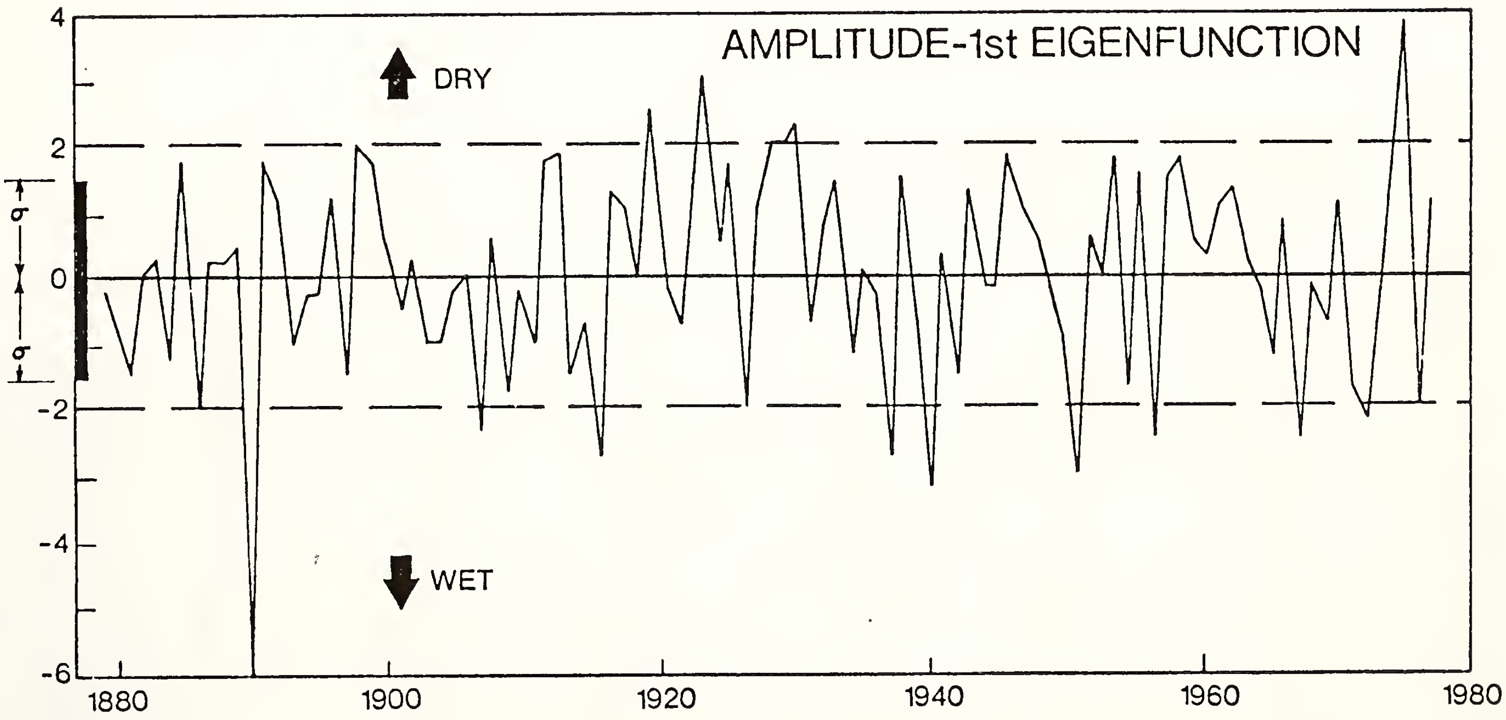

FIG. 11 THE PRINCIPAL COMPONENT OF THE FIRST EIGENFUNCTION IN FIG. (THE DATA CORRESPOND TO THE TIME SERIES OF THE AMPLITUDE OF EIGENFUNCTION 1). DASHED LINES AT AMPLITUDE = ±2 AND THE SOLID BAR DENOTING ± ONE STANDARD DEVIATION OF THE AMPLITUDE ARE SHOWN FOR REFERENCE. POSITIVE AMPLITUDES CORRESPOND TO BELOW NORMAL PRECIPITATION ALL ALONG THE U.S. COAST.

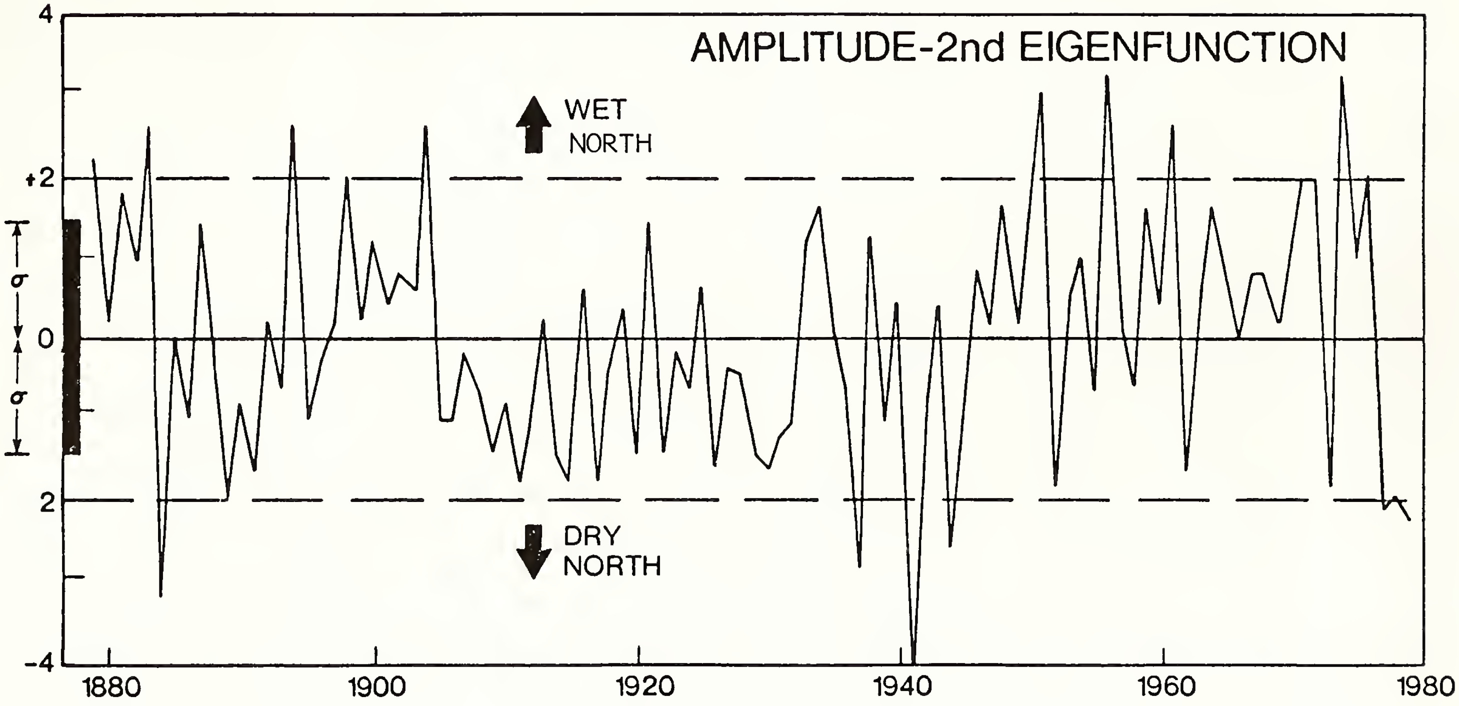

FIG. 12 THE PRINCIPAL COMPONENT OF THE SECOND EIGENFUNCTION IN FIG. 9. (THE DATA CORRESPOND TO THE TIME SERIES OF THE AMPLITUDE OF EIGENFUNCTION 2). DASHED LINES AT AMPLITUDE = ±2 AND THE SOLID BAR DENOTING ± ONE STANDARD DEVIATION OF THE AMPLITUDE ARE SHOWN FOR REFERENCE. POSITIVE AMPLITUDES CORRESPOND TO WETTER THAN NORMAL NORTHERN STATIONS AND DRIER THAN NORMAL SOUTHERN STATIONS.

# The Statistical Relationship Between Mean Summer Precipitation in the United States and the Concurrent Tropospheric Pressure Distribution

by

Robert Harnack

Department of Meteorology & Physical Oceanography
Rutgers - The State University
New Brunswick, New Jersey 08903

As part of a larger study, whose aim is the assessment of the predictability of summer season precipitation using statistical methods, an initial study was conducted to investigate the relationship between summer season precipitation and the concurrent summer season circulation. The primary purpose of this is the formulation of a precipitation statistic which relates well, and hopefully optimally, to the concurrent circulation so that the chances of finding a useful relationship between summer precipitation and antecedent predictors of some sort will be improved. The large degree of discontinuity of precipitation in both space and time, which makes the task especially difficult for finding useful predictive relationships on a seasonal time scale, requires that some experimentation be done with various smoothing procedures. The effectiveness of the smoothing procedures for predictive purposes was determined by comparing specification relationships, particularly in terms of explained variances and statistical significance, when both the type of summer precipitation statistic and tropospheric circulation statistic were varied in form. Multiple regression analysis was used.

Secondary benefits of this type of study include: (1) the development of specification equations for summer season precipitation using summer circulation which could be used later in conjunction with prediction models of summer circulation in order to predict summer precipitation from summer circulation, (2) the increased knowledge about the nature and degree of relationship between summer precipitation and circulation as compared to other time scales and seasons such as five-day winter relationships studied previously, and (3) the increased knowledge about geographical variations of summer precipitation specification, which suggests where skillful predictions are mostly likely to occur.

Table 1 summarizes the degree of statistical relationship between surface weather parameters and concurrent circulation found in several previous studies. This table gives one some idea of the very limited work performed on the specification of seasonal precipitation thus far.

Table 2 lists the types of specification relationships determined in the current study, while Figure 1 shows the locations of the 72 climatological divisions used when individual CD precipitation was employed. Table 3, and Figures 2-3 give information regarding EOF analyses performed and a few summer precipitation EOF patterns respectively. Figure 4 indicates the 20 subareas used for calculating most of the area-averaged precipitation values used in specification models.

Figures 5-10 are maps of explained variances for various specification relationships formulated. They were selected from a large number of similar maps in order to illustrate the important findings of this study. They should be examined in pairs.

Figures 5 and 6 can be compared in order to determine the effect of using individual CD precipitation versus using area-averaged precipitation in a similar type specification relationship. This comparison, and others not shown, indicate that spatial averaging of CD precipitation raises the explained variance only slightly over that obtained when individual CD precipitation is used. This improvement was generally confined to regions where specification was already best.

Figures 7 and 8 show the differences obtained for explained variance when the 700 mb height EOFs are derived from a large, less dense grid point domain (105 points) compared to a smaller, more dense grid point domain (40 points). Use of the small domain resulted in slightly higher explained variances in much of the East and Midwest, but generally lower in the West.

Comparison of Figure 6 with Figure 9 illustrates the effect of using actual summer precipitation versus using category summer precipitation in the specification equations. Very little, if any, overall differences were noted for this comparison.

Comparison of Figure 5 with Figure 10 allows for an assessment of the effect of using sea level pressure EOFs in place of 700 mb EOFs. Clearly, better specification occurs when 700 mb EOFs are used. The range of explained variances is 5-15% using SLP, but 5-30% using 700 mb heights.

Overall, it was noted that specification of summer precipitation is best for the Central Plains, Ohio Valley, Great Lakes, and Great Basin regions (i.e., 20-30% explained variance using two EOFs as predictors). Poor specification was achieved in the Gulf States, Northern Plains, West Coast, and Northeast (i.e., < 15% explained variance.

Finally, in trials not illustrated, it was found that summer season precipitation specification was not significantly improved by using transformed actual precipitation (i.e., taking the square-root); using objectively derived boundaries for area-averages or by using the time series of summer precipitation EOF amplitudes in place of individual CD actual precipitation.

Table 1. Some previously formulated specification models for forecast parameters in the extended range.

| Model | Reference | Main result |
|---|---|---|
| 30-day precip. by states correlated with hts/pressure at various levels | Stidd (1953) | Typical maximum correlations of ± .5 to .7 for winter months, but ± .3 to .4 for summer months. |
| 5-day precip. from 700 mb hts. for winter (subarea categories used for precip.) | Klein (1963) | ~25-75% exp. var. via screening regression; min. in NE & N. Plains, max. on W. Coast, ave. of 35% for 2 predictor models. |
| 30-day temp. from SLP for winter (EOFs used) | Gilman (1957) | 48% exp. var. on dependent sample, 43% when applied to indep. sample. |
| 5-day temp. from 700 mb hts., SLP, and thickness for winter | Klein (1959, 1964) | ~80% exp. var. using thickness, 50-60% using hts. |
| 30-day temp from 700 mb hts. using 5-day eqs; all seasons | Klein (1962) | ~45-55% exp. var. |

Table 2. Specification Models Formulated Relating Summer (June-August) Precipitation to Summer Circulation

| Predictors / Predictands | 700 mb ht. EOFs (105 Pt. Grid)[5] | 700 mb ht. EOFs (40 Pt. Grid)[6] | SLP EOFs (105 Pt. Grid) |
|---|---|---|---|
| Actual precipitation (CDs)[2] | X | X | X |
| Category precipitation (CDs)[3] | X | | |
| Actual precipitation (subareas)[1] | X | | X |
| Category precipitation (subareas) | X | | |
| Precipitation EOFs | X | | |
| Transformed precipitation (CDs)[4] | X | | |
| Transformed precipitation (subareas) | X | | |

Notes:
(1) Several subarea types formulated: 6 "key areas," 20 subareas, 18 subareas.
(2) 72 climatological divisions (CDs) used.
(3) 3 precipitation categories used for "category precipitation."
(4) "Transformed precipitation" means square-root of actual precipitation used.
(5) 105 point grid for 700 mb height EOF analysis covers: 20°-80°N by 10°, 120°E-40°E by 20°.
(6) 40 point grid for 700 mb height EOF analysis covers: 20°-60°N by 10°, 60°W-130°W by 10°.

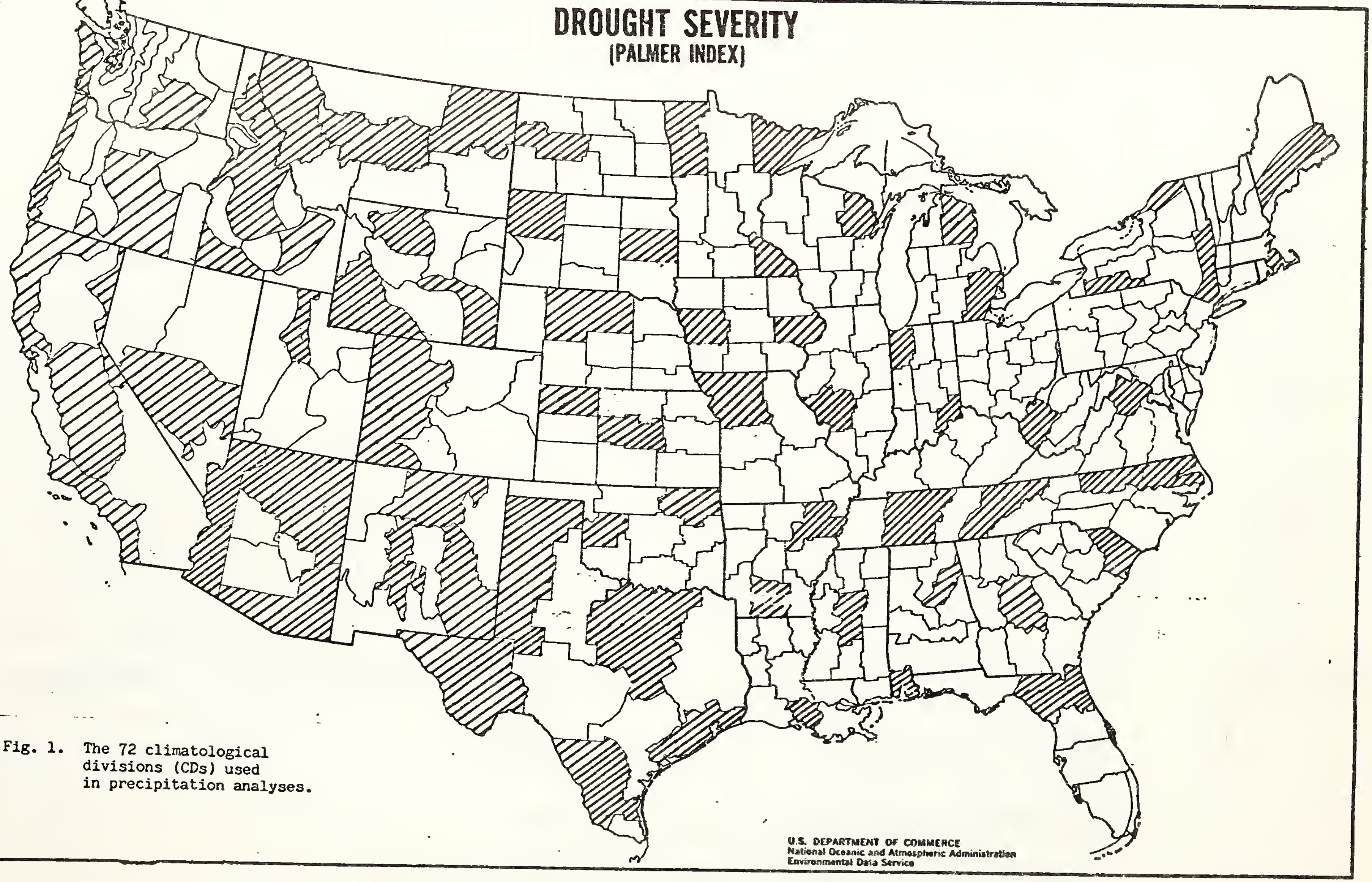
DROUGHT SEVERITY
(PALMER INDEX)
U.S. DEPARTMENT OF COMMERCE
National Oceanic and Atmospheric Administration
Environmental Data Service

Fig. 1. The 72 climatological divisions (CDs) used in precipitation analyses.

TABLE 3. EXPLAINED VARIANCE BY SIGNIFICANT EOFs (5% LEVEL)

| FIELD | EOF NUMBER |  |  |  |
|---|---|---|---|---|
|  | 1 | 2 | 3 | CUM |
| SUMMER PRECIPITATION (72 CDs) | 20% | 13 | 9 | 42 |
| SUMMER 700 MB HTS. (105 GRID PTS.) | 29 | 14 |  | 43 |
| SUMMER SLP (105 GRID PTS.) | 14 | 11 | 8 | 33 |

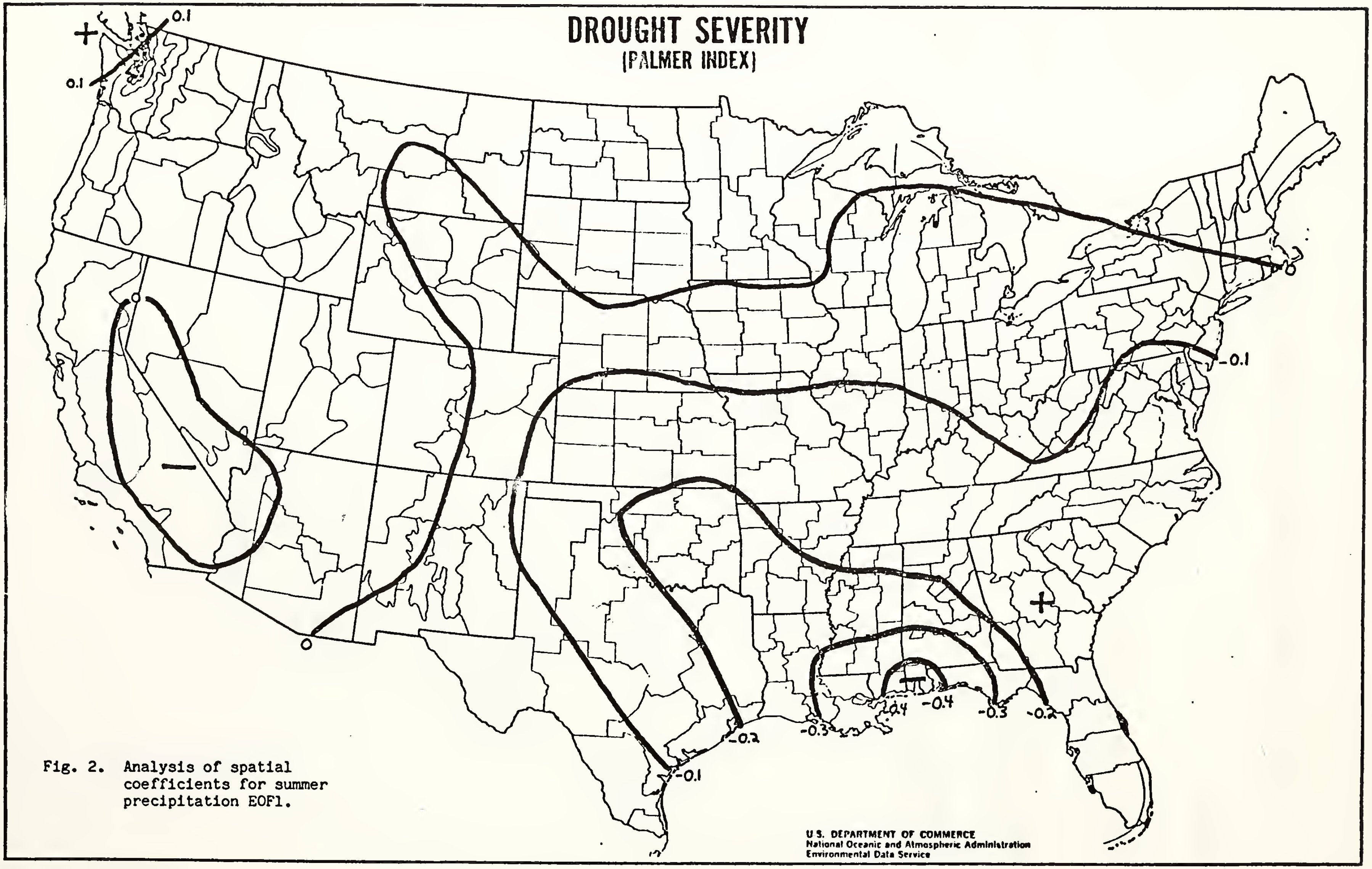
DROUGHT SEVERITY
(PALMER INDEX)
+
0.1
0.1
−
0
0
-0.1
-0.1
-0.2
-0.3
-0.4
-0.4
-0.3
-0.2
-0.1
+
U.S. DEPARTMENT OF COMMERCE
National Oceanic and Atmospheric Administration
Environmental Data Service

Fig. 2. Analysis of spatial coefficients for summer precipitation EOF1.

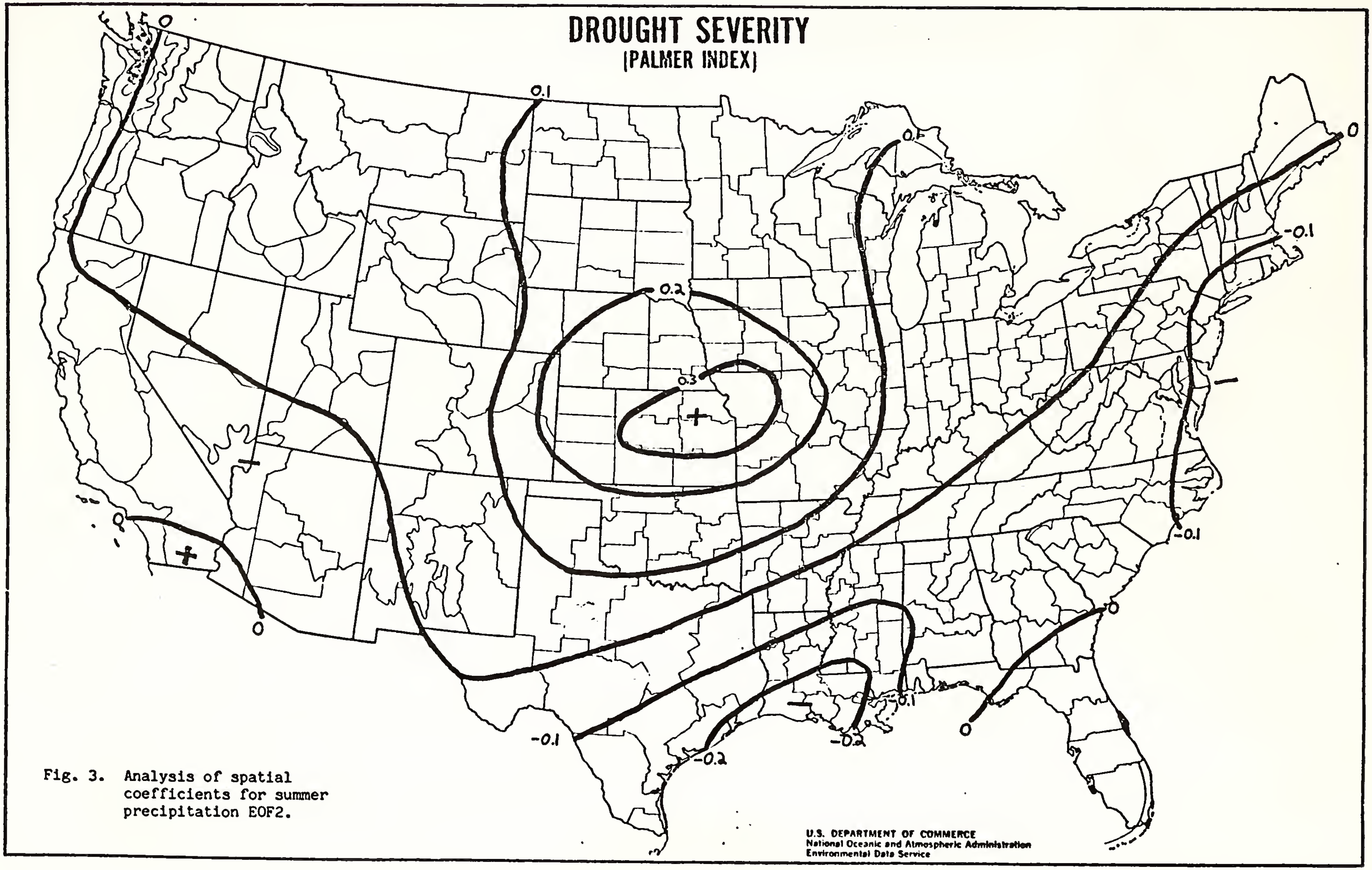
DROUGHT SEVERITY
(PALMER INDEX)
0
0.1
0.2
0.3
+
0.1
0
-0.1
-0.1
-0.1
-0.2
-0.2
0.1
0
0
+
0
U.S. DEPARTMENT OF COMMERCE
National Oceanic and Atmospheric Administration
Environmental Data Service

Fig. 3. Analysis of spatial coefficients for summer precipitation EOF2.

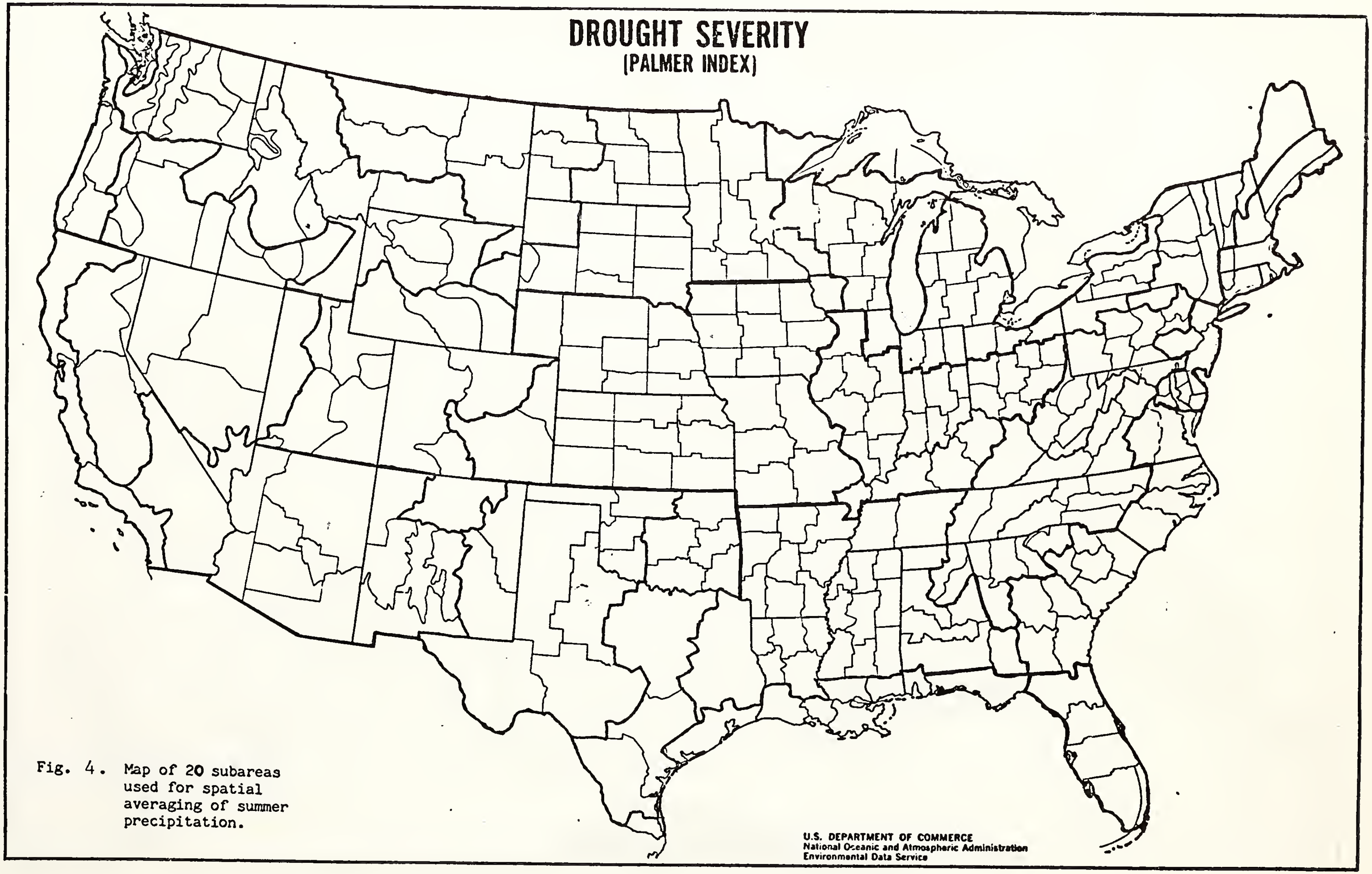
DROUGHT SEVERITY
(PALMER INDEX)
U.S. DEPARTMENT OF COMMERCE
National Oceanic and Atmospheric Administration
Environmental Data Service

Fig. 4. Map of 20 subareas used for spatial averaging of summer precipitation.

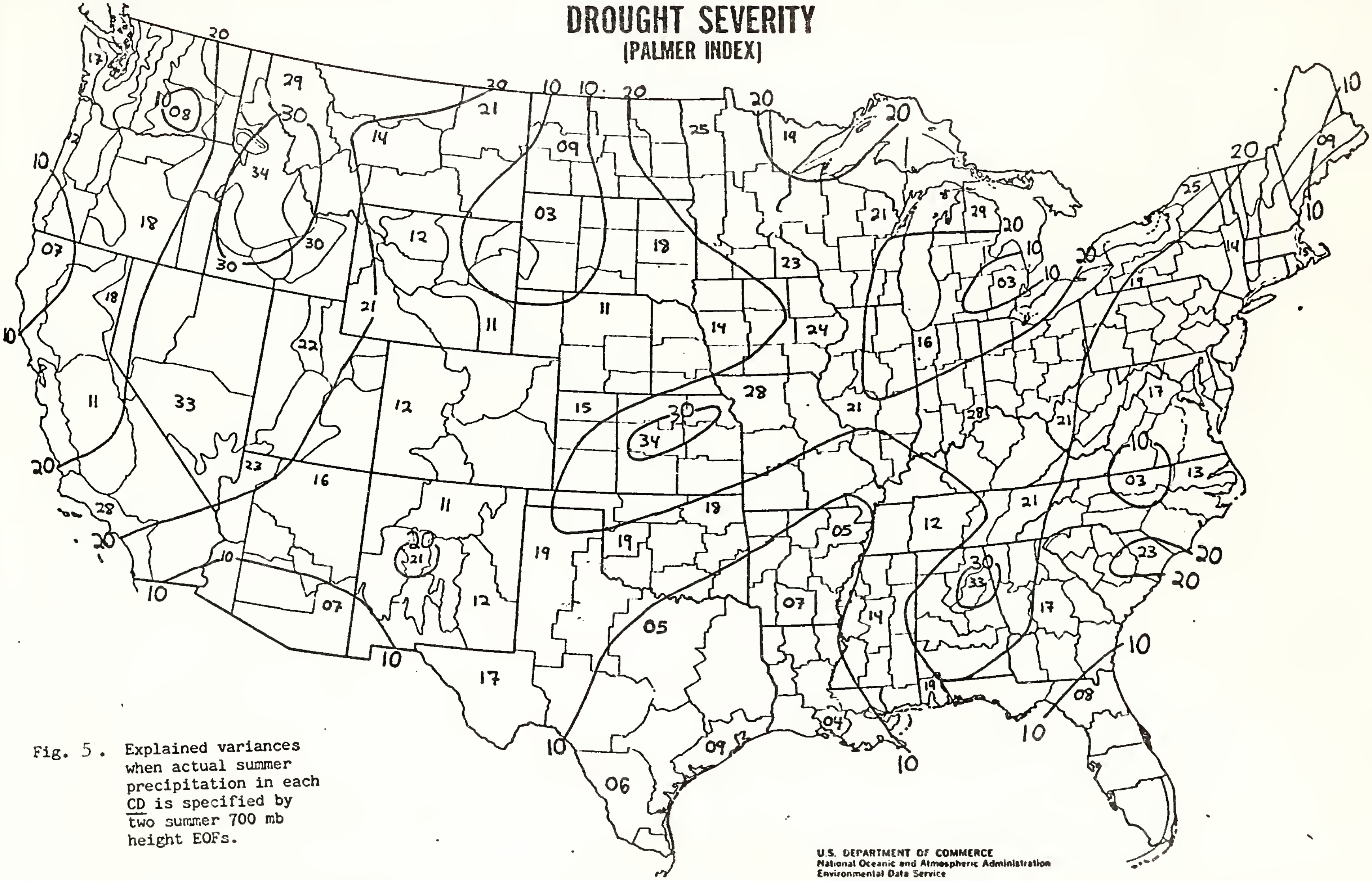

Fig. 5. Explained variances when actual summer precipitation in each CD is specified by two summer 700 mb height EOFs.

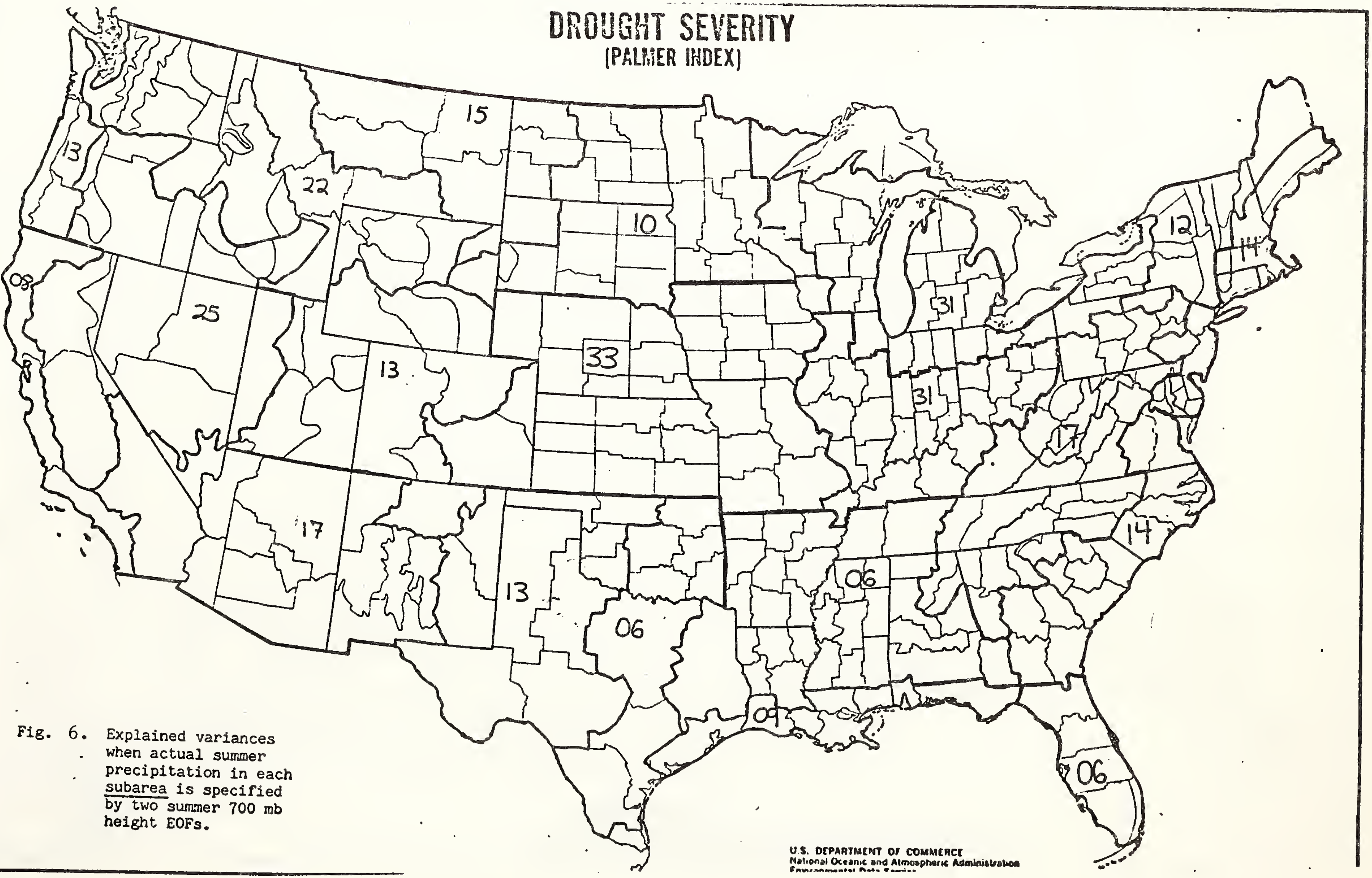
DROUGHT SEVERITY
(PALMER INDEX)
13
15
22
10
12
14
08
25
31
33
13
31
17
17
14
13
06
06
09
06
U.S. DEPARTMENT OF COMMERCE
National Oceanic and Atmospheric Administration

Fig. 6. Explained variances when actual summer precipitation in each subarea is specified by two summer 700 mb height EOFs.

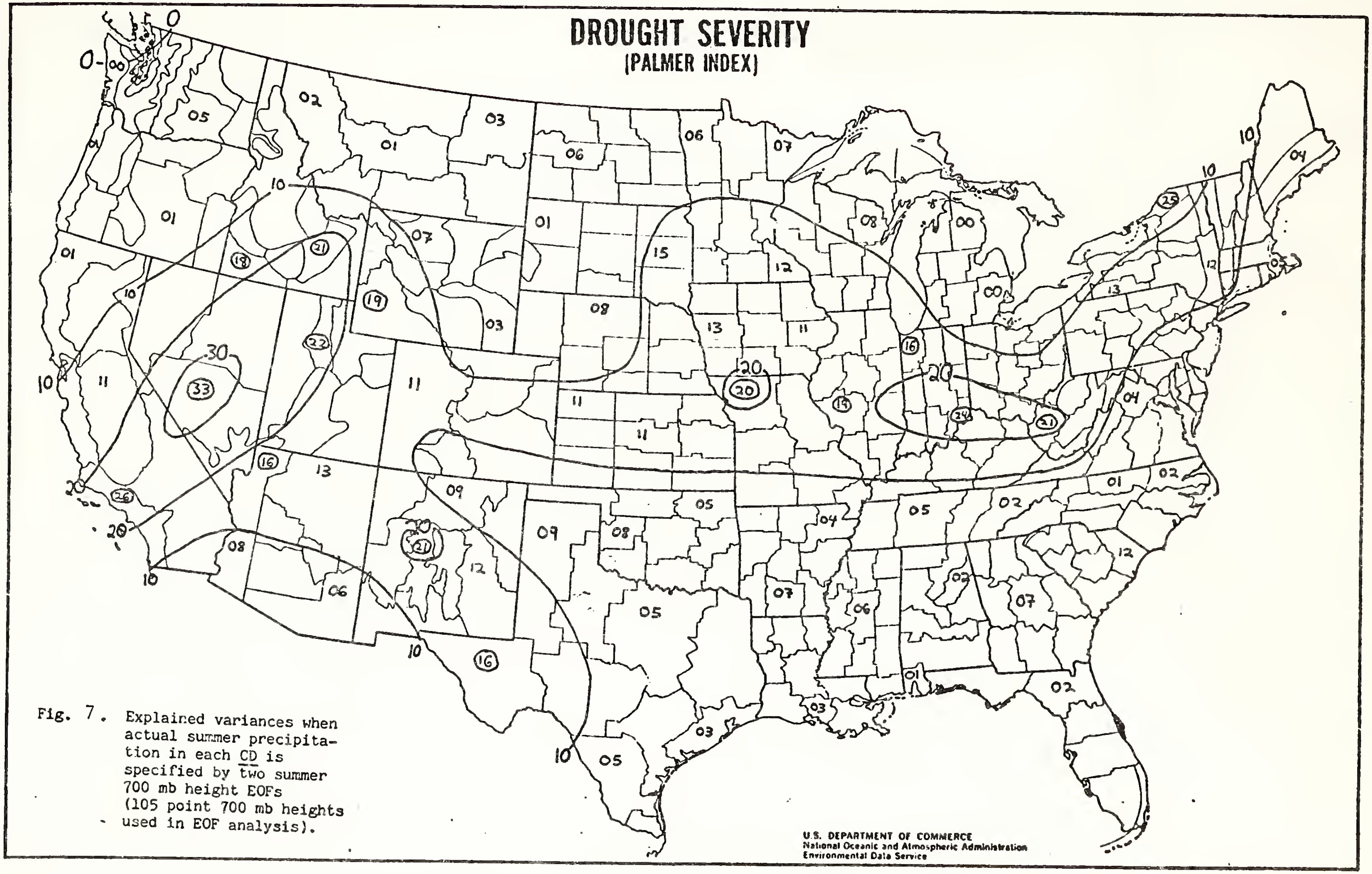
DROUGHT SEVERITY
(PALMER INDEX)
U.S. DEPARTMENT OF COMMERCE
National Oceanic and Atmospheric Administration
Environmental Data Service
10
20
30
(33)
(21)
(18)
(19)
(22)
(16)
(26)
(20)
(19)
(16)
(24)
(21)
(25)
(16)
(21)

Fig. 7. Explained variances when actual summer precipitation in each CD is specified by two summer 700 mb height EOFs (105 point 700 mb heights used in EOF analysis).

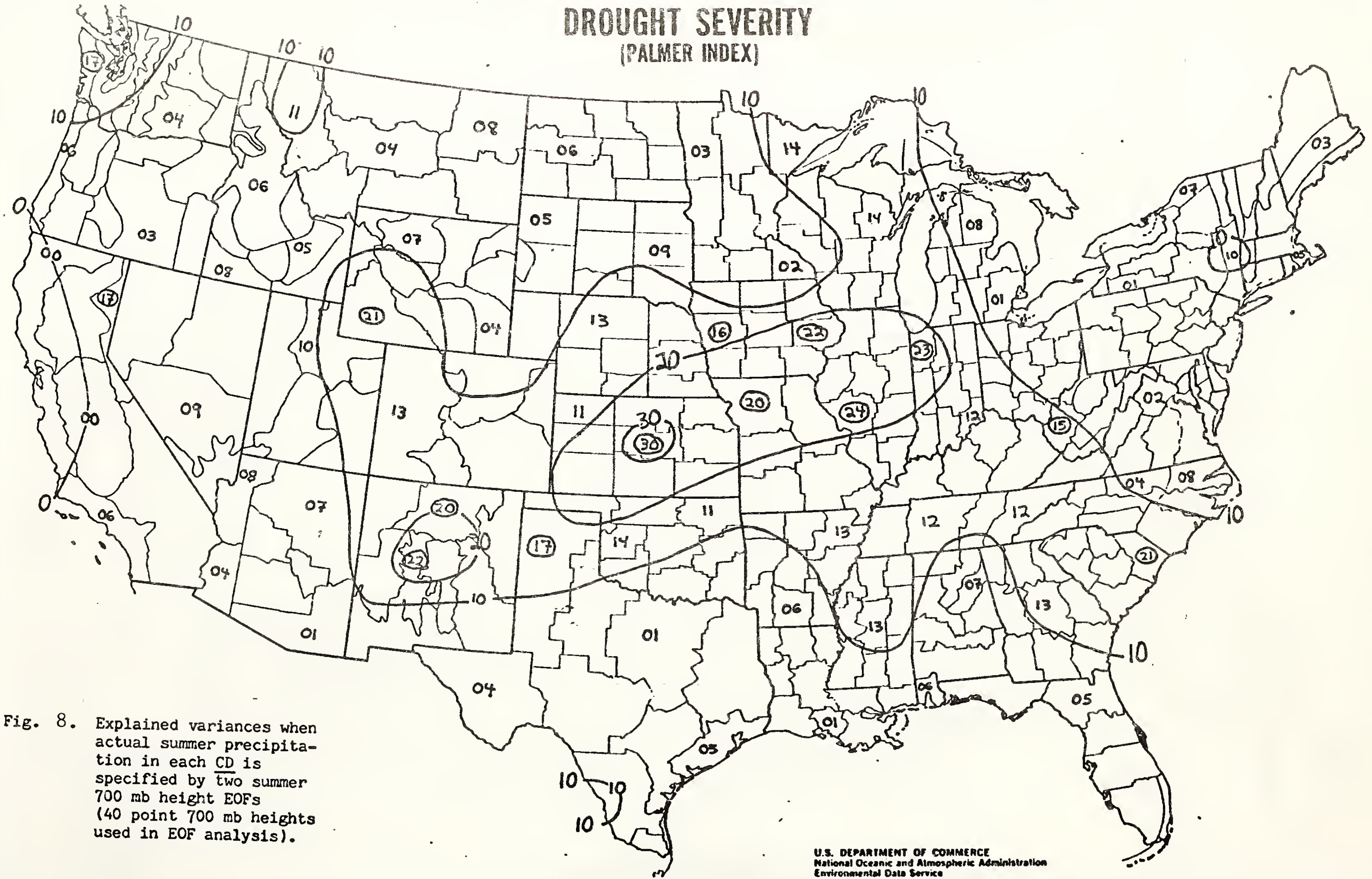
DROUGHT SEVERITY
(PALMER INDEX)
U.S. DEPARTMENT OF COMMERCE
National Oceanic and Atmospheric Administration
Environmental Data Service

Fig. 8. Explained variances when actual summer precipitation in each CD is specified by two summer 700 mb height EOFs (40 point 700 mb heights used in EOF analysis).

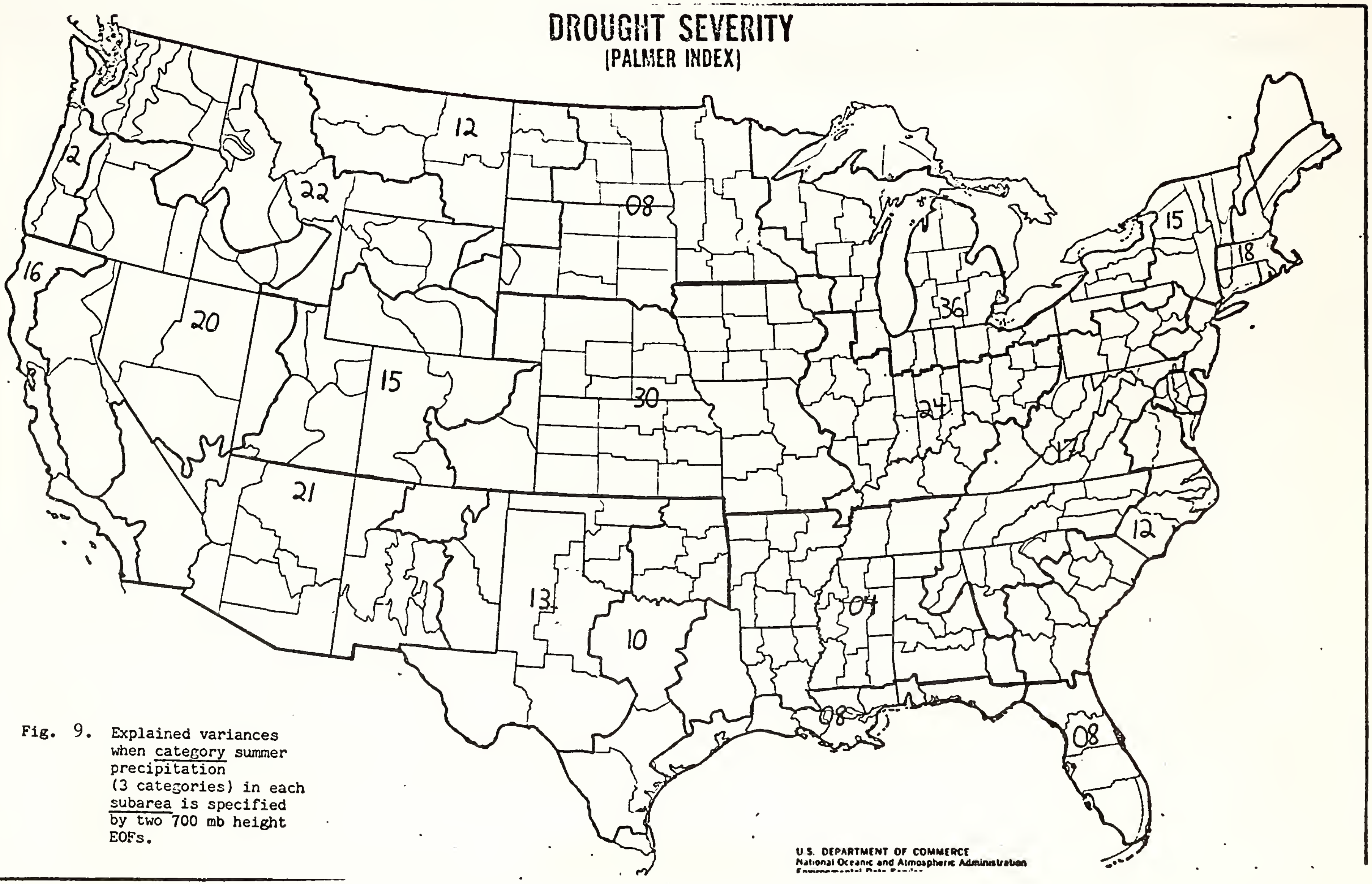

DROUGHT SEVERITY
(PALMER INDEX)
2
12
22
08
16
20
15
30
36
24
15
18
17
12
21
13
10
04
08
08
U.S. DEPARTMENT OF COMMERCE
National Oceanic and Atmospheric Administration

Fig. 9. Explained variances when category summer precipitation (3 categories) in each subarea is specified by two 700 mb height EOFs.

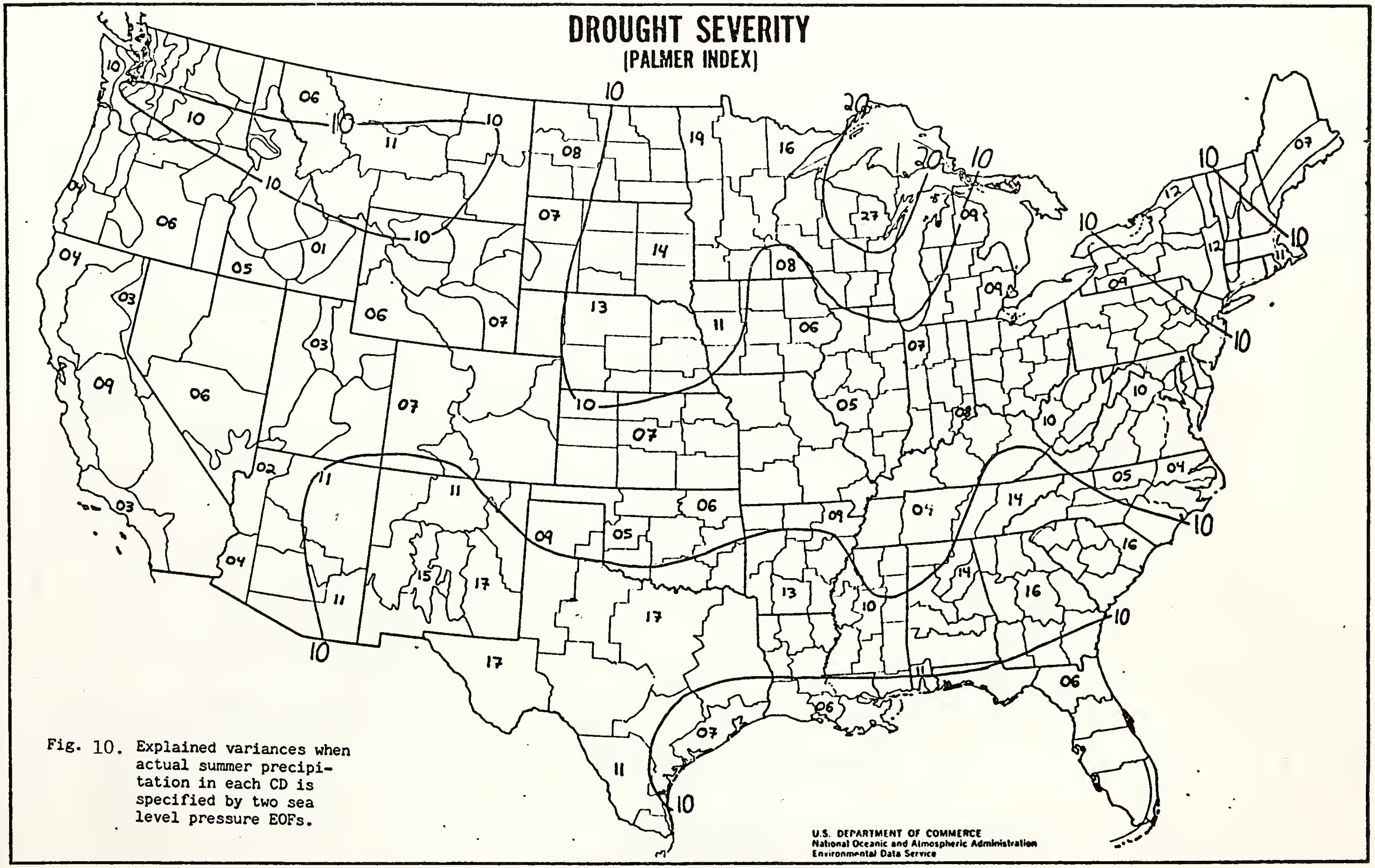
DROUGHT SEVERITY
(PALMER INDEX)
U.S. DEPARTMENT OF COMMERCE
National Oceanic and Atmospheric Administration
Environmental Data Service

Fig. 10. Explained variances when actual summer precipitation in each CD is specified by two sea level pressure EOFs.

# Airstream Source Regions of the Northern Hemisphere

Wayne M. Wendland
Illinois State Water Survey
and
Department of Geography
University of Illinois-Urbana

and

Reid A. Bryson
Director, Institute for Environmental Studies
University of Wisconsin-Madison

One method to quantitatively describe the climate of a given location is to document the length of time that site is dominated by the various airmasses "available" to that region. For example, the July climate of Urbana, Illinois may be understood to be experienced from 45% of the month dominated by maritime tropical, air; 50% by maritime polar air and 5% by continental tropical air (Bryson, 1966). Since airmasses tend toward similar temperature and humidity characteristics during similar seasons, the following corrolary offered: Sites with similar airmass dominances experience similar temperature and humidity climates.

For the purposes of this conference, mean airmass frequencies may not be as important or interesting as changes in airmass frequencies at one place from time to time. Anomalous years, seasons or months may differ from the longer term mean, because of anomalous distributions of airmass frequencies. Airmass frequencies are a forcing function of climate, and therefore site-specific anomalies may be meaningfully extrapolated into adjacent areas, in accordance with typical confluence - difluence patterns between and within airmasses over the area in question.

The present study deals with mean locations of sources and boundaries of airstreams of the Northern Hemisphere. These locational characteristics are presumably related to the mean temperature and humidity climate. Deviations in the location of airstream sources and primarily, airstream boundaries are related to anomalous temperature and humidity experienced in the area of displaced streamlines.

The present study is a preliminary analysis of mean airstream source regions and outer boundaries for the Northern Hemisphere. The sources were identified by drawing streamlines congruent to mean monthly resultant winds for each $3^{\circ}$ by $3^{\circ}$ latitude-longitude "square". Streamlines are equivalent to trajectories when using mean data, and hence the streamlines identify the location of monthly sources of the various airstreams. One airstream source may represent two airmasses, since the northern and southern trajectories from one common source may pass over considerably different surfaces thus modifying and character of the air, e.g., the Pacific subtropical anticyclone is the source of both maritime tropical and maritime polar air.

Fifteen sources for the hemisphere were identified, three being present all months of the year (sources over the Pacific and Atlantic, and air of the Southern Hemisphere), three for eleven months of the year (sources over the Arctic, Sinkiang and Africa), and nine airstream sources which exist for ten months per year or less. Figure 1 identifies the sources, while the encompassing lines identifiy the area covered by the airstream for the specified number of months per year.

The two subtropical highs are prominant features, each covering about 20% of the hemisphere for six months of the year. Air of Southern Hemispheric origin is found immediately to their south. The lines with parallel dots indicate the area covered by the specified airstreams half the year.

The area poleward of about 45°N is the sources of most airstreams of the hemisphere. It is also the area of steepest climatic gradients, as indicated by the variety of sources within close proximity to each other, and the absence of airstreams which dominate for many-most months of the year.

Research is currently underway at the Illinois State Water Survey to investigate year-to-year changes in airstream boundaries and related temperature and precipitation anomaly patterns.

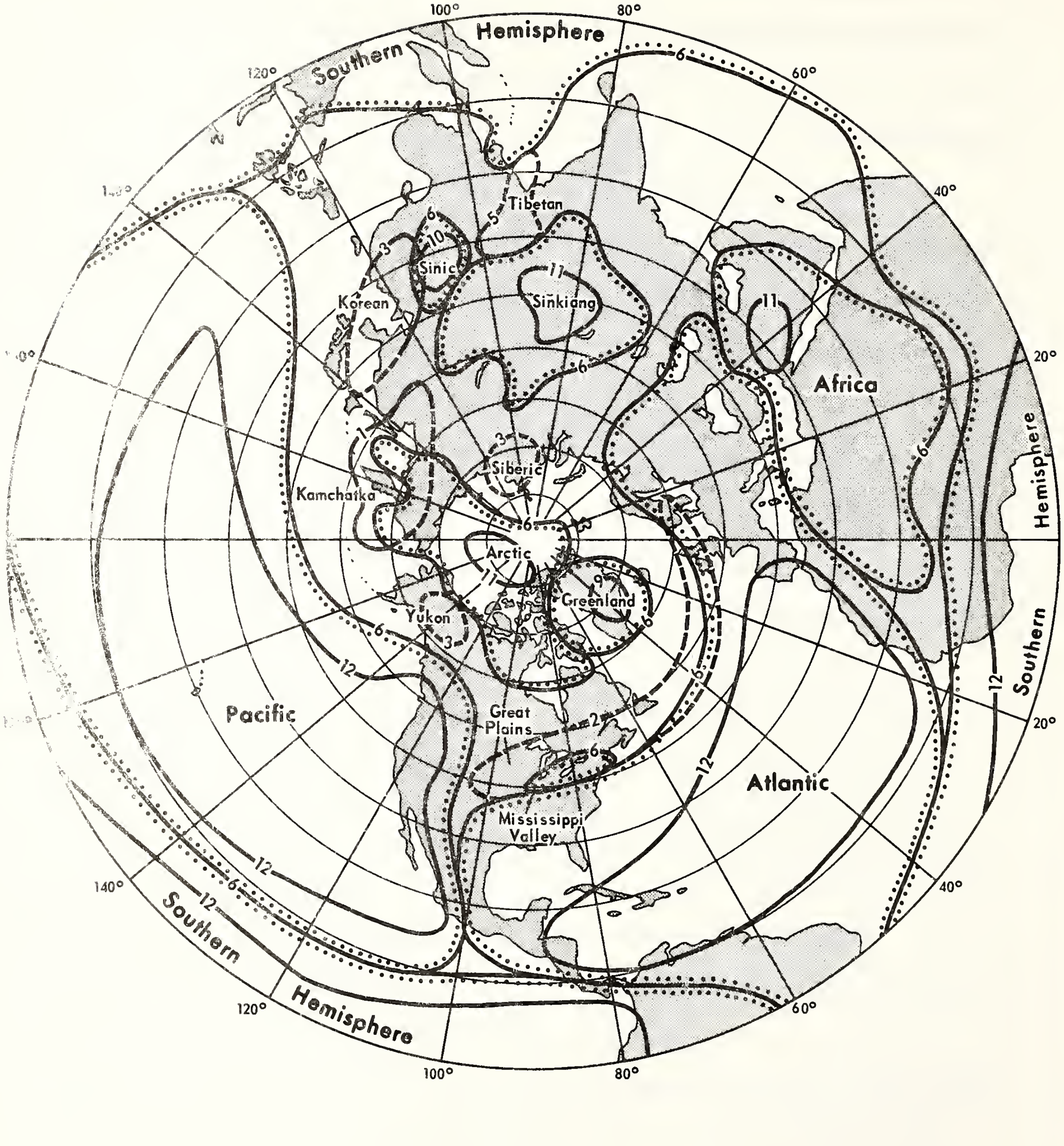
100°
80°
Southern
Hemisphere
120°
60°
40°
Tibetan
Sinic
Korean
Sinkiang
Africa
20°
Hemisphere
0°
Southern
Siberic
Kamchatka
Arctic
Yukon
Greenland
Pacific
Great Plains
Atlantic
Mississippi Valley
20°
40°
140°
Southern
Hemisphere
120°
60°
100°
80°
12
6
11
10
3
5
9
2

Figure 1

# VARIATIONS OF ATMOSPHERIC WATER VAPOR AND THE WATER VAPOR TRANSPORT VECTOR DURING A FIFTEEN-YEAR PERIOD

David A. Salstein and Richard D. Rosen
Environmental Research & Technology, Inc.
Concord, Massachusetts 01742

We have carefully chosen a set of radiosonde stations which are distributed as evenly as possible throughout the Northern Hemisphere and which reported frequently during the period 1958-1973 in order to look at the interannual variability of water vapor and its transports. Vertically integrated water vapor, $\overline{W} = 1/g \int q dp$, and the zonal and meridional transports of water vapor, $\overline{Q}_\lambda = 1/g \int qu dp$ and $\overline{Q}_\phi = 1/g \int qv dp$ respectively were computed at each of 91 stations for annual periods which are referred to as Years 1-15. Additional information about these quantities appear in Rosen et al. (1979).

In order to examine the variability, the technique of principal component analysis (empirical orthogonal functions) was used, with the long-term mean subtracted from each annual period. In this way, time correlations among different areas can be investigated.

The average annual field of precipitable water vapor is shown in Fig. 1, revealing an expected decrease from equator to pole with additional lower values over deserts and high altitude regions. The first two modes of $\overline{W}$ variability and their corresponding time series in Figs. 2 and 3 explain 44.1% and 18.7% of the variance respectively. Both of these fields show rather large-scale features, but the most striking observations concerning the first eigenvector are that (1) the African stations (positive) act oppositely to most of the rest of the hemisphere, especially the Pacific region, which is the strongest negative region and (2) the time series is negative in the whole interval years 1-7 and positive in 8-15. Thus, the atmospheric system seems to act in two regimes. During the first period, Africa is drier than average and the Pacific moister, and vice versa during the second period. The second mode is strong only in the years where the first mode is weak, that is years 7-9.

In order to assess the statistical significance of the results, we took each station independently and randomly permuted its 15 years of data to correspond to a different order of the years. Identical EOF analysis was then done several times on the randomly rearranged data sets, and eigenvalues and eigenvectors were obtained. The highest value of the first eigenvalue was chosen as a base value, above which the significance of other results was assurred. This is similar to the technique of Preisendorfer and Barnett (1977). Eigenvectors whose eigenvalues are below the base value are not necessarily insigificant if their spatial patterns are homogeneous across large scales, since the random eigenvectors tend to change sign frequently between nearby grid points. The eigenvalues obtained plus the base random eigenvalues are shown in Table 1.

Typical annual maps of $\overline{Q}_\lambda$ and $\overline{Q}_\phi$ can be seen in Rosen et al. (1979), which are similar to the 15-year averages. The first mode in the variability of $\overline{Q}_\lambda$ (Fig. 4) also shows a Pacific-African contrast in the strength of the zonal transports as well as a change of sign during the 15-year period into two regimes. Since easterly transports prevail in the tropics, years 1-7 have weaker transports in Africa and stronger in the Pacific, whereas years 8-15 show the opposite. 25.3% of the variance is explained by the first mode of $\overline{Q}_\lambda$. However, only 18.7% of the variance is explained by the first mode in the $\overline{Q}_\phi$ field (Fig. 5) and no obvious regime structure exists in the variability of the meridional transports.

Actually, the question of whether the two components of the transport vector can be studied independently was examined by a technique using complex empirical orthogonal functions and time series to represent the vector quantity (see Hardy and Walton, 1978). The resulting eigenvector (Fig. 6), which explains 23.9% of the variance, has small arrows at stations proportional to their magnitude. Different distinct areas of flow can be noted throughout the hemisphere. The corresponding time series (Fig. 7) is presented using curves of magnitude and direction. The direction switches from close to 0° to near 180° after year 7, which indicates that the flow then shifts at each of the stations by 180° (the arrows reverse direction). The Pacific and African arrows of the eigenvector again are pointed in opposite directions. However, most of the arrows largely have a zonal orientation, and so the $\overline{Q}_\lambda$ component seems to have a more important share of the variance. Thus, the separation of the two components appears to have been a useful technique.

We wished to test the hypothesis that the tropical areas respond more predictably (more uniformly from year to year) than do the extra-tropical regions, which are forced more stochastically (see Charney and Shukla, 1979). We thus divided the stations into two groups, south and north of 30°N, and performed EOF analysis on each group independently. The eigenvectors of zonal transport did exhibit quite a difference in the variance explained. The tropical model 1 showed large scale features, a change in sign of the time series after year 7 and an explanation of 31.2% of the variance. However, the extratropical vector explains only 19.5% of the variance and shows little uniformity. These results suggest that a climate signal in the tropics is stronger than in the extratropics. The tropics seem to dominate in the hemispheric total eigenvector. Further details and discussion are presented by Salstein et al. (1980).

## References

Charney, J. and J. Shukla, 1979: Predictability of monsoons, Monsoon Dynamics, J. Lighthill and R.P. Pierce (eds), Cambridge University Press (in press).

Hardy, D.M. and J.J. Walton, 1978: Principal components analysis of vector wind measurements, J. Appl. Met., 17, 1153-1162.

Preisendorfer, R.W. and T.P. Barnett, 1977: Significance tests for empirical orthogonal functions, Preprint volume: Fifth Conference on Probability and Statistics, Nov. 15-18, 1977, Las Vegas, Nevada, American Met. Soc., 169-172.

Rosen, R.D., D.A. Salstein and J.P. Peixoto, 1979: Variability in the annual fields of large-scale atmospheric water vapor transport, Mon. Wea. Rev., 107, 26-37.

Salstein, D.A., Rosen, R.D. and J.P. Peixoto, 1980: Water vapor and its transport fields principal component analysis, manuscript in preparation.

# TABLE 1

## PERCENT VARIANCE EXPLAINED BY EOFs OF FIELDS STUDIED AND CORRESPONDING BASE VALUES

| Mode | Fields - % explained | Base - % explained |
|---|---|---|
| $\overline{W}$ - Mode 1 | 44.1 | 19.6 |
| Mode 2 | 17.3 | |
| $\overline{Q}_\lambda$ - Mode 1 | 25.3 | 18.2 |
| $\overline{Q}_\phi$ - Mode 1 | 18.7 | 16.8 |
| $\overline{Q}_\lambda$ - Tropical - Mode 1 | 31.2 | 22.3 |
| $\overline{Q}_\lambda$ - Extratropical - Mode 1 | 19.5 | 18.7 |

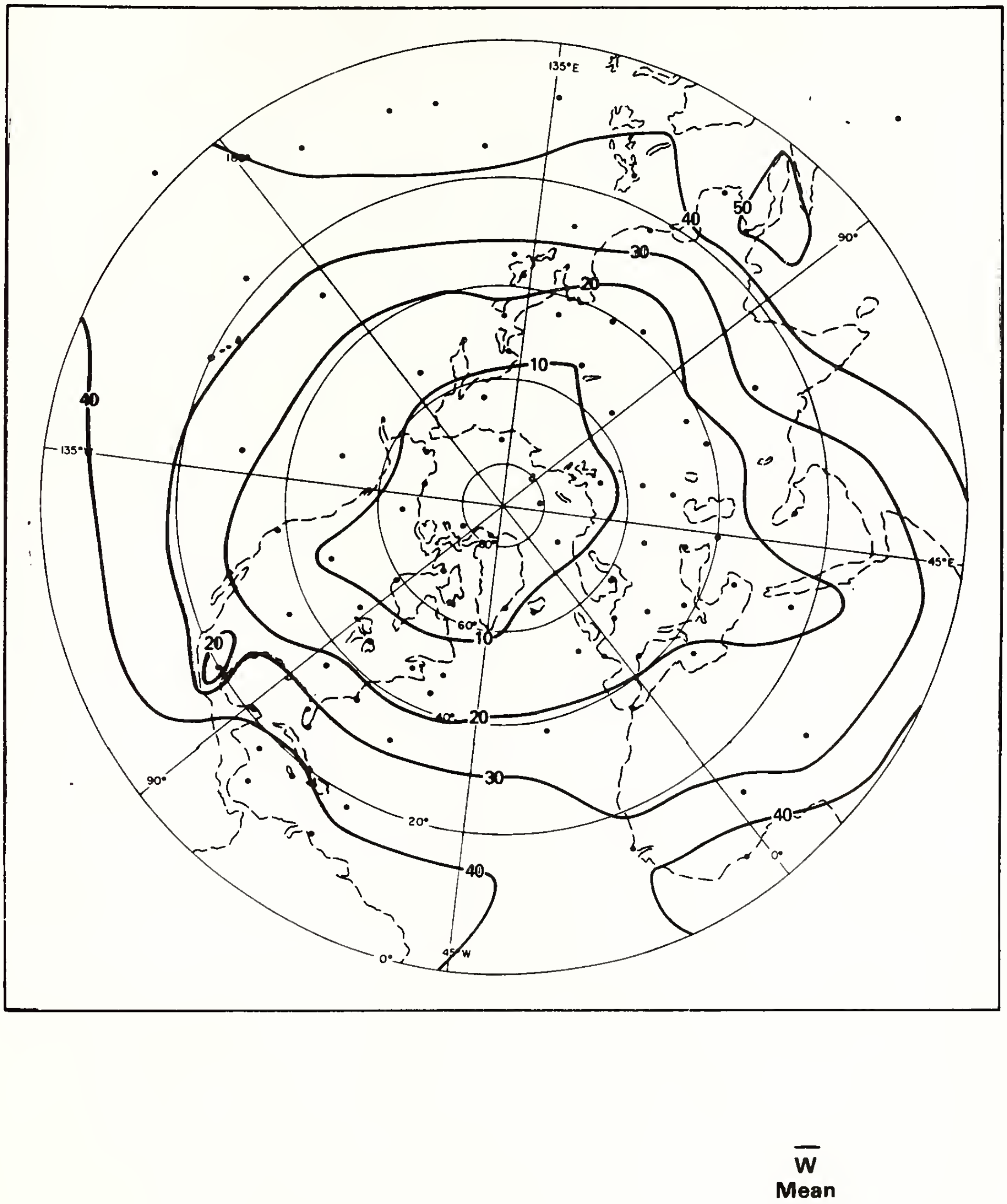

Figure 1 Average annual field of precipitable water, $\overline{W}$. Units are kg $m^{-2}$.

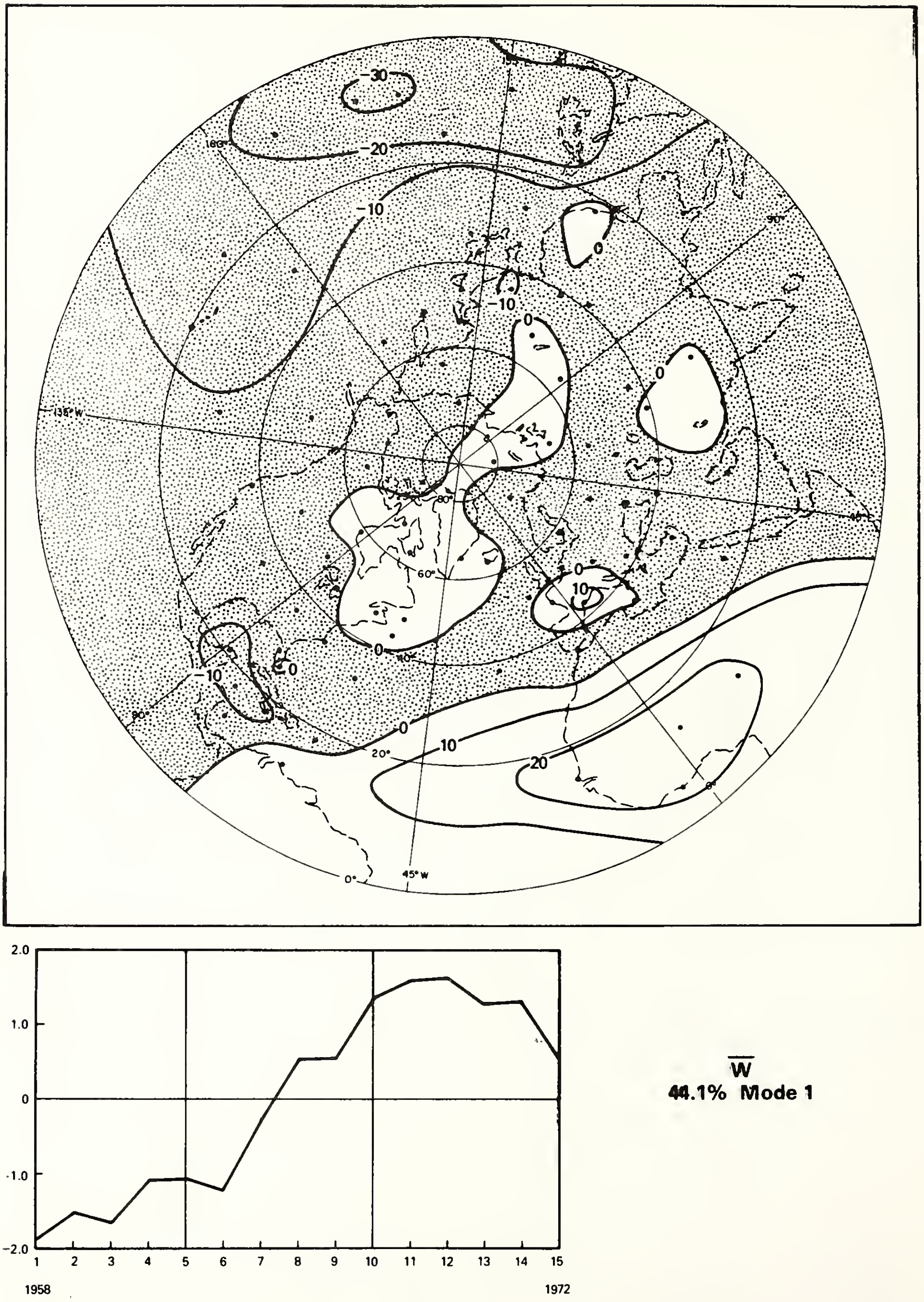

Figure 2 First EOF of $\overline{W}$ variability. Eigenvector units are x .01. Time series in 10 kg $m^{-2}$.

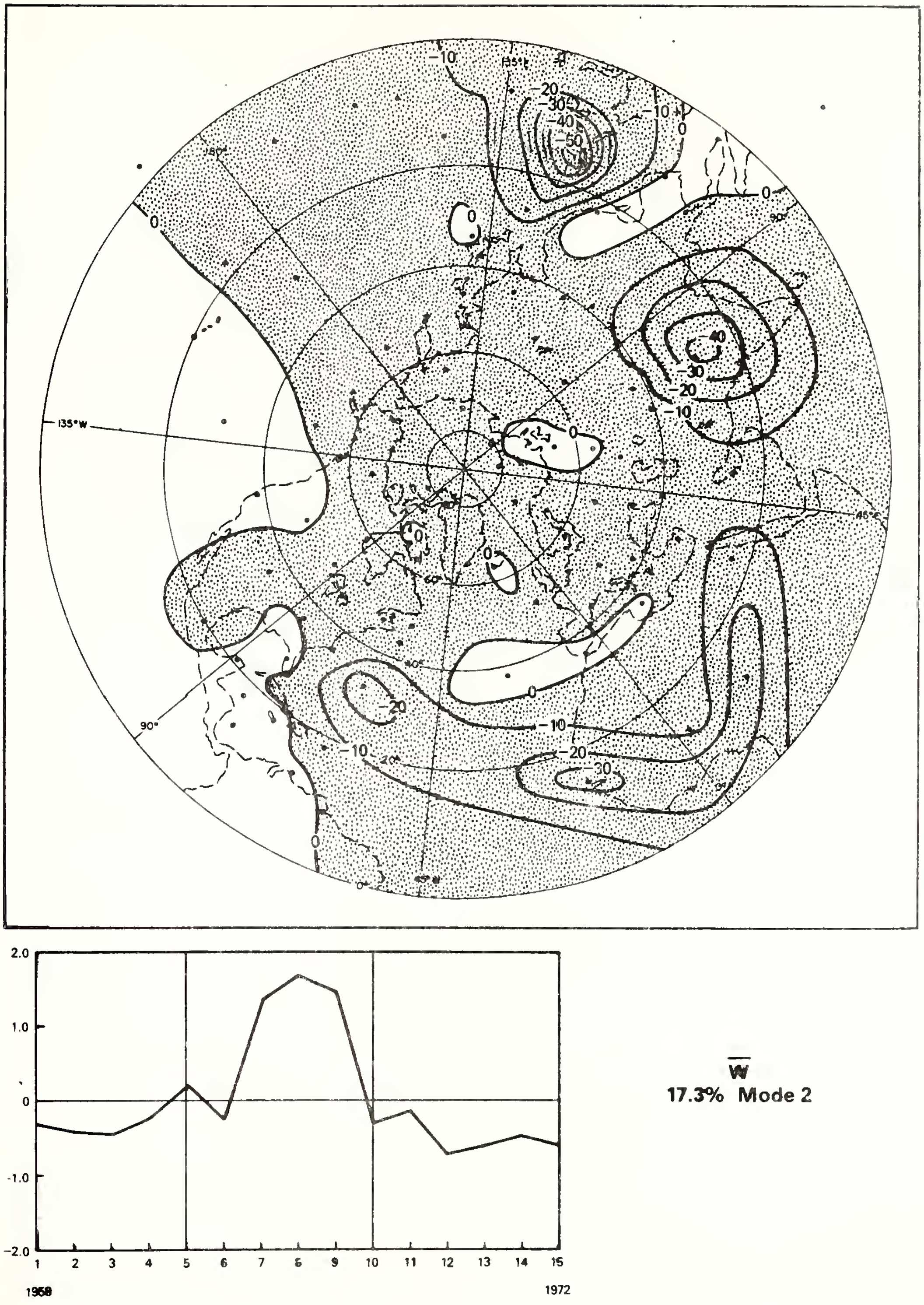

Figure 3 Second EOF of $\overline{W}$ variability. Eigenvector units are x .01. Time series in 10 kg $m^{-2}$.

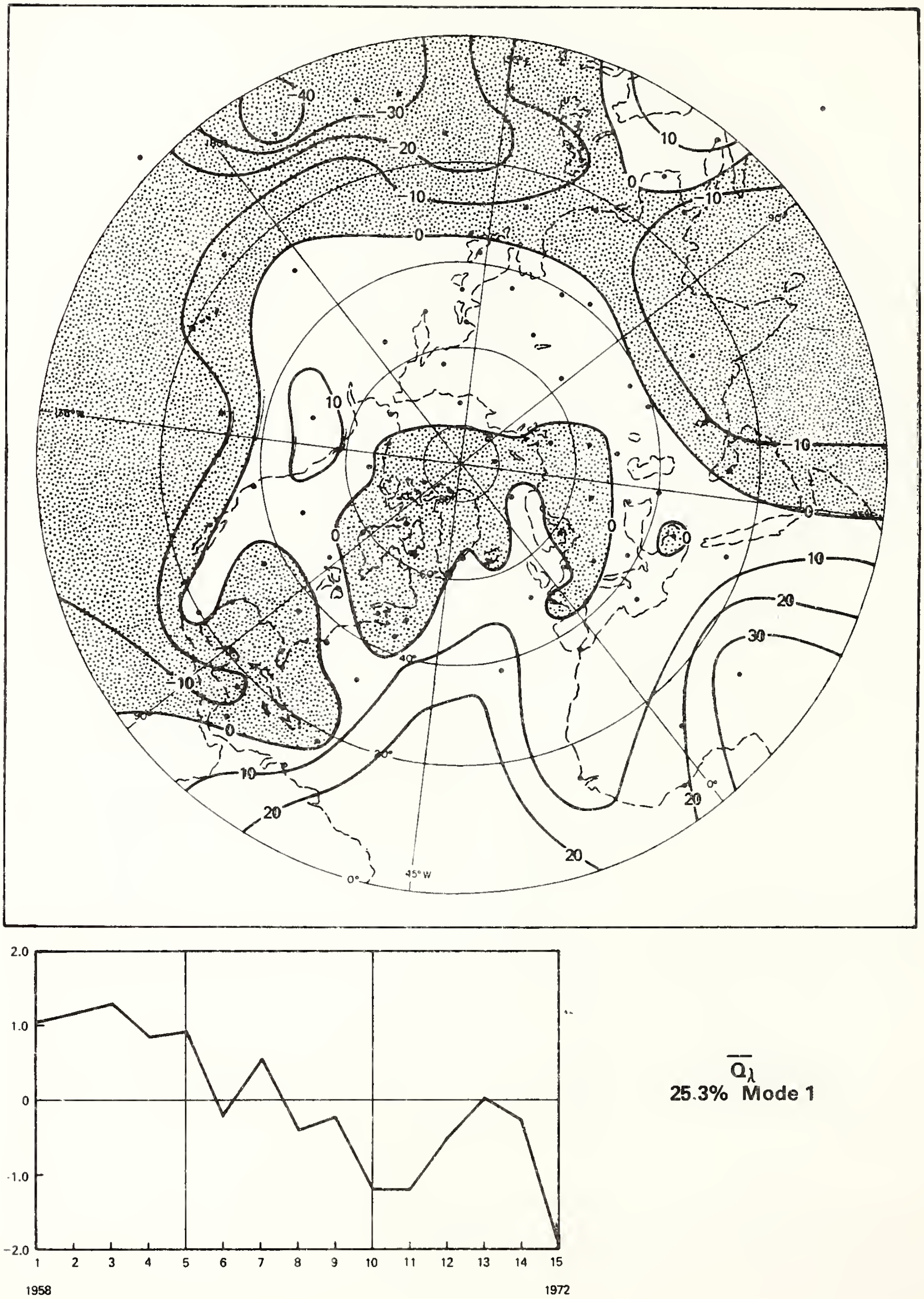

Figure 4 First EOF of $\overline{Q}_\lambda$ variability. Eigenvector units are x .01. Time seres in 100 kg $m^{-1}$ $s^{-1}$.

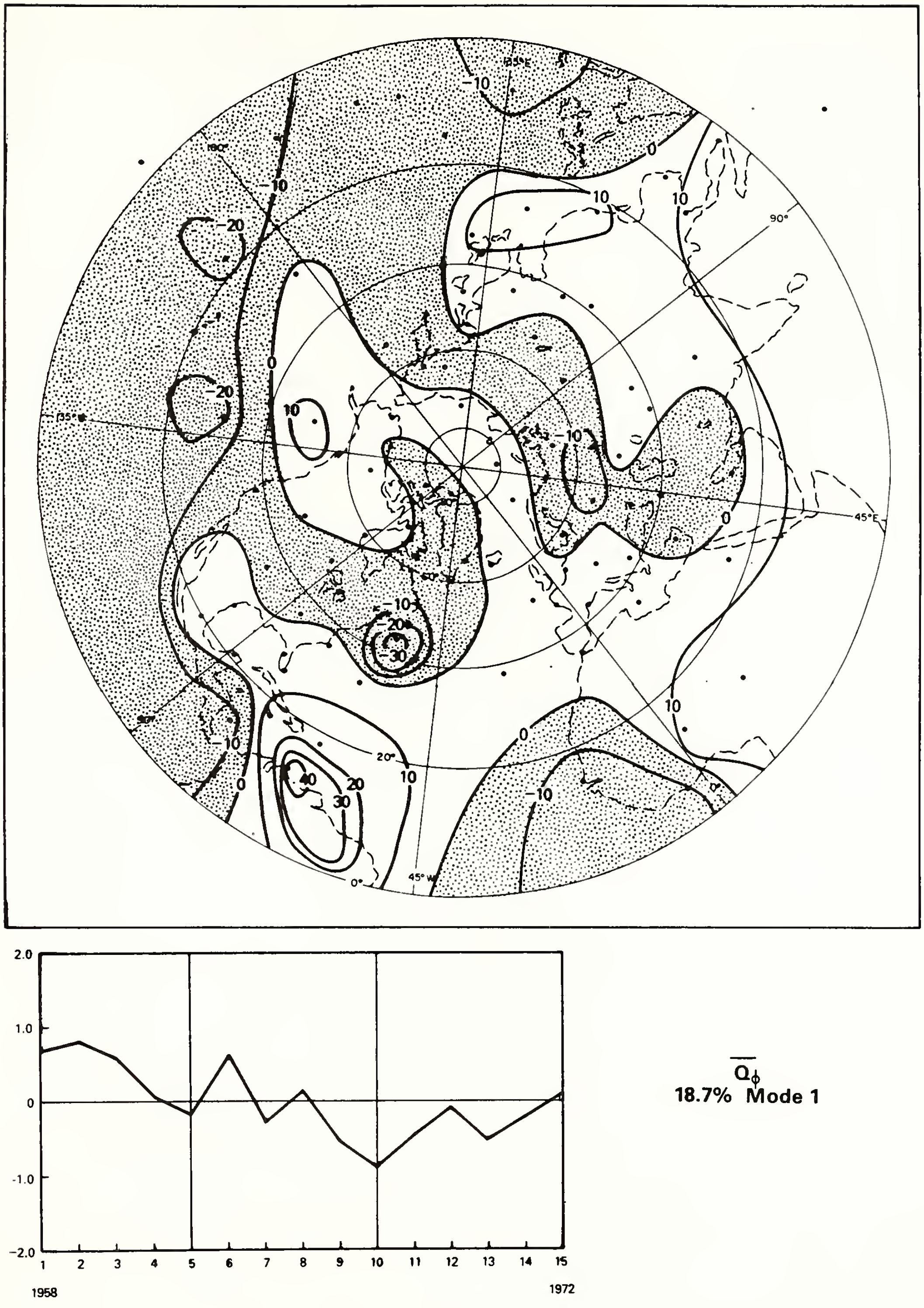

Figure 5 First EOF of $\overline{Q}_\phi$ variability. Eigenvector units are x .01. Time series in 100 kg $m^{-1}$ $s^{-1}$.

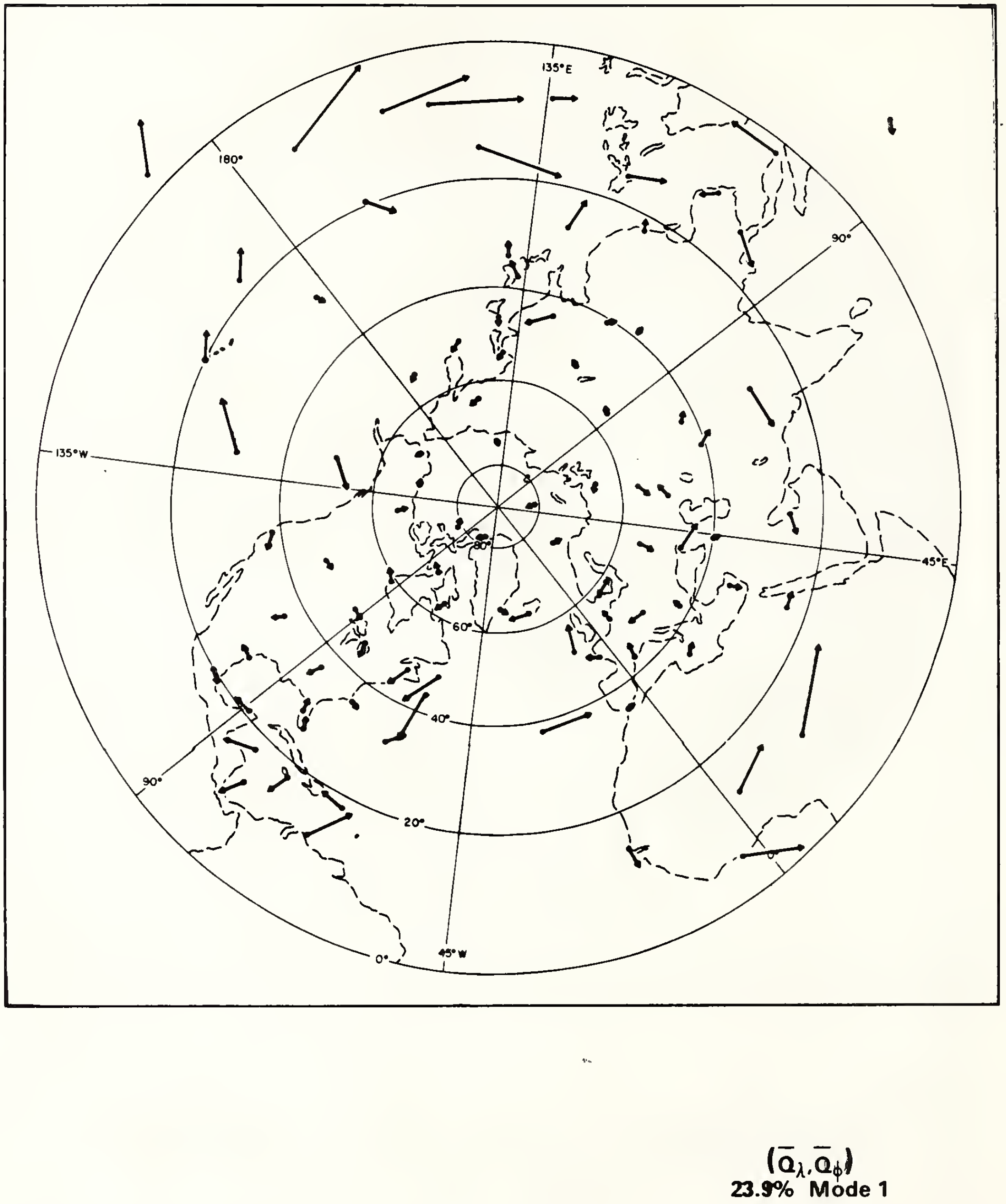

Figure 6 First EOF eigenvector of $(\overline{Q}_\lambda, \overline{Q}_\phi)$ variability.

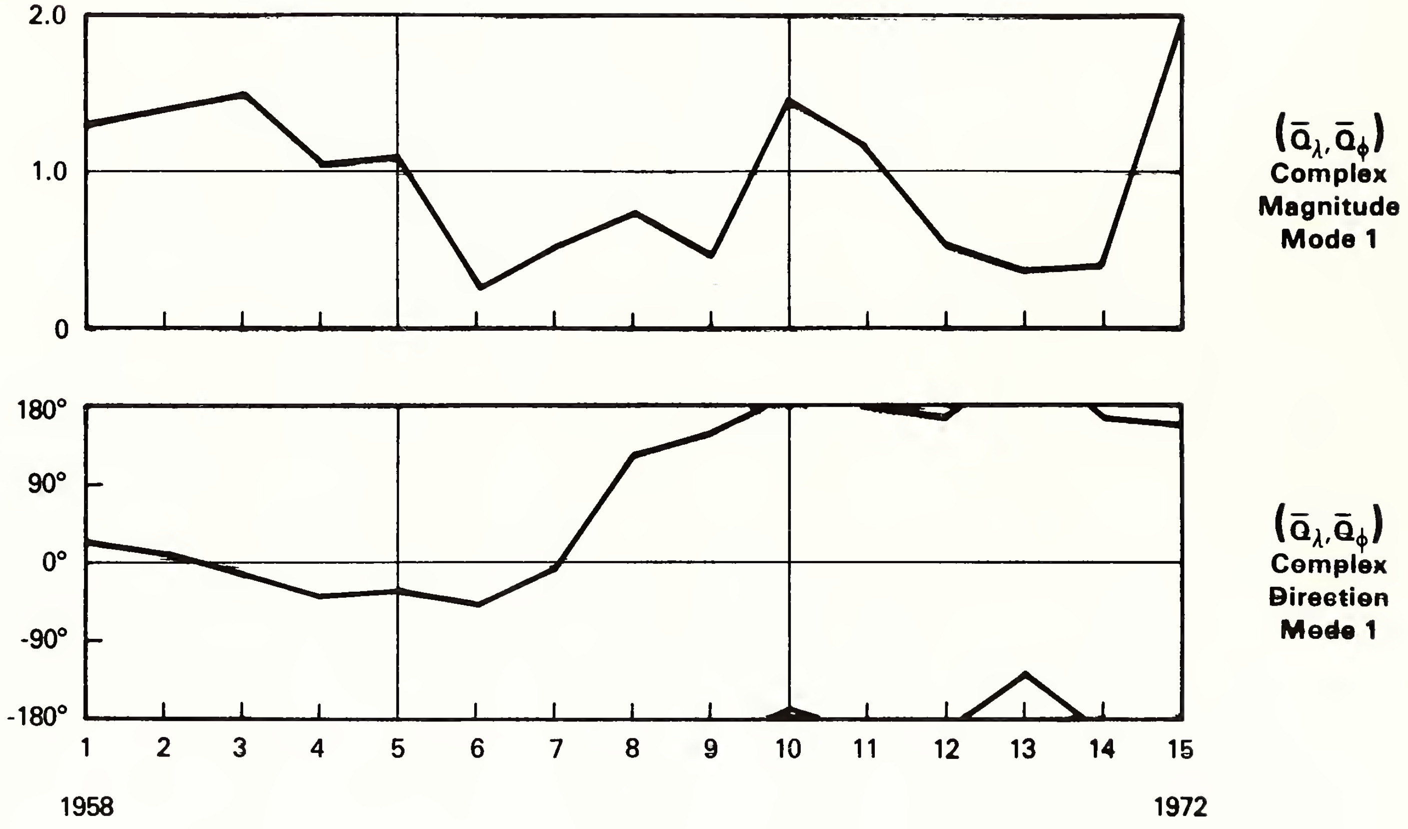

Figure 7 Time series for first EOF eigenvector of $(\bar{Q}_\lambda, \bar{Q}_\phi)$ variability. Magnitude in 100 kg $m^{-1}$ $s^{-1}$

# Climatic Variability in the Northern Hemisphere

by

George J. Boer
K. Higuchi

Canadian Climate Centre

An analysis of variance of the 1000-500 mb thickness field is performed to investigate climatic variability from 1949 to 1975. The thickness field and its variance, averaged over the Northern Hemispheric cap from 25°N latitude to the pole, are obtained and the resulting time series are analyzed for their trends and inter-relationships.

The figure displays, in order, the long term behaviour of the mean thickness and the standing eddy, transient eddy and north-south variance measures. The dashed line is a quadratic fitted to the data.

Analysis of the mean thickness and measures of transient eddy, standing eddy, and north-south variance shows a statistically significant linear trend in mean thickness and significant quadratic trend in standing eddy and north-south variance measures. No significant trend is found in transient eddy variance.

Correlation analysis of the time series shows a significant relationship between standing and transient eddy variances. No significant correlation between the mean thickness and the eddy terms nor between the north-south variance and the eddy terms is found.

The results of this study do not support the contention that the climate has become significantly more variable, nor do they support a connection between variability and either mean temperature or north-south variation of temperature.

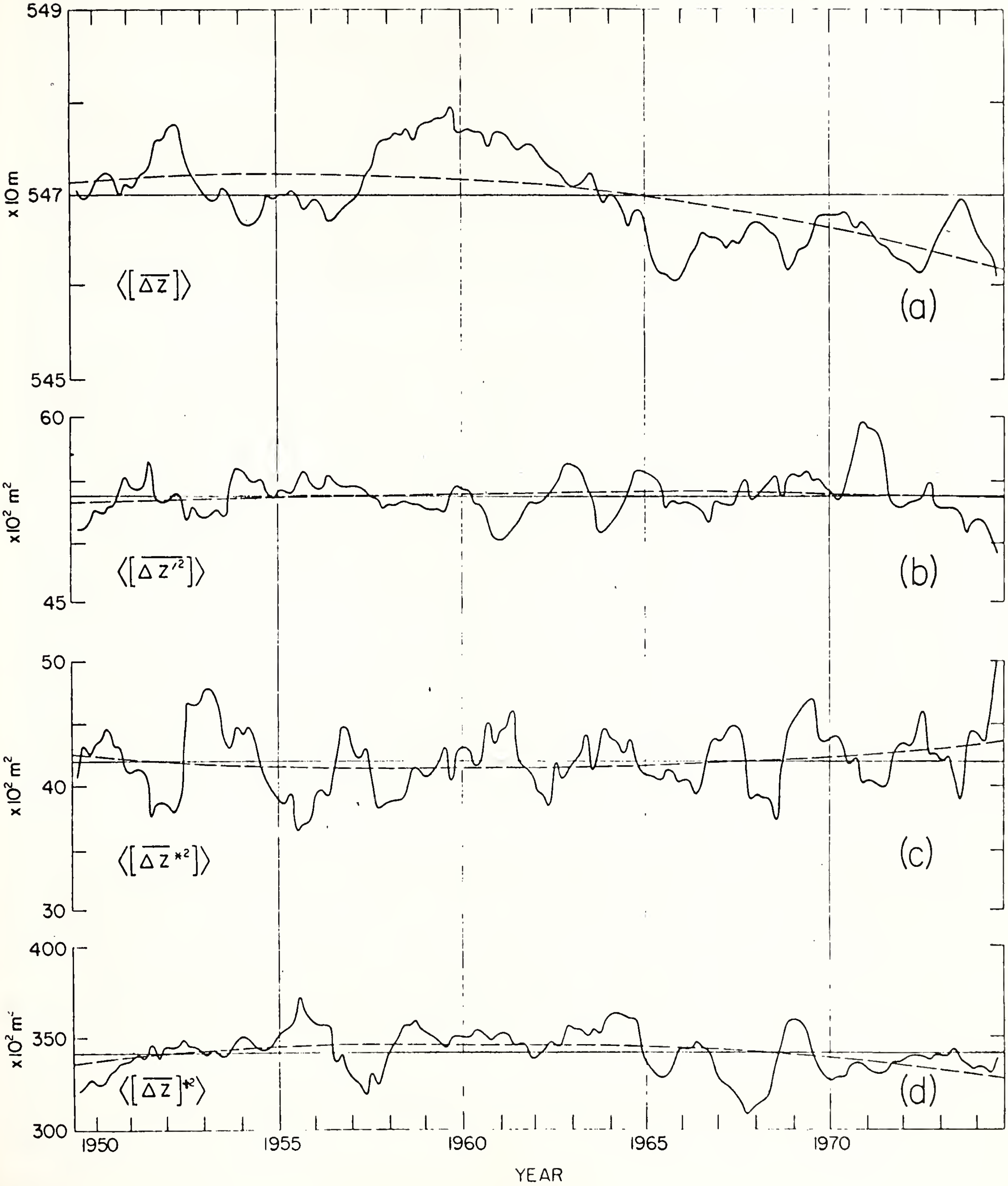
549
547
545
x 10 m
$\langle[\overline{\Delta z}]\rangle$
(a)
60
45
x10² m²
$\langle[\overline{\Delta z'^2}]\rangle$
(b)
50
40
30
x10² m²
$\langle[\overline{\Delta z^{*2}}]\rangle$
(c)
400
350
300
x10² m²
$\langle[\overline{\Delta z}]^{*2}\rangle$
(d)
1950
1955
1960
1965
1970
YEAR

# Trends of 700 mb Temperature in Winter and Their Connection with Changes in Stationary-Eddy Heat Fluxes

H. van Loon
National Center for Atmospheric Research[1]
Boulder, Colorado 80307

The changes from one year to another of the amplitude and position of the quasistationary waves and the attending changes in their transfer of atmospheric properties are naturally important to studies of climate changes. Below is a brief description of some associations between the transfer of sensible heat by the quasistationary waves in winter (DJF) and temperature, temperature gradients, wind, and pressure. Overbars will denote winter averages and brackets zonal averages, so that, e.g., $[\overline{v^*T^*}]$ will be the seasonally and zonally averaged transfer of sensible heat by the stationary eddies.

Figure 1 shows the correlation between the zonal averages of this transfer and temperature gradients at 700 mb. The correlation coefficients are negative between a given $[\overline{v}^*\overline{T}^*]$ and the gradients in the same area and immediately to the north, whereas they are positive between $[\overline{v}^*\overline{T}^*]$ and the region 25 or so degrees to the south. In other words, when the poleward heat flux in the stationary waves is strong near its peak at middle latitudes, the temperature gradients there and to the north tend to be weak while the gradients at lower latitudes tend to be steep, and conversely when $[\overline{v}^*\overline{T}^*]$ is weak. From this follows that the thermal wind and zonal wind will be related to the heat flux in the same manner. The correlation coefficients in Fig. 2 delineate the relationship between $[\overline{v}^*\overline{T}^*]$ at 850 mb and 50N and $[\overline{u}_g]$ everywhere below the 10-mb level. The zonal wind in the subtropics evidently tends to increase when the poleward heat transfer at middle latitudes is strong in the stationary waves, and to decrease north of 50N when it is weak. This may also be interpreted in terms of stronger cyclonic shear in the wind at lower latitudes when $[\overline{v}^*\overline{T}^*]$ is intense and weaker shear when $[\overline{v}^*\overline{T}^*]$ abates, and *vice versa* at higher latitudes. From this one may deduce that the frequency of cyclogenesis and of storm tracks tends to increase at lower latitudes when $[\overline{v}^*\overline{T}^*]$ increases at middle latitudes.

Intensifying $[\overline{v}^*\overline{T}^*]$ at middle latitudes is accompanied by larger heat-flux divergence to the south, and one must therefore expect an inverse relationship between $[\overline{v}^*\overline{T}^*]$ and the $[\overline{T}]$ on its south side. The correlation coefficients in Fig. 3 describe this relationship; for instance, $[\overline{v}^*\overline{T}^*]$ at 45-50N is correlated with $[\overline{T}]$ at 40N by -0.82. The time series of $[\overline{v}^*\overline{T}^*]$ at 50N and $[\overline{T}]$ at 40N in Fig. 4 demonstrate that this large correlation coefficient stems not only from quite frequent parallel changes from one winter to another but also from slow parallel changes over several years.

---

[1] The National Center for Atmospheric Research is sponsored by the National Science Foundation.

As the temperature at 40N drops while the stationary-eddy transfer of sensible heat increases to the north, the temperature gradients at lower latitudes become steeper and cyclonic activity increases in these latitudes while it decreases at high latitudes. It is thus reasonable to expect sea level pressure in the Arctic to rise while the 700 mb temperature drops at 40N, and *vice versa*; and a comparison of the pressure at Angmagssalik (66N, 38W) at the bottom of Fig. 4 with $[\overline{T}_{700\ \mathrm{mb}}]$ at 40N at the top of the diagram indicates that the trends of the two elements are indeed opposite. The correlation between them is -0.40. The record of sea level pressure at Angmagssalik began in 1895, and by means of this record and the linear regression equation between the pressure at Angmagssalik and $[\overline{T}_{700}]$ at 40N during 1949-1979 we can get a broad indication of the range of $[T_{700}]$ at 40N within the last century. The linear regression suggests that the temperature at 40N can be about 1°C lower than the lowest value observed since the winter of 1948/1949 which was -9.6°C; and that it can be as much as 2.5°C higher than the highest value observed since 1948/1949 of -6.5°C.

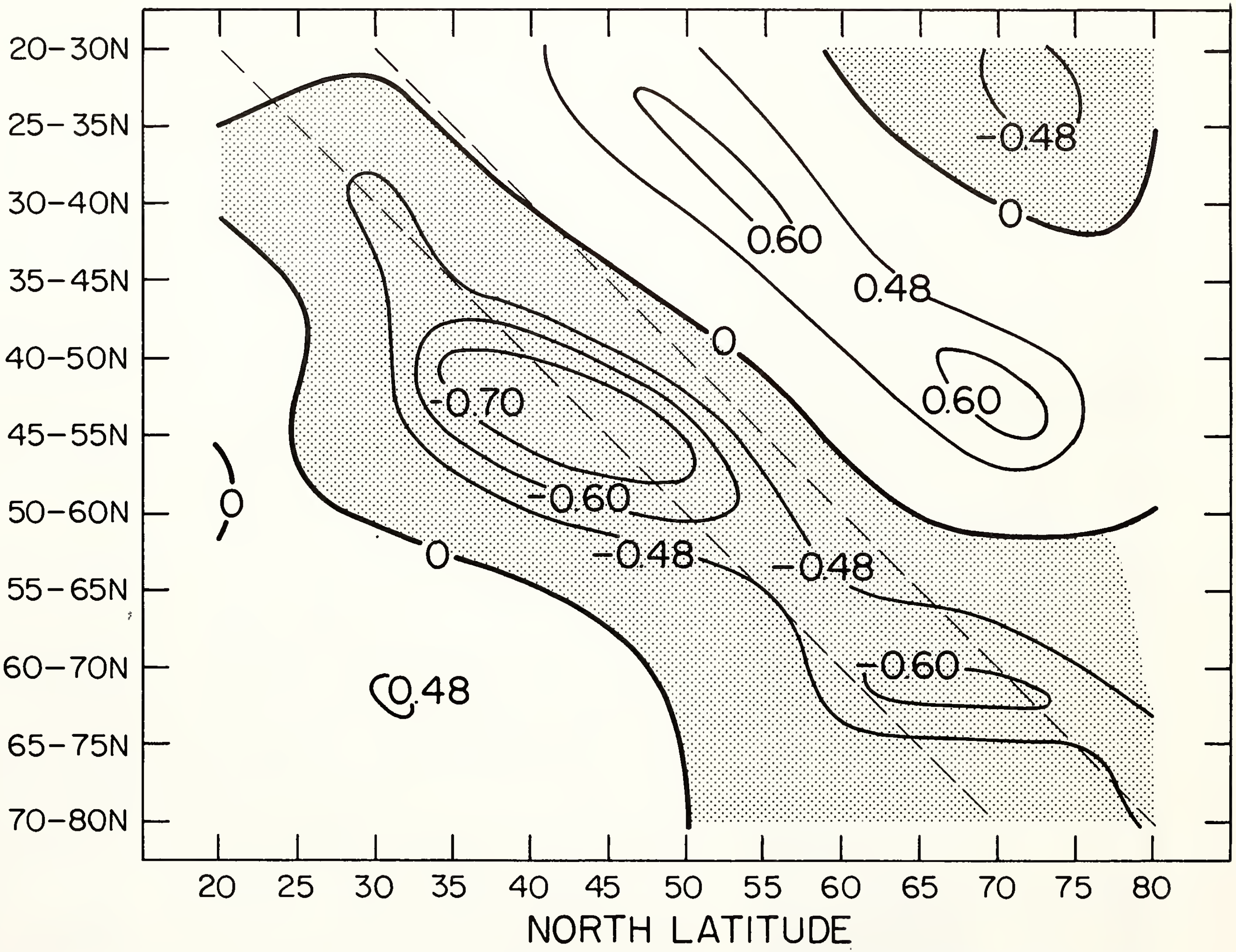

Fig. 1 The correlation between the zonal means of stationary-eddy transfer of sensible heat and the temperature gradient per 10 degrees of latitude at 700 mb for 29 winters. r = 0.48 is the 99% confidence limit.

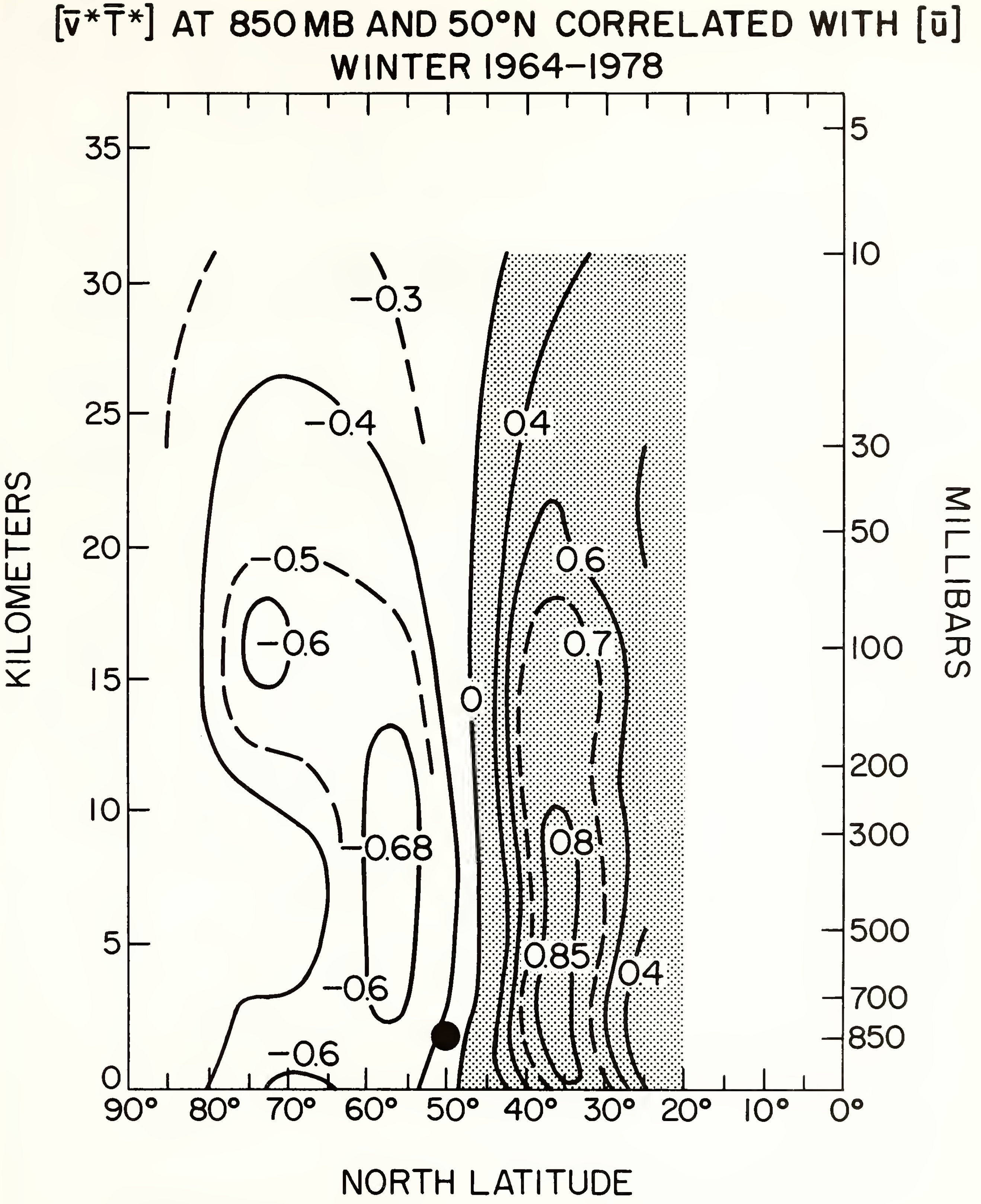

Fig. 2 The correlation between the zonal means of the stationary-eddy transfer of sensible heat at 50N and 850 mb and the zonal geostrophic wind for 15 winters. r = 0.67 is the 99% confidence limit.

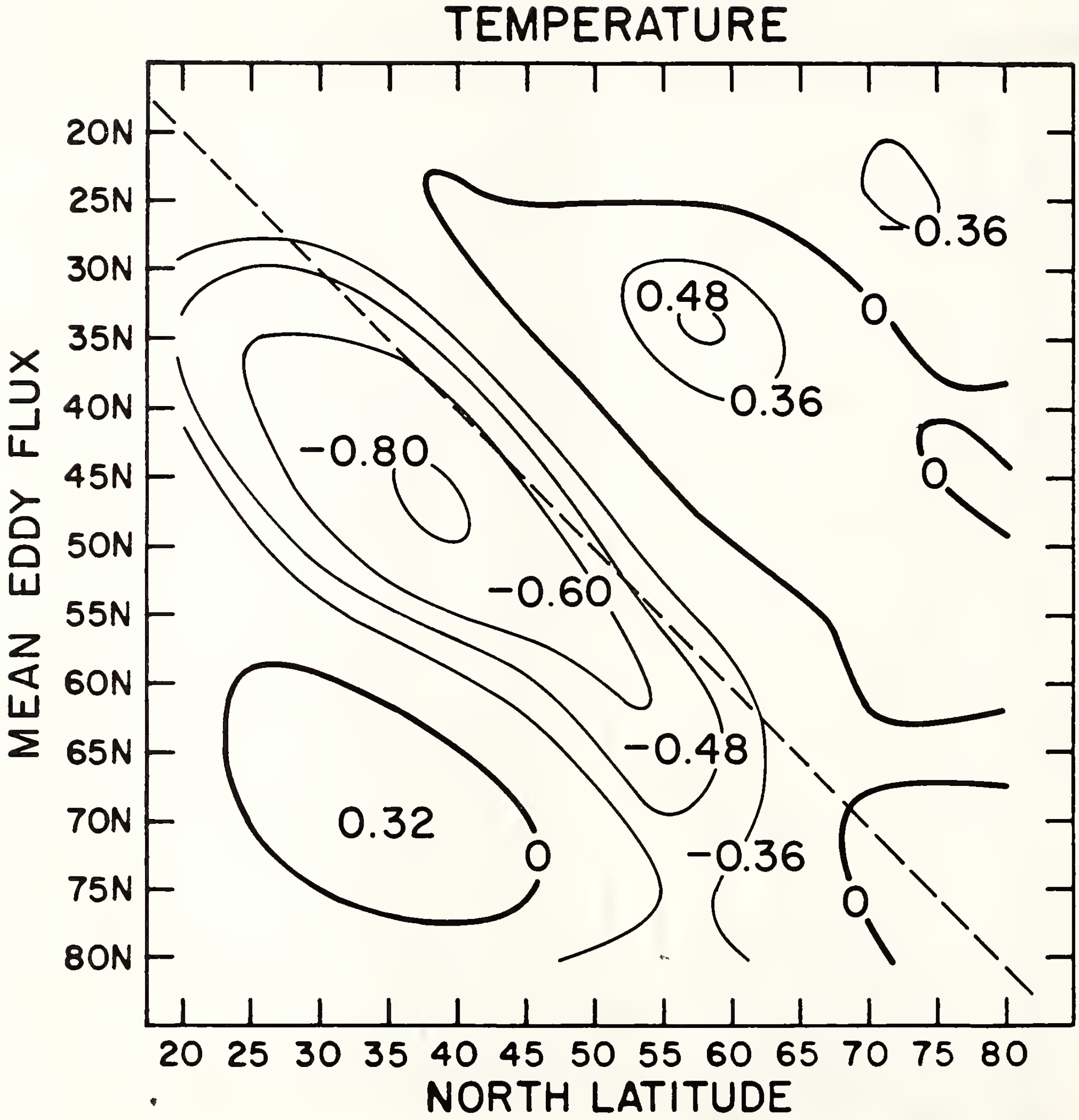

Fig. 3 The correlation between the zonal means of the stationary-eddy transfer of sensible heat and the zonally averaged temperature at 700 mb for 29 winters. r = 0.48 is the 99% confidence limit.

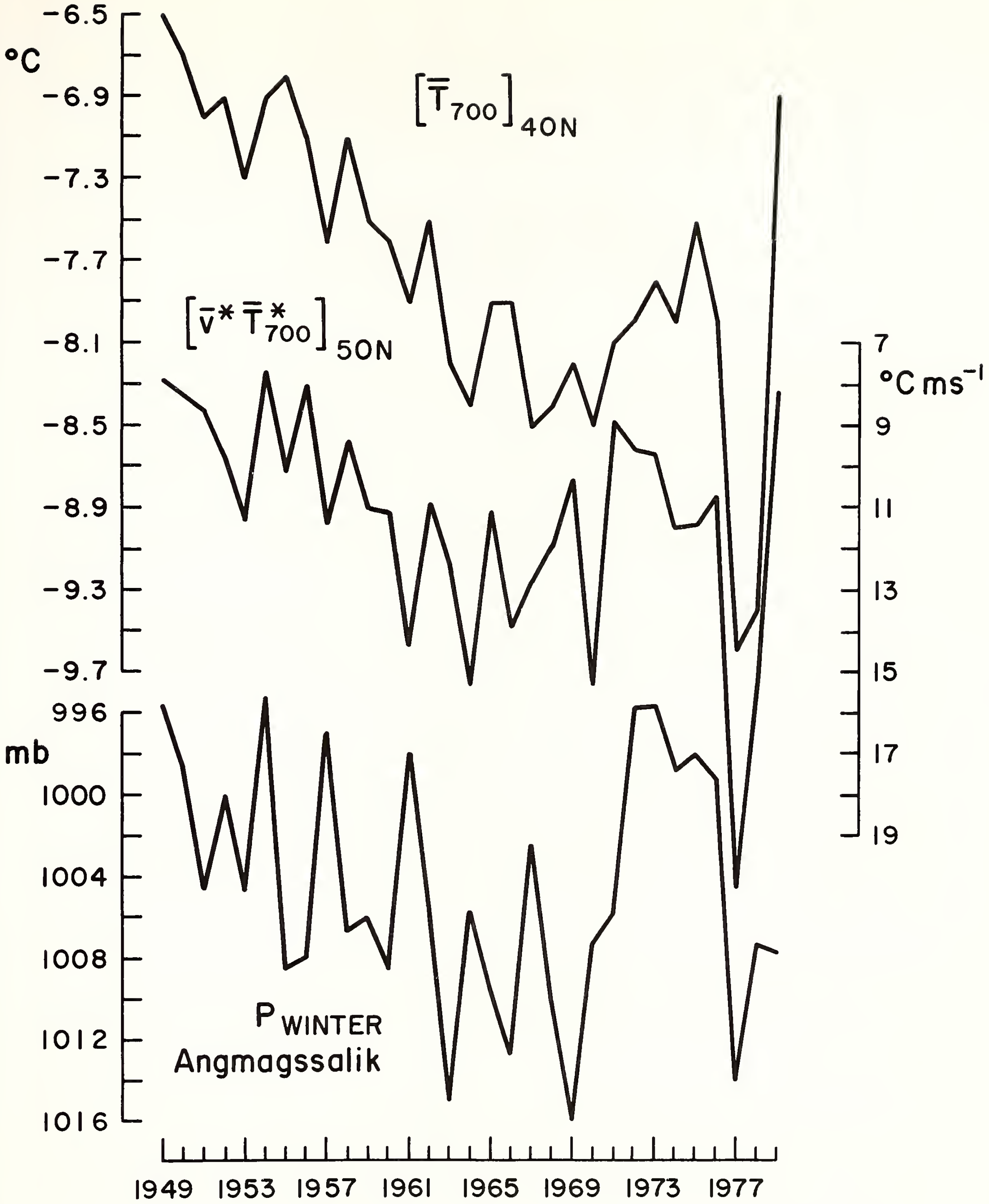

Fig. 4 Time series for winter of Top: the zonally averaged 700 mb temperature at 40N. Middle: the zonally averaged transfer of sensible heat by the quasistationary waves (°C $ms^{-1}$). Bottom: The sea level pressure at Angmagssalik at 66N, 38W. Note that the values of heat transfer and pressure increase downward, whereas 700 mb temperature increases upward.

# A Statistical Model of Planetary Scale Waves in the 500 mb Geopotential

J. Padro and S. Woronko
Atmospheric Environment Service
Downsview, Ontario. M3H 5T4

Experiments are being conducted to determine the level of skill which can be attained with a linear regression model in forecasting the time averaged large scale anomalies from the long-term mean in the 500 mb geopotential field. The initial test case reported here is based on parameters averaged over two-month intervals, with the predictand period being December - January. In the "first-order" model, the predictors are the October - November anomalies from the long-term mean, and additional predictors from the August - September period are also included in the "second-order" model.

The data consisted of daily and twice-daily analyzed 500 mb geopotential height fields from NCAR for the period 1946-1972, and from the Canadian Meteorological Center for the period 1973-1979. The data from 1971 onwards was reserved as an independent sample.

In order to reduce the number of degrees of freedom to a suitably small number, the fields were highly filtered with Fourier decomposition in the east-west dimension, and with empirical orthogonal functions of the Fourier coefficients in the north-south dimension. Truncation was based on the retention of those components explaining the highest portion of the dependent sample variance. Approximately 50% of the variance was accounted for with 6 components, and 70% with 12 components.

The 6 component set included east-west wavenumbers 0 to 3, and the 12 component set, 0 to 4. The statistical prediction was based on a canonical correlation analysis of the correlations between linear combinations of the predictors and linear combinations of the predictands (Glahn, 1968).

The results are summarized in the Table below. The score is the space correlation of the forecast field (on a 455 point grid) with the unfiltered verifying field. The score limit represents the best possible score, given that the forecasts are filtered. Since persistence shows skill on this time scale, its score is included as a control.

| PERIOD | MODEL | FORECAST SCORE | PERSISTENCE SCORE | SCORE LIMIT |
|---|---|---|---|---|
| 1946-70 | 12 component, first order | .59* | .13 | .84 |
| 1946-70 | 6 component, second order | .15* | .13 | .68 |
| 1946-70 | 6 component, first order | .17* | .13 | .68 |
| 1971-76 | 12 component, first order | .08 | .17 | .83 |
| 1971-76 | 6 component, second order | .21 | .17 | .69 |
| 1971-78 | 6 component, first order | .15 | .11 | .69 |
|  | (* Dependent Sample Scores) |  |  |  |

The first conclusion is that the 12 component version has too many degrees of freedom for the correlations to apply to independent samples. For a discussion of this problem see Lorenz, 1959. The 6 component models seem to carry their skill to independent data samples, but the skill is not significantly better than persistence.

More extensive analysis of these and other results will be necessary to reach general conclusions, but these results suggest that it will be very difficult to attain skill superior to persistence, given that the amount of historical data available drastically limits the number of degrees of freedom that can be used to describe the fields.

## References

Glahn, H.R., 1968: Canonical correlation and its relationship to discriminant analysis and multiple regression. J. Atmos. Sci., 25, 23-31

Lorenz, E.N., 1959: Prospects for statistical weather forecasting. Final report, Statistical Forecasting Project, Mass. Inst. Tech., Dept. of Meteoro., January 1959.

# On the Heat Budget of Hydrosphere and Atmosphere in the Indian Ocean

Stefan Hastenrath
University of Wisconsin
Madison, Wisconsin 53706

Abstract:

The heat budget of the atmosphere-ocean-land system in the realm of the Indian Ocean and its peripheries (30 - 120 E, 30 S - 30 N) is studied on the basis of oceanic heat budget calculations from long-term ship observations and satellite-derived net radiation at the top of the atmosphere.

The hydrosphere to the North of the Equator acts as an effective exporter to other parts of the globe, at an annual rate of 5 x $10^{14}$ W, whereas seasonal variations in oceanic heat gain approximately cancel in the Southern tropical Indian Ocean. Annual mean oceanic heat transport is directed southward, reaching a maximum of 8 x $10^{14}$ W at 10 - 15 S. An annual mean upwelling of about 6 x $10^{-7}$ m $s^{-1}$ is calculated for the Indian Ocean North of the Equator, with compensatory downwelling taking place largely outside the tropical Indian Ocean. Residual heat export within the atmosphere to the North of the Equator amounts to a surplus of 18 and 4 x $10^{14}$ W during the Northern summer and winter half years, respectively; and export from the Southern hemisphere domain is effected at an annual rate of 19 x $10^{14}$ W, with little seasonal variation. During the Northern summer, atmospheric energy export from the Southern Indian Ocean is mainly in the form of latent heat, transport being directed northward across the Equator. The water vapor flux divergence is related to the vigorous evaporation, which is maintained in part by the seasonal depletion of oceanic heat content. The Southern tropical Indian Ocean is the major source of atmospheric water vapor carried across the coastline of Southern Asia during the Northern summer Southwest monsoon.

In the Southern tropical Indian Ocean, the atmosphere must dispose of both the net radiative heat input at the top of the system and the heat import within the oceanic water body. In the equatorial and Northern Indian Ocean, atmosphere and hydrosphere cooperate in the lateral energy export.

# Empirical Orthogonal Function Analysis of Satellite-Observed Outgoing Longwave Radiation during Winter

## Part II. Short-Period (4-6 Day) Oscillations

T. Murakami

Department of Meteorology
University of Hawaii
Honolulu, Hawaii 96822

Empirical orthogonal function analysis was applied to outgoing longwave radiation (OLR) data over the South China Sea, western Pacific, and Indonesian Seas region, during the three winters of 1974-75, 1975-76, and 1976-77. Composite maps were constructed by truncating the eigenvector series of 4-6 day filtered OLR anomalies for each winter at 70 percent representation. An attempt was then made to investigate the phase propagations of 4-6 day OLR perturbations.

The winters of 1974-75 and 1976-77 have similar features in 4-6 day OLR disturbances, with systematic westward phase propagation in equatorial latitudes over the western North Pacific and the South China Sea (Fig. 1). In contrast, the 1975-76 winter is of a different character with distinct eastward propagation of OLR perturbations, against the prevailing northeasterly trades, over the equatorial zones (0°-10°N) of the North Indian Ocean and South China Sea. These large year-to-year changes in phase propagation appear to be related to interannual differences in nonlinear coupling with midlatitude westerly (eastward propagating) regimes over southern and southeastern Asia.

Monsoonal surges, associated with midlatitude baroclinic systems, appear to be pronounced during the winter of 1975-76. This can be seen by the large (>10 units) standard deviations to the south of Japan at around 30°N, 140°E (Fig. 2, bottom-left). It should also be noted that standard deviations exceed 10 (5) units to the north (south) of the Persian Gulf (Tibetan Plateau) during the 1975-76 winter, which is indicative of equatorward penetration of midlatitude westerly regimes into southern and Southeast Asia. In contrast, the smaller standard deviations of the 1974-75 and 1976-77 winters over these same regions, suggest that midlatitude disturbances (and monsoonal surges) were weaker during these years.

As shown in Fig. 2, standard deviations associated with 4-6 day OLR perturbations are relatively small over the large islands of Sumatra, Borneo, Celebes, and New Guinea. This stands in sharp contrast with the pronounced diurnal convective activity observed over and around the large islands. The smallness of OLR standard deviations probably indicates that the large islands inhibit the development and/or movement of synoptic disturbances. Perhaps, this is associated with the large amounts of latent heat in diurnal cloud activity since heating induces ascending motions, just as vertical motions are induced by flow over mountains. Such a heating distribution may be referred to as being an "equivalent mountain" (refer to Stern and Malkus, 1953); namely, pronounced and deep diurnal cloud systems may act in the same manner as high mountains and exert some measure of control over the movement of synoptic disturbances.

Interestingly, 4-6 day OLR disturbances never seem to cross over regions of high (> 2,000 ft) mountains (Fig. 1). For example, during the 1975-76 winter, the trajectory of 4-6 day OLR disturbances is directed northeastward (parallel to the northwest coast of Borneo) over the South China Sea and crosses over the Philippines between the high mountains of Luzon and Mindanao. From this point east of the Philippines, the trajectory then turns southward and travels into the Southern Hemisphere tropics between the high mountains of New Guinea and Celebes.

The horizontal scale of 4-6 day OLR disturbances is about 3,000 km, which is much greater than any of the islands scattered throughout the WMONEX region. Yet, Fig. 1 clearly indicates the strong influence of these islands upon the movement of 4-6 day OLR disturbances.

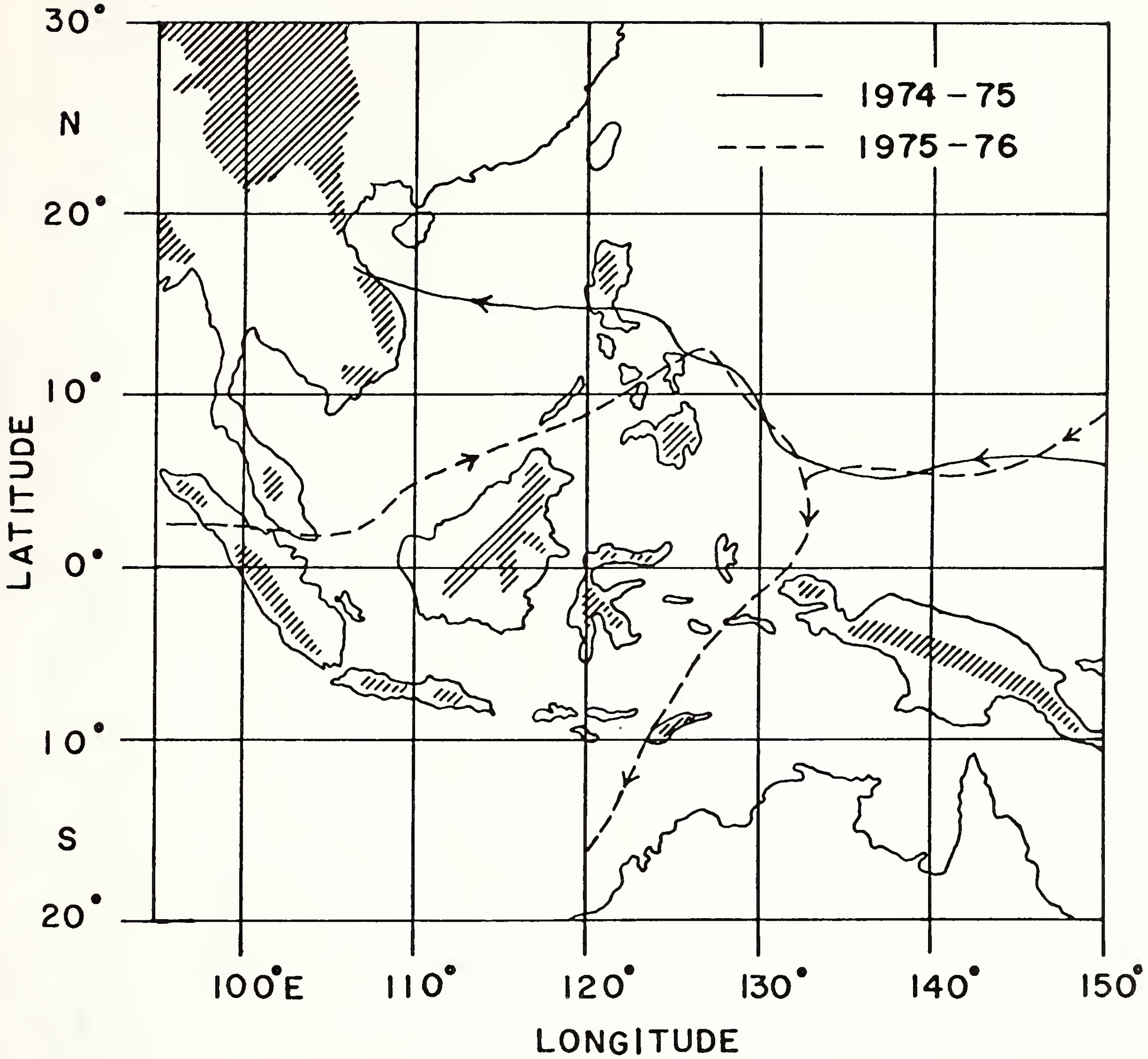

Figure 1. Trajectories of 4-6 day OLR perturbations during the 1974-75 (full line) and 1975-76 (dashed line) winters. Shading indicates mountains with elevations higher than 2,000 ft.

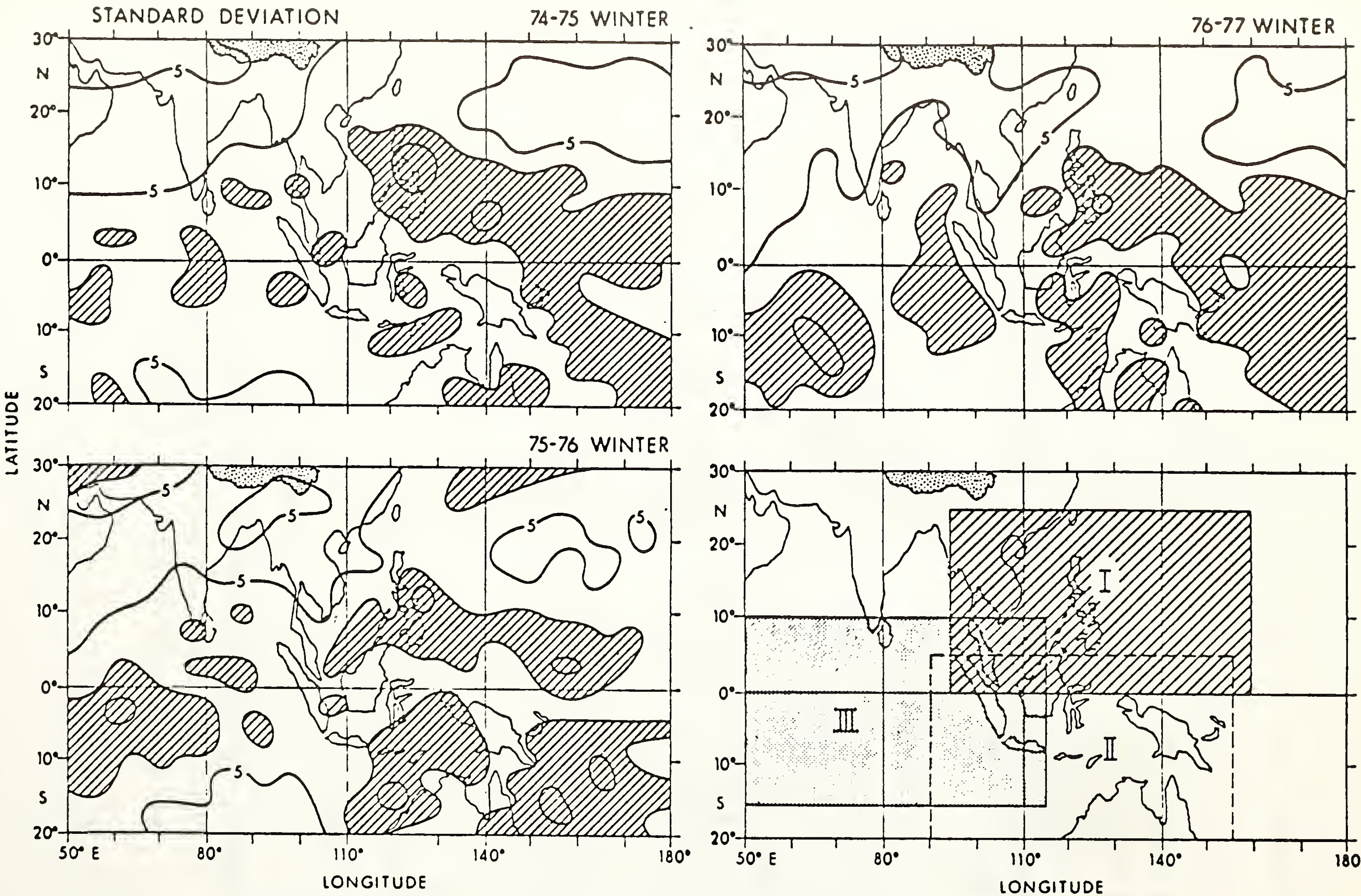

Figure 2. Standard deviations of 4-6 day filtered OLR data (10 W $m^{-2}$) during the three winters (December-February) of 1974-75 (top-left), 1975-76 (bottom-left), and 1976-77 (top-right). Interval 5 units. Regions of greater than 10 units are shaded. Also shown in the bottom-right diagram are regions 1 to 3, to which empirical orthogonal function analysis was applied.

# The False El Niño and Recent Related Climatic Changes in the Southeast Pacific

William H. Quinn
School of Oceanography, Oregon State University

We have heard much about El Niño, the large-scale climatic changes that relate to it, and the devastating affect it has on the Peruvian anchoveta fishery. Here we discuss a similar phenomenon which at times adversely affects the jack mackerel and anchoveta fishery off northern Chile. Cañon (1978) calls it the false El Niño, involving an intrusion of subtropical surface water (salinity 35.2°/$_{oo}$). Although it occurs near the time of El Niño, the transequatorial flow of warm surface water identified with El Niño has a much lower salinity.

A tongue of warm water extending southeastward from the area south of the Galapagos to the region off northern Chile was noted by Bjerknes (1961), and this we consider to be a likely source of warm water for the false El Niño. However, this tongue is a seasonal feature which appears every year and the false El Niño, like El Niño, occurs infrequently. Figs. 1 and 2 from Wyrtki (1964) show typical summer and winter sea surface temperature (SST) patterns. In general he finds the tongue located from October to May to the west of the cold upwelling water off Peru. Fishing Information analyses usually show the tongue to be most fully developed in January and February.

Wyrtki (1977), using two years (1975-76) of satellite derived SST maps to study advection in the subtropical oceanic gyre, noted the advance and retreat of the tongue of cool water stretching from the subtropical coast of Chile to the northwest under the southeast trade winds. He discussed the seasonal nature of the cool tongue and related its different behavior during the two years to the occurrence of the 1976 El Niño event. He found that advection in the subtropical gyre during 1976 was much weaker than during the year before.

The cool tongue is just to the west of the warm tongue (Fig. 1). It appears that seasonal and interannual changes in the warm and cool tongues are likely to be interrelated and caused by seasonal and interannual changes in the South Pacific subtropical high. In the mean this high lies farthest north during southern hemisphere (S.H.) winter (25°S) and moves southward during S.H. spring reaching its farthest south position (31°S) in S.H. summer (Allison, et al., 1972). As a result, the band of stronger southeast trades on the northeast flank of the high moves southward and further away from the NW-SE oriented coast of Peru; and, the warm tongue occurs in the zone of weak and variable winds that lies between the strong southeast trade band and the southerly coastal wind system that prevails along Peru during the S.H. summer. This tends to explain the interrelated nature of the cool and warm tongue developments noted on Wyrtki's (1964) S.H. spring through early fall charts.

Surface waters in the southeastern part of the warm tongue are identified as subtropical by Sandoval and Hott (1975). The high SST's in the southeastern lobe of the tongue during S.H. summer are attributed to: (1) the subtropical origin, (2) in situ summer heating, and (3) the weak winds limiting vertical mixing and latent heat loss.

Interest was focused on effects of interannual change on warm tongue and coastal water temperatures. Ordinarily south to north coastal circulation and coastal upwelling are sufficient to prevent warm tongue waters from penetrating in to the coast. However, when the southeast trades and associated coastal oceanic circulation become unusually weak the warm tongue waters are allowed to penetrate coastward, causing SST's to be 2, 3, or more degrees above normal. (The invading warm, saline surface layer is 25 to 50 meters thick near the coast.) The southeast extremity of the tongue is usually quite narrow with highest temperatures in a zone 80 to 150 miles wide. Projections from Fishing Information analyses, indicate the tongue axis is most likely to reach the coast between 19° and 22°S latitude.

Fig. 3 shows plots of some of the meager coastal and offshore data. The value of the Antofagasta SST plot is quite limited since observations are taken at the protected location of the sea level gauge. Fig. 4 and Table 1 data were included to provide a precedent for using air temperature trends to represent SST trends at west coast South American sites. Fig. 5 shows monthly air temperature anomaly trends during the stronger events of recent years at certain sites where data were available. There is no way of knowing where the tongue axis was in relation to the station involved, but it was most likely near Iquique in January 1973. In some cases, e.g. the 1957 and 1965 El Niños, the positive anomalies show up several months earlier in the Marsden Square (MS) 379 data (Fig. 3) than it does in the Lima/Callao/La Punta data (Fig. 4). SST data for the northern quadrants of MS 379 may, therefore, be useful at times when making El Niño predictions.

Although the false El Niño appears to be a companion type development to El Niño, it is more directly associated with changes in the South Pacific subtropical high and its related southeast trades. From Table 2 we can see that changes in the subtropical high are likely to lead those in the equatorial low by several months. Therefore, monthly mean 850 mb height data for Easter, Antofagasta and Quintero were used in Easter-Antofagasta and Easter-Quintero height difference indices. Fig. 6 shows 3-month running mean plots of the index anomalies which are being used to represent interannual changes in strength of the low level flow (south to north components) over that part of the southeast Pacific with which we are concerned. Although this upper level data record is short, the interannual changes related to the 1972-73 and 1976-77 El Niño events are clearly evident. The indices should be useful for monitoring and predicting the false El Niño occurrence.

There is a need for further study of the false El Niño due to its adverse affect on the increasingly important north Chilean jack mackerel and anchoveta fishery, its relationship to El Niño, and the involved larger-scale marine climatic ramifications. Hydrographic data indicate the details pertaining to this development are quite complex.

During my review of the available SST analyses in Fishing Information, it appeared that there might be a long-term rising trend in SST's over this part of the southeast Pacific with which we are concerned. Fig. 7 shows a 3-month running mean plot of Easter I. sea level pressure anomalies and a similar plot of anomalies of the maximum SST noted in the square running from 17°S to 24°S and 70°W to 77°W (area penetrated by the warm tongue). The long-term fall in Easter pressure would be compatible with a long-term rise in SST over the southeast Pacific. I called Dr. Joe Fletcher (NOAA-ERL) who has been studying SST changes on a global basis, and he had also noted this long-term change over the southeast Pacific. This will of course add to the compexity of studies in this region.

I thank the Chief of the Naval Weather Service and the Director of the Hydrographic Institute of the Armada de Chile; the President of the Instituto del Mar del Peru; the Department of Fisheries, University of

the North, Antofagasta; Mr. Forrest R. Miller of the Inter-American Tropical Tuna Commission and Mr. Richard Evans of the Southwest Fisheries Center, National Marine Fisheries Service, NOAA; Dr. J. O. Fletcher, Environmental Research Laboratories, NOAA; and Mr. Clayton Creech, OSU Marine Science Center, for their support to this study. I also thank the National Science Foundation for support under the Climate Dynamics Program of the Division of Atmospheric Sciences through NSF Grant No. ATM-7820419.

Table 1. Lag/lead correlation coefficients between anomalies in the following variables pertaining to the Lima/Callao/La Punta locale: sea level (SL), sea surface temperature (SST), air temperture (AT), and sea level pressure (SLP).

| Lag/lead in months | SL vs. SST | SL vs. AT | SL vs. SLP | SST vs. AT | SST vs. SLP | AT vs. SLP |
|---|---|---|---|---|---|---|
| -3 | .500 | .528 | -.504 | .670 | -.614 | -.556 |
| -2 | .607 | .616 | -.578 | .781 | -.667 | -.639 |
| -1 | .732 | .725 | -.630 | .874 | -.702 | -.720 |
| 0 | .842 | .818 | -.662 | .913 | -.714 | -.776 |
| 1 | .885 (SL leads) | .855 (SL leads) | -.661 | .876 | -.694 | -.773 |
| 2 | .841 | .820 | -.641 | .779 | -.643 | -.709 |
| 3 | .725 | .723 | -.600 | .651 | -.571 | -.609 |
| 4 | .588 | .596 | -.537 | .518 | -.484 | -.505 |
| 5 | .463 | .460 | -.444 | .398 | -.387 | -.416 |
| 6 | .365 | .341 | -.330 | .297 | -.281 | -.332 |
| Period of record | 1956-74 | 1950-74 | 1950-74 | 1956-77 | 1956-77 | 1950-78 |

Table 2. Lag/lead correlation coefficients between pressure anomalies at South Pacific subtropical ridge sites (Easter and Rapa) and Darwin

| Lag/lead in months | Easter vs. Darwin | Rapa vs. Darwin |
|---|---|---|
| -3 | -.340 | -.339 |
| -2 | -.420 | -.436 |
| -1 | -.494 | -.527 |
| 0 | -.559 | -.608 |
| 1 | -.613 | -.674 |
| 2 | -.656 | -.725 |
| 3 | -.685 | -.759 |
| 4 | -.700 Easter leads | -.774 Rapa leads |
| 5 | -.700 | -.772 |
| 6 | -.684 | -.755 |
| Period of record | 1948-78 | 1951-78 |

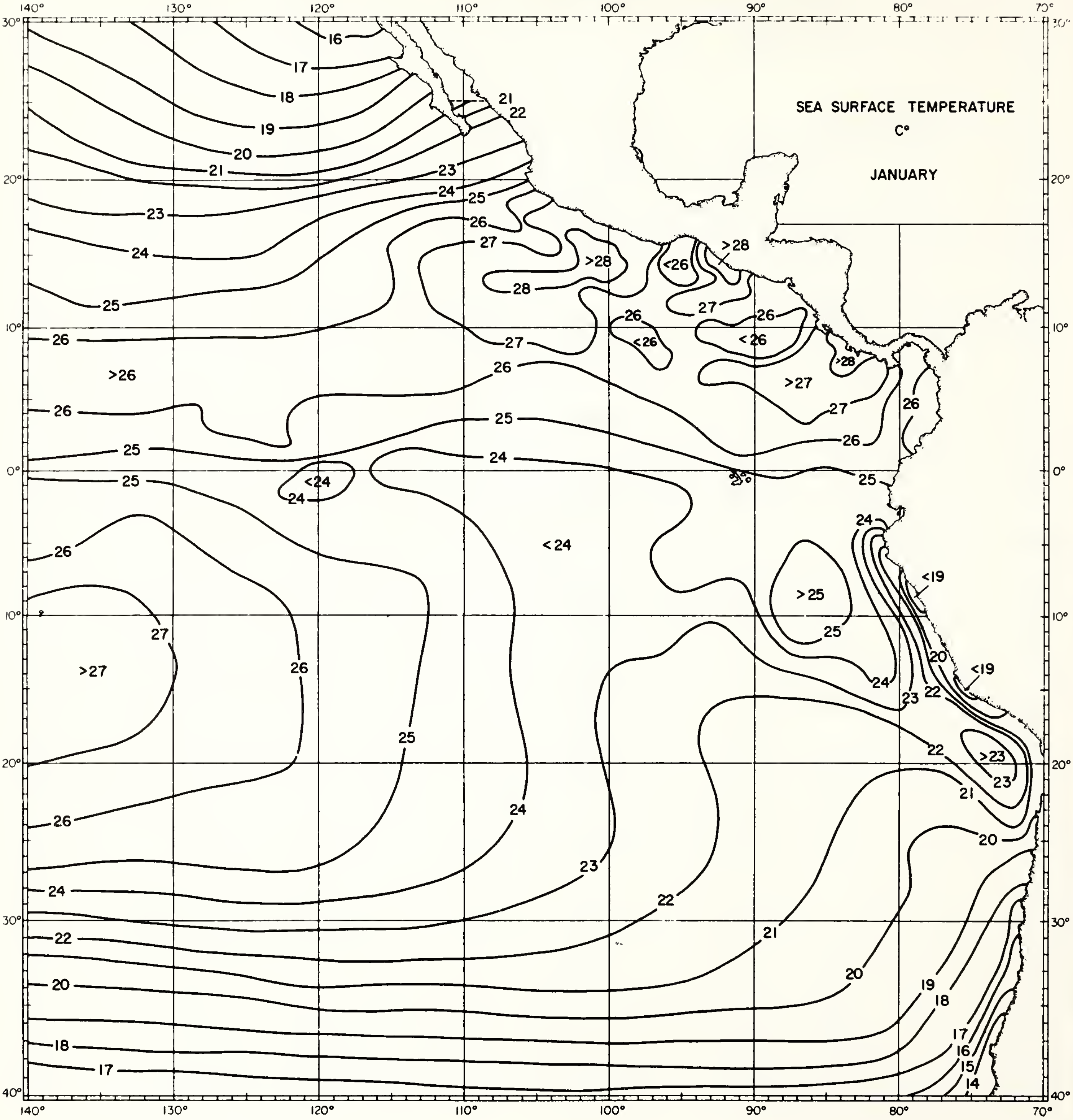

Fig. 1. Distribution of sea surface temperature for January (from Wyrtki, 1964).

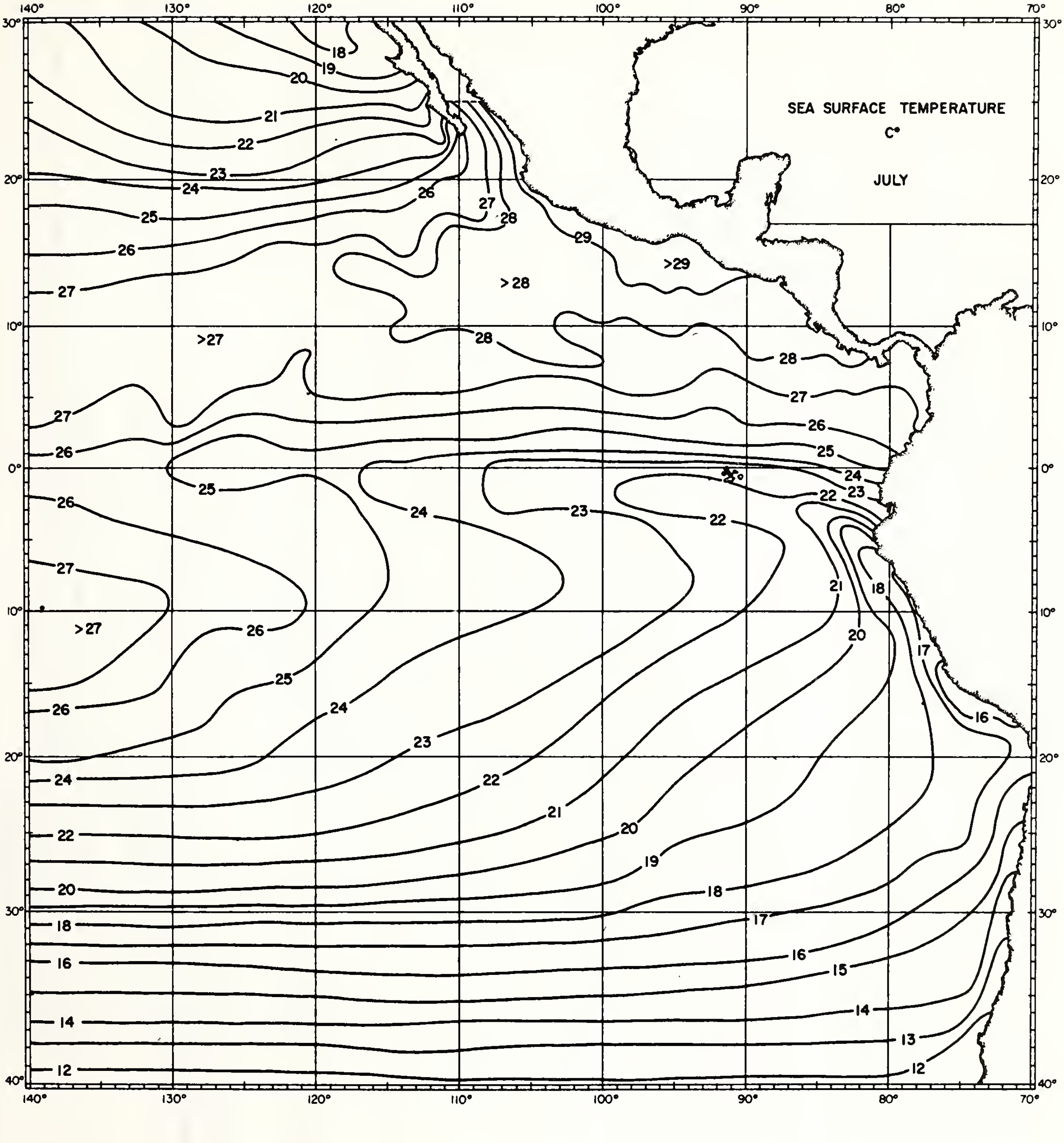

Fig. 2. Distribution of sea surface temperature for July (from Wyrtki, 1964).

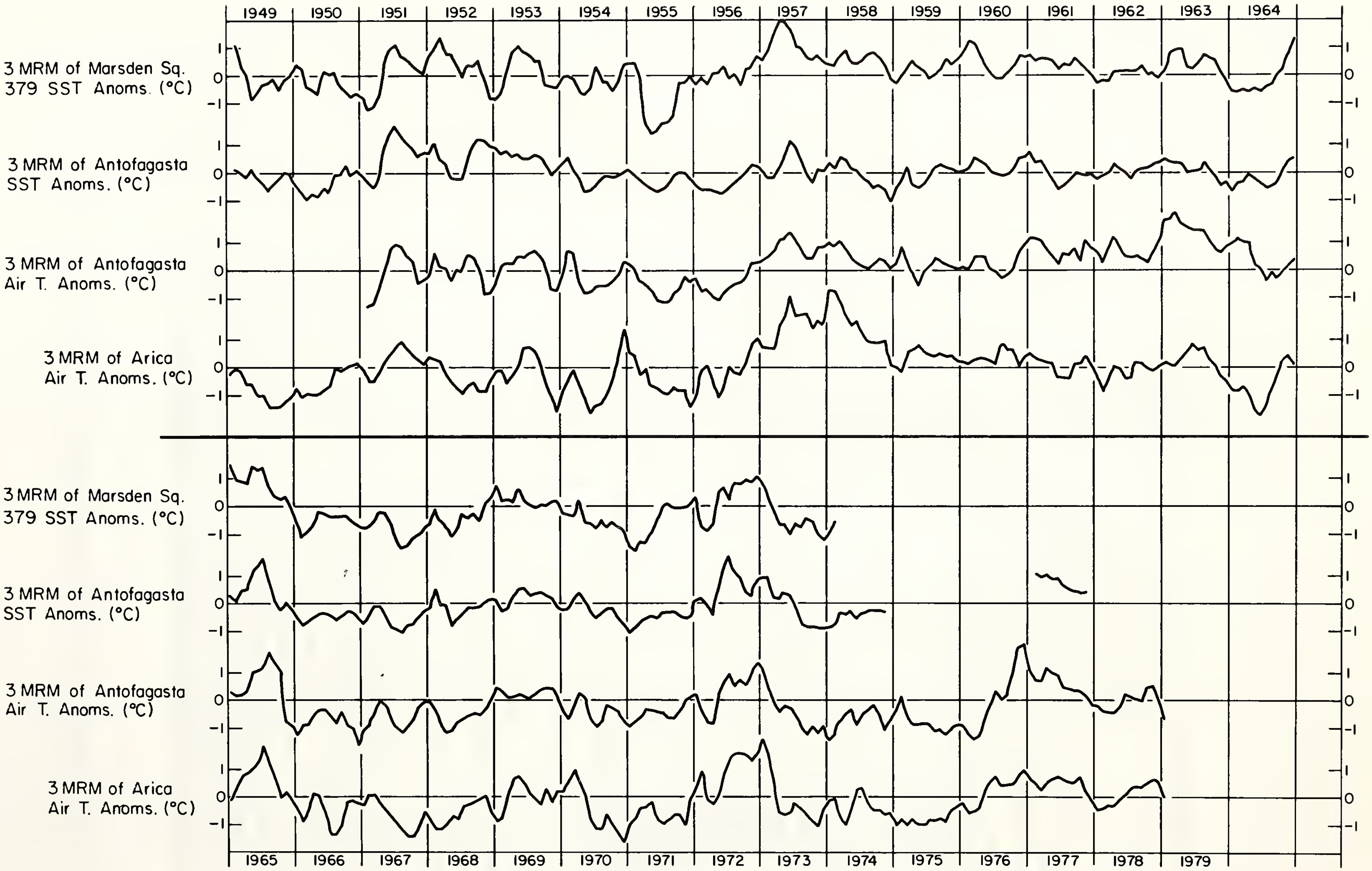

Fig. 3. Three month running mean plots of sea surface temperature (SST) anomalies for Marsden Square 379 (20°-30°S, coast of Chile to 80°W), of SST and air temperature anomalies for Antofagasta (23°28'S, 70°21'W), and of air temperature anomalies for Arica (18°22'S, 70°21'W) for 1949-78.

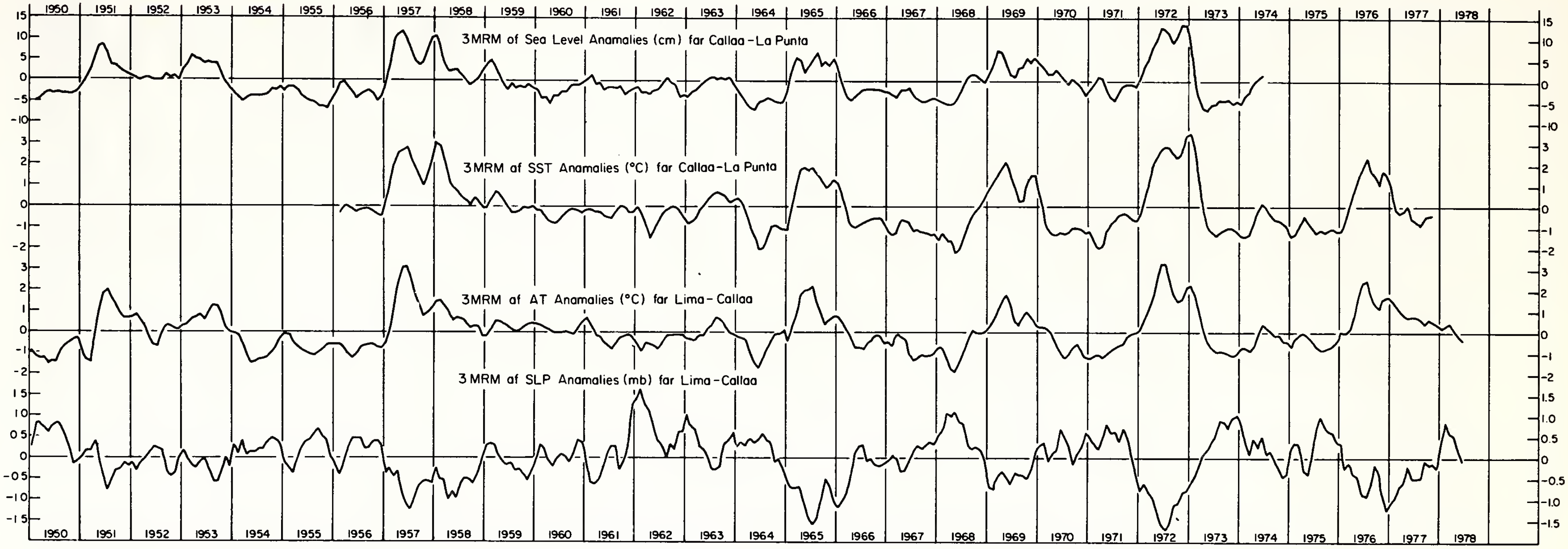

Fig. 4. Three month running mean plots of anomalies in sea level (cm), sea surface temperature (°C), air temperature (°C), and sea level pressure (mb) for the Lima/Callao/La Punta vicinity (12°S, 77°W) of Peru for 1950-77.

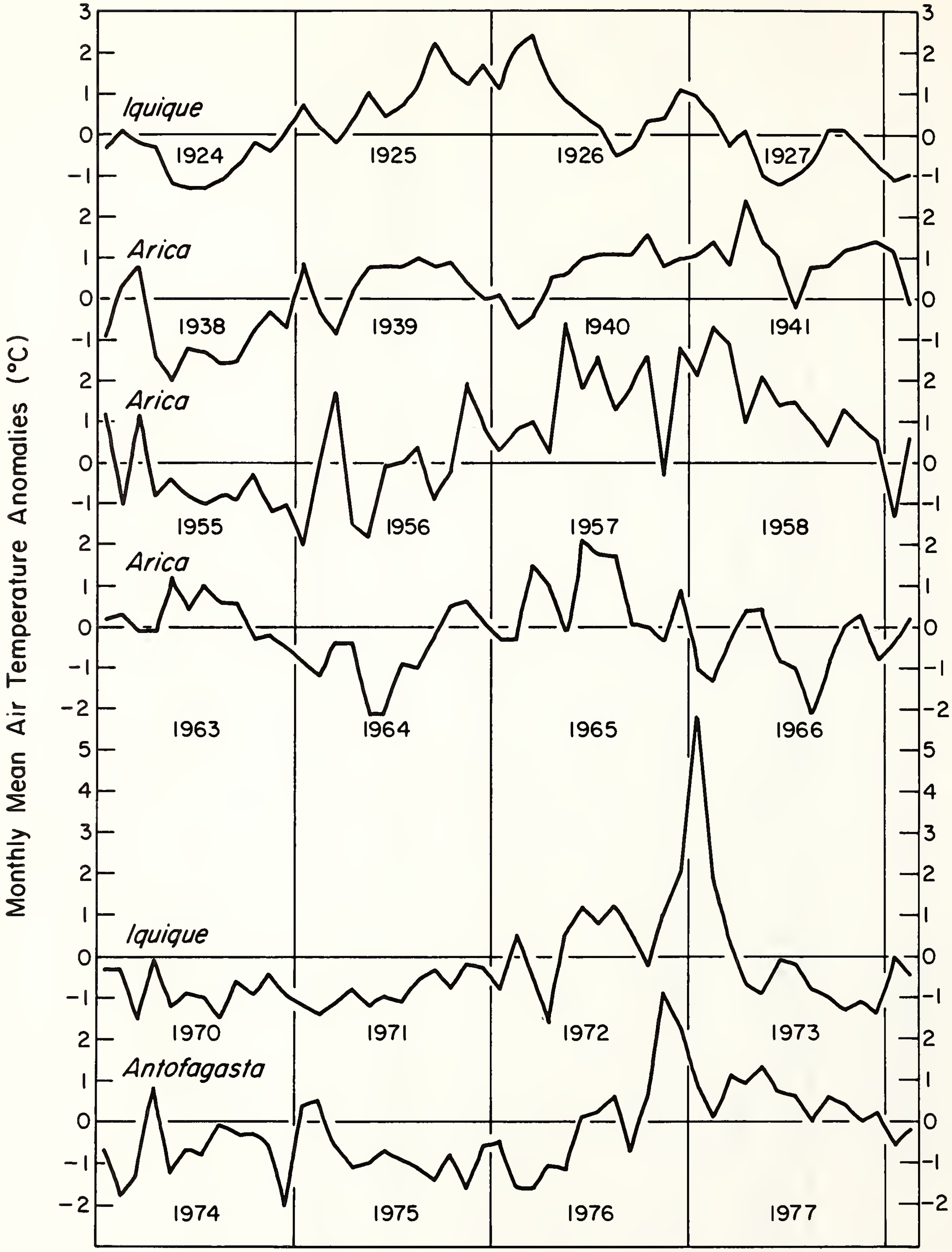

Fig. 5. Monthly air temperature anomaly trends prior to and during the stronger El Niños of recent years at Arica (18°22'S, 70°21'W), Iquique (20°13'S, 70°09'W) and Antofagasta (23°38'S, 70°26'W), as indicated.

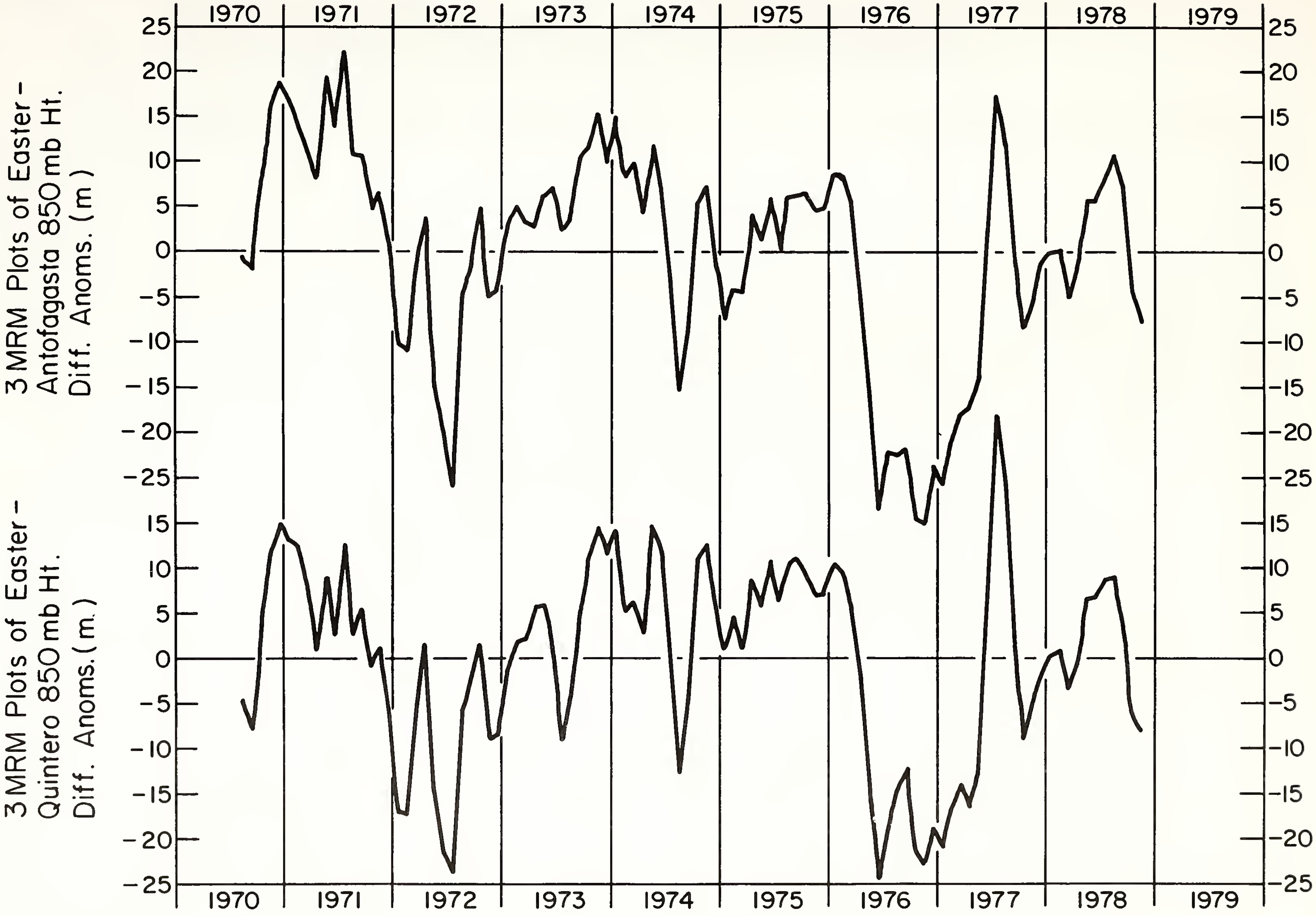

Fig. 6. Three month running mean plots of 850 mb height difference anomalies (m) for Easter (27°10'S, 109°26'W)-Antofagasta (23°28'S, 70°26'W) and Easter-Quintero (32°47'S, 71°32'W) for 1970-78.

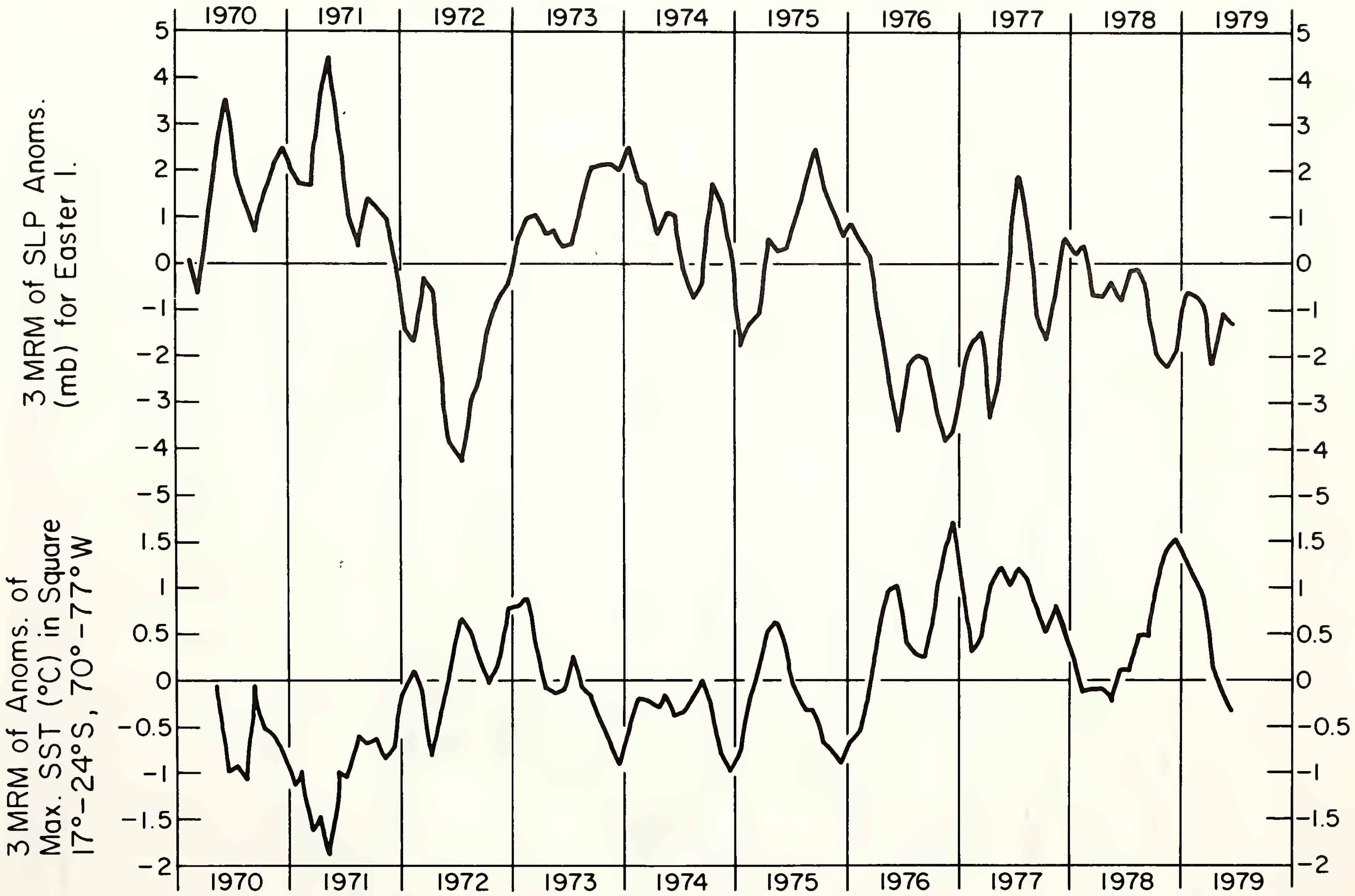

Fig. 7. Three month running mean plots of anomalies of sea level pressure for Easter (27°10'S, 109°26'W) and anomalies of the maximum sea surface temperature noted in the square running from 17°S to 24°S and from 70°W to 77°W for 1970-79.

# Coherent Fluctuations of the Ocean/Atmospheric System on the Time Scale of Decades and Centuries

by

Joseph O. Fletcher
Environmental Research Laboratories, NOAA
Boulder, Colorado 80303

Magnetic tapes containing shipboard weather observations have been obtained from the WMO Historical Sea Surface Temperature Project. These tapes contain monthly averages of sea surface temperature, air temperature, scalar wind speed, and vector wind magnitude and direction. They cover the time period from 1861 through 1960, and the Pacific and Indian Oceans, but are not yet available for the Atlantic Ocean.

For the Pacific Ocean, the monthly summaries have been extended to 1976 by additional data from the National Climate Center, and for the shorter time period of 1948-1972: monthly summaries for the Atlantic Ocean have been obtained from the Woods Hole Oceanographic Institute.

Analyses of these data have revealed the existence of two distinct ocean-wide modes of variability. One of these has a typical time scale of a few years; its most pronounced regional expression is the occasional warming of the ocean surface which spreads throughout the equatorial regions and often is referred to as El Nino. The other mode has a time scale of the order of 100 years, and takes the form of substantial large-scale anomalies in both wind and sea surface temperature lasting several decades, followed by rapid transitions to equally large and persistent anomalies of the opposite sign. There is indirect evidence that this sequence has recurred repeatedly over historical times.

In selected regional wind records, both modes of variability have also been identified, and it has been possible in some cases to infer from the wind changes long-term changes in the pressure patterns. For instance, the wind direction anomalies during the 1860s imply that the subtropical high pressure cells of the eastern Pacific during that time were displaced toward the equator and westward from their normal positions. Calculations of the surface zonal wind stress show large long-term changes in the driving force for ocean currents and the torque driving the circulation of the Pacific. However, the relationship between changes in surface wind and sea surface temperature seems not to be a simple one.

A paper describing some of these results has been submitted for presentation at the General Assembly of the IUGG in December 1979, and a more extensive paper is in preparation.

# SOME EXAMPLES OF ATMOSPHERIC DYNAMICAL EFFECTS ON ATMOSPHERIC TRACE CONSTITUENTS

by

Kirby Hanson, James Peterson, Bernard Mendonca, and Walter Komhyr
Air Resources Laboratories
Environmental Research Laboratories
NOAA, Boulder, Colorado, 80303

The role of atmospheric trace constituents affecting climate is generally recognized to be through modification of atmospheric processes. A lesser studied aspect of this relationship is the reverse. That is, concentrations of atmospheric trace constituents can be modified, to some degree, by atmospheric processes, namely, dynamic processes. Thus, for studies of biogeochemical cycles that utilized atmospheric measurements of trace constituents, due attention must be given to the question:

- What atmospheric conditions do trace constituent measurements represent?

In this presentation we give examples of the effect of changing atmospheric circulation on atmospheric trace constituent concentrations.

## 1. Barrow, Alaska

Atmospheric $CO_2$ concentrations are measured continuously at the NOAA baseline observatory at Barrow, Alaska. Daily average $CO_2$ is shown in Figure 1 and 2 for January through May of 1977 and 1978, respectively. The smooth curves in the figures are cubic spline least-square best-fits to the data with knots on the first of each month. The January-to-April period is characterized by quasi-cyclical variations with amplitudes of 1 to 3 ppm about the spline curve. These variations are of special interest here.

To investigate a meteorological cause for these variations we obtained air trajectories for 1977 and 1978 based on rawinsonde wind speed and direction measurements over the height interval 300 to 2000 m above ground. The trajectories are a general indicator of the path of air arriving at Barrow at a given time. The trajectory paths often persisted from the same general location for several days. An example of such persistence is shown in Figure 3.

Several periods were selected with $CO_2$ clearly above or below the spline "average" for at least three days during late January to March. The trajectories for one day of each period (indicated by the arrows in Figure 1 and 2) are presented in Figure 4. Days with above average $CO_2$ are represented by dashed lines and days with below average $CO_2$ by solid trajectory paths. The open circles indicate one-day travel times. The trajectories (Figure 4) are distinctly separated between those associated with high vs. low $CO_2$ values. All five cases with high $CO_2$ had associated trajectories with air flowing from the Arctic Basin. All air trajectories associated with low $CO_2$ concentrations came from the south.

The higher concentrations with northerly flow imply a source of $CO_2$ to the north of Barrow. We suggest two possibilities for such a source. The first is the Arctic Ocean itself. During winter there is a transfer of $CO_2$ to the atmosphere through the annual sea ice, which can be quite porous because of brine channels. The second possible source of $CO_2$ "north" of Barrow is advection from mid-latitude anthropogenic sources, primarily the northeastern U.S. or western Europe, across the North Atlantic Ocean to the Arctic.

## 2. Mauna Loa, Hawaii (Mauna Loa Observatory)

The histogram of 700 mb wind direction at Hilo, Hawaii (Figure 5) shows a bimodal distribution in winter, about half the winds being from the east and the other half from the west. An analysis of the Mauna Loa Observatory monthly mean $CO_2$ departure from a 2-year mean for these east-wind and the west-wind cases shows that the mean value for east- and west-wind cases are in agreement to within a few hundredths of a part per million (ppm). Thus, the $CO_2$ concentration at Mauna Loa Observatory does not appear to be significantly dependent on mean monthly wind direction at about the height of and regional location of the Observatory.

In an attempt to see whether the $CO_2$ concentration is dependent on the general atmospheric circulation over a large portion of the North Pacific, we have identified three major circulation patterns at 700 mb during January using 18 of the 19 Januaries during the period 1959-77, inclusive. For discussion purposes these are called types "A", "B", and "C". Composite of the major centers of height departure from normal (DN) are given in Figures 6, 7, and 8 for the three circulation types. Composite zonal profiles for the 700 mb high DN along 170°W longitude are given in Figures 9, 10, and 11 for the three circulation types. Finally, histograms of the 700 mb wind direction at Hilo, Hawaii are given in Figures 12, 13, and 14 for the three circulation types. It is clear that the wind direction at Hilo is determined by the general circulation in the Pacific -- west winds with type "A" and "C", and east winds with type "B".

An analysis of the composite mean January Mauna Loa Observatory $CO_2$ departure from a 2-year average for each circulation type shows (Table 1) a difference of about 0.35 ppm for $CO_2$ concentration between type "A" and "C". The standard deviations are also given.

## 3. Samoa

The $CO_2$ concentration measured at the GMCC Observatory in Samoa is, at times, variable with excursions lasting over 10 to 15 day periods. Typical excursions during 1977 are shown in Figure 15. We have examined satellite data and find that these excursions are associated with the movement of the intertropical convergence zone, normally north of Samoa, to latitudes south of Samoa. The March 1-15, 1977 anomaly in $CO_2$ is an excellent example and satellite cloud photos were shown at the meeting to show the association.

## Figure Captions

Fig. 1. Daily average $CO_2$ concentration (ppm) measured at Barrow, Alaska, January-May, 1977. Values are relative, expressed on the Scripps 1959 Adjusted Index Scale. Vertical arrows refer to days used in trajectory analyses.

Fig. 2. As in Figure 1, except for 1978.

Fig. 3. Five-day trajectories of airflow arriving at Barrow, Alaska at 1200 GMT on the indicated dates.

Fig. 4. Five-day trajectories of airflow arriving at Barrow, Alaska at 1200 GMT on the indicated dates. Open circles indicate one day travel time. Dashed lines correspond to days with high $CO_2$ at Barrow and solid lines to days with low $CO_2$.

Fig. 5. Frequency of occurrence of 700 mb wind direction at Hilo, Hawaii (1958-1977) for bimonthly periods.

Fig. 6. Type "A", 700 mb height DNs.

Fig. 7. Type "B", 700 mb height DNs.

Fig. 8. Type "C", 700 mb height DNs.

Fig. 9. Type "A", composite 700 mb height DN. Zonal profile along 170°W longitude.

Fig. 10. Type "B", otherwise as Fig. 9.

Fig. 11. Type "C", otherwise as Fig. 9.

Fig. 12. Type "A", frequency of occurrence of 700 mb wind direction at Hilo, Hawaii.

Fig. 13. Type "B", otherwise as Fig. 12.

Fig. 14. Type "C", otherwise as Fig. 12.

Fig. 15. Daily average $CO_2$ concentrations (ppm) measured at American Samoa January-June, 1977. Values are relative, expressed on the Scripps 1959 Adjusted Index Scale.

## Table Caption

Table 1. Average $CO_2$ concentration for Types "A", "B", and "C". The average is composed of the individual January $CO_2$ departures from a 2-year mean. Seven Januaries for Type "A"; seven Januaries for Type "B"; and four Januaries for Type "C".

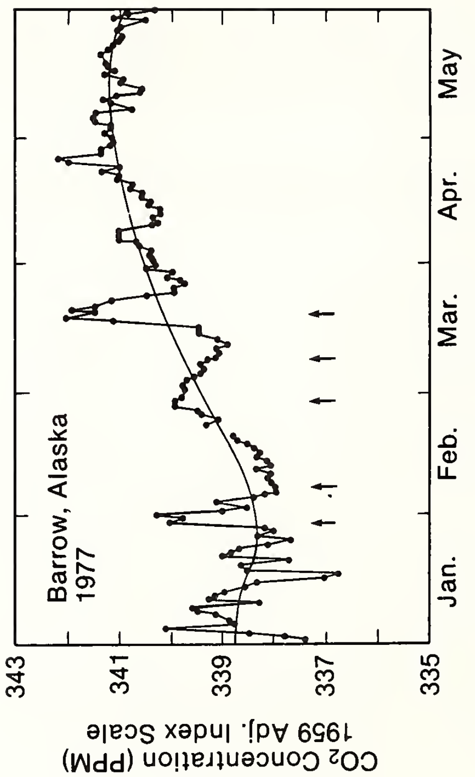
Barrow, Alaska
1977
343
341
339
337
335
CO2 Concentration (PPM)
1959 Adj. Index Scale
Jan.
Feb.
Mar.
Apr.
May

Figure 1

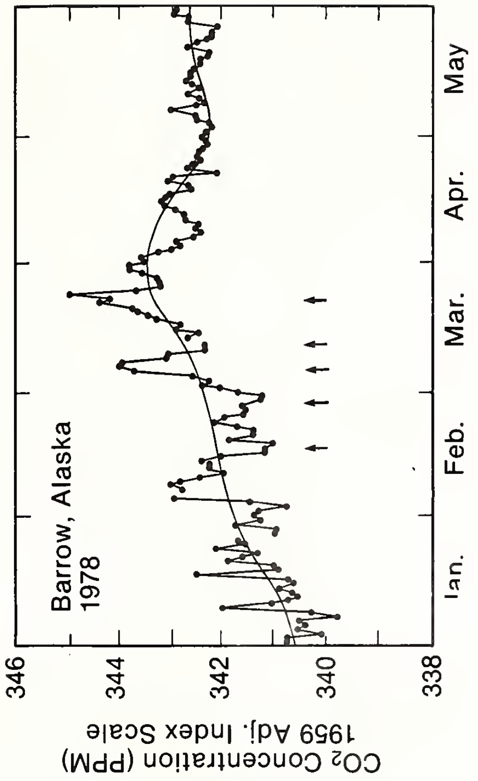
Barrow, Alaska
1978
346
344
342
340
338
CO₂ Concentration (PPM)
1959 Adj. Index Scale
Jan.
Feb.
Mar.
Apr.
May

Figure 2

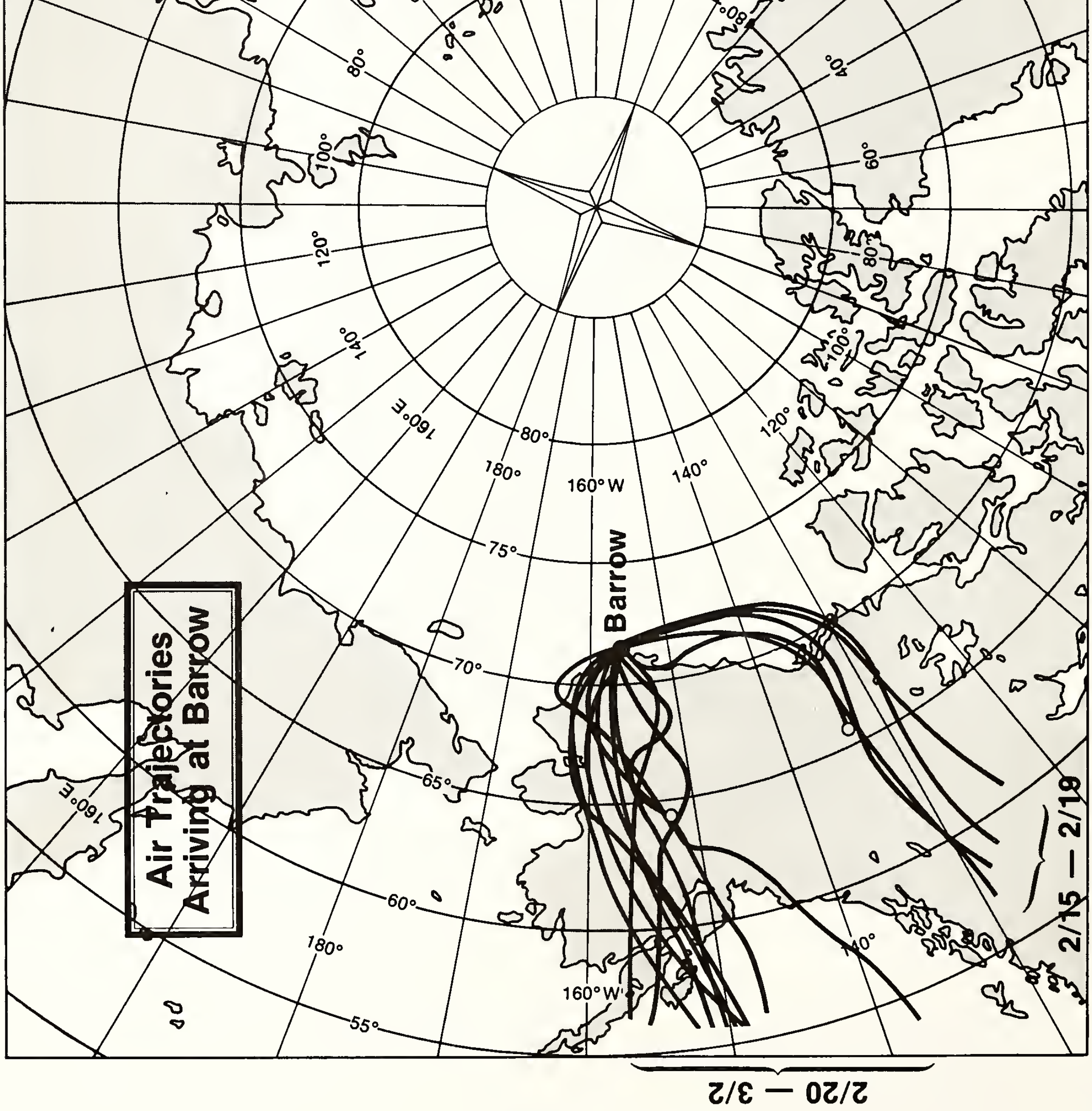
Air Trajectories Arriving at Barrow
Barrow
2/15 — 2/19
2/20 — 3/2
160° W
140°
120°
100°
80°
60°
40°
20°
0°
180°
160° E
140°
120°
100°
80°
60°
40°
20°
80°
75°
70°
65°
60°
55°

Figure 3

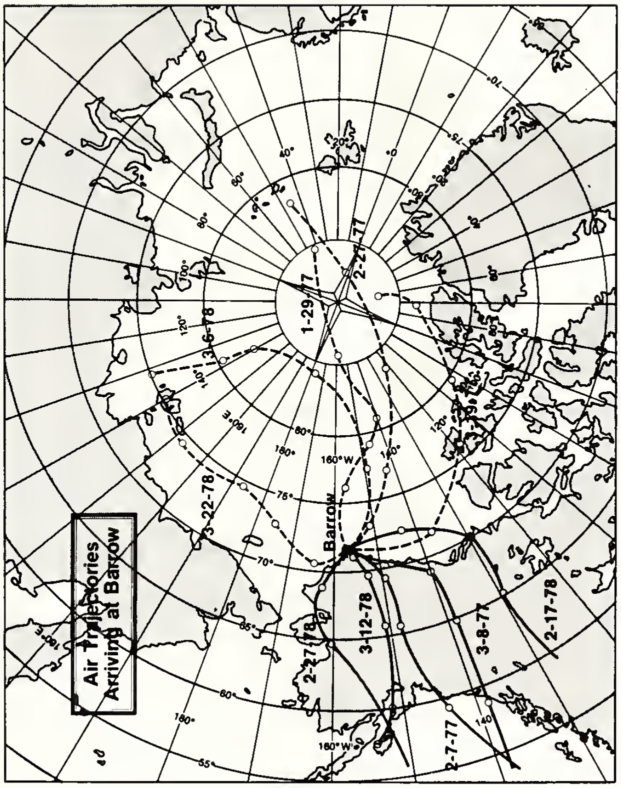
Air Trajectories
Arriving at Barrow
Barrow
1-29-77
2-27-77
3-6-78
3-22-78
2-27-78
3-12-78
3-8-77
2-17-78
2-7-77
160° W
180°
160° E
140°
120°
100°
80°
60°
40°
20°
0
75°
70°
65°
60°
55°

Figure 4

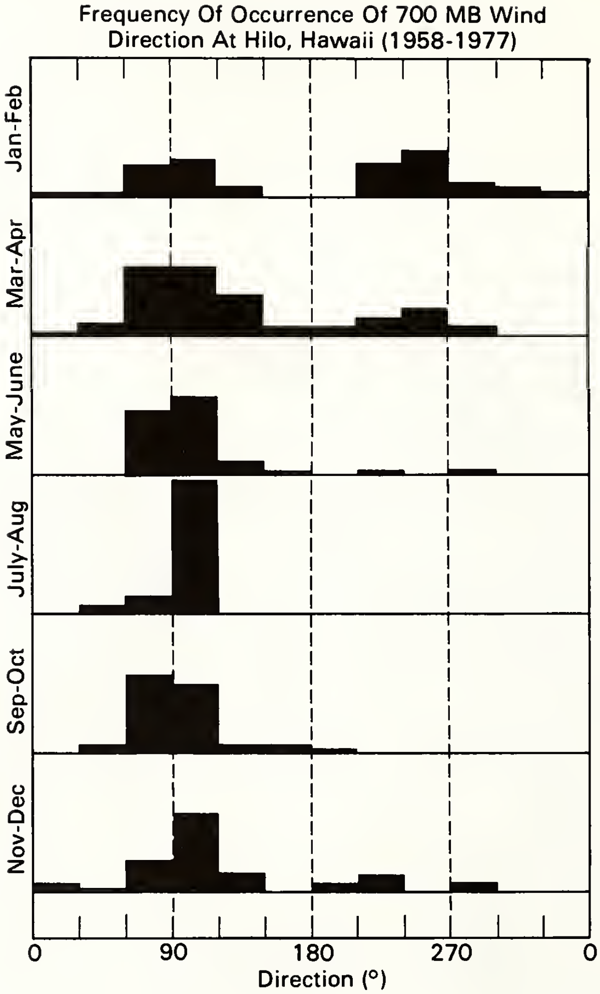 
Frequency Of Occurrence Of 700 MB Wind Direction At Hilo, Hawaii (1958-1977)

Figure 5

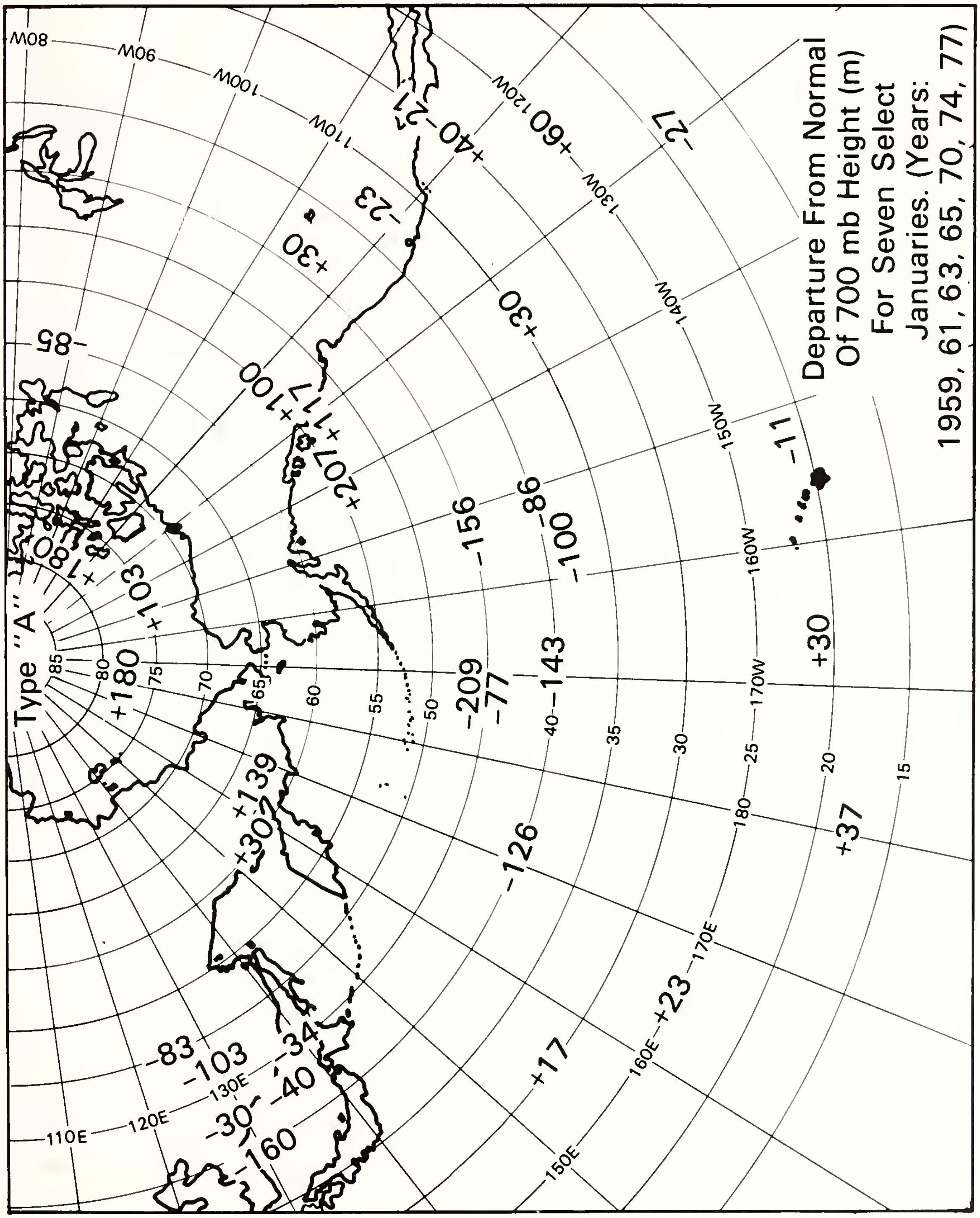
Type "A"
Departure From Normal
Of 700 mb Height (m)
For Seven Select
Januaries. (Years:
1959, 61, 63, 65, 70, 74, 77)
80W
90W
100W
110W
120W
130W
140W
150W
160W
170W
180
170E
160E
150E
130E
120E
110E
85
80
75
70
65
60
55
50
40
35
30
25
20
15
-85
+30
-23
+40
-21
+60
-27
+30
+100
+177
+207
-156
-86
-100
-11
+103
+180
-209
-77
-143
+30
+139
+30
-126
+37
+23
+17
-83
-103
-34
-40
-30
-160

Figure 6

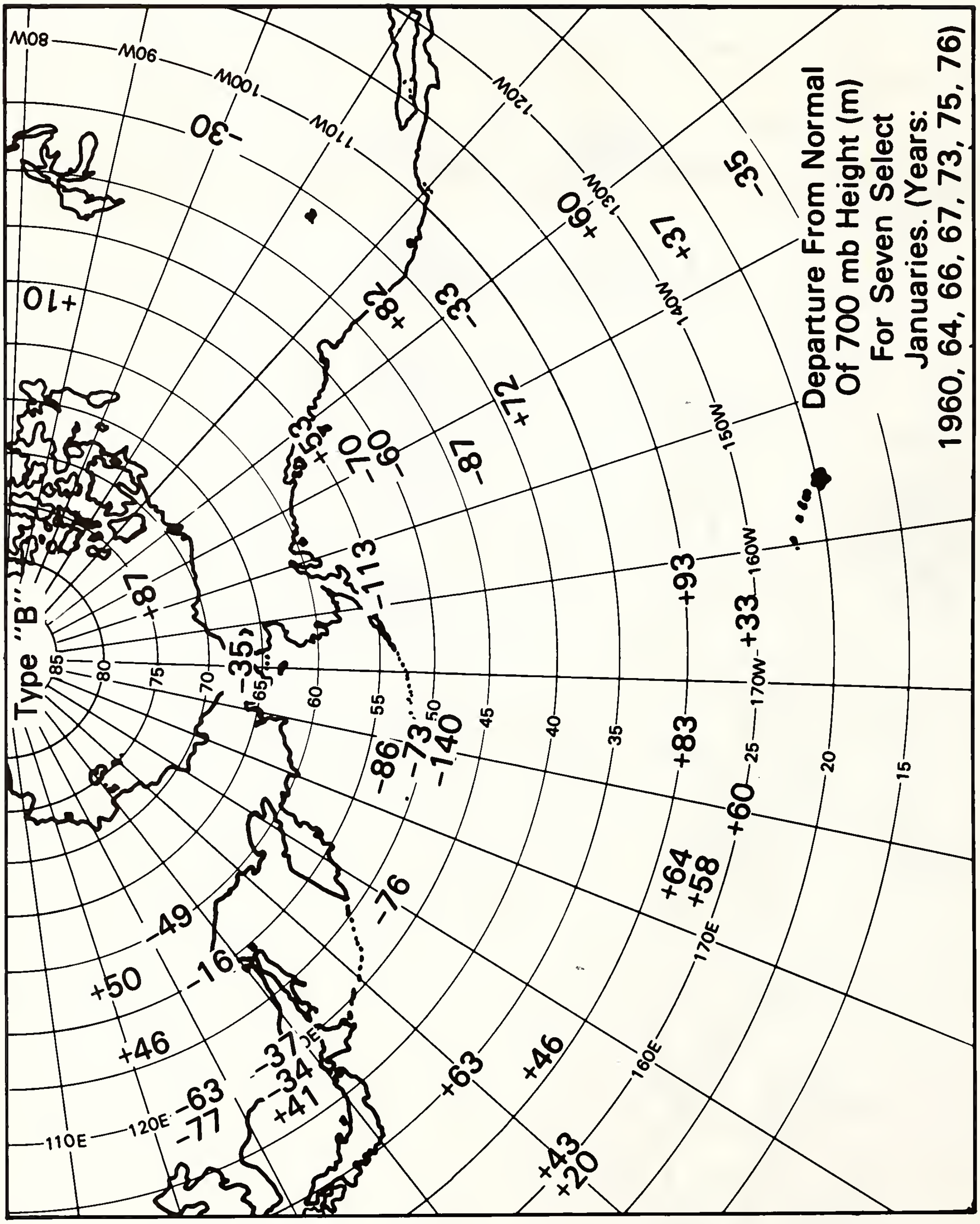
Type "B"
Departure From Normal
Of 700 mb Height (m)
For Seven Select
Januaries. (Years:
1960, 64, 66, 67, 73, 75, 76)
80W
90W
100W
110W
120W
130W
140W
150W
160W
170W
170E
160E
110E
120E
85
80
75
70
65
60
55
50
45
40
35
25
20
15
+10
-30
-35
+60
+37
+82
-33
+72
-87
+53
-70
-60
-113
+93
+33
+87
-35
-86
-73
-140
+83
+60
+64
+58
-76
-49
-16
+50
+46
-37
-34
+41
-63
-77
+63
+46
+43
+20

Figure 7

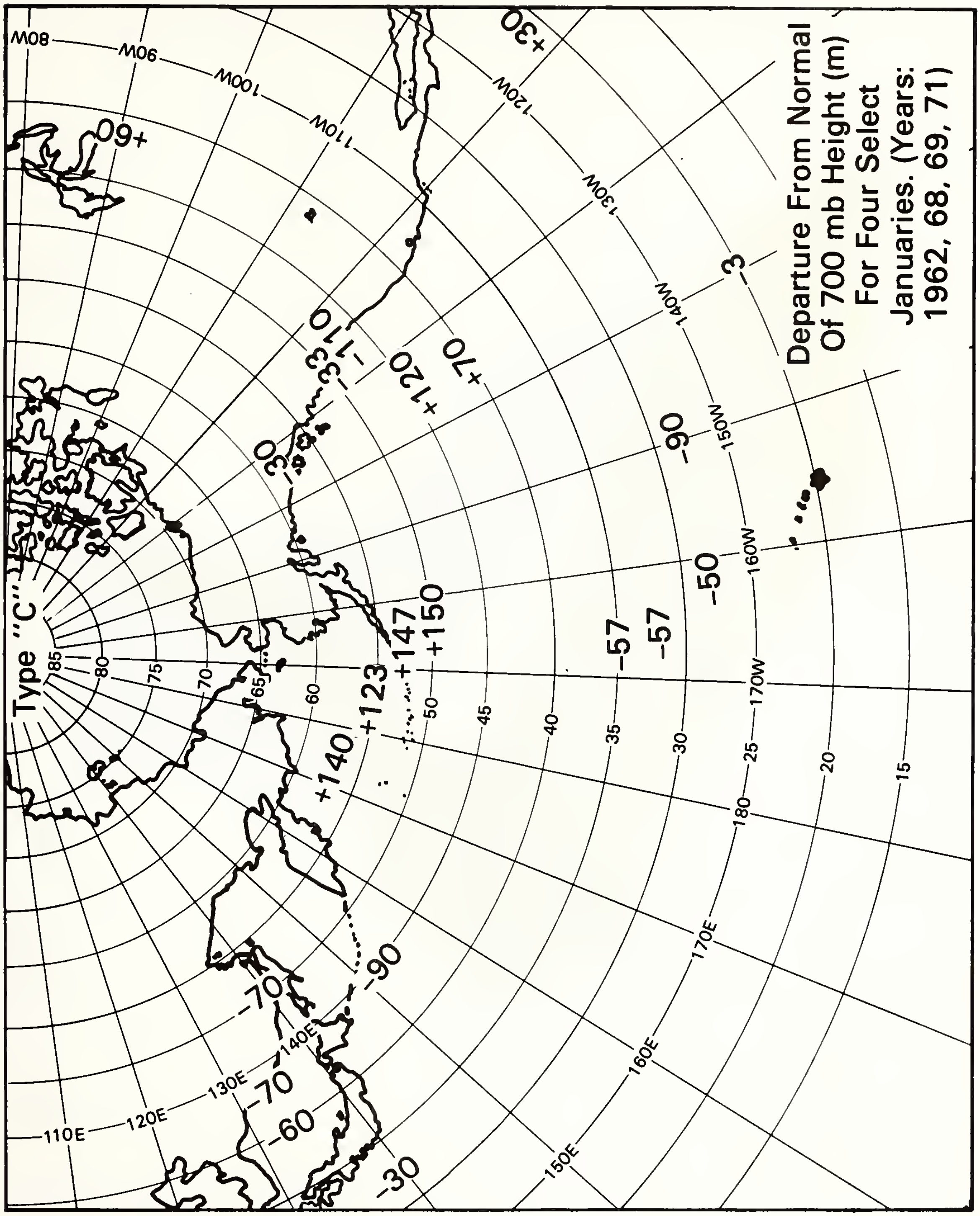

Type "C"

Departure From Normal Of 700 mb Height (m) For Four Select Januaries. (Years: 1962, 68, 69, 71)

Figure 8

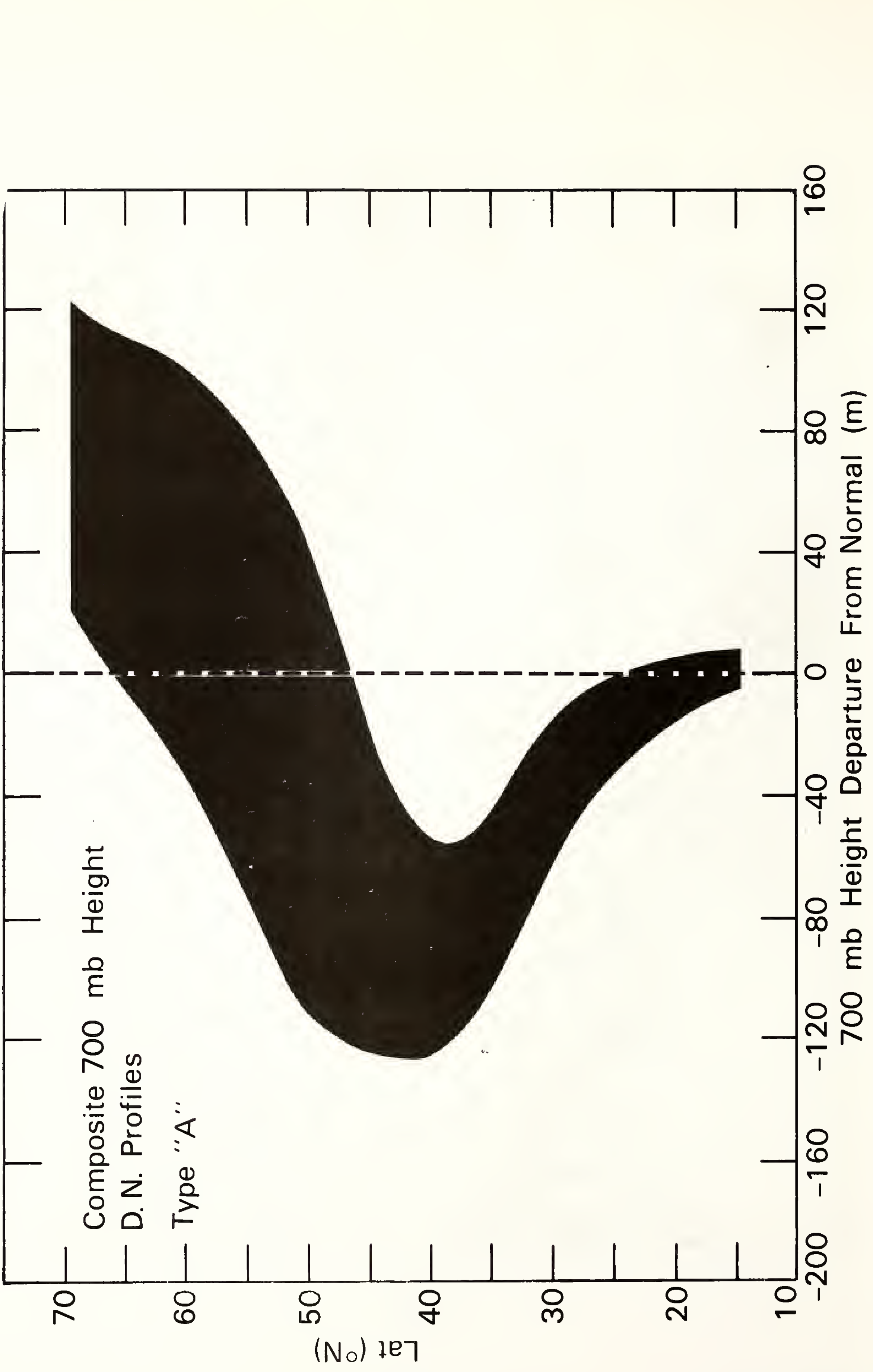
Composite 700 mb Height
D.N. Profiles
Type "A"
70
60
50
40
30
20
10
Lat (°N)
-200
-160
-120
-80
-40
0
40
80
120
160
700 mb Height Departure From Normal (m)

Figure 9

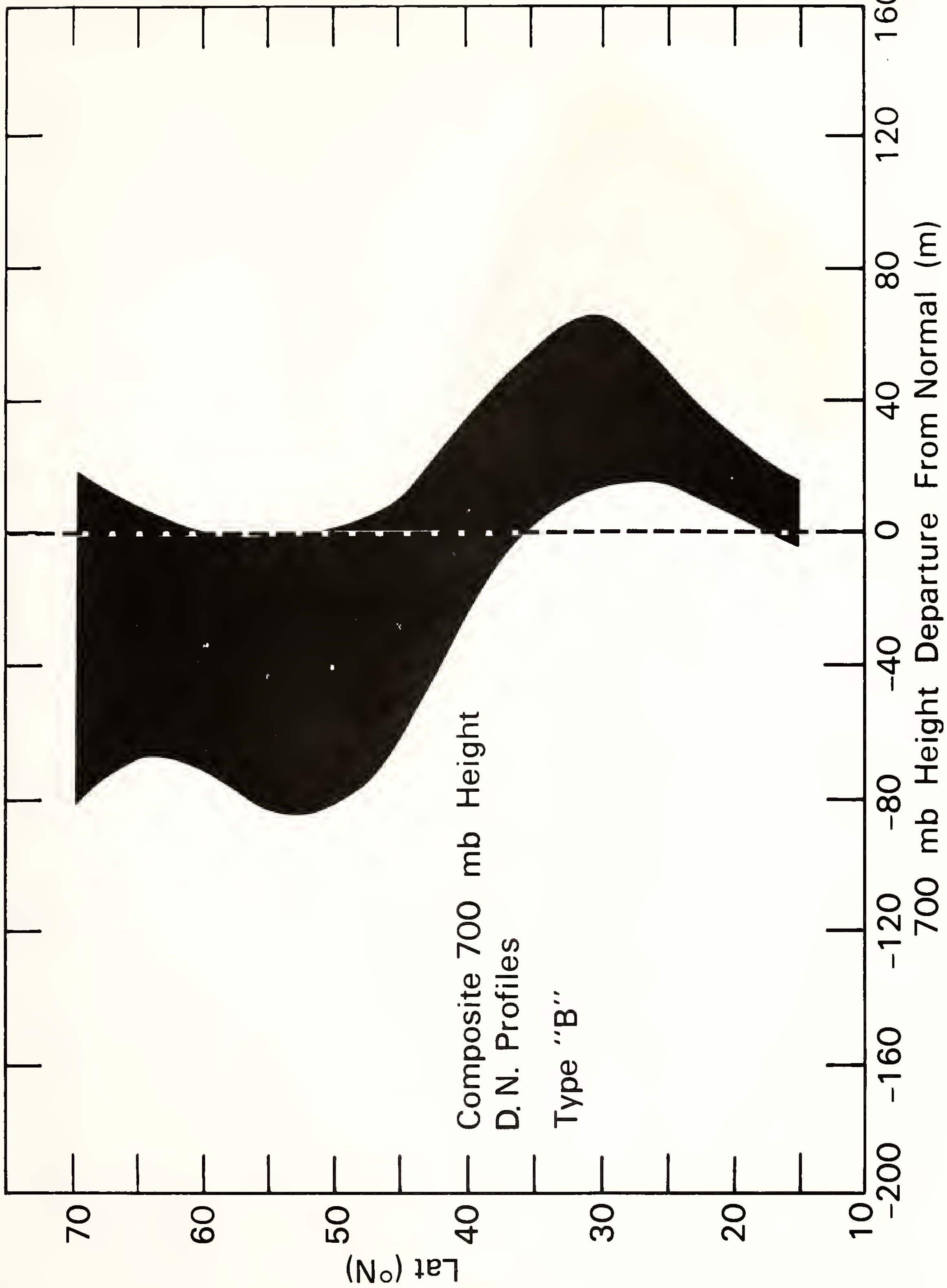
Composite 700 mb Height
D.N. Profiles
Type "B"
70
60
50
40
30
20
10
Lat (°N)
−200
−160
−120
−80
−40
0
40
80
120
160
700 mb Height Departure From Normal (m)

Figure 10

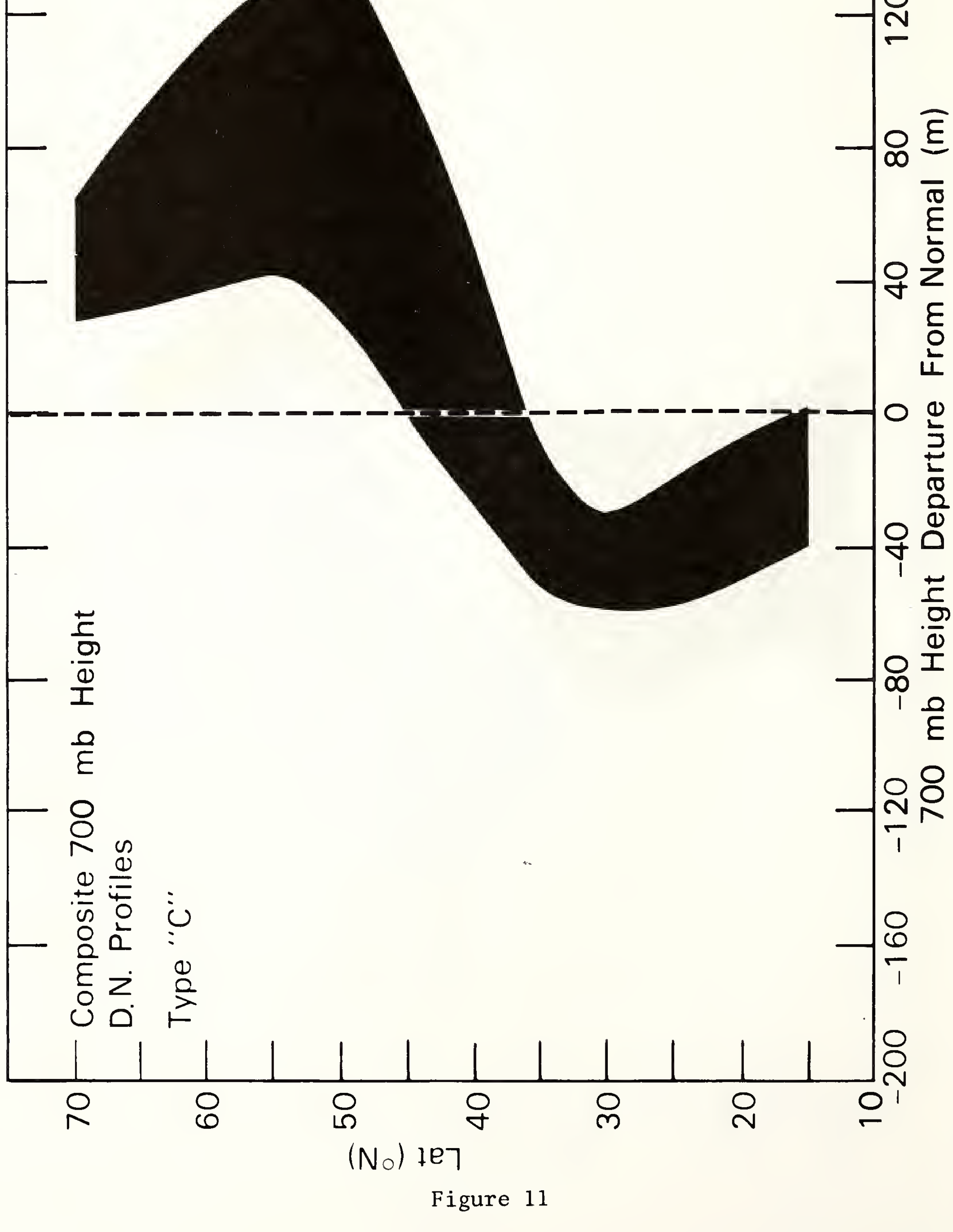
Composite 700 mb Height
D.N. Profiles
Type "C"
Lat (°N)
10
20
30
40
50
60
70
700 mb Height Departure From Normal (m)
-200
-160
-120
-80
-40
0
40
80
120
160

Figure 11

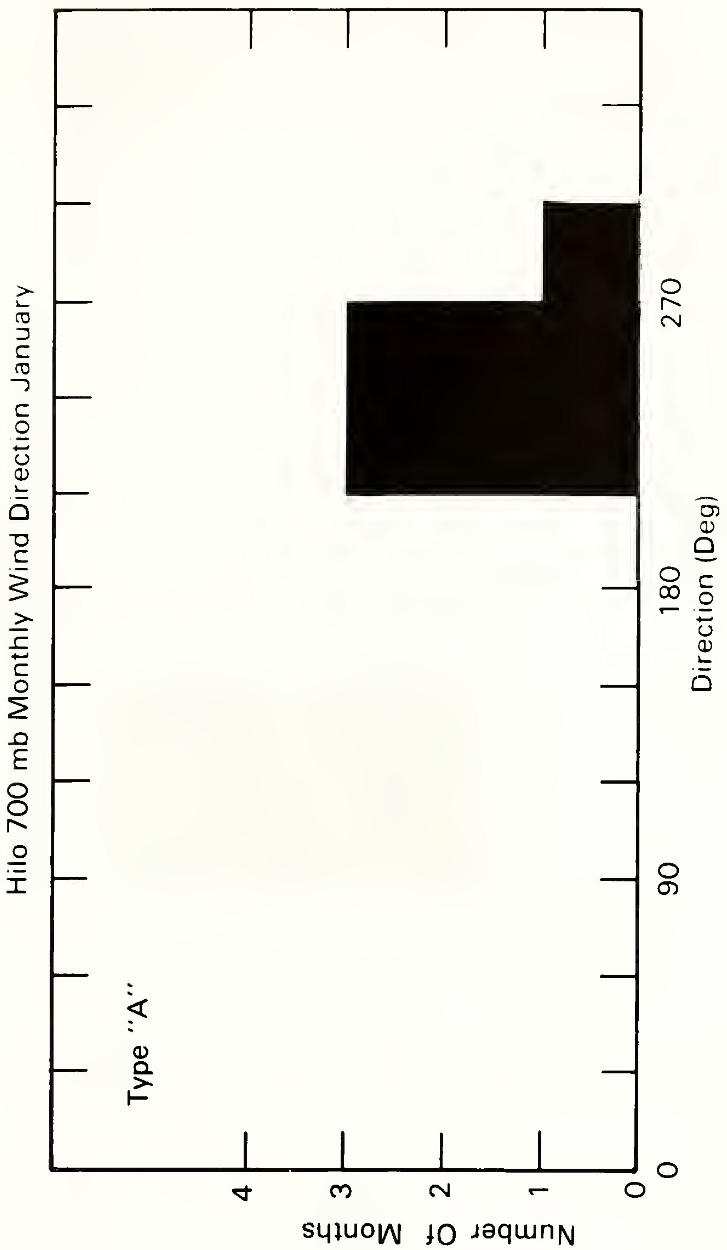
Hilo 700 mb Monthly Wind Direction January
Type "A"
Number Of Months
0
1
2
3
4
0
90
180
270
Direction (Deg)

Figure 12

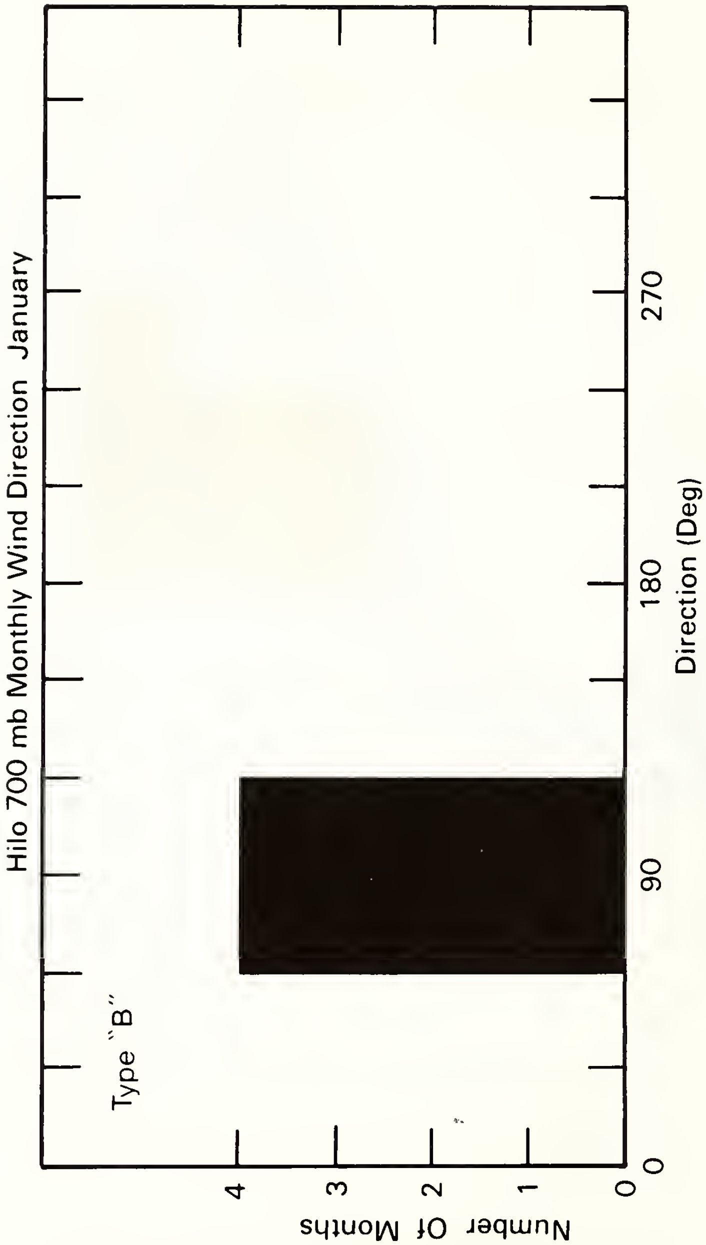
Hilo 700 mb Monthly Wind Direction January
Type "B"
Number Of Months
0
1
2
3
4
0
90
180
270
Direction (Deg)

Figure 13

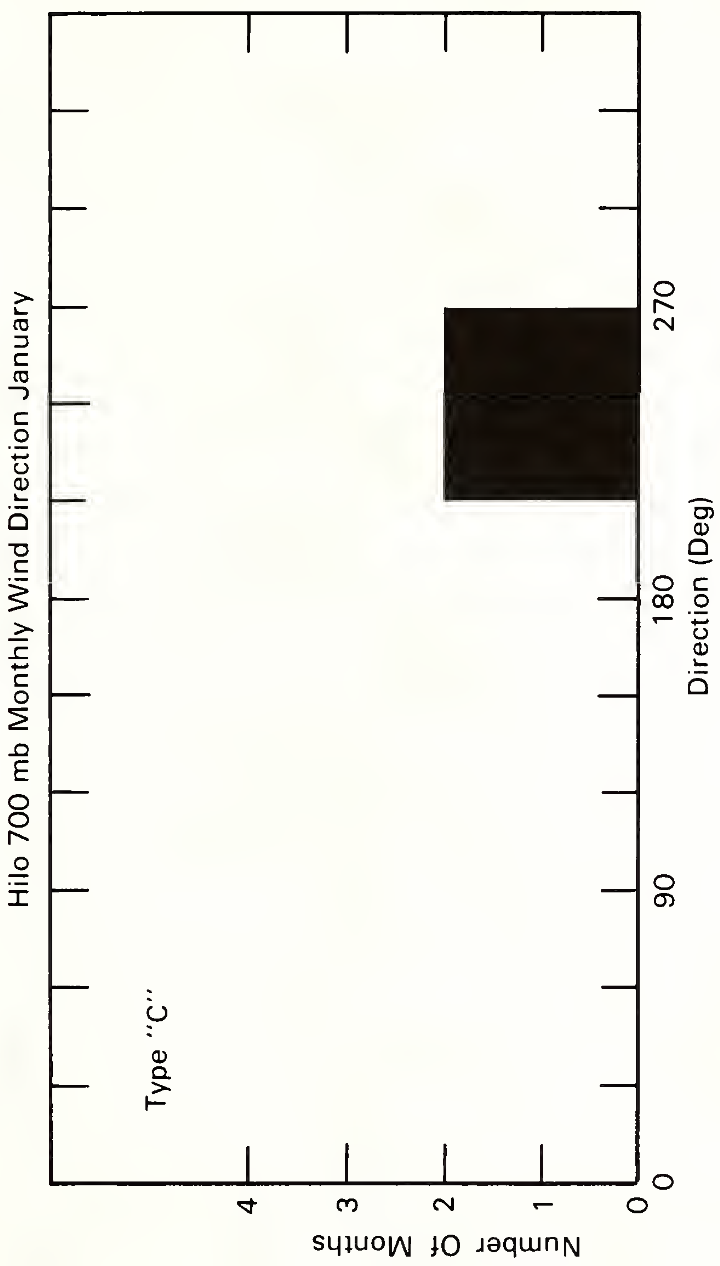
Hilo 700 mb Monthly Wind Direction January
Type "C"
Number Of Months
0
1
2
3
4
0
90
180
270
Direction (Deg)

Figure 14

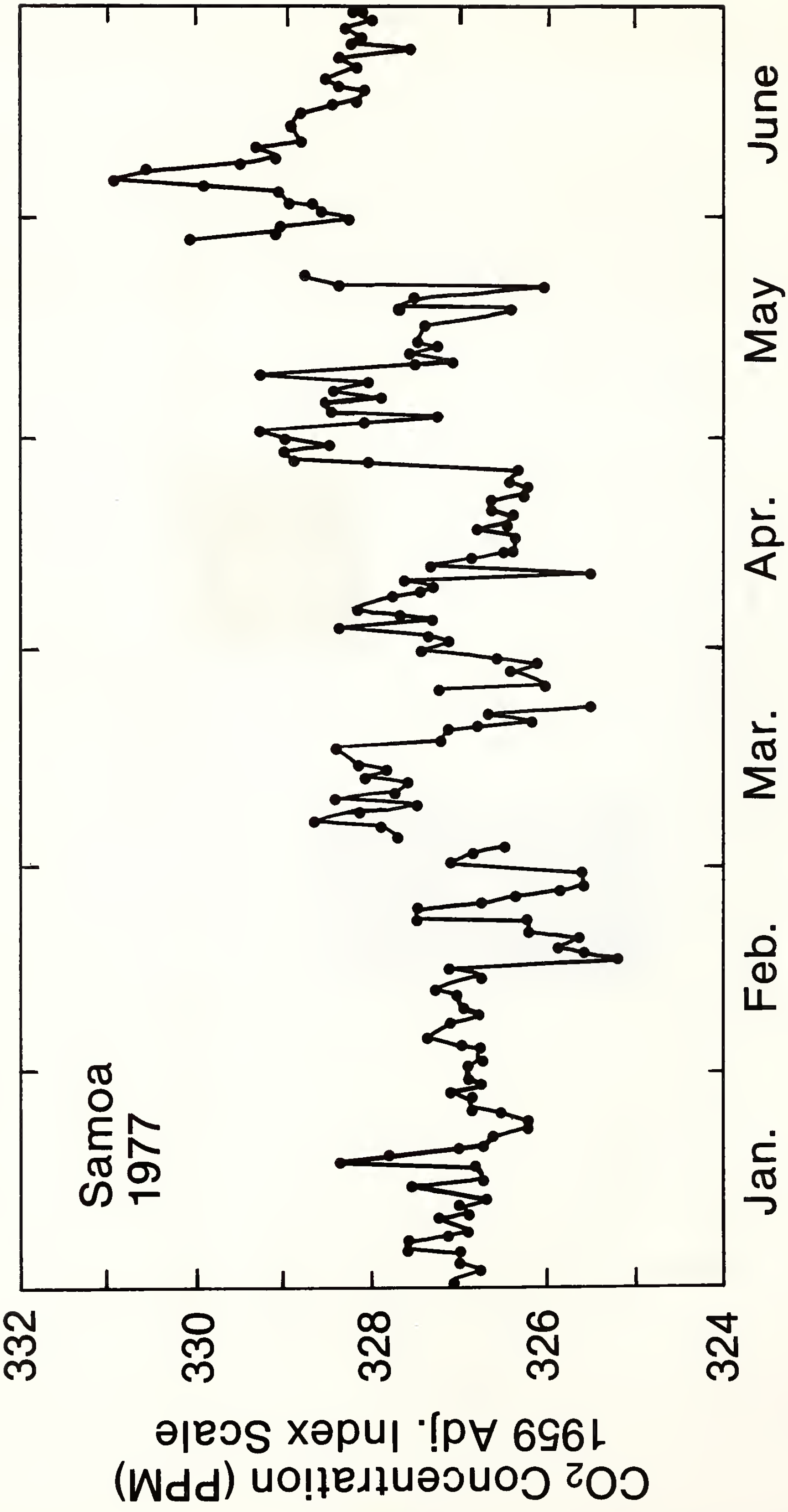
Samoa
1977
Jan.
Feb.
Mar.
Apr.
May
June
332
330
328
326
324
CO2 Concentration (PPM)
1959 Adj. Index Scale

Figure 15

Table 1

| | Type<br>"A" | <br>"B" | <br>"C" |
|---|---|---|---|
| Departure Of January Mean $CO_2$ Concentration At Mauna Loa Observatory From 2-Year Mean | −0.28 (ppm)<br>±0.20 | −0.01 (ppm)<br>±0.28 | +0.07 (ppm)<br>±0.13 |

# Current and Planned Activities of NOAA's Climate Analysis Center

Jay S. Winston
NOAA, NWS, CAC, Washington, D. C.

The Climate Analysis Center (CAC) was formed within the National Meteorological Center, National Weather Service at the World Weather Building near Washington, D. C. in 1978. It consists of personnel and some functions that were formerly part of the Environmental Data and Information Service and the National Environmental Satellite Service, as well as the National Weather Service. The CAC constitutes a major new element of the NOAA Climate Program. Its mission is to maintain a continuous watch on short-term climate fluctuations and to diagnose and predict them. These efforts are designed to assist agencies both inside and outside the Federal Government in coping with such climate-related problems as food supply, energy allocation, and water resources (Fig. 1).

The organization of the CAC is shown in Fig. 2. Some details of the functions and activities of the individual branches of CAC are given in the ensuing figures.

Figures 3 and 4 treat the Prediction Branch. It is anticipated that the R&D objectives (Fig. 4) will be met by applying enhanced worldwide climate observations in new statistical studies which may employ more sophisticated and thorough statistical methodology. However, this work will be guided by diagnostic studies of climate variations to be carried on within the Diagnostics Branch and elsewhere.

Note that the R&D emphasis of statistics over numerical modeling is based on the concept that routine skillful forecasts for months and seasons by numerical methods are at least a decade away. Also, since NOAA's Geophysical Fluid Dynamics Laboratory is concerned with application of numerical modeling to prediction of climate variations, the CAC will depend on keeping abreast of developments there and at other centers for possible future application of such models in operational monthly and seasonal predictions.

The Diagnostics Branch's functions and activities are covered in Figs. 5-7. In the next few years it is clear that the Diagnostics Branch will be deeply involved in developing a real-time climate diagnostics data base consisting of analyzed fields and indices determined to be most significant for maintaining awareness of current global and regional climate. This diagnostics data base will be highly dependent on analyzed products and data compilations available from the NMC and NESS operational processing of worldwide data on the Suitland computers. The concept of this diagnostic data base is shown schematically in Fig. 8.

Functions and activities of the Analysis and Information Branch are shown in Figs. 9-13. This Branch has the principal responsibility for providing data and information to CAC's users (except for monthly and seasonal predictions which are issued directly by the Prediction Branch). It is involved in implementing and maintaining routine production and dissemination of the diagnostics data base as well as climate assessment support data. One of the users for the latter is the Joint Agricultural Weather Facility located at the U. S. Department of Agriculture Weather Facility located at the U. S. Department of Agriculture in Washington (Fig. 11). Of importance for both streams of CAC data is a careful system of quality control to which considerable effort is being devoted (Fig. 12). Also in the Analysis and Information Branch is a stratospheric analysis and monitoring program (Fig. 13), much of which carries on work of NMC's Upper Air Branch which formed the principal base of CAC's Analysis and Information Branch. This program's emphasis is now shifting more strongly toward climatic trends and variations in stratospheric behavior.

CAC supports research and development in climate diagnostics and prediction at a number of research institutions. A listing of grants, contracts, and transfers within NOAA for Fiscal Year 1979 is presented in Fig. 14. CAC also receives some support from NASA, NESS, and other agencies for its stratospheric work and from ERL for work on the Equatorial Pacific Ocean Climate Studies (EPOCS).

## FUNCTIONS OF CLIMATE ANALYSIS CENTER

- Applies new technology and approaches to analysis, diagnosis, and projection of short-term climate fluctuations, regionally and globally.

- Maintains awareness of current climate anomalies and provides information on these anomalies and their projected changes to a wide variety of users.

- Cooperates and coordinates its activities with:
  - U. S. and NOAA Climate Program Offices
  - Other elements of NMC and NWS.
  - NESS (Offices of Research and Operations)
  - EDIS (CCEA and NCC)
  - NASA
  - Department of Energy
  - Department of Agriculture
  - Department of Defense
  - Foreign climatic services
  - WMO
  - Research community

- Supports research studies in climate diagnosis and prediction at universities, private research organizations, and other government agencies.

Figure 1

# ORGANIZATION OF THE CLIMATE ANALYSIS CENTER

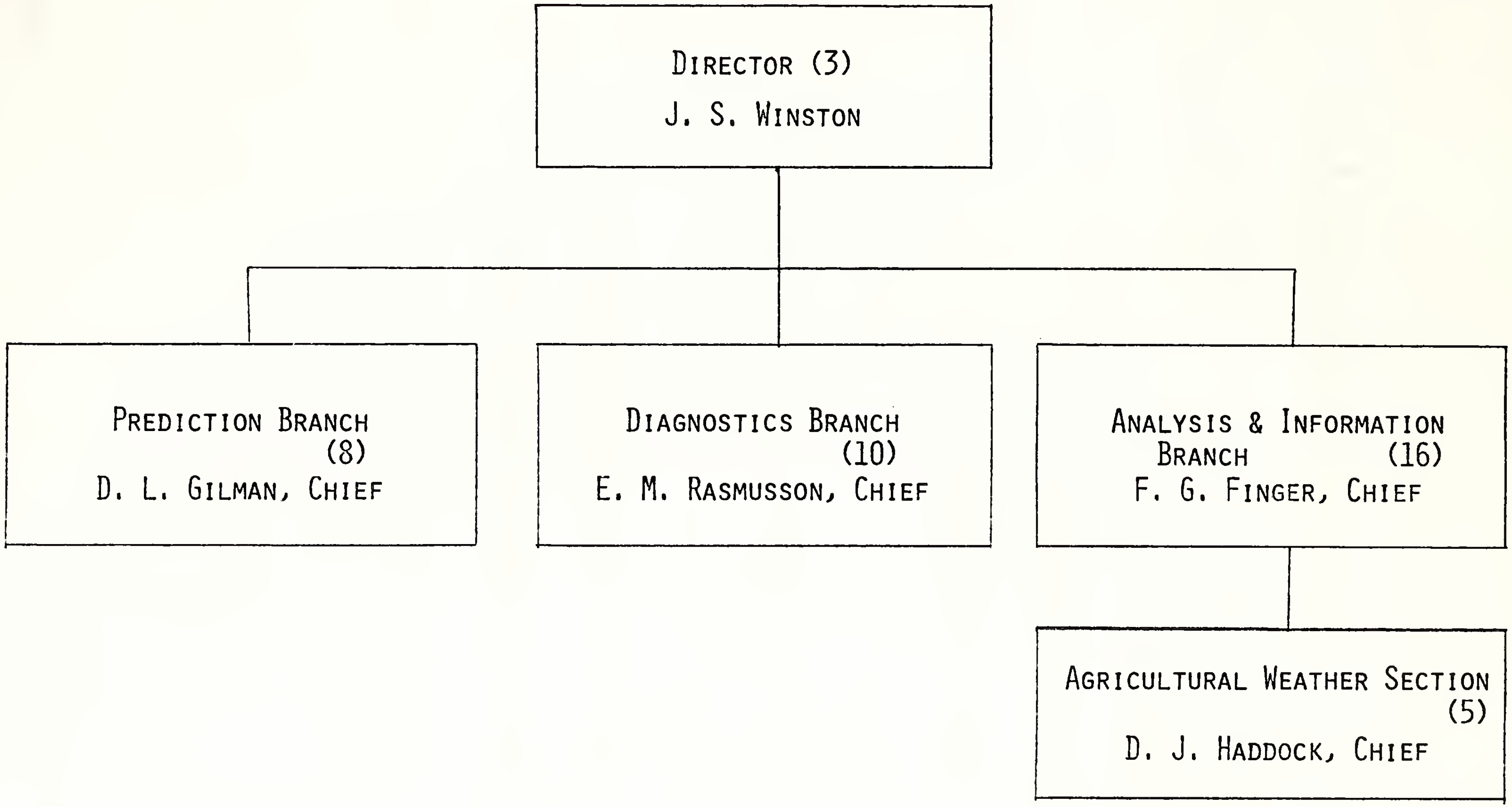

( ) Full Time Permanent Positions

Figure 2

# PREDICTION BRANCH

FUNCTIONS

- PREDICTION
- TEST AND EVALUATION
- FORECAST DEVELOPMENT

PRODUCTS

- MONTHLY OUTLOOKS
- SEASONAL OUTLOOKS
- DEGREE-DAY SUMMARIES AND PROJECTIONS
- MONTHLY AND ANNUAL WEATHER REVIEWS

FIGURE 3

## R & D OBJECTIVES

- INCREASE OUTLOOK ACCURACY, EXTENT, AND INFORMATION CONTENT
- STRETCH SEASONAL OUTLOOK LEAD TIME TO 3 - 9 MONTHS.

## R & D EMPHASES

- STATISTICS OVER NUMERICAL MODELLING
- IN-HOUSE PLUS GRANTS
- INTERACTION WITH EXPERIMENTAL FORECAST CENTERS
- EVALUATION STUDIES

FIGURE 4

# DIAGNOSTICS BRANCH

- Provide accurate climate diagnosis
  - Describe monthly - interannual fluctuations
    - case studies
    - statistical analyses
  - Specify important physical factors
    - energy balance
    - interactions
    - forcing

- Develop new climate indices
  - Distill key information
  - Satellite and conventional data
    - global radiation budget
    - atmospheric circulation
    - land surface and sea-air interface
    - snow cover and sea ice
    - upper ocean

- Support development of empirical - statistical prediction techniques
  - Document spatial relationships (teleconnections)
  - Identify lag relationships

Figure 5

# CURRENT ACTIVITIES

- Diagnostic Studies (in house)
  - 1978-79 Climate behavior
    - Tropical Circulation
    - Heavy Spring Rainfall
    - Long-wave Fluctuations
  - Equatorial Pacific Ocean Climate Studies (EPOCS)*
    - Large Scale Sea-air Interaction
    - Tropical-extratropical Interaction
    - Surface Marine and Upper Air Analysis
  - Climate Variability Studies
    - Global Radiation Budget 1974-78
    - Global SLP Variations 1947-77

* Jointly funded by CAC and ERL

Figure 6

# CURRENT ACTIVITIES

- DEVELOPMENT OF CLIMATIC INDICES
    - GENERAL STRATEGY
    - HISTORICAL DATA ANALYSIS
        - GLOBAL RADIATION BUDGET (SATELLITE)
        - TROPICAL/N. HEM. UPPER AIR ANALYSES

- DATA BASE DEVELOPMENT
    - CLIMATE DIAGNOSTIC DATA BASE (PLANNING)
        - REAL TIME MONITORING
        - DIAGNOSTIC CASE STUDIES
    - GLOBAL SEA SURFACE TEMPERATURE FIELDS 1946-77
    - REFORMATTING U. S. DAILY DATA

- FOURTH ANNUAL CLIMATE DIAGNOSTIC WORKSHOP (OCT. 16-18)
    - CLIMATE FLUCTUATIONS 9/78 - 8/79
    - DIAGNOSTIC STUDIES
    - CLIMATE INDICES
    - MODELLING RESULTS
    - VOLCANIC ACTIVITY AND CLIMATE

FIGURE 7

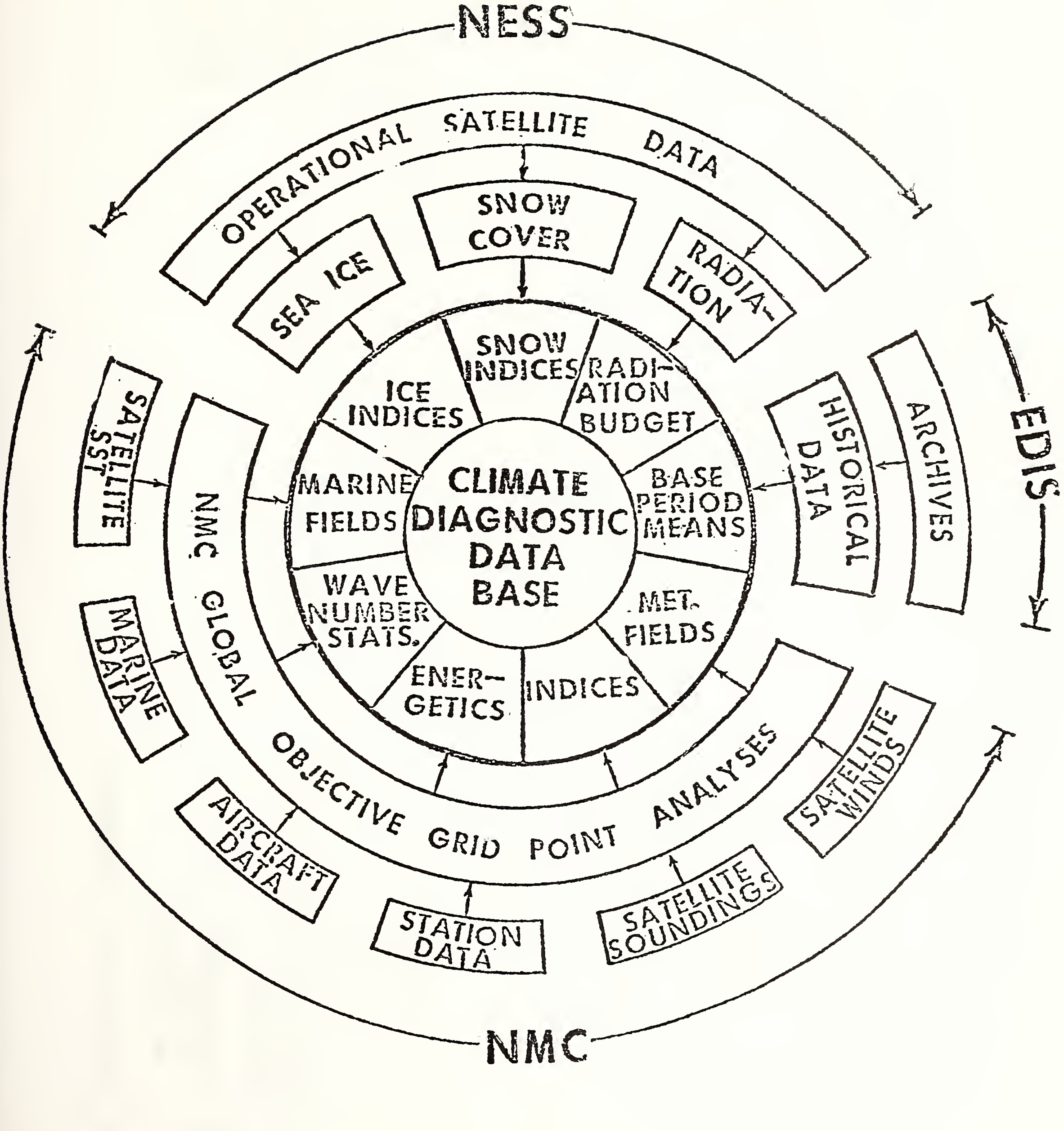
NESS
OPERATIONAL SATELLITE DATA
SNOW COVER
SEA ICE
RADIATION
EDIS
ARCHIVES
HISTORICAL DATA
SATELLITE SST
MARINE DATA
NMC GLOBAL OBJECTIVE GRID POINT ANALYSES
CLIMATE DIAGNOSTIC DATA BASE
SNOW INDICES
RADIATION BUDGET
ICE INDICES
MARINE FIELDS
BASE PERIOD MEANS
WAVE NUMBER STATS.
MET. FIELDS
ENERGETICS
INDICES
AIRCRAFT DATA
STATION DATA
SATELLITE SOUNDINGS
SATELLITE WINDS
NMC

FIGURE 8

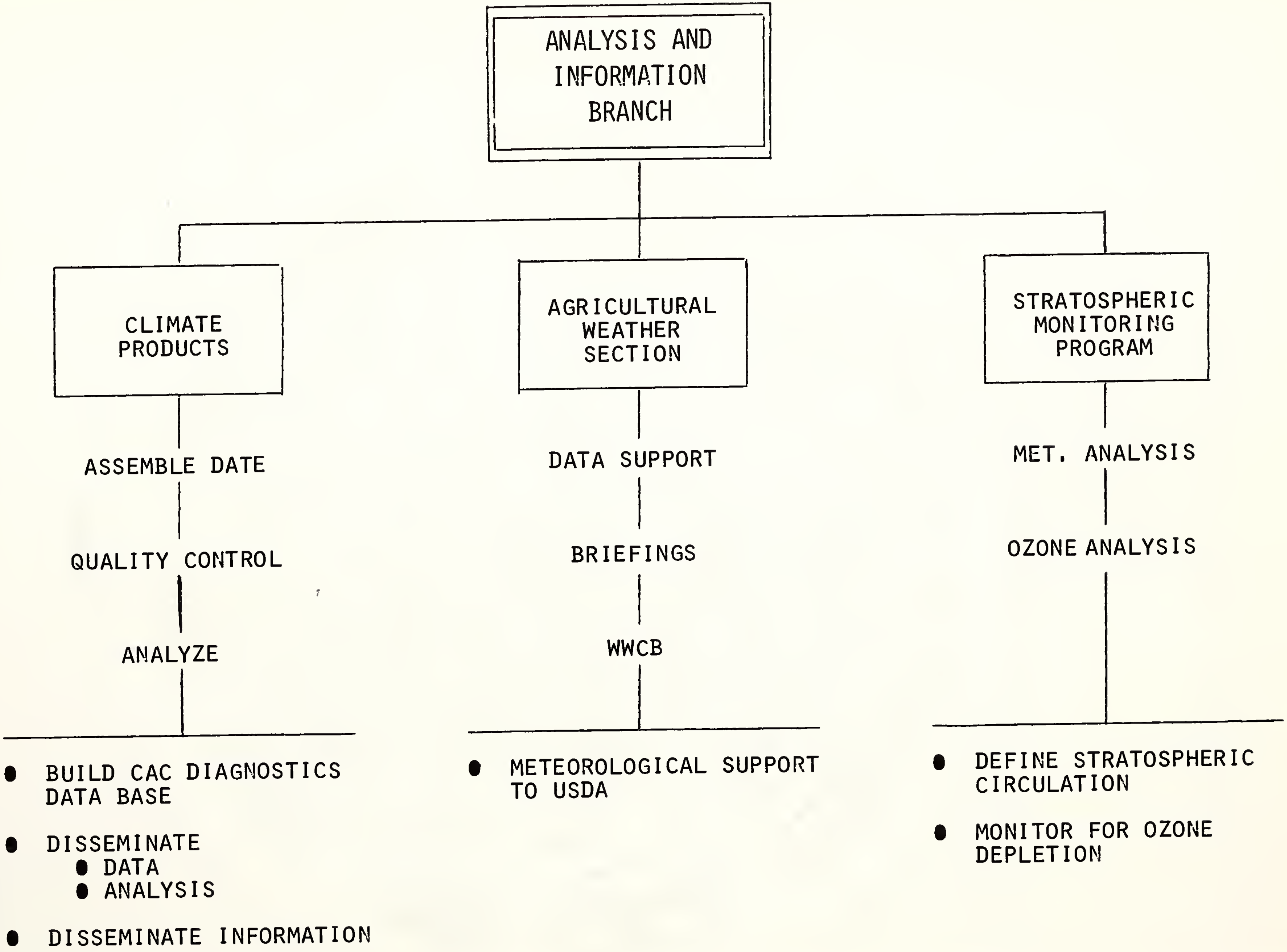
ANALYSIS AND INFORMATION BRANCH
CLIMATE PRODUCTS
AGRICULTURAL WEATHER SECTION
STRATOSPHERIC MONITORING PROGRAM
ASSEMBLE DATE
QUALITY CONTROL
ANALYZE
● BUILD CAC DIAGNOSTICS DATA BASE
● DISSEMINATE
● DATA
● ANALYSIS
● DISSEMINATE INFORMATION
DATA SUPPORT
BRIEFINGS
WWCB
● METEOROLOGICAL SUPPORT TO USDA
MET. ANALYSIS
OZONE ANALYSIS
● DEFINE STRATOSPHERIC CIRCULATION
● MONITOR FOR OZONE DEPLETION

FIGURE 9

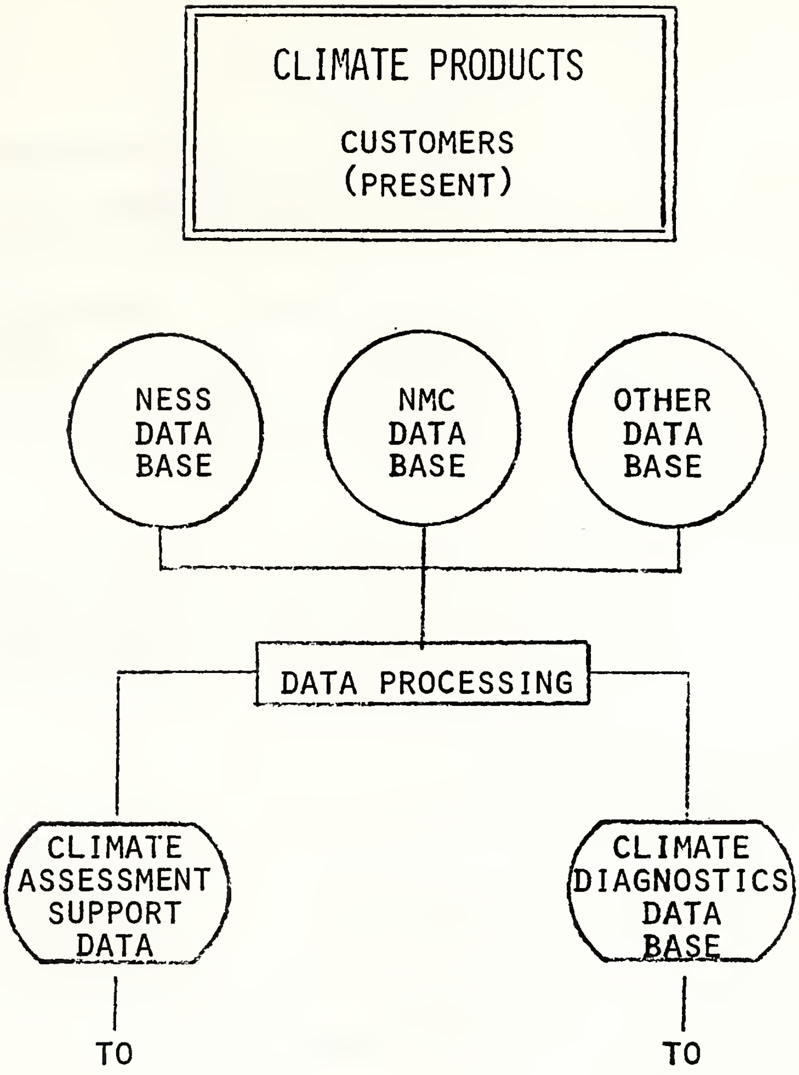

- CEAS - WASHINGTON
  COLUMBIA
- USDA - WASHINGTON
  HOUSTON
- AGRISTARS - HOUSTON
- NCC - ASHEVILLE
- CIA - WASHINGTON
- CAC - WASHINGTON

- CAC WASHINGTON
- USERS FOR DIAGNOSTICS AND PREDICTION RESEARCH

FIGURE 10

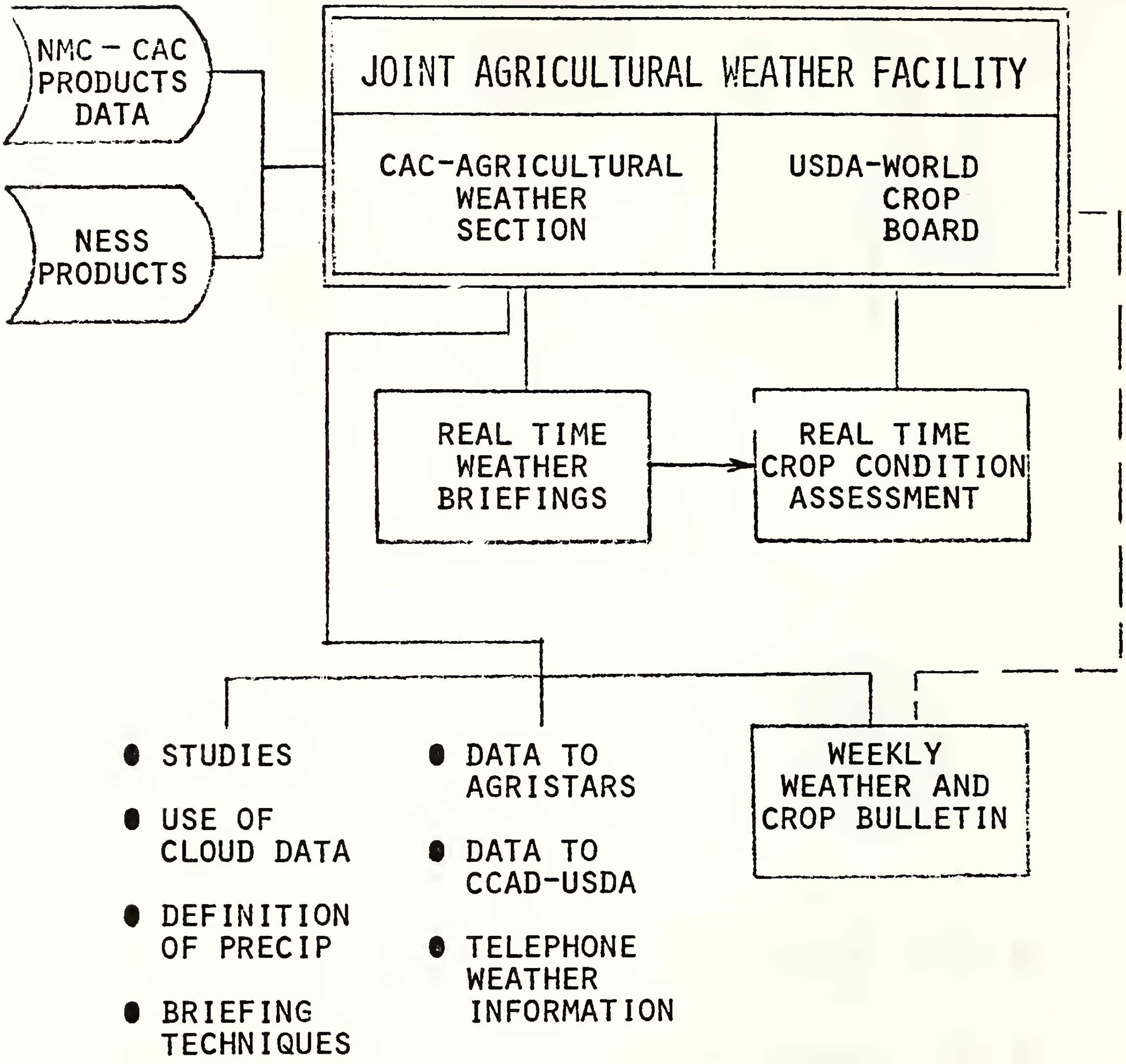
NMC - CAC PRODUCTS DATA
NESS PRODUCTS
JOINT AGRICULTURAL WEATHER FACILITY
CAC-AGRICULTURAL WEATHER SECTION
USDA-WORLD CROP BOARD
REAL TIME WEATHER BRIEFINGS
REAL TIME CROP CONDITION ASSESSMENT
STUDIES
USE OF CLOUD DATA
DEFINITION OF PRECIP
BRIEFING TECHNIQUES
DATA TO AGRISTARS
DATA TO CCAD-USDA
TELEPHONE WEATHER INFORMATION
WEEKLY WEATHER AND CROP BULLETIN

FIGURE 11

# PLANNED QUALITY CONTROL PROGRAM

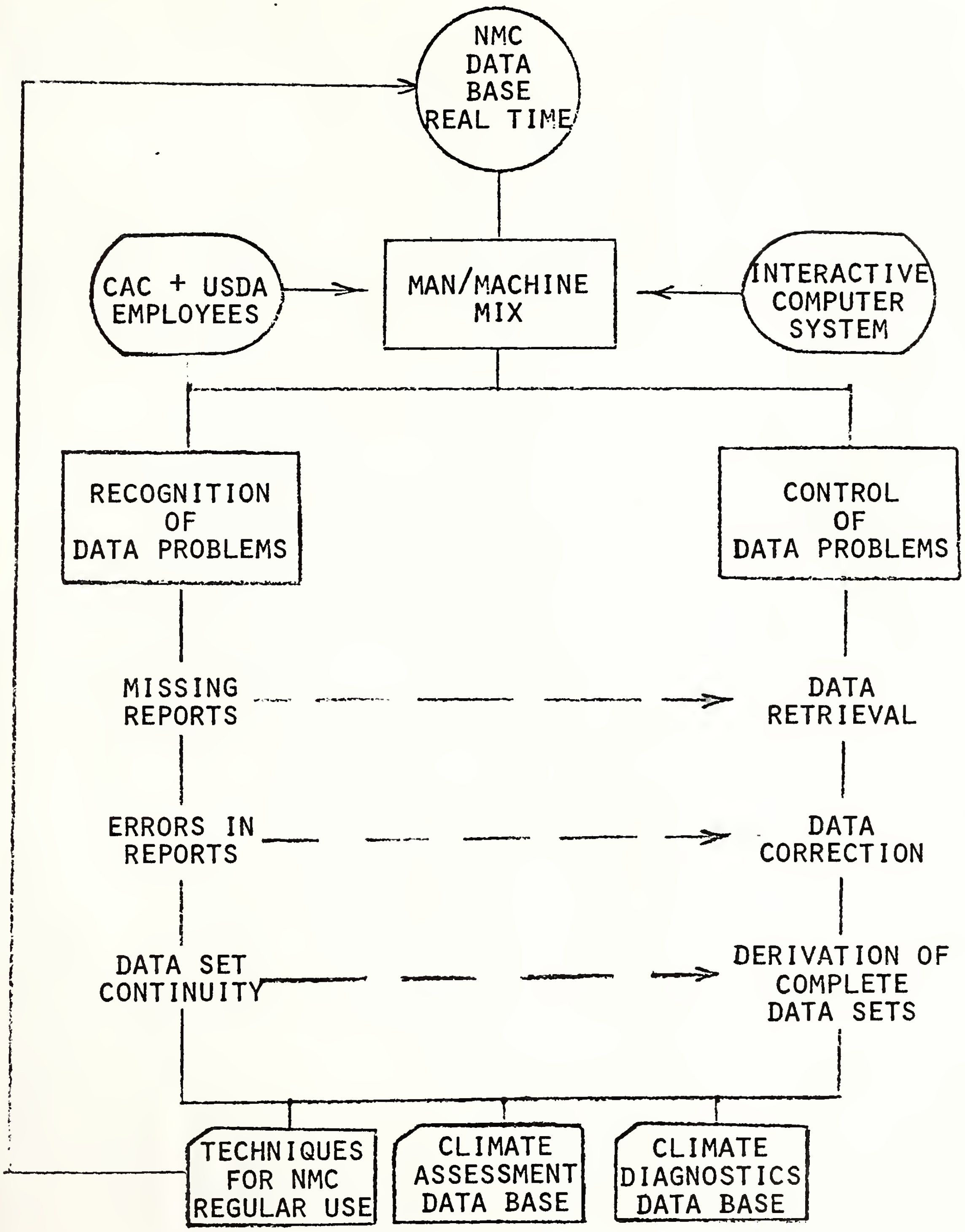
NMC DATA BASE REAL TIME
CAC + USDA EMPLOYEES
MAN/MACHINE MIX
INTERACTIVE COMPUTER SYSTEM
RECOGNITION OF DATA PROBLEMS
CONTROL OF DATA PROBLEMS
MISSING REPORTS
DATA RETRIEVAL
ERRORS IN REPORTS
DATA CORRECTION
DATA SET CONTINUITY
DERIVATION OF COMPLETE DATA SETS
TECHNIQUES FOR NMC REGULAR USE
CLIMATE ASSESSMENT DATA BASE
CLIMATE DIAGNOSTICS DATA BASE

FIGURE 12

# STRATOSPHERIC MONITORING PROGRAM
## NOAA RESPONSIBILITY UNDER PUBLIC LAW 95-95

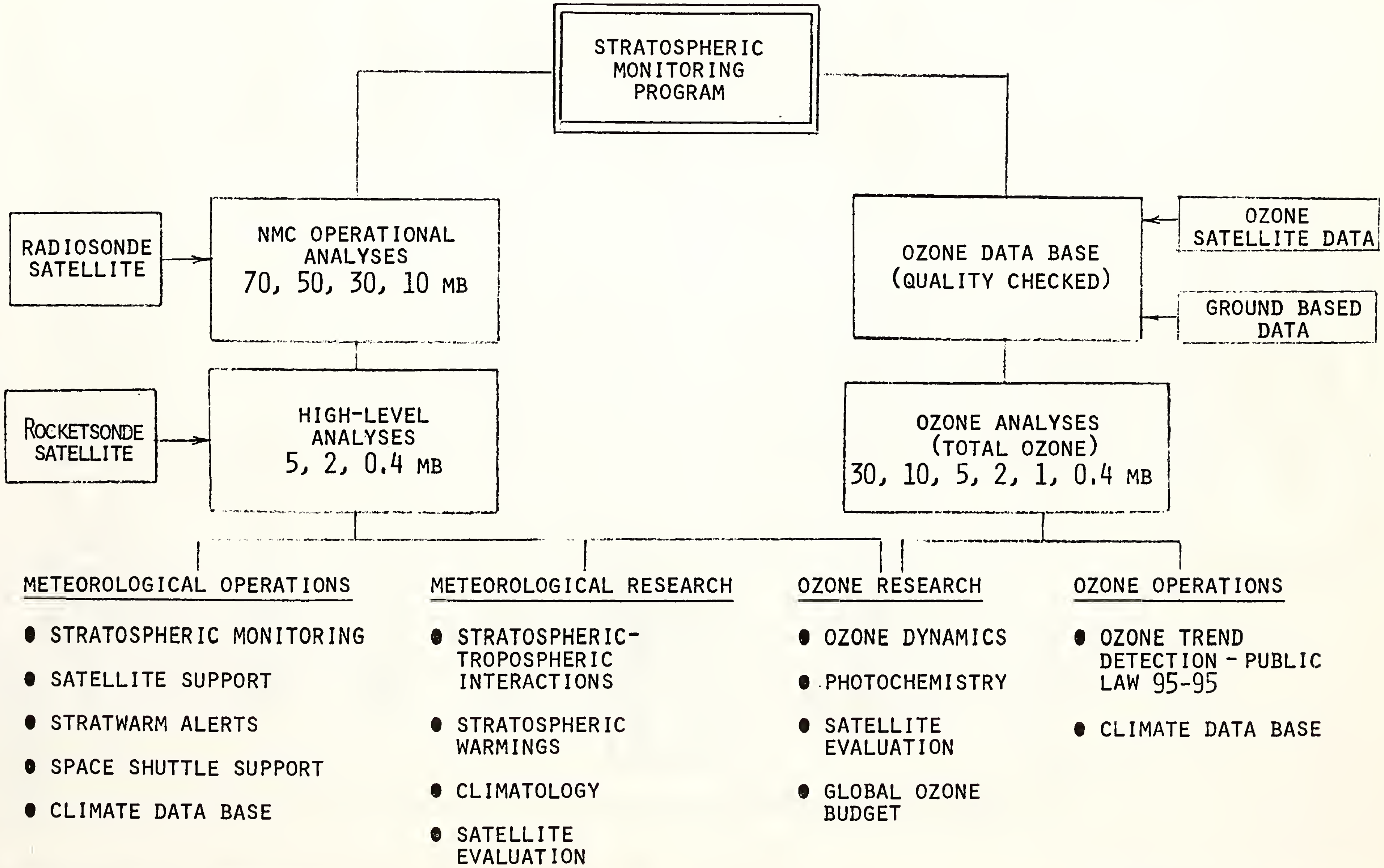

FIGURE 13

## CAC Grants, Contracts, Transfers (FY-79)

| Starting Date | Type | Institution | Title | Principal Investigator(s) | Monitor | Amt. (K) |
|---|---|---|---|---|---|---|
| 10/1/78 (1 yr.) | G | Florida State University | Diagnostic Studies of Climatic Anomalies | Krishnamurti | Krueger | $ 39 |
| 1/1/79 (1 yr.) | G | University of Hawaii | Synoptic Studies of Summer & Winter Monsoons | Murakami | Krueger | 38 |
| 1/15/79 (6 mo.) | G | Solar Climate Res. Inst. | Development of a Statistical Homogeneous Proxy Series of a Northern Hemispheric Grid of Monthly Mean 500 mb Heights, 1899-1977 Inclusive | Willett | Gilman | 28 |
| 3/1/79 (1 yr.) | G | Columbia Univ. - Lamont-Doherty Geological Observ. | A Low Resolution Thermodynamic Model: Modification and Application | Adem, Donn | Shuman | 59 |
| 4/1/79 (1 yr.) | C | Naval Postgrad. School | Study of Relationships Between Planetary-Scale Circulation and Synoptic Scale Wave Disturbances Through Analysis of Digitized Heat Budget, Wind Fields and Other MONEX Data Sets | Chang | Gray | 14 |
| 8/1/79 (1 yr.) | C | Meteorology International | A System for Producing Historical Sequences of Analyzed Sea Surface Temperature Fields for Application to Studies of Climate Trends and Regimes | Holl | Rasmusson | 70 |
|  | T | National Climate Center | Reformat the NCC Summary of the Day File (Coop Data) and Rehabilitation of Surface Marine Observations, | Mitchell | Rasmusson | 65 |
| 9/1/79 (1 yr.) | G | University of Wisconsin | Diagnostic Studies of Northern Hemisphere Wintertime Circulation Patterns and their Fluctuations on Time-Scales of Weeks and Months | Kutzbach | Rasmusson | 28 |
| 9/30/79 (1 yr.) | G | University of Wisconsin | Diagnostics of Climatic Hazards | Hastenrath | Erickson | 25 |
| 9/30/79 (1 yr.) | G | Scripps Inst. of Oceanography | Climate Research and Prediciton | Namias, Barnett | Gilman | 150 |

FIGURE 14

# Survey of Climate Indices
# Useful to the Climate Analysis Center

by

E. M. Rasmusson and W. Y. Chen
Climate Analysis Center
National Oceanic and Atmospheric Administration
Washington, D. C. 20233

## 1. Introduction

This review covers a few topics from a survey aimed at identifying climate indices which might be routinely computed and monitored at the CAC. Three general areas are considered, (1) zonally and globally averaged quantities, (2) teleconnections and regional indices, and (3) indices from satellite data. Time scales in the range of weeks to a few years are of primary interest. Most of the data for evaluating those indices will be in the form of operational analyses and derived data products rather than basic observations.

## 2. Zonally and Globally Averaged Indices

The use of latitudinally averaged zonal westerly indices dates back to the 1940's. Polar (55-70N), Temperate (35-55N) and Subtropical (20-35N) Indices are still routinely monitored by the CAC Prediction Branch. The problem of distinguishing between changes in strength and shifts in latitude, which arises when using an average over a latitude band, can be avoided by using data for the entire profile. Month to month profile changes can be effectively expressed in terms of Empirical Orthogonal Functions (EOF's). Figure 1 shows the first three EOF's for the winter profile (Dec.-Feb.) of zonally averaged geostrophic westerly wind component. Three EOF's explain 90, 88, 85 and 86 percent of the total winter, spring, summer and autumn variance, respectively. Thus, the profile can be characterized quite well by the three EOF amplitude coefficients, in place of the three index values. Note that EOF 1, which accounts for 45% of the winter variance, represents a latitudinal shift of the westerlies, rather a change in strength.

During the years since the development of the zonal indices, a more physical and comprehensive framework has emerged for describing the state of the general circulation. Particularly suitable for CAC use is the "4 Box" energy formulation introduced by Lorenz (1955). NMC computer facilities and data analysis products allow the necessary computations to be performed on a routine basis. A significant step in this direction was taken by Miller et al. (1975) when they developed the NMC Operational Energy Program.

These energy computations offer a wealth of diagnostic information. In terms of indices, they provide degrees of compaction ranging from integrals over the entire atmosphere, to zonally averaged quantities at a single level.

Analyses in the wave number domain offer another important method for summarizing global scale climate information. The relationship of planetary scale standing waves, particularly wave number 2, to climate variability on both the global and regional scale is discussed by Quiroz (1979) and van Loon (1979) in other papers of these proceedings.

### 3. Teleconnections and Regional Indices

Although useful for many purposes, global or zonally averged indices reduce or eliminate information on regional anomalies. Regional indices have been developed which use factors such as the location and intensity of circulation features, pressure differences between stations or between circulation features, and trough and ridge positions.

The concept of teleconnections assumes that there are favored modes for coupling large scale circulation and climate anomalies. In designing regional indices and in treating the basic data, the time and space scales of the regional teleconnection systems must be carefully considered. For example, Trenberth (1976b) and Wright (1977) point out that the Southern Oscillation (S.O.) signal is dominated by the higher frequency "noise" in mean monthly data. Thus the S.O. is an important mechanism only on time scales of seasons or longer. Teleconnection systems may be non-stationary in nature. Troup (1956) found the S.O. to be less marked during recent decades when compared to the period Walker studied. Similarly, Trenberth (1976b) found temporal variations in both the character and amplitude of the S.O. Wright (1977) computed quite different S.O. index spectra for three separate periods of record. Most teleconnection systems also exhibit distinct seasonal variations. Walker and Bliss (1932, 1937) recognized this in the oscillations they examined. Similarly, the teleconnection statistics of O'Connor (1969) and Namias (1978) are computed separately for each season or month.

Among the objective aids for digesting and distilling the mass of information from large data sets, and identifying and quantifying teleconnection systems, there are three particularly powerful tools of statistical analysis: (1) cross correlation analysis, (2) empirical orthogonal function (EOF) analysis, and (3) objective classification by factor analysis. It is important to emphasize that these techniques provide only statistical information, which may or may not aid in the physical interpretation of the data.

Cross correlation analysis was used by Martin (1955) and later by O'Connor (1969) to develop maps showing the correlation between 5-day mean 700 mb height departures at a given grid point with those of all other grid points over the Northern Hemisphere. Namias (1978) has updated and extended these computations. The results of more recent cross correlation analysis are described by Wallace and Gutzler (1979) in a separate proceedings paper.

EOF analysis was first applied to the problem of 30-day forecasting by Gilman (1957). In a more diagnostic application, Kutzbach (1970) used EOF analysis to describe the dominant modes of variation in the January and July monthly mean sea level pressure fields. The method was highly recommended by the WMO Working Group on Climate Change, and is now widely used, as attested to by the many applications described in these workshop proceedings.

Unlike harmonic analysis, the EOF's have no predetermined form but rather are determined by the statistical properties of the data. Although the functions are defined only at data points, it is common practice to construct isolines from the point values.

A major advantage of the EOF formulation is the very effective compression of a data set by separating the meaningful information from the redundancy and noise and expressing it in terms of a few characteristic modes of variability. The necessity of viewing the variations in component form can be turned to advantage if the preferred configurations of departure fields, represented by the EOF's, correspond with well-defined oscillations or teleconnection systems, e.g. Kidson (1975), Trenberth (1976a), van Loon (1978).

In these cases, the EOF amplitude coefficients can be used as an index, or the results of the analysis can serve as the basis for designing a simple index from station data, e.g. Trenberth (1976a), Wright,(1977). In many cases the EOF analysis will merely point the way to other types of analyses.

Conventional EOF analysis may be thought of as describing variations in terms of standing waves, as they are limited to showing variations as either in phase or 180 degrees out of phase. Rasmusson et al. (1978), illustrated a further development of the EOF approach, referred to as Hilbert Singular Decomposition (HSD). This technique describes the variations of a scalar field in terms of complex EOF's, thus allowing for the full range of phase variations. Complex EOF analysis can be directly applied to a vector field, as was described by Salstein and Rosen (1979) in another proceedings paper.

EOF's are ordered in such a way that the important characteristics of the data matrix are contained in the leading terms, with successive terms describing less and less of the main features and more and more of the specific details. There are many situations in which an EOF does not represent a distinct circulation type but rather a second order variation in phase, shape or position of a more basic oscillation described by a lower order EOF. A simple example is shown in Fig. 2 taken from Jalickee and Ropelewski (1979). "A" shows the two leading EOF's for the low level profile of potential temperature derived from the GARP Atlantic Tropical Experiment (GATE) structuresonde data. EOF 1 represents a general warming or cooling at all levels, while EOF 2 shows a tendency for out of phase temperature changes in the upper and lower levels. While EOF 1 can be viewed as a characteristic profile shape, EOF 2 cannot. In order to obtain characteristic shape functions, the authors used an objective classification scheme which is a generalization of the method of "factor rotation" commonly used in factor analysis. Essentially, the results of an EOF analysis are recombined to obtain functions characteristic of mutually exclusive subgroups or "classes" of the data, in contrast to the original EOF components, which are ordered in importance. The new patterns or classes are generally not independent or orthogonal. In this case, the two profile classes clearly represent the "disturbed" and "undisturbed" atmospheric states. Specification of a higher number of classes revealed no meaningful, new, profile types. This type of analysis results in each individual profile, or map, as the case may be, being characterized by a set of coefficients, which quantify its affinity to each of the classes.

### 4. Indices from Satellite Data

In separate proceedings papers, Sadler (1979), and Matson et al. (1979), describe the use of satellite data for obtaining tradewind and continental snow cover indices, respectively. We shall briefly describe the use of satellite radiation budget data as proxy data for monitoring cloud and precipitation systems. Finally, we shall make a few comments concerning the monitoring of variations in sea ice cover.

Ground-based observations of cloudiness and precipitation are for the most part inadequate, particularly over ocean areas. Therefore, indices derived from satellite data offer an attractive proxy method for monitoring the large scale fluctuations in these parameters. As an example, our colleague, Phillip Clapp, has experimented with an index for the equatorial Pacific based on satellite measurements of absorbed solar radiation. Fig. 3 shows the 5-month running mean anomaly of Rapa (27.6S, 144.3W) minus Darwin (12.4S, 130.9E) sea level pressure. This is similar to Quinn's triple 6-month running mean S.O. index for the same stations and time interval.

Also shown is the 5 month running mean of Clapp's Pacific Dry Zone Absorbed Radiation Anomaly Index. This index is defined as the maximum absorbed shortwave radiation near the Equator in the 60-degree sector 135W-75W (segment 3) minus that in the sector 165E to 135W (segment 4). These specific longitude bands were chosen simply because they correspond to sector averages routinely produced by the Meteorological Satellite Laboratory of NESS. Due to the short data record, each anomaly value represents a departure from an average of only 3 or 4 monthly values.

Comparison with the S.O. Index, i.e. Rapa-minus Darwin pressure, suggests systematic shifts in cloudiness between segments 3 and 4 during the S.O. Index cycle. During the high index state (August 1975) there was less cloudiness in segment 3 than in segment 4, as the main area of convection was far to the west over Indonesia. Also contributing to the difference may have been the occurrence of widespread stratus clouds in the eastern equatorial Pacific and along the South American coast associated with the upwelling cold water in that area.

During the low-index phase (September 1976) the main area of convection shifted eastward from Indonesia, and even extended east of 180° as shown by Krueger and Winston (1979). Coupled with this may have been the diminishing of stratus clouds in the eastern Pacific associated with the warmer sea surface temperatures.

Our colleague, Tom Heddinghaus, has recently completed a global EOF analysis of outgoing longwave (IR) radiation. Fig. 4 shows the amplitude time series for EOF 1 of the IR monthly anomalies, together with Quinn's Rapa-Darwin S.O. Index (reversed from customary sign), and an index of Tarawa rainfall anomalies. Note when comparing the curves that the values of the EOF amplitude time series are unsmoothed. The correspondence of the 3 curves is apparent with both Tarawa rainfall and the amplitude coefficients lagging the S.O. Index by 2-4 months. EOF 1 (Fig. 5) shows the eastward shift in the Indonesia precipitation area characteristic of a low S.O. Index, and indicates a tie-in with the South Pacific Convergence Zone (SPCZ). The chart also shows other areas where the IR anomalies varied with the S.O. Index in a coherent manner during this period. In some cases, these appear to correspond with features of Kidson's EOF 1 for tropical precipitation, which he identified with the S.O. Although the period of record is short, these results encourage additional more detailed analyses.

Until recently, the collection and analysis of snow and ice data has been done primarily on a regional basis. It is only since the advent of satellite observations in the 1960's that uniform sets of sea ice and snow cover data became available. The description of Arctic Sea ice variations and their relationship to atmospheric parameters has recently been addressed by Walsh and Johnson (1979a; 1979b). Using monthly mean data spanning the period 1953-77, they described the variations in the area of Arctic ice coverage in terms of EOF's. Because much of the area of analysis is either perpetually ice covered or perpetually ice free, they expressed the data as a one dimensional function of longitude, i.e., in terms of the area covered by ice in each of 36 ten degree longitude sectors. The 4 leading EOF's (unnormalized) are shown in Fig. 6. Use of unnormalized data has the advantage of not artifically weighing the fluctuations in those longitudes (i.e., the Canadian Archipelago and Siberian Arctic) where a negligible wintertime variance in ice area, due to the land boundary, lowers the total variance for the longitude sector. As shown by the EOF's, heavy ice conditions do not generally occur at all longitudes. The major variability is concentrated in 3 sectors: the Bering Sea, Baffin Bay-Davis Strait, and the Greenland Sea-Iceland area. An area of lesser variabliity is found in the Barents-Kara Sea area. The amplitude coefficients of the leading EOF's can be used as indices of these variations. Alternately, it may be possible to accurately express the amplitude coefficients in terms of linear combinations of data from only these sectors. One can entirely avoid viewing the variations in component form by simply using as indices the average ice cover for the 3 or 4 areas of major variability (Walsh and Johnson, 1979b).

The newly created Navy/NOAA Joint Ice Center now routinely prepares real time map analyses of ice cover for both the North and South Polar regions. Practical considerations require that these data be available on a current basis in either area averaged or digital form if they are to meet the needs of the CAC. At present, however, these data are not being digitized on a current basis.

# References

Gilman, D.L., 1957: Empirical Orthogonal Functions Applied to Thirty-Day Forecasting. Sci. Rpt. No. 1. Contract No: AF19(604)1283 Dept. of Meteorology, Mass. Inst. of Tech., Cambridge, Mass., 129 pp.

Jalickee, J.B. and C.P. Ropelewski, 1979: An Objective Analysis of the Boundary Layer Thermodynamic Structure during GATE. Part I: Method. Mon. Weather Rev., 107, 68-76.

Kidson, J. W. 1975: Tropical Eigenvector Analysis and the Southern Oscillation. Mon. Weather Rev., 103, 197-216.

Krueger, A.F. and J. S. Winston, 1979: Further Analysis of Recent Fluctuations in Circulation and Cloudiness (rainfall) over the Tropics. Proceedings of the Fourth Annual Climate Diagnostics Workshop, Oct. 16-18, 1979, U. of Wisconsin, Madison, Wisc.

Kutzbach, J.E., 1970: Large Scale Features of Monthly Mean Northern Hemisphere Anomaly Maps of Sea-Level Pressure. Mon. Weather Rev., 98, 708-716.

Lorenz, E.N., 1955: Available Potential Energy and the Maintenance of the General Circulation. Tellus, 7, 157-167.

Martin, D.E., 1955: Atlas of 700 mb Five-Day Mean Northern Hemisphere Anomaly Charts. Air Weather Service Technical Report 105-100/2, Hq. Air Weather Service, MATS, USAF, Washington, D.C. 39 pp.

Matson, M., D.A. Wiesnet, C.P. Berg, and E.P. McClain, 1979: New Data and New Products: The NOAA/NESS Continental Snow Cover Data Base. Proceedings at the Fourth Annual Climate Diagnostic Workshop, October 16-18, 1979, U. of Wisconsin, Madison, Wisc.

Miller, A.J., W. Collins, and D. Dubofsky, 1975: The NMC Operational Global Energy Program, Office Note 109, National Meteorological Center, NOAA, 13 pp.

Namias, J, 1978: Recent Drought in California and Western Europe. Rev. of Geophys. and Space Phys., 16, 435-458.

O'Connor, J. F., 1969: Hemispheric Teleconnections of Mean Circulation Anomalies at 700 Milibars. ESSA Tech. Report WB 10, Environmental Sciences Services Administration, U.S. Dept. of Commerce, Washington, D. C. 103 pp.

Quinn, W. H., 1979: Monitoring and Predicting Short-term Climatic Changes in the South Pacific Ocean. Paper presented at the International Conference on Marine Science and Technology, March 26-30, 1979, Catholic University, Valparaiso, Chile.

Quiroz, R. S., 1979:; The stratosphere and Troposphere during the 1978-79 Winter. Proceedings of the Fourth Annual Climate Diagnostics Workshop, October 16-18, 1979, U. of Wisconsin, Madison, Wisc.

Rasmusson, E.M., J.B. Jalickee, P.A. Arkin, and W.Y. Chen, 1978: Biennial Variations in Surface Temperatures over the United States as Revealed by Singular Decomposition. *Proceedings of the Third Annual Climate Diagnostics Workshop*, U.S. Dept. of Commerce, NOAA.

Sadler, J.C., 1979: Trade Wind Index from Satellite Winds. *Proceedings of the Fourth Annual Climate Diagnostic Workshop*, October 16-18, 1979,

Salstein, D.A. and R. D. Rosen, 1979: Variations of Atmospheric Water Vapor and the Water Vapor Transport Vector during a 15Year Period. *Proceedings of Fourth Annual Climate Diagnostic Workshop*, Oct. 16-18, U. of Wisconsin, Madison, Wisc.

Trenberth, K.E., 1976a: Fluctuations and Trends in Indices of the Southern Hemispheric Circulation. *Quart. J. Roy. Meteor. Soc.*, 102, 25-35.

________________ 1976b: Spatial and Temporal Variations in the Southern Oscillation. *Quart. J. Roy. Meteor. Soc.*, 102, 639-653.

Troup, A.J., 1965: The Southern Oscillation. *Quart. J. Roy. Meteor. Soc.*, 91, 490-506.

van Loon, H., 1979: Trends of 700 mb Temperature and Their Connection with Changes in Stationary Eddy Heat Fluxes and Circulation at the Surface. *Proceedings of the Fourth Annual Climate Diagnostics Workshop*, Oct. 16-18, 1979, U. of Wisconsin, Madison, Wisc.

van Loon, H., and J. C. Rodgers, 1978: The Seesaw in Winter Temperatures between Greenland and Northern Europe. Part I. General Description. *Mon. Weather Rev.*, 106, 296-310.

Walsh, J.E. and C. M. Johnson, 1979a: An Analysis of Arctic Sea Ice Fluctuations 1953-77. *J. Physical Oceanogr.*, 9, 580-591.

____________ and ______________, 1979b: Interannual Atmospheric Variability and Associated Fluctuations in Arctic Sea Ice Extent. *J. Geophys. Res.* (to be published November 79).

Wright, P. B., 1977: The Southern Oscillation Patterns and Mechanisms of the Teleconnections and the Persistence. *Report HIG-77-13*, Hawaii Institute of Geophysics, U. of Hawaii, 107 pp.

Walker, G. T., and E. W.Bliss, 1932: *World Weather V. Mem. Roy. Meteor. Soc.*, 4(36), 53-84.

_______________ and ____________, 1937: World Weather VI, *Mem. Roy. Meteor. Soc.*, 4(39), 119-139.

Wallace, J. M. and D. S. Gutzler, 1979: Horizontal Teleconnections during the Northern Hemisphere Winter Season. *Paper presented at the Fourth Climate Diagnostic Workshop*, October 16-18, U. of Wisconsin, Madison, Wisc.

# List of Figures

Fig. 1 EOF's 1-3 for the winter (Dec.-Feb.) zonally averaged geostrophic westerly component. Superimposed is the mean winter westerly profile. Bounding latitudes for the Polar, Temperate and Subtropical Westerly Indices are also shown.

Fig. 2 (a) Leading EOF's of the GATE structuresonde potential temperature data set (see text); (b) Characteristic shape functions resulting from the classification for the potential temperature profiles; and (c) time series of classification coefficients. (From Jalickee and Ropelewski, 1979).

Fig. 3 (a) Average field of absorbed solar radiation. Latitudinally averaged values for segment 3 and 4 were used by Clapp for index computations (see text); (b) 5-month running means of Rapa minus Darwin pressure anomaly and Clapp's Pacific Dry Zone Absorbed Radiation Anomaly Index (see text).

Fig. 4 Values of (a) Darwin minus Rapa pressure anomaly difference smoothed with a triple pass 6-month running mean (from Quinn, 1979); (b) Tarawa rainfall anomaly with similar smoothing, and (c) the unsmoothed amplitude time series for EOF 1 for the IR radiation anomalies.

Fig. 5 EOF 1 and amplitude time series for the IR radiation anomalies.

Fig. 6 The first 4 hemispheric EOF's of unnormalized arctic ice extent (from Walsh and Johnson, 1979b). Sectors of maximum variability are indicated.

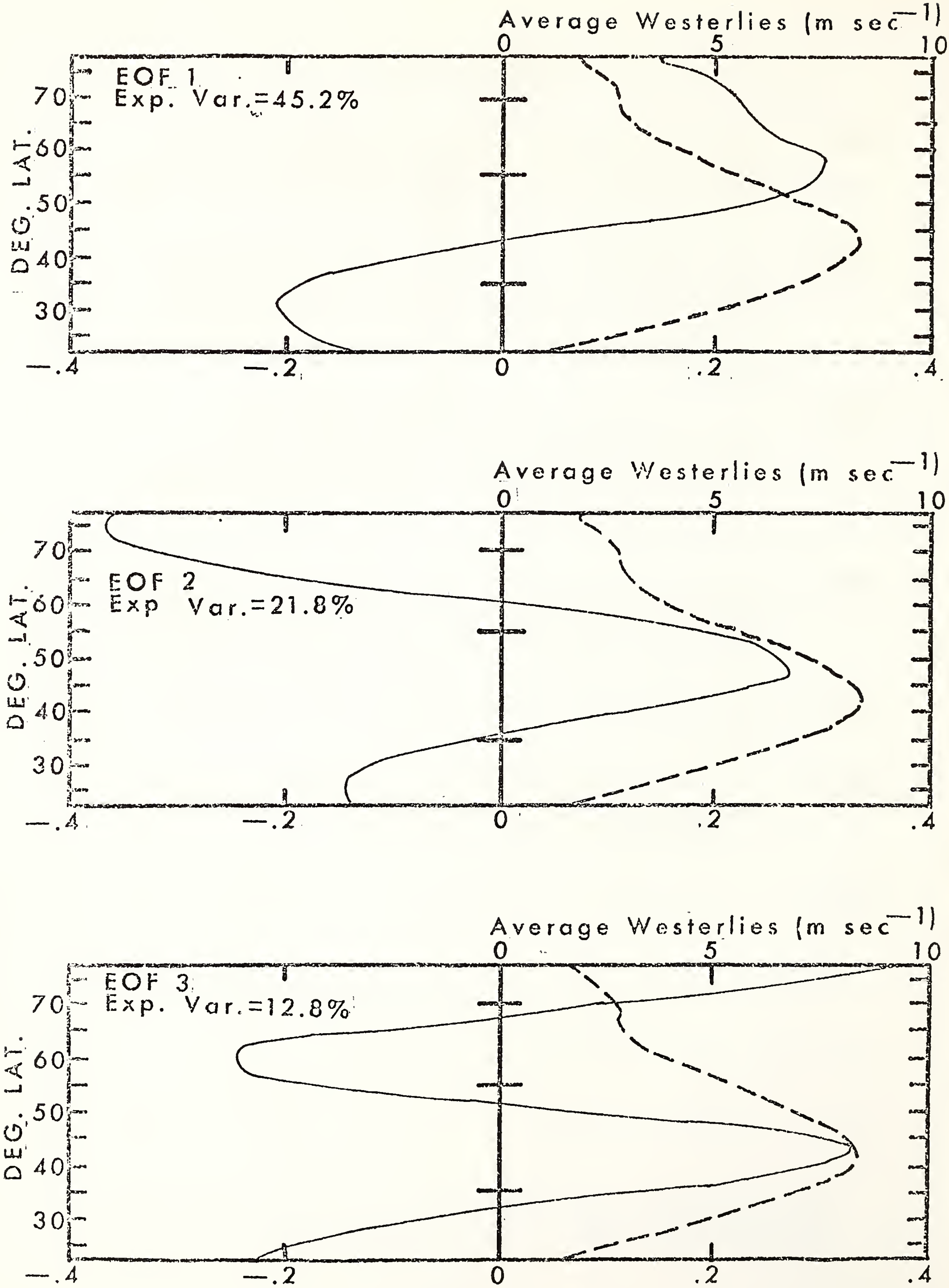
Average Westerlies (m sec$^{-1}$)
0
5
10
EOF 1
Exp. Var.=45.2%
DEG. LAT.
70
60
50
40
30
—.4
—.2
0
.2
.4
Average Westerlies (m sec$^{-1}$)
0
5
10
EOF 2
Exp Var.=21.8%
DEG. LAT.
70
60
50
40
30
—.4
—.2
0
.2
.4
Average Westerlies (m sec$^{-1}$)
0
5
10
EOF 3
Exp. Var.=12.8%
DEG. LAT.
70
60
50
40
30
—.4
—.2
0
.2
.4

Figure 1

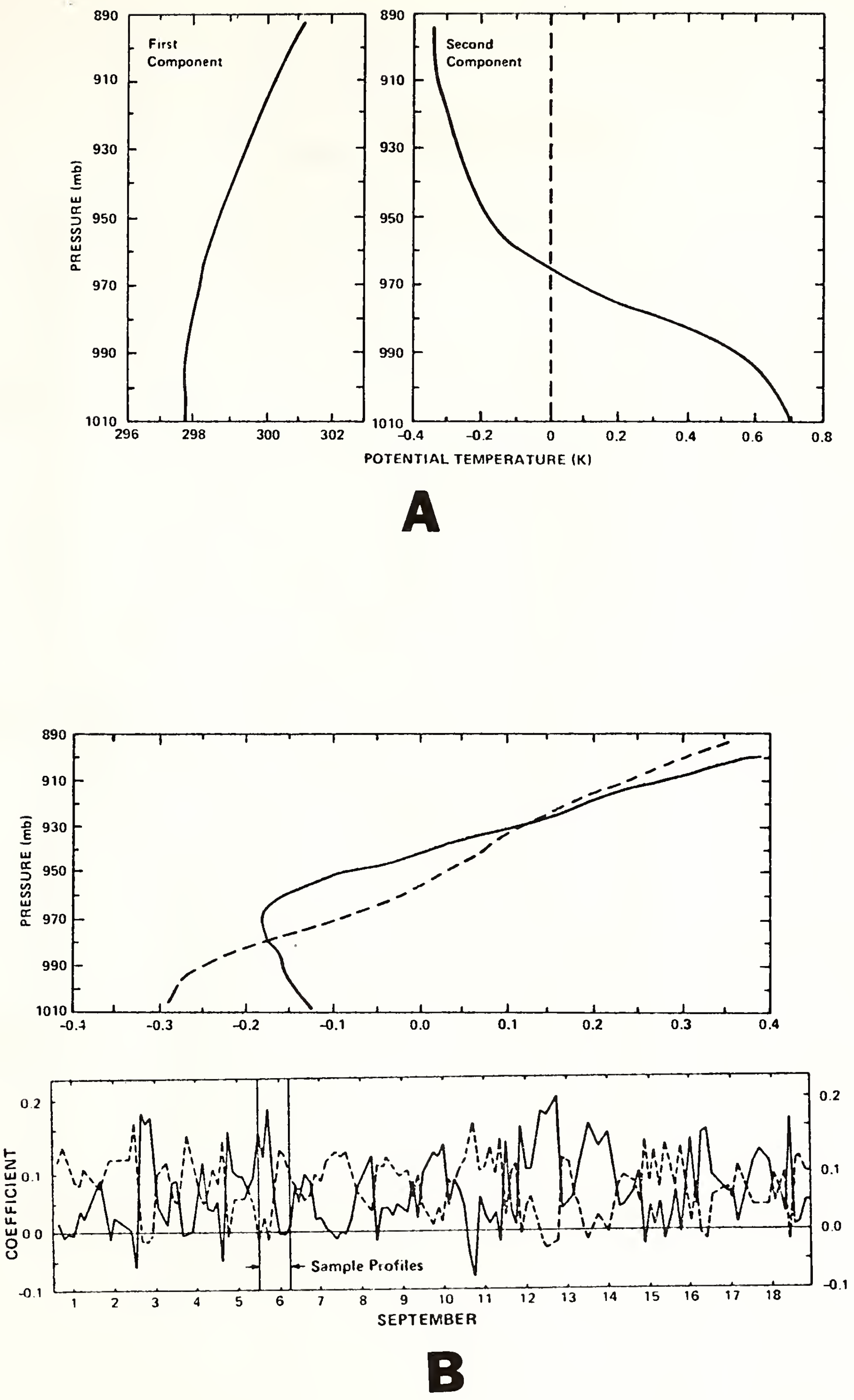
First Component
Second Component
PRESSURE (mb)
890
910
930
950
970
990
1010
296
298
300
302
-0.4
-0.2
0
0.2
0.4
0.6
0.8
POTENTIAL TEMPERATURE (K)
A
-0.4
-0.3
-0.2
-0.1
0.0
0.1
0.2
0.3
0.4
COEFFICIENT
0.2
0.1
0.0
-0.1
Sample Profiles
1
2
3
4
5
6
7
8
9
10
11
12
13
14
15
16
17
18
SEPTEMBER
B

FIGURE 2

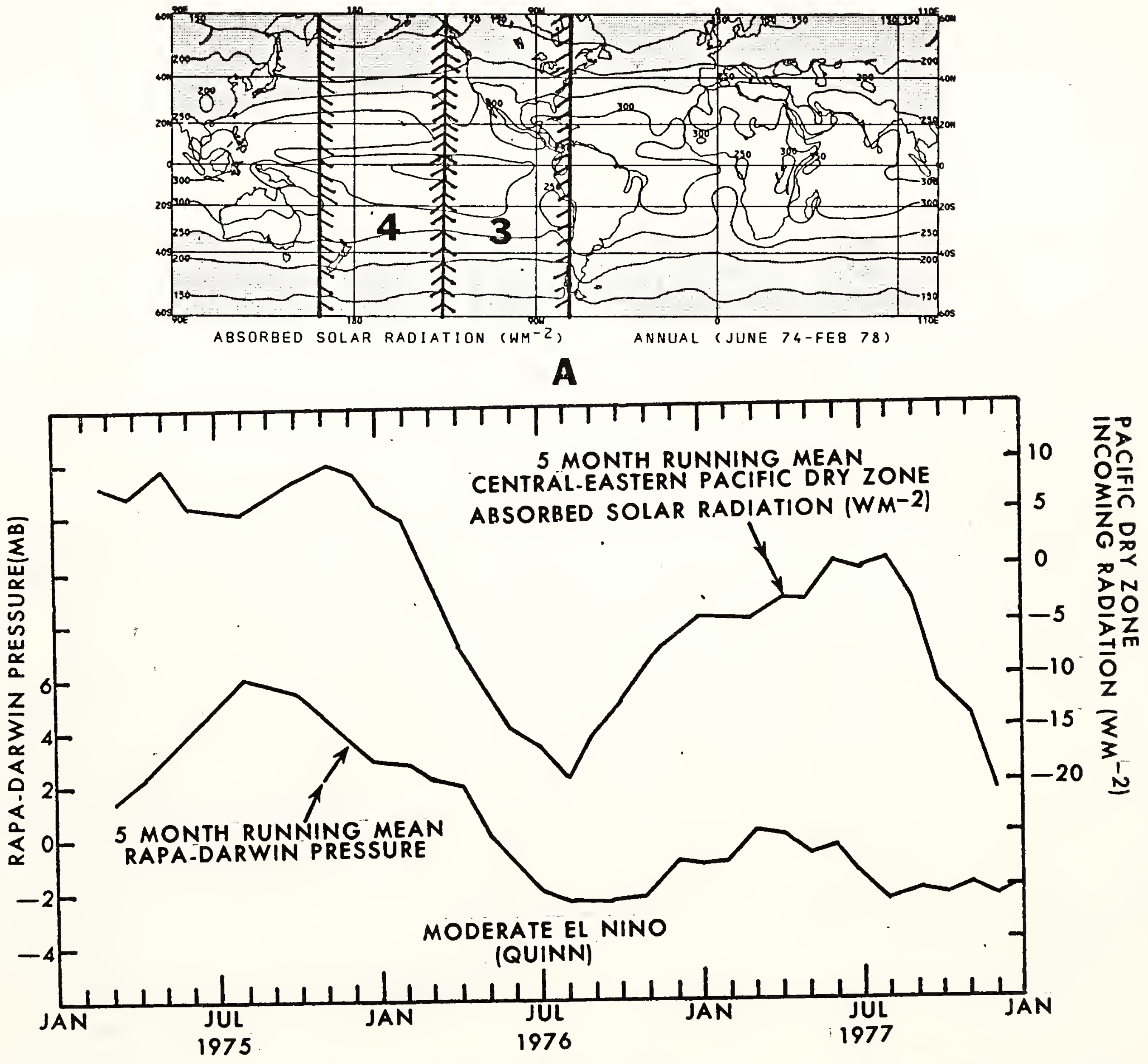

FROM CLAPP(1979)

**B**

Figure 3

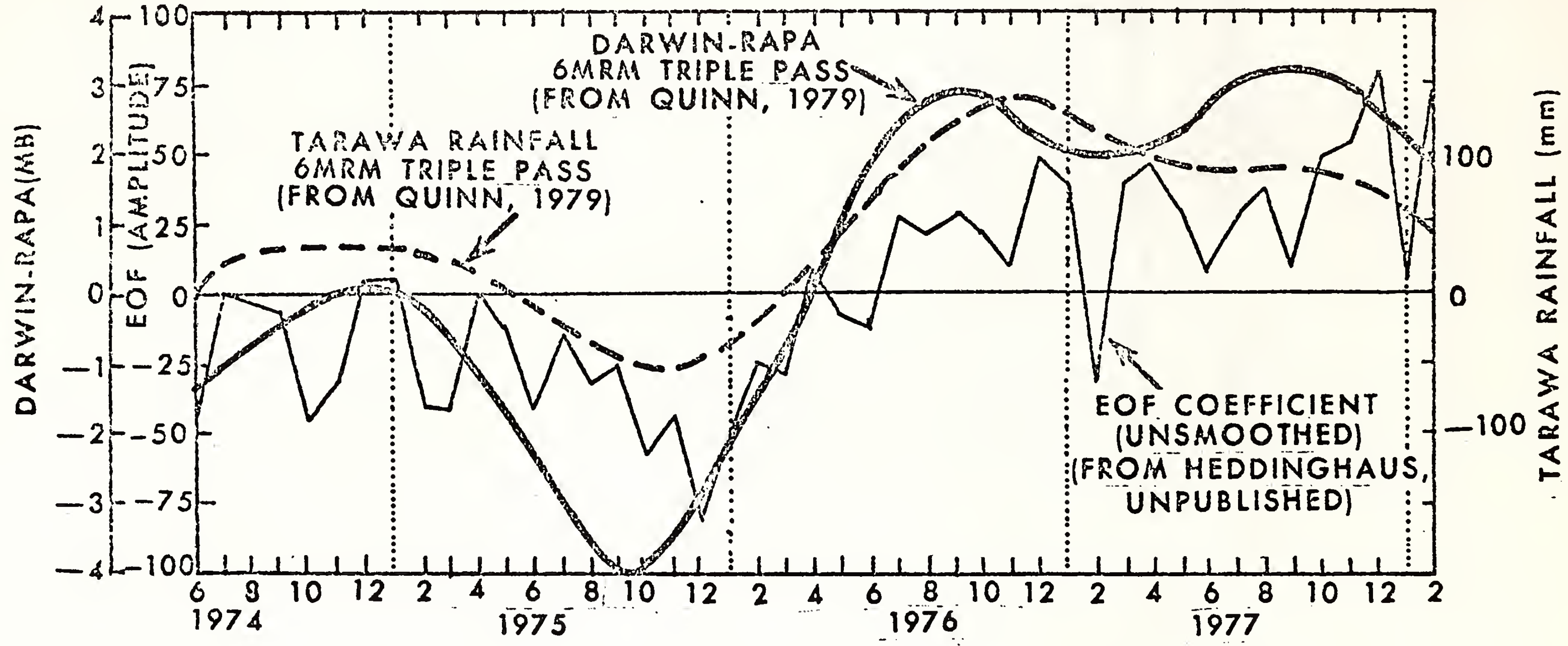
DARWIN-RAPA 6MRM TRIPLE PASS (FROM QUINN, 1979)
TARAWA RAINFALL 6MRM TRIPLE PASS (FROM QUINN, 1979)
EOF COEFFICIENT (UNSMOOTHED) (FROM HEDDINGHAUS, UNPUBLISHED)
DARWIN-RAPA(MB)
EOF (AMPLITUDE)
TARAWA RAINFALL (mm)
4
3
2
1
0
−1
−2
−3
−4
100
75
50
25
0
−25
−50
−75
−100
100
0
−100
6
8
10
12
2
4
6
8
10
12
2
4
6
8
10
12
2
4
6
8
10
12
2
1974
1975
1976
1977

Figure 4

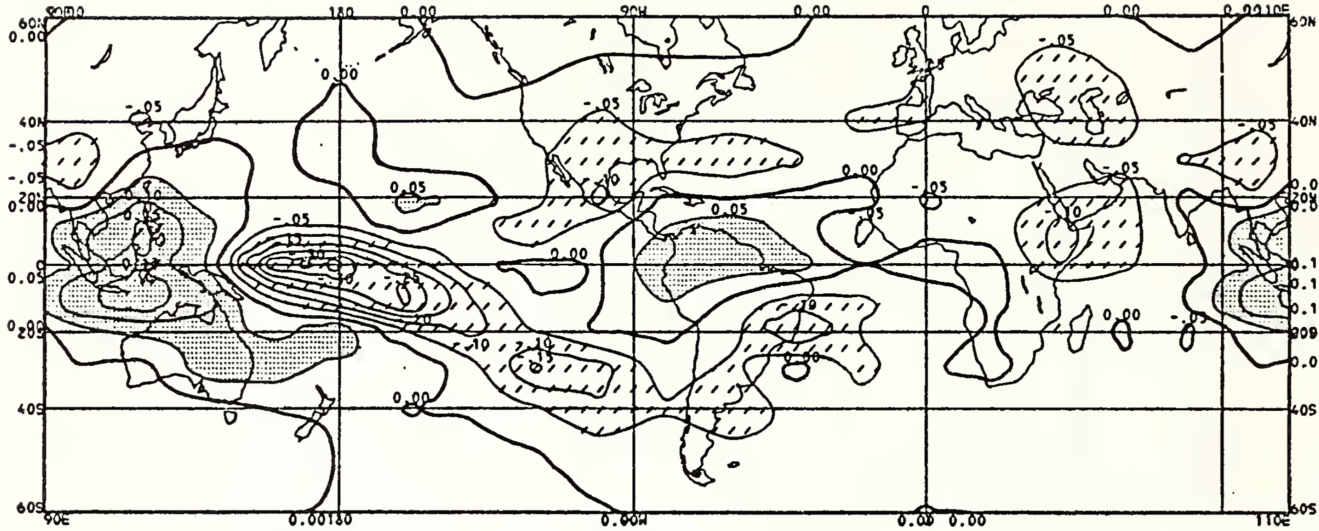

EIGENVECTOR 1 IN THE IR UNNORMALIZED WITH THE A&S CYCLES REMOVED

PERCENT OF TOTAL VARIANCE 13.06 CUMULATIVE VARIANCE 13.06

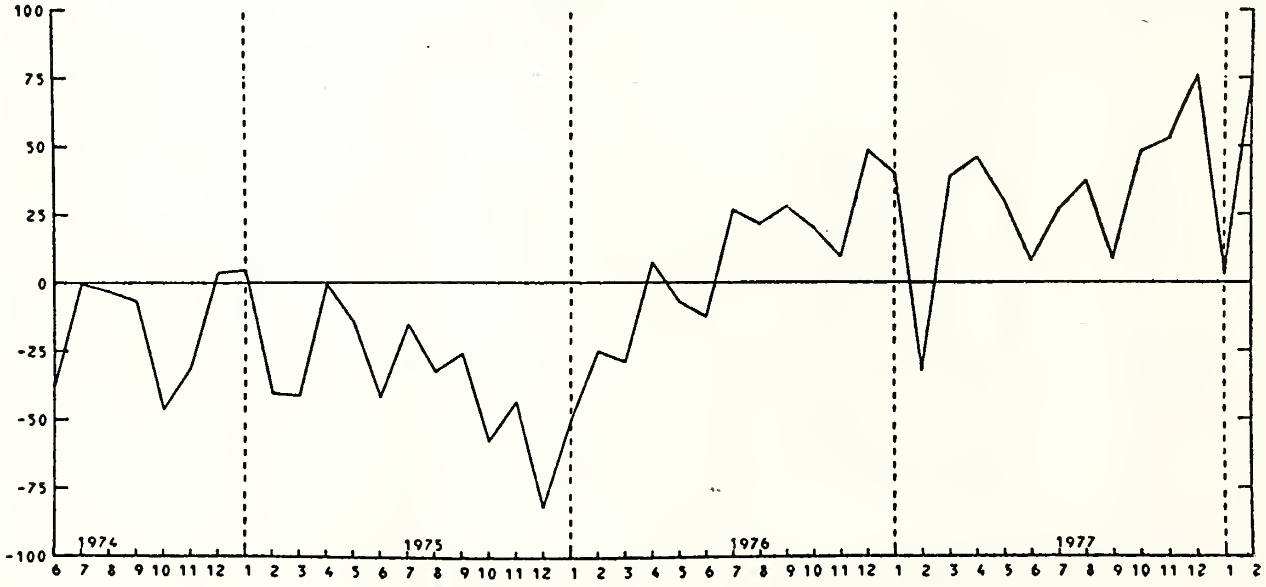

Figure 5

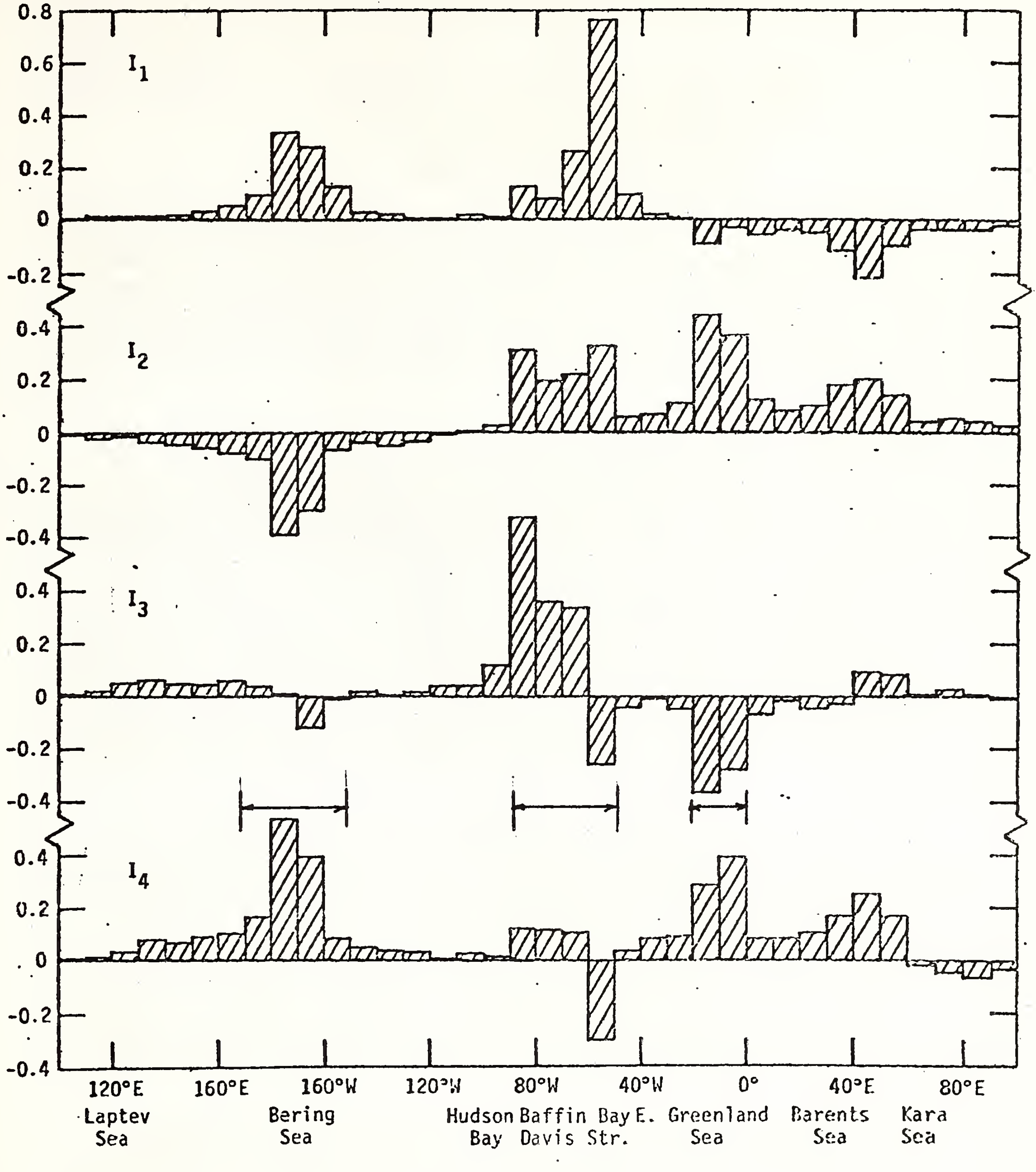

0.8
0.6
0.4
0.2
0
-0.2
0.4
0.2
0
-0.2
-0.4
0.4
0.2
0
-0.2
-0.4
0.4
0.2
0
-0.2
-0.4
$I_1$
$I_2$
$I_3$
$I_4$
120°E
160°E
160°W
120°W
80°W
40°W
0°
40°E
80°E
Laptev Sea
Bering Sea
Hudson Bay
Baffin Bay
Davis Str.
E. Greenland Sea
Barents Sea
Kara Sea

FIGURE 6

# Horizontal teleconnections during the Northern Hemisphere winter season

by

John M. Wallace and David S. Gutzler
Department of Atmospheric Sciences
University of Washington
Seattle, Washington 98195

Cross-correlation analysis of wintertime monthly mean 500 mb heights reveals the existence of five "teleconnection patterns" distributed over the Northern Hemisphere. Each pattern consists of two or more distinctly separated, geographically fixed centers whose 500 mb anomalies are strongly correlated with the anomalies at each other center. Thus, the teleconnection patterns represent standing oscillations in the 500 mb height field.

The primary data set used in this study contains monthly means of twice-daily NMC 5° x 5° gridded analyses for December, January, and February for fifteen winters beginning with the 1962-3 winter and ending with the 1976-77 winter. Individual cross-correlation maps, in which 500 mb heights at every grid point over the hemisphere are correlated with the simultaneous 500 mb height at a fixed base grid point, were calculated using each grid point as the base point. Fig. 1 was then constructed by plotting the magnitude of the lowest negative correlation from each individual cross-correlation map at the location of the base grid point. Regions which are not strongly correlated with distant points (lowest negative correlation not lower than -0.6) are unshaded; regions very strongly correlated with distant points (lowest negative correlation lower than -0.75) are stippled heavily. Arrows connect the strongest correlations.

We defined five patterns by examining in detail the regions of strongest correlation appearing in Fig. 1. Two patterns are spread over the eastern oceans and western continents. The Eastern Pacific (EP) pattern has centers at 20°N 160°W, 45°N 165°W, 55°N 115°W, and 30°N 85° W. The Eastern Atlantic (EA) pattern has centers at 25°N 25°W, 55°N 20°W, and 50°N 40°E. Representative cross-correlation maps (of the type used to construct Fig. 1) for an EP and an EA pattern center are shown in Fig. 2. The four cross-correlation maps having EP pattern centers as base points look remarkably similar, as do the three maps based on EA pattern centers.

A pattern index, defined as a linear combination of the height anomalies from the 15-month mean at each pattern center, was used as a basis for compositing. The sign of the index was defined so that positive EP and EA indices represented positive height anomalies at 55°N 115°W and 55°N 20°W, respectively. Defined in this way, a positive index is found to be associated with blocking over the west coast. EP composites are shown in Fig. 3; the EA composites are completely analogous.

Two additional patterns are north-south oriented "seesaws" situated in the western oceans near the axes of mean troughs in the 500 mb height field. The cross-correlation maps based on the northern centers of these patterns are shown in Fig. 4. These patterns are associated with the intensity of the major Northern Hemisphere mid-latitude jet streams; negative anomalies at the northern center and positive anomalies to the south represent a strong jet, and anomalies in the opposite sense represent a weak jet.

A fifth pattern covers the Eurasian continent, with centers located at 55° 20°E, 55°N 75°E, and 40°N 145°E. Two of these individual cross-relation maps are shown in Fig. 5.

Maps showing the correlation between each pattern index and simultaneous 500 mb heights over the hemisphere were calculated. The ± 0.6 correlation isolines from each of these five maps are shown superimposed upon the mean 500 mb height field in Fig. 6. A comparison of this summary plot with Fig. 1 shows that the five teleconnection patterns, taken together, cover a large fraction of the total "teleconnected area" of the hemisphere.

The reproducibility of the patterns was demonstrated using an independent data set containing 700 mb heights for the thirteen winters (1949-50 to 1961-62) preceding the winters contained in the primary 500 mb data set. One center from each pattern was preselected as the base point of a cross-correlation map using the 700 mb data set to determine if the same pattern observed during the later period was reproduced. The four oceanic patterns proved highly reproducible; the Eurasian pattern somewhat less so.

The first four modes of an eigenvector expansion of the 500 mb data set (Fig. 7) are composed of the same "centers of action" appearing in the five teleconnection patterns. The eigenvectors are optimized to explain the largest amount of hemispheric variance with fewer predictors than any other analysis scheme. However, the teleconnection patterns explain more variance locally, and they appear to be easier to interpret physically.

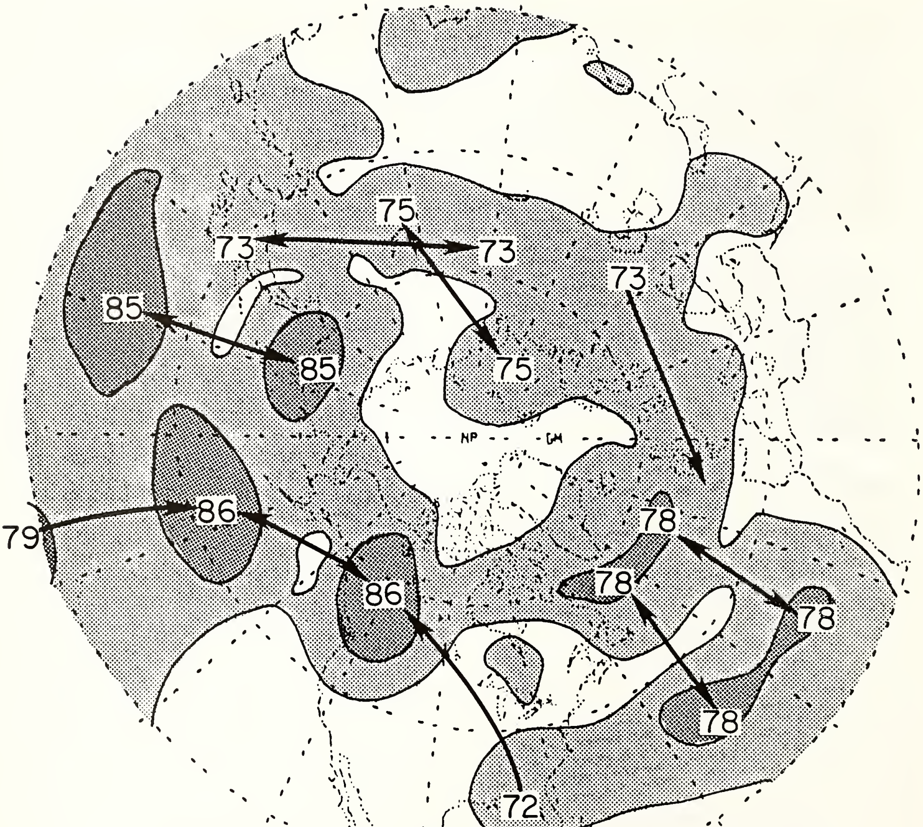

Fig. 1 Magnitude of the lowest negative correlation (R) found on each individual cross-correlation map, plotted at the location of the base grid point. Strongest correlations are labeled, with arrows locating the site of the correlation. R < • 6 unshaded, • 6 < R < • 75 lightly stippled, •75 < R heavily stippled.

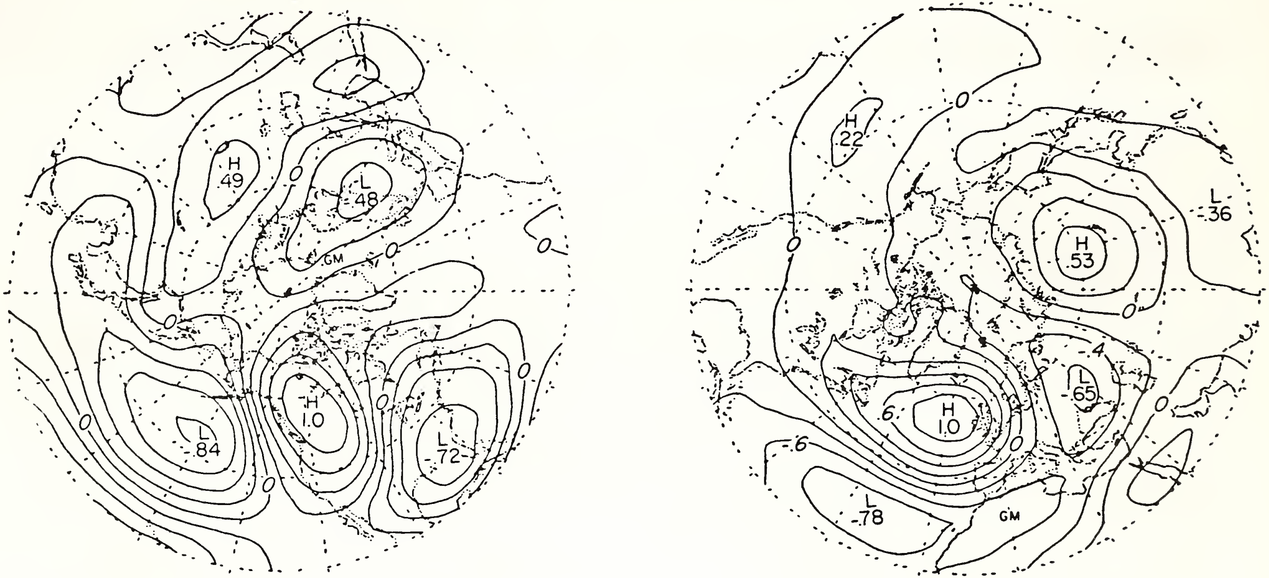

Fig. 2 Correlation coefficient between Northern Hemisphere 500 mb height and 500 mb height at (a) 55°N 115°W (b) 55°N 20°W. Contour interval 0.2.

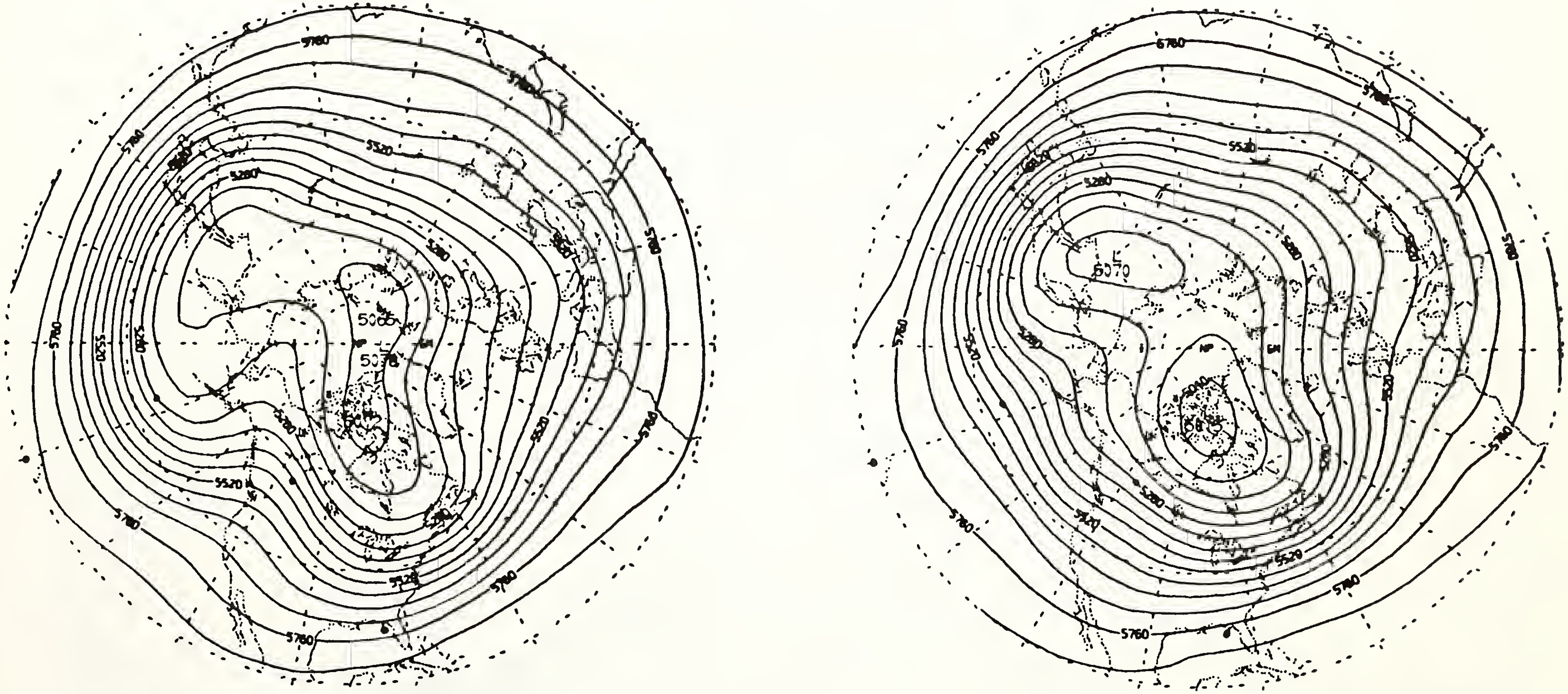

Fig. 3 500 mb composite for the twelve winter months with (a) highest (b) lowest values of the Eastern Pacific pattern index: index = z'(20°N 160°W) - z'(45°N 165°W) + z'(55°N 115°W) - z'(30°N 85°W)

Contour interval 60 m.

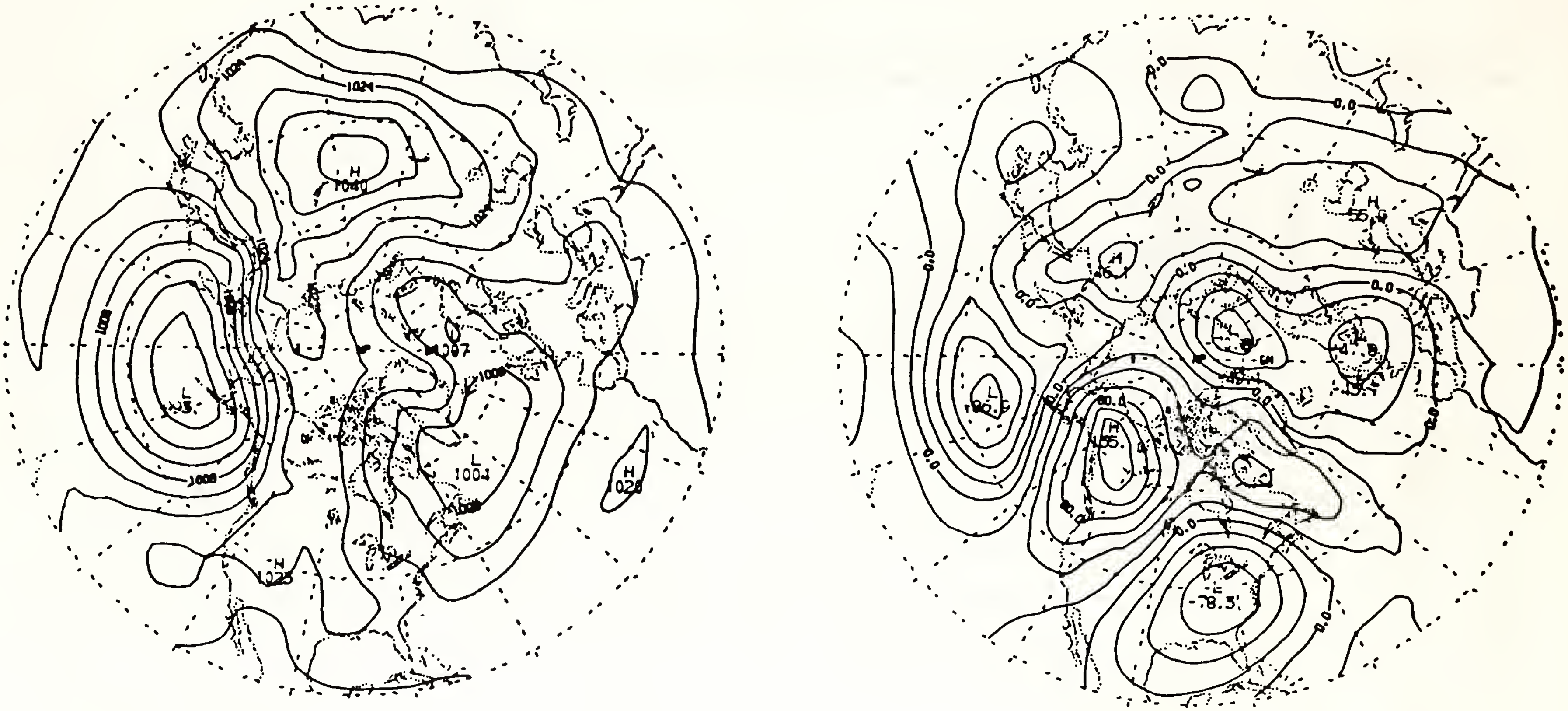

Fig. 3 c) Sea level pressure composite for the same months used in Fig. 3(a). Contour interval 4 mb.

d) Difference between the thickness composite for months used in Fig. 3(a) and months used in Fig. 3(b). Contour interval 20 m.

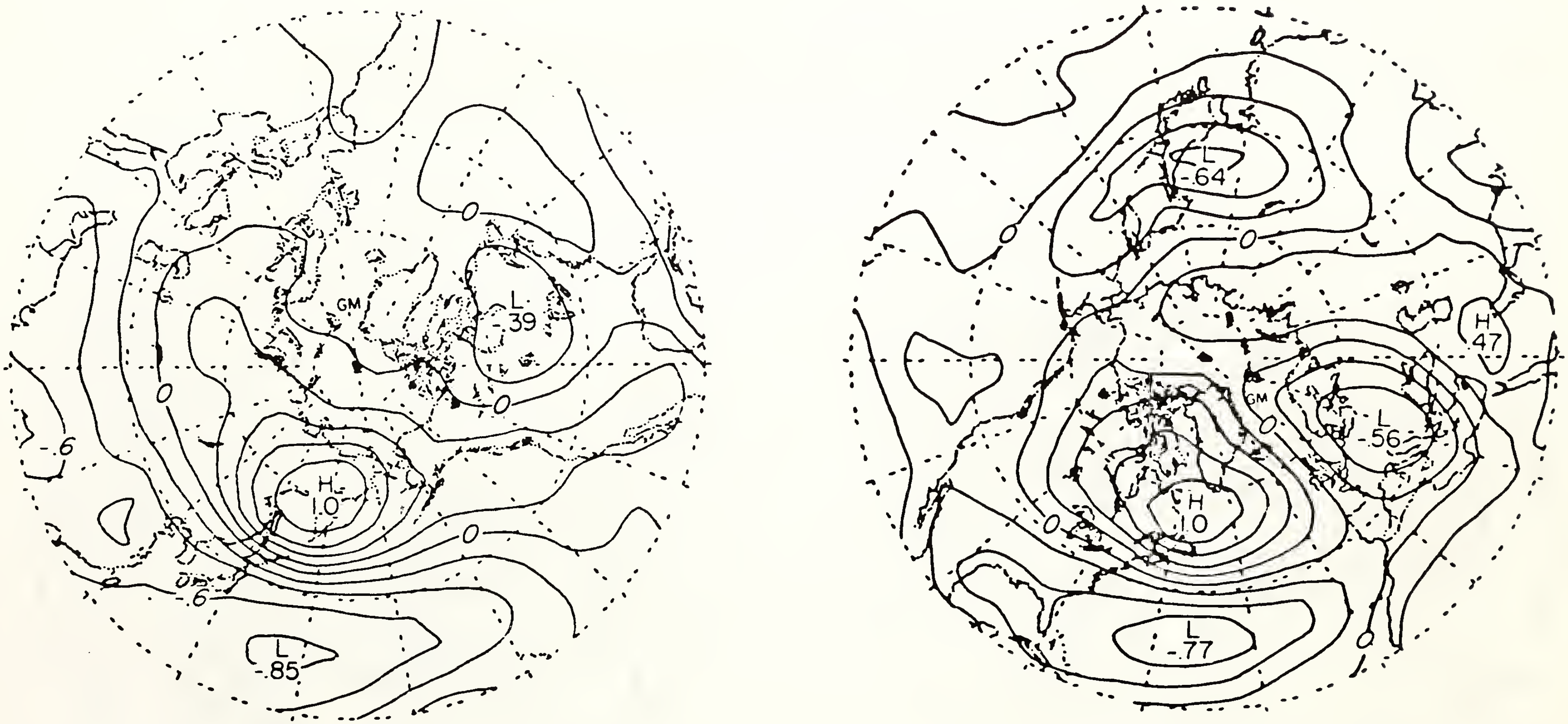

Fig. 4 Correlation coefficient between Northern Hemisphere 500 mb height and 500 mb height at
(a) 60°N 155°E

(b) 55°N 55°W

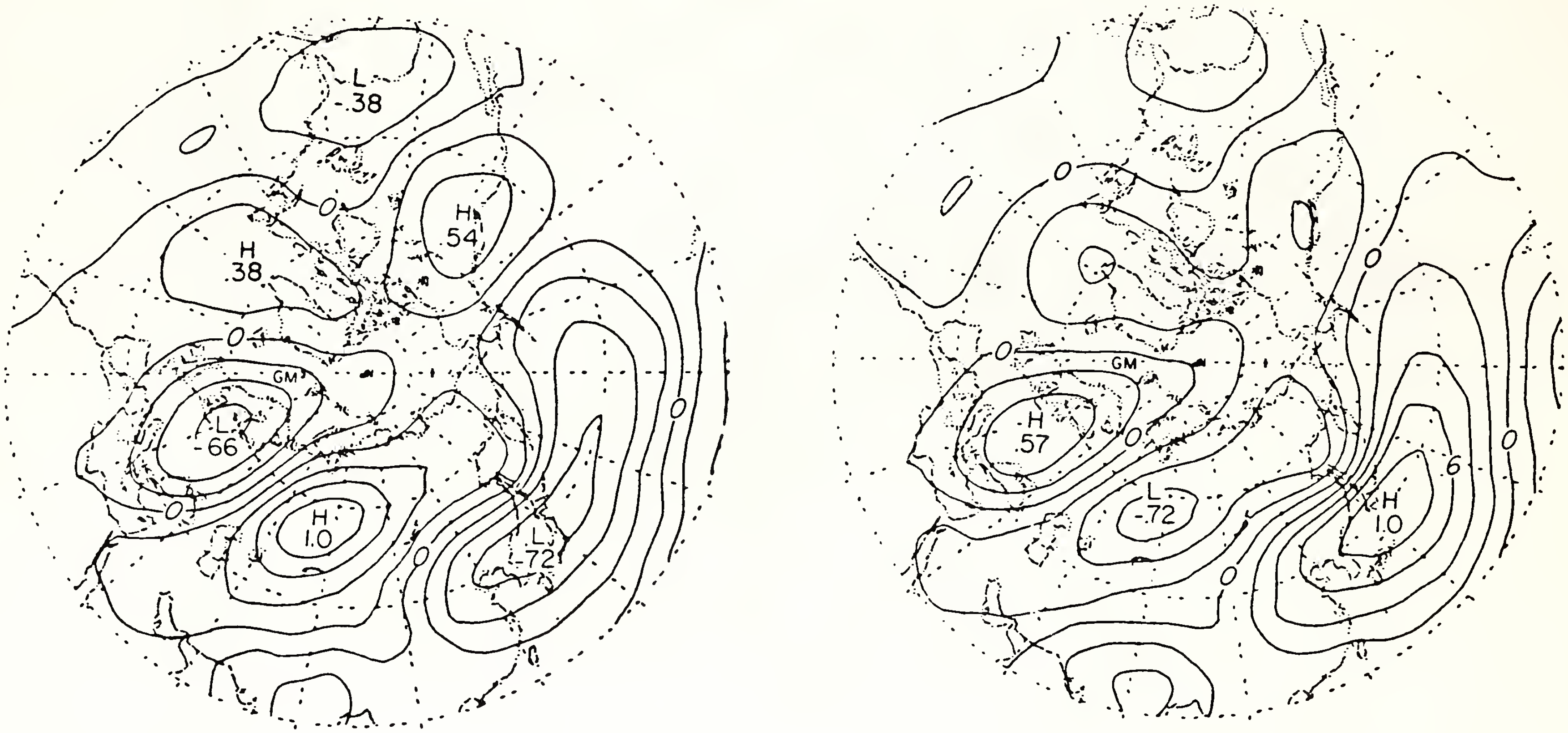

Fig. 5 Correlation coefficient between Northern Hemisphere 500 mb height and 500 mb height at
(a) 55°N 75°E
(b) 40°N 145°E

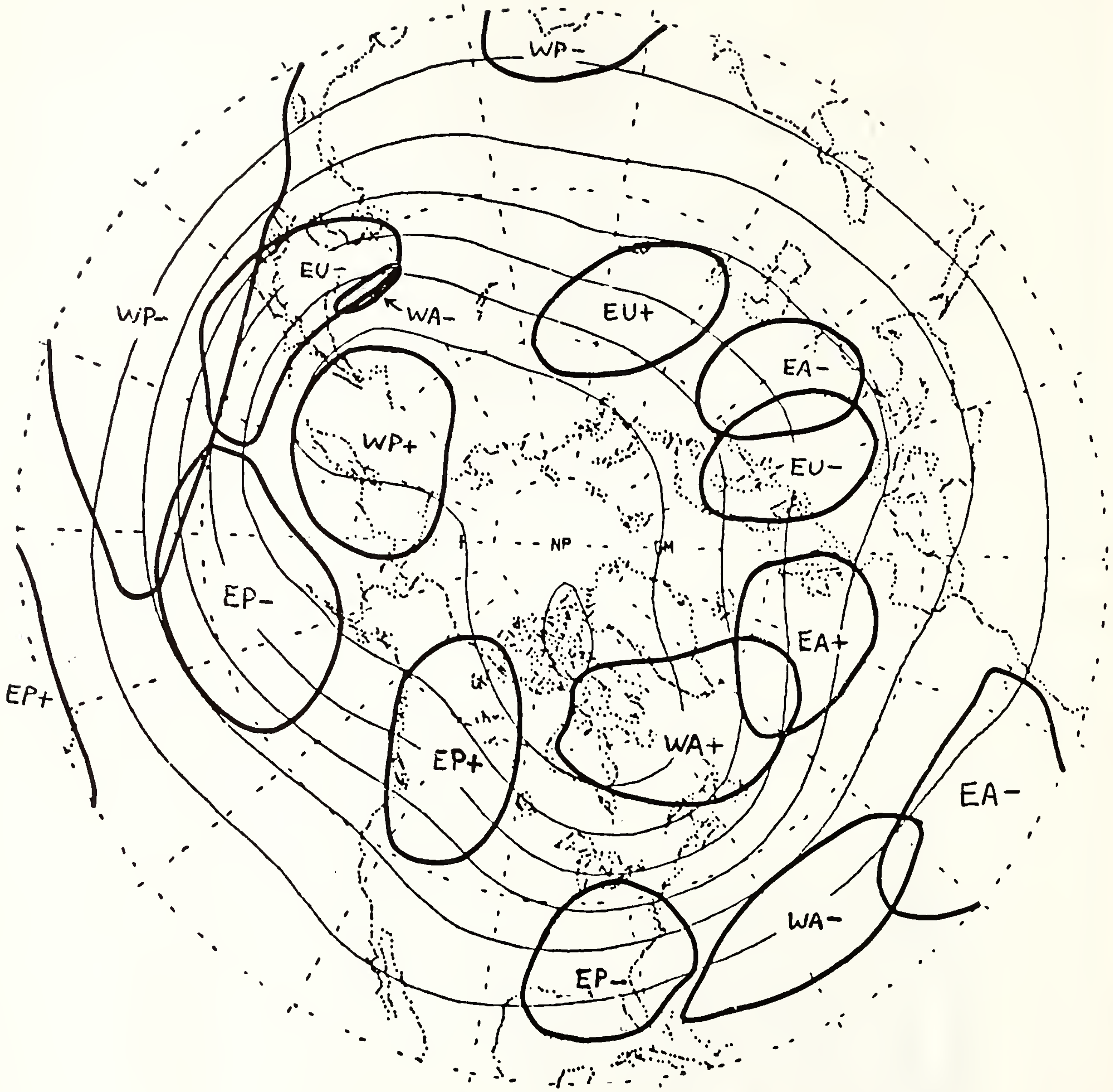

Fig. 6 Isolines of + 0.6 correlation adapted from maps for each pattern correlating the pattern index with Northern Hemisphere 500 mb height.

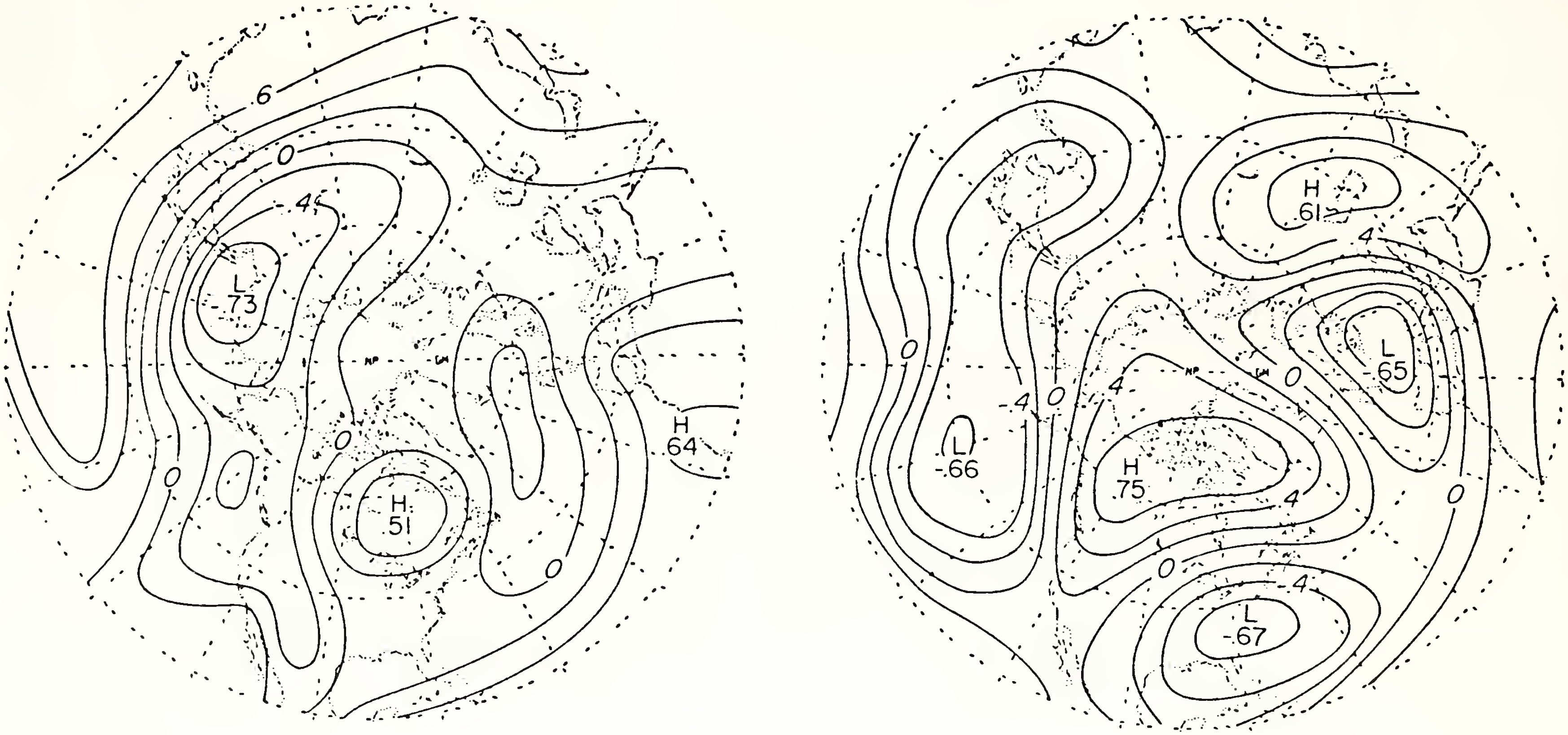

(a)

(b)

Fig. 7 Correlation coefficient between Northen Hemisphere 500 mb height and the (a) first (b) second (c) third (d) fourth mode of an eigenvector expansion.

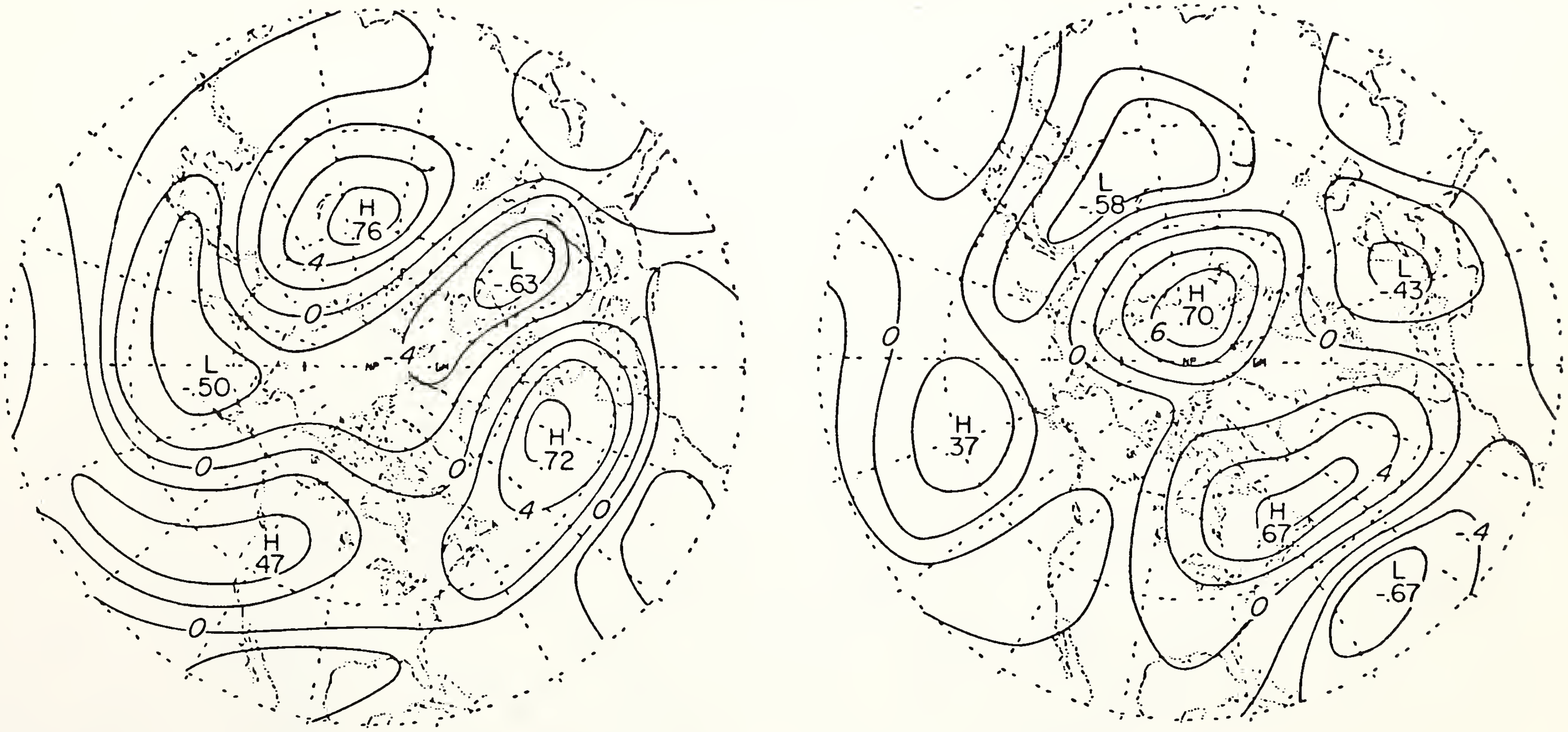

(c)

(d)

Fig. 7

# TRADE WIND ANOMALIES USING SATELLITE CLOUD MOTION VECTORS

James C. Sadler
Department of Meteorology
University of Hawaii
Honolulu, Hawaii

## 1. INTRODUCTION

Winds derived from geostationary satellite observed cloud drifts have been extensively evaluated by many people. Most evaluations have been in a research mode whereby carefully derived cloud vectors are compared individually with nearby rawinsonde observations with the consensus being that they are of equal quality. A few evaluations have also been made of time averaged satellite wind fields especially derived for projects such as data system tests. The results have been favorable notwithstanding the meteorological bias of the satellite winds. However, to my knowledge no comprehensive evaluation has been made of the winds derived routinely by the National Environmental Satellite Service (NESS). This is the data base which must be exploited for climate purposes over the tropical oceans. Toward this goal, we have been evaluating the NESS winds from the GOES East and GOES West satellites under the NORPAX, sponsored by the NSF. The work includes both the high- and low-level winds; however, in this presentation we will restrict the discussion to the low level and even further to the trade wind zone within the low-level wind field. The reasons for concentrating on the trade wind zones are many: (1) they are large scale and relatively homogeneous; (2) the quantity of satellite winds are a maximum over the zones because of persistent low-level cloudiness and infrequent obscuration by high-level cloud systems; (3) the directional shear is small from the surface to the cloud level thereby permitting better "ground truth" comparison with known climatological features obtained from ship reports; and (4) the intriguing scientific roles being hypothesized for the trade wind systems in the climatic scenes, particularly the Southern Oscillation.

## 2. DATA BASE, ANALYSIS AND EXTRACTION

The daily sawins from NESS are obtained through the NORPAX data center at monthly intervals, then averaged over grid sizes of 2° latitude by 10° longitude, plotted with model showing monthly resultant wind direction and speed, number of observations and steadiness. The number of observations per grid over the trade wind zones vary typically between 50 and 150 compared to ship winds of 0 to 10 per month.

A typical monthly analysis is shown in Fig. 1. The directional confluence line shown on Fig. 1 as a heavy line near 10N separates the northeast and southeast trades. For compatibility with previous work using averaged ship winds of 4.5 m/s, the trade index is defined as the area between the subtropical ridges with wind speeds $\geq$ 8 m/s. Initially we used the area x wind speed weighted average; however, as shown in Fig. 2 this is identical to using the simple method of just the area $\geq$ 8 m/s because when the core speed increases the area within the 8 m/s isotach increases proportionately.

## 3. TRADE WIND INDICES

The monthly NE and SE trade indices for the Pacific east of 180° since December 1975 are shown in Fig. 3 and the first 3-year average is in Fig. 4.

The 3-year average compares very favorably with the long-term average from ship reports. The N.H. index has an annual cycle with the maximum in March and April and the minimum in September and October whereas the S.H. index has a semiannual cycle with maxima in January and July and minima in April and November. The annual average index of the S.H. is approximately twice that of N.H.

## 4. TRADE WINDS AND THE SOUTHERN OSCILLATION

1976 experienced warm water anomalies along the equator and from the normally maintained indices of pressure, SST, and central equatorial Pacific cloudiness and rainfall; it was classed as a moderate El Niño year beginning in May. Ship observations have never been sufficient to determine a monthly trade wind index; however, the general hypothesis has the trade winds weaker than normal during an El Niño.

The sawin trade index anomalies shown in Fig. 5 confirm the hypothesis and further show that only the S.H. trades are responsible for the low index anomaly of the total trades.

## 5. SPATIAL ANOMALIES

We are beginning the production of monthly anomaly maps from the four to five-year satellite data base to further evaluate the data by comparison with known events. Figs. 6-9 show the anomaly fields over the Pacific between 30N and 30S for the Decembers of 1975-78, respectively. In 1975 (Fig. 6), the stronger trades of 1 to 4 m/s in the S.H. agree with the hypothesis that prior to the El Niño event of 1976 the trades should be stronger than normal. The N.H. trades would not have participated in this hypothesized buildup of sea level in the western Pacific, but in fact just the opposite, for the NE trades in the east-central Pacific were 1 to 4 m/s weaker than average.

During the El Niño December of 1976 (Fig. 7), the trades were weaker than normal by 1 to 6 m/s over most of the SE trades region or just the opposite of 1975. Again the NE trades anomaly in the east-central Pacific was opposite to that of the SE trades. The weakening of the SE trades and the more northerly anomaly of the NE trades west of 130W may account for the slight equatorward shift of the convergence zone which is observed by the satellite cloudiness during an El Niño.

During December 1977 (Fig. 8), there was no large regionwide anomaly pattern; however, the pattern west of 140W in the equatorial and south Pacific corresponds well to the meteorological events observed during the NORPAX Hawaii to Tahiti shuttle conducted by research aircraft and ships along 150W and 158W. The more easterly anomaly south of 15S and the strong westerly anomaly in the equatorial zone produced a rather strong zone of cyclonic shear extending from 10S 175W to 15S 145W which coincided with a very active zone of tropical depression formations with one attaining near hurricane force winds on 6 December at 13S 150W. The strong equatorial westerly anomaly was related to a record monthly rainfall at Canton Island.

Very strong trade winds occurred in the Hawaiian Islands during early December 1978, resulting in the loss of the research ship Holo Holo and its entire crew. This strong anomaly as depicted in Fig. 9 extended only to 15N. Again in December 1978 westerly anomalies occurred in the equatorial region of the central Pacific which was the third winter in succession. As mentioned earlier these are related to positive rainfall anomalies and in a teleconnection fashion to an increase in strength of the subtropical jet across the southern United States which has been observed for the past three winters.

In summary, I have demonstrated the satellite derived low-level winds to be an excellent data base for observing the climatic variations of the trade wind systems. We should now exploit these data to not only test the many hypotheses which have included the poorly observed trades from infrequent ship reports but to explore their true role in climate fluctuations.

Maximum benefit from satellite winds can be achieved only by establishing a global standard methodology for deriving the winds. This seemingly obvious requirement is not even mentioned in the FGGE planning.

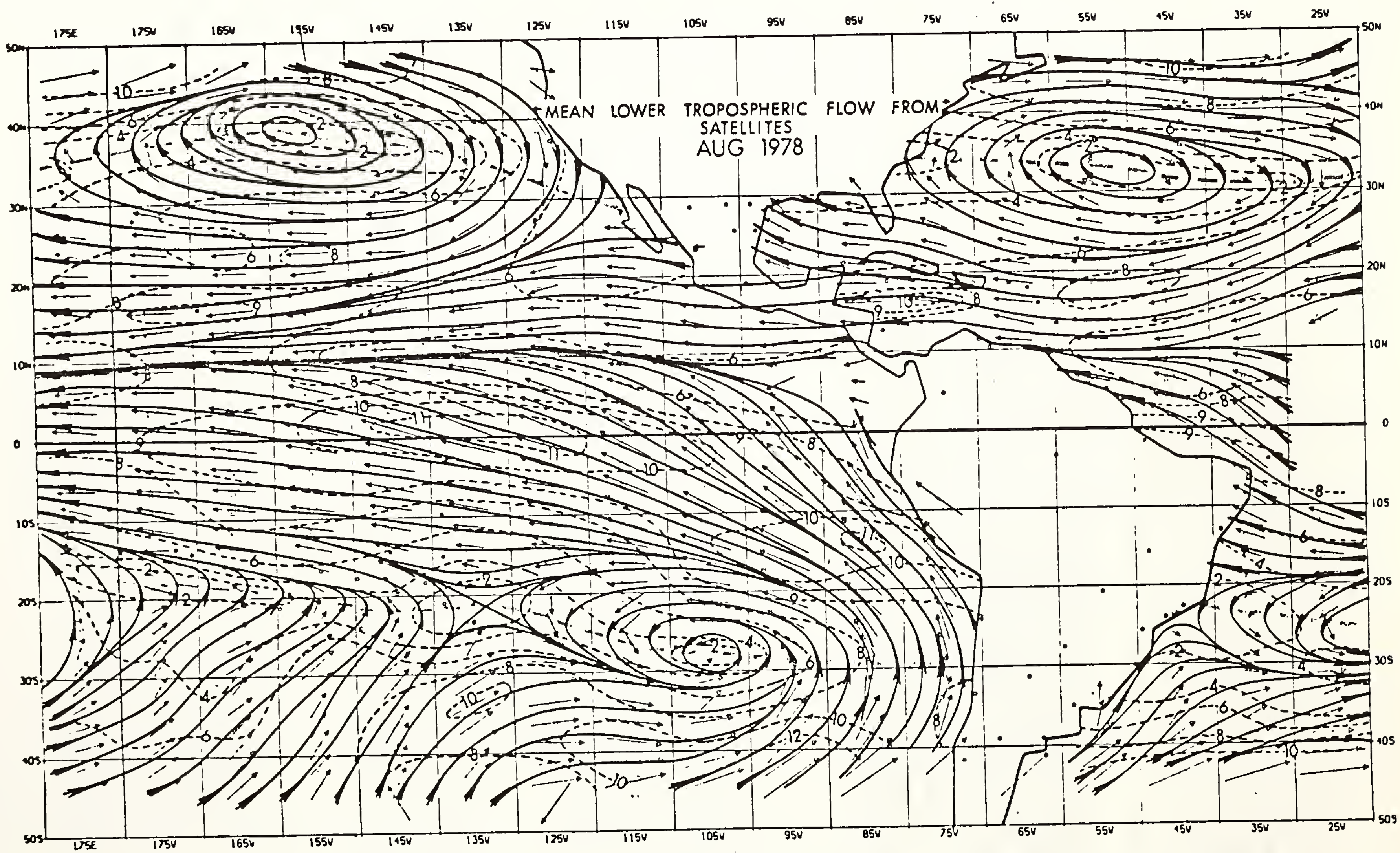

Fig. 1 Mean low-level wind analysis for August 1978 using GOES satellite observed cloud vectors. Units: m/sec.

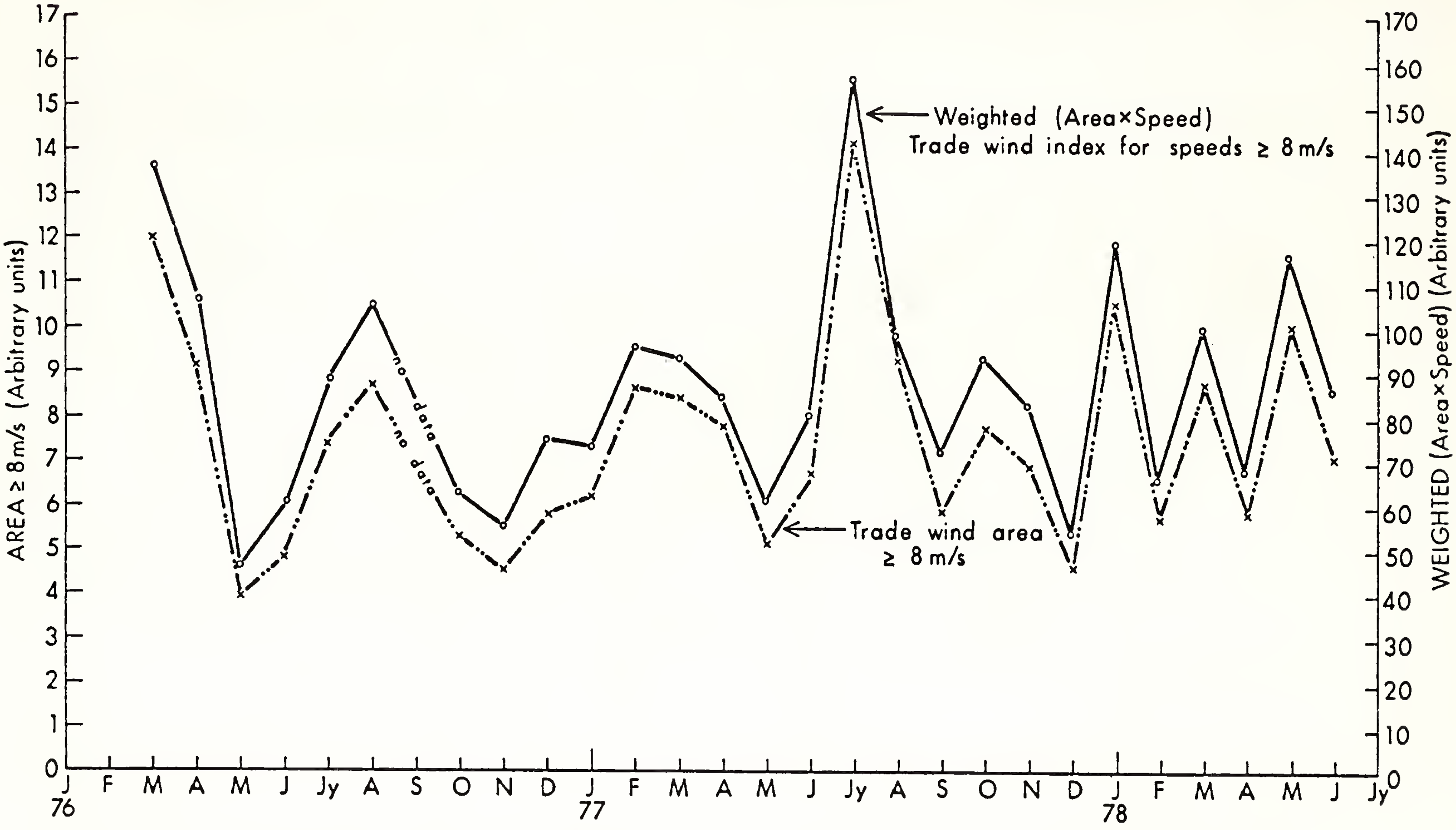

Fig. 2 Relative comparison of trade wind index curves determined from weighted area x speed method and simple area $\geq$ 8 m/s method.

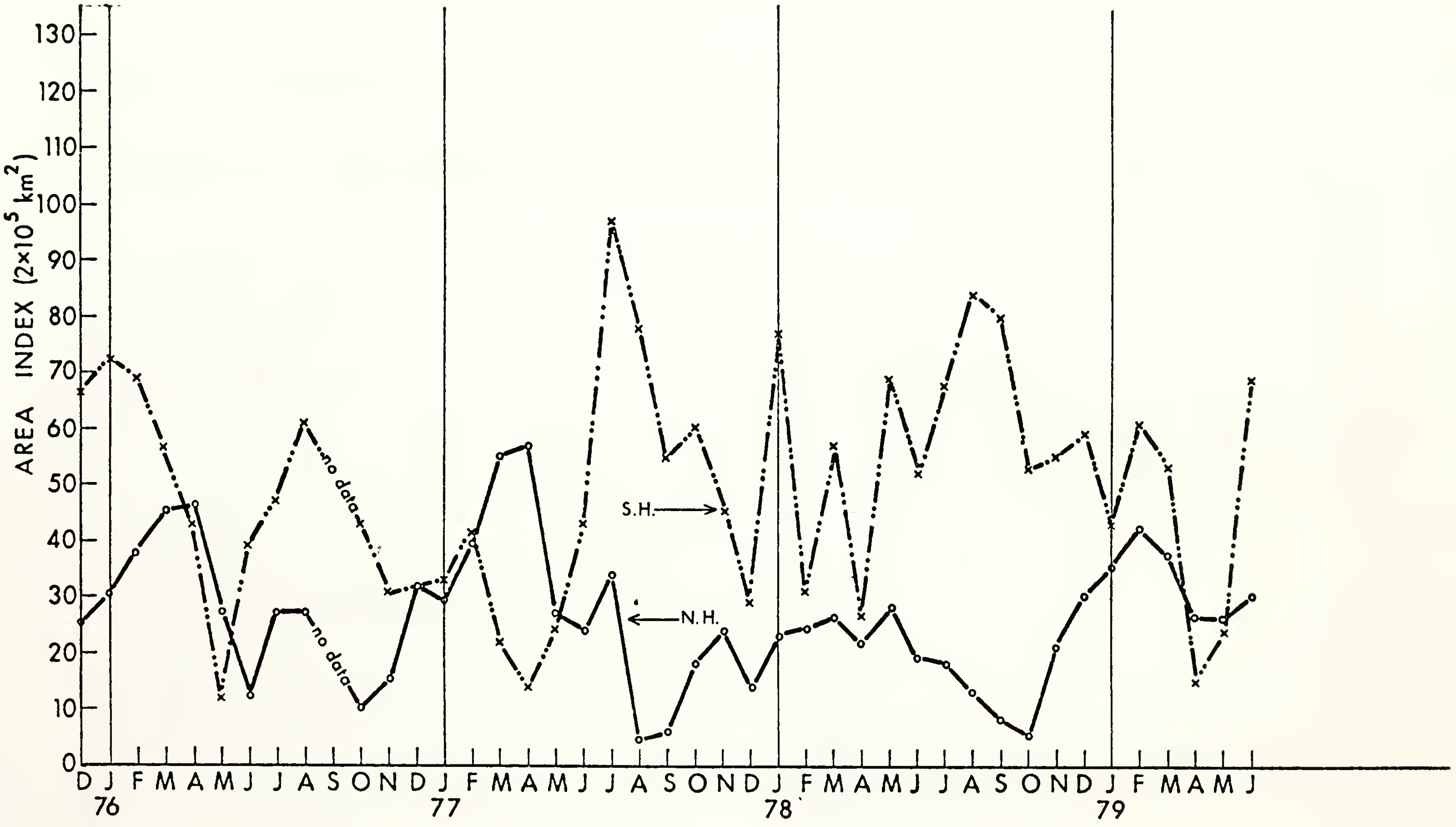

Fig. 3 Monthly indices of the Northern Hemisphere and Southern Hemisphere trades between 180 and the west coast of the Americas.

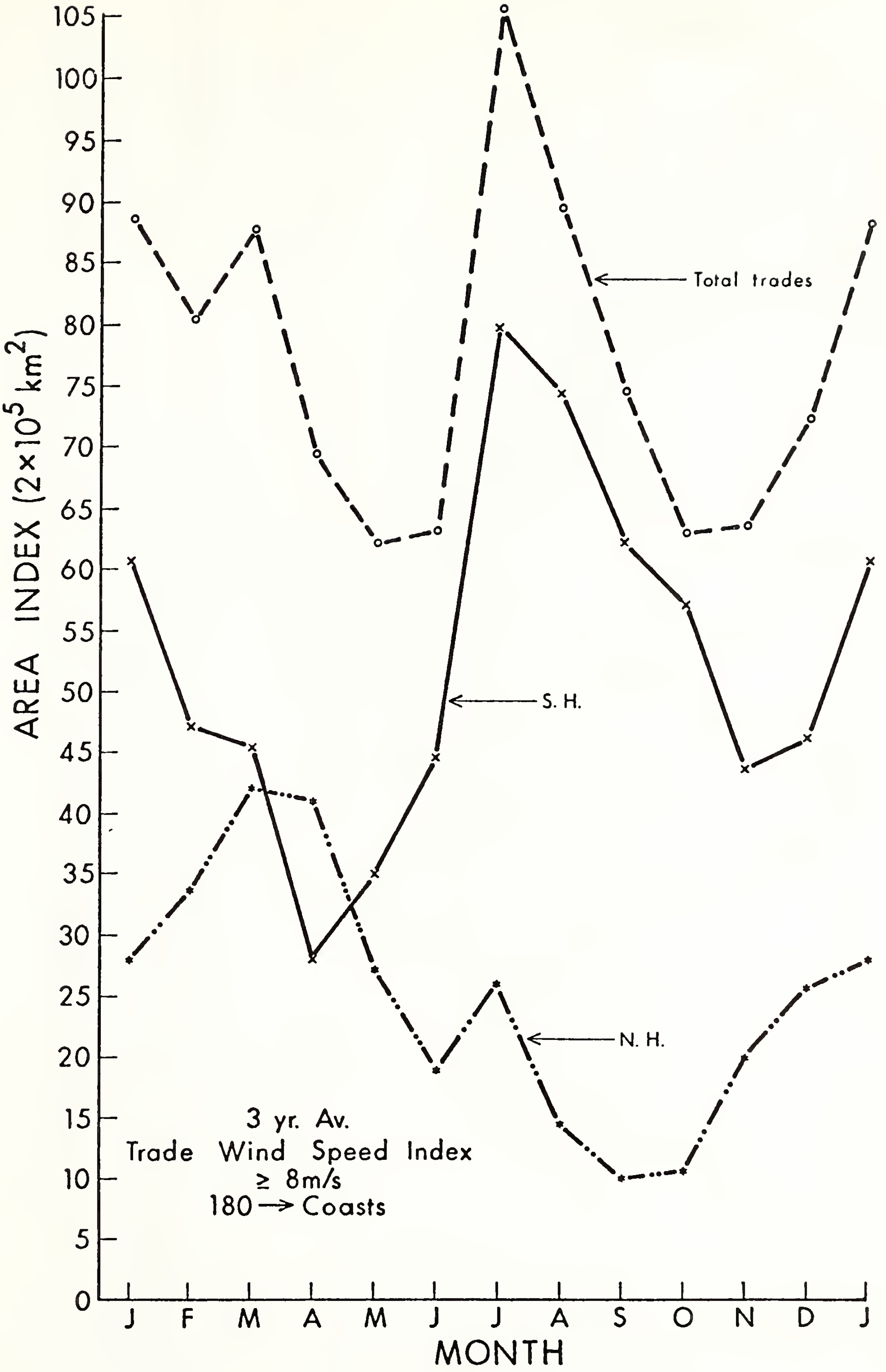

Fig. 4 Three-year average trade wind indices.

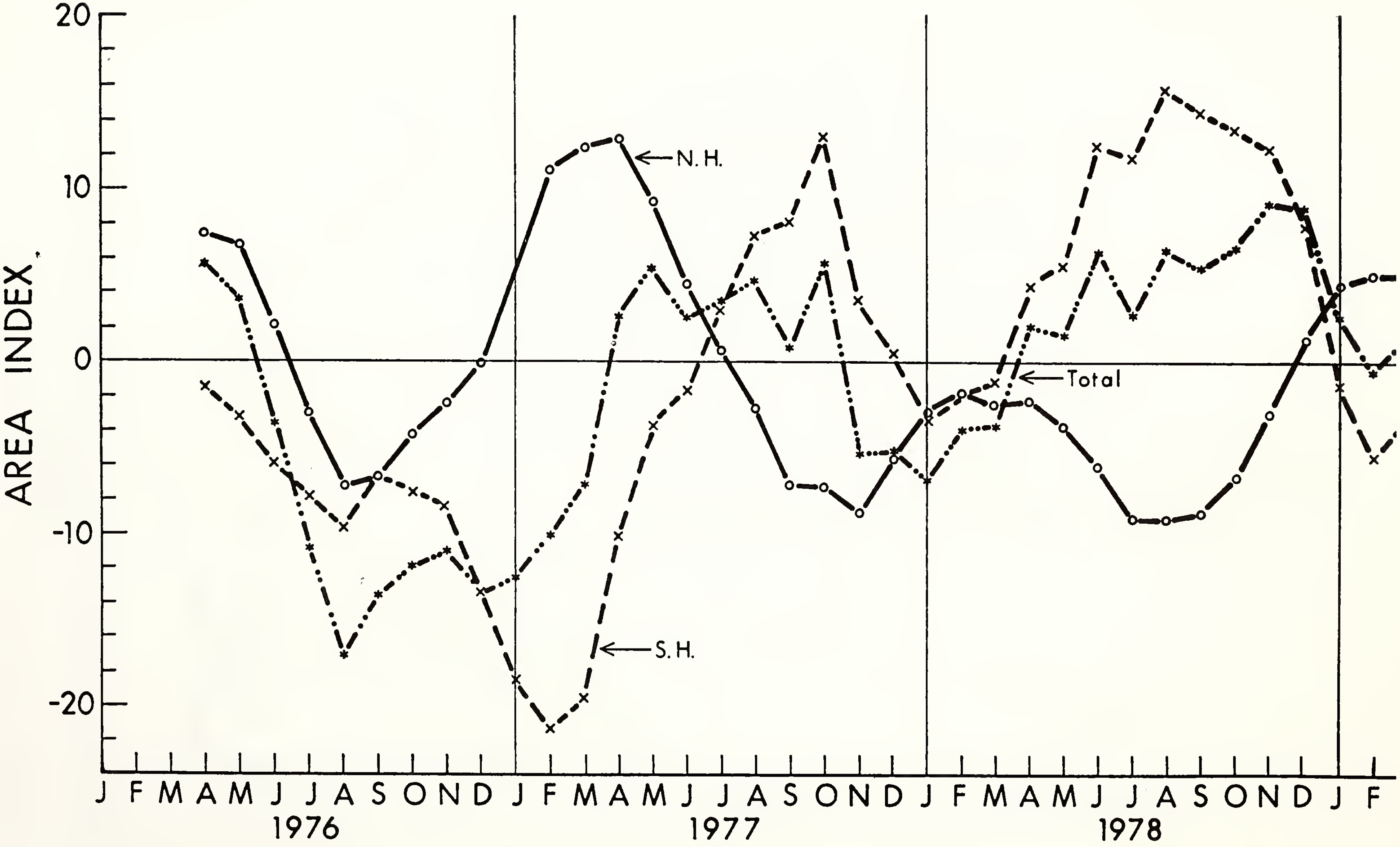

Fig. 5 Seven-month running means of East Pacific trade wind indices expressed as departures from 3-year annual mean.

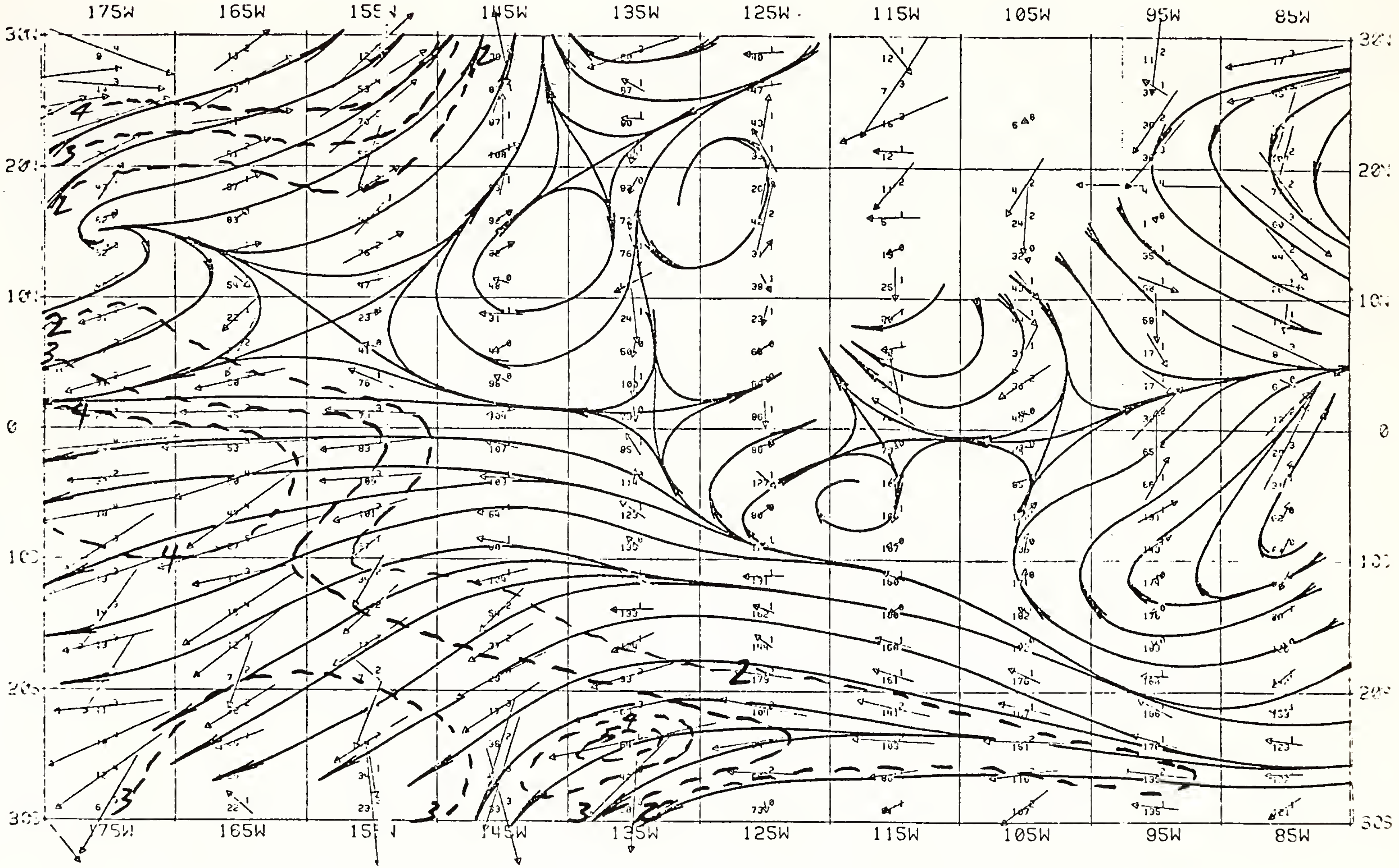

Fig. 6 LOWER LEVEL SAT WINDS (M/S) DECEMBER 1975 ANOMALY FROM 5 YR MEAN

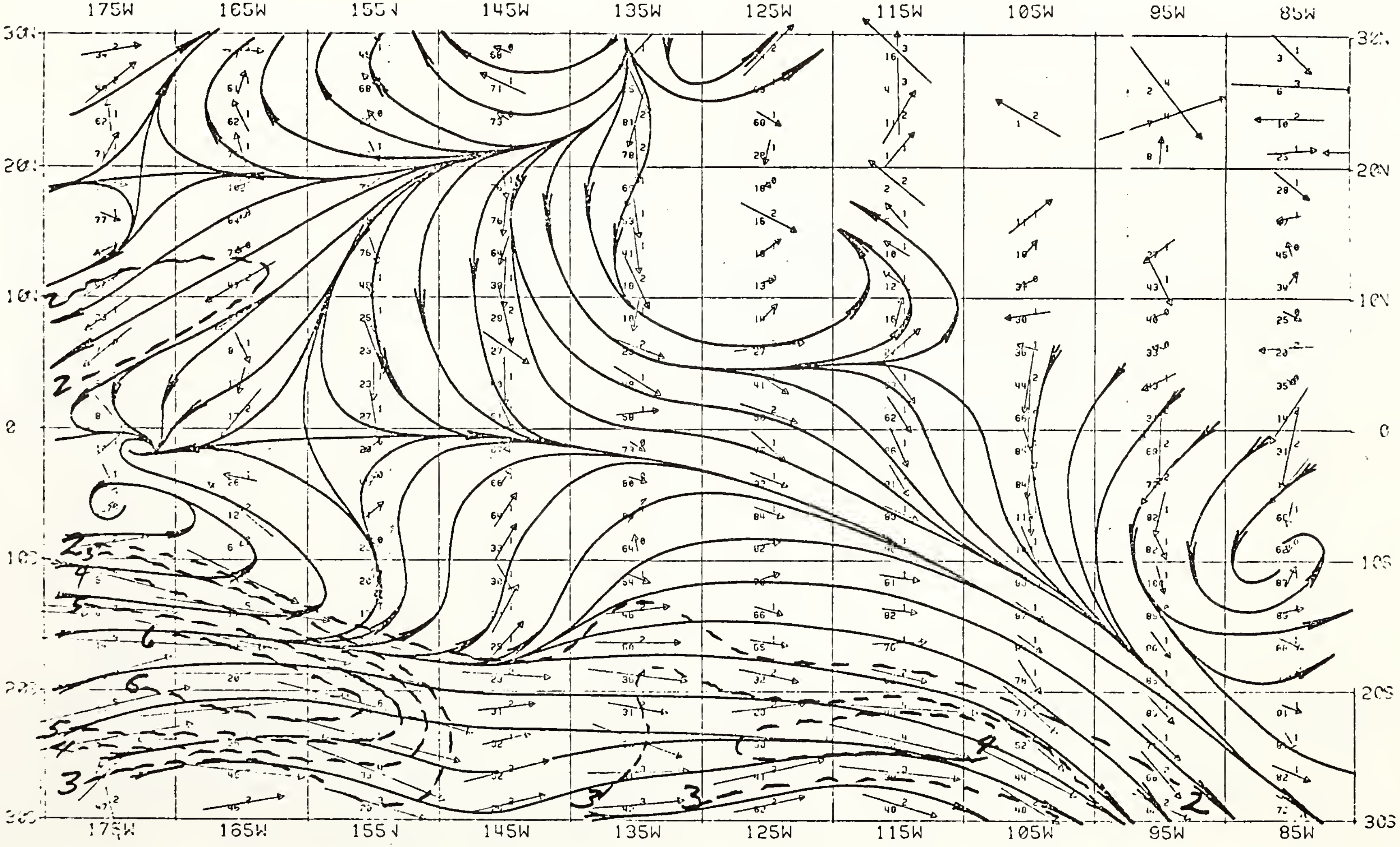

Fig. 7 LOWER LEVEL SAT WINDS (M/S) DECEMBER 1976 ANOMALY FROM 5 YR MEAN

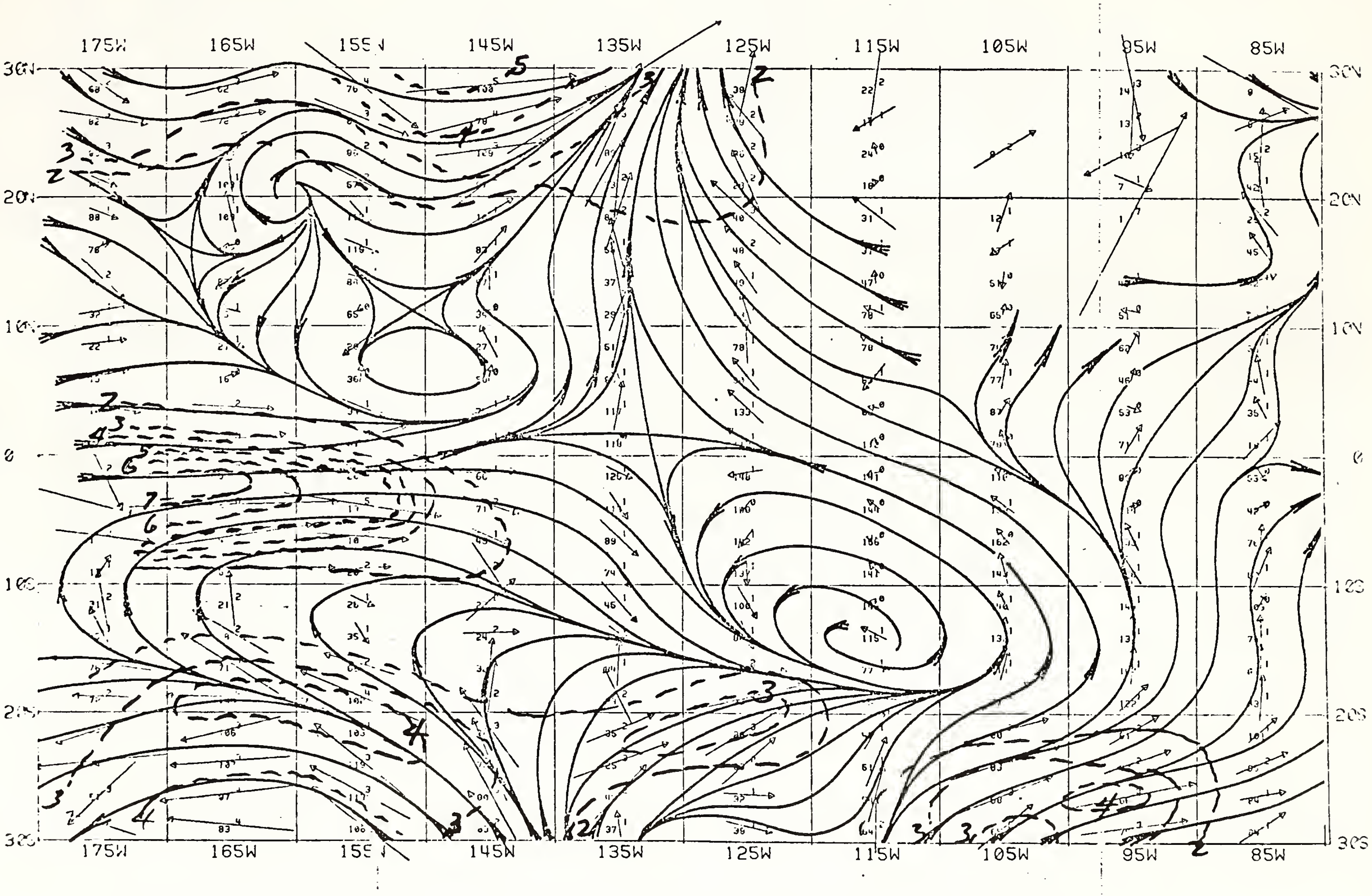

Fig. 8 LOWER LEVEL SAT WINDS (M/S) DECEMBER 1977 ANOMALY FROM 5 YR MEAN

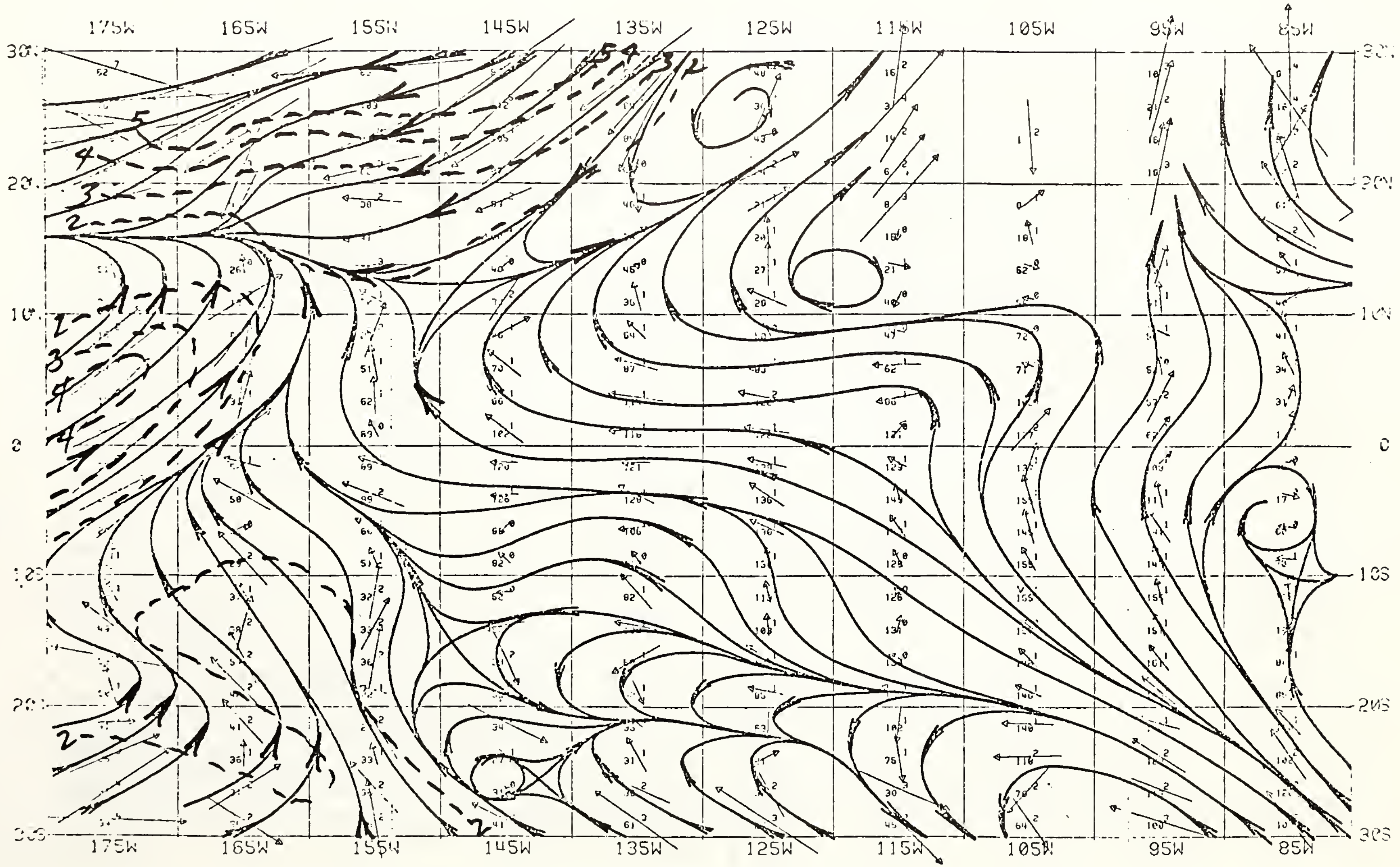

Fig. 9 LOWER LEVEL SAT WINDS (M/S) DECEMBER 1978 ANOMALY FROM 5 YR MEAN

# THE NMC OPERATIONAL ENERGY CODE
## Its Use In Date Base Evaluation

A. J. Miller and T. G. Rogers
Analysis and Information Branch/CAC/NMC/NOAA
Washington, D. C.

## I. Introduction

Throughout the course of this workshop, definitions of climate have been presented that are considerably varied, but with essentially one element in common. That is, to determine the climate we need a data base. But not just a data base, one that is stable and controlled in time. The reality, however, is that when considering the global aspect of climate, we are using a data base that is very much non-stationary in time. Our observational systems are constantly evolving and we must wage a continual battle to determine the effects.

For example, in Figure 1 is presented a map of rawinsonde stations (dots) and pilot balloon stations (crosses) for the 1976-1977 winter (Rosen and Salstein, 1979). Included also (triangles) are the positions of several stations that have been deleted from the data base since the early 1960's (Oort and Rasmusson, 1971). The impact of the removal of these stations is to increase the gaps in the data especially in the Atlantic Ocean area and Rosen and Salstein (1979) discuss the impact.

One recourse is to utilize the satellite retrievals that have been produced operationally for some time. The difficulties with this approach are that winds are not generally provided in the global sense and the data are not over the same spot on a day-to-day basis. This means that an analysis technique would have to be developed or alternatively we may utilize the operational analysis products available from the NWS. Here again, the product is undergoing constant evolution and Table 1 lists several major changes in the analysis system that have been incorporated since 1975. The magnitude of the impact of each of these changes on a climate data base have not been determined and clearly their utilization as such requires some caution.

Since January 1975 the National Meteorological Center has been running, twice daily, an atmospheric energy budget (or at least certain terms thereof) from the global final analyses (Miller et al., 1975). While our original interest in developing this program was on the basis of climate research, over the years the emphasis has actually been in evaluating the data base for the impacts of some of the changes described above. Our purpose here is to present a few examples of this type of effort that should illustrate the problems of data base management.

The parameters utilized in this study are AZ and AE, the zonal and eddy available potential energy, respectively, and KZ and KE the zonal and eddy kinetic energies. These are defined by

$$AZ=\frac{R}{2}\frac{1}{p_0^{\kappa}}\frac{p^{\kappa-1}\overline{\theta''^2}}{-\overline{\dfrac{\partial\theta}{\partial p}}},$$

$$AE=\frac{R}{2}\frac{1}{p_0^{\kappa}}\frac{p^{\kappa-1}[\theta^{*2}]}{-\dfrac{\partial\bar{\theta}}{\partial p}},$$

$$KZ=\tfrac{1}{2}(\overline{[u]^2}+\overline{[v]^2}),$$

$$KE=\tfrac{1}{2}[\overline{u^{*2}+v^{*2}}],$$

Where R is the universal gas constant, P the pressure (subscript zero referring to 1000 mb), k the gas constant divided by the specific heat at constant pressure, Θ the potential temperature and u and v are, respectively, the zonal and meridional wind speeds. The following is a list of additional symbols;

| | |
|---|---|
| [S] | average around a latitude circle or zonal average |
| S* | departure of S at any point from the zonal average |
| $\overline{S}$ | areal average |
| S" | departure of the zonal average from the areal average [S] - $\overline{S}$ |

In essence, AZ and KZ define the zonal mean mass gradient and motion, respectively, while AE and KE describe variance about these mean states.

## II. Tropical Energy

The first example is shown in Figure 2 which shows the average monthly zonal (KZ) and eddy (KE) kinetic energy at 200 mb for the tropical strip 20 N - 20 S, 1975-1979. Also indicated (arrows) are the times of the modifications made to the analyses at NMC. It was originally suggested by Arthur Krueger that the wave patterns in the tropics seemed greater than previously when the OI analysis was introduced in late 1978. We see that the KE results are in fact, slightly greater than the previous 2 years, but if we disregard the large values in January '76 for the moment, this increase seems part of a trend from 1975. Is this trend real or an artifact of the changing analyses - we do not know. It is interesting, however, to note that the large peak in KE in January '76 was during the DST test when major modifications were made to the analysis and also the large minimum in KZ in February '77 was the month after the 6 hour forecast-analysis cycle was introduced.

In summary, it is clear from this diagram that the analysis procedures must be considered as an integral part of the climate diagnostics.

## III. August 1975 Data Systems Test

The second example is one taken from a recent publication by Miller and Hayden (1978) on the impact of satellite-derived temperature profiles on the NMC analyses during the August '75 Data Systems Test. Miller and Hayden (1978) and Tracton and McPherson (1977) discuss in detail the nature of the systems test and this is summarized in Table 2. We see that for the Northern Hemisphere there were 3 parallel analyses produced for the period 18 August - 4 September. System 1 included all data, System 2 all but the satellite temperature retrievals and System 3 all but the radiosonde reports.

Figure 3 presents the average (Aug. 18-23) AZ and KZ values integrated over the domain 20 N - Pole for each system and plotted as a function of pressure. In addition, on the right is listed the ratio of the values Sys 3/ Sys 2 and Sys 1/Sys 2. Here we see that the impact of the satellite data is to reduce the zonal mean mass gradient in the lower atmosphere, but that the available radiosonde etc. reports help compensate for this effect. In a somewhat similar fashion the zonal kinetic energy diagram indicates that while the analysis of the satellite temperature retrieval data has a tendency to reduce the zonal kinetic energy, the addition of the radiosonde data is able to bring the values for System 1 and 2 generally within about 1% of each other. This suggests that the radiosonde observations overwhelm the analysis wind law.

For the wave motion fields, AE and KE, the results are presented in Figure 4, and are very different from the zonal gradient components. The System 3 AE is considerably reduced from that of System 2, the ratios indicating about a 40% reduction at the AE maximum at 300 mb. Including the radiosonde data tends to diminish the reduction, but it cannot compensate completely such that about a 20% reduction is maintained. The eddy wind component, KE, indicates that the System 3 reduction is quite apparent as would be expected from the AE results, but System 1 and System 2 results are nearly identical. Once again, this suggests that the wind observation overwhelm the analysis wind law in controlling the analyses.

In summary, the results of this experiment for which the satellite data are very similar to that currently available on the Tiros-N series spacecraft, indicates a profound effect on the NMC temperature analyses. While a similar experiment has not yet been carried out for the current operational analysis system, our purpose here is to point out the type of problem that can exist and to raise the question as to how to handle it from the climate point of view.

## IV Hemispheric Diurnal Cycle

The final example of data base evaluation is one that has perplexed us for quite some time and is indicated in Table 3. In this table is presented the 3 year average ratio of the 00 GMT energy values to the 12 GMT values by month. Current values are quite consistent with these numbers. We see that the AZ component is quite consistent throughout the year with a 00-12 GMT variation which appars to be related to the stability, though we have not yet examined this in detail. The AE term, on the other hand, shows a marked seasonal variation of the ratio with the maxiumum impact during the summer of about 15%. Both KZ and KE, in contrast to this, indicate virtually no 00-12 GMT variation.

While it is clear that we might expect some evidence of a summertime diurnal variation in the energy cycle, these results were confusing to us on two points:

1. With a 15% variation in the mass field (AE) why is there no indication of variation in the energy wind field?

2. Kung (1967) has examined the 00-12 GMT kinetic energy variations from station data over the United States, and found a very strong cycle in the available to kinetic conversion team with 00 GMT much greater than 12 GMT. The K values themselves were approximately the same at both times.

Concerned about these discrepancies, we have examined the cycle further by looking at some of the basic components of the energy calculations and in Figure 5 is shown the monthly average 00/12 GMT ratio for June 1979 of the latitudinal temperature variance as a function of pressure and latitude. The shaded areas are for a ratio less than 1.00 and cross-hatched areas less than 0.80. Obviously, the diurnal cycle is quite widespread, but the maximum effect, on the order of 30%, is in the lower layers, 1000-700 mb.

With these results suggesting a surface or land-sea contrast problem we proceeded to examine the variations as evidenced in the actual surface temperatures and also those in the 6 hour analyses (00, 06, 12, 18 GMT) available at NMC. The results at this time are not yet complete, but it appears that the 1000 mb vs surface temperature patterns appear realistic and that the diurnal cycle in AE is basically real. The variation in KE, or lack thereof, is, however, still open to question and is related to the way the operational 6 hourly analysis-forecast product cycles. We have seen from the previous section that the observed winds tend to overwhelm the wind analyses so that the 06 and 18 GMT analyses, which include only very sparse wind observations, must be considered with caution. The possibility of a diurnal variation in KE with a peak at 0600 or 18 GMT, for example, cannot be verified or disproven at this time.

## V Final Remarks

As stated above, our purpose here is to call attention to the types of problems encountered when considering a hemispheric or global data set suitable for climate application. While many aspects of the problem have been tacitly recognized previously, it seems clear that the question of a stable, long-term data set must be resolved if we are to obtain meaningful results. Among the options that might be considered are:

1. Limit climate depiction to regions where sufficient data exist.

2. Utilize station data, only, rather than analyses. These data suffer from incomplete spatial coverage, but they may be more easily quality controlled.

3. Establish a "climate analysis system" that is based on quantity and quality of available data and limited in scope to particular parameters.

4. Establish a "climate" verification/calibration of operational analyses based on parallel runs with and without modification.

## References

1 Kung, E., 1967: Diurnal and long-term variations of the kinetic energy generation and dissipation for a five-year period. Mo. Wea. Rev., 95, 593-606.

2 Miller, A. J., W. Collins and D. Dubofsky, 1975: The NMC operational global energy program. National Meteorological Center Office Note 109, 13 pp.

3 Miller. A. J. and C. M. Hayden, 1978: The impact of satellite-derived temperature profiles on the energetics of NMC analyses and forecasts during the August 1975 Data Systems Test. Mo. Wea. Rev., 106, 390-398.

4 Oort, A. H. and E. R. Rasmusson, 1971: Atmospheric circulation statistics. NOAA Professional Paper 5. U. S. Department of Commerce, 323 pp.

5 Rosen, R. D. and D. A. Salstein, 1979: A comparison of two methods for computing general circulation statistics. Manuscript submitted for review.

6 Tracton, S. and R. McPherson, 1977: On the impact of radiometric sounding data upon operational numerical weather prediction at NMC. Bull. Amer. Meteor. Soc., 58, 1201-1209.

# List of Tables

Table 1. Major changes incorporated into NMC operational analysis since 1975.

Table 2. Data bases used in comparative DST analysis/forecast cycles.

Table 3. Three year average (1975-1978) by month of ratio of 00 GMT to 12 GMT for energy components.

Table 1. Major changes incorporated into NMC operational analysis since 1975.

| | |
|---|---|
| February 1975 | Zonal wave number in Hough analysis increased from 13 to 24. |
| December 1975 | Satellite data and bogus removed from analysis cycle. |
| March 1976 | Satellite data and bogus reinstated into final analysis cycle. |
| May 1976 | 9 layer model replaced 8 layer model (provides 1st guess for analysis) |
| September 1978 | Optimum interpolation replaced Hough analysis |
| ∿ April 1979 | Tiros N satellite data replaced VTPR |

TABLE 2. Data bases used in comparative DST analysis/forecast cycles.

| Data type | System 1 | System 2 | System 3 |
|---|---|---|---|
| Surface observations | X | X | X |
| Radiosonde reports | X | X | |
| NESS cloud-tracked winds | X | X | X |
| Wisconsin cloud-tracked winds | X | X | X |
| NESS VTPR | | | |
| Northern Hemisphere | X | | X |
| Southern Hemisphere | X | X | X |
| Nimbus 6 | | | |
| Northern Hemisphere | X | | X |
| Southern Hemisphere | X | | X |
| Aircraft | X | X | X |
| TWERLE | X | X | X |
| Bogus reports | | | |

Table 3. Three year average (1975-1978) by month of ratio of 00 GMT to 12 GMT for energy components.

NORTHERN HEMISPHERE AVERAGE (1975-1978)

Ratio $\frac{00\ Z}{12\ Z}$ 100-10 KPA

| | AZ | AE | KZ | KE |
|---|---|---|---|---|
| January | 0.98 | 1.01 | 1.01 | 0.99 |
| February | 0.98 | 1.02 | 1.01 | 0.99 |
| March | 0.99 | 0.96 | 1.00 | 1.00 |
| April | 0.99 | 0.93 | 1.01 | 1.00 |
| May | 0.99 | 0.86 | 1.00 | 1.00 |
| June | 0.99 | 0.83 | 1.00 | 1.00 |
| July | 0.98 | 0.84 | 0.99 | 1.00 |
| August | 0.97 | 0.85 | 1.01 | 1.00 |
| September | 0.97 | 0.91 | 0.98 | 0.99 |
| October | 0.98 | 0.97 | 0.98 | 0.99 |
| November | 0.98 | 1.00 | 1.00 | 1.00 |
| December | 0.98 | 1.01 | 1.00 | 1.00 |

## List of Figures

Figure 1. Location of rawinsonde (dots) and pilot ballons sites (crosses) for winter '76-'77 from Rosen and Salstein (1979). Triangles are stations deleted since early 1960's from Oort and Rasmusson (1971).

Figure 2. Monthly average area-integrated (20N-20S) values of KZ (solid) and KE (dashed) at 200 mb (00GMT). Units : J/kg.

Figure 3. Area integrated values (20N-pole) of the zonal available potential energy (AZ) and zonal kinetic energy (KZ) as a function of pressure for the three analysis systems. Numbers at right are ratio of results for System 1/ System 2 and System3/System 2.

Figure 4. Same as Figure 2 for eddy available potential energy (AE) and eddy kinetic energy (KE).

Figure 5 Ratio, 00GMT/12GMT, of June 1979 temperature variance around latitude circle as a function of pressure and latitude. Shaded areas less than 1.0 and cross-hatched areas less than 0.8.

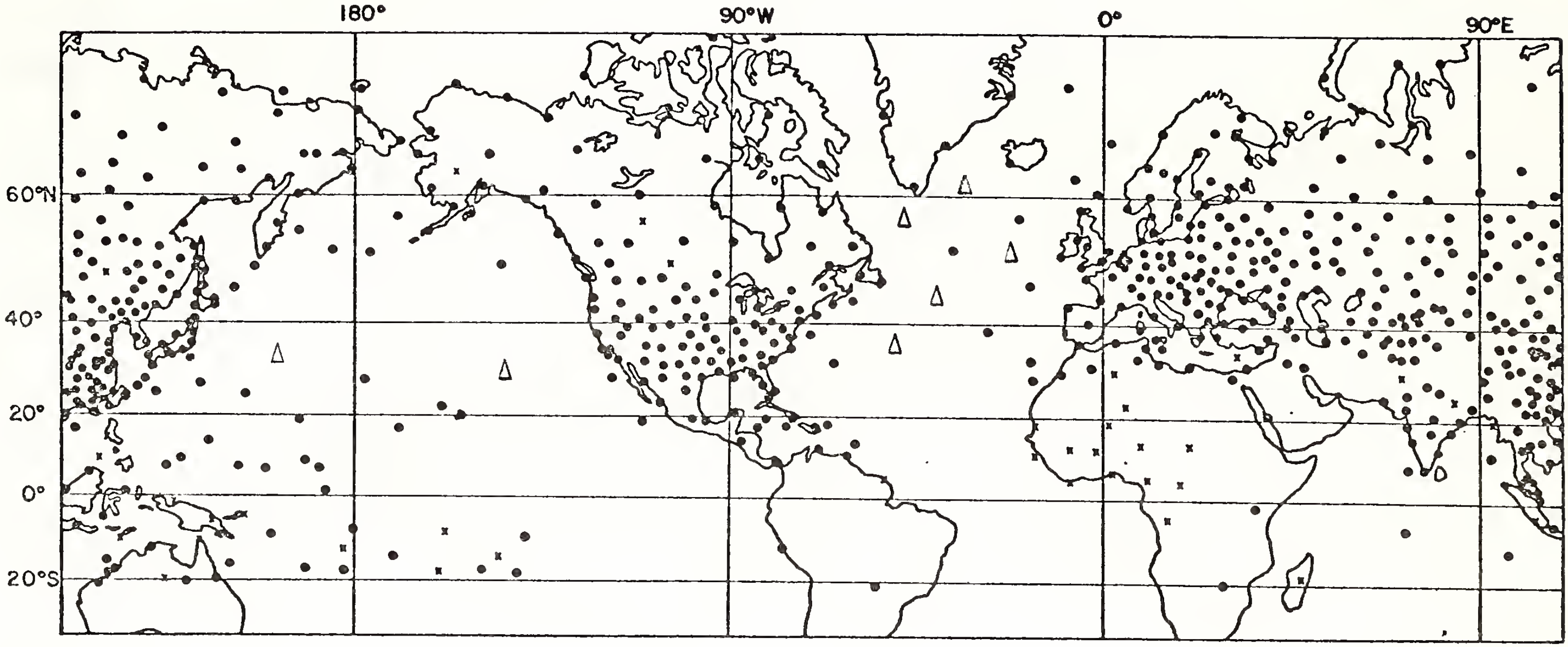

Figure 1

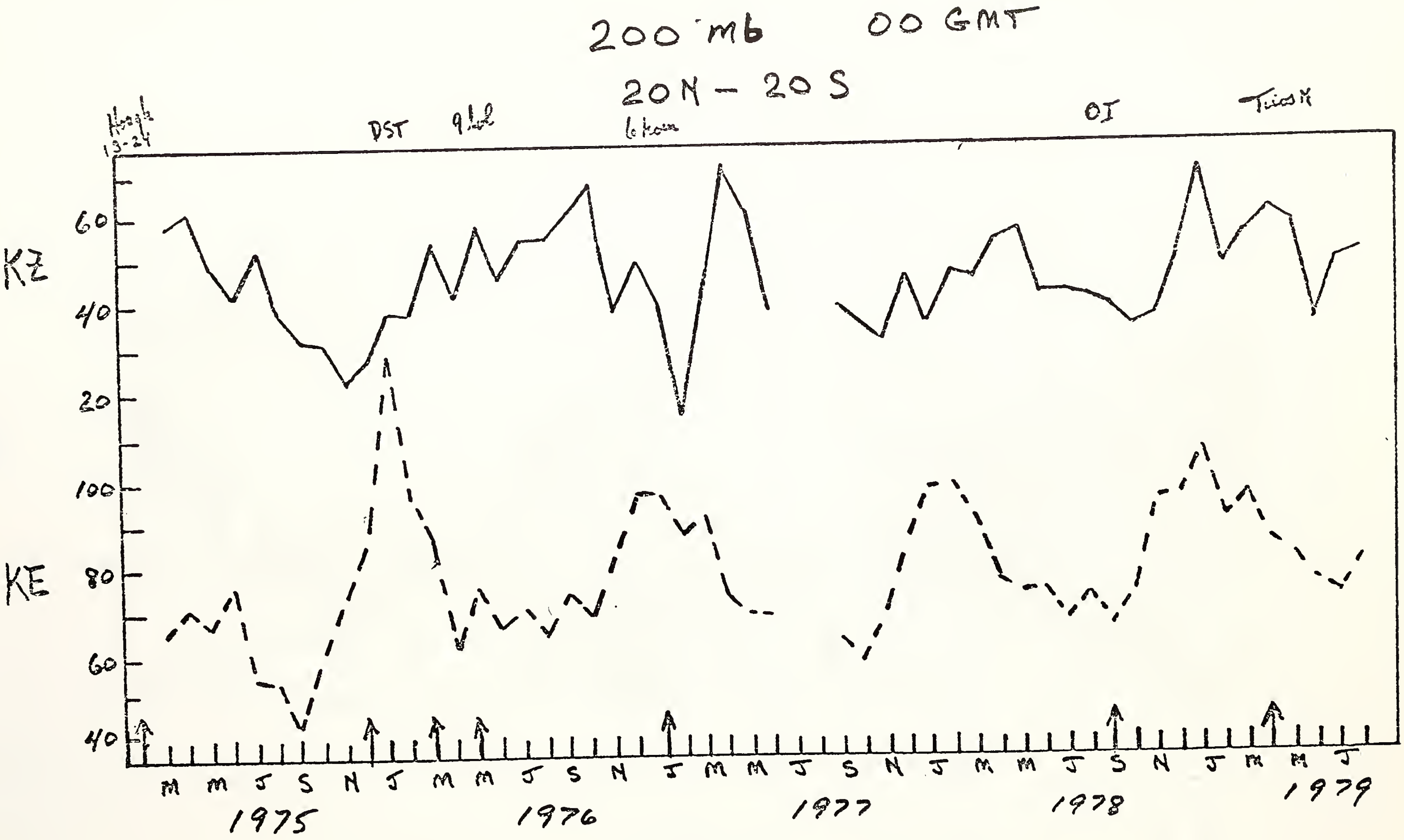
200 mb 00 GMT
20N – 20S
13-24
DST
OI
Tiros N
KZ
KE
60
40
20
100
80
60
40
M M J S N J M M J S N J M M J S N J M M J S N J M M J
1975
1976
1977
1978
1979

Figure 2

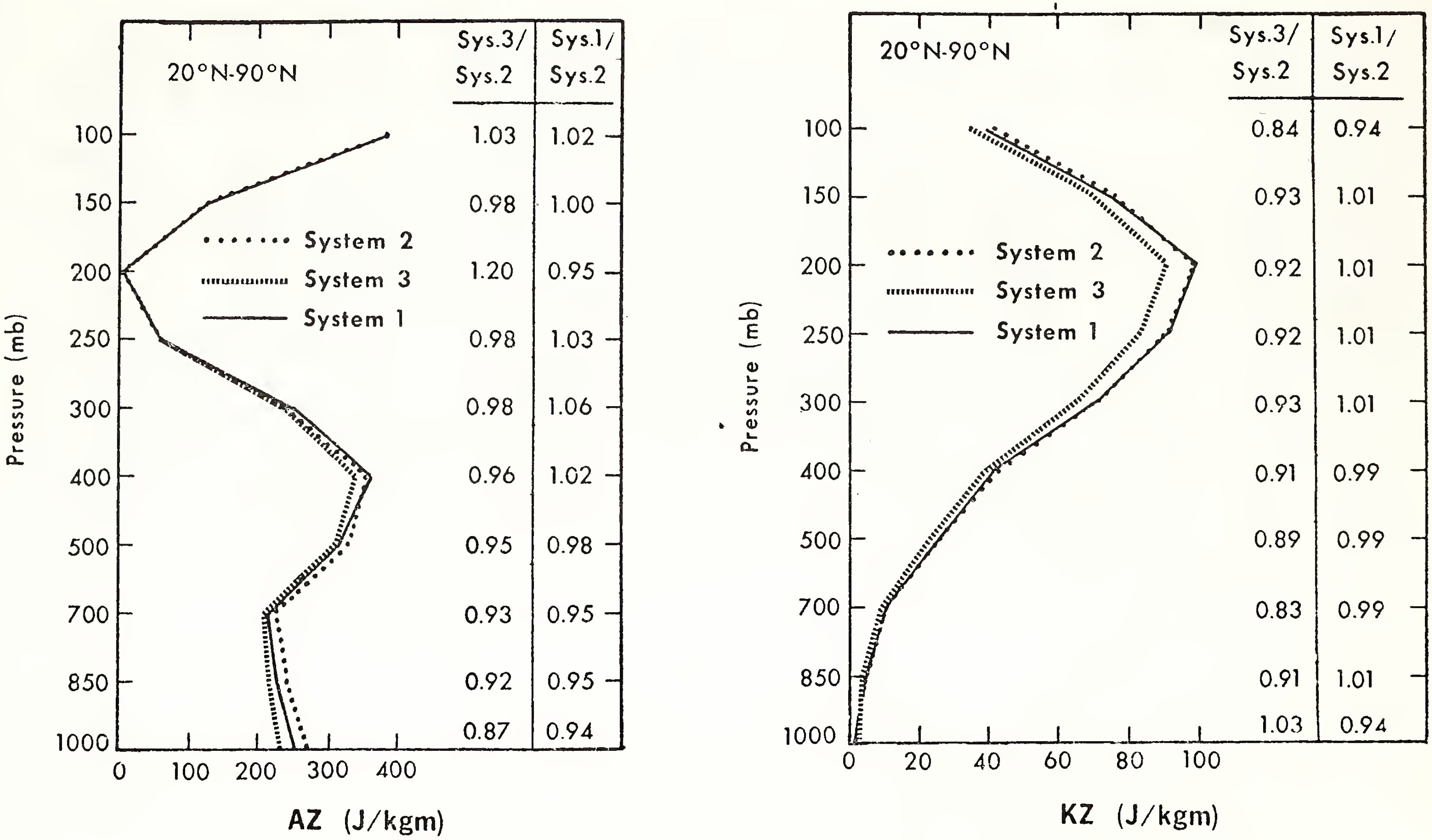
20°N-90°N
Pressure (mb)
100
150
200
250
300
400
500
700
850
1000
System 2
System 3
System 1
Sys.3/ Sys.2
1.03
0.98
1.20
0.98
0.98
0.96
0.95
0.93
0.92
0.87
Sys.1/ Sys.2
1.02
1.00
0.95
1.03
1.06
1.02
0.98
0.95
0.95
0.94
0
100
200
300
400
AZ (J/kgm)
20°N-90°N
Pressure (mb)
100
150
200
250
300
400
500
700
850
1000
System 2
System 3
System 1
Sys.3/ Sys.2
0.84
0.93
0.92
0.92
0.93
0.91
0.89
0.83
0.91
1.03
Sys.1/ Sys.2
0.94
1.01
1.01
1.01
1.01
0.99
0.99
0.99
1.01
0.94
0
20
40
60
80
100
KZ (J/kgm)

Figure 3

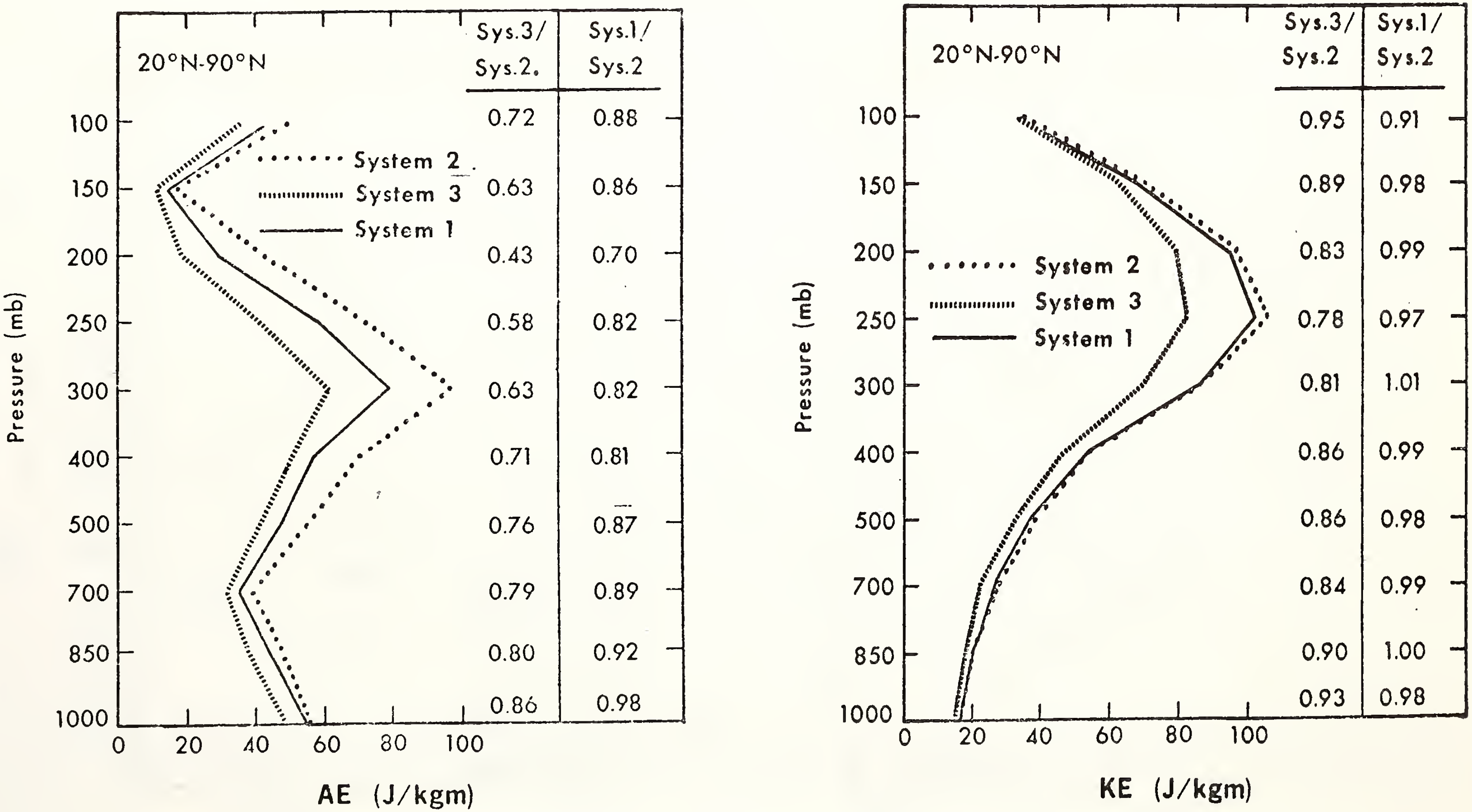
20°N-90°N
Sys.3/ Sys.2.
Sys.1/ Sys.2
System 2
System 3
System 1
Pressure (mb)
100
150
200
250
300
400
500
700
850
1000
0.72
0.63
0.43
0.58
0.63
0.71
0.76
0.79
0.80
0.86
0.88
0.86
0.70
0.82
0.82
0.81
0.87
0.89
0.92
0.98
0
20
40
60
80
100
AE (J/kgm)
20°N-90°N
Sys.3/ Sys.2
Sys.1/ Sys.2
System 2
System 3
System 1
Pressure (mb)
100
150
200
250
300
400
500
700
850
1000
0.95
0.89
0.83
0.78
0.81
0.86
0.86
0.84
0.90
0.93
0.91
0.98
0.99
0.97
1.01
0.99
0.98
0.99
1.00
0.98
0
20
40
60
80
100
KE (J/kgm)

Figure 4

JUNE '79 [T*2] 00/12

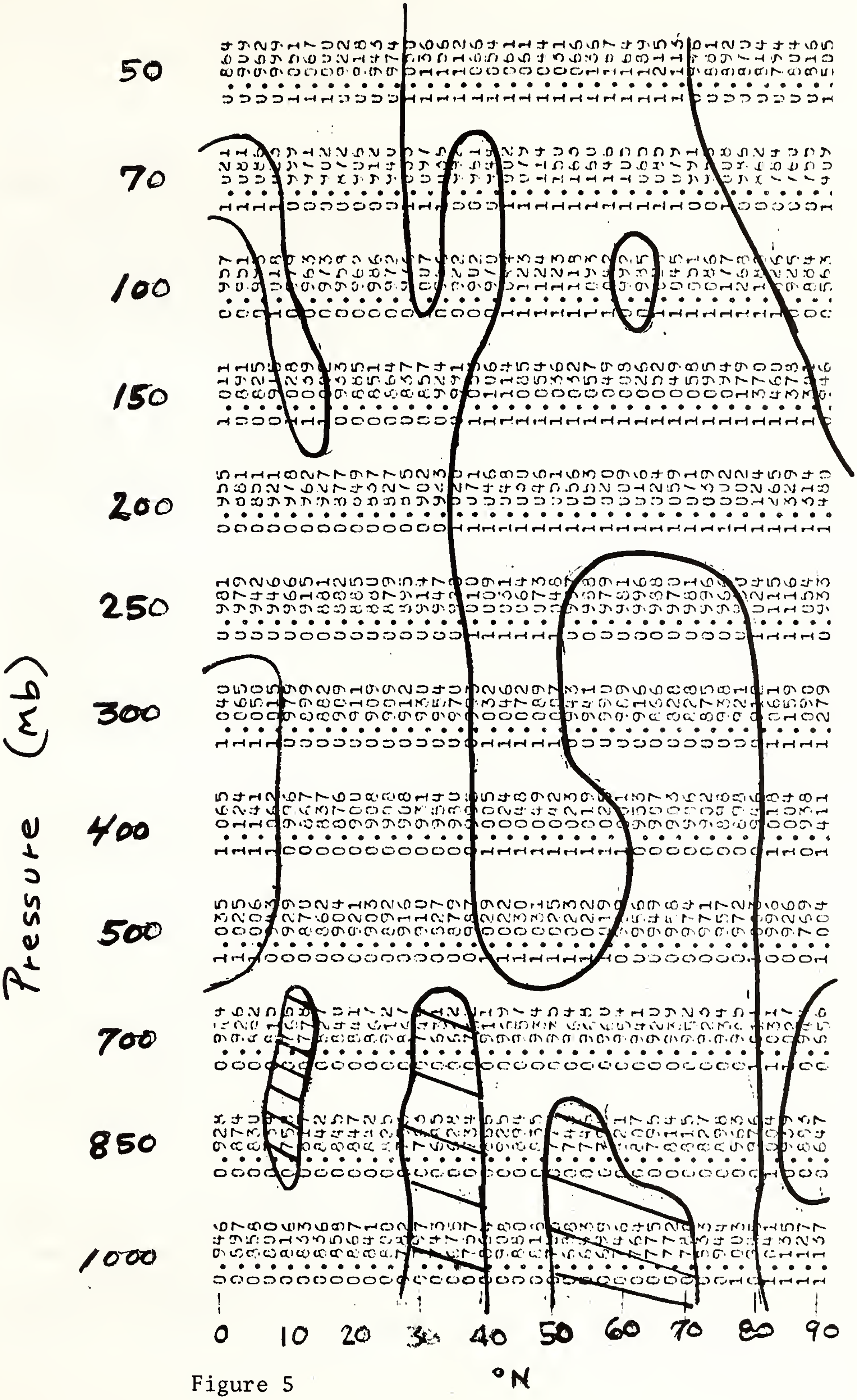

Figure 5

# A Comparison Between Circulation Statistics Computed from Conventional Data and NMC Hough Analyses

Richard D. Rosen and David A. Salstein
Environmental Research & Technology, Inc.
Concord, Massachusetts 01742

The traditional source of information concerning the general circulation has been the analysis of data collected from the hemispheric network of upper-air station soundings (the compilation by Oort and Rasmusson is a classic example of this approach). Unfortunately, the task of organizing and analyzing such data is both tedious and expensive, so that work along these lines has not progressed beyond data for April 1973. Moreover, as Fig. 1 suggests, the conventional data network has begun to deteriorate, particularly with the recent disappearance of key ocean weather ships.

An alternate source of upper-air information covering the entire NH is provided by the NMC global Hough analysis, which was introduced around 1973. A distinct advantage provided by this data set is that its values are already located on a regular grid, thus eliminating the need for one's own objective analysis procedure.

For the purpose of comparing statistics derived from these two very different sources, we selected the winter of 1976-77. As Fig. 2 illustrates, the fields of $[\bar{u}]$ compare favorably. However, closer inspection of $\bar{u}$ at 200 mb in Fig. 3 shows that the weaker zonal average jet in the station data results from an important void in the radiosonde network over the North Pacific. Presumably, the gridded Hough data have benefitted in this region from the incorporation of aircraft data and the use of a forecast field as an initial guess.

On the other hand, the Hough data do exhibit a serious shortcoming, in that they have been constrained to yield $[\bar{v}] = 0$. Thus, while the station data exhibit the expected three cell mass streamfunction pattern (Fig. 4), no cells are present in the gridded data.

The absence of mean meridional overturnings in the gridded data does not, however, seem to seriously affect their measure of eddy fluxes. Both the standing and transient eddy fluxes of angular momentum (Figs. 5 and 6) computed from the gridded data appear reasonable when compared with the station data. Some differences do exist, but it is not always clear which approach is the more truthful, given the problems associated with each data set. One interesting point of agreement is that both analyses produce a maximum in the transient eddy flux at 250 mb, rather than at the 200 mb level previously associated with this feature.

The analyses of the zonal mean temperature field (Fig. 7) also agree quite well, although the gridded equatorial stratosphere is colder than that yielded by the station data analysis. The standing and transient eddy heat fluxes (Figs. 8 and 9) compare favorably, thus affording us some reassurance that the Hough data can be used for studying midlatitude waves and their transports. However, as the profiles of total integrated meridional heat flux (Fig. 10) demonstrate, the lack of a Hadley cell in the Hough data limit their usefulness in studies of atmospheric transports in the tropics.

Moisture fluxes in the tropics are also poorly treated by the gridded Hough data, but not only because of the lack of a Hadley cell. As Fig. 11 shows, the gridded data yield much more water vapor than do the station data. The reasons for this disparity are not yet known, but are surprising in light of the good agreement in $[\overline{T}]$ noted earlier. In any event, the high humidities and zonal winds in the gridded data account for the more intense picture of the (non-divergent) moisture streamfunction with these data (Fig. 12). Interestingly, the station data this winter completely miss the small, but intense, moisture circulation off the east African coast near Somalia.

In summary, because of gaps in the conventional observing network, the station data have proven an uncertain yardstick against which to measure the gridded data. Basically, though, the gridded data examined here have proven easy to work with and seem reliable for studies of mid-latitude waves. For studies in which the mean meridional circulations play a major role or for studies involving water vapor, caution is needed with the Hough data. Finally, we recommend a study similar to this one be made for the optimum interpolation global analysis scheme currently being used at NMC.

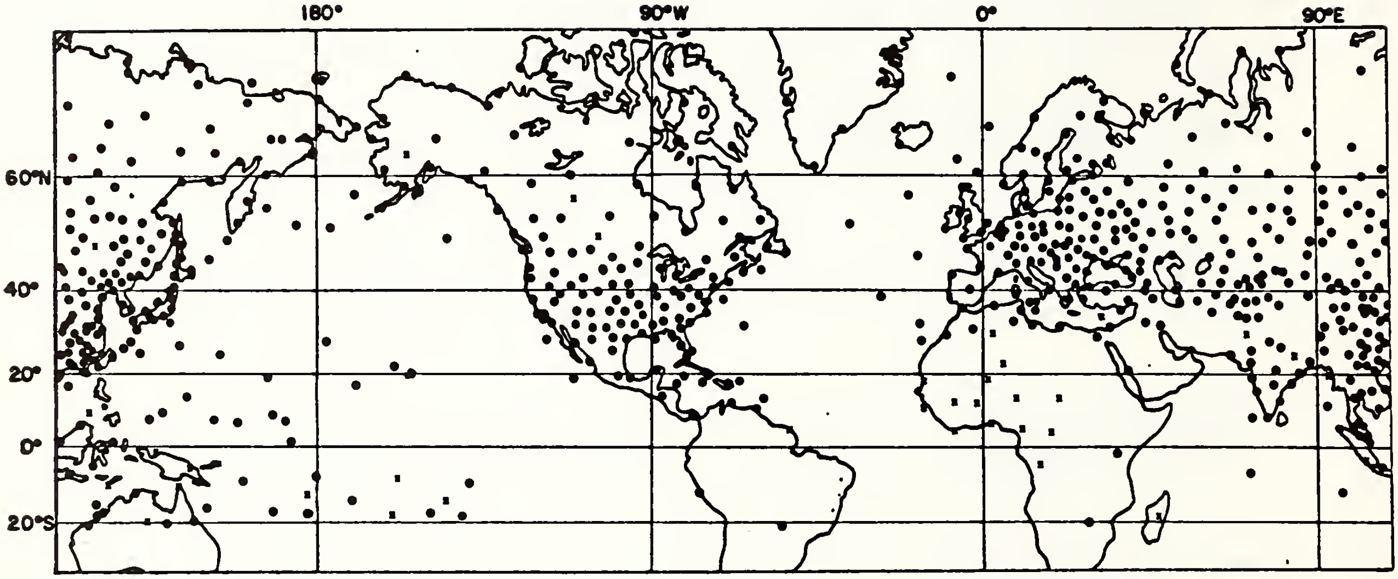

Fig. 1. Map of rawinsonde stations (dots) which were used in the analysis of 00 GMT wind and temperature fields at 850 mb for the 1976-77 winter. Pilot balloon stations (crosses) provided wind data only.

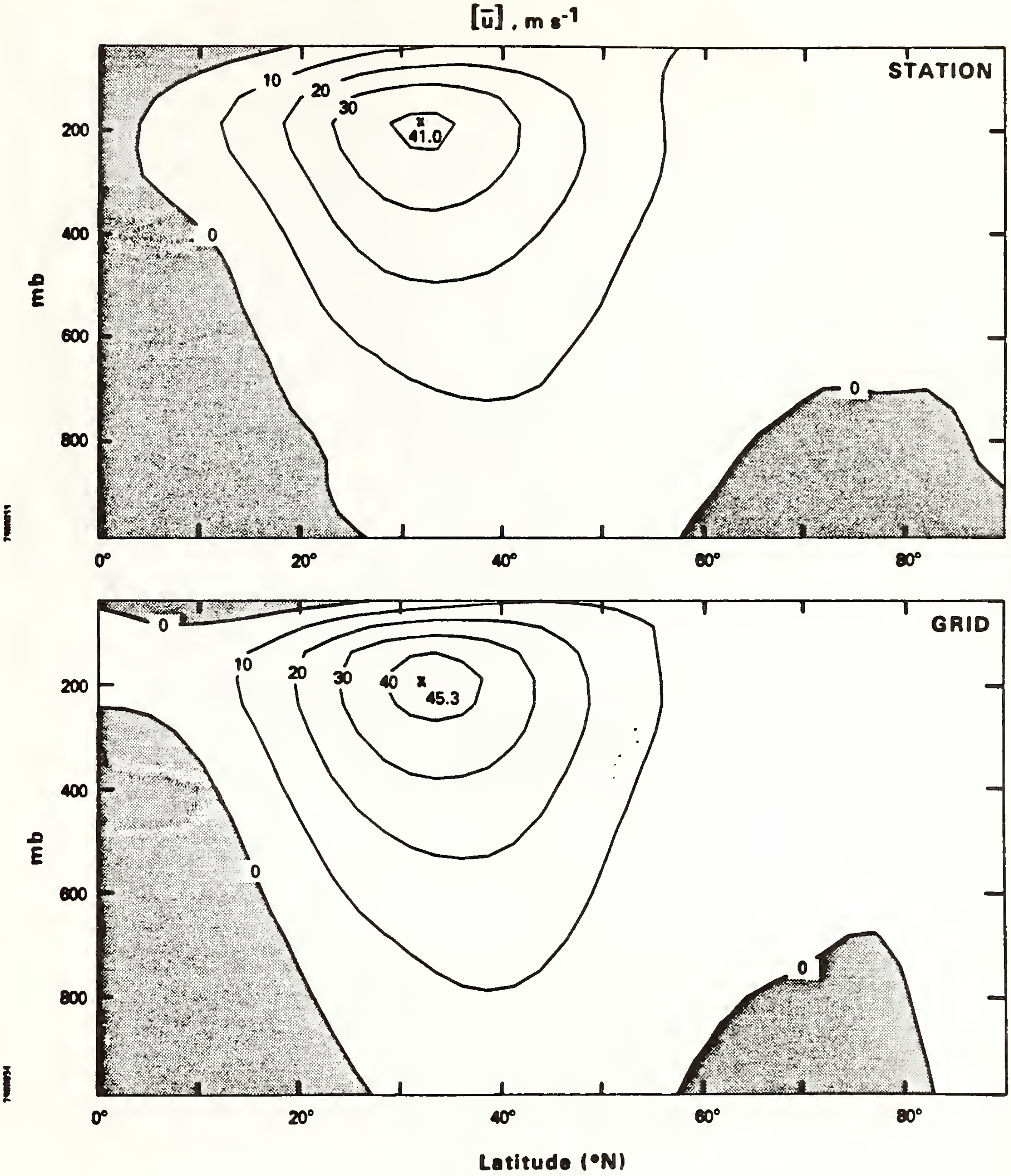

Fig. 2. Cross sections of the zonally averaged mean zonal wind obtained from station and grid data for the 1976-77 winter. Negative values are shaded and indicate flow toward the east.

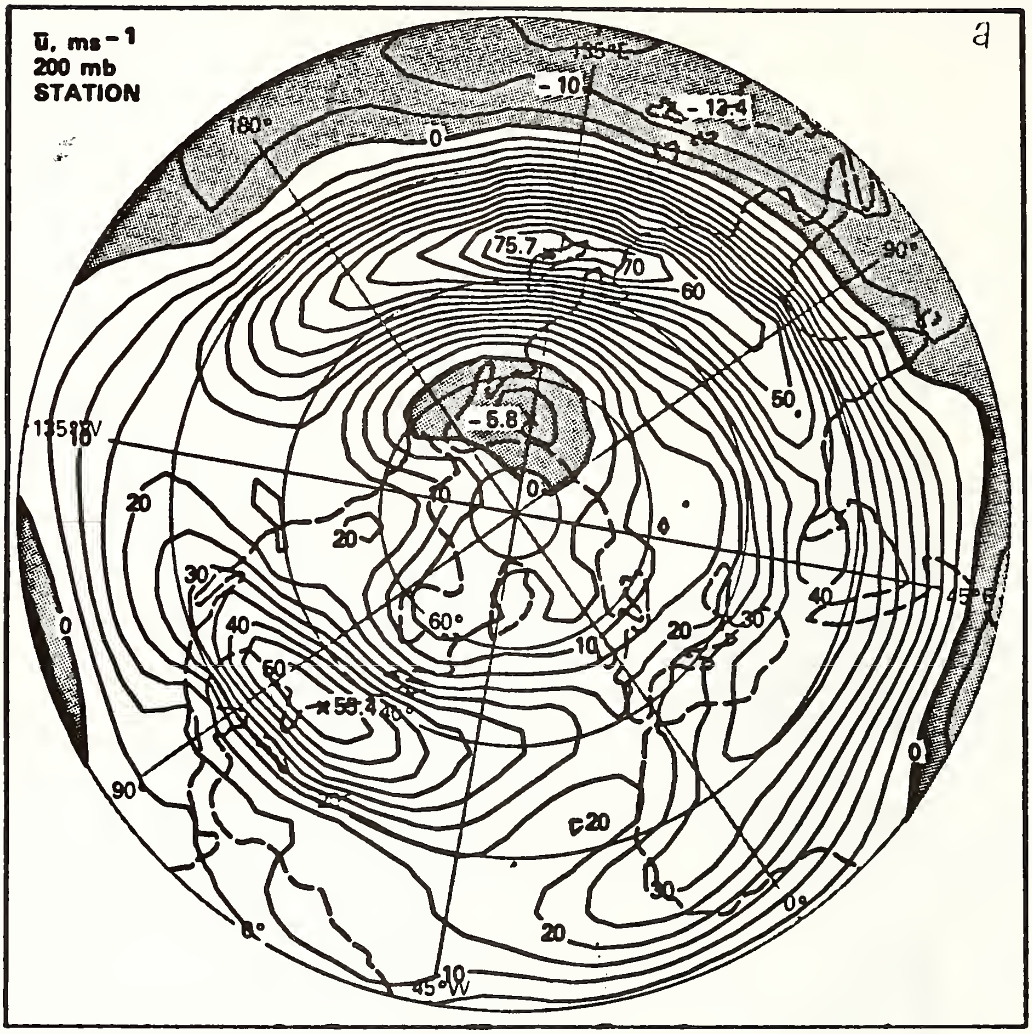

Fig. 3. Hemispheric maps of the mean zonal velocity at 200 mb obtained from the station (part a) and grid (part b) data for the 1976-77 winter. Negative values are shaded and indicate flow toward the east. Also, in part c, the hemispheric map of the field in part a minus the field in part b. Here, negative values are shaded and indicate regions of stronger westerlies or weaker easterlies in the grid data.

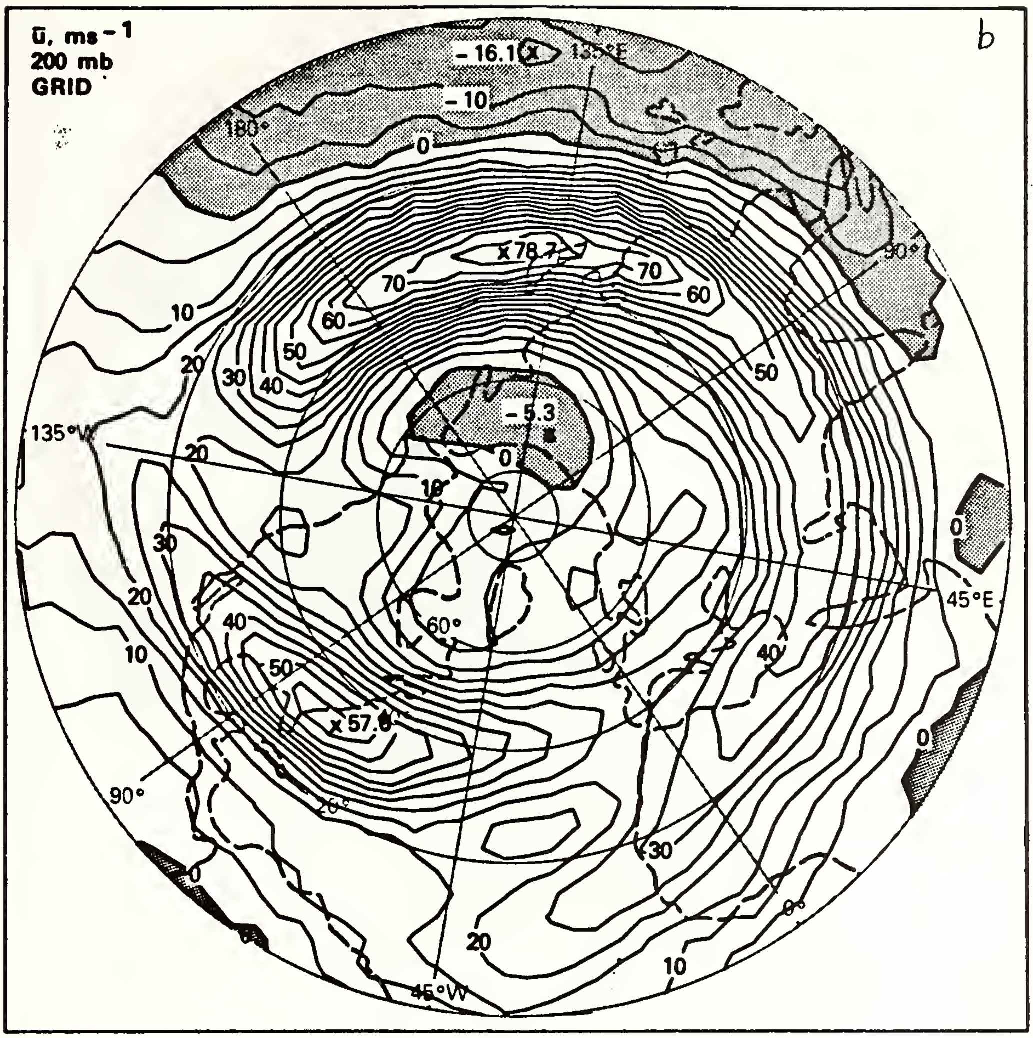

ū, ms - 1
200 mb
GRID
b
- 16.1 x
135°E
- 10
180°
0
x 78.7
70
70
60
60
50
10
20
30
40
50
- 5.3
0
135°W
20
10
90°
0
45°E
30
20
40
60°
10
40
50
x 57.8
0
90°
20°
30
0
0°
20
10
45°W

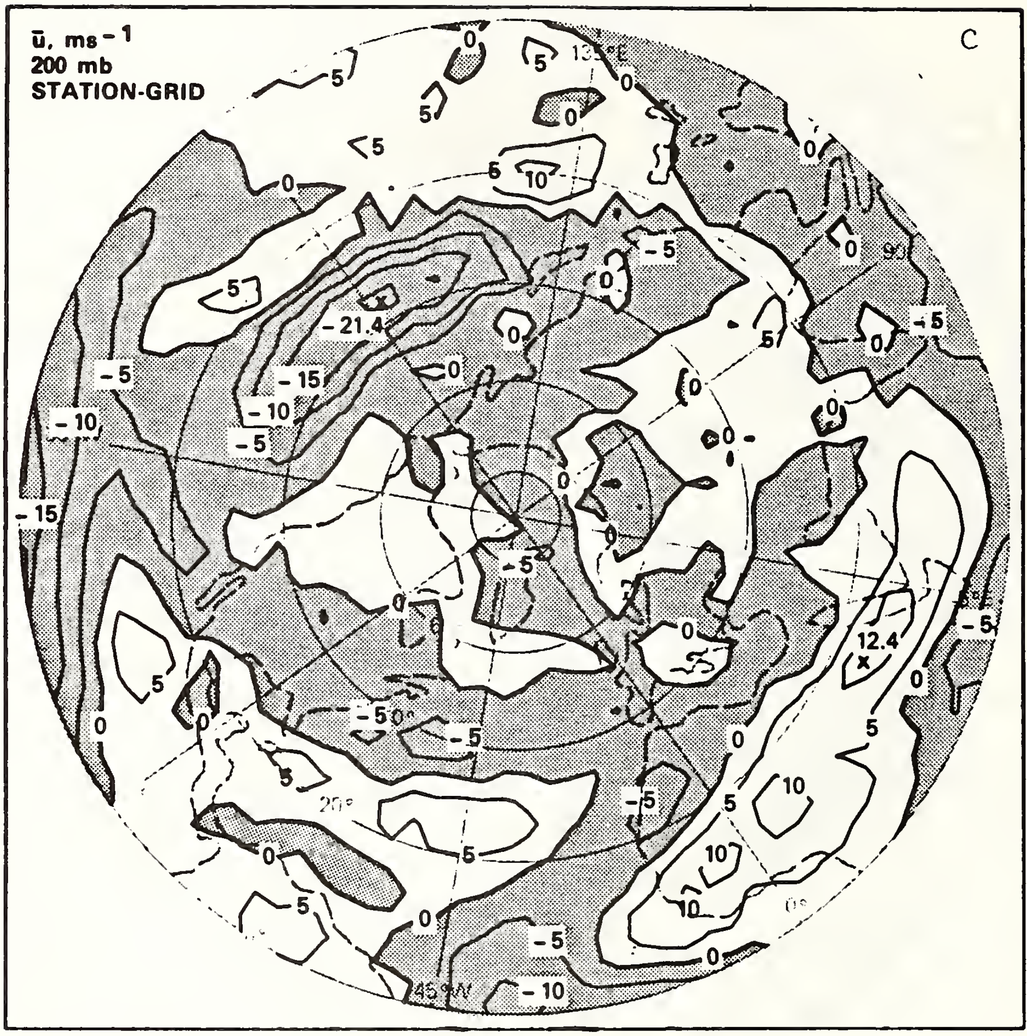
ū, ms⁻¹
200 mb
STATION-GRID
C
-21.4
-15
-10
-5
0
5
10
12.4
135°E
90°
45°W
20°

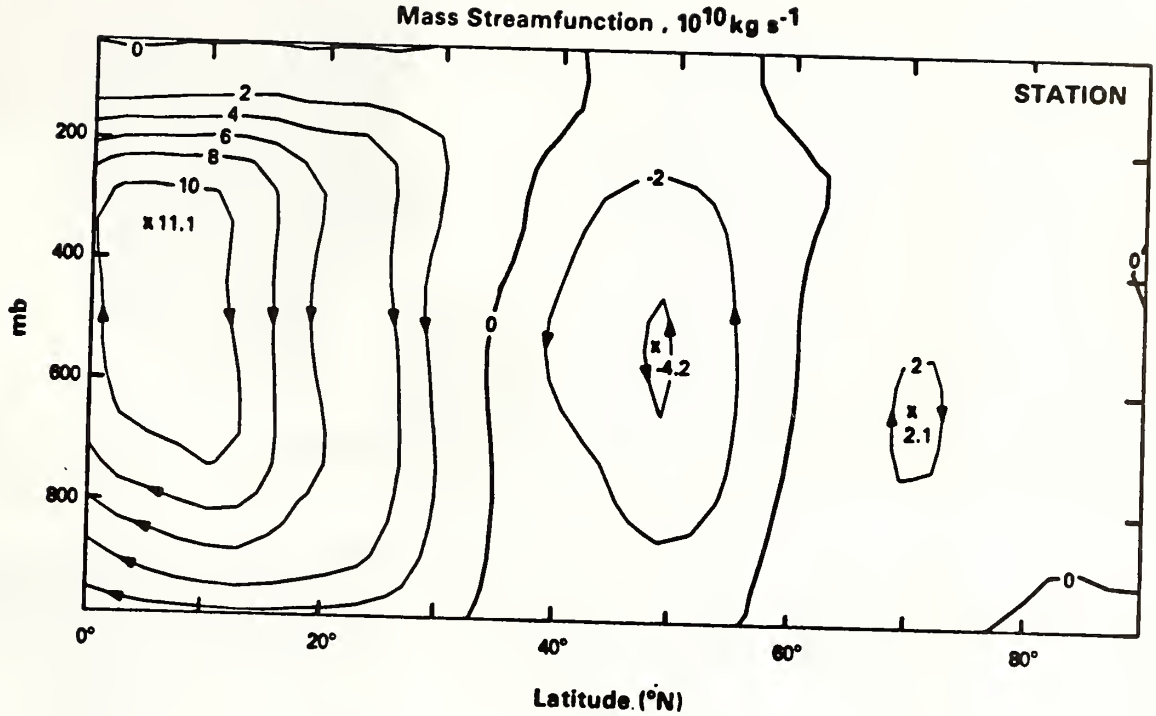

Fig. 4. Cross section of the mass streamfunction for the mean meridional circulation. Positive values indicate clockwise circulation.

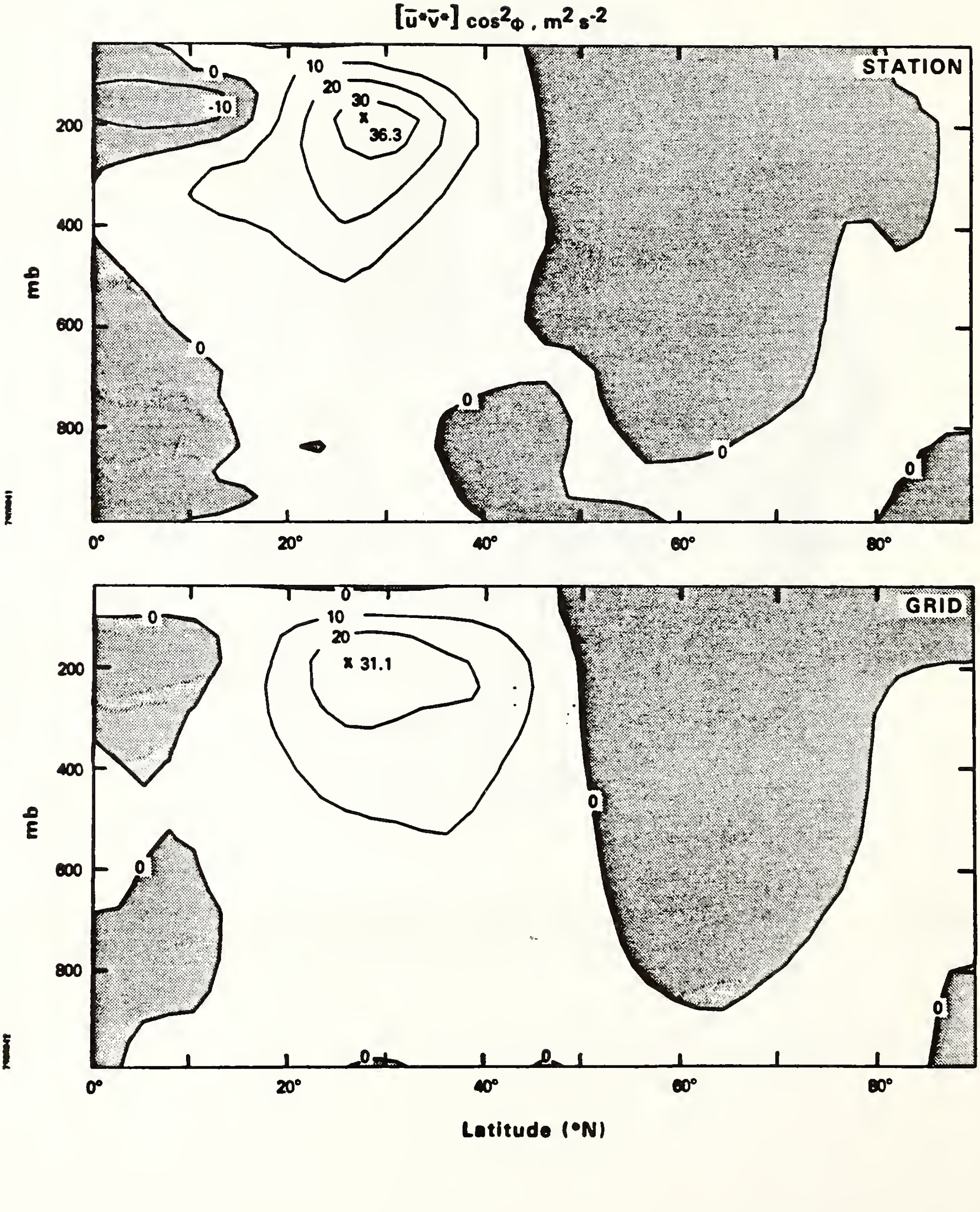

Fig. 5. Cross sections of the standing eddy angular momentum flux ($\div 2\pi a^2$) obtained from station and grid data for the 1976-77 winter. Negative values are shaded and indicate a southward flux.

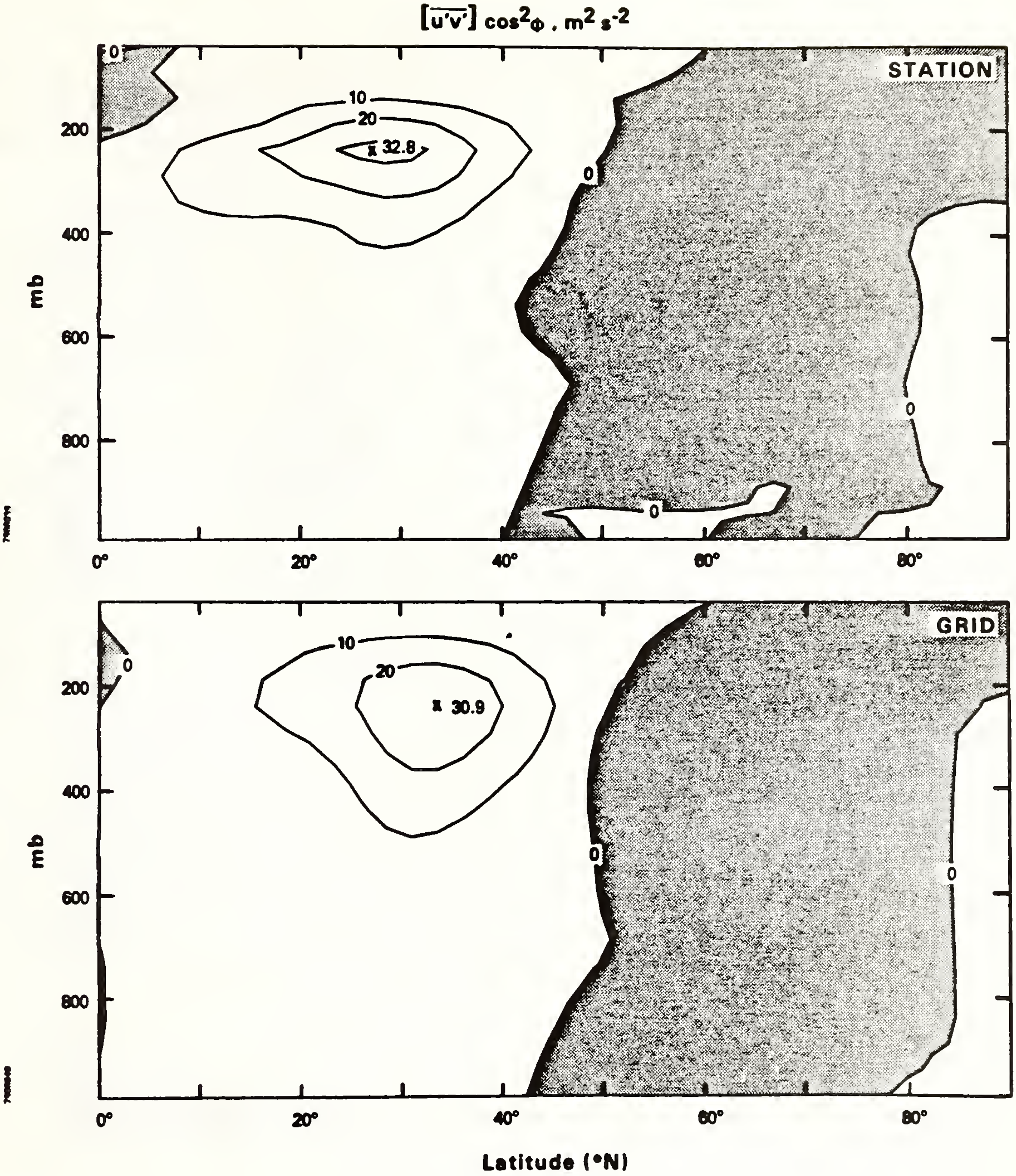

Fig. 6. Cross sections of the transient eddy angular momentum flux ($\div 2\pi a^2$) obtained from station and grid data for the 1976-77 winter. Negative values are shaded and indicate a southward flux.

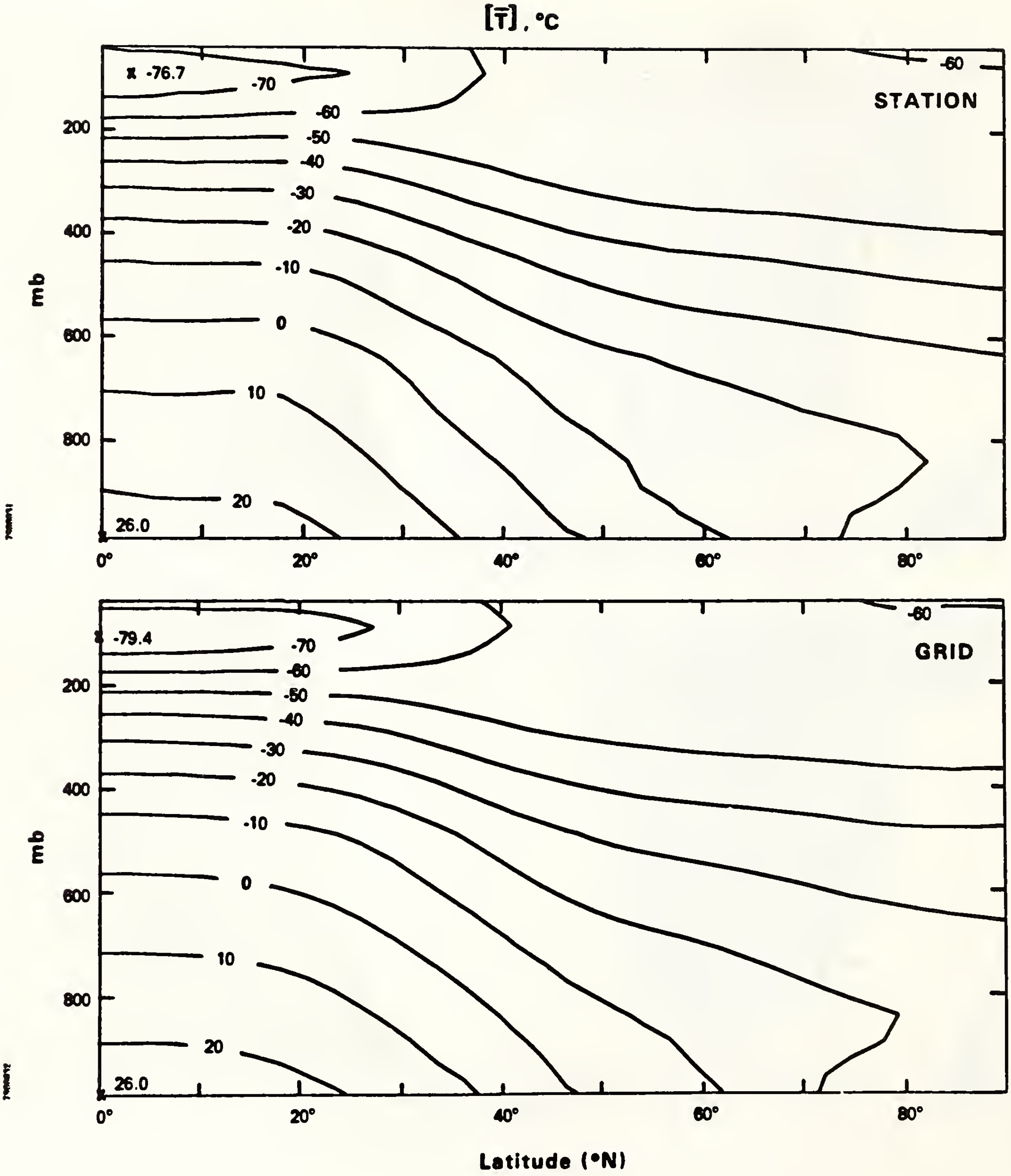

Fig. 7. Cross sections of the zonally averaged mean temperature obtained from the station and grid data for the 1976-77 winter.

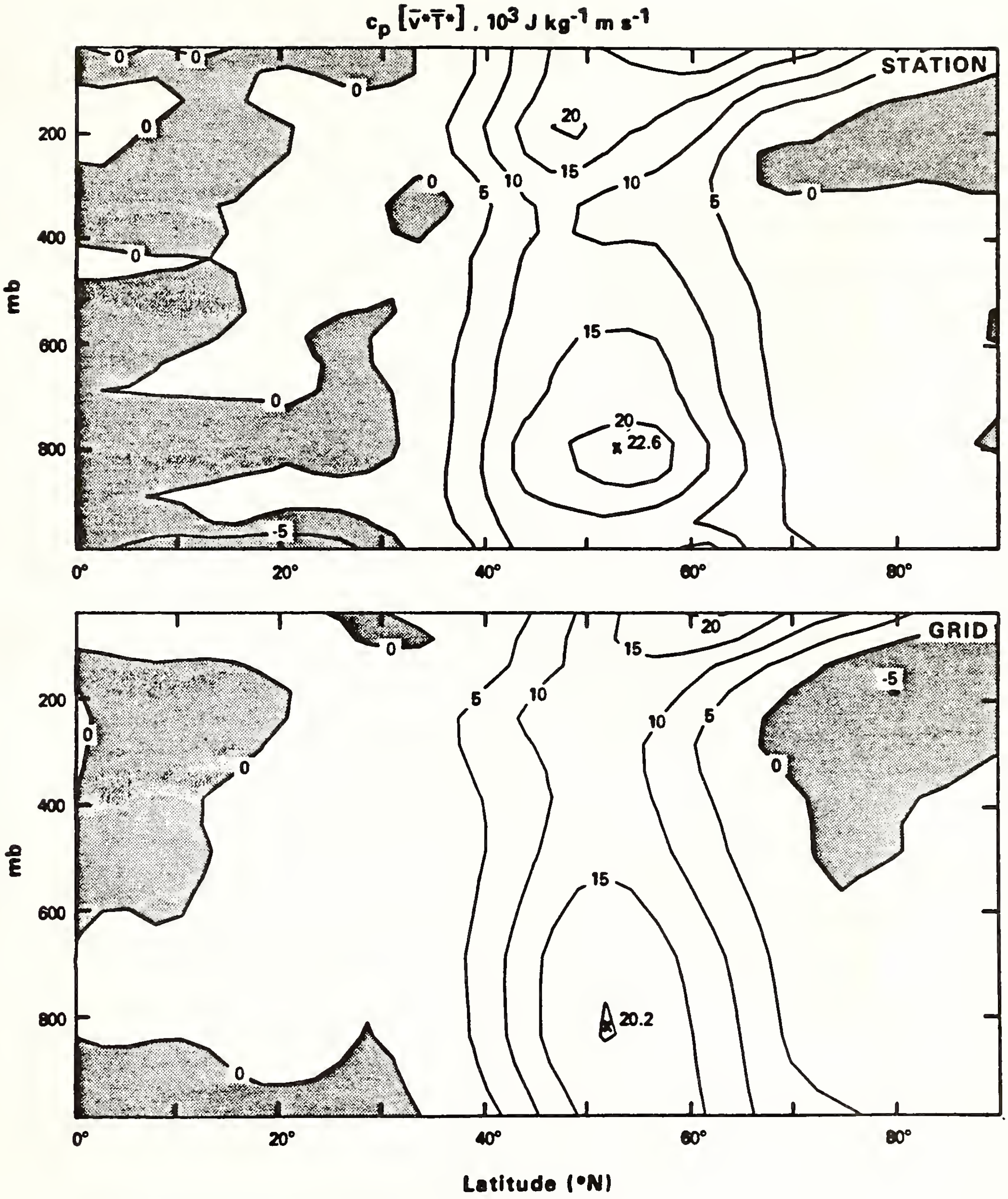

Fig. 8. Cross sections of the standing eddy sensible heat flux ($\div\ 2\pi a \cos\phi$) obtained from station and grid data for the 1976-77 winter. Negative values are shaded and indicate a southward flux.

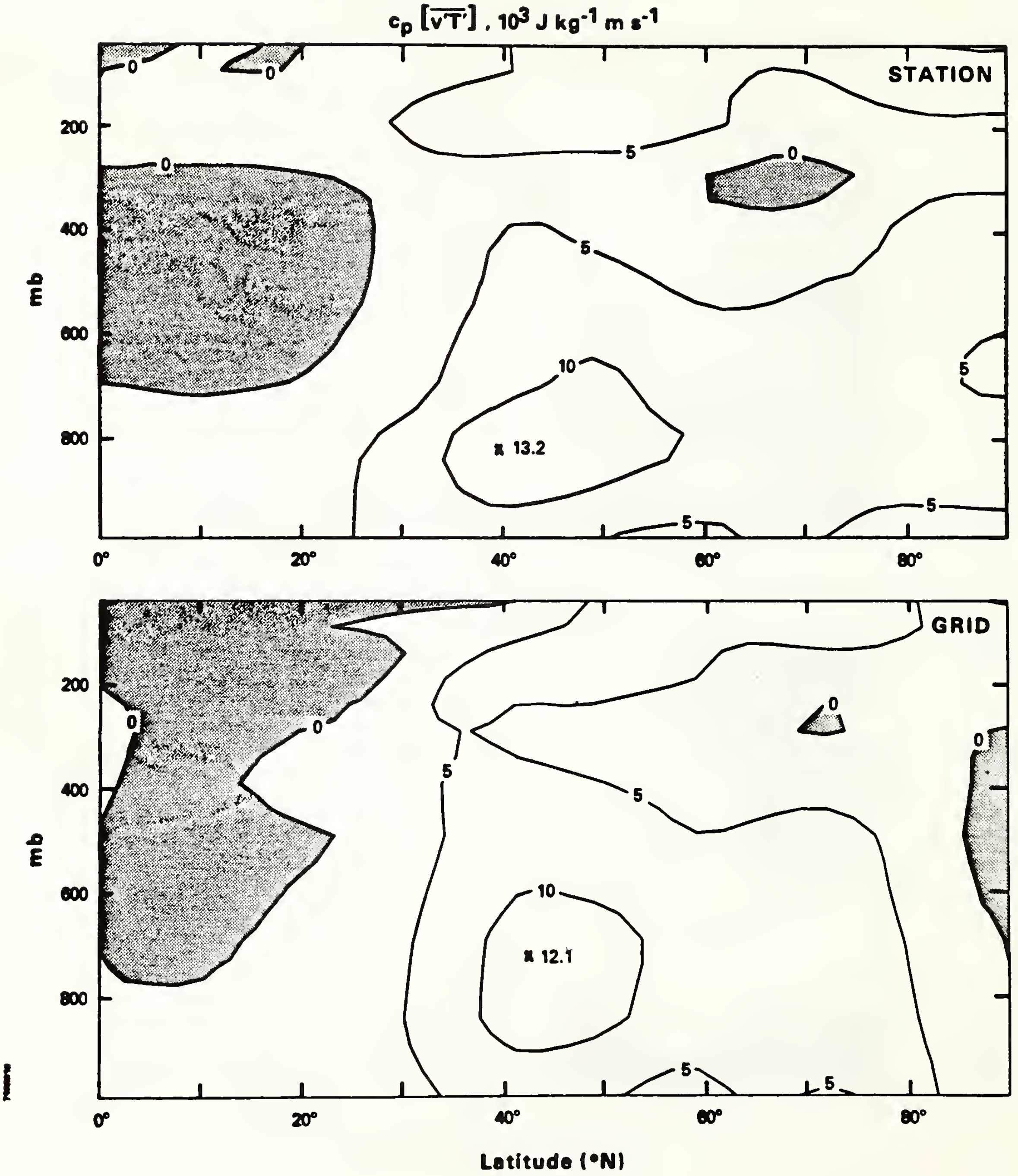

Fig. 9. Cross sections of the transient eddy sensible heat flux (÷ 2πa cosϕ) obtained from station and grid data for the 1976-77 winter. Negative values are shaded and indicate a southward flux.

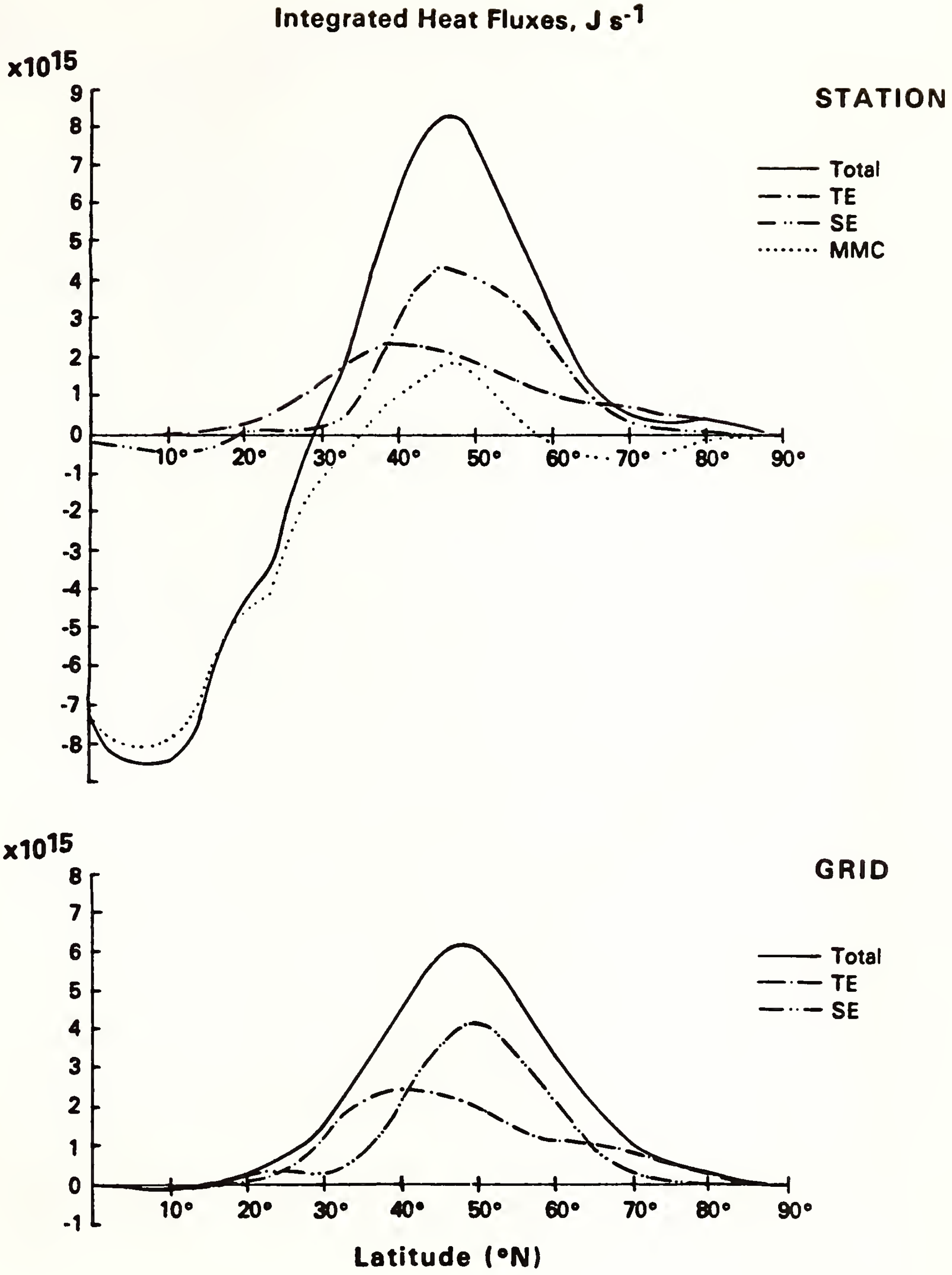

Fig. 10. Meridional profiles of the vertically integrated northward flux of total sensible heat and its component parts for the 1976-77 winter.

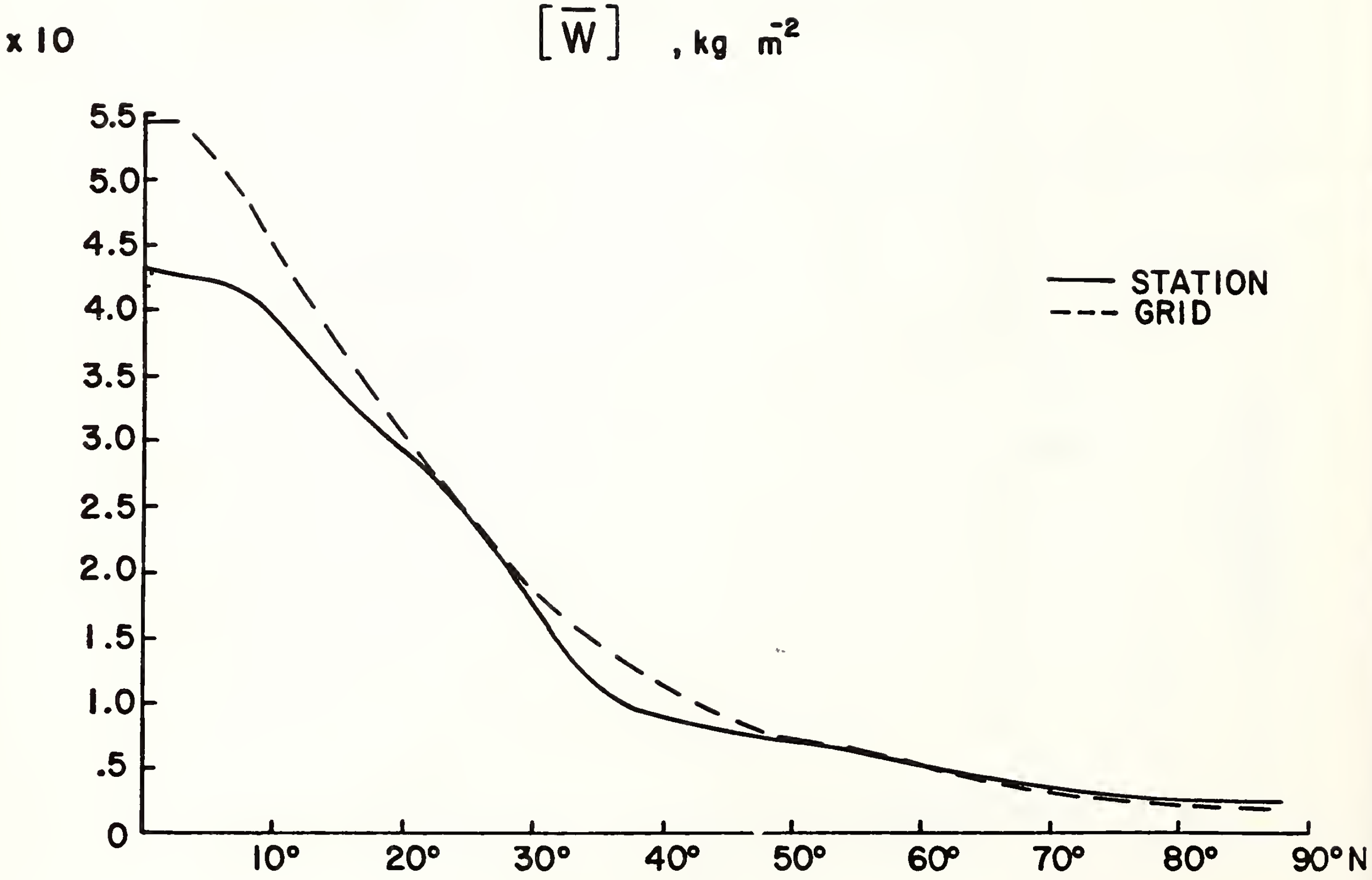

Fig. 11. Meridional profiles of the vertically integrated mean moisture content obtained from station and grid data for the 1976-77 winter.

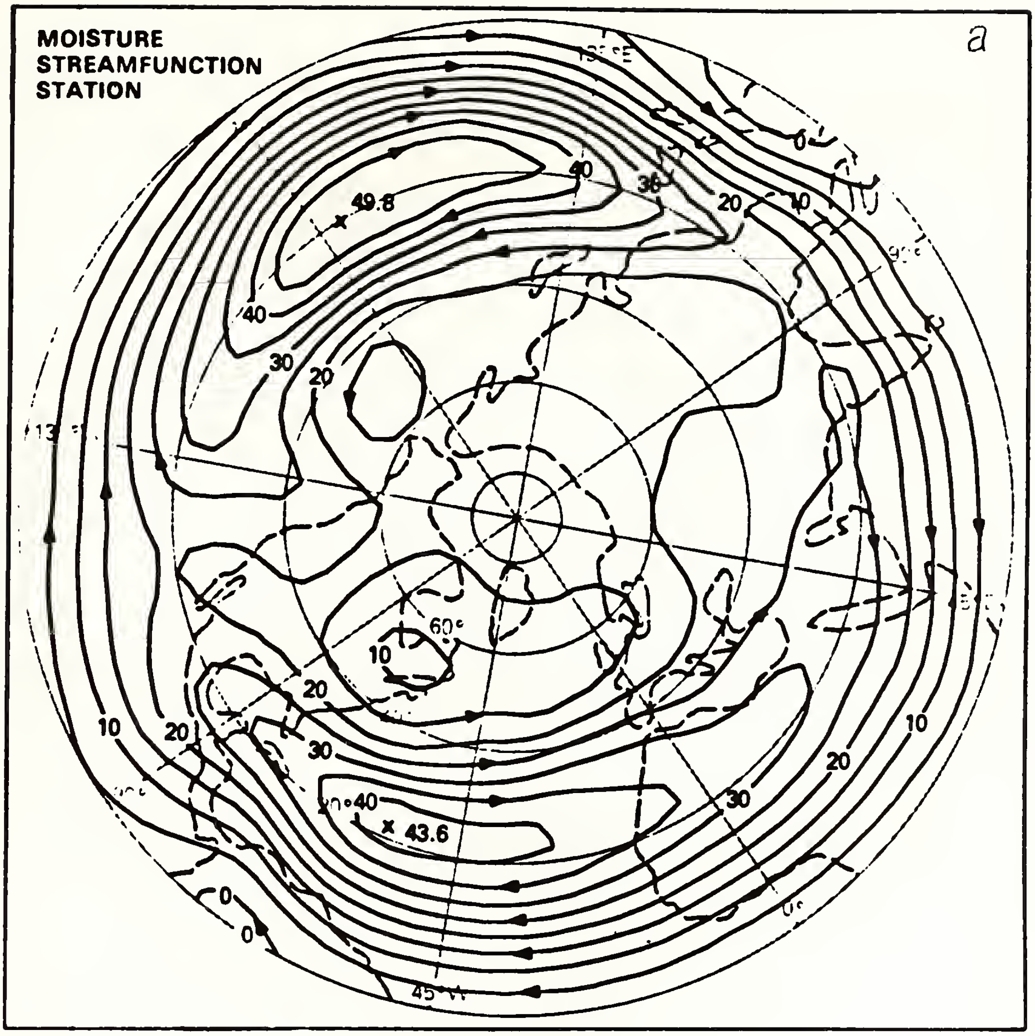

Fig. 12. Hemispheric maps of the streamfunction field for the vertically integrated moisture transport obtained from station and grid data for the 1976-77 winter. Units are x $10^7$ kg $s^{-1}$ and arrows indicate the sense of the circulation.

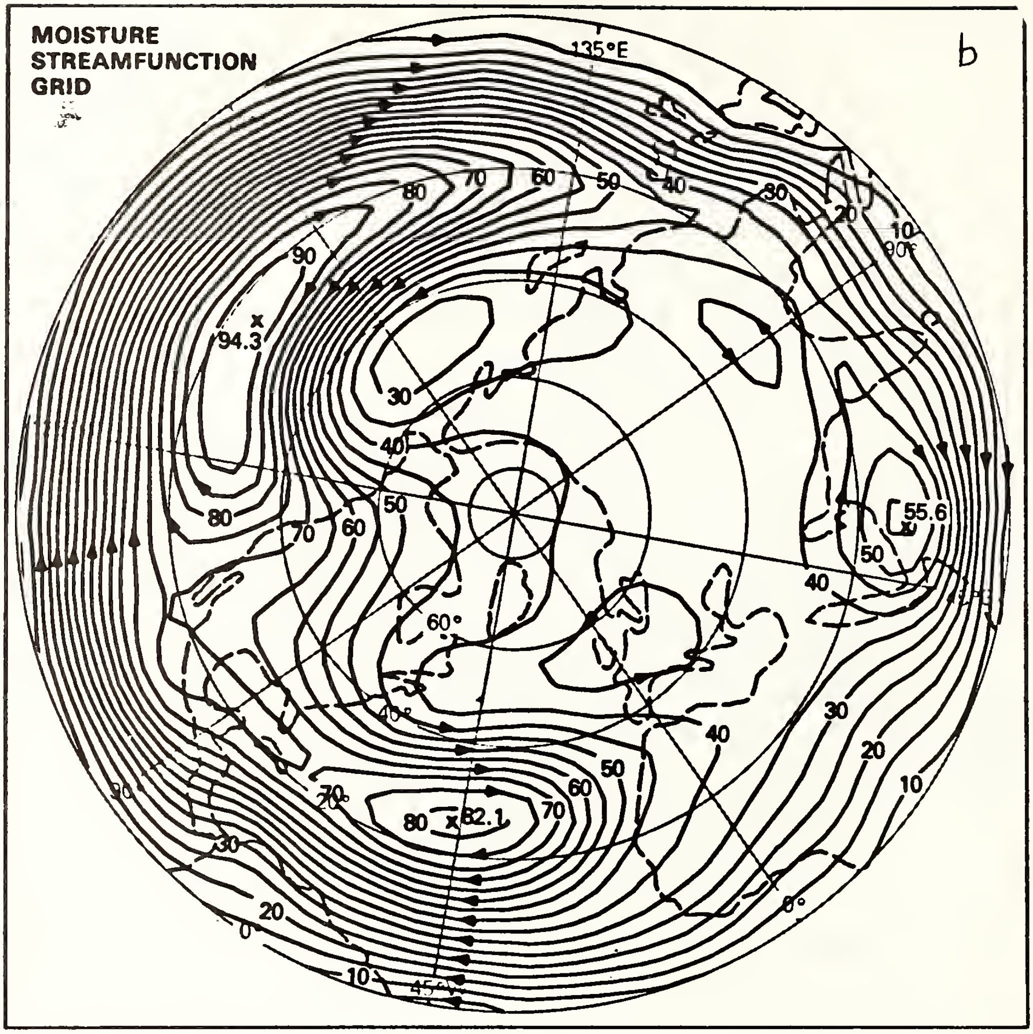
MOISTURE
STREAMFUNCTION
GRID
b
135°E
80
70
60
50
40
30
20
10
90°E
90
94.3
30
40
80
70
60
50
55.6
50
40
60°
40°
30
20
10
40
50
60
70
80
82.1
70
70
20°
90°
30
20
0
10
45°W
0°

# New Data and New Products: The NOAA/NESS Continental Snow Cover Data Base

by

Michael Matson, Donald R. Wiesnet, Craig P. Berg, and E. Paul McClain
NOAA/National Environmental Satellite Service

If anyone's impression of climatic variability was one of slowly evolving fluctuations of the atmosphere-cryosphere-ocean system about some mean value, the severe Eurasian winter of 1971-72 and the memorable North American winters of 1976-77, 1977-78, and 1978-79 dispelled this impression. All four winters certainly demonstrated the dynamic nature of the climatic system and its socio-economic impact. One parameter reflective of the dynamic nature of climate is snow cover. Until 1966 the monitoring of the areal extent of continental snow cover was limited to point measurements and extrapolations between these points. Mountainous and sparsely inhabited areas were poorly represented in this type of monitoring. In October 1966 the first satellite-derived Northern Hemispheric Weekly Snow and Ice Cover Chart was produced by the National Environmental Satellite Service (NESS) of NOAA. Since that time continental snow-cover extent has been monitored on a weekly basis by means of satellite data. The purpose of this paper is (1) to present the satellite record of continental snow cover during the winter of 1978-79, and (2) to describe the NOAA/NESS satellite-derived snow-cover products now available to climate researchers.

Figures 1 through 4 show the winter (December through March) snow lines for 1978-79 as compared with the 10-year mean snow lines. During all four months the North American snow line lay south of the 10-year mean snow line. With the exception of March, each of the winter months in North America exceed one standard deviation from the 10-year mean in snow-cover extent (see figures 5 and 6). January and February 1979 was the second consecutive year in which North American snow-cover extent exceeded the 10-year mean by more than one standard deviation. The increase in North American winter snow-cover extent is also shown in figure 7, a graph of the seasonal average of snow cover, December through February. The graph shows that since 1975 North American winter snow-cover extent has increased by 8 percent.

During the winter of 1978-79 Eurasian snow-cover extent exceeded the 10-year mean, principally in Europe (see figures 1 through 4). Figures 8 and 9 show that only January snow cover exceeded one standard deviation from the 10-year mean. The 1978-79 seasonal average Eurasian snow-cover extent, December through February, declined from the previous winter (see figure 10). The cyclic pattern is intriguing but the data set is too short to confirm the continuity of the cycle.

Table 1 is a listing of NOAA/NESS satellite-derived continental snow-cover products. The snow charts and related products provide a continental snow-cover index, which it is hoped will prove useful to climate researchers and modellers. One of the more promising of the new snow-cover products is the computer-derived 7-day Composite Minimum Brightness (CMB) chart (see figure 11). Over the 7-day compositing period, which is updated daily, only the minimum satellite-derived brightness value is retained for each 20 by 20 km spot. The filtering process objectively retains relatively permanent snow and ice fields. In general clouds are sufficiently transient to assure that they are not retained in the final product. Occasionally cloudiness will be so persistent in a particular region that the CMB technique fails to filter it out completely. Such time-composited cloud areas, however, are not usually as bright as composited snow and ice fields. Polar night coverage of the snow and ice fields is accomplished through the use of the accompanying 7-day Composite Maximum Temperature (CMT) charts (see figure 11). All temperature values above 0°C are depicted in black while all temperature values 0°C or less are depicted in increasing brightness levels from gray to white. To date the CMB and CMT product represents the only objective technique capable of delineating snow and ice fields on a continental scale. The daily nature of the CMB's and CMT's allows the construction of movie "loops" depicting the areal dynamics of hemispheric snow and ice cover extent throughout an annual cycle. Digital archival of the CMB data, currently not done, would provide a means whereby hemispheric snow and ice cover extent could be readily quantified, regionalized, and compared with other climatic parameters.

TABLE 1. NOAA/NESS SATELLITE-DERIVED CONTINENTAL SNOW COVER PRODUCTS

| PRODUCT | COVERAGE | TIME PERIOD | FORMAT |
|---|---|---|---|
| NORTHERN HEMISPHERE WEEKLY SNOW AND ICE COVER CHART | NORTHERN HEMISPHERE | WEEKLY, 1966-PRESENT | 1:50,000,000 POLAR STEREOGRAPHIC PROJECTION |
| NORTHERN HEMISPHERE MONTHLY MEAN SNOW COVER CHART | NORTHERN HEMISPHERE | MONTHLY, 1966-PRESENT | 1:50,000,000 POLAR STEREOGRAPHIC PROJECTION |
| 7-DAY COMPOSITE MINIMUM BRIGHTNESS (CMB) CHART | NORTHERN HEMISPHERE | DAILY, 1979-PRESENT | 1:110,000,000 POLAR STEREOGRAPHIC PROJECTION |
| MONTHLY MEAN SNOW COVER VALUES | NORTH AMERICA, EURASIA, AND NORTHERN HEMISPHERE | 1966-PRESENT | TABULATED COMPUTER PRINTOUT |
| SEASONAL SNOW COVER VALUES | NORTH AMERICA, EURASIA, AND NORTHERN HEMISPHERE | 1966-PRESENT | GRAPHS ON MICROFILM |
| 12 MONTH RUNNING MEAN SNOW COVER VALUES | NORTH AMERICA, EURASIA, AND NORTHERN HEMISPHERE | 1966-PRESENT | GRAPHS ON MICROFILM |
| PERCENT OF CONTINENT COVERED BY AVERAGE WINTER (DEC.-MAR.) SNOW COVER | NORTH AMERICA AND EURASIA | 1966-PRESENT | GRAPHS ON MICROFILM |

NOTE: The snow cover charts and the CMB chart are available as NOAA/NESS operational products. The printouts and plots of the snow cover values are currently NOAA/NESS research-related products and available only by individual requests to the authors.

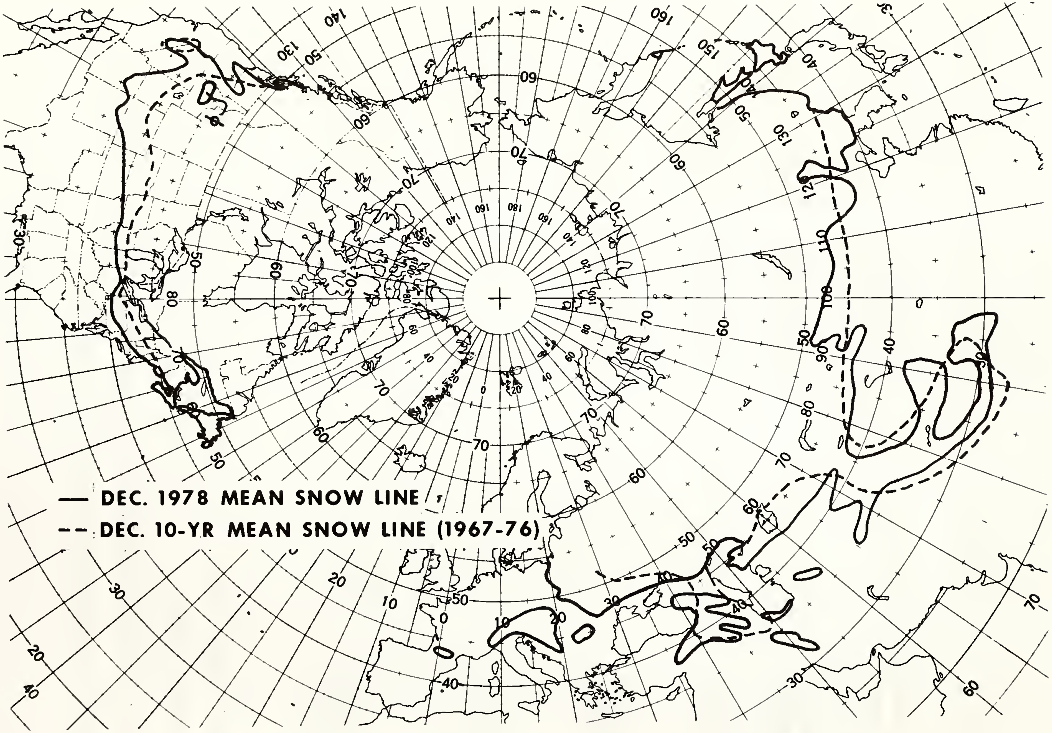
— DEC. 1978 MEAN SNOW LINE
-- DEC. 10-YR MEAN SNOW LINE (1967-76)

Fig. 1. Comparison of the satellite-derived mean snow line for December 1978 (solid line) with the 10-year satellite-derived mean snow line (dashed line). The snow line is terminated at 52°N because of insufficient solar illumination for satellite visible data.

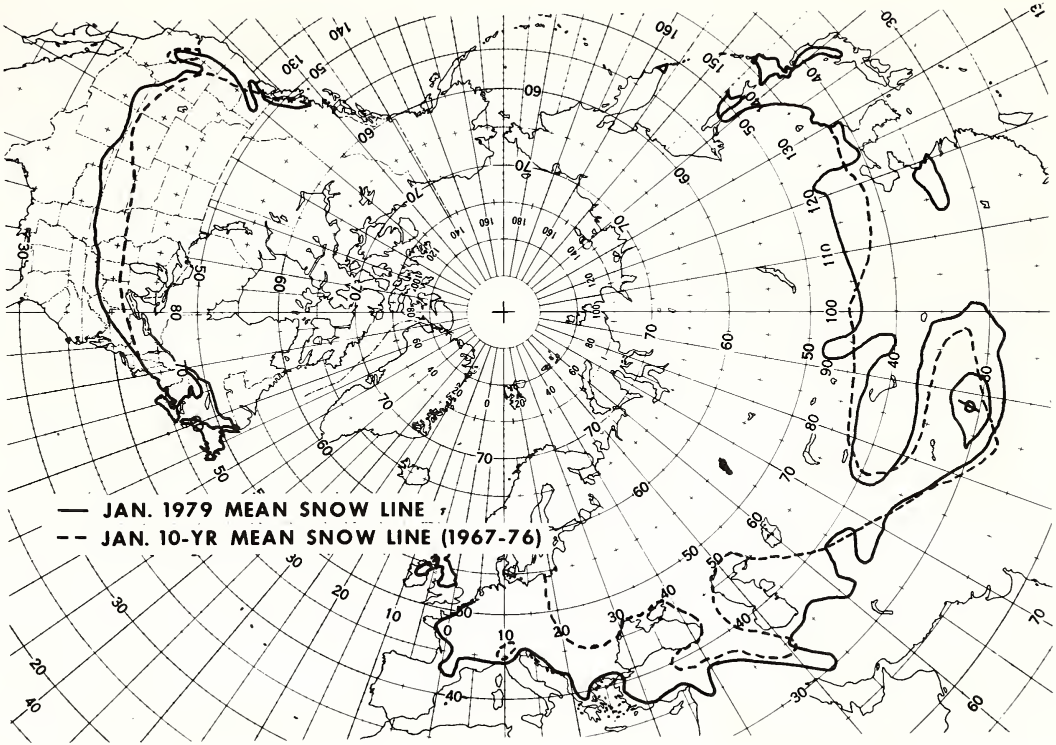
— JAN. 1979 MEAN SNOW LINE
-- JAN. 10-YR MEAN SNOW LINE (1967-76)

Fig. 2. Comparison of the satellite-derived mean snow line for January 1979 (solid line) with the 10-year satellite-derived mean snow line (dashed line).

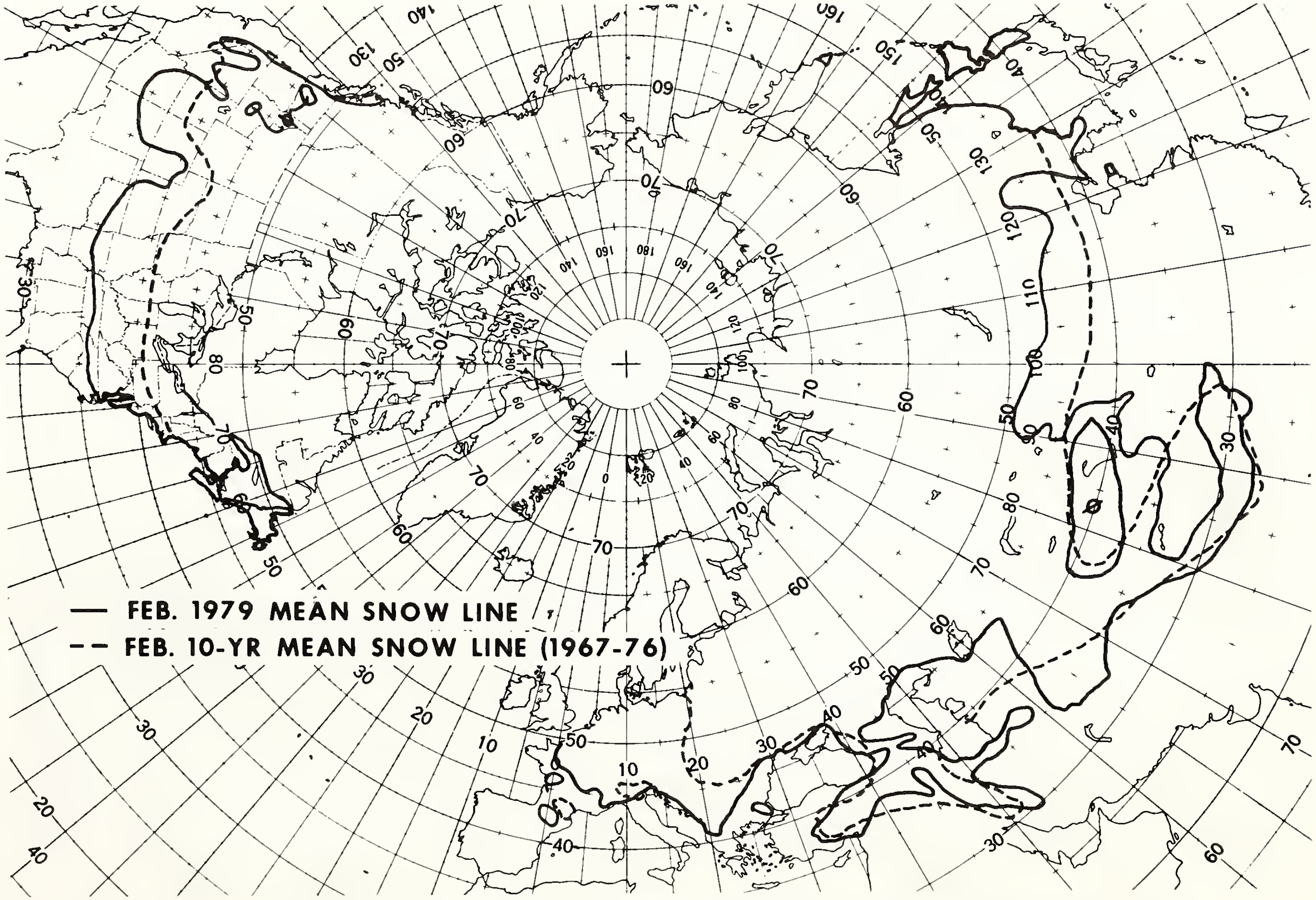
— FEB. 1979 MEAN SNOW LINE
-- FEB. 10-YR MEAN SNOW LINE (1967-76)

Fig. 3. Comparison of the satellite-derived mean snow line for February 1979 (solid line) with the 10-year satellite-derived mean snow line (dashed line).

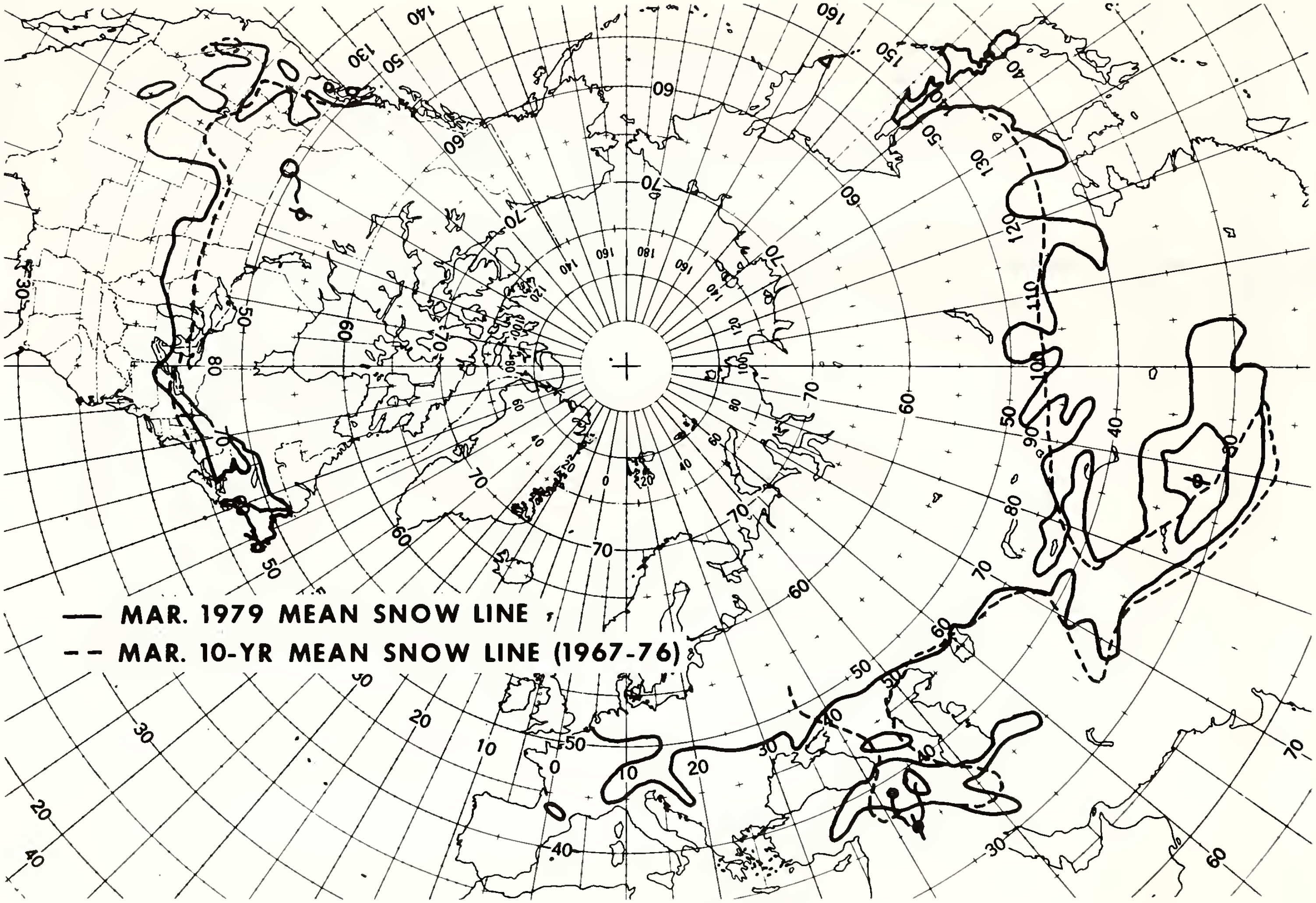
— MAR. 1979 MEAN SNOW LINE
-- MAR. 10-YR MEAN SNOW LINE (1967-76)

Fig. 4. Comparison of the satellite-derived mean snow line for March 1979 (solid line) with the 10-year satellite-derived mean snow line (dashed line).

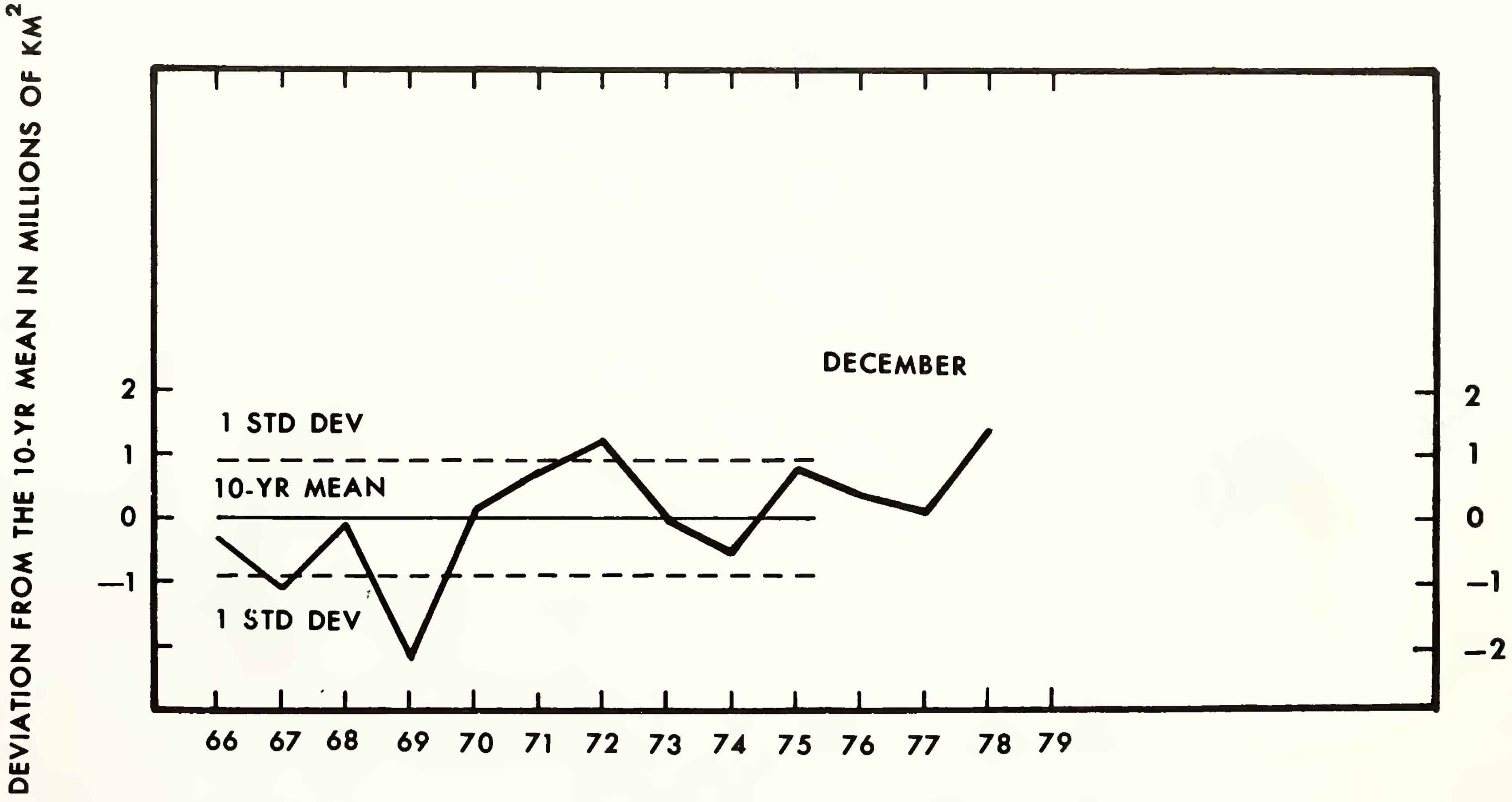

VARIABILITY OF DECEMBER SNOWCOVER IN NORTH AMERICA, 1966-1978

Fig. 5. Variability of monthly mean December snow cover in North America as determined from NOAA satellite data, 1966-1978.

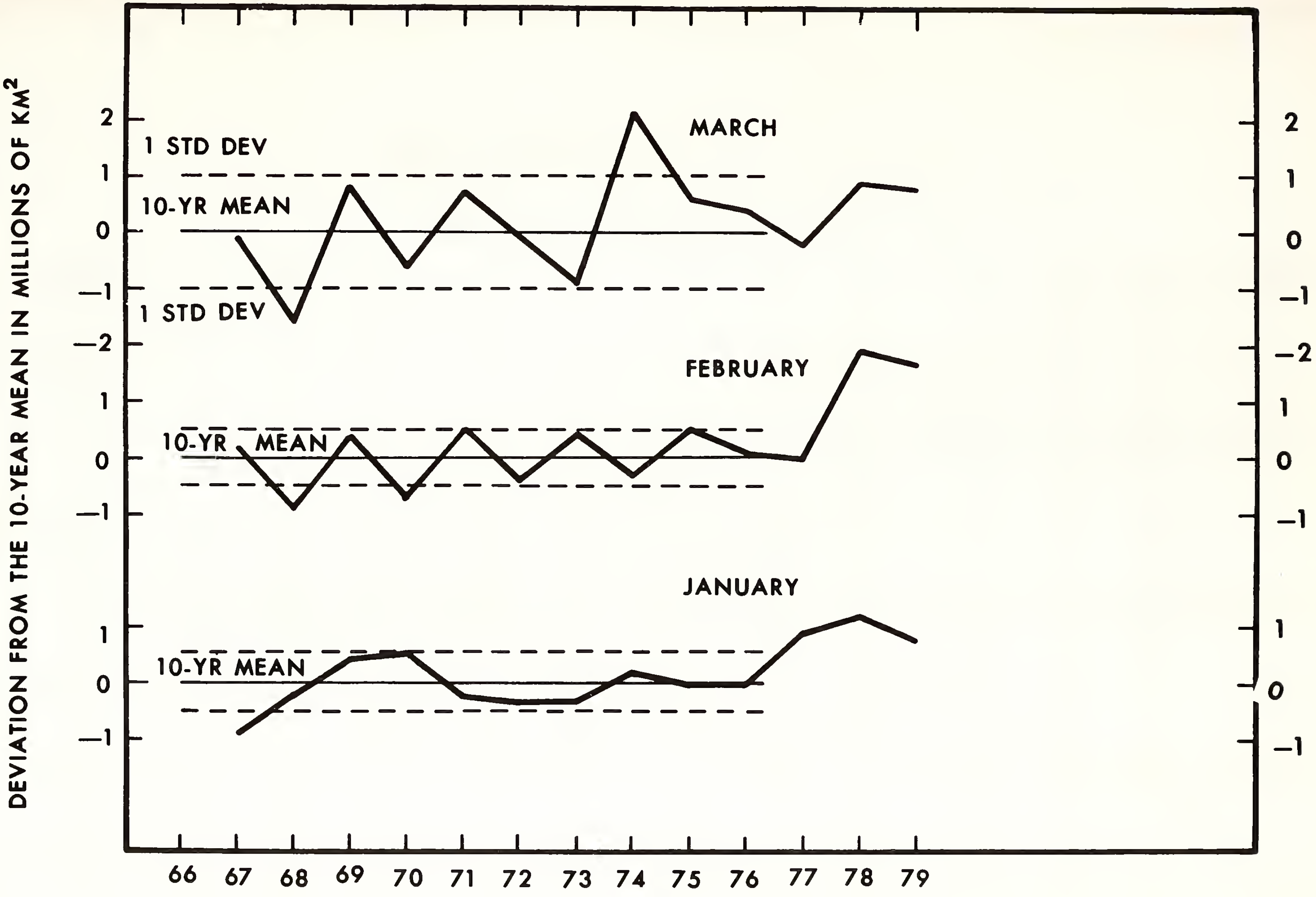

VARIABILITY OF JANUARY, FEBRUARY, AND MARCH SNOWCOVER IN NORTH AMERICA, 1967-1979

Fig. 6. Variability of monthly mean January, February, and March snow cover in North America as determined from NOAA satellite data, 1967-1979.

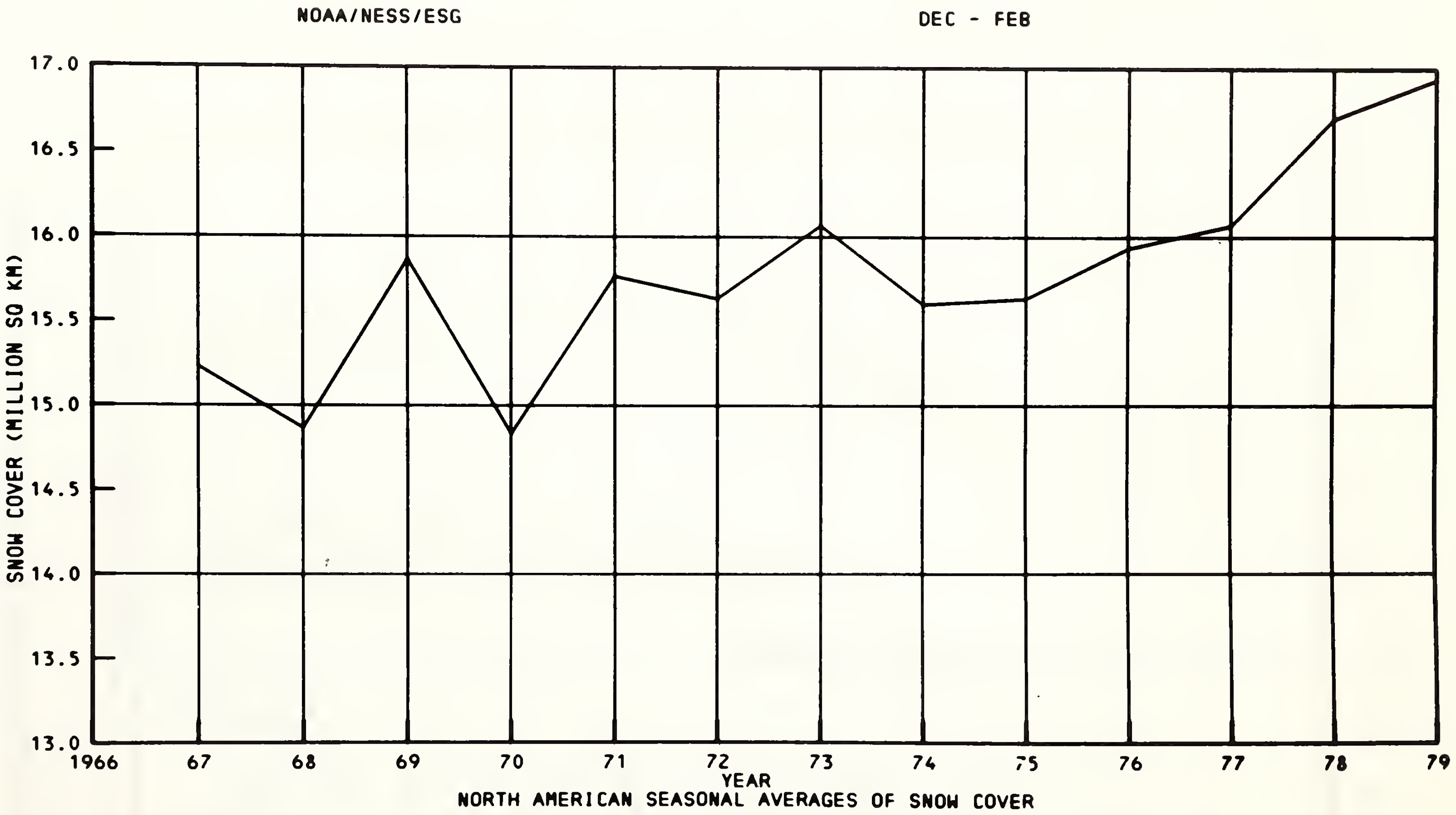

Fig. 7. North American December through February average snow-cover extent, 1967-1979.

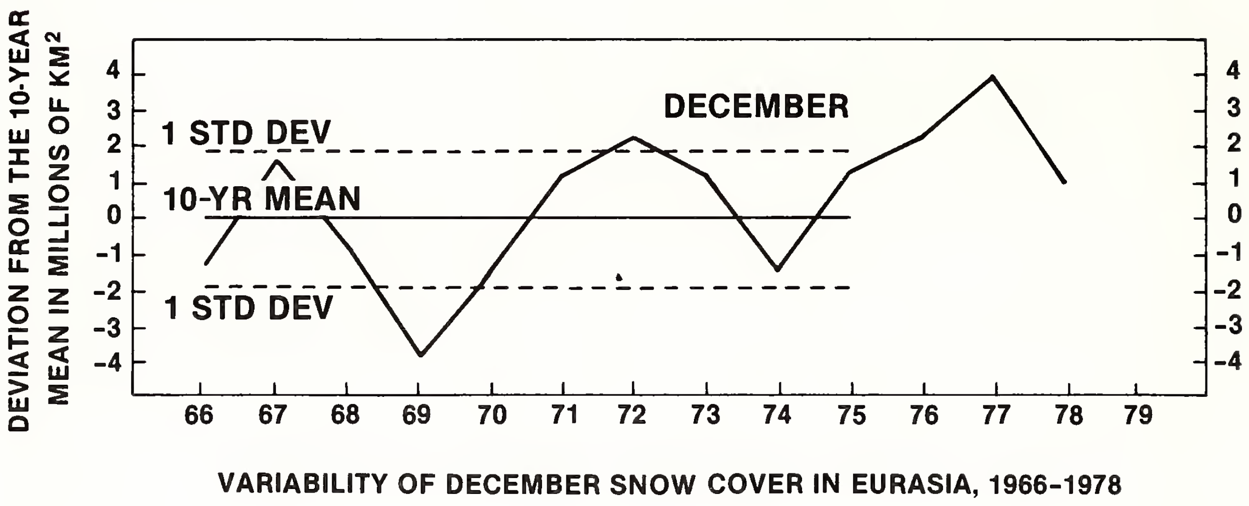

Fig. 8. Variability of monthly mean December snow cover in Eurasia as determined from NOAA satellite data, 1966-1978.

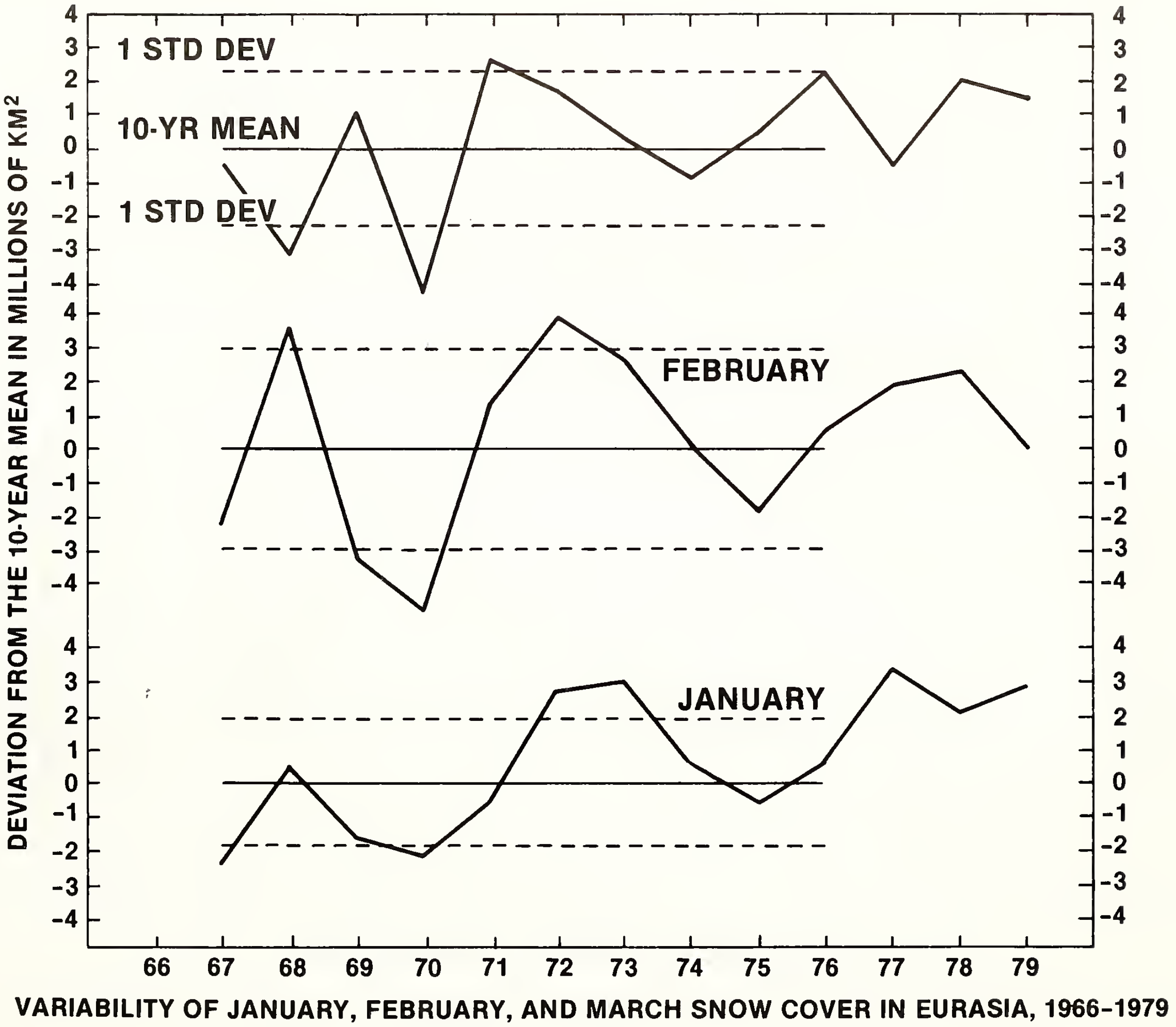

Fig. 9. Variability of monthly mean January, February, and March snow cover in Eurasia as determined from NOAA satellite data, 1967-1979.

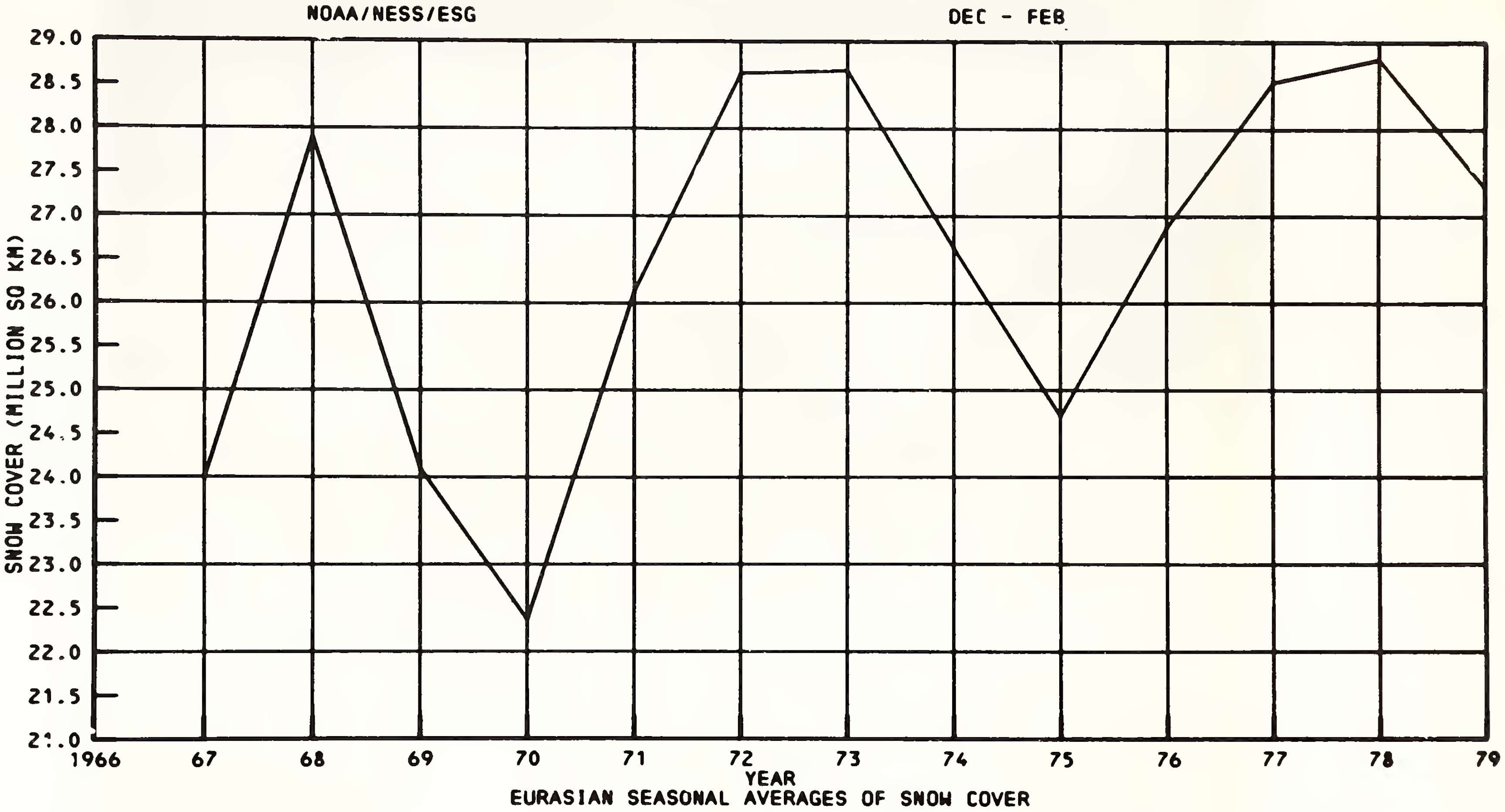

Fig. 10. Eurasian December through February average snow-cover extent, 1967-1979.

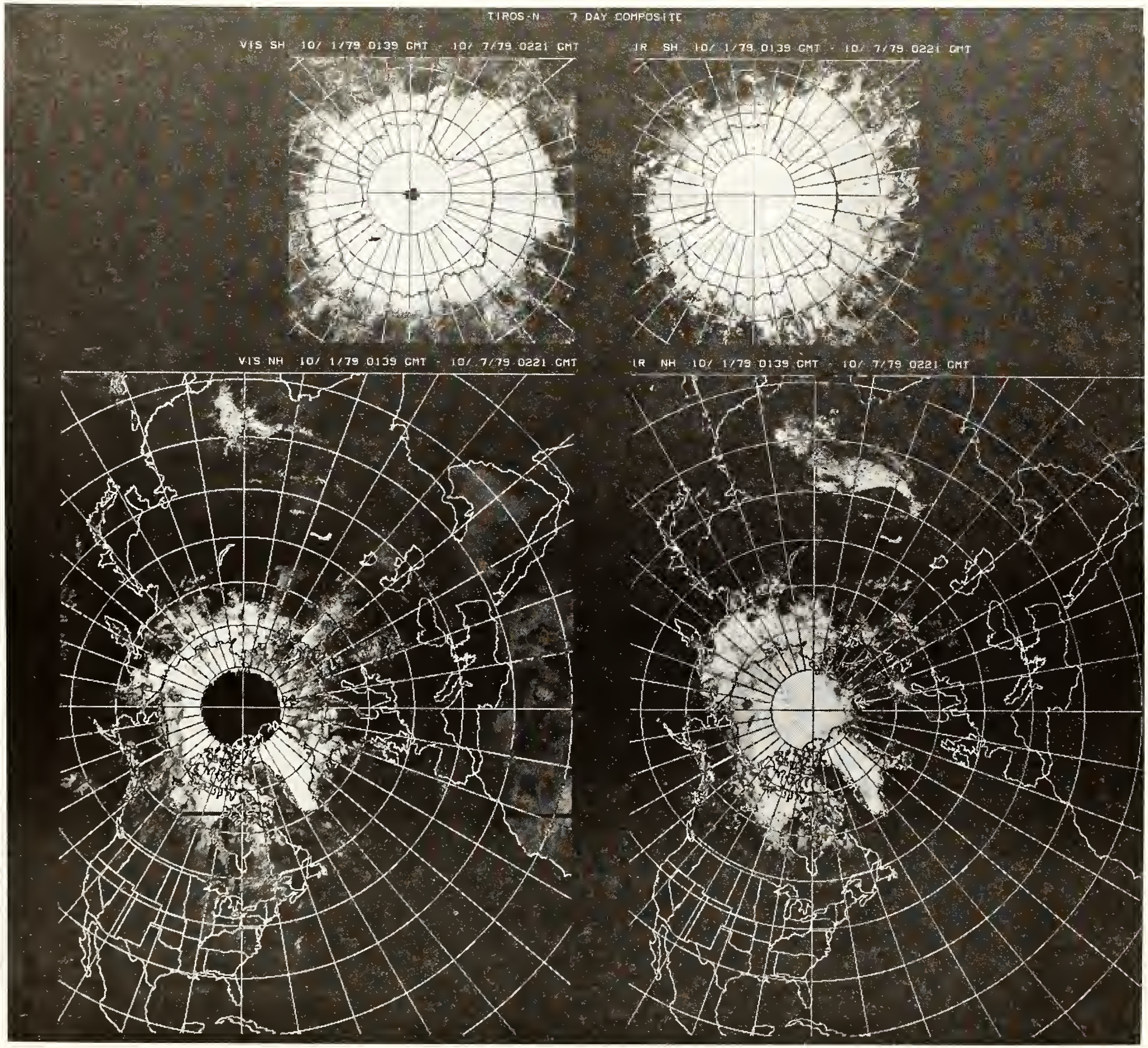
TIROS-N 7 DAY COMPOSITE
VIS SH 10/ 1/79 0139 GMT - 10/ 7/79 0221 GMT
IR SH 10/ 1/79 0139 GMT - 10/ 7/79 0221 GMT
VIS NH 10/ 1/79 0139 GMT - 10/ 7/79 0221 GMT
IR NH 10/ 1/79 0139 GMT - 10/ 7/79 0221 GMT

Fig. 11. 7-day Composite Minimum Brightness (CMB) chart for the period October 1 through October 7, 1979 (the two charts on the left). The 7-day Composite Maximum Temperature (CMT) charts are represented by the two charts on the right.

# The Northern Hemisphere sea level pressure data set: Trends, errors and discontinuities.

Kevin E. Trenberth and Daniel A. Paolino, Jr.
Laboratory for Atmospheric Research
University of Illinois
Urbana, Illinois 61801

A detailed examination of the Northern Hemisphere monthly mean sea level grid point pressures shows a disappointingly large number of problems. The data set extends from 1899-1977 but has originated from eight different sources (see Table 1) and discontinuities have been identified with every change in source.

Comparisons of grid point with station data for each month has revealed many serious errors. Their distribution as a function of space and time are shown in Tables 2 and 3. Most of the errors are over Asia, and are predominant before about 1922 or during World War II. They have been corrected or set to missing. Table 4 shows the number of missing values in the original and corrected data set. The number of points departing from the mean by 3.0, 3.2, 3.5 and 4.0 standard deviations in the final version of the data set which also includes corrections for several discontinuities are presented in Table 5, along with comparable values for a normal distribution.

The discontinuities were corrected for by (i) identifying the time of the discontinuity from grid point-station values comparisons, and (ii) assuming no trend between the subperiods on either side of the discontinuity. Results are shown for the following:

(a) March 1902 - August 1909 in the vicinity of Dawson (Fig. 1);
(b) over Asia for the discontinuities between 1) June and July 1939; and 2) December 1945 and January 1946; and 3) during 1956.

Fig. 2 shows the student-t values for the differences between the means of each subperiod 1) 1899(1)-1939(6), 2) 1937(7)-1945(12), 3) 1946(1)-1956(5) and subperiod 4) 1956(6)-1977(12). Fig. 3 shows the area over Asia where the discontinuities are present--note the resemblance with the region of high orography (Fig. 4). The correction patterns for the first three subperiods relative to subperiod 4 are shown in Fig. 5.

Other problems still remain in the corrected data set as shown by station versus grid-point time series in Fig. 6.

An analysis of the zonal mean pressures and hemispherically averaged mean pressures is shown in Fig. 7. Values before the discontinuity analyses are presented and compared to those after the corrections were applied. Some of the remaining apparent trends are spurious.

Both U.S. Navy and U.S.N.M.C. operational analyses have been used in this data set. A comparison of monthly means from each source for December 1975 - February 1976 has been made and results are shown in Fig. 8. The discrepancy appears to be mainly due to errors in the N.M.C. analyses.

It is clear that a greater effort is desirable in archiving quality controlled climatological data with a need for accompanying documentation to be as complete as possible.

Table 1 Sources of sea level pressure data grids. All are based on daily analyses except as noted. Continual updates of this series are made from time to time.

| | Dates Year(month) | Source | Comment | Time |
|---|---|---|---|---|
| 1 | 1899(1)-1939(6) | N.C.C. | Historical map series 75, 85, 90N missing | (13Z) |
| 2 | 1939(7)-1944(11) | M.I.T. | 85N missing | (12Z) |
| 3 | 1944(12) | | All missing | |
| 4 | 1945(1)-1945(12) | Scripps Inst. Oceanog. | Monthly means only | |
| 5 | 1946(1)-1955(3) | N.C.C. (Navy contracts) | Digitized with curve follower and objectively analyzed by Navy | (12Z) |
| 6 | 1960(4)-1962(6) | | | (12Z) |
| 7 | 1955(4)-1960(3) | N.M.C. | 433L-ESSPO Project (hand drawn analyses) | (00 Z, 12Z) |
| 8 | 1962(6)-1977(12) | Navy | Operational objective analyses | (00 Z, 12Z) |

N.C.C. = National Climatic Center (Asheville, NC)
M.I.T. = Massachusetts Institute of Technology

Table 2. Distribution of errors of status 0 and 1 for bands 5-120E (Asia), 125E-120W (Pacific), 120W-0 (N. Am-Atlantic) and 10 degree latitude bands.

| latitude | 20-25 | 30-35 | 40-45 | 50-55 | 60-65 | 70-75 | TOTAL |
|---|---|---|---|---|---|---|---|
| Asia | 920 | 427 | 348 | 58 | 62 | 7 | 1882 |
| Pacific | 500 | 32 | 59 | 7 | 223 | 136 | 957 |
| N. Am-Atlantic | 323 | 19 | 8 | 0 | 87 | 47 | 484 |
|  | 1743 | 478 | 415 | 65 | 372 | 190 | 3263 |

Table 3. Number of errors in each "decade", N.

| Interval | 1899-1910 | 1911-20 | 1921-30 | 1931-40 | 1941-50 | 1951-60 | 1961-70 | 1971-77 |
|---|---|---|---|---|---|---|---|---|
| N | 1092 | 510 | 269 | 418 | 724 | 206 | 26 | 18 |

Table 4. Numbers of missing data in the corrected and original data set.

|  | 1899(1)-1939(6) | 1939(7)-1945(12) | 1946(1)-1956(5) | 1956(6)-1977(2) |
|---|---|---|---|---|
| original | 10,018 | 136 | 0 | 0 |
| corrected | 11,747 | 565 | 150 | 172 |

Table 5. Number of points departing from the long term mean by 3.0, 3.2, 3.5, and 4.0 standard deviations compared to a normal distribution (ND).

|  | N | >3.0 | >3.2 | >3.5 | >4.0 |  |
|---|---|---|---|---|---|---|
| 1899(1)-1939(6) | 408157 | 776 | 331 | 49 | 10 | Data |
|  |  | 1102 | 561 | 190 | 26 | ND |
| 1899(1)-1977(2) | 805574 | 1785 | 824 | 153 | 50 | Data |
|  |  | 2175 | 1106 | 374 | 51 | ND |

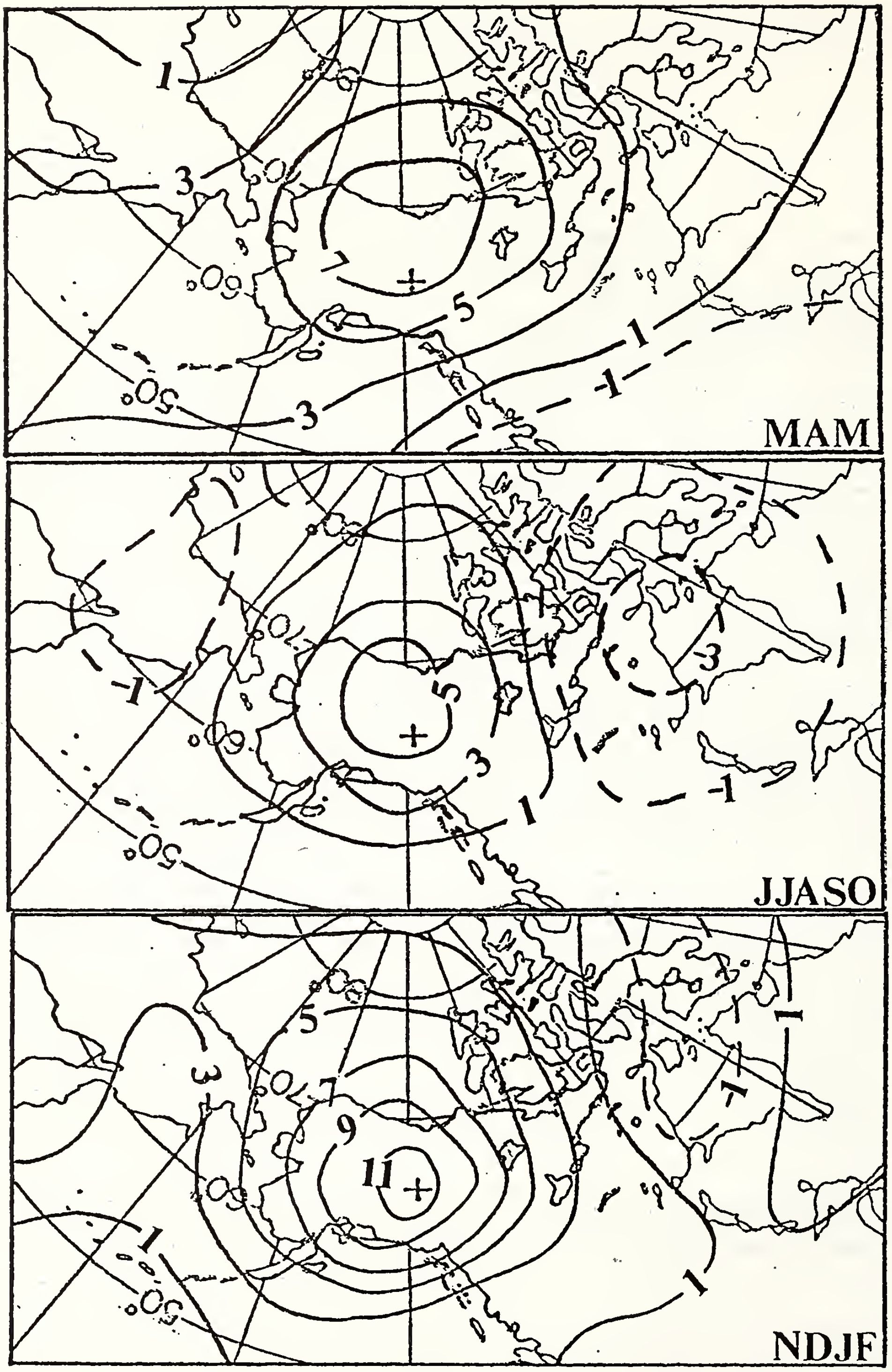

Fig. 1 Differences in analyzed sea level pressure (mb) between March 1902 - July 1909 and August 1909 - August 1916 for three sets of months (a) March, April and May, (b) June, July, August, September and October, and (c) November, December, January and February. The + indicates the location of Dawson. Negative contours are dashed.

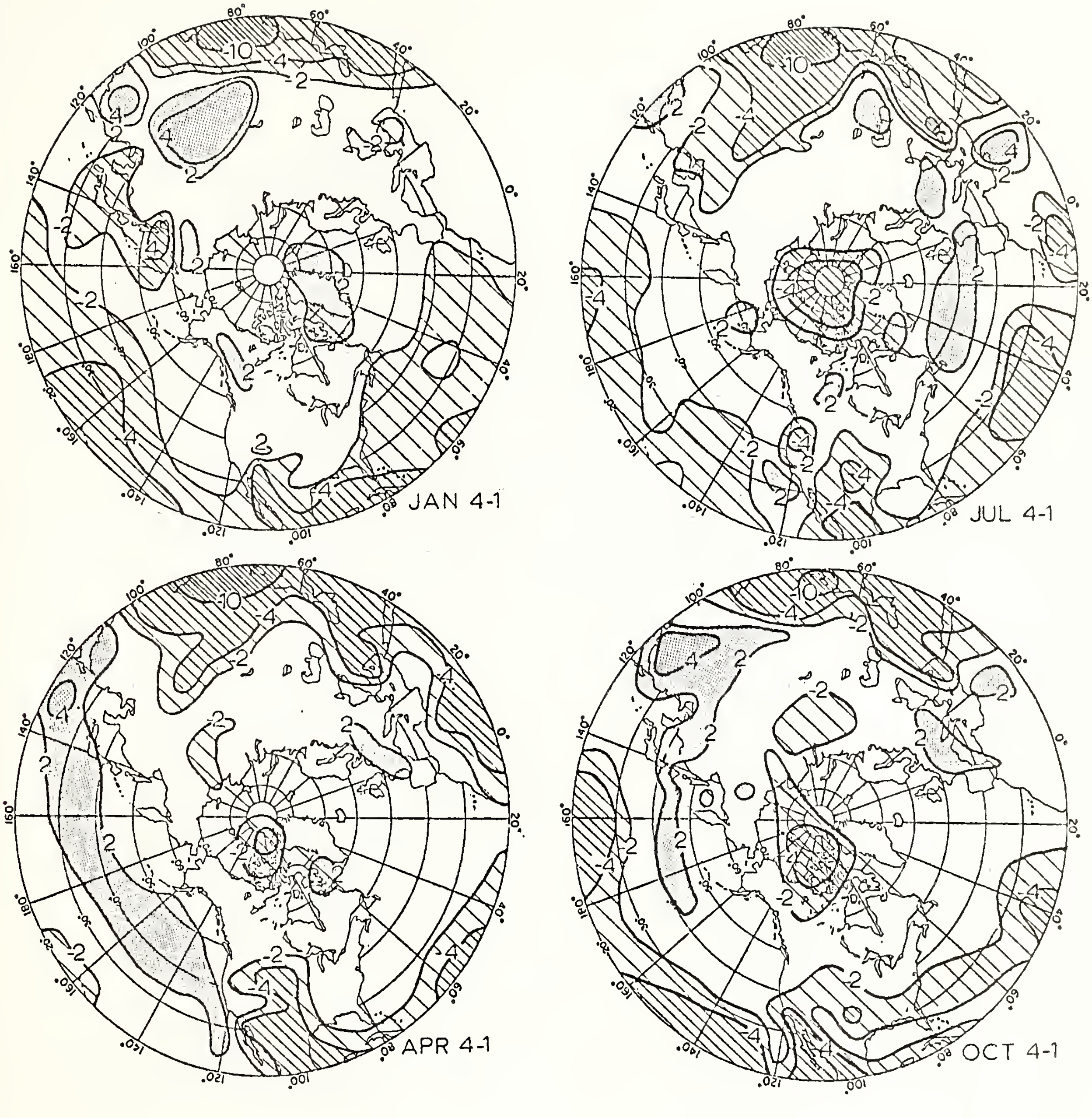

Fig. 2a Student-t test values in the comparison of the means for subperiods 1) 1899(1) - 1939(6), 2) 1939(7) - 1945(12), 3) 1946(1) - 1956(5) with subperiod 4) 1956(6) - 1977(12). t-magnitudes of 2 (95% significance), 4 (99.99% significance) and 10 are plotted for January, April, July and October. Positive values indicate pressures were higher in subperiod 4.

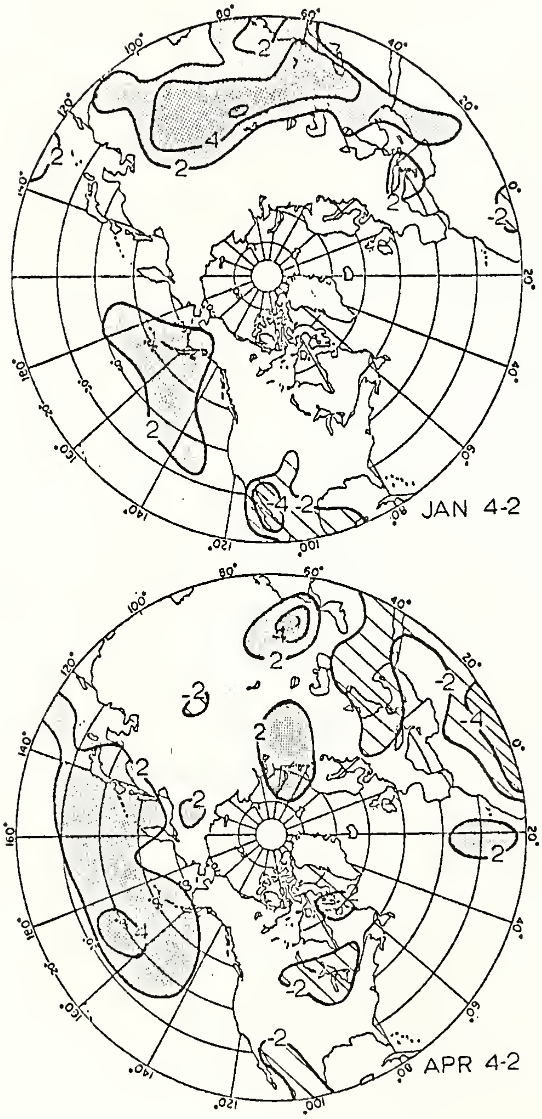

Fig. 2b Student-t test values in the comparison of the means for subperiods 1) 1899(1) - 1939(6), 2) 1939(7) - 1945(12), 3) 1946(1) - 1956(5) with subperiod 4) 1956(6) - 1977(2). t-magnitudes of 2 (95% significance), 4 (99.99% significance) and 10 are plotted for January, April, July and October. Positive values indicate pressures were higher in subperiod 4.

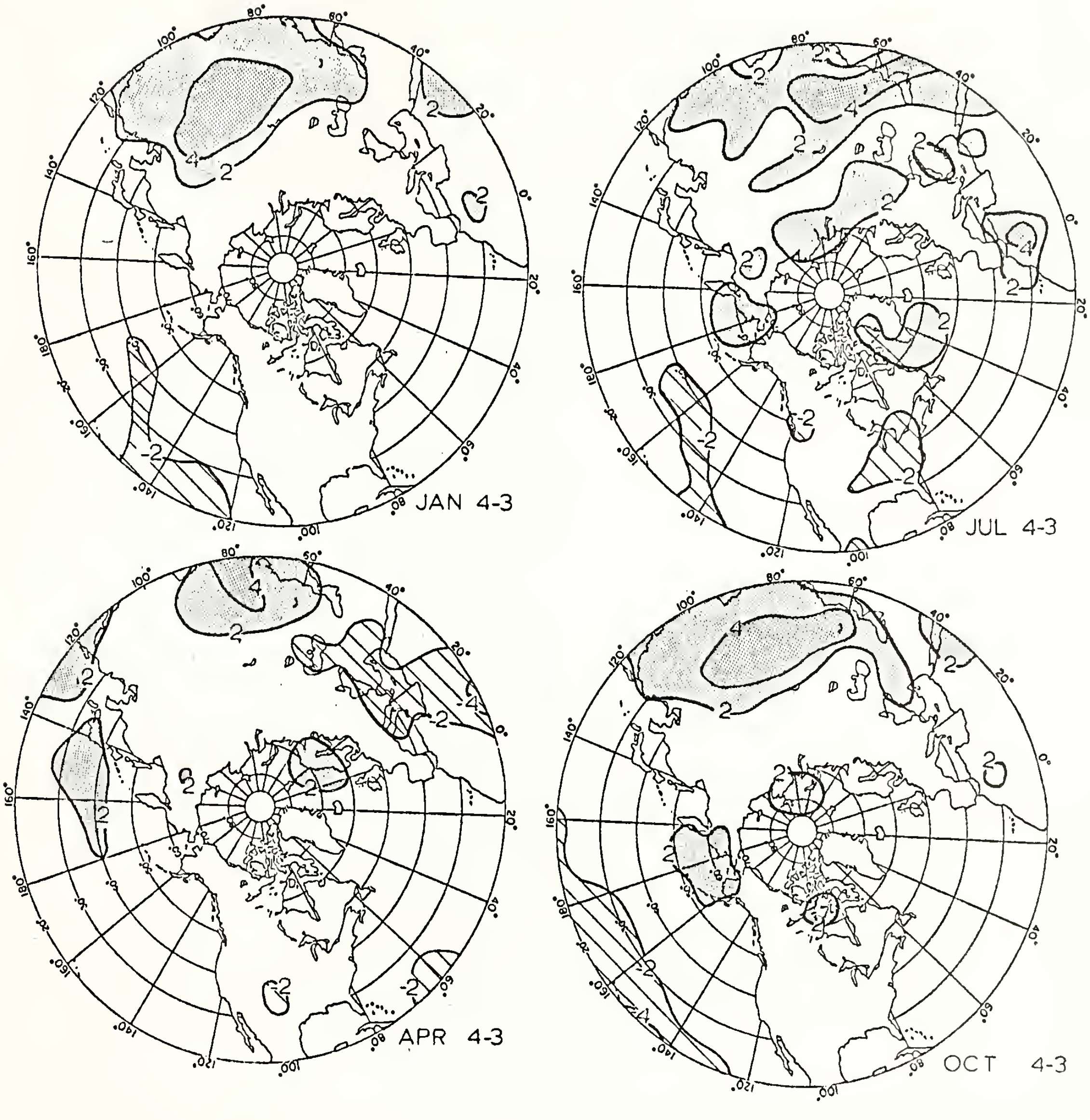

Fig. 2c Student-t test values in the comparison of the means for subperiods 1) 1899(1) - 1939(6), 2) 1939(7) - 1945(12), 3) 1946(1) - 1956(5) with subperiod 4) 1956(6) - 1977(2). t-magnitudes of 2 (95% significance), 4 (99.99% significance) and 10 are plotted for January, April, July and October. Positive values indicate pressures were higher in subperiod 4.

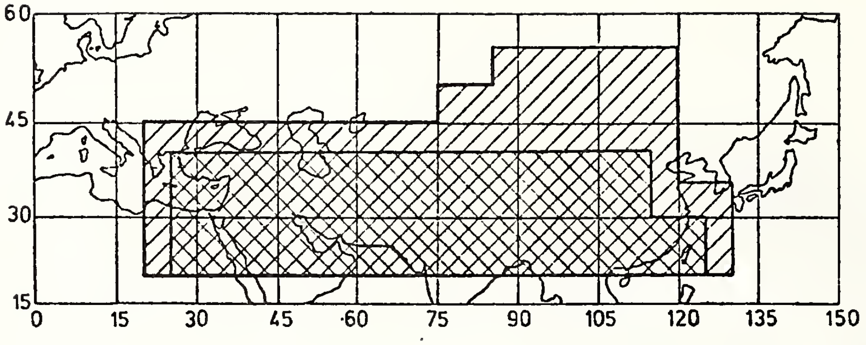

Fig. 3 Area affected by the three major discontinuities. Inside the cross-hatched area the discrepancy is assumed totally due to the discontinuity. The single hatched area is the merge region and at the outer points it is assumed that half the discrepancy was caused by the discontinuity.

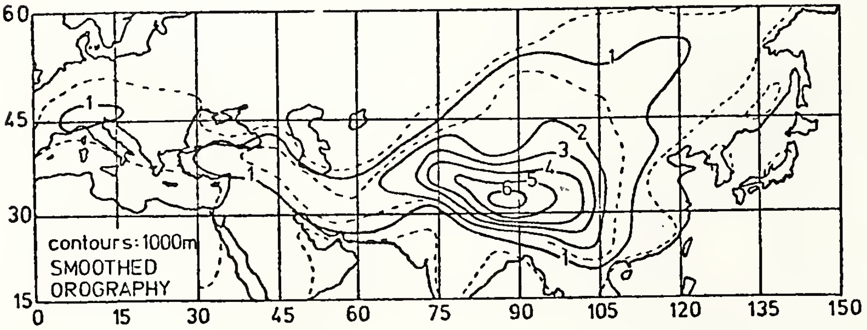

Fig. 4 Smoothed orography, with 1000 m contours, adapted from Berkofsky and Bertoni (1955).

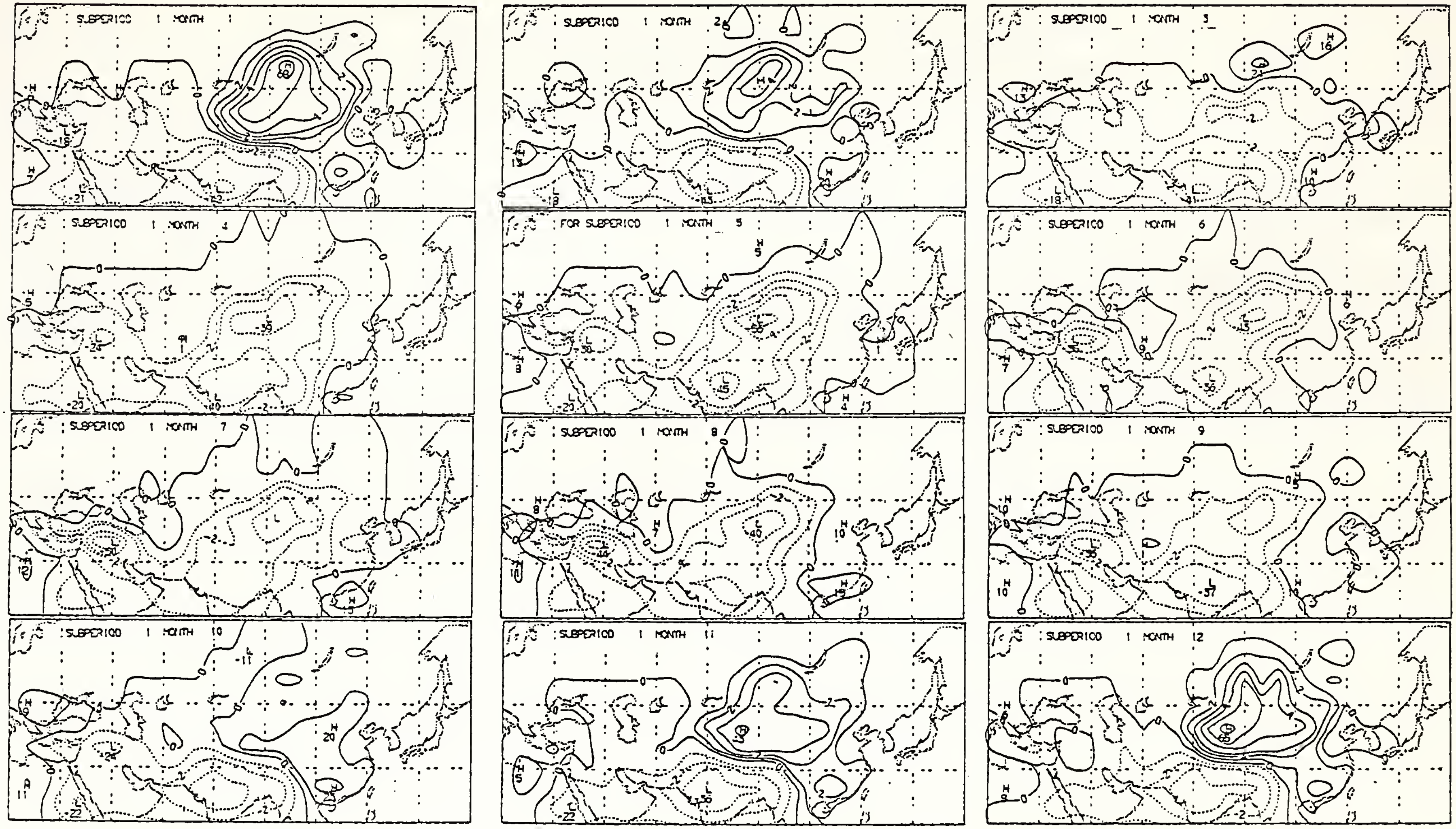

Fig. 5a Correction patterns for subperiods 1, 2 and 3 compared to subperiod 4. Values are in mb and the contour interval is 1 mb. Highs and lows are given in tenths of mb. The domain contoured extends from 15-60N, 15-150E with latitude and longitude lines every 15°.

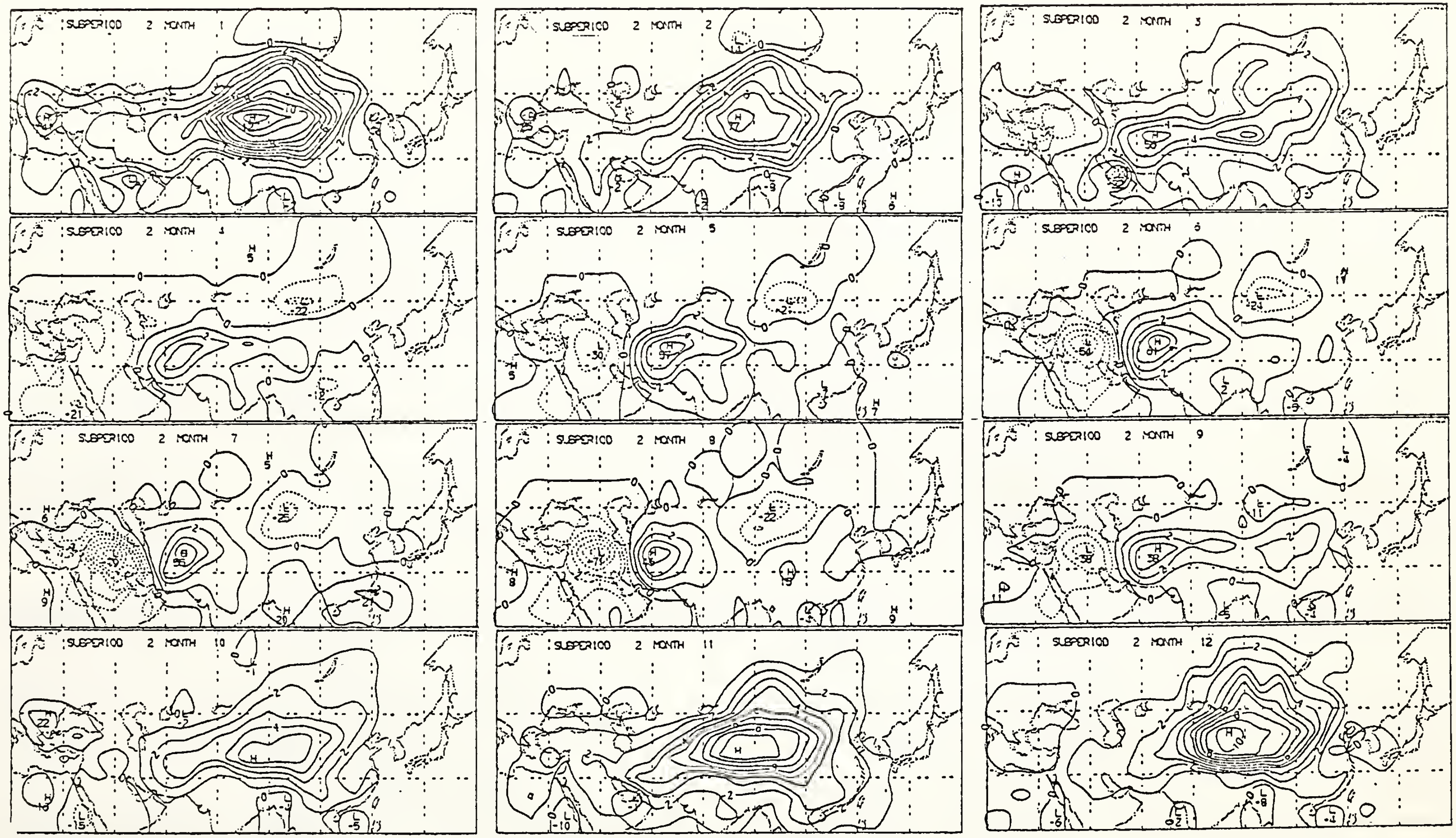

Fig. 5b Correction patterns for subperiods 1, 2 and 3 compared to subperiod 4. Values are in mb and the contour interval is 1 mb. The domain contoured extends from 15-60N, 15-150E with latitude and longitude lines every 15°.

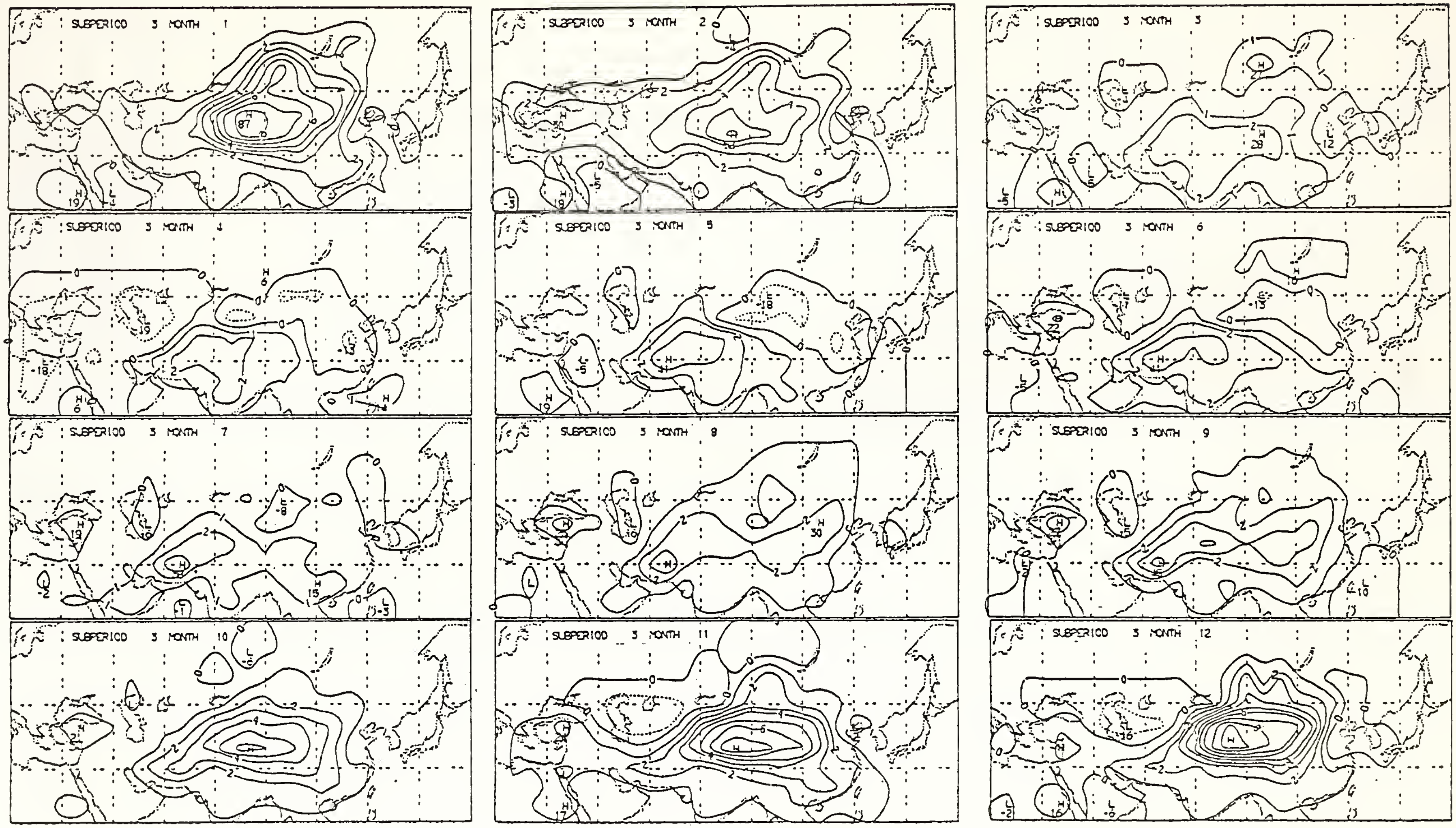

Fig. 5c Correction patterns for subperiods 1, 2 and 3 compared to subperiod 4. Values are in mb and the contour interval is 1 mb. The domain contoured extends from 15-60N, 15-150E with latitude and longitude lines every 15°.

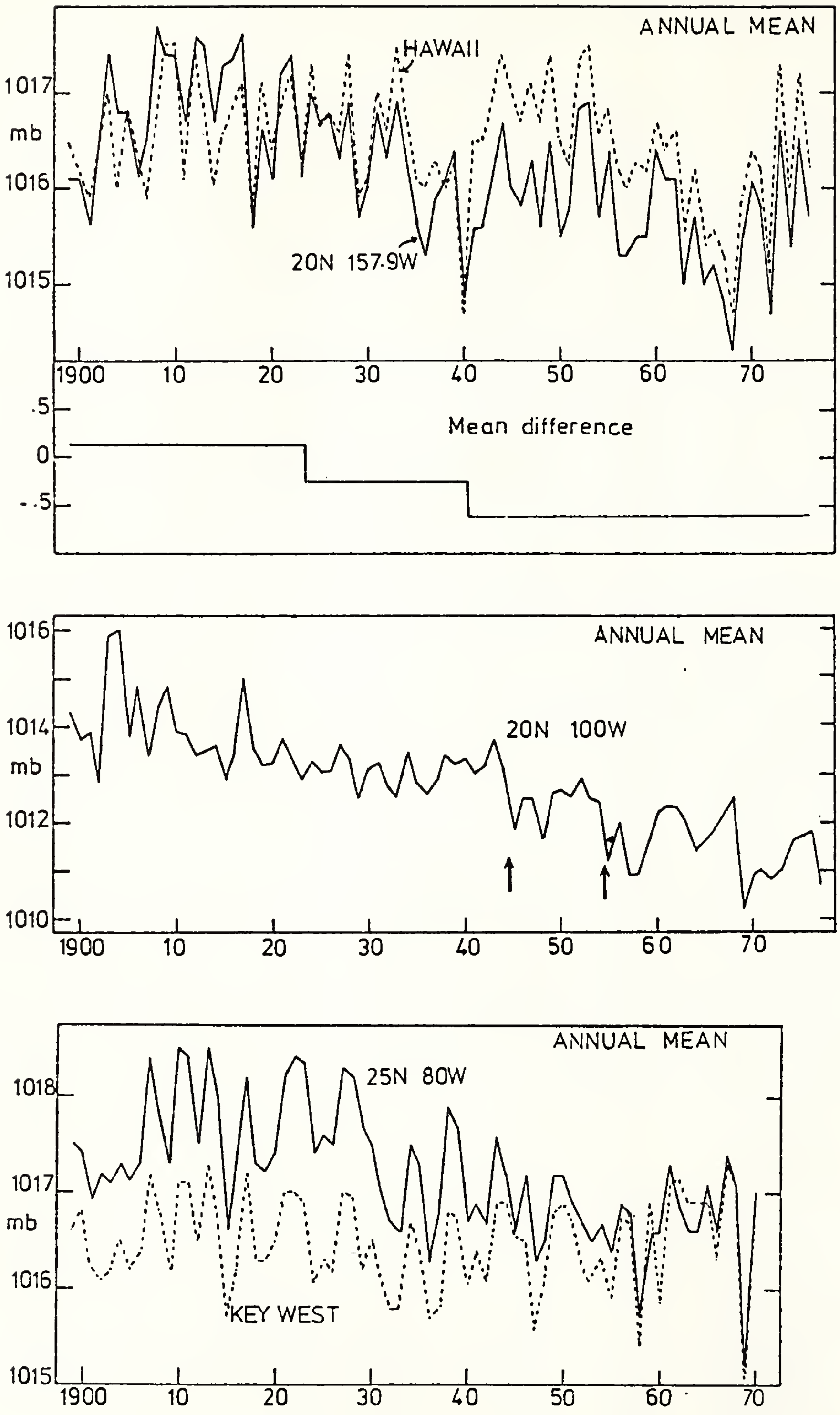

Fig. 6 Time series of annual mean pressures

(a) Grid point values interpolated to 20N 157.9W versus Hawaii (21.3N 157.9W), and the mean difference between them;

(b) Grid point values at 20N 100W (Mexican highlands) with two discontinuities indicated by heavy arrows;

(c) Grid point values at 25N 80W versus Key West (24.6N 81.8W).

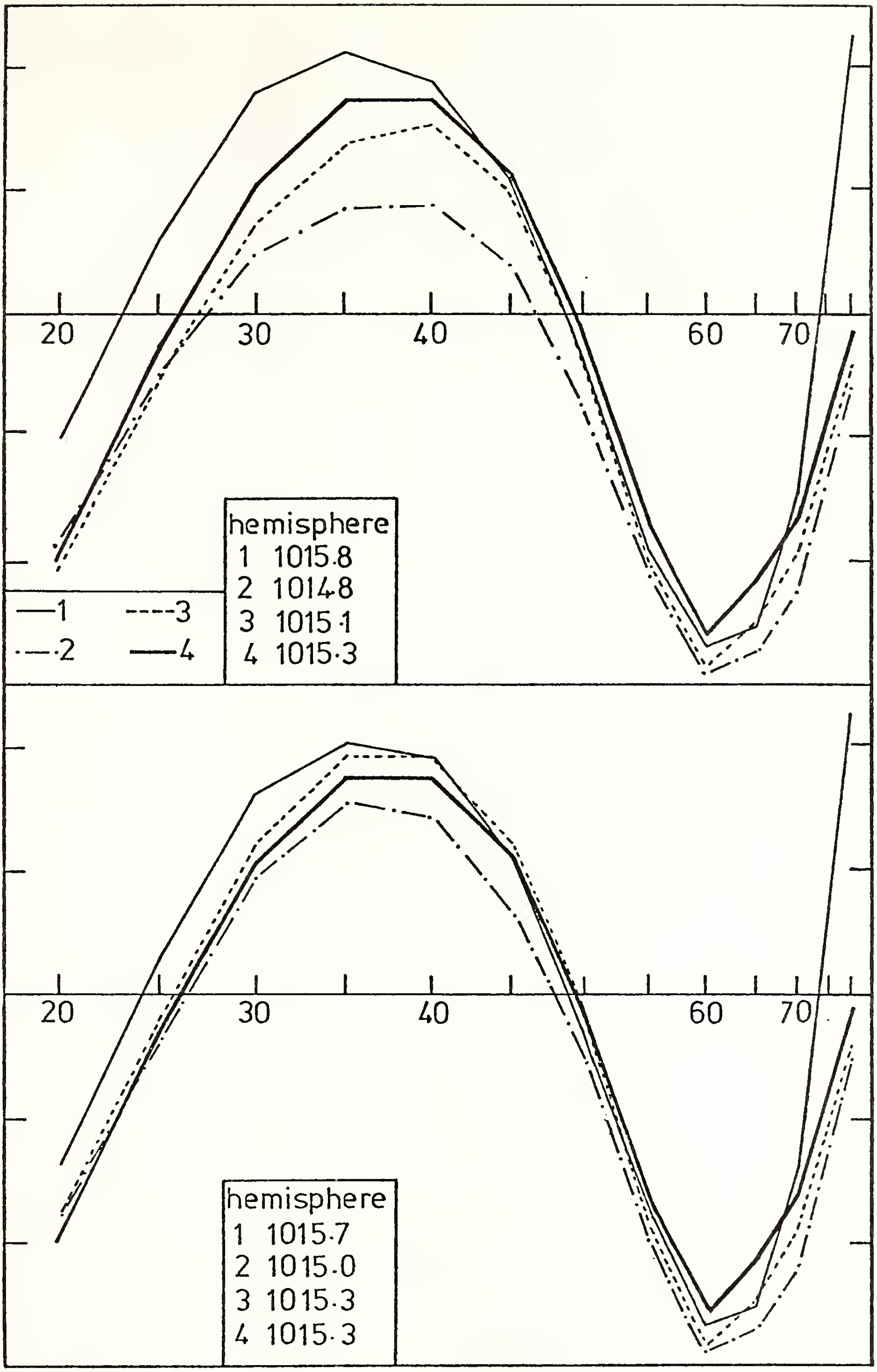

Fig. 7 Zonally averaged annual mean sea level pressure as a function of the sine of the latitude and the hemispheric (17.5N - 87.5N) value for the four subperiods 1) 1899(1) - 1939(6); 2) 1939(7) - 1945(12); 3) 1946(1) - 1956(5); 4) 1956(6) - 1977(12). (a) Values after correcting for errors but prior to discontinuity correction; (b) After discontinuity has been corrected.

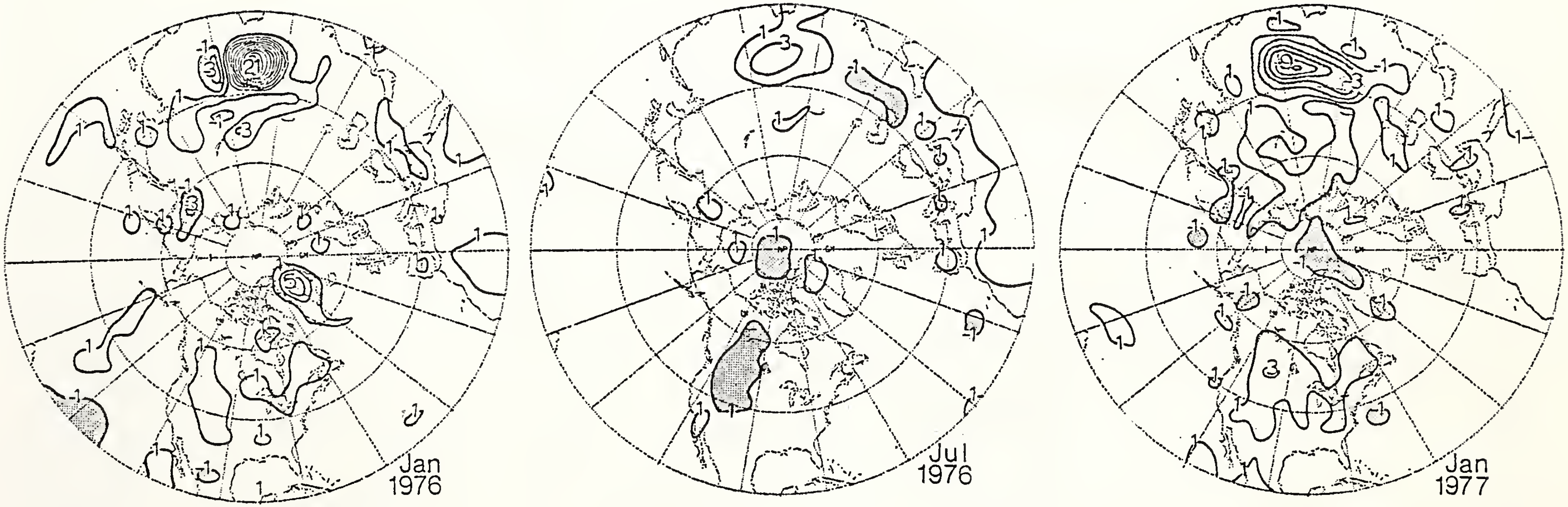

Fig. 8 Differences between monthly mean sea level pressure analyses by N.M.C. and the Navy, (N.M.C.-Navy), for (a) Jan 1976, (b) July 1976, (c) Jan 1977. Contours are every 2 mb and values less than -1 are shaded.

# PRELIMINARY ANALYSIS OF THE SEASONAL AND INTERANNUAL VARIABILITY SIMULATED BY THE OSU TWO-LEVEL ATMOSPHERIC GENERAL CIRCULATION MODEL

M. E. Schlesinger and W. L. Gates
Climatic Research Institute
and
Department of Atmospheric Sciences
Oregon State University, Corvalis, Oregon

## 1. Introduction

To assess the capability of an atmospheric general circulation model (AGCM) to simulate a climatic change for which there are no verifying observations, such as that resulting from an increase in atmospheric carbon dioxide, it is necessary to evaluate the model's performance in simulating climatic changes for which there are verifying observations. Since the seasons are the best known climatic changes, it is particularly important that the seasonal performance of a model be evaluated.

Such evaluations of the seasonal performance of the two-level AGCM have been made by Gates and Schlesinger (1977) and Schlesinger and Gates (1979). However, because of the model's computational requirement on the then-available computer (8.5 minutes per simulated day on an IBM 360-91), those evaluations were based only on the model's simulated solstice climates as obtained from a pair of two-month integrations for December-January and June-July. While such "snapshot" evaluations have been useful in identifying and correcting several systematic model errors, it is desirable to evaluate the model's seasonal performance over a complete annual simulation. It is also of interest to evaluate the interannual climate variations simulated by the model during an extended integration.

## 2. Initial and boundary conditions

With the availability of the CRAY 1 computer at the National Center for Atmospheric Research, it is now possible to perform multi-year simulations with the OSU two-level AGCM. We have therefore re-coded the OSU model to run on the CRAY (on which it requires 32 seconds per simulated day), and have performed an integration over 39 simulated months with a version of the two-level model similar to that described by Schlesinger and Gates (1979).

The two-level model was initialized at 1 December of year 0 as in the December-January simulation reported by Schlesinger and Gates (1979), except that the permanent snow mass over glacial land ice was initialized at 500 g $cm^{-2}$; the model was then integrated for 39 months through February of year 4. The earth-sun distance and solar declination were updated once a day through their annual cycle. The distributions of sea-surface temperature and sea ice were prescribed from the monthly tabulated data of Alexander and Mobley (1976). The sea-surface temperatures were updated once a day through their annual cycle, while the sea ice distribution was updated once a month through its annual cycle. Therefore the prescribed boundary conditions did not vary from year to year during the integration.

## 3. Results

In the following we shall discuss both the "normal" climatology simulated by the model (defined as the 3-year mean during the last 36 months of the simulation) and the simulated interannual anomalies from that "normal" climatology. Thus, the normal monthly mean for each of the months March through December is taken as the average of the respective monthly means for years 1, 2 and 3, while the normal monthly mean for January and February is taken as the average of the respective monthly means for years 2, 3 and 4.

### a. *Sea-level pressure*

The sea-level pressure distributions and anomalies for January of years 2, 3 and 4 are shown in Figs. 1a-c. Considering these three Januaries together, we see that the simulated sea-level pressure varies locally from year to year by as much as 14 mb in the middle and higher latitudes of both hemispheres, and that there are distinct regions of maximum variability. This is confirmed by the distribution of the standard deviation of the three January monthly means (not shown) which reveals maximum interannual variability from the central Pacific to western North America, and in the northeastern Atlantic, north-central Siberia, and the north polar region. In the Southern Hemisphere, the maximum interannual variability is found in areas near 70°S, 120°W; 60°S, 160°E; and in the Drake passage. The year-to-year variation of sea-level pressure in the tropics and subtropics is considerably smaller than in high latitudes, and is generally less than 4 mb.

The sea-level pressure distributions and anomalies for July of years 1, 2 and 3 are presented in Figs. 2a-c. Considering the three July

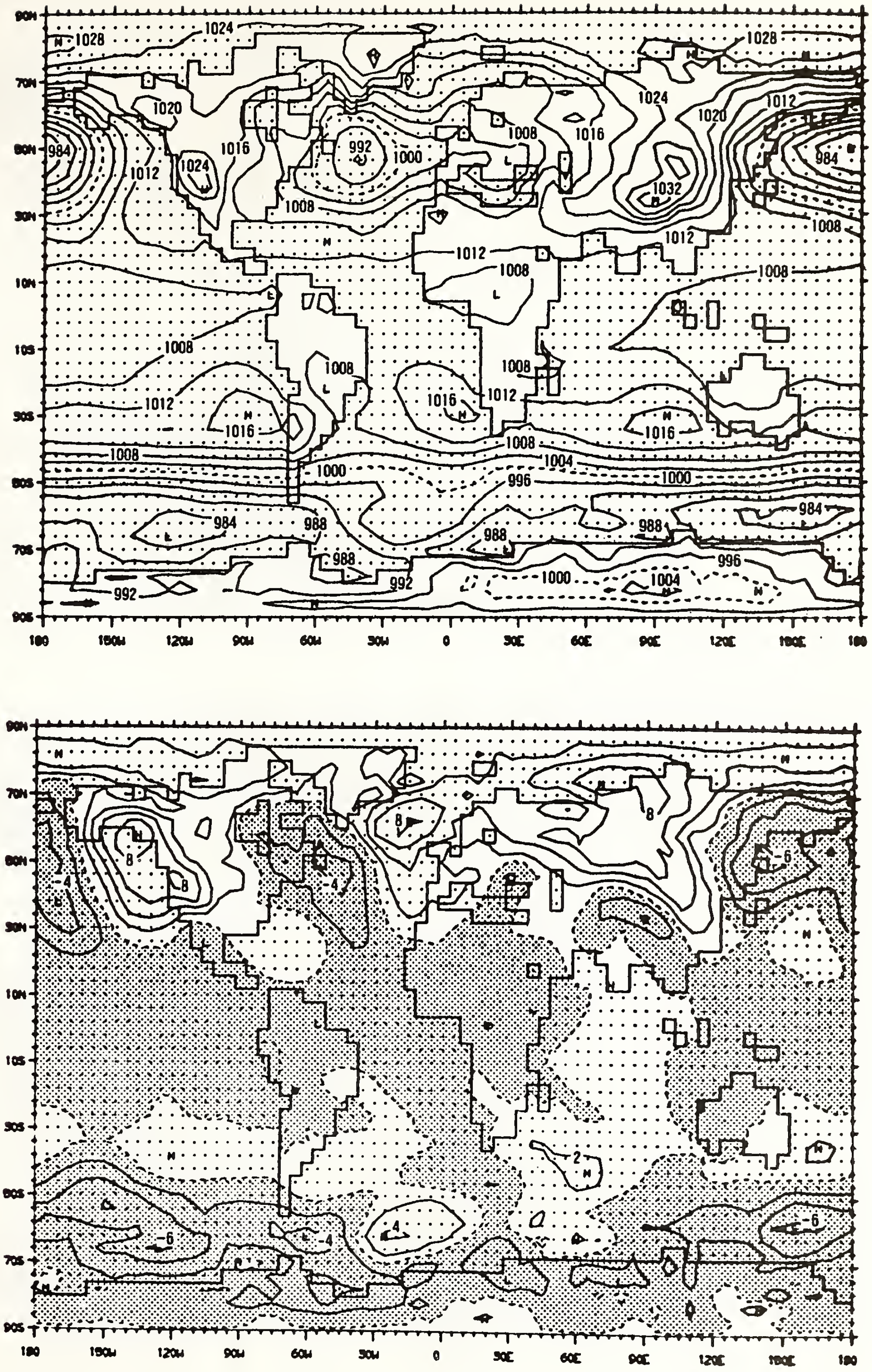

Fig. 1a. The simulated sea-level pressure (mb) for January of year 2 (above), and the anomaly (mb) with respect to the 3-year January mean (below). Negative anomalies are shaded.

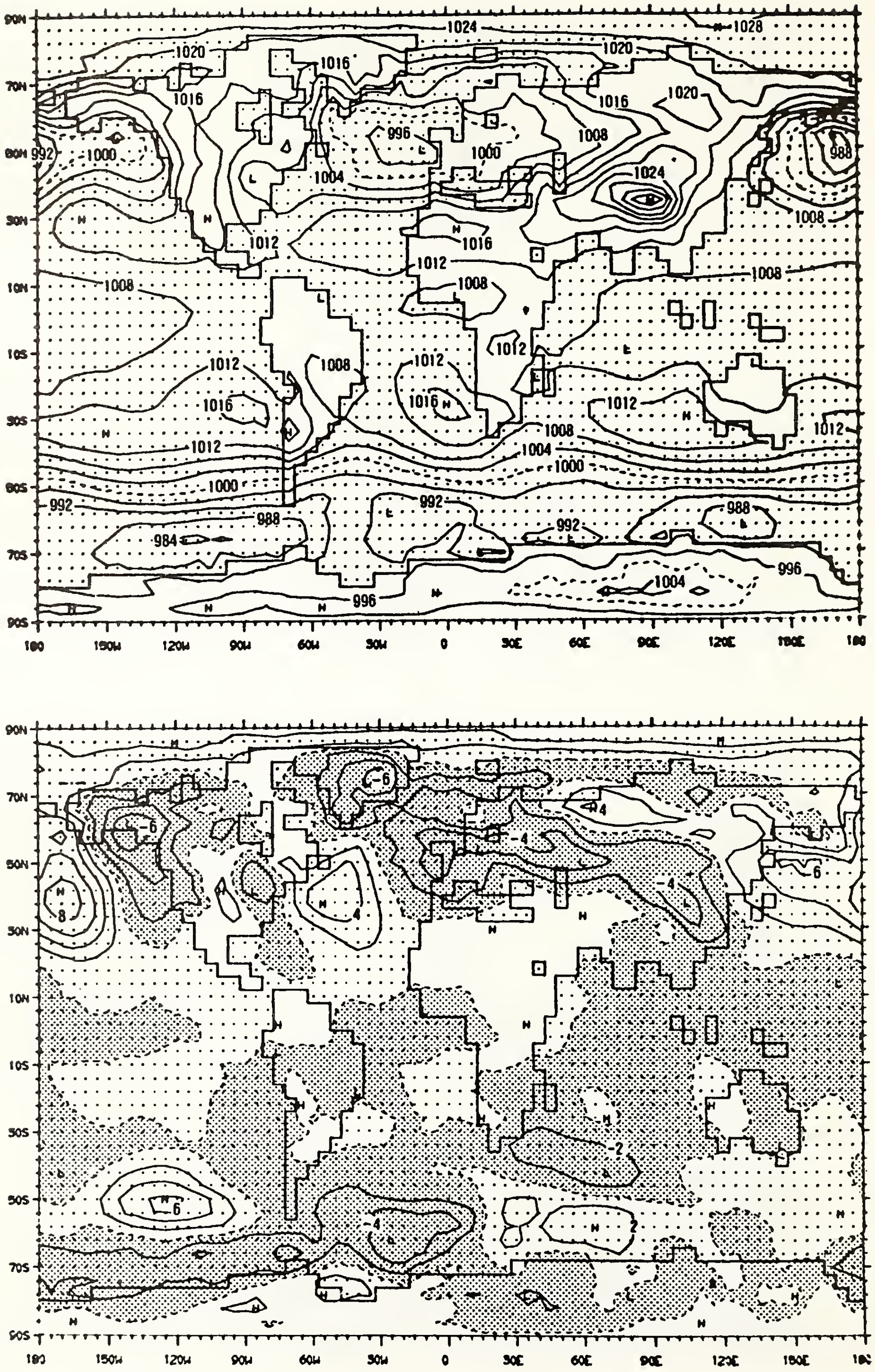

Fig. 1b. As in Fig. 1a except for January of year 3.

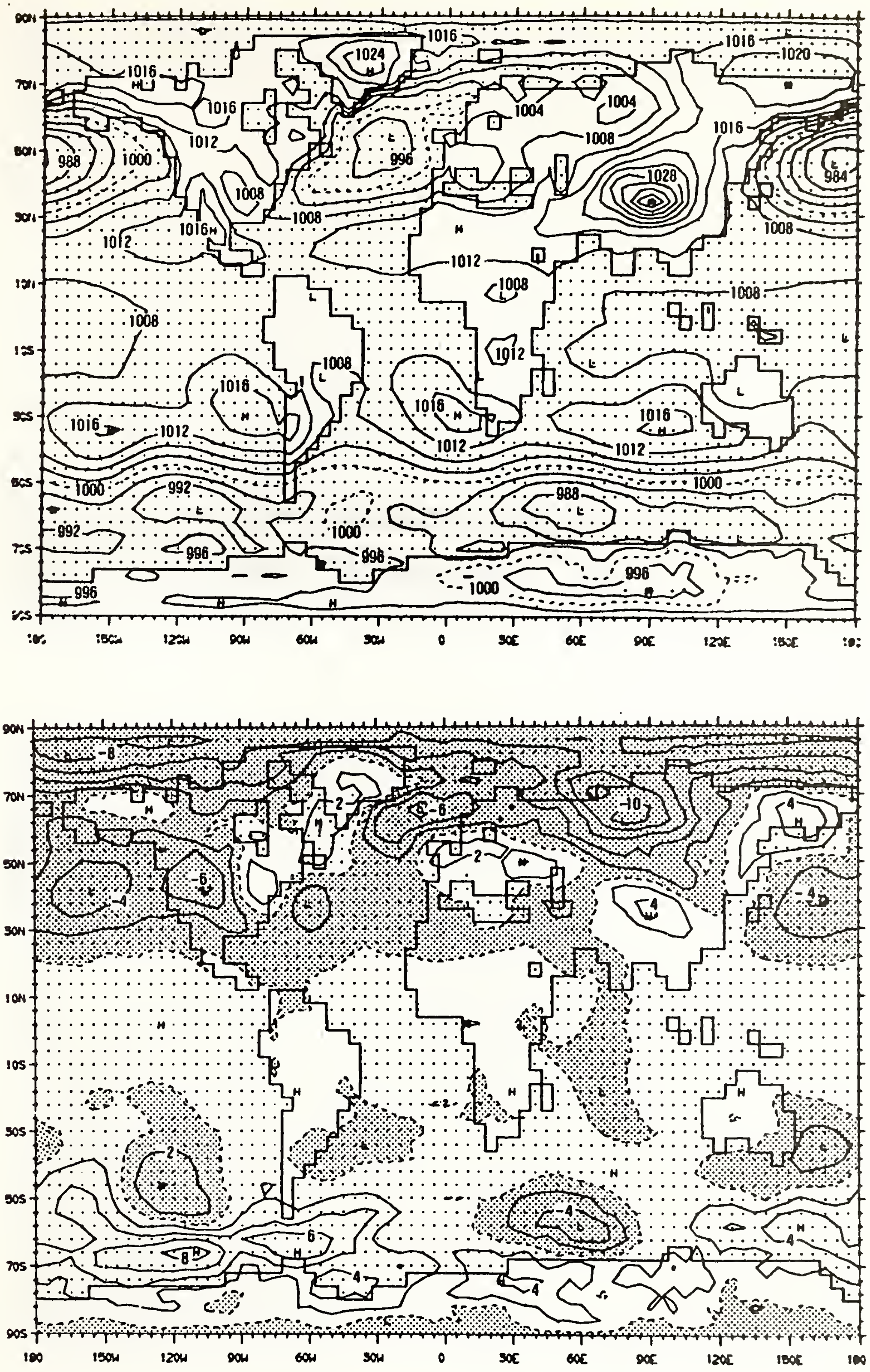

Fig. 1c. As in Fig. 1a except for January of year 4.

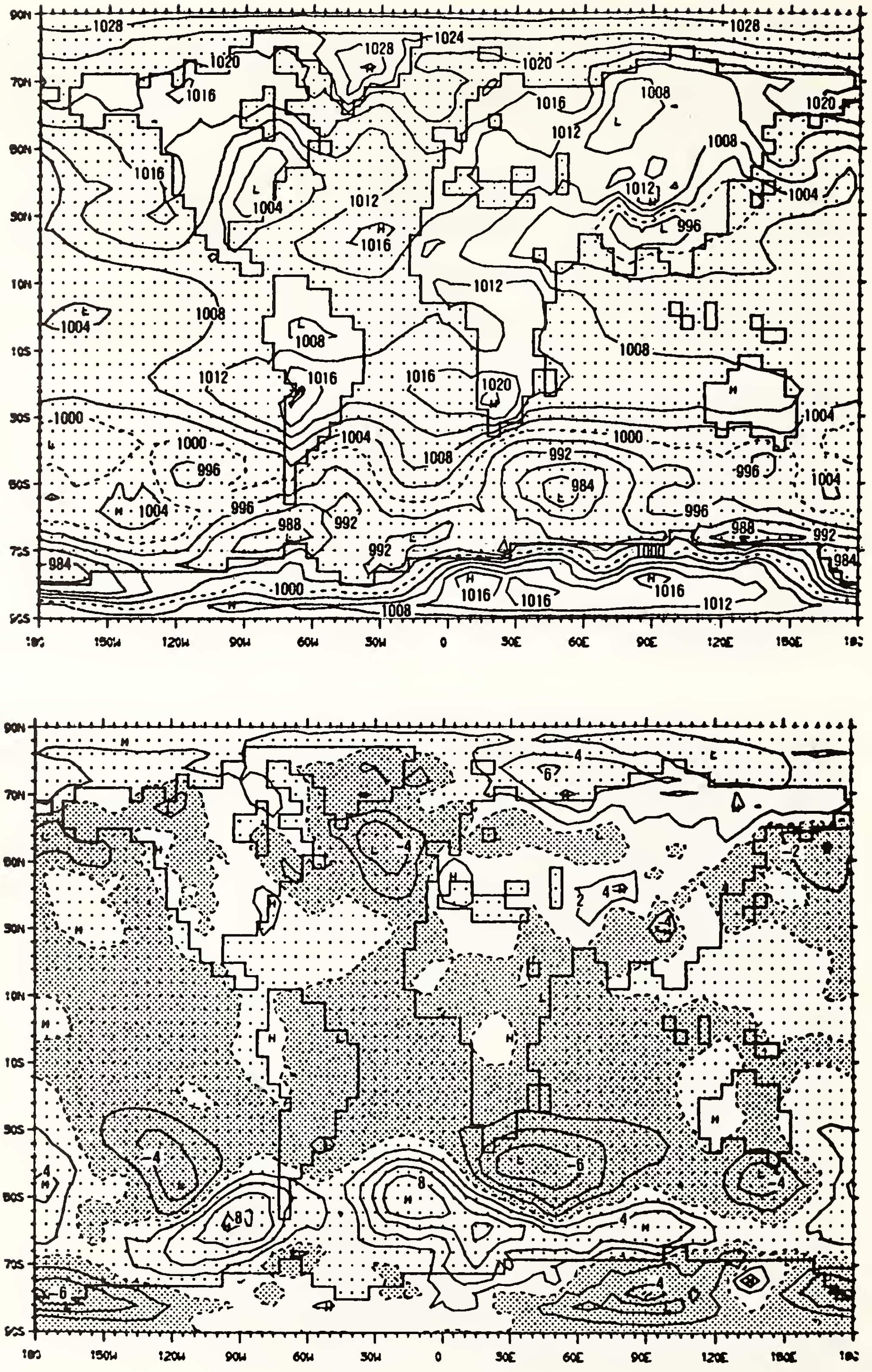

Fig. 2a. The simulated sea-level pressure (mb) for July of year 1 (above), and the anomaly (mb) with respect to the 3-year July mean (below). Negative anomalies are shaded.

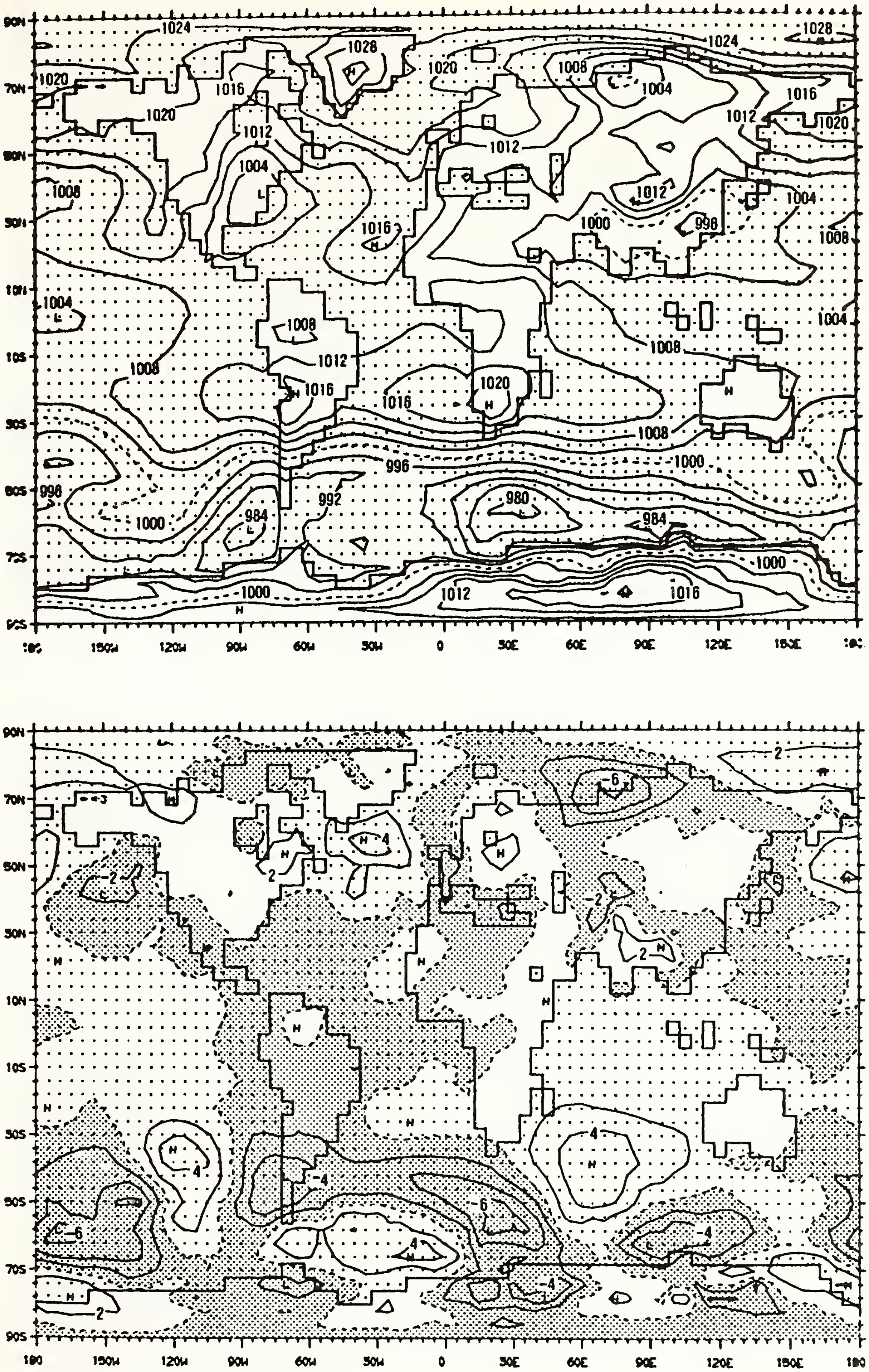

Fig. 2b. As in Fig. 2a except for July of year 2.

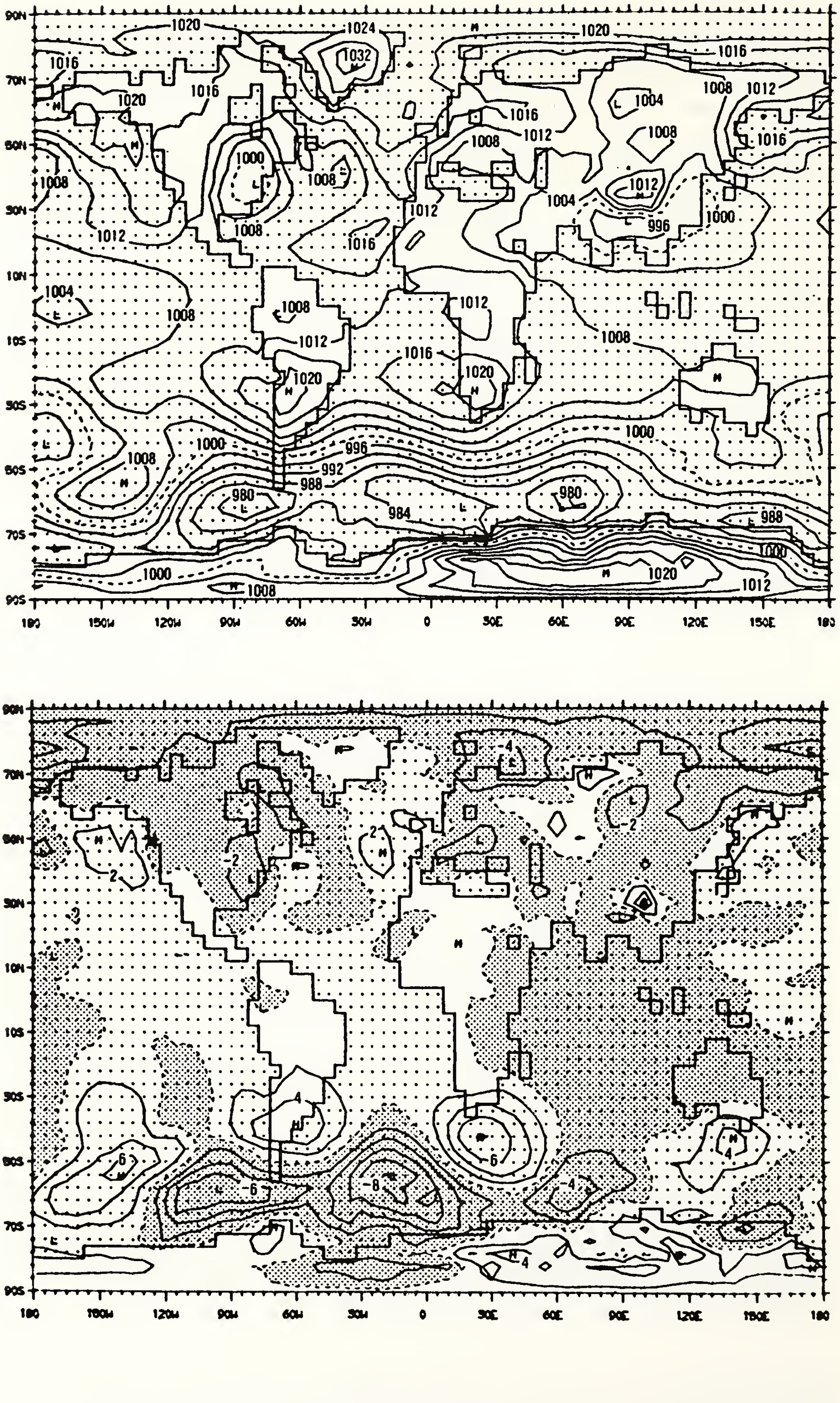

Fig. 2c. As in Fig. 2a except for July of year 3.

simulations together, we see that the anomalies are generally larger in the middle and high latitudes in the Southern (winter) Hemisphere than in the Northern (summer) Hemisphere, and that the anomalies are generally small in the tropics and subtropics. The distribution of the standard deviation of the July means (not shown) confirms this hemispheric difference in the interannual variability of the July sea-level pressure, and shows maxima near Cape Horn and the Cape of Good Hope.

It should be noted that the interannual variability of the January and July sea-level pressure distributions presented above is not due to interannual variations of the prescribed solar insolation, sea-surface temperature or sea ice distribution. As will be recalled, these boundary conditions were assigned a climatological seasonal variation and therefore displayed no anomalies whatsoever. Thus the interannual variability of sea-level pressure simulated by the model may represent an essentially unpredictable component of the year-to-year variations.

### b. *Precipitation*

The simulated normal annual cycle of the zonal-mean precipitation rate is shown in Fig. 3, together with the observed climatological zonal-mean precipitation rate from Jaeger (1976). Here we see that the present model has simulated the annual cycle of both the intensity and position of the ITCZ precipitation belt with good accuracy, although the simulated ITCZ band is somewhat narrower than the observed. The present model is also successful in simulating the positions and intensities of the subtropical dry belts in both hemispheres, although the simulated precipitation rate is twice the observed in the northern hemisphere subtropics during fall and winter. In the mid-latitude rainbelt of the Northern Hemisphere the wintertime precipitation rate is overestimated as a consequence of the excessive rain off the east coasts of North America and Asia. In the Southern Hemisphere the simulated maximum precipitation is located about 10 degrees equatorward of the observed latitude, and the observed summertime maximum is not simulated by the model. In the high latitudes of both hemispheres, the simulated precipitation rate decreases toward the pole as does the observed, but there are phase errors near both poles.

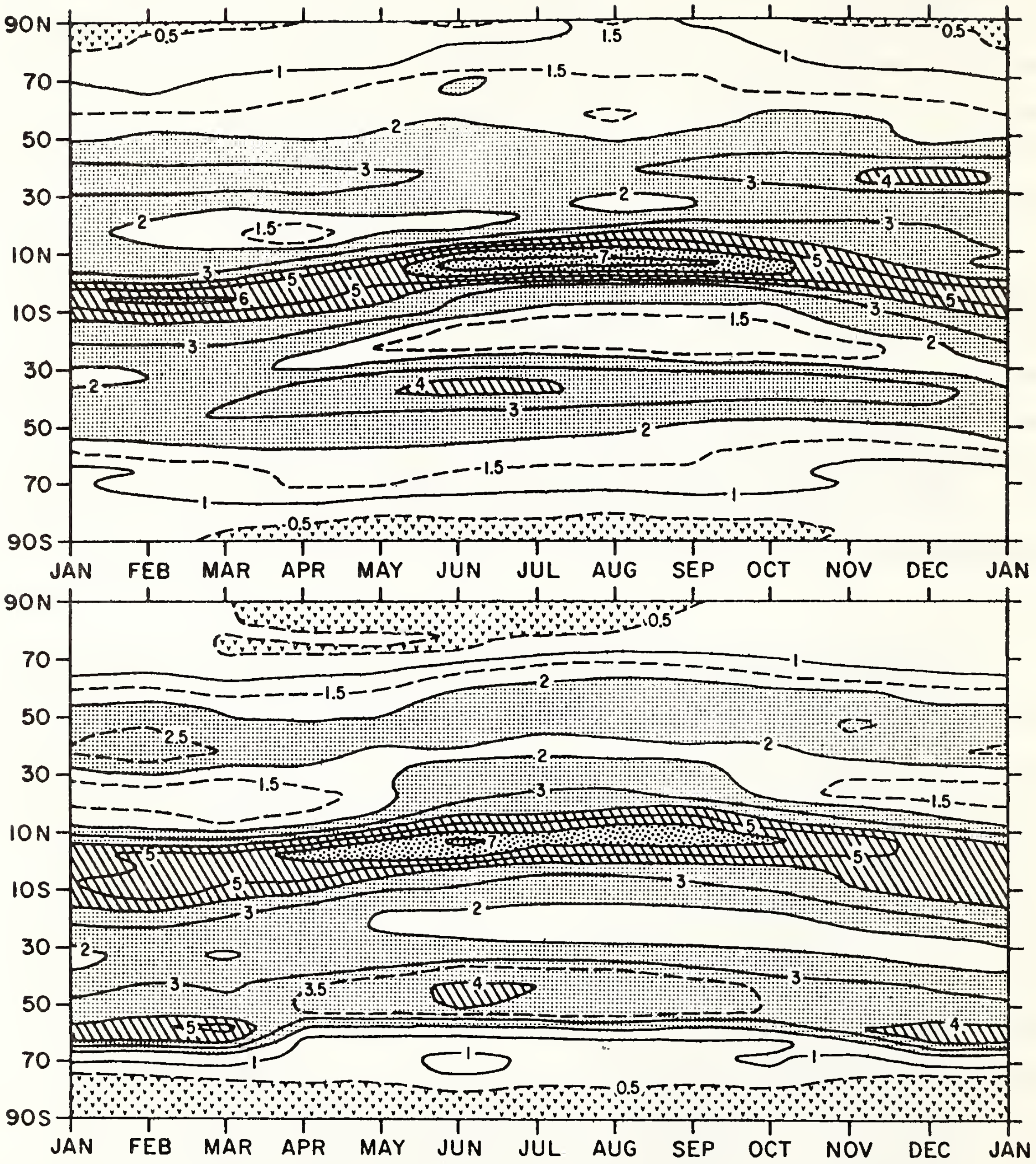

Fig. 3. The simulated (above) and observed (below) normal annual cycle of zonal-mean precipitation rate (mm $day^{-1}$). The observed data are from Jaeger (1976).

### *c. Surface air temperature*

The simulated and observed normal annual cycle of the zonal-mean surface air temperature is shown in Fig. 4. This figure shows that the model is quite successful in simulating most features of the observed annual cycle. While this is gratifying, it should be remembered that the annual cycle of the sea-surface temperature was prescribed from observation, and that the sea-surface temperature strongly controls the surface air temperature over about 70 percent of the earth. Nevertheless, this simulated distribution will serve as a useful reference for the more critical future test with a coupled ocean-atmosphere model.

### *d. Net radiation at the top of the atmosphere*

The net radiation at the top of the model atmosphere $N_o$ is given by $N_o = (S_i - AS_{st}) - S_r - R_o$, where $S_i$ is the incoming solar radiation (at pressure = 0 mb), $AS_{st}$ the solar radiation absorbed by a prescribed ozone distribution above the 200 mb isobaric top of the model atmosphere (see Schlesinger and Gates, 1979), $S_r$ the reflected and scattered solar radiation, and $R_o$ the net outgoing longwave radiation at the 200 mb surface. The simulated annual cycle of the zonal-mean $N_o$ is shown in Fig. 5, along with the observed net radiation $N_\infty = S_i - S_r - R_\infty$ determined by Ellis and Vonder Haar (1976) from satellite measurements. Figure 5 shows that the annual cycle of net radiation at the top of the atmosphere is successfully simulated by the model. Since $N_\infty - N_o = AS_{st} + R_o - R_\infty$ and $R_\infty > R_o$, the observed $N_\infty$ is slightly more negative than the simulated $N_o$ during winter in both hemispheres. The principal simulation errors appear to be in the high latitudes of the summer hemisphere where the simulated $N_o$ is of opposite sign from the observed $N_\infty$. This error is most likely due to the simulated high latitude summertime cloudiness.

The normal annual cycle of the global-mean net radiation budget at the top of the model atmosphere is shown in Fig. 6, along with the corresponding observations. In Fig. 6a we see that the simulated normal annual cycle of global-mean $N_o$ shows good agreement with the observed values of $N_o$ given by Ellis *et al.* (1978) except during March-June, although during March the simulated $N_o$ agrees closely with the observations of Newell *et al.* (1974). From this we conclude that the

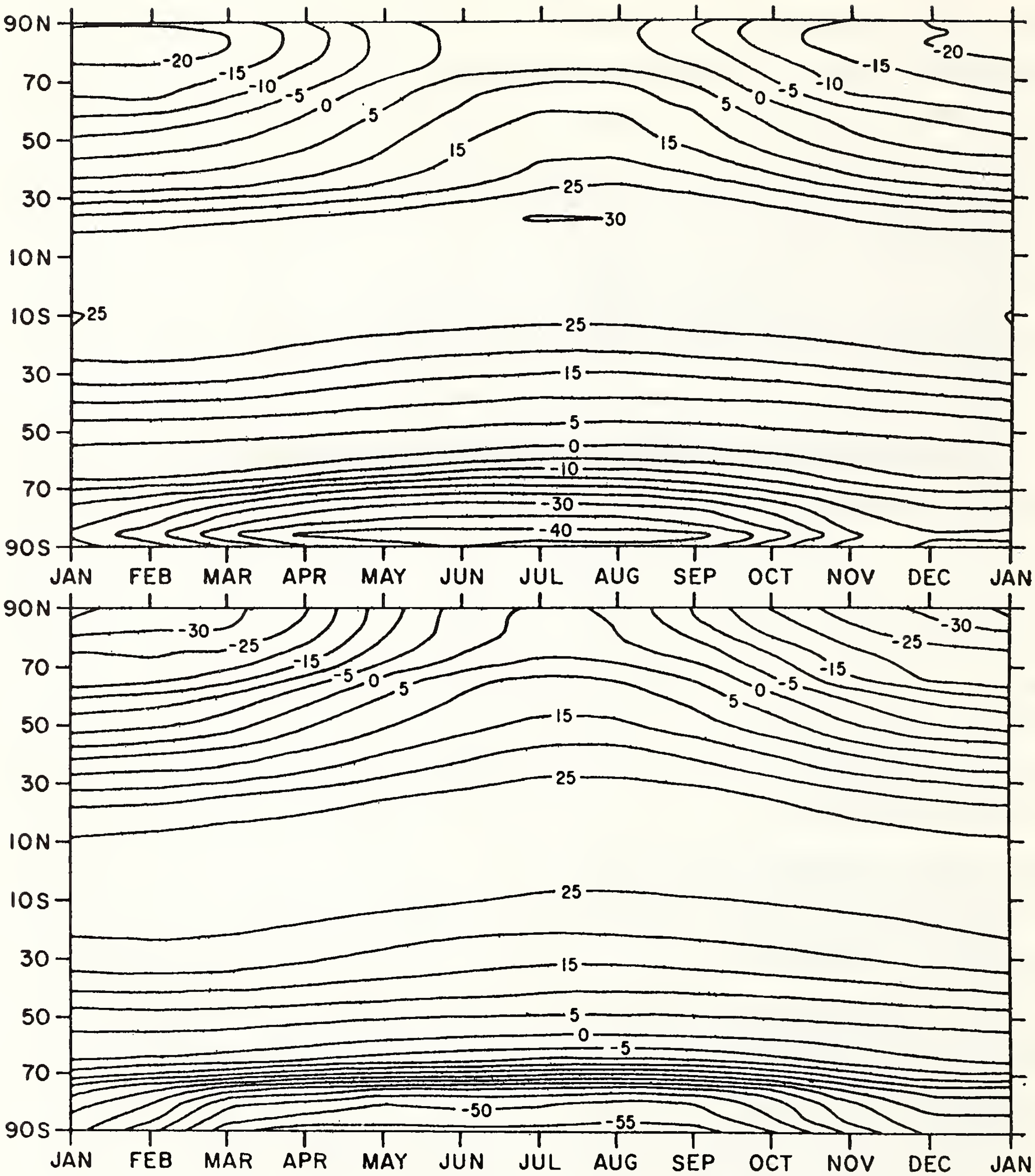

Fig. 4. The simulated (above) and observed (below) normal annual cycle of zonal-mean surface air temperature (°C). The observed data are based on Crutcher and Meserve (1970) and Taljaard *et al.* (1969), and were obtained from the National Center for Atmospheric Research (see Jenne, 1975).

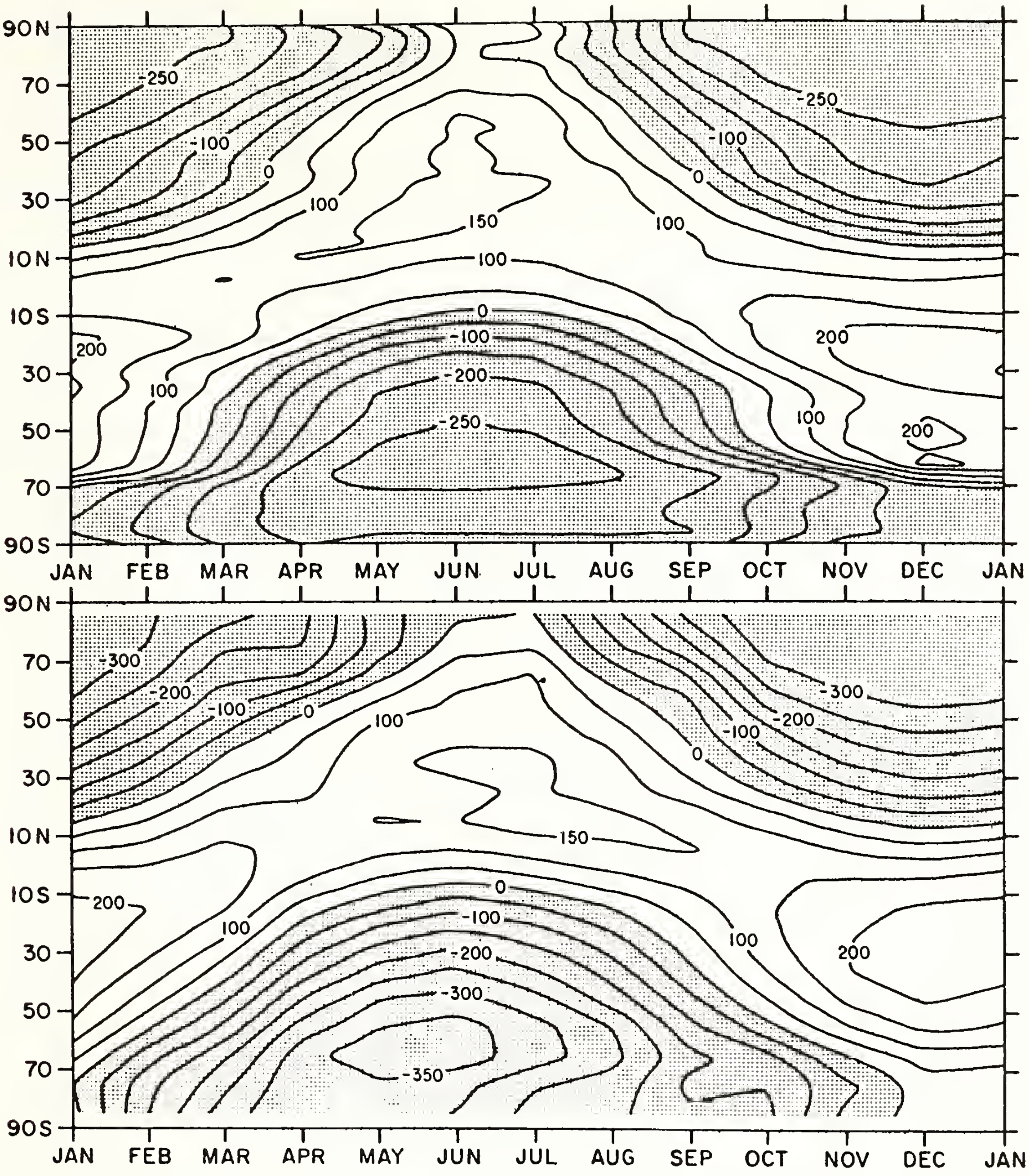

Fig. 5. The simulated (above) and observed (below) normal annual cycle of net radiation at the top of the atmosphere (ly day$^{-1}$). The observed data are from Ellis and Vonder Haar (1976).

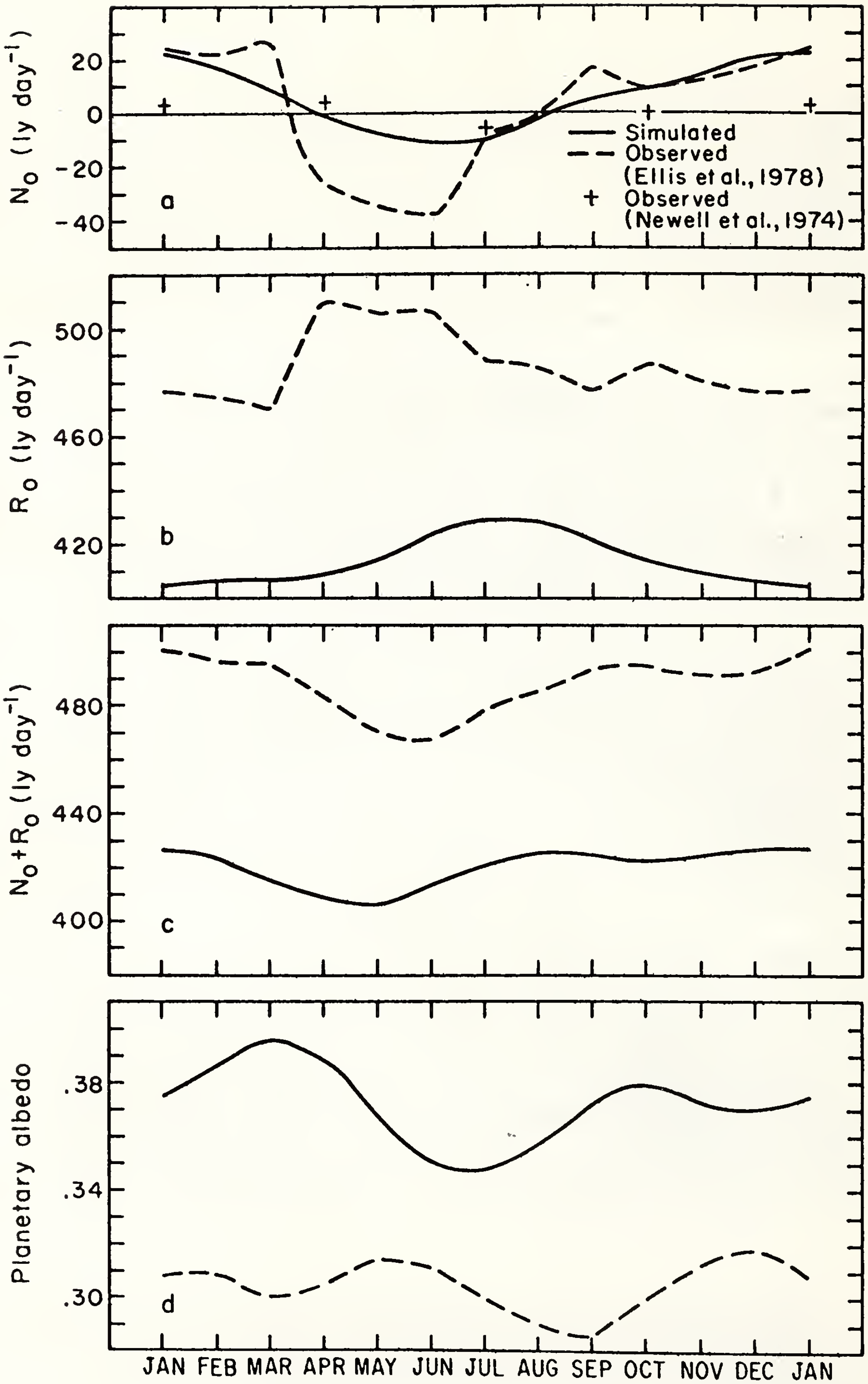

Fig. 6. The simulated and observed normal annual cycle of the components of the global-mean radiation budget at the top of the atmosphere.

simulated $N_o$ agrees with the observations within their uncertainty.

The components of the radiation budget at the top of the model and actual atmospheres are shown in Figs. 6b and c; in the latter figure, $N_o + R_o$ represents the absorption of solar radiation by the atmosphere. Fig. 6b shows that the simulated $R_o$ is systematically smaller than the observed $R_\infty$. While we expect this because the atmosphere above the 200 mb surface is generally cooled by the longwave flux divergence, it is not clear that this difference should be as large as that shown (approximately 70 ly day$^{-1}$). The absorbed solar radiation simulated by the model (Fig. 6c) is also approximately 70 ly day$^{-1}$ smaller than the observed, but this underestimate by the model is due to the fact that the simulated planetary albedo is approximately 7 percent higher than the observed in the annual mean (see Fig. 6d). Thus, while the annual cycles of both the zonal-mean and global-mean $N_o$ are reasonably well simulated by the model, this success is achieved in part by compensating errors in the radiation budget components.

### *e. Net heating*

The normal annual cycles of the global-mean net diabatic heating of the earth-atmosphere system, the net diabatic atmospheric heating, and the net surface heating are shown in Figs. 7a, b and c, respectively. The net surface heating $B_s$ is given by $B_s = N_s - LE_s - H_s - Q_d$, where $N_s$ is the net surface radiation; $E_s$ the surface evaporation (or sublimation) rate, with L the latent heat of vaporization (or fusion); $H_s$ the surface sensible heat flux; and $Q_d$ the conduction heat flux through sea ice only (see Schlesinger and Gates, 1979 for detailed description). The net atmospheric heating $B_a$ is given by $B_a = N_o - N_s + H_s + LP$, where P is the precipitation rate, and the other symbols are as previously defined. The net diabatic heating of the earth-atmosphere system $B_{ea}$ is given by $B_{ea} = B_a + B_s + Q_d = N_o + L(P - E_s)$. Fig. 7a shows that the simulated net heating of the earth-atmosphere system $B_{ea}$ is well approximated by the simulated net radiation at the top of the model atmosphere, $N_o$. This is true, of course, because the simulated net moisture source $E_s - P$ is quite close to zero for each month. Assuming that this is also true in the actual atmosphere, we

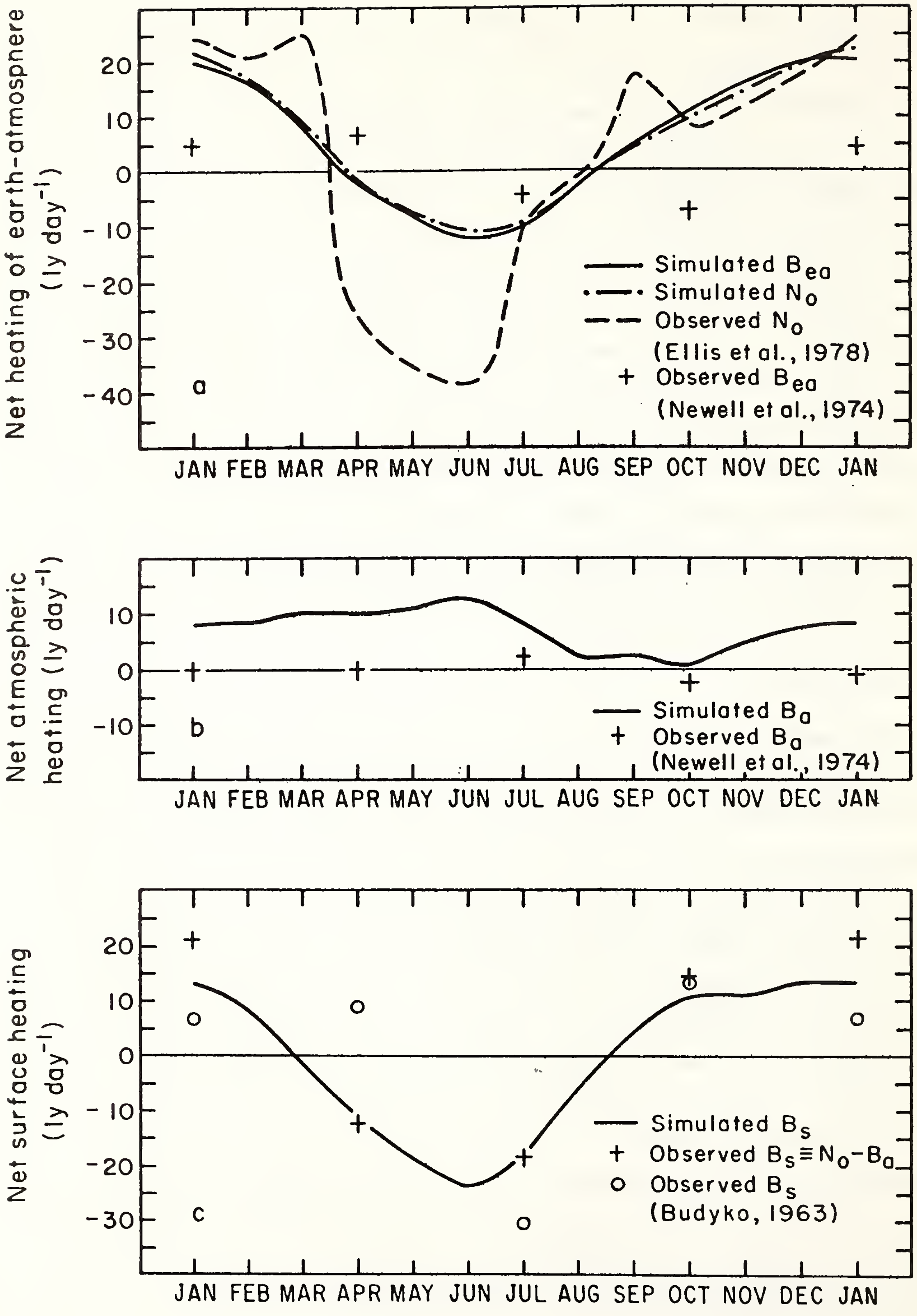

Fig. 7. The simulated and observed normal annual cycle of the global-mean net heating of the earth-atmosphere system (top), the atmosphere alone (middle), and at the earth's surface (bottom).

may compare the model's simulated $B_{ea}$ with the observed values of $N_\infty$ given by Ellis *et al.* (1978). This comparison, as that between the simulated $N_o$ and observed $N_\infty$ presented in Fig. 6a, shows that, with the exception of April-June, the model simulates the observed $B_{ea}$ with reasonable accuracy. However, the simulated $B_{ea}$ is quite close to the observed $B_{ea}$ reported by Newell *et al.* (1974) for April, but disagrees with Newell's observations for January and October. From this we conclude that the model simulates the observed net heating of the earth-atmosphere system within the observational uncertainity.

The net atmospheric heating $B_a$ simulated by the model (Fig. 7b) is positive throughout the annual cycle with an annual mean of about 6 ly day$^{-1}$. This is in contrast to the observed values of $B_a$ given by Newell *et al.* (1974), for which the annual mean is very near zero. It may thus appear that the net positive annual heating of the atmosphere is a systematic model error; however, this net diabatic atmospheric heating is required to balance the model's frictional dissipation of kinetic energy.

Considering the net surface heating simulated by the model (Fig. 7c), we see that the simulated normal annual cycle is in good agreement with that determined from the $N_\infty$ observations of Ellis *et al.* (1978) and the $B_a$ observations of Newell *et al.* (1974) (shown by +'s). However, both this observation and the simulation display differences with respect to the surface heating data of Budyko (1963). We therefore again conclude that the model has reproduced the observed net surface heating within the uncertainty of the observations.

## 4. Conclusions

We have presented here only a sample of the results from the 39-month-long integration which has been carried out to assess the seasonal and interannual performance of the OSU two-level atmospheric general circulation model. The analysis of those results is continuing, and the discussion presented here should therefore be regarded as preliminary. Further analyses of this valuable simulated data set are planned, including studies of the budgets of angular momentum, vorticity, energy, heat and water vapor, as well as studies of the simulated seasonal and interannual variability using empirical orthogonal function and space-time filtering techniques.

## Acknowledgements

We would like to thank Robert Mobley for his programming of the model on the CRAY 1 computer and for the production of the output statistics. This research was supported by the National Science Foundation under Grant ATM-77-26406.

# REFERENCES

Alexander, R. C., and R. L. Mobley, 1976: Monthly average sea-surface temperatures and ice-pack limits on a $1^{\circ}$ global grid. *Mon. Wea. Rev., 104,* 143-148.

Budyko, M. I., 1963: *Atlas of the Heat Balance of the Earth.* Gidrometeorizdat, Moscow, USSR, 69 pp.

Crutcher, H. L., and J. M. Meserve, 1970: *Selected Level Heights, Temperatures and Dew Points for the Northern Hemisphere,* NAVAIR 50-1C-52, Naval Weather Service Command, Washington, D.C.

Ellis, J. S., and T. H. Vonder Haar, 1976: Zonal average earth radiation budget measurements from satellites for climate studies. *Atmos. Sci. Paper* 240, Colorado State University, Ft. Collins, Colorado, 50 pp.

Ellis, J. S., T. H. Vonder Haar, S. Levitus and A. H. Oort, 1978: The annual variation in the global heat balance of the earth. *J. Geophys. Res., 83,* 1958-1962.

Gates, W. L., and M. E. Schlesinger, 1977: Numerical simulation of the January and July global climate with a two-level atmospheric model. *J. Atmos. Sci., 34,* 36-76.

Jaeger, L., 1976: Monatskarten des Niederschlags für die ganze Erde. *Ber. Deutsch. Wetterdienstes,* Nr. 139, Offenbach, 38 pp.

Jenne, R., 1975: Data sets for meteorological research. NCAR Tech. Note TN/1A-111, National Center for Atmospheric Research, Boulder, Colorado, 194 pp.

Newell, R. E., J. W. Kidson, D. G. Vincent and G. J. Boer, 1974: *The General Circulation of the Tropical Atmosphere and Interactions with Extratropical Latitudes.* Vol. 2, MIT Press, Cambridge, Massachusetts, 371 pp.

Schlesinger, M. E., and W. L. Gates, 1979: Numerical simulation of the January and July global climate with the OSU two-level atmospheric general circulation model. Report No. 9, Climatic Research Institute, Oregon State University, Corvallis, Oregon, 102 pp.

Taljaard, J. J., H. van Loon, H. L. Crutcher and R. L. Jenne, 1969: *Climate of the Upper Air: Southern Hemisphere, Vol. 1, Temperatures, Dew Points and Heights at Selected Pressure Levels.* NAVAIR 50-1C-55, Naval Weather Service Command, Washington, D.C.

# Simulation of Atmospheric Variability

Douglas G. Hahn and Syukuro Manabe
Geophysical Fluid Dynamics Laboratory/NOAA
Princeton University
Princeton, New Jersey 08540

As a first step toward investigating mechanisms responsible for climate variation, an attempt has been made to simulate atmospheric variability with a highly truncated spectral model of the atmosphere. The model has a global computational domain, realistic geography and topography, and prescribed seasonally varying sea surface temperature and insolation. In addition, the processes of snow-albedo feedback and soil moisture feedback are incorporated. This model, which is described in more detail by Manabe et al. (1978), was time integrated for a period of nearly 18 years.

It was found that the model successfully reproduces some of the characteristics of the daily and monthly fluctuations of the atmosphere. Figures 1 and 2 illustrate the success of the model in simulating the standard deviation of daily and monthly mean geopotential height at the 1000 mb surface.

The results depicted in Fig 3 suggest that, in mid-latitudes, the model is very successful in simulating the variability of daily and monthly means. In the tropics, the model underestimates the variability of both daily and monthly means. Moreover, in tropical regions, the model is able to simulate a higher percentage of the observed daily variability than that of the monthly variability, suggesting that the model tropics is missing relatively long period fluctuations.

The results presented here are only preliminary and clearly do not constitute a complete analysis of model performance. However, it is hard not to be surprised by the fidelity of this highly truncated spectral model in simulating the variability of the actual atmosphere in middle latitudes, particularly in light of the fact that the interannual variability of the prescribed underlying sea surface temperature field is precisely zero. If these model results are not fortuitous, they suggest that air-sea interactions play a relatively small role in contributing to the atmospheric variability in mid-latitudes. However, in the tropics, the model is unable to simulate relatively long period fluctuations. One can speculate that this missing element of the model tropics is a result of the lack of some boundary forcing (e.g., air-sea interaction, surface albedo feedback, etc.) with a long time constant. These speculations suggest avenues for future research.

Refer to the paper by Lau (1979) published herein for additional discussion of the results from the same model integration.

## References

Jenne, R. L., 1975: Data sets for meteorological research. NCAR Tech. Note TN/IA111, National Center for Atmospheric Research, Boulder, Colo., 172 pp.

Lau, N. C., 1979: The three-dimensional structure of monthly anomalies appearing in a 15-year simulation of a GFDL general circulation model. Proceedings of the Fourth Annual Climate Diagnostics Workshop, October 16-18, 1979, Madison, Wisconsin, NOAA, U.S. Dept. of Commerce.

Manabe, S., D. G. Hahn and J. L. Holloway, Jr., 1978: Climate simulations with GFDL spectral models of the atmosphere: Effect of spectral truncation. Submitted to the Proceedings of the JOC Study Conference on Climate Models, Washington, D.C.

Oort, A. H., 1977: The interannual variability of atmospheric circulation statistics. NOAA Prof. Paper No. 8, U.S. Government Printing Office, Washington, D.C.

## Figure Captions

Fig. 1. Standard deviation of daily geopotential height (meters) at the 1000 mb surface as compiled for the Dec., Jan., Feb. season. Top: computed from the last 15 years of model simulation. Bottom: observed from 5 years of data, Oort (1977).

Fig. 2. Standard deviation of monthly mean geopotential height (meters) at the 1000 mb surface as compiled for the Dec., Jan., Feb. season. Top: computed from the last 15 years of model simulation. Bottom: observed from 5 years of data, Oort (1977).

Fig. 3. Zonal means of standard deviation of daily and monthly mean geopotential height at the 1000 mb surface as compiled for the Dec., Jan., Feb. season. Observed distributions are from 5 years of data, Oort (1977) and 71 years of data, Jenne (1975).

# STANDARD DEVIATION OF DAILY GEOPOTENTIAL HEIGHT (1000mb)

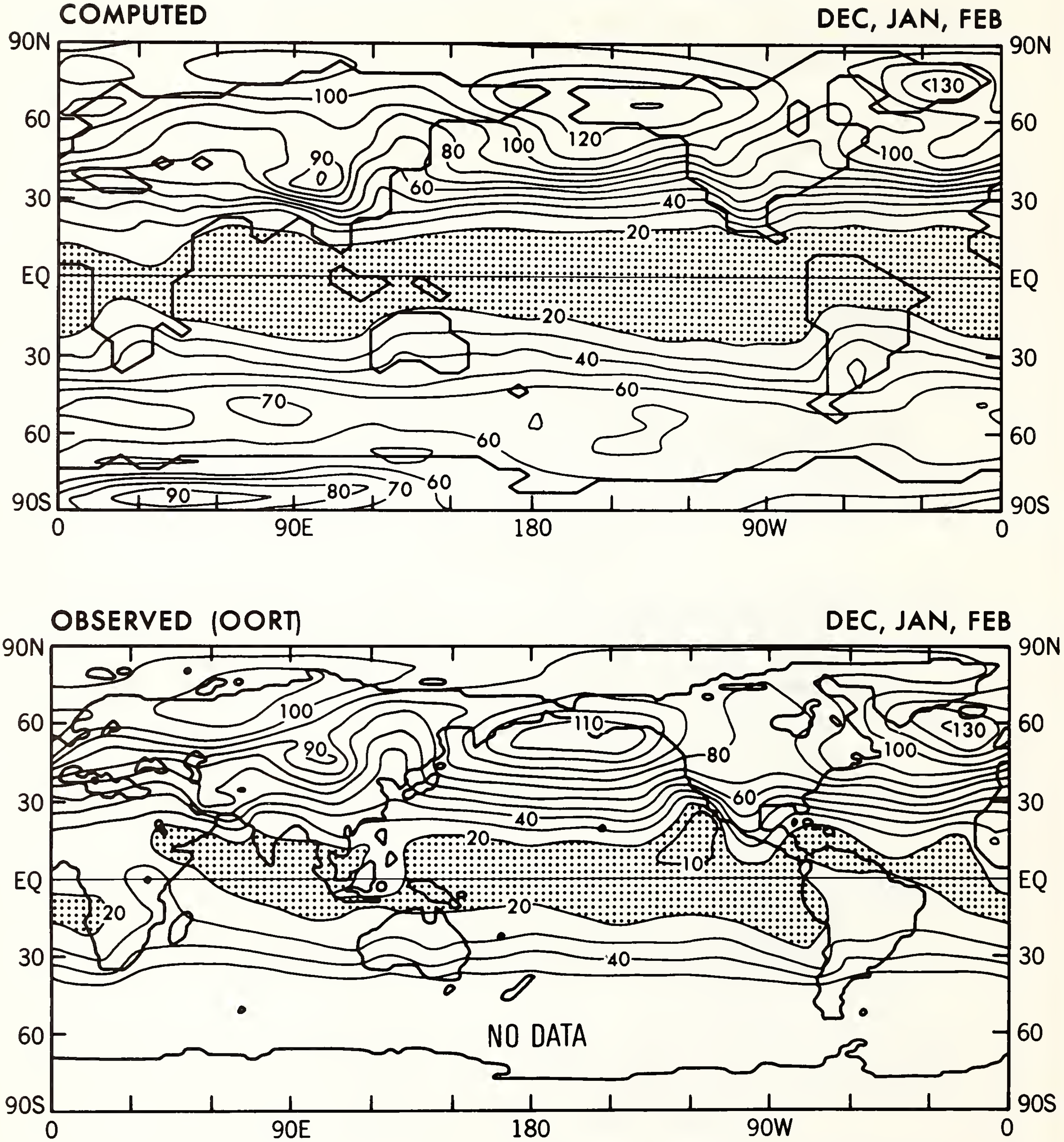

Figure 1

STANDARD DEVIATION OF MONTHLY MEAN GEOPOTENTIAL HEIGHT (1000mb)

**COMPUTED** **DEC, JAN, FEB**

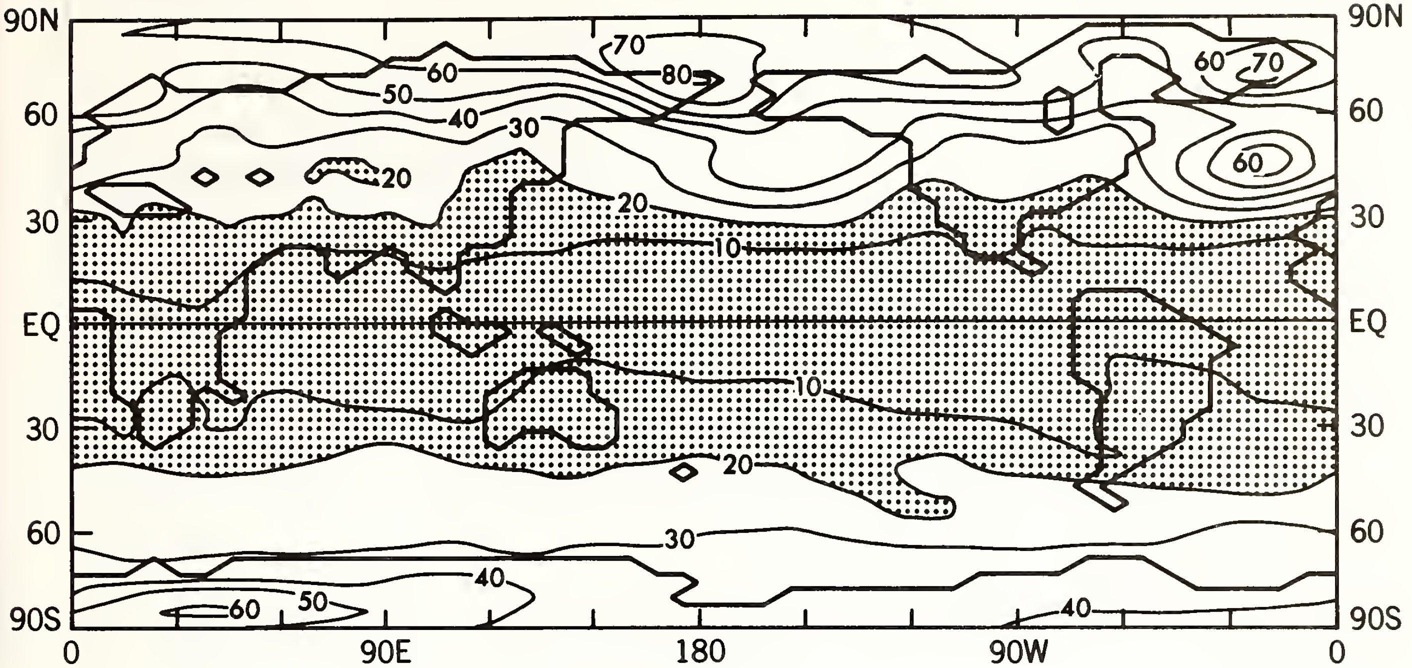

**OBSERVED (OORT)** **DEC, JAN, FEB**

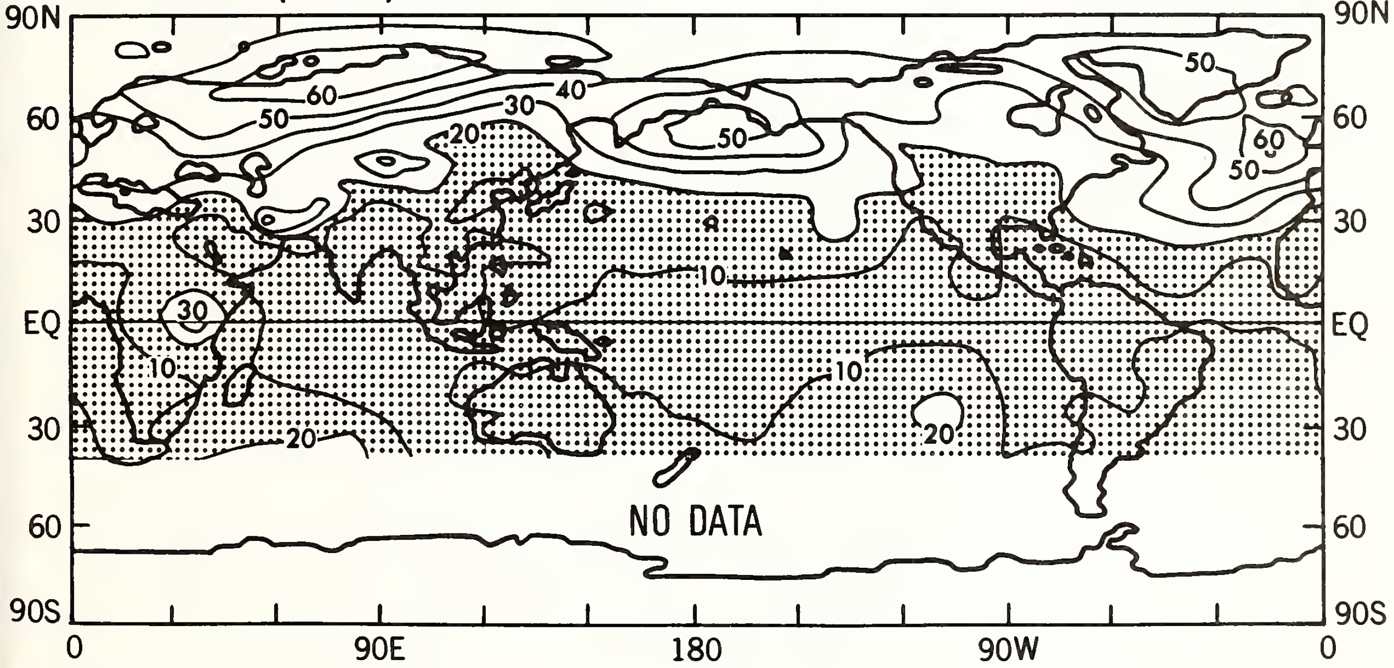

Figure 2

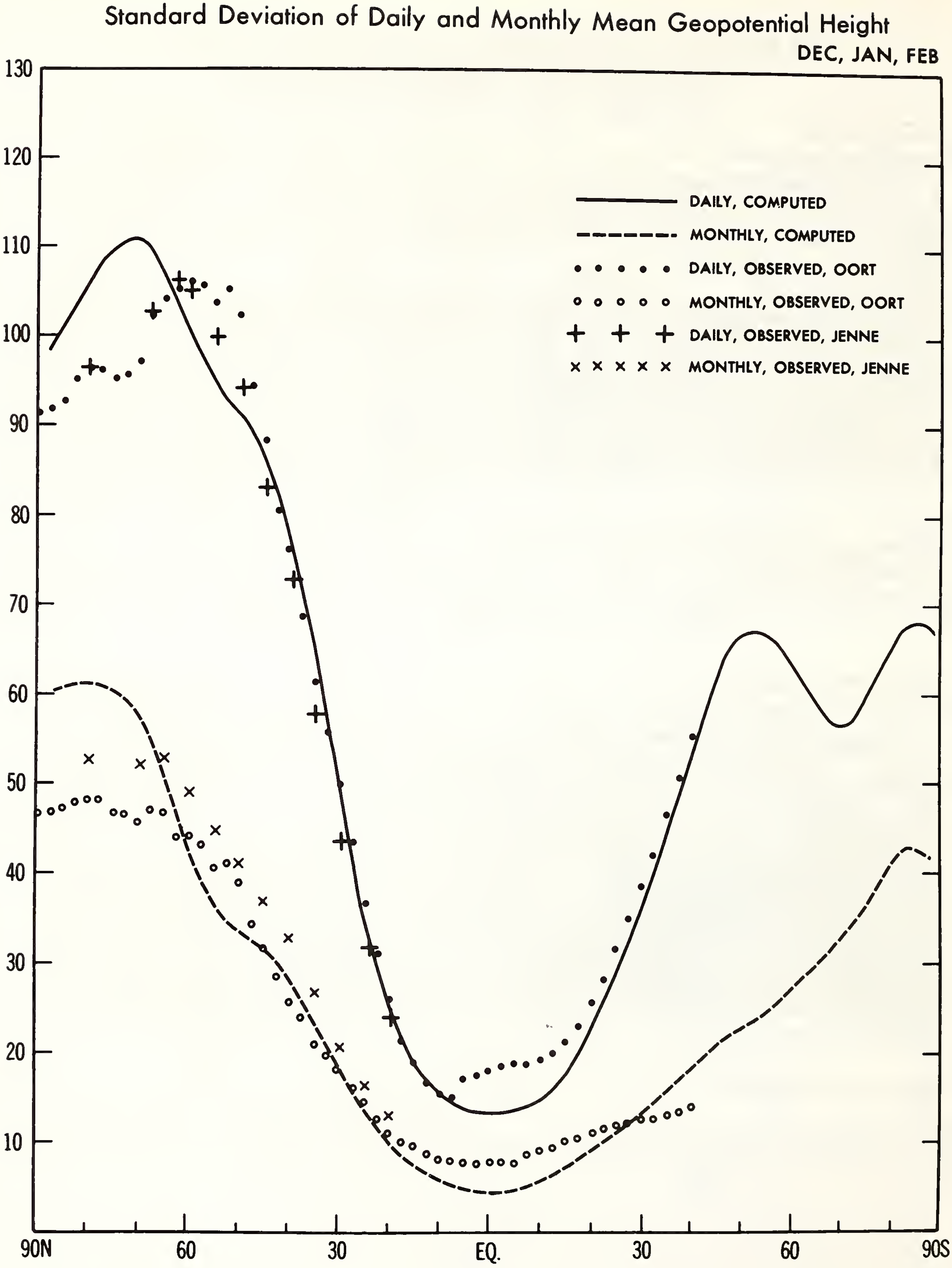
Standard Deviation of Daily and Monthly Mean Geopotential Height
DEC, JAN, FEB
130
120
110
100
90
80
70
60
50
40
30
20
10
DAILY, COMPUTED
MONTHLY, COMPUTED
DAILY, OBSERVED, OORT
MONTHLY, OBSERVED, OORT
DAILY, OBSERVED, JENNE
MONTHLY, OBSERVED, JENNE
90N
60
30
EQ.
30
60
90S

Figure 3

# The Three-dimensional Structure of Monthly Anomalies Appearing in a 15-year Simulation of a GFDL General Circulation Model

Ngar-Cheung Lau
Geophysical Fluid Dynamics Program
Princeton University
Princeton, N.J. 08540

As a result of the rapid advances in numerical techniques and computer technology during the past few years, it is now feasible to perform multi-year integrations of three-dimensional general circulation models (GCM's) of the earth's atmosphere. The diagnosis of these model experiments should provide physical insights into variability of atmospheric circulation systems on time-scales of weeks and months. Our synoptic experience as well as several recent observational studies reported by van Loon, Wallace and their colleagues (van Loon and Rodgers, 1978; Rodgers and van Loon, 1979; Meehl and van Loon, 1979, Blackmon et al. 1979; and Wallace and Gutzler, 1979) suggest that the monthly and seasonal anomalies in the real atmosphere are characterized by well-organized horizontal and vertical structures. It is hence evident that a comprehensive analysis of the model simulations should attempt to address the following issues:

a) Given the dynamical framework and imposed boundary forcings in the GCM, are there any indications that the simulated circulation patterns exhibit some degree of interannual variability?

b) If the prevalent weather patterns in the model do fluctuate from year to year, are the amplitudes and time scales of these circulation anomalies realistic? Do the spatial patterns of these anomalies bear any resemblance to those appearing in the real atmosphere?

The primary objective of the present study is to answer these questions by identifying the dominant circulation regimes in the model and by comparing the geographical patterns of the simulated anomalies with observations. It is only possible to present a highly condensed version of this investigation here because of space limitations.

The GCM which provided the history tapes for this study was developed at the Geophysical Fluid Dynamics Laboratory. The prognostic variables are represented spectrally by spherical harmonics with a truncation limit of 15 total wave numbers. This corresponds to an equivalent horizontal resolution of approximately 7.5° and 4.5° in the zonal and meridional directions, respectively. The effects of mountains are treated by using a sigma coordinate system consisting of nine levels. The physical processes incorporated in the model include prescribed seasonal variation of solar radiation and sea surface temperature, zonally uniform cloud cover, radiative heating and cooling, moist convective adjustment and a hydrological cycle. The 15-year global integration described here was performed using the Advanced Scientific Computer developed by Texas Instruments. The entire run was completed in about one week of central processing unit (CPU) time. This long-term simulation also provided the data base for the analysis by Hahn and Manabe on climate variability. The results of their study are summarized in a separate report in these proceedings.

The results presented in Figs. 1-5 are all based on the monthly mean data for 45 winter months (December, January and February) in the 15-year model experiment. Except for the composites shown in Fig. 4, the seasonal cycle was removed by subtracting the 15-year mean for each respective calendar month to obtain deviations.

In Fig. 1 is shown the hemispheric distribution of the standard deviation of monthly means of geopotential height at 500 mb. This pattern may be compared with the corresponding observational result presented by Blackmon et. al. (1979, Fig. 1b) based on NMC analyses for 15 winter seasons. The regions of maximum variability over the northern Pacific and Atlantic are reproduced by the model. The amplitudes of the geopotential height fluctuations in the model over these active centers are approximately 70% of those observed.

The horizontal structure of the anomaly pattern which accounts for the largest fraction of the variance in 500 mb height is delineated by the first mode of the empirical orthogonal functions (EOF's), shown in Fig. 2. The data used in this EOF analysis were normalized by the local standard deviations, so that the matrix in the eigenvalue problem was composed of correlation coefficients. The first EOF mode consists of four major centers of extremum. The three centers over East China Sea, central Pacific and western Atlantic are of the same sign. The fourth center located north of the Alaskan Peninsula exhibit a marked tendency to protrude into lower latitudes along the west coast of the North American continent. The geostrophic circulation associated with this mode is characterized by meridional displacements of the jet axes relative to their climatological mean positions over the Pacific and Atlantic; and by intensification of the meridional flow component in the sector between 120° W and 160° W.

It is not difficult to identify wintertime anomalies in the observed atmosphere which bear a close resemblance to the pattern in Fig. 2. Of particular interest are the circulations in January 1963 (O'Conner, 1963) and January 1977 (Wagner, 1977), which correspond to two of the most severe winter months on record over the eastern half of the United States. Both months are characterized by deepening and broadening of the semi-permanent trough over the western and central Pacific; and by intensification of the trough over the eastern United States. The stationary pressure ridge along the west coast of North America was highly amplified. The jet axis over the central Pacific was shifted equatorward of the normal position in both cases; and the circulation acquired a strong poleward component over the eastern Pacific.

An alternative method to describe the spatial patterns of circulation anomalies in the model is the construction of teleconnection maps (for further details on this approach, please refer to the report by Wallace and Gutzler in these proceedings). In Fig. 3 is shown the distribution of the correlation coefficients between the monthly means of 500 mb geopotential height at (42.75°N, 75°W) and the corresponding data at all other grid points in the Northern Hemisphere. This reference point was chosen so as to maximize the correlations and anticorrelations with those "centers of action" which are located in the vicinity of the North American continent. It is evident that a strong correspondence exists between the patterns in Figs. 2 and 3.

In order to provide for a synoptic description of those patterns in the model which exhibit the most extreme departures from the 15-winter climatology, the following "anomaly index" is assigned to each month $\underline{i}$ :

$$\begin{aligned} I_i \equiv Z'_i\,(74.25^\circ\ \mathrm{N},\ 150^\circ\ \mathrm{W}) - Z'_i\,(33.75^\circ\mathrm{N},\ 157.5^\circ\ \mathrm{W}) \\ -Z'_i\,(42.75^\circ\mathrm{N},\ 75^\circ\mathrm{W}), \end{aligned} \qquad (1)$$

where $\underline{Z_i'\,(x)}$ is the deviation of the 500 mb height in month $\underline{i}$ at point $\underline{x}$ from the long-term mean. The three grid points chosen for deriving this anomaly index correspond closely to the locations of extrema in the first EOF mode (Fig. 2) and the teleconnection map (Fig. 3).

In Fig. 4 is shown the composite pattern of 300 mb height for those nine winter months with the (a) highest and (b) lowest anomaly indices defined in Eqn. (1). The distinction between the circulations over the western hemisphere shown in this pair of figures is quite striking.

The vertical structure of the monthly anomalies may be examined by computing the correlation coefficient between the heights at 500 and 1000 mb, shown in Fig. 5. The geographical pattern presented here bears a close resemblance to the corresponding observational result presented by Blackmon et al. (1979, Fig. 2). The correlations in the vicinity of the grid points used in Eqn. (1) are very high, indicating that the anomalies over these locations are characterized by an equivalent barotropic structure.

The selected set of results presented above indicates that the GCM is capable of reproducing some of the essential features of the observed circulation anomalies in the atmosphere. The relative importance of various possible mechanisms in the formation and maintenance of the simulated anomalies has yet to be assessed by performing detailed diagnoses of this and other future sensitivity experiments.

## References

Blackmon, M.L., R.A. Madden, J.M. Wallace and D.S. Gutzler, 1979: Geographical variations in the vertical structure of geopotential height fluctuations. J. Atmos. Sci., 36, in press.

Meehl, G.A., and H. van Loon, 1979: The seesaw in winter temperatures between Greenland and Northern Europe. Part III: Teleconnections with Lower latitudes. Mon. Wea. Rev., 107, 1095-1106.

O'Conner, J.F., 1963: The weather and circulation of January 1963 -

one of the most severe months on record in the United States and Europe. Mon. Wea. Rev., 91 . 209-218.

Rogers, J.C., and H. van Loon, 1979: The seesaw in winter temperatures between Greenland and northern Europe. Part II: sea ice, sea surface temperatures, and winds. Mon. Wea. Rev., 107, 509-519.

van Loon, H. and J.C. Rogers, 1978: The seesaw in winter temperatures between Greenland and northern Europe. Part 1: General description. Mon. Wea. Rev., 106, 296-310.

Wagner, A.J., 1977: Weather and circulation of January - the coldest month on record in the Ohio Valley. Mon. Wea. Rev., 105, 553-560.

Wallace, J.M. and D.S. Gutzler, 1979: Horizontal teleconnections during the Northern Hemisphere winter season. Proceedings of the Fourth Annual Climate Diagnostics Workshop, October 16-18, 1979, Madison, Wisconsin NOAA, Department of Commerce.

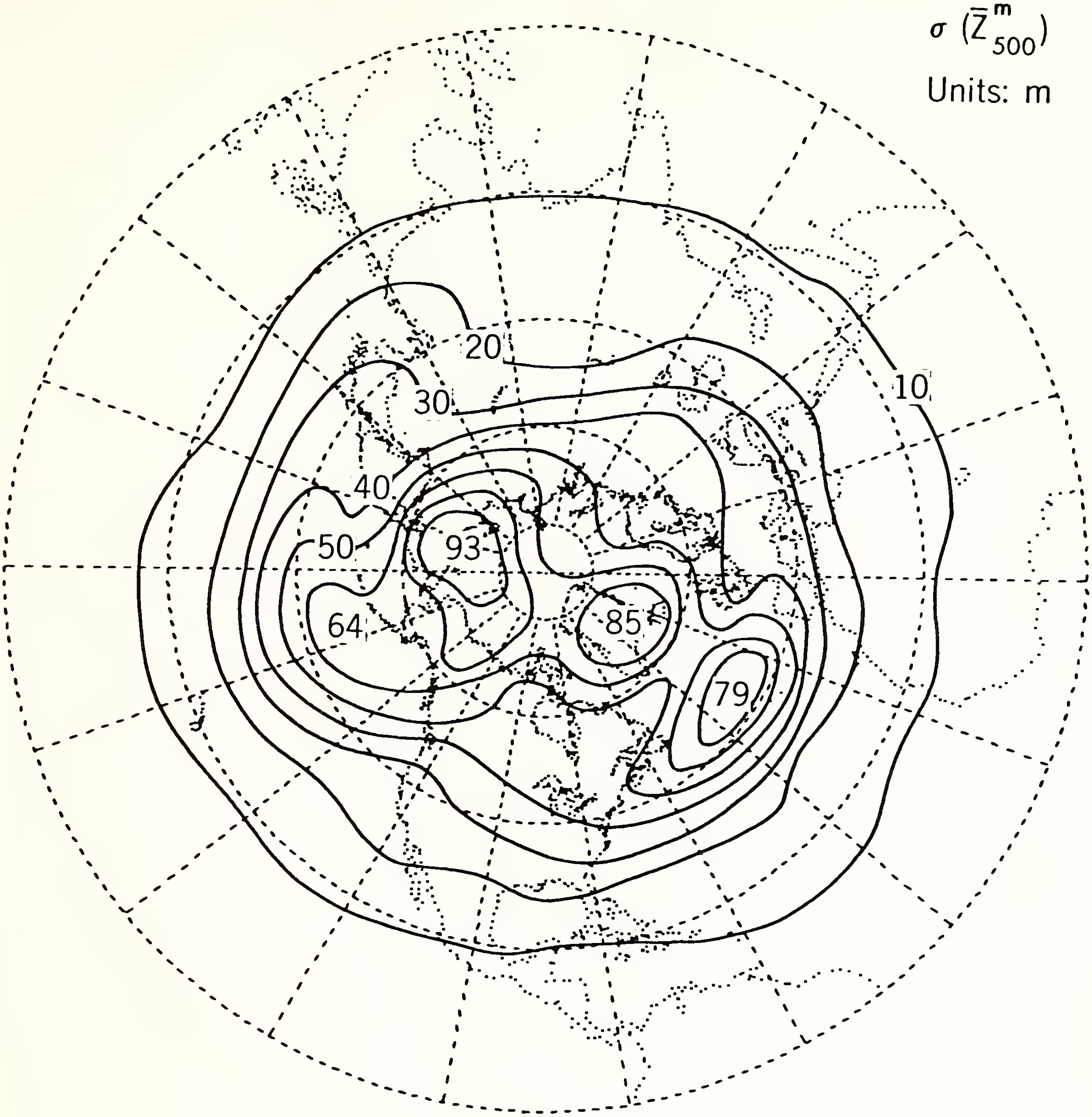

Fig. 1. The standard deviation of the monthly means of geopotential height at 500 mb, based on model data for 45 winter months. Contour interval: 10m. The meridians and latitude circles are drawn at intervals of 20°. The outermost latitude circle represents the equator.

FIRST MODE

EOF

$\overline{Z}^{m}_{500}$ DJF

Variance Explained: 22%

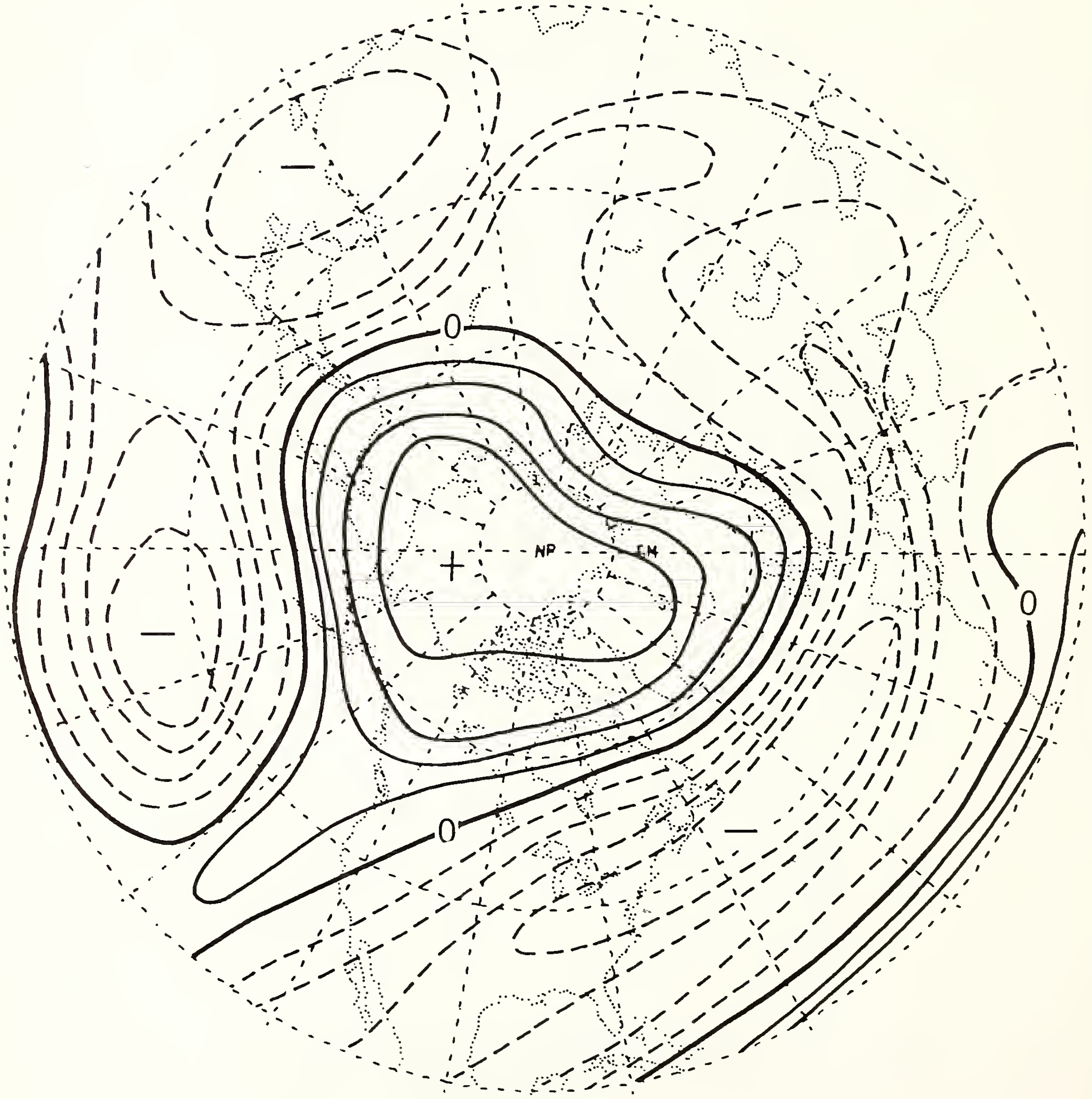

Fig. 2. The first mode of empirical orthogonal functions for monthly mean data of 500 mb height during the winter season. Note that the outermost latitude circle represents 20° N.

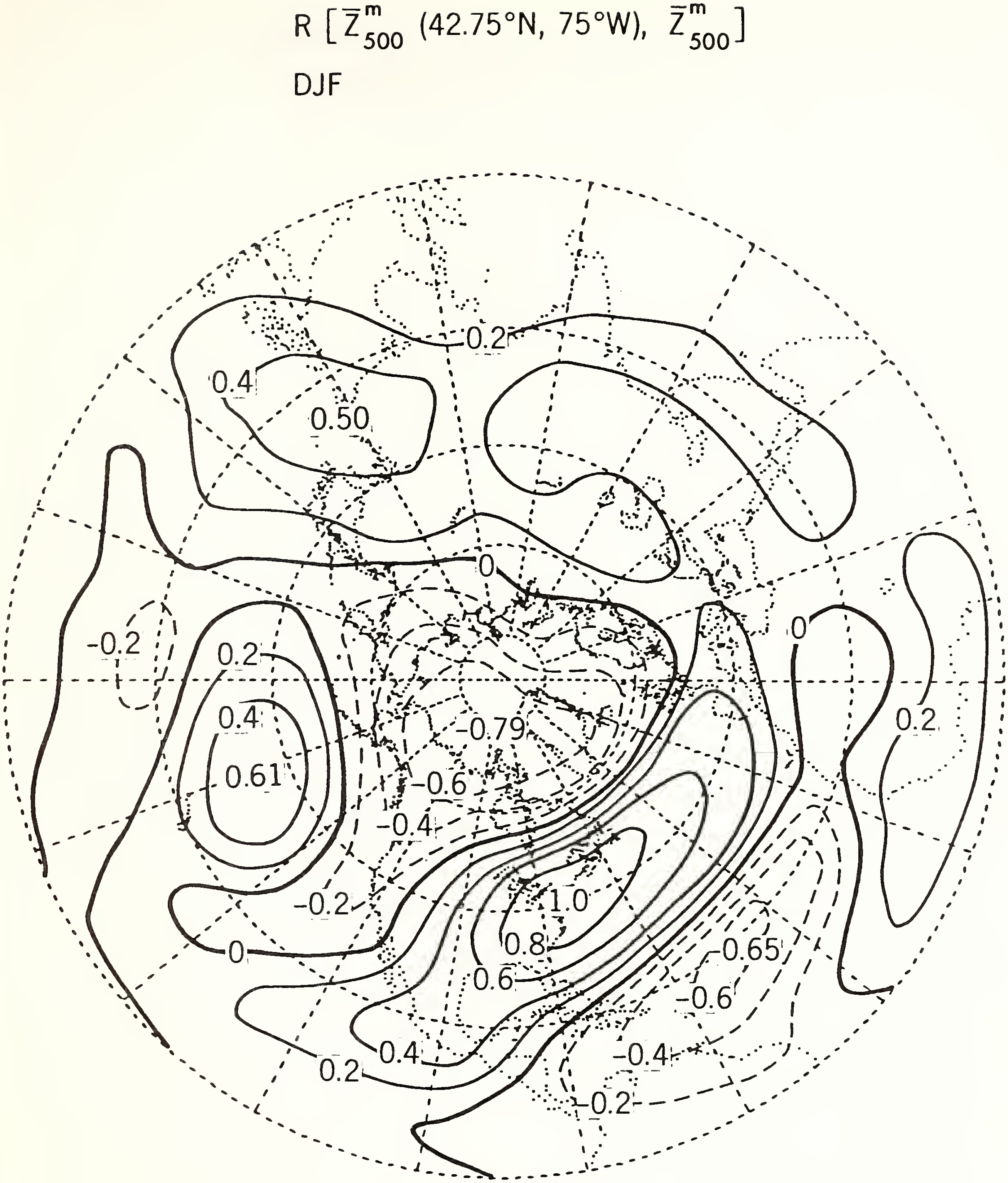

$R\left[\bar{Z}^m_{500}\ (42.75°N,\ 75°W),\ \bar{Z}^m_{500}\right]$

DJF

Fig. 3. The correlation coefficient between monthly mean of 500 mb height at (42.75° N, 75° W) and the corresponding data at all other grid points during the winter season. Contour interval: 0.2. The outermost latitude circle represents the equator.

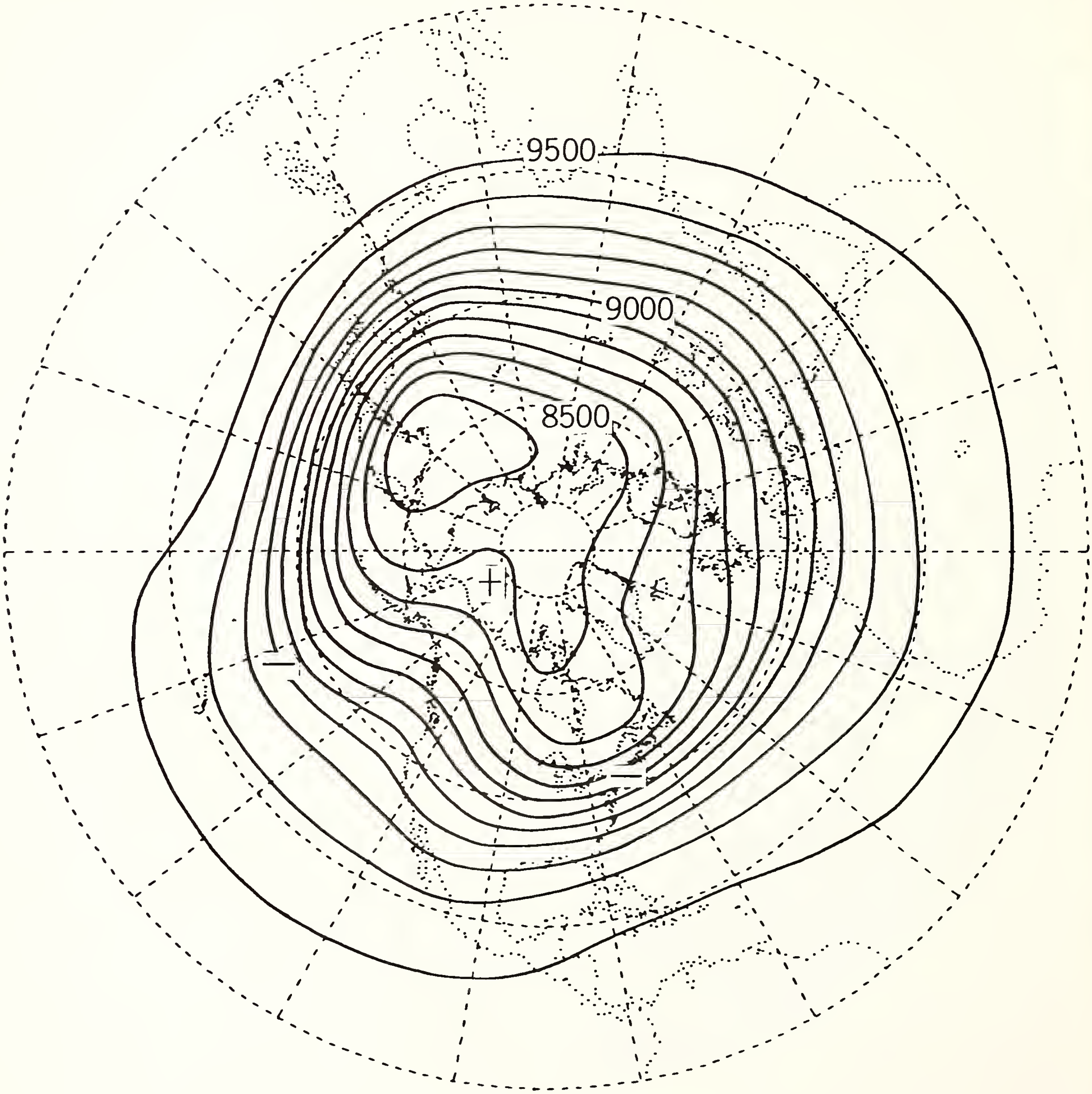

$\bar{Z}^{m}_{300}$

COMPOSITE OF 9 WINTER MONTHS WITH HIGHEST ANOMALY INDICES

Fig. 4a. Composite of 300 mb height for the nine winter months with the highest anomaly indices as defined in Eqn. (1). Contour interval: 100 m.

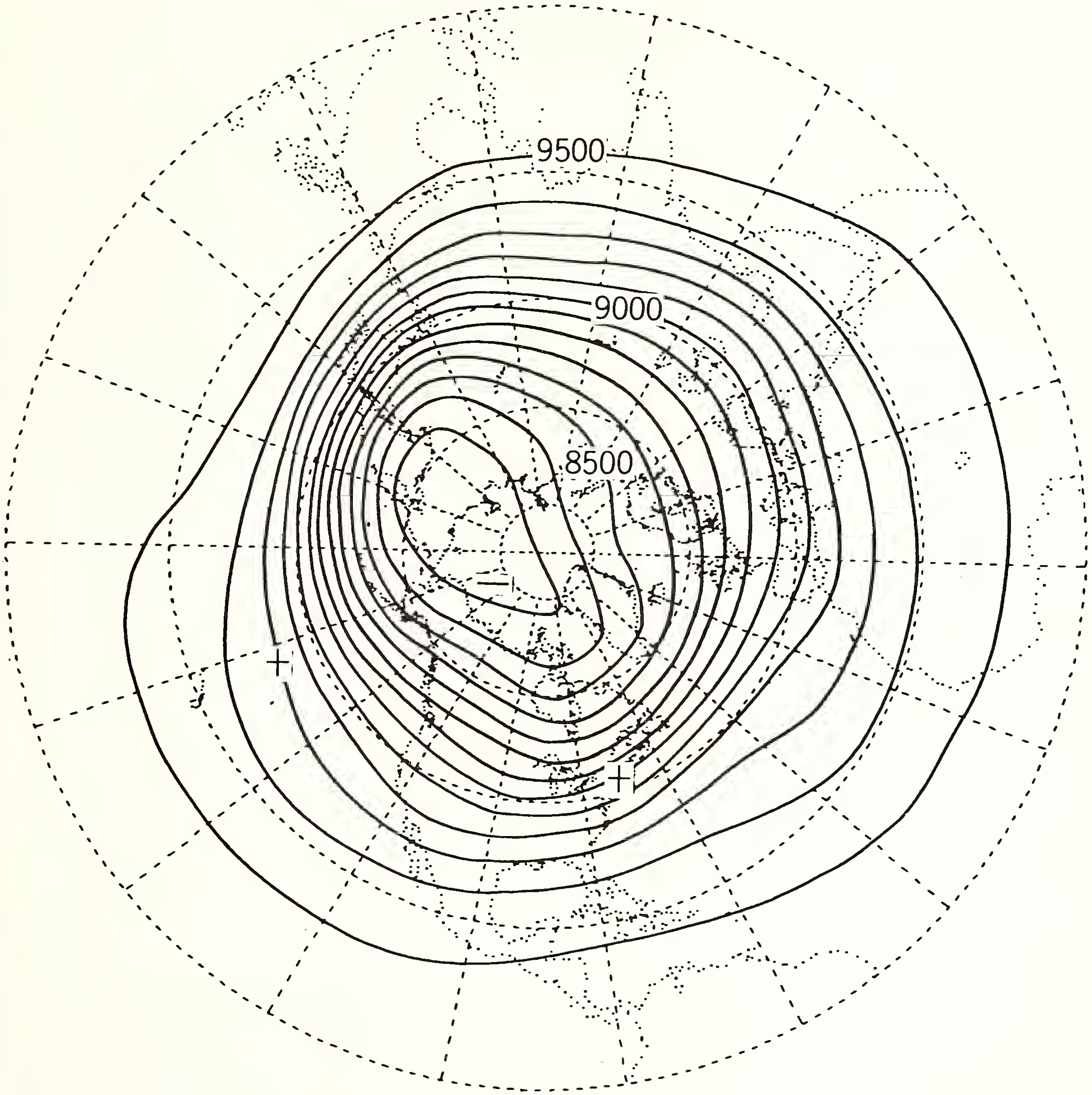

$\bar{Z}^{m}_{300}$

COMPOSITE OF 9 WINTER MONTHS WITH LOWEST ANOMALY INDICES

Fig 4b. Composite of 300 mb height for the nine winter months with the lowest anomaly indices defined in Eqn. (1). Contour interval: 100 m.

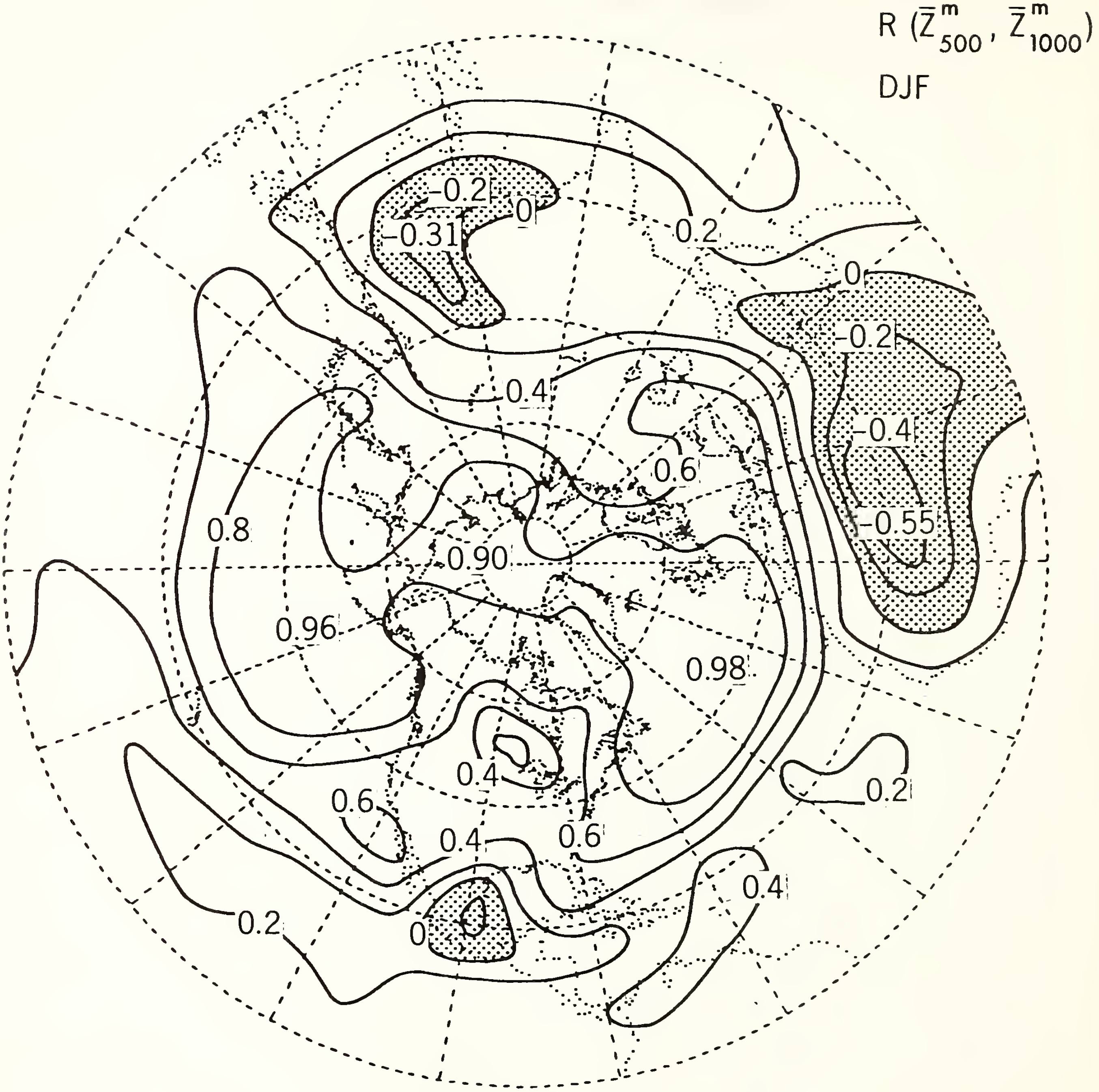

Fig. 5. Correlation coefficient between monthly means of 1000 and 500 mb heights during the winter season. Contour interval: 0.2.

# Prediction Experiments with a Coarse-Mesh Global Model

Jerome Spar
The City College
New York, N. Y.

A global general circulation model (GCM) has been developed for climate simulation studies by a group under J. Hansen at the Goddard Institute for Space Studies (GISS) in New York. The model can be operated with a horizontal grid of 8° of latitude by 10° of longitude and 7 layers in the vertical. With this resolution, one month of meteorological history can be computed in about 2 hours on an IBM 360/95 computer.

The model has been exercised in a set of prediction runs by initializing it with global gridded data from the National Meteorological Center (NMC) for the first day of each of 5 months: October 1976 - February 1977. The output for each one-month run was averaged to obtain a set of 5 monthly mean "forecasts", and these were verified against the monthly mean NMC data. Climatological monthly mean sea-surface temperatures (adjusted daily) are specified as surface boundary conditions over the oceans for these forecast runs.

Figures 1, 2, and 3 illustrate the "forecast" and "observed" global monthly mean fields of 850 mb temperature (T8), 500 mb geopotential height (Z5), and sea-level pressure (SLP) for December 1976. Table 1 presents northern hemisphere forecast statistics for all 5 months for both the model forecasts (F) and "forecasts" of climatology (C).

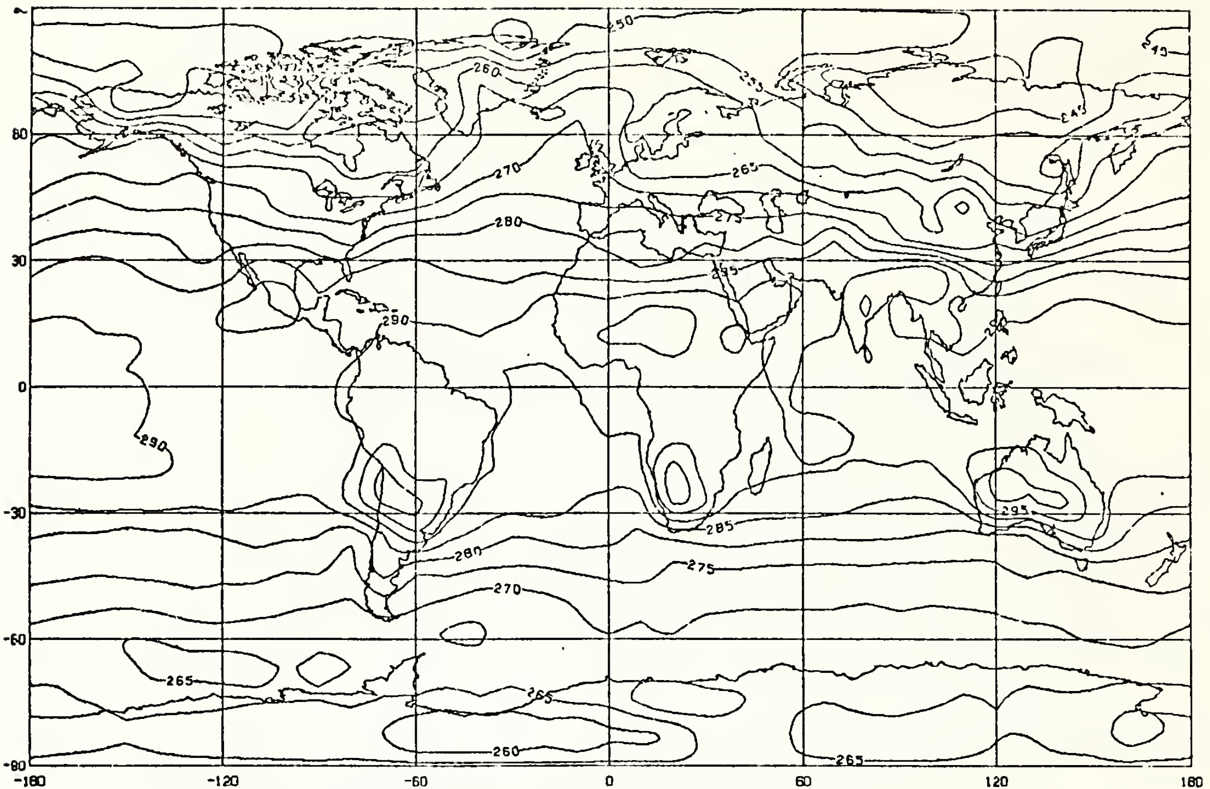

1976 DECEMBER FORECAST 850MB TEMPERATURE

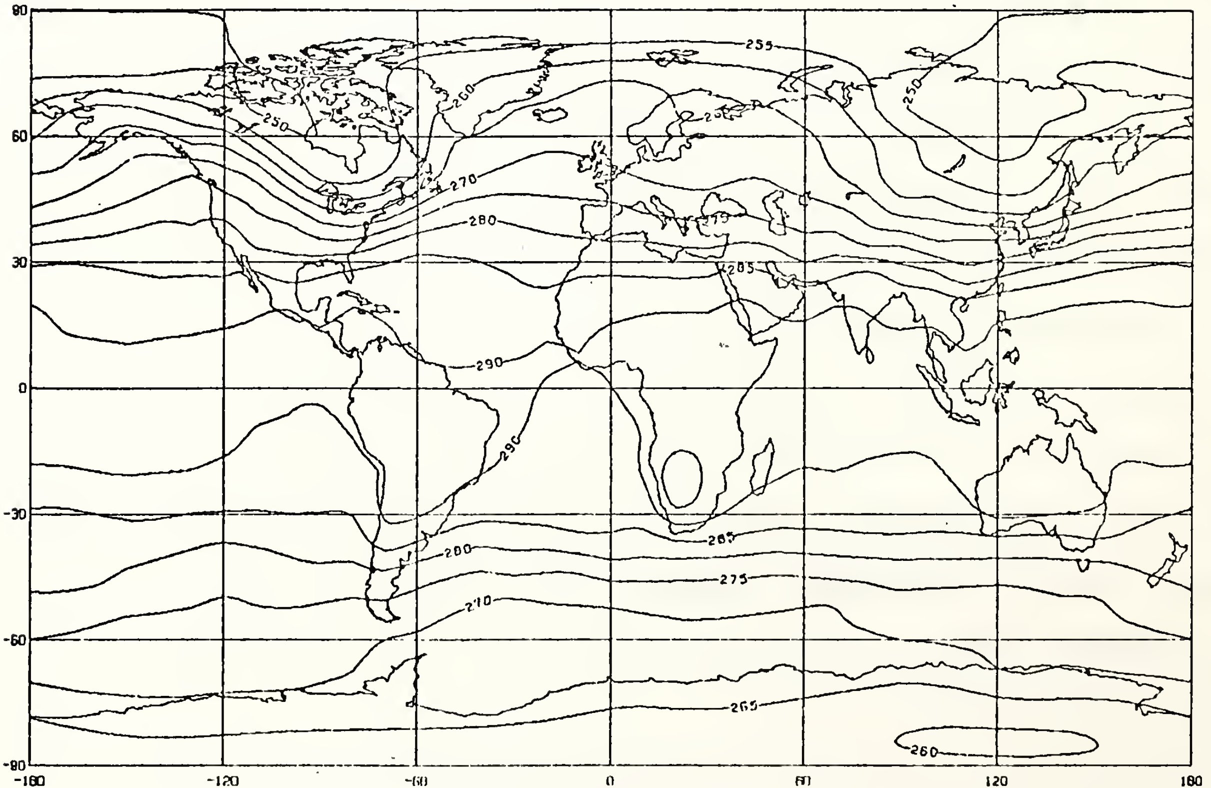

1976 DECEMBER OBSERVED 850MB TEMPERATURE

Fig. 1

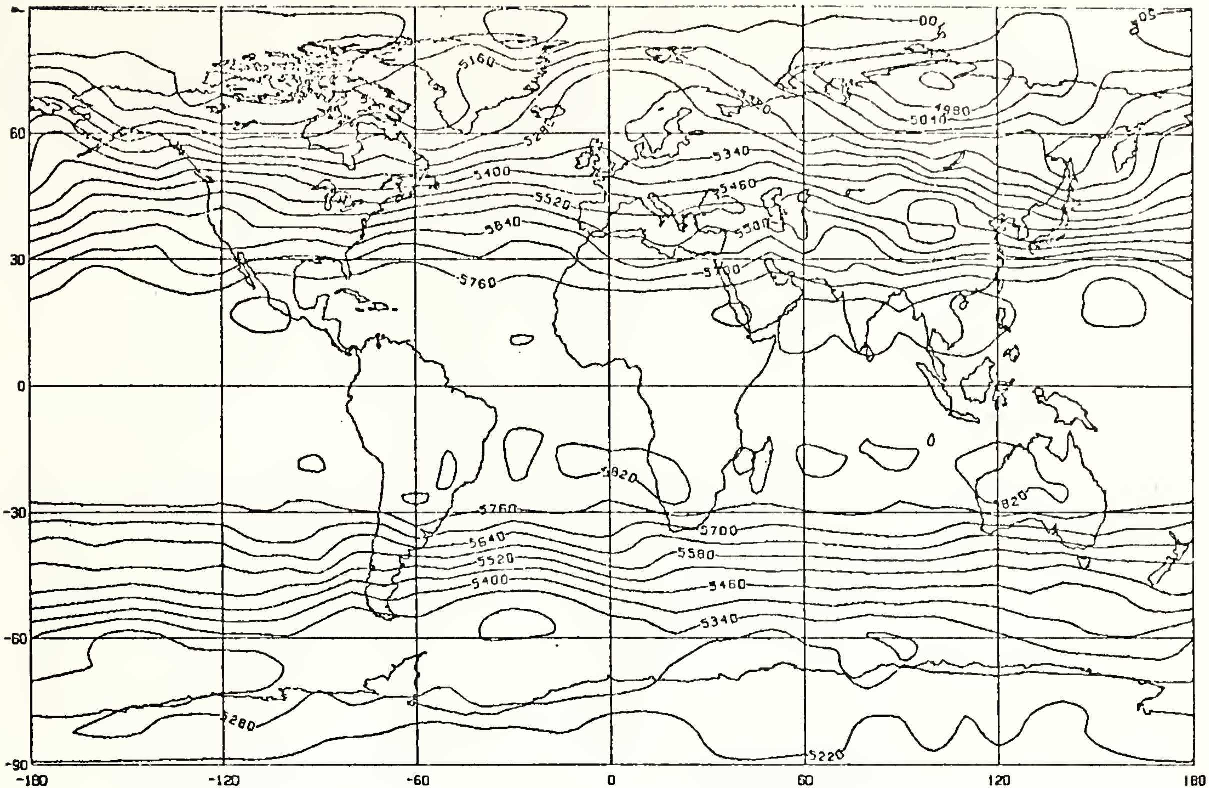

1976 DECEMBER FORECAST 500MB GEOPOTENTIAL HEIGHT

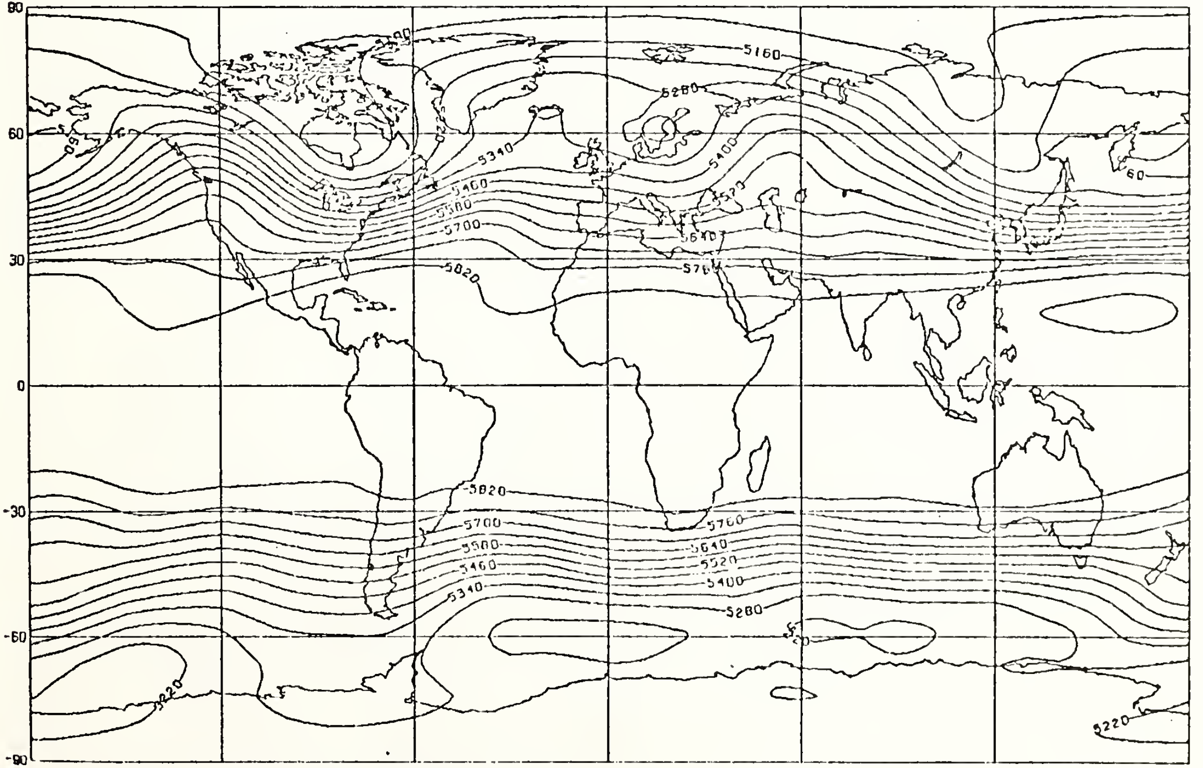

1976 DECEMBER OBSERVED 500MB GEOPOTENTIAL HEIGHT

Fig. 2

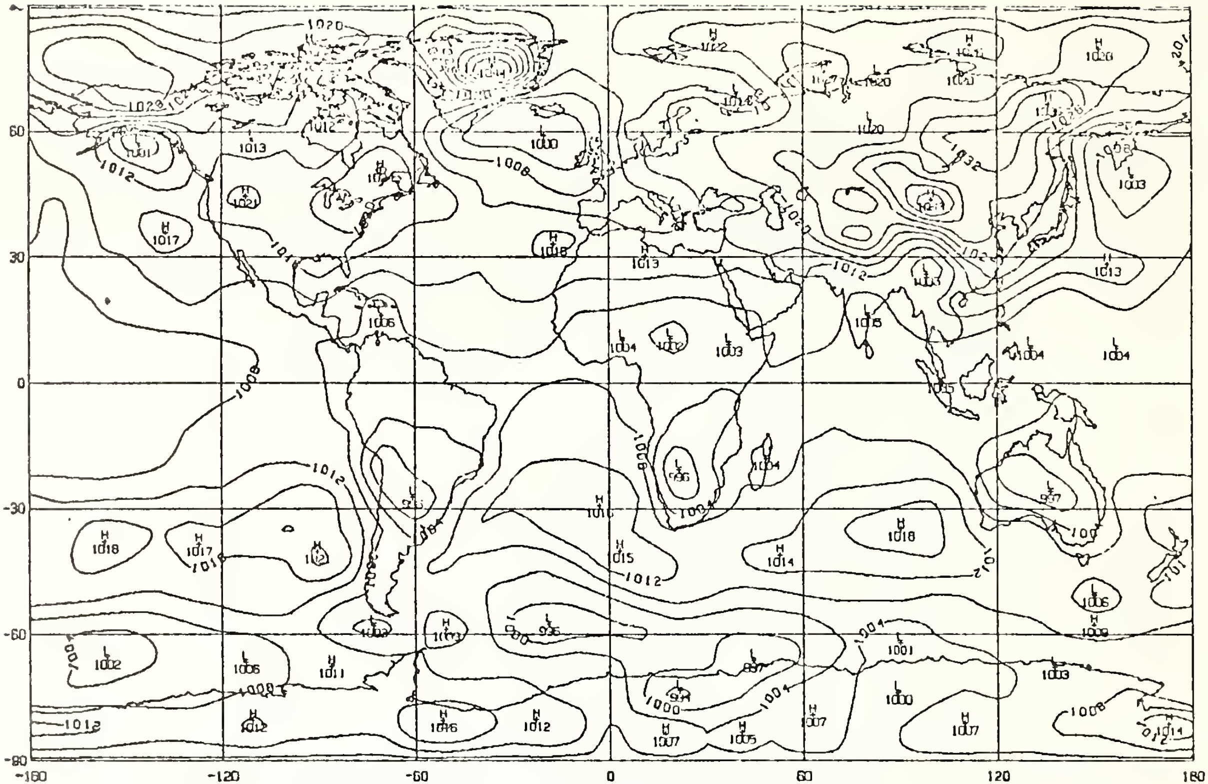

1976 DECEMBER FORECAST SEA LEVEL PRESSURE

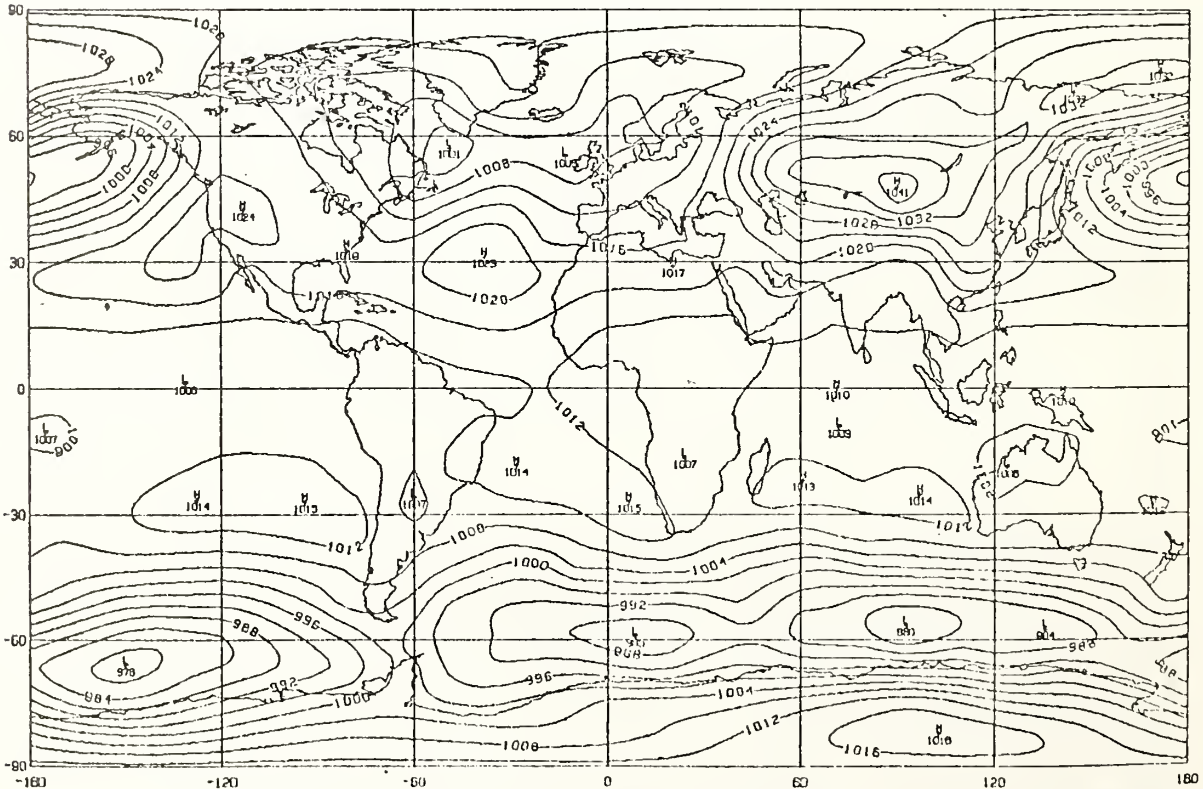

1976 DECEMBER OBSERVED SEA LEVEL PRESSURE

Fig. 3

Table 1 Climate model (MX500H7) forecast statistics for Northern Hemisphere. October 1976 - February 1977.

F=model (control) forecast. C=climatology forecast. (See text for details.

| Month | Field | | Bias | Root-mean-Square error (rmse) | Skill Score (S1) | Correlation coefficient (r) |
|---|---|---|---|---|---|---|
| October '76 | T8 | F | -0.5K | 3.2K | 65 | +0.56 |
| | | C | -0.4K | 2.2K | 49 | |
| | Z5 | F | -39m | 62m | 63 | +0.30 |
| | | C | + 4m | 39M | 47 | |
| | SLP | F | -2.4mb | 6.0 mb | 99 | +0.39 |
| | | C | -0.2mb | 3.0 mb | 65 | |
| November '76 | T8 | F | -1.0K | 3.8K | 66 | +0.20 |
| | | C | -0.7K | 2.1K | 47 | |
| | Z5 | F | -37m | 72m | 66 | -0.11 |
| | | C | + 3m | 40m | 42 | |
| | SLP | F | -1.6mb | 7.1 mb | 90 | -0.21 |
| | | C | +0.0mb | 2.9 mb | 53 | |
| December '76 | T8 | F | -0.4K | 3.4K | 62 | +0.15 |
| | | C | -0.4K | 1.9K | 39 | |
| | Z5 | F | -32m | 71m | 63 | -0.03 |
| | | C | + 4m | 43m | 43 | |
| | SLP | F | -2.1mb | 5.8 mb | 84 | +0.33 |
| | | C | -0.0mb | 3.5 mb | 51 | |
| January '77 | T8 | F | -0.9K | 4.3K | 61 | +0.07 |
| | | C | -0.5K | 2.7K | 51 | |
| | Z5 | F | -45m | 91m | 66 | +0.17 |
| | | C | + 2m | 73m | 57 | |
| | SLP | F | -2.5mb | 6.8mb | 83 | +0.56 |
| | | C | -0.7mb | 5.9mb | 64 | |
| February '77 | T8 | F | -0.9K | 4.2K | 68 | +0.20 |
| | | C | -0.7K | 2.3K | 43 | |
| | Z5 | F | -38m | 80m | 60 | +0.12 |
| | | C | - 5m | 55m | 48 | |
| | SLP | F | -2.0mb | 7.5mb | 85 | +0.05 |
| | | C | -0.3mb | 4.4mb | 62 | |

"Bias" denotes the area-weighted algebraic mean error. The root-mean-square error is also area-weighted, as are the Teweles-Wobus S1 (gradient) skill score, and the correlation coefficient, r, between forecast and observed deviations from climatology. Although the predicted fields look realistic, the forecast statistics indicate no skill relative to climatology.

A "model climatology" (M) was generated for each month by running the model for 5 simulated years. Figures 4, 5, and 6 illustrate the model climatology for December compared with the actual (NCAR) climatology (C for the same month in terms of the fields of T8, Z5, and SLP. Difference statistics for M vs. C, indicate that the "climatology errors" are of the same magnitude as the "forecast errors" (Table 1).

While the model climatology does differ from that of the real atmosphere, it is nevertheless possible that the response of the model to initial conditions may resemble that of the real atmosphere. To test this hypothesis, a "response error" was evaluated by computing the correlations, r*, between deviations of model forecast from model climatology (F - M) with the observed anomalies (O-C). In Table 3, r* is compared with r, the correlation between forecast (F - C) and observed (O - C) anomalies, but the values are seen to be no greater.

Model simulation of real monthly climatic anomalies is clearly a difficult task, requiring further model development as well as improved global data sets.

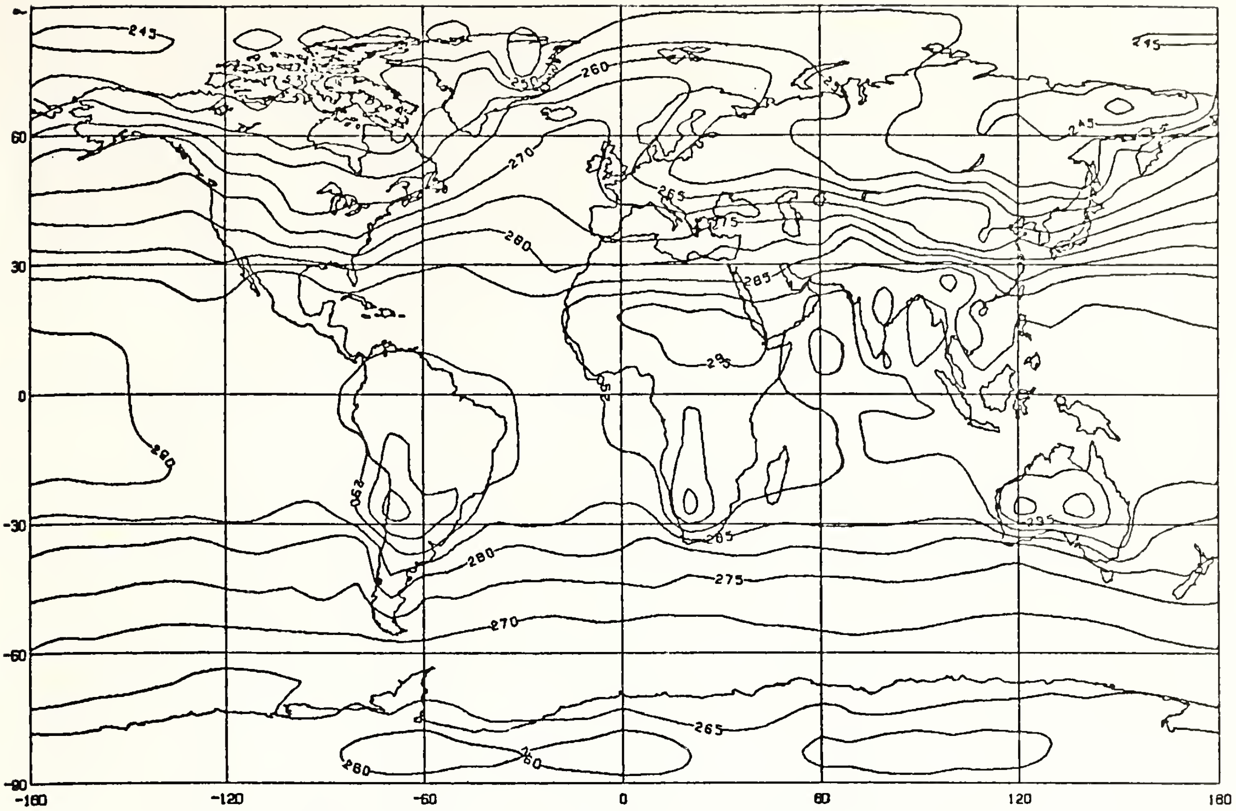

DECEMBER MODEL CLIMATOLOGY 850MB TEMPERATURE

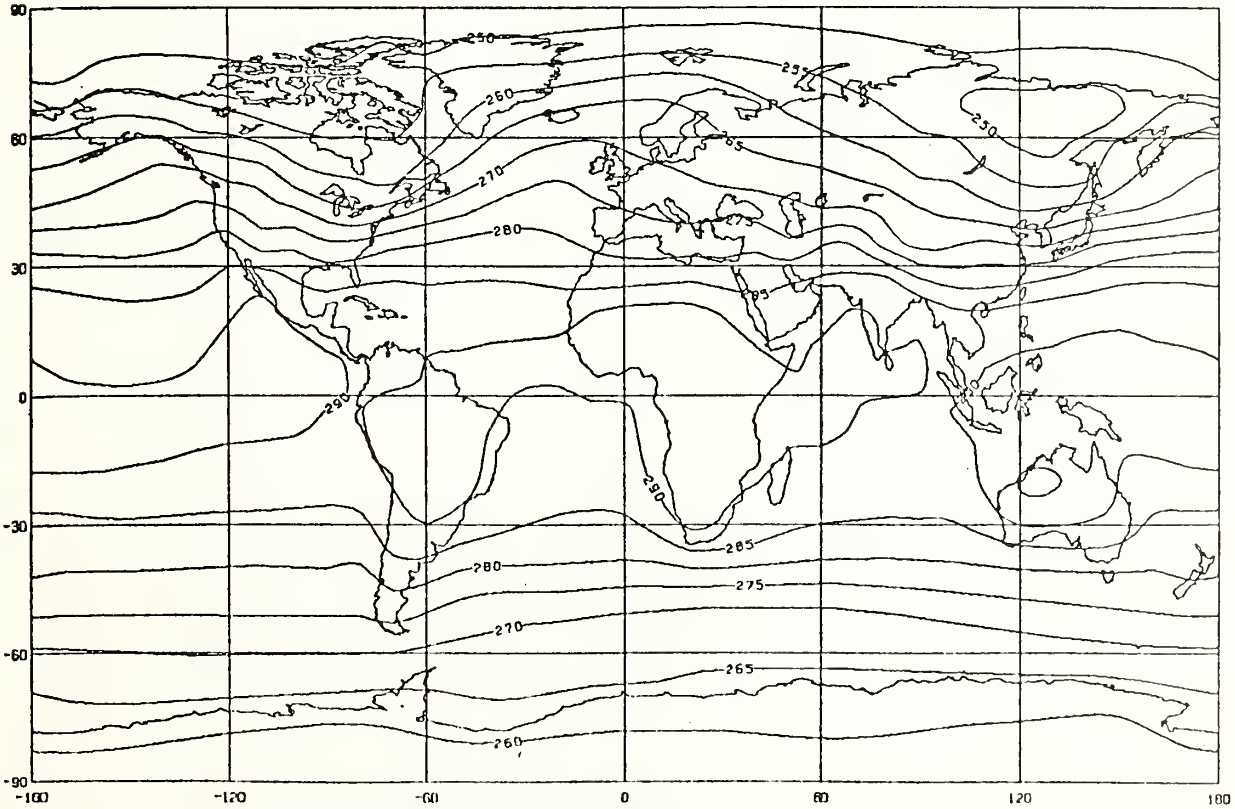

DECEMBER CLIMATOLOGY 850MB TEMPERATURE Fig. 4

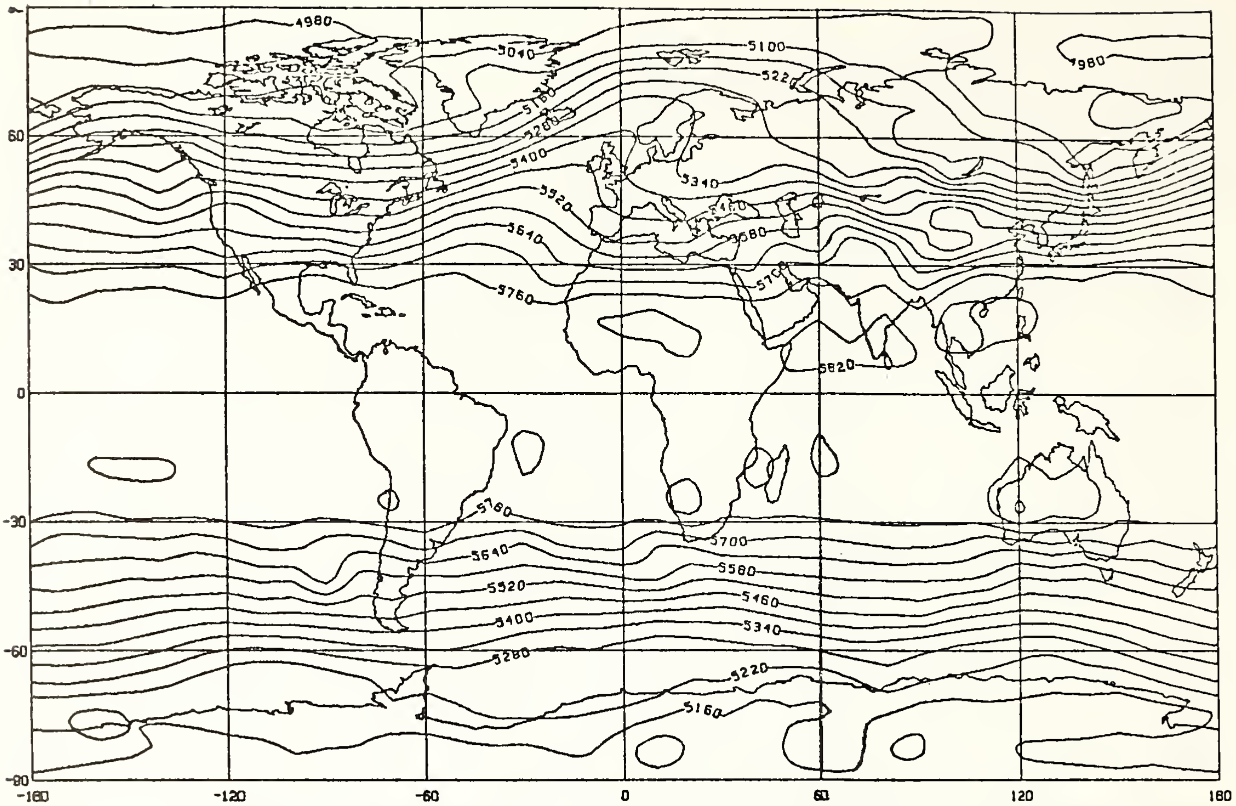

DECEMBER MODEL CLIMATOLOGY 500MB GEOPOTENTIAL HEIGHT

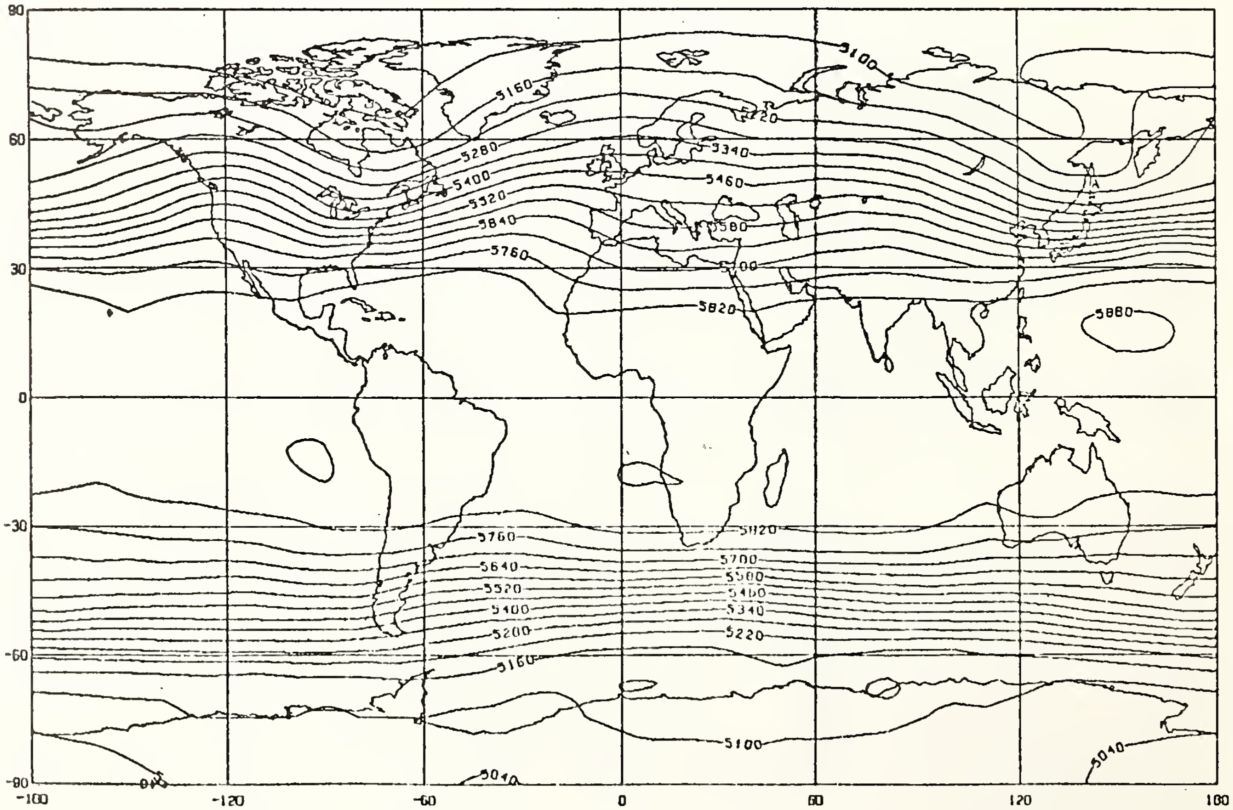

DECEMBER CLIMATOLOGY 500MB GEOPOTENTIAL HEIGHT Fig. 5

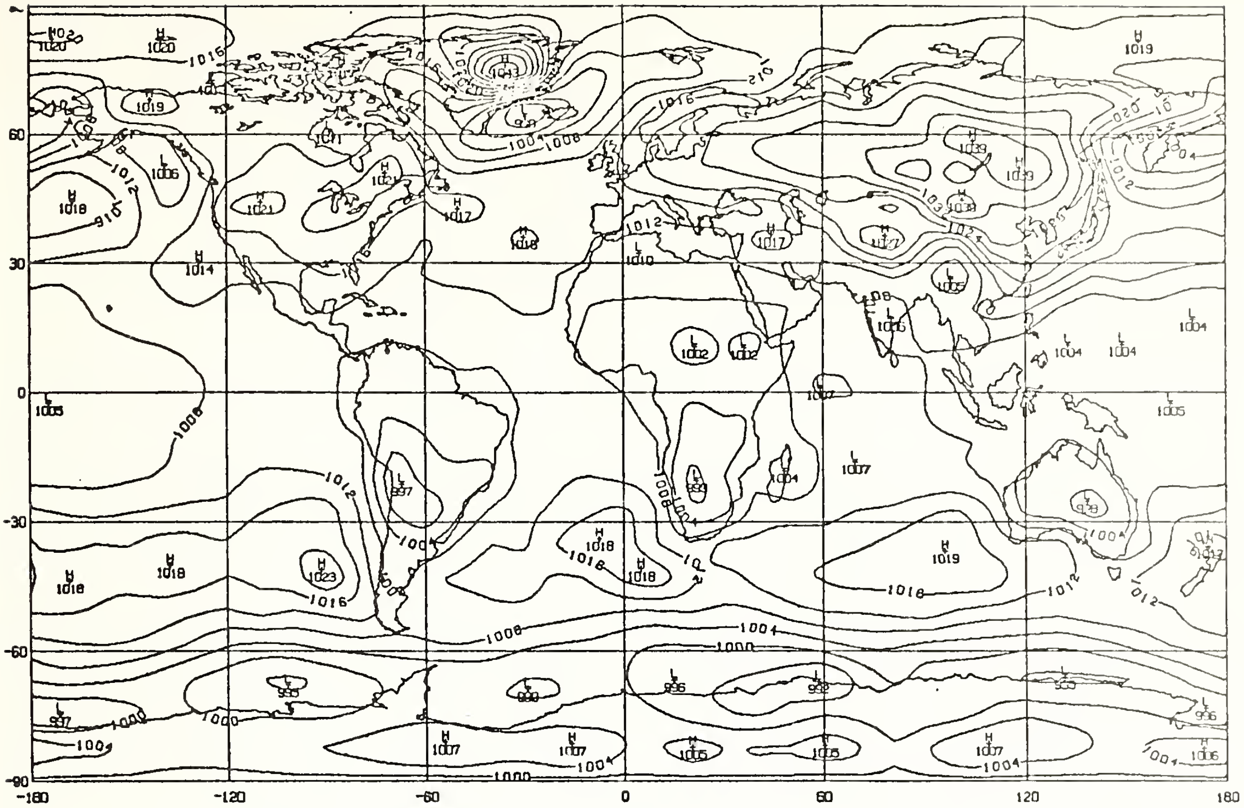

DECEMBER MODEL CLIMATOLOGY SEA LEVEL PRESSURE

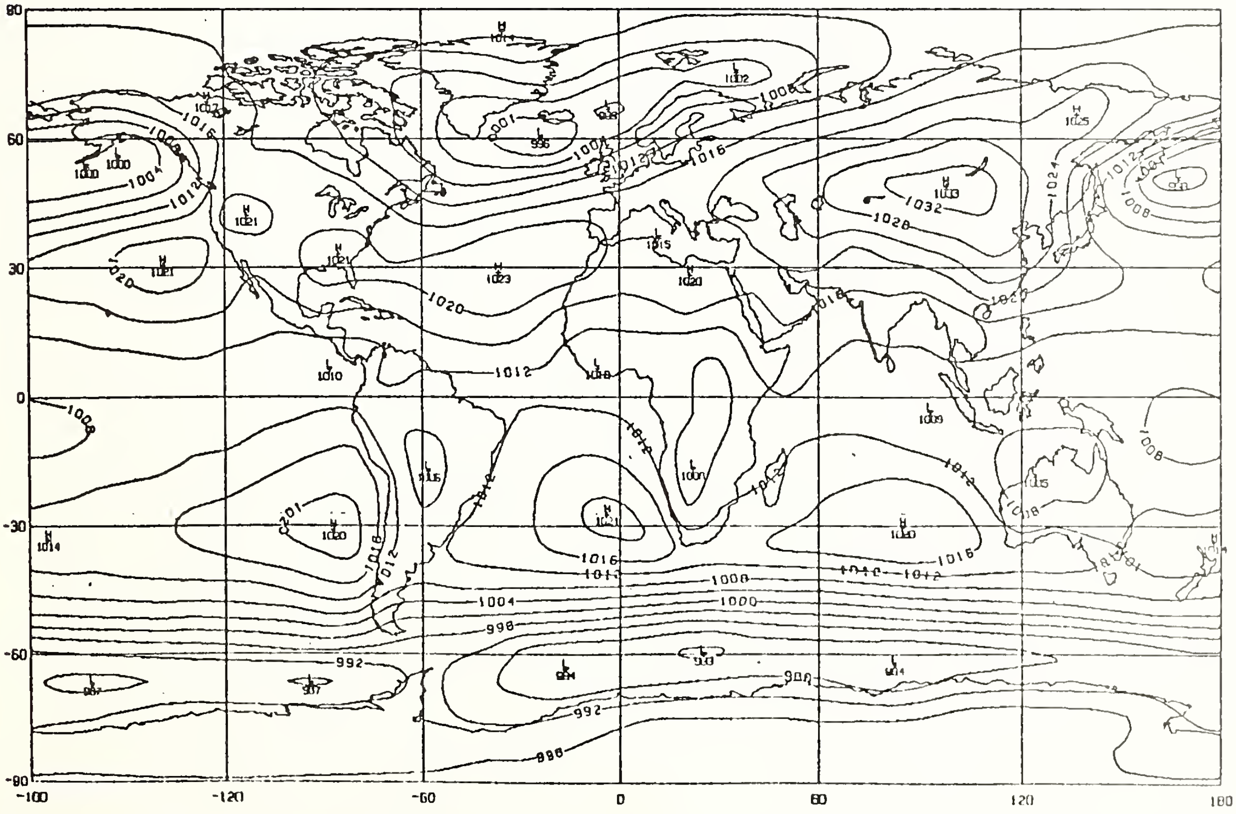

DECEMBER CLIMATOLOGY SEA LEVEL PRESSURE Fig. 6

Table 2. Five year "model climatology" versus observed (NCAR) climatology. (M-C) difference statistics over the Northern Hemisphere.

|  | Bias | RMS | SI |
|---|---|---|---|
| **October** |  |  |  |
| T8 | -0.2 K | 3.8 K | 72 |
| Z5 | -29 m | 51 m | 57 |
| SLP | -1.2 mb | 6.9 mb | 98 |
| **November** |  |  |  |
| T8 | -0.5 K | 4.0 K | 70 |
| Z5 | -40 m | 61 m | 52 |
| SLP | -1.6 mb | 6.2 mb | 89 |
| **December** |  |  |  |
| T8 | -0.5 K | 3.5 K | 58 |
| Z5 | -44 m | 66 m | 54 |
| SLP | -2.1 mb | 6.1 mb | 87 |
| **January** |  |  |  |
| T | -0.5 K | 3.8 K | 60 |
| Z5 | -53 m | 77 m | 54 |
| SLP | -2.4 mb | 6.1 mb | 89 |
| **February** |  |  |  |
| T8 | -0.6 K | 4.1 K | 61 |
| Z5 | -52 m | 76 m | 53 |
| SLP | -2.8 mb | 6.2 mb | 91 |

Table 3. Correlation coefficient r*, between model anomaly, F-M, and observed anomaly, O-C, compared with correlation coefficient, r, between forecast anomaly, F-C, and observed anomaly. Northern Hemisphere. October 1976 - February 1977

| Month | Field | r* | r |
|---|---|---|---|
| October '76 | T8 | +0.08 | +0.56 |
| | Z5 | +0.39 | +0.30 |
| | SLP | +0.20 | +0.39 |
| November '76 | T8 | +0.05 | +0.20 |
| | Z5 | +0.17 | -0.11 |
| | SLP | +0.03 | -0.21 |
| December '76 | T8 | -0.05 | +0.15 |
| | Z5 | +0.14 | -0.03 |
| | SLP | +0.28 | +0.38 |
| January '77 | T8 | +0.00 | +0.07 |
| | Z5 | +0.34 | +0.17 |
| | SLP | +0.32 | +0.36 |
| February '77 | T8 | +0.07 | +0.20 |
| | Z5 | +0.14 | +0.12 |
| | SLP | +0.17 | +0.05 |

# Observed Interannual Aerosol Optical Depth Variations for the Northern Hemipshere

by

Brian M. Goodman and Reid A. Bryson

Institute for Environmental Studies
University of Wisconsin-Madison
Madison, Wisconsin 53706

Starting with Benjamin Franklin in 1758, the idea has emerged that climatic variation in time might be related to variations in the amount of solar radiation reaching the earth's surface. Observations of the intensity of the direct beam solar radiation have been made routinely in the Northern Hemisphere since 1883. Variations in this quantity could be due to either changes in the solar output or to changes in the transparency of the atmosphere by aerosol loading from volcanic, anthropogenic, or other natural sources.

The upper curve in figure 1 was constructed after a careful reanalysis of the pyrheliometric and actinometric measurements of the intensity of the direct beam solar radiation received at 42 observing sites situated around the Northern Hemisphere between 20 and 65N. This is essentially the entire body of data available in the literature. The measurements were converted to optical depths with a simple wavelength-integrated form of Beer's Law, removing differences in air mass, altitude, scaling factors, and time of year. These individual values were then combined into a time series of annual means, which were representative of the year-to-year variations in the total optical depth of the Northern Hemisphere. For those years when only one station was available an annual mean was based upon a regression equation for that station's record against the annual means for years where the one station's and other stations' records were available. The upper curve in figure 1 is the residual optical depth attributable to aerosols after removing that part due to clean air, water vapor, ozone, and other molecular components. The latter contributions are treated as a constant, approximately 0.212 for the Northern Hemisphere using mean hemispheric and mean annual values from the literature.

As mentioned before any variations in the solar output will be implicit in the data. However, it is unlikely that changes in the solar constant are responsible for the observed fluctuation (or at least a major portion of them) in the upper curve of figure 1. Past estimates of the solar constant and recent satellite measurements suggest that the observed variations if due only to variations in the solar constant are of an order of magnitude larger than the largest likely change which could have occurred. Indeed, the most successful simulations of the course of hemispheric or zonal surface temperatures over the past century have not been based on the assumption of a time varying solar constant, but on the assumption that the transparency of the cloudless atmosphere has varied, specifically, in response to variations of volcanically produced turbidity.

In part, these models help distinguish between the sun and volcanic debris changing the aerosol optical depth as the source of variations in the direct beam solar radiation received at the earth's surface. For example, the sensitivity of the hemispheric mean surface temperature to a 1% change in the solar constant is between 1.0-1.2 K. The observed aerosol optical depth values increased from 0.04 to 0.08 during the period 1945-1975, which corresponds to a decrease in the atmospheric transparency at an air mass of M = 2 from 60% to 55%, or in other words a decrease of 5% in the direct beam solar radiation. If this decrease were due only to variations in the solar constant, then the mean hemispheric surface temperature during this time should have decreased 6-10 K. This is clearly much larger than the 0.3-0.4 K decrease which has been observed by Borzenkova. On the other hand, if the turbidity of the atmosphere had varied enough to reduce the direct beam solar radiation by 5%, then the mean hemispheric surface temperature should have decreased only by about 0.85 K according to the Bryson-Dittberner climate model. This is because the increased turbidity increases the amount of diffuse radiation almost as much as it decreases the direct beam radiation. Correcting this value for the effect of increasing carbon dioxide (about 12 ppm from 1945-1975), a temperature increase of about 0.30-0.35 K, gives a calculated decrease in the mean hemispheric surface temperature of 0.50-0.55 K. This is much closer to the observed decrease than the value obtained with the assumption of a variable solar constant. If we also take into account the lag produced by the heat storage in the hydrosphere the match would become even closer.

The lower curve in figure 1 is drawn from the listing of about 6000 historically recorded eruptions in the files of the Center for Climatic Research at the University of Wisconsin-Madison. This is approximately ten times the number of eruptions compiled in the Lamb chronology, which has been used by many authors for assessing climate-volcano interactions. While the numbers used for the lower curve in figure 1 are only of those eruptions classified as being of a "great" magnitude, there are also far more "moderate" and "small" type eruptions recorded for the early years of this century and for this past decade than during the 1925-1955 period when the observed aerosol optical depths were at a minimum and the mean hemispheric surface temperature anomalies computed by Borzenkova was at its highest. Indeed, the course of general volcanic activity and of the mean aerosol optical depth in this century are remarkably the inverse of the hemispheric mean surface temperature, see figure 2. The volcano count per year of all eruptions (middle curve in figure 2) only goes back to 1925 because before this time there is considerable sampling bias on the "small" type eruption counts. From 1945 to 1970 the annual eruption numbers roughly doubled from 16-18 per year to 37-40 per year. During this same interval the aerosol optical depth also doubled from about 0.04 to 0.08. This is in good agreement with recent ice core analyses which report an observed doubling in the amount of non-organic impurities deposited on the Greenland Ice Sheet between times of low and high volcanic activity over the past 300 years.

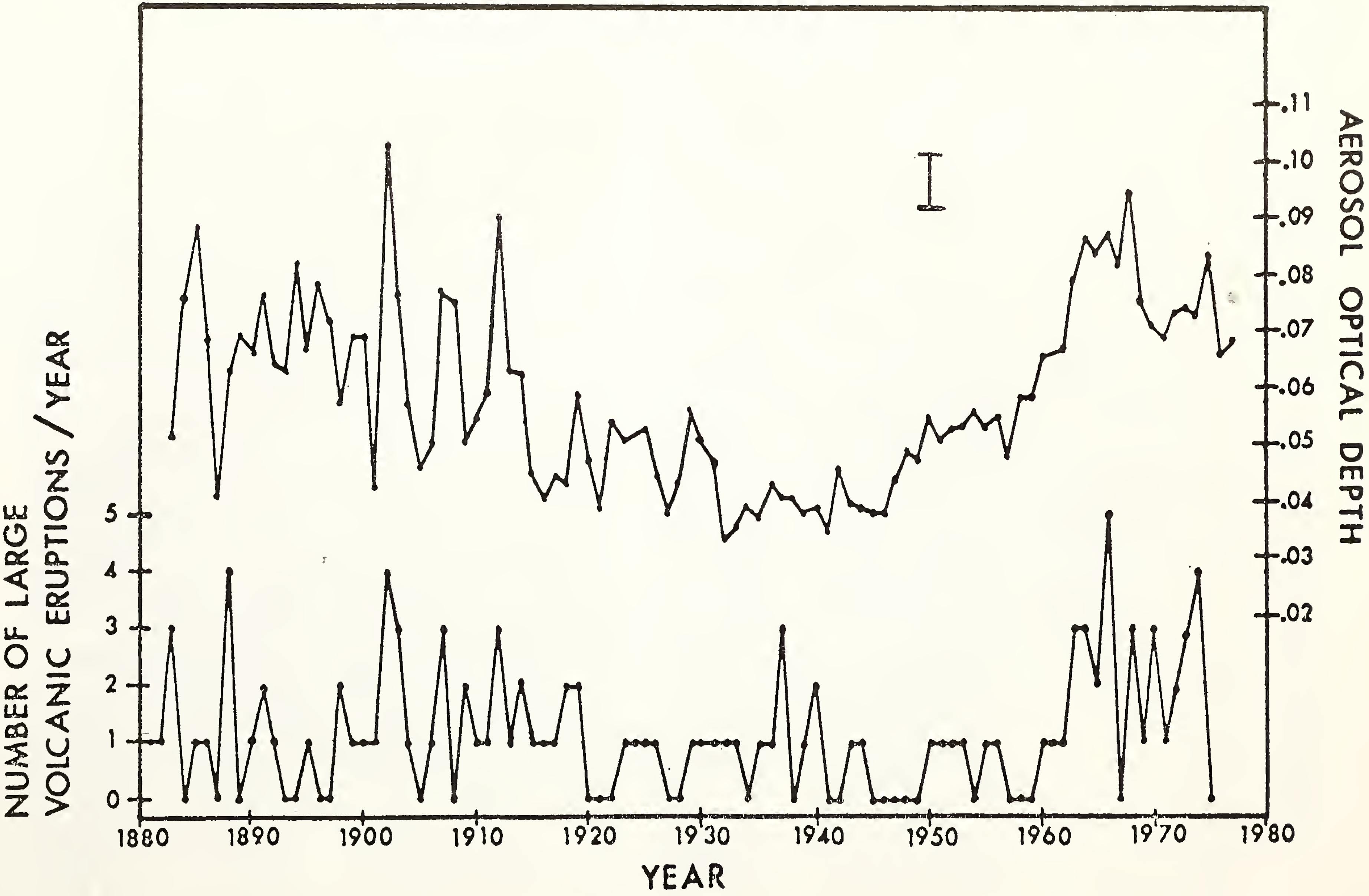

Figure 1. Mean annual aerosol optical depth, based on 42 stations between 20 and 65N (upper curve) and number of volcanic eruptions between 10S and 90N of large magnitude per year (lower curve).

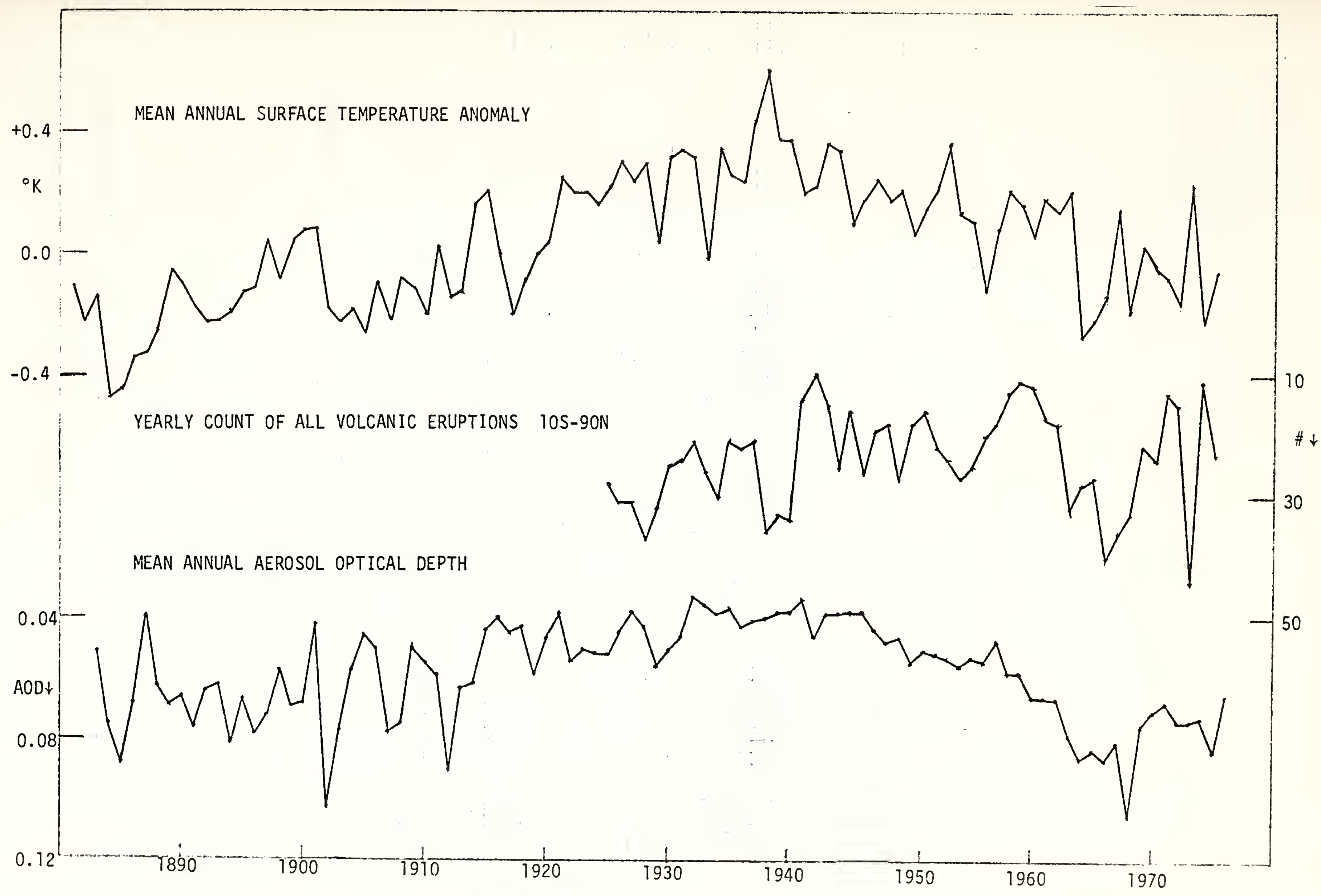

**Figure 2.** Mean annual surface temperature anomaly for the Northern Hemisphere from 1881-1975 by Borzenkova (upper curve), the inverse of the number of volcanic eruptions between 10S and 90N of all magnitudes per year (middle curve), and the inverse of the mean annual aerosol optical depth, based on 42 stations between 20N and 65N (lower curve).

# Influence of Volcanic Aerosols and Oceanic Surface Temperatures on Tropospheric Temperatures

by Alfredo R. Navato

Department of Meteorology
Massachusetts Institute of Technology

For many years now climatologists have been aware of the influence of the presence of volcanic dust and aerosol in the atmosphere on tropospheric temperatures (e.g., Lamb, 1970; Newell and Weare, 1976; Bryson and Dittberner, 1976; Hansen, Wang, and Lacis, 1978). The influence of oceanic sea surface temperatures (SST) on tropospheric temperatures has also been investigated, e.g., by Newell and Weare (op. cit.). however, none of the previous studies included the Indian Ocean. This report summarizes results of a study to estimate the sensitivity of the tropical (20°N to 20°S) tropospheric temperatures (TTT) to SST's of the Pacific Ocean, Atlantic Ocean, and Indian Ocean, and to atmospheric dust and aerosol concentrations over the northern tropics and over the southern hemisphere. When the SST and aerosol time series are used as predictors in a regression equation for tropospheric temperatures, the time lags required for the predictors in order to achieve the maximum explanation of variance of tropospheric temperatures will be suggestive of the answer to the question: does the atmosphere drive the ocean, or is it the other way around? A multiple regression model of the "air-SST-aerosol" interaction was developed and the relative influence of the various oceans and aerosols on tropospheric temperatures was deduced from the values of the regression coefficients.

A stepwise regression procedure (explained, e.g., in Draper and Smith, 1966) was used to select five predictors (at the appropriate lags) among the set of predictors shown in Figure 1. This procedure results in a maximum explanation of variance of the predictand TTT with the chosen number of predictors. We then arrived at a regression model in which the ocean SST's and aerosols either led, or were contemporaneous with,TTT. We found that TTT would increase by about 0.3 standard deviations for every standard deviation increase in SST's of any one of the three oceans, and about 0.15 standard deviations for every standard deviation increase in aerosol concentration over the tropics or over the southern hemisphere. The SST's and aerosols were intercorrelated, and so, may tend to increase or decrease together. A fuller report of this research has been submitted to the Monthly Weather Review.

The predictand TTT represents nonseasonal anomalies of monthly tropospheric mean temperatures (i.e., departures from long-term 1958-1972 monthly means for each calendar month) following Angell and Korshover's (1975) method of using the average 700-300 mb geopotential height differences estimated from seven tropical stations located near 20°N and 20°S (see Table 1). The nonseasonal anomalies averaged over the five stations north of the equator had a positive correlation of

0.459 with the corresponding average for the two stations south of the equator. Oceanic SST's were represented by the time series coefficients of the empirical orthogonal function (EOF) representation of the nonseasonal SST monthly anomalies (e.g., Weare, Navato, and Newell, 1976 for a similar EOF representation of Pacific Ocean SST's and Weare, 1977 for Atlantic Ocean SST's). EOF time series from unnormalized monthly average anomalies, and from anomalies after normalization with respect to the corresponding grid square standard deviation were included in the set of possible predictors. Only the time series of the principal function (that which explains the largest fraction of the variance of the SST's) for each ocean was used. Data for the Pacific Ocean covered the area from 60°N to 30°S but excluded the area west of 125°E and another area south of 10°N and west of 180°W. The EOF used here was calculated by Billing (1979) and explains 18.4% of the variance. This variability was mainly contributed by the equatorial regions and by an area in the North Pacific in its eastern sector. A positive value in the time series represents warm anomalies in these two areas. The Atlantic Ocean analysis (by Hsiung, 1978) covered the area between 70°N and 30°S. The principal normalized mode used in the regression equation explained 9.7% of the variance. A positive value in the time series represents cold anomalies in the central 30°N to 50°N region, large warm anomalies around 20°N, off Scotland, near the equator, and off Southwest Africa. The Indian Ocean analysis (paper in preparation) covered the area south of 25°N to 35°S from 20°E to 120°E, and two small areas north and south of Australia. The principal normalized mode used explained 13.8% of the variance. A positive value in the time series represents warm anomalies in the entire region north of 30°S and cold anomalies between 55°E and 75°E south of 30°S, at the northern edge of the "roaring forties."

To represent aerosol over the tropics we used the apparent solar transmittance at Mauna Loa at 19°N (see Pueschel, Machta, Cotton, Flowers, and Peterson, 1972) kindly provided by the National Oceanic and Atmospheric Administraion. Aerosol over the southern hemisphere was represented by the Aspendale (38°S) dust index provided by Dyer as seasonal data (Dyer, 1974).

To obtain estimators for the regression coefficients which would have the minimum variance (i.e., maximum precision) among all unbiased linear estimators, one important condition is that the time series of residuals (the difference between the dependent variable and the sum of the independent variables and their corresponding regression coefficients) be not serially correlated (see, e.g., Goldberger, 1964). Ordinary least squares procedures applied to the regression equation we obtained by the stepwise procedure gave residuals which were serially correlated. We then had to resort to a generalized least squares procedure (see, e.g., Goldberger, op. cit.) and obtained the following regression model, now with no violations for the validity of the statistical procedures used:

$$TTT_t = 0.293\ P_{t-6} + 0.266\ A_t + 0.306\ I_{t-1} + 0.127\ M_t - 0.152\ AD_{t-2}$$

| | | | | | |
|---|---|---|---|---|---|
| std. error | 0.0733 | 0.0579 | 0.0664 | 0.0543 | 0.0594 |
| t-statistic | 4.24 | 4.28 | 4.71 | 2.09 | -2.47 |

where $TTT_t$ = topical tropospheric temperature at time t

$P_{t-6}$ = Pacific Ocean SST unnormalized EOF time series coefficient for month t-6

$A_t$ = Atlantic Ocean SST normalized EOF time series coefficient for month t

$I_{t-1}$ = Indian Ocean SST normalized EOF time series coefficient for month t-1

$M_t$ = Mauna Loa apparent solar transmittance for month t

$AD_{t-2}$ = Aspendale dust index for month t-2

The right-hand side of the equation explains 50.2% of the variance of the left-hand side. All the variables are standardized, i.e., they are deviations from their long-term means divided by their long-term standard deviations. The deviations for TTT, P, A, and I are nonseasonal. All assumptions of the asymptotic theory for the estimates of standard errors, t-statistics, and fraction of variance explained were verified to be fulfilled. The coefficients all differed from zero at a significance level better than 2.5%. It may be noted that the number of degrees of freedom involved in estimates of the standard errors and t-statistics are taken from the uncorrelated residuals of the generalized least squares procedure, and hence, are equal to the length of the time series reduced by the number of independent variables increased by one.

It is interesting to note that in the Northern Pacific where space and time scales of oceanic surface flows are not long, Davis (1976) found that the atmosphere leads oceanic SST's while for the whole Pacific we found that the ocean leads the tropical troposphere.

# REFERENCES

J.K. Angell and J. Korshover: Estimate of the global achange in tropospheric temperature between 1958 and 1973, Mon. Wea. Rev. 103 (1975), 1007.

C. Billing: Unpublished M.S. thesis, Department of Meteorology, Massachusetts Institute of Technology (1979).

R.A. Bryson and G.J. Dittberner: Non-equilibrium model of hemispheric mean surface temperature, J. Atmosph. Sc. 31 (1976), 2094.

R.E. Davis: Predictability of sea surface temperature and sea level pressure anomalies over the North Pacific Ocean, J. Phys. Oceanogr. 6 (1976), 249.

N.R. Draper and H. Smith. Applied Regression Analysis, Wiley, New York (1966).

A. J. Dyer: The effect of volcanic eruptions on global turbidity, and an attempt to detect long-term trends due to man, Quart. J. R. Met. Soc. 100 (1974), 563.

A.S. Goldberger: Econometric Theory, Wiley, New York (1964).

J. E. Hansen, W.-C. Wang, and A.A. Lacis: Mount Agung eruption provides test of a global climatic perturbation, Science 199 (1978), 1065.

J. Hsiung: Unpublished M.S. thesis, Department of Meteorology, Massachusetts Institute of Technology (1978).

H.H. Lamg: Volcanic dust in the atmosphere; with a chronology and assessment of its meteorological significance, Philo. Trans. R. Soc. London A 266 (1970), 425.

R.E. Newell and B.C. Weare: Factors governing tropospheric mean temperature, Science 194 (1976), 1413.

R.F. Pueschel, L. Machta, G.F. Cotton, E.C. Flowers and J. T. Petersen: Normal incidence radiation trends on Mauna Loa, Hawaii, Nature 240 (1972), 545.

B.C. Weare, A. R. Navato and R. E. Newell: Empirical orthogonal analysis of Pacific sea surface temperatures, J. Phys. Oceanogr. 6 (1976), 671.

B.C. Weare: Empirical orthogonal analysis of Atlantic Ocean surface temperatures, Quart. J.R. Met. Soc. 103 (1977), 467.

## Table 1

## UPPER AIR STATIONS

| Name | Latitude | Longitude |
|---|---|---|
| Tropical Stations (between 20°N and 20°S) | | |
| Pt. Hedland | 20.23°S | 118.37°E |
| Wake Island | 19.17°N | 166.39°E |
| Nandi | 17.45°S | 177.27°E |
| Hilo | 19.43°N | 155.04°W |
| San Juan | 18.26°N | 66.0°W |
| Dakar | 14.44°N | 17.3°W |
| Khartoum | 15.36°N | 32.33°E |

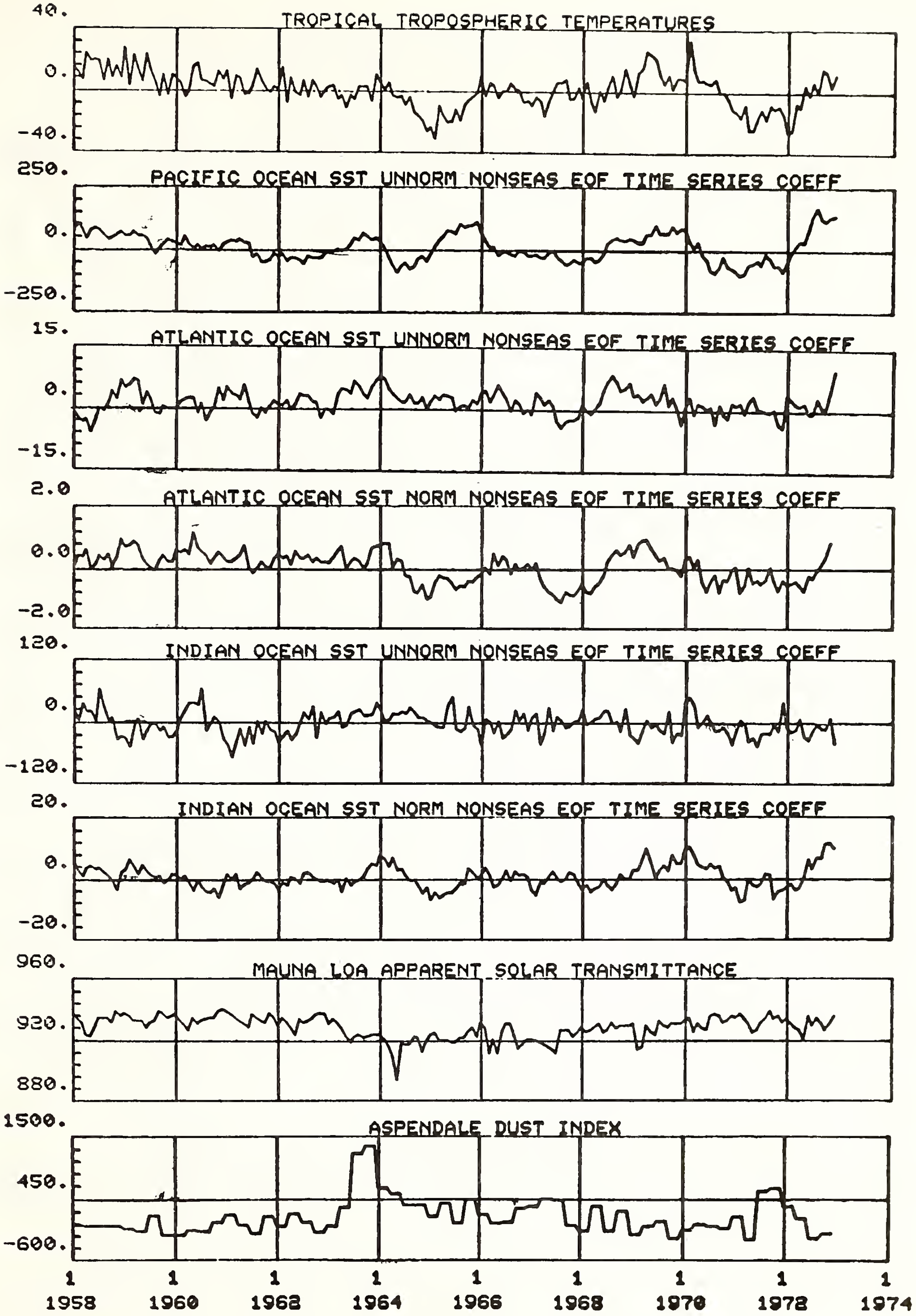

Figure 1a: Set of possible predictor time series and TTT

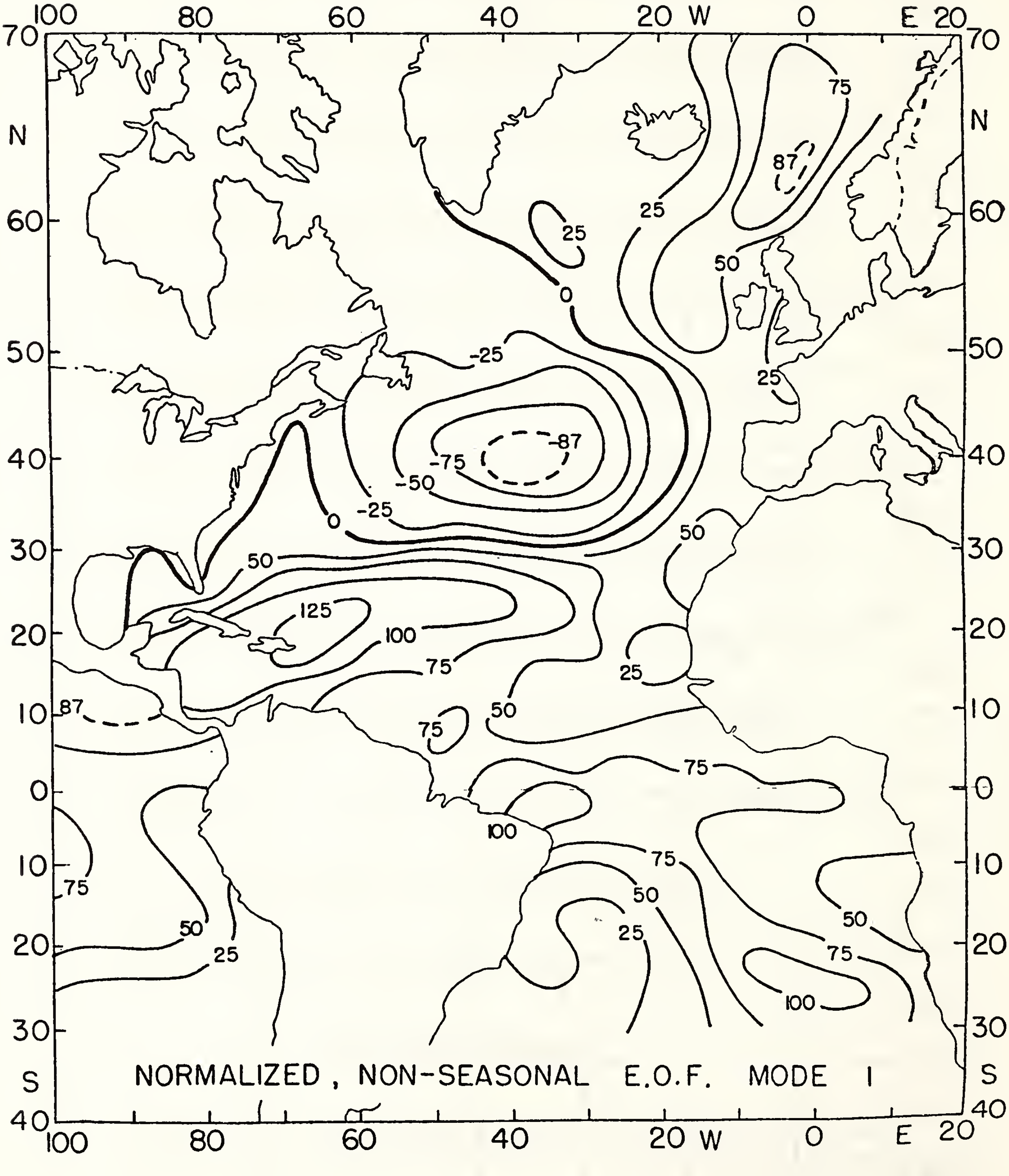

NORMALIZED, NON-SEASONAL E.O.F. MODE 1

Figure 1b: Atlantic Ocean empirical orthogonal function analysis

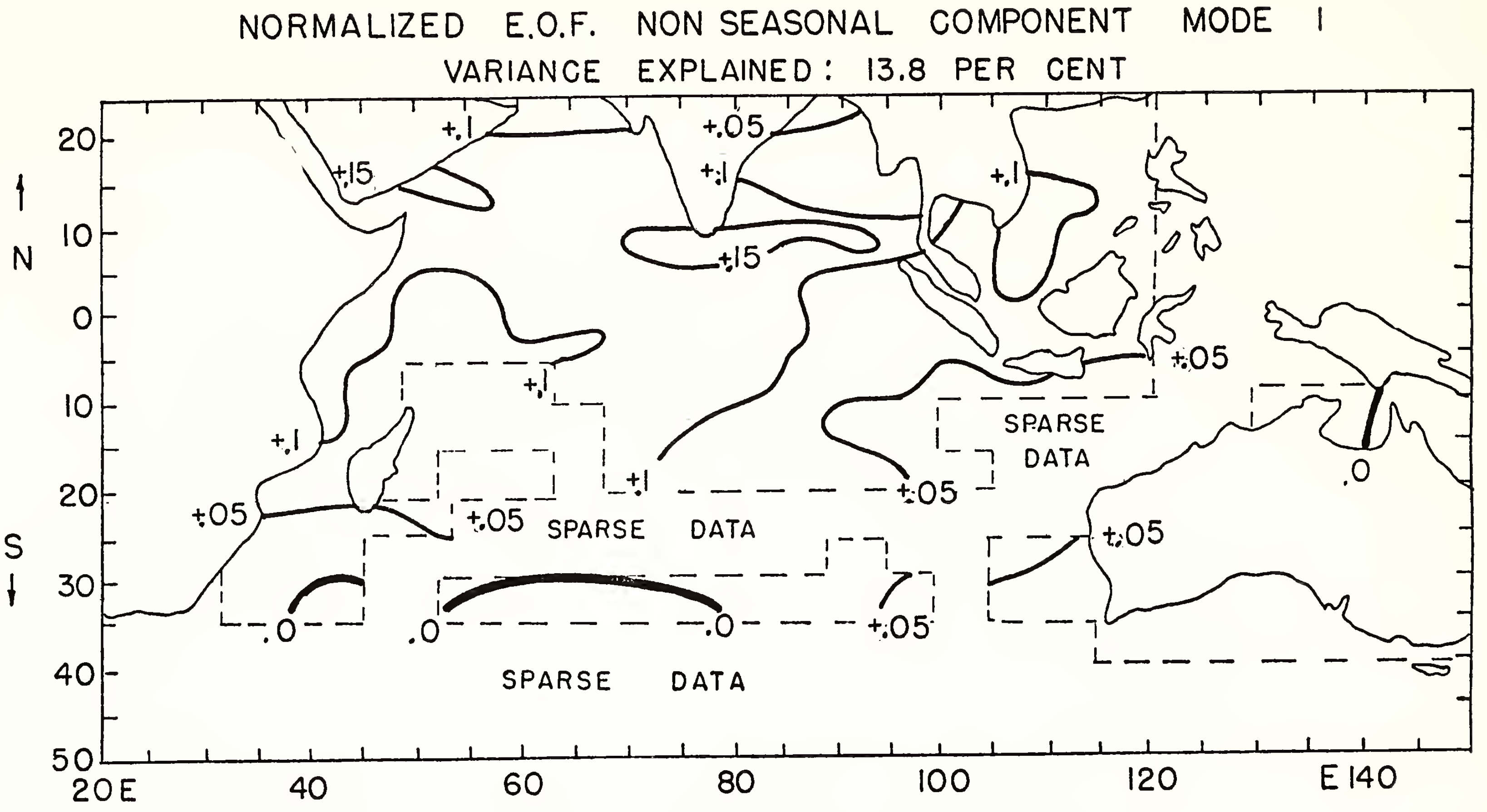

Figure 1c: Indian Ocean empirical orthogonal function (EOF) analysis

☆U.S. GOVERNMENT PRINTING OFFICE: 1980-311-046/98

PENN STATE UNIVERSITY LIBRARIES
A000072022467

NOAA--S/T 80-150